

MoDOT Pavement Preservation Research Program Volume V. Site-Specific Pavement Condition Assessment



Prepared by

Neil Anderson, PhD, PEng

Lesley Sneed, PhD, PE

Brent Rosenblad, PhD

Ronaldo Luna, PhD, PE

Missouri University of Science and Technology Departments of Geological Sciences &
Geological & Petroleum Engineering and Civil, Architectural & Environmental Engineering
University of Missouri-Columbia Department of Civil & Environmental Engineering



Final Report Prepared for Missouri Department of Transportation
November 2015

Project TRyy1141

Report cmr16-004

TECHNICAL REPORT DOCUMENTATION PAGE

1. Report No. cmr 16-004	2. Government Accession No.	3. Recipient's Catalog No.
4. Title and Subtitle MoDOT Pavement Preservation Research Program. Volume V, Site-Specific Pavement Condition Assessment		5. Report Date August 15, 2015 Published: November 2015
7. Author(s) Neil Anderson, PhD, PEng; Lesley Sneed, PhD, PE; Brent Rosenblad, PhD, PE; Ronaldo Luna, PhD, PE		6. Performing Organization Code
9. Performing Organization Name and Address Missouri University of Science and Technology Department of Geological Sciences & Geological & Petroleum Engineering 1400 N. Bishop, Rolla, MO 65409 Department of Civil, Architectural & Environmental Engineering 1401 N. Pine St., Rolla, MO 65409 University of Missouri-Columbia Department of Civil & Environmental Engineering E 2509 Lafferre Hall Columbia, MO 65211		8. Performing Organization Report No. NUTC R300
12. Sponsoring Agency Name and Address Missouri Department of Transportation (SPR) http://dx.doi.org/10.13039/100007251 Construction and Materials Division P.O. Box 270 Jefferson City, MO 65102 Center for Transportation Infrastructure and Safety/NUTC program Missouri University of Science and Technology 220 Engineering Research Lab Rolla, MO 65409		10. Work Unit No. 11. Contract or Grant No. MoDOT project #TRyy1141 (Task 4) NUTC project #00039112 USDOT contract #DTRT06-G-0014
15. Supplementary Notes Conducted in cooperation with the U.S. Department of Transportation, Federal Highway Administration. MoDOT research reports are available in the Innovation Library at http://www.modot.org/services/or/byDate.htm . This report is available at http://library.modot.mo.gov/RDT/reports/TRyy1141/cmr16-004v5.pdf .		13. Type of Report and Period Covered Final report (June 2012-August 2015)
16. Abstract The overall objective of Task 4 was to thoroughly assess the cost-effectiveness and utility of selected non-invasive technologies as applicable to MoDOT roadways. Non-invasive imaging technologies investigated in this project were Ultrasonic Surface Waves (USW), Impact Echo (IE), Ground-coupled Ground Penetrating Radar (GPR) (400 MHz and 1500 MHz antennae), Electrical Resistivity Tomography (ERT), Multichannel Analyses of Surface Waves (MASW), Falling Weight Deflectometer (FWD), Rolling Dynamic Deflectometer (RDD), and Air-launched Ground Penetrating Radar (GPR). USW, IE, ground coupled GPR (1500 MHz antennae), ERT, MASW, FWD, and RDD were used to acquire non-invasive data along eight designated project-level roadways. GPR (400 MHz) and air-launched GPR were used to acquire non-invasive data along two designated network-level roadways. High-frequency air-launched GPR is recommended for primary consideration for network-level investigations, and is recommended along all segments of pavement where ARAN data are collected. This data can be used to spot developing problems where further project-level investigations may be needed. USW, GPR, and FWD techniques are recommended for primary consideration for project-level investigations, where in situ properties of the pavement are needed, or for quality assurance purposes. At its current stage of development, RDD is recommended for secondary consideration for project-level investigations. ERT is recommended for primary consideration of the base, and MASW is recommended for secondary consideration, or where engineering properties of the base material are desired.		14. Sponsoring Agency Code

17. Key Words Evaluation and assessment; Level of service; Maintenance equipment; Pavement maintenance; Pavement management systems; Pavement performance; Preservation; Rehabilitation (Maintenance)		18. Distribution Statement No restrictions. This document is available through the National Technical Information Service, Springfield, VA 22161.	
19. Security Classif. (of this report) Unclassified.	20. Security Classif. (of this page) Unclassified.	21. No. of Pages 400	22. Price

Form DOT F 1700.7 (8-72)

Reproduction of completed page authorized

MoDOT PAVEMENT PRESERVATION RESEARCH PROGRAM
MoDOT TRyy1141

FINAL REPORT

VOLUME V
SITE-SPECIFIC PAVEMENT CONDITION ASSESSMENT

August 15, 2015

Prepared for
Missouri Department of Transportation

by

Neil Anderson Ph.D., P.Eng.
Professor

Department of Geological Sciences & Geological & Petroleum Engineering
Missouri University of Science and Technology

Lesley Sneed, Ph.D., P.E.
Associate Professor

Department of Civil, Architectural & Environmental Engineering
Missouri University of Science and Technology

Brent Rosenblad, Ph.D.
Associate Professor

Department of Civil & Environmental Engineering
University of Missouri

Ronaldo Luna, Ph.D., P.E.
Professor

Department of Civil, Architectural & Environmental Engineering
Missouri University of Science and Technology

The opinions, findings, and conclusions expressed in this publication are those of the investigators. They are not necessarily those of the Missouri Department of Transportation, U.S. Department of Transportation, or Federal Highway Administration. This information does not constitute a standard or regulation.

EXECUTIVE SUMMARY

The overall objective of the MoDOT Pavement Preservation Research Program, Task 4: *Site Specific Pavement Condition Assessment* was to thoroughly assess the cost-effectiveness and utility of selected non-invasive technologies as applicable to MoDOT roadways. The intent was to develop a guidance document focused on the utility and cost-effectiveness of project-applicable and network-applicable non-invasive imaging technologies. The optimal utilization of appropriate non-invasive imaging technologies will result in more accurate pavement assessments at significantly reduced costs. Assessment of the utility and cost-effectiveness of the tested *network*-applicable non-invasive imaging tools was based, in large part, on the analyses of data acquired along two designated roadways. Assessment of the utility and cost-effectiveness of the tested *project*-applicable non-invasive imaging tools was based, in large part, on the analyses of data acquired along eight designated roadways.

Non-invasive imaging technologies investigated in this project were Ultrasonic Surface Waves (USW), Impact Echo (IE), Ground-coupled Ground Penetrating Radar (GPR) (400 MHz and 1500 MHz antennae), Electrical Resistivity Tomography (ERT), Multichannel Analyses of Surface Waves (MASW), Falling Weight Deflectometer (FWD), Rolling Dynamic Deflectometer (RDD), and Air-launched Ground Penetrating Radar (GPR). To thoroughly assess the cost-effectiveness and utility of these technologies, corresponding field data were acquired across/along designated MoDOT roadways. USW, IE, ground coupled GPR (1500 MHz antennae), ERT, MASW, FWD, and RDD were used to acquire non-invasive data along eight designated project-level roadways. GPR (400 MHz) and air-launched GPR were used to acquire non-invasive data along two designated network-level roadways. Pavement cores extracted from each site served as ground truth for the non-invasive imaging technology results. Results of each investigation are summarized in the main body of this report and are summarized by technology.

Based on the findings summarized in this section, high-frequency air-launched GPR is recommended for primary consideration for network-level investigations of MoDOT pavements, and is recommended along all segments of pavement where ARAN data are collected. This data can be used to spot developing problems where further project-level investigations may be needed. USW, GPR, and FWD techniques are recommended for primary consideration for project-level investigations of MoDOT pavements, where in situ properties of the pavement are needed, or for quality assurance purposes. At its current stage of development, RDD is recommended for secondary consideration for project-level investigations of MoDOT pavements. ERT is recommended for primary consideration of the base, and MASW is recommended for secondary consideration, or where engineering properties of the base

material are desired. Appendix A includes the **Guidance Document** based on the results of the project-level and network-level investigations conducted.

This study was sponsored by the Missouri Department of Transportation and the National University Transportation Center at the Missouri University of Science and Technology in Rolla, Missouri. This research was performed by the Missouri University of Science and Technology and the University of Missouri. The report fully documents the research.

AUTHOR ACKNOWLEDGEMENTS

The research reported herein was sponsored by the Missouri Department of Transportation (MoDOT) and the National University Transportation Center (NUTC) at the Missouri University of Science and Technology (Missouri S&T). The research was performed by Missouri S&T and the University of Missouri-Columbia. At Missouri S&T, the principal investigator for this task (Task 4) was Lesley Sneed, and the technical lead was Neil Anderson. The co-principal investigator was Ronaldo Luna. The co-principal investigator at the University of Missouri-Columbia was Brent Rosenblad. The principal investigator for the overall project was David Richardson. Major contributions to the project were made by Evgeniy Torgashov, Brittany Coppedge, Adel Elkry, Brandon Goodwin, Dan Iffrig, Aleksey Khamzin, Mengxing Li, Stanley Nwokebuihe, Aleksandra Varnavina, David Willey, and Brandon Wolk. The assistance of each of these individuals is gratefully acknowledged.

TABLE OF CONTENTS

	Page
EXECUTIVE SUMMARY	ii
AUTHOR ACKNOWLEDGEMENTS.....	iv
TABLE OF CONTENTS.....	v
LIST OF FIGURES.....	ix
LIST OF TABLES.....	xxxvi
1 INTRODUCTION.....	1
1.1 Objectives.....	1
1.2 Justification	2
1.3 Scope of Work.....	4
1.4 Organization of the Report	5
1.5 Links to Report Sections on Individual Pavement Sections	6
2 DESCRIPTION OF PROJECT- AND NETWORK-LEVEL ROADWAYS.....	6
2.1 Project- and Network-Level Roadways: Survey Objectives	6
2.1.1 Project-Level Sites.....	6
2.1.2 Network-Level Sites	6
2.2 Project- and Network-Level Roadways: Investigation Dates and Weather Conditions	9
2.3 Project- and Network-Level Roadways: Visual Assessments	11
2.3.1 Project-Level Sites.....	11
2.3.1.1 Project-Level Site 1 (US 63).....	11
2.3.1.2 Project-Level Site 2 (US 54).....	12
2.3.1.3 Project-Level Site 3 (MO 179).....	14
2.3.1.4 Project-Level Site 4 (HWY AT).....	14
2.3.1.5 Project-Level Site 5 (I-55 Pemiscot County).....	16
2.3.1.6 Project-Level Site 6 (I-55 Perry County).....	17
2.3.1.7 Project-Level Site 7 (HWY U).....	18
2.3.1.8 Project-Level Site 8 (I-35).....	19
2.3.2 Network-Level Sites	20
2.3.2.1 Network-Level Site 9 (I-70)	20
2.3.2.2 Network-Level Site 10 (MO 465)	23
2.4 Project- and Network-Level Roadways: Core Assessments.....	25
2.4.1 Project-Level Sites.....	25
2.4.1.1 Project-Level Site 1 (US 63).....	25
2.4.1.2 Project-Level Site 2 (US 54).....	28
2.4.1.3 Project-Level Site 3 (MO 179).....	31
2.4.1.4 Project-Level Site 4 (HWY AT).....	34
2.4.1.5 Project-Level Site 5 (I-55 Pemiscot County).....	37
2.4.1.6 Project-Level Site 6 (I-55 Perry County).....	40
2.4.1.7 Project-Level Site 7 (HWY U).....	42
2.4.1.8 Project-Level Site 8 (I-35).....	44
2.4.2 Network-Level Sites	47

2.4.2.1	Network-Level Site 9 (I-70)	47
2.4.2.2	Network-Level Site 10 (MO 465)	49
3	PROJECT-LEVEL ULTRASONIC SURFACE WAVE AND IMPACT ECHO INVESTIGATIONS	52
3.1	Introduction	52
3.2	PSPA Data Acquisition, Processing, and Interpretation	53
3.2.1	PSPA Data Acquisition	53
3.2.2	PSPA Data Processing and Interpretation	54
3.2.2.1	Ultrasonic Surface Wave Data Analyses	54
3.2.2.2	Impact Echo Data Analyses	57
3.2.3	Typical Elastic Modulus of Asphalt Concrete (AC; Bituminous Mix (BM)) and Portland Cement Concrete (PCC)	59
3.3	Project-Level PSPA Data: USW and IE	60
3.3.1	Project-Level Site 1 (US 63)	60
3.3.1.1	Ultrasonic Surface Wave Data	60
3.3.1.2	Impact Echo Data	71
3.3.2	Project-Level Site 2 (US 54)	72
3.3.2.1	Ultrasonic Surface Wave Data	72
3.3.2.2	Impact Echo Data	82
3.3.3	Project-Level Site 3 (MO 179)	83
3.3.3.1	Ultrasonic Surface Wave Data	84
3.3.3.2	Impact Echo Data	93
3.3.4	Project-Level Site 4 (HWY AT)	94
3.3.4.1	Ultrasonic Surface Wave Data	95
3.3.4.2	Impact Echo Data	104
3.3.5	Project-Level Site 5 (I-55 Pemiscot Co.)	105
3.3.5.1	Ultrasonic Surface Wave Data 06	106
3.3.5.2	Impact Echo Data	118
3.3.6	Project-Level Site 6 (I-55 Perry County)	119
3.3.6.1	Ultrasonic Surface Wave Data	120
3.3.6.2	Impact Echo Data	127
3.3.7	Project-Level Site 7 (HWY U)	128
3.3.7.1	Ultrasonic Surface Wave Data	129
3.3.7.2	Impact Echo Data	136
3.3.8	Project-Level Site 8 (I-35)	137
3.3.8.1	Ultrasonic Surface Wave Data	138
3.3.8.2	Impact Echo Data	145
3.4	Concluding Remarks	146
4	PROJECT-LEVEL HIGH-FREQUENCY GROUND PENETRATING RADAR INVESTIGATIONS	147
4.1	Introduction	147
4.2	Overview of Project-Level High-Frequency GPR Investigations	149
4.3	Project-Level High-Frequency GPR (1.5 GHz) Data	152
4.3.1	Project-Level Site 1 (US 63)	152
4.3.2	Project-Level Site 2 (US 54)	160
4.3.3	Project-Level Site 3 (MO 179)	166

4.3.4	Project-Level Site 4 (HWY AT)	171
4.3.5	Project-Level Site 5 (I-55 Pemiscot Co.)	178
4.3.6	Project-Level Site 6 (I-55 Perry Co.)	184
4.3.7	Project-Level Site 7 (HWY U).....	191
4.3.8	Project-Level Site 8 (I-35).....	197
4.4	Concluding Remarks.....	202
5	PROJECT-LEVEL LOW-FREQUENCY GROUND PENETRATING RADAR INVESTIGATIONS	204
5.1	Introduction	204
5.2	Overview of Project-Level Low-Frequency GPR Investigations.....	204
5.3	Project-Level Low-Frequency GPR (400 MHz) Data.....	205
5.3.1	Project-Level Site 1 (US 63).....	205
5.3.2	Project-Level Site 2 (US 54).....	206
5.3.3	Project-Level Site 3 (MO 179)	207
5.3.4	Project-Level Site 4 (HWY AT)	208
5.3.5	Project-Level Site 5 (I-55 Pemiscot County).....	209
5.3.6	Project-Level Site 6 (I-55 Perry County).....	210
5.3.7	Project-Level Site 7 (HWY U).....	211
5.3.8	Project-Level Site 8 (I-35).....	213
5.4	Concluding Remarks.....	213
6	SURFACE WAVE AND ELECTRICAL RESISTIVITY TOMOGRAPHY INVESTIGATIONS	216
6.1	Introduction	216
6.1.1	Electrical Resistivity Tomography (ERT).....	216
6.1.2	Multi-Channel Analyses of Surface Wave (MASW)	217
6.2	Overview of Project-Level ERT and MASW Investigations	218
6.3	Overview of Data Acquisition, Processing, and Interpretation	222
6.3.1	Electrical Resistivity Tomography (ERT).....	222
6.3.2	Multi-Channel Analyses of Surface Wave (MASW)	223
6.4	Project-Level ERT and MASW Data.....	225
6.4.1	Project-Level Site 1 (US 63).....	225
6.4.1.1	Electrical Resistivity Tomography Data.....	225
6.4.1.2	Multi-Channel Surface Wave Analyses Data	226
6.4.2	Project-Level Site 2 (US 54).....	228
6.4.2.1	Electrical Resistivity Tomography Data.....	228
6.4.2.2	Multi-Channel Surface Wave Analyses Data	229
6.4.3	Project-Level Site 3 (MO 179)	231
6.4.3.1	Electrical Resistivity Tomography Data.....	231
6.4.3.2	Multi-Channel Surface Wave Analyses Data	232
6.4.4	Project-Level Site 4 (HWY AT)	234
6.4.4.1	Electrical Resistivity Tomography Data.....	234
6.4.4.2	Multi-Channel Surface Wave Analyses Data	235
6.4.5	Project-Level Site 5 (I-55 Pemiscot County).....	237
6.4.5.1	Electrical Resistivity Tomography Data.....	237
6.4.5.2	Multi-Channel Surface Wave Analyses Data	238
6.4.6	Project-Level Site 6 (I-55 Perry County).....	240

6.4.6.1	Electrical Resistivity Tomography Data.....	240
6.4.6.2	Multi-Channel Surface Wave Analyses Data	241
6.4.7	Project-Level Site 7 (HWY U).....	243
6.4.7.1	Electrical Resistivity Tomography Data.....	243
6.4.7.2	Multi-Channel Surface Wave Analyses Data	244
6.4.8	Project-Level Site 8 (I-35).....	246
6.4.8.1	Electrical Resistivity Tomography Data.....	246
6.4.8.2	Multi-Channel Surface Wave Analyses Data	247
6.5	Concluding Remarks.....	249
7	ROLLING DYNAMIC DEFLECTOMETER (RDD) AND FALLING WEIGHT DEFLECTOMETER (FWD) INVESTIGATIONS.....	251
7.1	Introduction	251
7.2	FWD Data Acquisition, Processing, and Interpretation	255
7.2.1	FWD Data Acquisition	255
7.2.2	FWD Data Processing and Interpretation	256
7.3	RDD Data Acquisition, Processing, and Interpretation.....	257
7.3.1	RDD Data Acquisition	257
7.3.2	RDD Data Processing and Interpretation.....	259
7.4	RDD and FWD Results	262
7.4.1	Project Level Site 1 (US 63)	262
7.4.2	Project Level Site 2 (US 54)	267
7.4.3	Project Level Site 3 (HWY 179)	271
7.4.4	Project Level Site 4 (HWY AT)	275
7.4.5	Project Level Site 5 (I-55, Pemiscot County).....	276
7.4.6	Project Level Site 6 (I-55, Perry County)	280
7.4.7	Project Level Site 7 (HWY U)	280
7.4.8	Project Level Site 8 (I-35)	282
7.4.9	Additional Project-Level Site for RDD Testing (I-35 Southbound).....	286
7.5	Concluding Remarks on Application of the RDD to Missouri Pavement Management.....	288
8	NETWORK-LEVEL GROUND PENETRATING RADAR INVESTIGATIONS	290
8.1	Introduction	290
8.2	Overview of Network-Level GPR Investigations	290
8.3	Network-Level GPR Investigations.....	291
8.3.1	Network-Level Site 9 (I-70 WB).....	291
8.3.2	Network-Level Site 10 (MO 465)	309
8.4	Concluding Remarks.....	320
9	SUMMARY AND CONCLUSIONS	321
	Appendix A GUIDANCE DOCUMENT	331
	Appendix B PAVEMENT CORES AND AUGER SAMPLES	359

LIST OF FIGURES

	Page
Fig. 2.1–Map showing locations of eight project-level sites and two network-level sites.....	7
Fig. 2.2–Map showing network-level Site 9 (I-70). GPR data were acquired in the west-bound driving lane.	8
Fig. 2.3–Map showing network-level Site 10 (MO 465). GPR data were acquired in all four lanes (two north-bound; two south-bound).....	8
Fig. 2.4–Photograph of US 63 (Site 1). The pavement was observed to be in excellent condition with no visible surface defects.	12
Fig. 2.5–Photograph of US 54 (Site 2). The pavement appeared to be in fair condition with block crack, alligator cracks and rutting observed on the surface.	13
Fig. 2.6–Photograph of US 54 (Site 2). The pavement was observed to be in fair condition with evidence of patches as well as longitudinal and transverse cracks on the surface.	13
Fig. 2.7–Photograph showing typical condition of the MO 179 (Site 3) pavement site at the time of field investigation.	14
Fig. 2.8–Photograph of HWY AT (Site 4) pavement. Cracks were visible on the pavement surface.....	15
Fig. 2.9–Photograph showing cracks and patch observed on the HWY AT (Site 4) pavement surface.....	15
Fig. 2.10–Photograph of I-55 Pemiscot County (Site 5) pavement.	16
Fig. 2.11–Photograph of I-55 Perry County (Site 6). The pavement appeared to be in very good condition with few cracks on the surface.....	17
Fig. 2.12–Cracks, rutting, and patches observed on the pavement surface at HWY U (Site 7).	18
Fig. 2.13–I-35 (Site 8) showing evidence of cracks and patches on the pavement surface.....	19
Fig. 2.14–I-35 (Site 8) showing evidence of cracks on the pavement surface.	19
Fig. 2.15–Typical section of the network-level Site 9 (I-70) pavement. This paved surface was judged to be in good condition.	20
Fig. 2.16–Photograph of section of network-level Site 9 (I-70) showing cracked and patched surface of a bridge deck.....	21
Fig. 2.17–Photograph of section of network-level Site 9 (I-70) showing patched pavement near bridge.....	21
Fig. 2.18–Photograph of section of network-level Site 9 (I-70) showing transition from PCC to bituminous mix.....	22
Fig. 2.19–Photograph section of network-level Site 9 (I-70) showing cracks and patches on bridge deck.....	22
Fig. 2.20–Photograph of section of network-level Site 9 (I-70) showing pavement that was recently treated.	23
Fig. 2.21–MO 465 (network-level Site 10) pavement in good condition.	23
Fig. 2.22–Photograph of segment of network-level Site 10 (MO 465) bridge with recently applied treatment.....	24
Fig. 2.23– Section of network-level Site 10 (MO 465) pavement with evidence of cracks and rutting.	24

Fig. 2.24–Recently treated segment of MO 465 (network-level Site 10).	25
Fig. 2.25–Photographs of cores extracted at US 63 (project-level Site 1).	26
Fig. 2.26–Photographs of US 63 (project-level Site 1) cores split to evaluate degree of stripping.	27
Fig. 2.27–Photographs of cores extracted at US 54 (project-level Site 2).	29
Fig. 2.28–Photographs of US 54 (project-level Site 2) cores split to evaluate degree of stripping.	30
Fig. 2.29–Photographs of cores extracted at MO 179 (project-level Site 3).	32
Fig. 2.30–Photographs of MO 179 (project-level Site 3) cores split to evaluate degree of stripping.	33
Fig. 2.31–Photographs of cores extracted at HWY AT (project-level Site 4).	35
Fig. 2.32–Photographs of HWY AT (project-level Site 4) cores split to evaluate degree of stripping.	36
Fig. 2.33–Photographs of cores extracted at I-55 Pemiscot County (project-level Site 5).	38
Fig. 2.34–Photographs of I-55 Pemiscot County (project-level Site 5) cores split to evaluate degree of stripping.	39
Fig. 2.35–Photographs of cores extracted at I-55 Perry County (project-level Site 6).	41
Fig. 2.36–Photographs of cores extracted at HWY U (project-level Site 7).	43
Fig. 2.37–Photographs of cores extracted at I-35 (project-level Site 8).	45
Fig. 2.38–Photographs of I-35 (project-level Site 8) cores split to evaluate degree of stripping.	46
Fig. 2.39–Photographs of cores extracted at I-70 (network-level Site 9).	48
Fig. 2.40–Photographs of cores extracted at MO 465 (network-level Site 10).	50
Fig. 3.1–Photograph of the portable seismic property analyzer (PSPA). The PSPA is a portable system consisting of a data acquisition box, a high-frequency acoustic impact source and two vertically-polarized receiver transducers. The PSPA is connected to a laptop computer that controls the PSPA and automatically stores, processes and interprets the acoustic signals (surface wave and compressional wave) recorded by the receiver transducers. A transducer spacing of either 4 in. or 6 in. is normally employed.	52
Fig. 3.2–Not-to-scale sketch showing PSPA test grid (2 ft x 100 ft) employed for each project-level Sites 1-6 and 8 (a 1.5 ft x 100 ft grid was employed at Site 7). As shown, five PSPA data sets (e.g. 1-5, 6-10, etc.) were acquired every 100 ft along each project-level pavement section. In total, 55 PSPA data sets were acquired for each project-level investigation except Sites 7 and 8 (where 66 PSPA data sets were acquired). All PSPA data sets were acquired along a GPR traverse (see Section 4 of this report). The spacing (1 ft in figure) between the outermost PSPA test locations and the edge of pavement varied from site to site. Core locations also varied from site to site.	54
Fig. 3.3–The PSPA tool records both ultrasonic surface wave (UBW-USW caption) and reverberating compressional wave (IE caption) data. The ultrasonic surface wave (USW) data acquired at each test location were automatically transformed into a 1-D plot of elastic modulus. The reverberating compressional wave (IE; impact echo) data were used to estimate pavement layer thicknesses and/or to detect horizontal flaws (Gucunski et al., 2008). Receiver transducer spacing can be set at either 4 in. or 6 in.	55

Fig. 3.4—Example automated output for a single example PSPA test location. Calculated elastic moduli (ksi) are plotted over the depth range tested (2 in. - approx.7 in.); the average elastic modulus over this depth range is also plotted. The plotted elastic moduli range from 3405 ksi to 3825 ksi; the average elastic modulus is 3510 ksi. The reflector depths (4.0 in. and 5.3 in.) corresponding to the peaks on the “Echo Amp” plot ideally represent either pavement layer thicknesses or the depth to flaws (debonding or delaminations) within the pavement. In this case, 4.0 in. depth corresponds to the thickness of the overlying asphalt concrete. The 5.3 in. depth does not correspond to either a pavement layer or a known defect. Rather, it is thought to be caused by the flexural wave propagating within the upper asphalt concrete layer. 56

Fig. 3.5—The “ideal” amplitude spectrum for intact and layered/debonded concrete pavement (Source: 2007, Celaya et al). “ f_h ” is the resonance frequency of the reverberating compressional wave energy reflected from the base of pavement; “ f_d ” is the resonance frequency of the reverberating compressional wave energy reflected from the flaw within the pavement..... 59

Fig. 3.6—Photograph of PSPA tool placed on pavement at project-level Site 1 (US 63 N). 61

Fig. 3.7—Base map for project-level Site 1 showing PSPA test locations and core locations. PSPA data were acquired at 100 ft intervals along each GPR transverse. GPR traverse 1 was located 2 ft from the outer edge of the driving lane (shoulder). Only cores 1 and 4 were located within 10 ft of a PSPA location. 63

Fig. 3.8—Elastic modulus plot generated from PSPA USW data acquired in immediate proximity to core 01 (Fig. 3.7). The pavement consists of two BM layers over an existing PCC layer. No visible evidence of debonding or stripping was observed in core 01. The elastic modulus of the BM is consistently greater than 3200 ksi, even in proximity to the BM/PCC interface. The acoustic interface between the BM and PCC cannot be confidently identified. The apparent average elastic modulus of the PCC is 3250 ksi. 64

Fig. 3.9—Elastic modulus plot generated from PSPA USW data acquired in immediate proximity to core 04 (Fig. 3.7). The BM/PCC contact was debonded, however there was no evidence of chemical or physical degradation of the PCC. The elastic modulus of the BM is slightly less than 3100 ksi near the BM/PCC interface. The acoustic interface between the BM and PCC cannot be confidently identified. The apparent average elastic modulus of the PCC is 3386 ksi. 64

Fig. 3.10—Elastic modulus plot generated from PSPA USW data acquired about 30 ft from core 07 (Fig. 3.7). The pavement consists of two BM layers over an existing PCC layer. The interface between the second layer of BM and PCC was debonded. The elastic modulus of the BM is slightly less than 3100 ksi near the BM/PCC interface. The acoustic interface between the BM and PCC cannot be confidently identified. The apparent average elastic modulus of the PCC is 2654. This value is anomalously low compared to the PSPA data acquired at core locations 01 and 04. The core 07 PCC appears to be physically and chemically degraded. 65

Fig. 3.11—Cross-sections depicting variations in the elastic modulus (ksi) for BM for PSPA USW data acquired at the 0 ft to 400 ft intervals along the GPR traverses. The five PSPA USW data sets in each cross-section were acquired at 2 ft intervals starting 2 ft

from the edge of pavement (Fig. 3.7). Depth of investigation extends from 2 in. to approx. 3.7 in.	66
Fig. 3.12–Cross-sections depicting variations in the elastic modulus (ksi) for BM for PSPA USW data acquired at the 500 ft to 1000 ft intervals along the GPR traverses.	67
Fig. 3.13–Cross-sections depicting variations in the elastic modulus (ksi) for concrete for PSPA USW data acquired at the 0 ft to 300 ft intervals along the GPR traverses. The five PSPA USW data sets in each cross-section were acquired at 2 ft intervals starting 2 ft from the edge of pavement (Fig. 3.7). Depth of investigation extends from 4 in. to approx. 7.2 in.	68
Fig. 3.14–Cross-sections depicting variations in the elastic modulus (ksi) for concrete for PSPA USW data acquired at the 400 ft to 700 ft intervals along the GPR traverses.	69
Fig. 3.15–Cross-sections depicting variations in the elastic modulus (ksi) for concrete for PSPA USW data acquired at the 800 ft to 1000 ft intervals along the GPR traverses.	70
Fig. 3.16–Plot of the average elastic modulus (over depth range of 2 to 7.2 in.) along each GPR transverse. The GPR traverses are spaced at 2 ft intervals. GPR traverse 1 is 2 ft from the outer edge of the pavement.	71
Fig. 3.17–The PSPA IE calculated depth to shallowest identified reflector is plotted for all PSPA test locations (Fig. 3.7). The average calculated depth to this reflector (approx. 4 in.) measurement agrees well with the actual thickness (approx. 3.5 in.) of the BM layer.	72
Fig. 3.18–The calculated depth to the deeper reflector (corresponding to the lower peak frequency) was consistently about 5.2 in. (Fig. 3.17). The depth to the PSPA IE identified deeper reflector does not correlate to any known pavement interface. This resonant frequency is therefore attributed to noise (possibly the flexural wave propagating through the asphalt layer).	73
Fig. 3.19–Photograph of PSPA tool placed on pavement at project-level Site 2 (US 54).	74
Fig. 3.20–Base map for project-level Site 2 showing PSPA test locations and core locations. PSPA data were acquired at 100 ft intervals along each GPR transverse. GPR traverse 1 was located 2 ft from the outer edge of the paved driving lane (at the shoulder). Only cores 03, 04, 05 and 09 are located within 25 ft of a PSPA location.	75
Fig. 3.21–Elastic modulus plot generated from PSPA USW data acquired in immediate proximity to stripped and debonded core 03 (Fig. 3.20). The pavement consists of approx. 11 in. of BM. The PSPA USW average elastic modulus for core 03 is 1058 ksi indicating the BM is severely deteriorated BM (at an air temperature of 32 °F; Table 3.2).	76
Fig. 3.22–Elastic modulus plot generated from PSPA USW data acquired in immediate proximity to stripped and debonded core 04 (Fig. 3.20). The PSPA USW average elastic modulus for core 04 is 1914 ksi indicating the BM is severely deteriorated BM (at an air temperature of 32 °F; Table 3.2).	76
Fig. 3.23–Elastic modulus plot generated from PSPA USW data acquired in immediate proximity to stripped and debonded core 05 (Fig. 3.20). The PSPA USW average elastic modulus for core 05 is 1366 ksi indicating the BM is severely deteriorated BM (at an air temperature of 32 °F; Table 3.2).	77

Fig. 3.24—Elastic modulus plot generated from PSPA USW data acquired in immediate proximity to stripped and debonded core 09 (Fig. 3.20). The PSPA USW average elastic modulus for core 09 is 1858 ksi indicating the BM is severely deteriorated BM (at an air temperature of 32 °F; Table 3.2). 77

Fig. 3.25—Cross-sections depicting variations in the PSPA USW elastic modulus (ksi) of the BM at the 0 ft, 100 ft, and 200 ft intervals along the GPR traverses. The five PSPA USW data sets in each cross-section were acquired at 2 ft intervals starting 2 ft from the edge of pavement (Fig. 3.20). Depth of investigation extends from 2 in. to approx. 7.2 in. 78

Fig. 3.26—Cross-sections depicting variations in the PSPA USW elastic modulus (ksi) of the BM at the 300 ft, 400 ft, and 500 ft intervals along the GPR traverses. PSPA data could not be acquired at the 4 ft mark on the 300 ft profile because of the deteriorated nature of the paved surface. 79

Fig. 3.27—Cross-sections depicting variations in the PSPA USW elastic modulus (ksi) of the BM at the 600 ft, 700 ft, and 800 ft intervals along the GPR traverses..... 80

Fig. 3.28—Cross-sections depicting variations in the PSPA USW elastic modulus (ksi) of the BM at the 900 ft and 1000 ft intervals along the GPR traverses. PSPA data could not be acquired at the 8 ft mark on the 1000 ft profile because of the deteriorated nature of the paved surface. 81

Fig. 3.29—Plot of the average elastic modulus (over depth range of 2 to 7.2 in.) along each GPR transverse. The GPR traverses are spaced at 2 ft intervals. GPR traverse 1 is 2 ft from the outer edge of the pavement..... 82

Fig. 3.30—The PSPA IE calculated depth to shallowest identified reflector is plotted for all PSPA test locations (Fig. 3.20)..... 83

Fig. 3.31—Photograph of PSPA tool placed on pavement at project-level Site 3 (MO 179). 84

Fig. 3.32—Base map for project-level Site 3 showing PSPA test locations and core locations. PSPA data were acquired at 100 ft intervals along each GPR transverse. GPR traverse 1 was located 1 ft from the outer edge of the paved driving lane (shoulder). Only cores 01 and 02 are located within 20 ft of a PSPA location. 85

Fig. 3.33—Elastic modulus plot generated from PSPA USW data acquired in immediate proximity to intact core 01 (Fig. 3.32). The pavement consists of approx. 12 in. of BM. The PSPA USW average elastic modulus for core 01 is 3022 ksi indicating the BM is fair quality (at an air temperature of 32 °F; Table 3.2). 86

Fig. 3.34—Elastic modulus plot generated from PSPA USW data acquired in immediate proximity to intact core 02 (Fig. 3.32). The pavement consists of approx. 12 in. of BM. The PSPA USW average elastic modulus for core 01 is 3147 ksi indicating the BM is fair quality (at an air temperature of 32 °F; Table 3.2). 86

Fig. 3.35—Elastic modulus plot generated from PSPA USW data acquired within 12 ft of intact core 04 (Fig. 3.32). The pavement consists of approx. 12 in. of BM. The PSPA USW average elastic modulus for core 04 is 3582 ksi indicating the BM is fair quality (at an air temperature of 32 °F; Table 3.2). Core 04 was located about 12 ft from the PSPA location. 87

Fig. 3.36—Elastic modulus plot generated from PSPA USW data acquired within 20 ft of core 07 (Fig. 3.32). This core was debonded at a depth of approx. 4 in. (weak bonded

at a depth of 1.5 in.) The PSPA USW average elastic modulus for core 04 is 2522 ksi indicating the BM is poor quality (at an air temperature of 32 °F; Table 3.2). Note that the elastic modulus of the pavement decreases abruptly at a depth of 4 in. 87

Fig. 3.37–Cross-sections depicting variations in the PSPA USW elastic modulus (ksi) of the BM at the 0 ft, 100 ft, and 200 ft intervals along the GPR traverses. The five PSPA USW data sets in each cross-section were acquired at 2 ft intervals starting 1 ft from the edge of pavement. PSPA data could not be acquired at the 5 ft and 9 ft marks on the 0 ft traverse because of the deteriorated nature of the paved surface. 89

Fig. 3.38–Cross-sections depicting variations in the PSPA USW elastic modulus (ksi) of the BM at the 300 ft, 400 ft, and 500 ft intervals along the GPR traverses. PSPA data could not be acquired at several test locations because of the deteriorated nature of the paved surface. 90

Fig. 3.39–Cross-sections depicting variations in the PSPA USW elastic modulus (ksi) of the BM at the 600 ft, 700 ft, and 800 ft intervals along the GPR traverses. 91

Fig. 3.40–Cross-sections depicting variations in the PSPA USW elastic modulus (ksi) of the BM at the 900 ft and 1000 ft intervals along the GPR traverses. 92

Fig. 3.41–Plot of the average elastic modulus (over depth range of 2 in. to 7.2 in.) along each GPR transverse. The GPR traverses are spaced at 2 ft intervals. GPR traverse 1 is 1 ft from the outer edge of the pavement. 93

Fig. 3.42–The PSPA IE calculated depth to shallowest identified reflector is plotted for all PSPA test locations (Fig. 3.32). 94

Fig. 3.43–Photograph of PSPA tool placed on pavement at project-level Site 4 (HWY -AT). 95

Fig. 3.44–Base map for project-level Site 4 showing PSPA test locations and core locations. PSPA data were acquired at 100 ft intervals along each GPR transverse. GPR traverse 1 was located 1 ft from the outer edge of the paved driving lane (shoulder). Only cores 01, 03, 04, and 07 are located within 5 ft of a PSPA location. 97

Fig. 3.45–Elastic modulus plot generated from PSPA USW data acquired in immediate proximity to stripped core 01 (Fig. 3.44). The PSPA USW average elastic modulus for core 01 is 1160 ksi indicating the BM is fair quality (at an air temperature of 70 °F, Table 3.2). 98

Fig. 3.46–Elastic modulus plot generated from PSPA USW data acquired within 25 ft of debonded and stripped core 02 (Fig. 3.44). The core is comprised of approx. 8 in. of BM overlay and 6 in. of underling PCC. The average elastic modulus of the BM is 729 ksi which corresponds to poor quality at 70 °F (Table 3.2). The average “apparent” elastic modulus of the PCC is 609 ksi. This extremely low “apparent” average elastic modulus means the PCC is severely deteriorated (Table 3.1). 98

Fig. 3.47–Elastic modulus plot generated from PSPA USW data acquired in immediate proximity to debonded and stripped core 07 (Fig. 3.44). The core is comprised of approx. 7 in. of BM overlay and 6 in. of underlying PCC. The average elastic modulus of the BM is 885 ksi which corresponds to poor quality at 70 °F (Table 3.2). The average “apparent” elastic modulus of the PCC is 702 ksi. This extremely low “apparent” average elastic modulus means the PCC is severely deteriorated (Table 3.1). 99

Fig. 3.48—Elastic modulus plot generated from PSPA USW data acquired in immediate proximity to debonded and stripped core 09 (Fig. 3.44). The core is comprised of approx. 4 in. of BM overlay and 6 in. of underling PCC. The average elastic modulus of the BM is 594 ksi which corresponds to poor quality at 70 °F (Table 3.2). The average “apparent” elastic modulus of the PCC is 507 ksi. This extremely low “apparent” average elastic modulus means the PCC is severely deteriorated (Table 3.1). 99

Fig. 3.49—Cross-sections depicting variations in the PSPA USW elastic modulus (ksi) of the pavement at the 0 ft, 100 ft, and 200 ft intervals along the GPR traverses. The six PSPA USW data sets in each cross-section were acquired at 2 ft intervals starting 1 ft from the edge of pavement. The pavement at Site 4 is comprised of BM of variable thickness and underlying PCC. Inasmuch as the thickness of the BM is unknown at most PSPA test locations, no attempt has been made to differentiate the elastic modulus values of the overlying AC from the “apparent” elastic modulus of the underlying PCC. 100

Fig. 3.50—Cross-sections depicting variations in the PSPA USW elastic modulus (ksi) of the pavement at the 300 ft, 400 ft, and 500 ft intervals along the GPR traverses. No attempt has been made to differentiate the elastic modulus values of the overlying BM from the “apparent” elastic modulus of the underlying PCC. 101

Fig. 3.51—Cross-sections depicting variations in the PSPA USW elastic modulus (ksi) of the pavement at the 600 ft, 700 ft, and 800 ft intervals along the GPR traverses. No attempt has been made to differentiate the elastic modulus values of the overlying BM from the “apparent” elastic modulus of the underlying PCC. 102

Fig. 3.52—Cross-sections depicting variations in the PSPA USW elastic modulus (ksi) of the pavement at the 300 ft, 400 ft, and 500 ft intervals along the GPR traverses. No attempt has been made to differentiate the elastic modulus values of the overlying BM from the “apparent” elastic modulus of the underlying PCC. 103

Fig. 3.53—Plot of the average elastic modulus (over depth range of 3 in. to 11 in.) along each GPR transverse. The GPR traverses are spaced at 2 ft intervals. GPR traverse 1 is 1 ft from the outer edge of the pavement. 104

Fig. 3.54—The apparent thickness measurements for the pavement..... 105

Fig. 3.55—Photograph of PSPA tool placed on pavement at project-level Site 5 (I-55 N). 106

Fig. 3.56—Base map for project-level Site 5 showing PSPA test locations and core locations. PSPA data were acquired at 100 ft intervals along each GPR transverse. GPR traverse 1 was located 1 foot from the outer edge of the paved driving lane (shoulder). Only cores 01, 02, 03 and 04 are located within 5 ft of a PSPA location. 108

Fig. 3.57—Elastic modulus plot generated from PSPA USW data acquired in immediate proximity to debonding core 01 (Fig. 3.56). The tested pavement consists of 8.5 in. of PCC overlay above an 8.75 in. thick PCC layer. A 2.5 in. thick layer of asphalt (BM) is embedded between the two PCC layers. The upper layer of PCC and the underlying BM were debonded. The upper layer of PCC showed visible evidence of physical degradation..... 109

Fig. 3.58—Elastic modulus plot generated from PSPA USW data acquired in immediate proximity to stripped and debonded core 02 (Fig. 3.56). The tested pavement consists of 8.5 in. of overlay above an 8.75 in. thick PCC layer. A 2.5 in. thick layer of asphalt is

embedded between the two PCC layers. The upper layer of PCC and the underlying AC were debonded. The upper layer of PCC showed visible evidence of physical degradation.....	109
Fig. 3.59—Elastic modulus plot generated from PSPA USW data acquired in immediate proximity to intact core 06 (Fig. 3.56). The tested pavement consists of 8.5 in. of PCC overlay above an 8.75 in. thick PCC layer. A 2.5 in. thick layer of asphalt (BM) is embedded between the two PCC layers. No visible evidence of debonding was observed in core 06.	110
Fig. 3.60—Elastic modulus plot generated from PSPA USW data acquired in immediate proximity to intact core 08 (Fig. 3.56). The tested pavement consists of 8.5 in. of overlay above an 8.75 in. thick PCC layer. A 2.5 in. thick layer of asphalt (BM) is embedded between the two PCC layers. No visible evidence of debonding was observed in core 08.	110
Fig. 3.61—Cross-sections depicting variations in the elastic modulus (ksi) for PCC for PSPA USW data acquired at the 0 ft, 100 ft and 200 ft intervals along the GPR traverses. The five PSPA USW data sets in each cross-section were acquired at 2 ft intervals starting 1 ft from the edge of pavement (Fig. 3.56). Depth of investigation extends from 2 in. to 8.5 in.....	111
Fig. 3.62—Cross-sections depicting variations in the elastic modulus (ksi) for PCC for PSPA USW data acquired at the 300 ft, 400 ft, and 500 ft intervals along the GPR traverses.....	112
Fig. 3.63—sections depicting variations in the elastic modulus (ksi) for PCC for PSPA USW data acquired at the 600 ft, 700 ft, and 800 ft intervals along the GPR traverses.....	113
Fig. 3.64—Cross-sections depicting variations in the elastic modulus (ksi) for PCC for PSPA USW data acquired at the 900 ft and 1000 ft intervals along the GPR traverses.	114
Fig. 3.65—Cross-sections depicting variations in the apparent elastic modulus (ksi) of BM for PSPA USW data acquired at the 0 ft, 100 ft, 200 ft, and 300 ft intervals along the GPR traverses. Depth of investigation extends from 8.5 in. to 11 in.	115
Fig. 3.66—Cross-sections depicting variations in the apparent elastic modulus (ksi) of BM for PSPA USW data acquired at the 400 ft, 500 ft, 600 ft, and 700 ft intervals along the GPR traverses. Depth of investigation extends from 8.5 in. to 11 in.	116
Fig. 3.67—Cross-sections depicting variations in the apparent elastic modulus (ksi) of BM for PSPA USW data acquired at the 800 ft, 900 ft, and 1000 ft intervals along the GPR traverses. Depth of investigation extends from 8.5 in. to 11 in.	117
Fig. 3.68—Plot of the average elastic modulus (over depth range of 3 in. to 11 in.) along each GPR transverse. The GPR traverses are spaced at 2 ft intervals. GPR traverse 1 is 1 ft from the outer edge of the pavement.	118
Fig. 3.69—The PSPA IE calculated depth to identified reflector is plotted for all PSPA test locations (Fig. 3.56). The average calculated depth to this reflector (approx. 5 in.) measurement does not agree well with the actual thickness (approx. 8.75 in.) of the PCC layer.	119
Fig. 3.70—Photograph of PSPA tool placed on pavement at project-level Site 6 (I-55 S).	120
Fig. 3.71—Base map for project-level Site 6 showing PSPA test locations and core locations. PSPA data were acquired at 100 ft intervals along each GPR transverse. GPR traverse 1	

was located 1 ft from the outer edge of the paved driving lane (shoulder). Only cores 01 and 03 are located within 5 ft of a PSPA location.	121
Fig. 3.72–Elastic modulus plot generated from PSPA USW data acquired in immediate proximity to intact PCC core 01 (Fig. 3.71). Small pits are visible. The core, with an average elastic modulus of 5973 ksi is classified as good quality (Table 3.2)	122
Fig. 3.73–Elastic modulus plot generated from PSPA USW data acquired in immediate proximity to intact PCC core 03 (Fig. 3.71). Small pits are visible. The core, with an average elastic modulus of 5897 ksi is classified as good quality (Table 3.2).	122
Fig. 3.74–Cross-sections depicting variations in the elastic modulus (ksi) for concrete for PSPA USW data acquired at the 0 ft, 100 ft, and 200 ft intervals along the GPR traverses. The five PSPA USW data sets in each cross-section were acquired at 2 ft intervals starting 1 ft from the edge of pavement (Fig. 3.71). Depth of investigation extends from 4 in. to 9 in.....	123
Fig. 3.75–Cross-sections depicting variations in the elastic modulus (ksi) for concrete for PSPA USW data acquired at the 300 ft, 400 ft, and 500 ft intervals along the GPR traverses.....	124
Fig. 3.76–Cross-sections depicting variations in the elastic modulus (ksi) for concrete for PSPA USW data acquired at the 600 ft, 700 ft, and 800 ft intervals along the GPR traverses.....	125
Fig. 3.77–Cross-sections depicting variations in the elastic modulus (ksi) for concrete for PSPA USW data acquired at the 600 ft, 700 ft, and 800 ft intervals along the GPR traverses.....	126
Fig. 3.78–Plot of the average elastic modulus (over depth range of 3 in. to 9 in.) along each GPR transverse. The GPR traverses are spaced at 2 ft intervals. GPR traverse 1 is 1 ft from the outer edge of the pavement.....	127
Fig. 3.79–The PSPA IE calculated depth to identified reflector is plotted for all PSPA test locations (Fig. 3.71). The average calculated depth to this reflector (approx. 5.9 in.) measurement does not agree well with the actual thickness (approx. 8.5 in.) of the PCC layer.	128
Fig. 3.80–Photograph of PSPA tool placed on pavement at project-level Site 7 (HWY U).....	129
Fig. 3.81–Base map for project-level Site 7 showing PSPA test locations and core locations. PSPA data were acquired at 100 ft intervals along each GPR transverse. GPR traverse 1 was located 1.5 ft from the outer edge of the paved driving lane (shoulder). Reliable PSPA data could not be acquired at several locations because of severe surface cracking. Where necessary and possible, the PSPA locations were shifted by up to 1 ft, so that data could be acquired as close as possible to the planned test locations. Only cores 05 and 08 are located within 5 ft of a PSPA location.....	130
Fig. 3.82–Elastic modulus plot generated from PSPA USW data acquired in immediate proximity to stripped core 01 (Fig. 3.81). Only 1 in. of core was recovered.....	131
Fig. 3.83–Elastic modulus plot generated from PSPA USW data acquired in immediate proximity to stripped core 05 (Fig. 3.81). Only 4 in. of core was recovered.....	131
Fig. 3.84–Cross-sections depicting variations in the elastic modulus (ksi) for BM and for PSPA USW data acquired at the 0 ft, 100 ft, and 200 ft intervals along the GPR traverses. The six PSPA USW data sets in each cross-section were acquired at 2 ft	

intervals starting 1 ft from the edge of pavement (Fig. 3.81). Reliable PSPA data could not be acquired at several locations because of severe surface cracking. Where necessary and possible, the PSPA locations were shifted by up to 1 ft, so that data could be acquired as close as possible to the planned test locations. 132

Fig. 3.85–Cross-sections depicting variations in the elastic modulus (ksi) for asphalt (BM) for PSPA USW data acquired at the 300 ft, 400 ft, and 500 ft intervals along the GPR traverses..... 133

Fig. 3.86–Cross-sections depicting variations in the elastic modulus (ksi) for asphalt (BM) for PSPA USW data acquired at the 600 ft, 700 ft, and 800 ft intervals along the GPR traverses. PSPA data could not be acquired at several test locations because of the deteriorated nature of the paved surface. 134

Fig. 3.87–Cross-sections depicting variations in the elastic modulus (ksi) for asphalt (BM) for PSPA USW data acquired at the 900 ft and 1000 ft intervals along the GPR traverses. PSPA data could not be acquired at several test locations because of the deteriorated nature of the paved surface. 135

Fig. 3.88–Plot of the average elastic modulus (over depth range of 2 in. to 7.2 in.) along each GPR transverse. The GPR traverses are spaced at 1.5 ft intervals. GPR traverse 1 is 1.5 ft from the outer edge of the pavement. 136

Fig. 3.89–The calculated depth to the identified reflector varied significantly. The values clustered between 2 in. and 4 in. could represent reflections from the base of the BM layer or from flaws within the BM layer. 137

Fig. 3.90–Photograph of PSPA tool placed on pavement at project-level Site 8 (I-35 N). 138

Fig. 3.91–Base map for project-level Site 8 showing PSPA test locations and core locations. PSPA data were acquired at 100 ft intervals along each GPR transverse. GPR traverse 1 was located 1 ft from the outer edge of the paved driving lane (shoulder). Only cores 01,02,05 and 06 are located within 5 ft of a PSPA location. 139

Fig. 3.92–Elastic modulus plot generated from PSPA USW data acquired in immediate proximity to intact core 01 (Fig. 3.91). The tested pavement consists of approx. 7 in. of PCC overlay above a 9 in. thick PCC layer. A 1 in. thick layer of BM is embedded between the two PCC layers. There was no evidence of debonding or stripping in core 01. 140

Fig. 3.93–Elastic modulus plot generated from PSPA USW data acquired in immediate proximity to debonded core 02 (Fig. 3.91). The tested pavement consists of approx. 7 in. of PCC bonded overlay above a 9 in. thick PCC layer. A 1 in. thick layer of BM is embedded between the two PCC layers. Core 02 was debonded at PCC/BM interface with the depth of 7 in. 140

Fig. 3.94– Cross-sections depicting variations in the elastic modulus (ksi) for upper layer of PCC for PSPA USW data acquired at the 0 ft, 100 ft and 200 ft intervals along the GPR traverses. The five PSPA USW data sets in each cross-section were acquired at 2 ft intervals starting 1 ft from the edge of pavement (Fig. 3.91). Depth of investigation extends from 3 in. to 7 in. PSPA data could not be acquired at several test locations because of the deteriorated nature of the paved surface. 141

Fig. 3.95–Cross-sections depicting variations in the elastic modulus (ksi) for concrete for PSPA USW data acquired at the 300 ft, 400 ft, and 500 ft intervals along the GPR

traverses. PSPA data could not be acquired at several test locations because of the deteriorated nature of the paved surface.	142
Fig. 3.96—Cross-sections depicting variations in the elastic modulus (ksi) for concrete for PSPA USW data acquired at the 600 ft, 700 ft, and 800 ft intervals along the GPR traverses. PSPA data could not be acquired at several test locations because of the deteriorated nature of the paved surface.	143
Fig. 3.97—Cross-sections depicting variations in the elastic modulus (ksi) for concrete for PSPA USW data acquired at the 900 ft and 1000 ft intervals along the GPR traverses. PSPA data could not be acquired at several test locations because of the deteriorated nature of the paved surface.	144
Fig. 3.98—Plot of the average elastic modulus (over depth range of 3 in. to 11 in.) along each GPR transverse. The GPR traverses are spaced at 2 ft intervals. GPR traverse 1 is 1 ft from the outer edge of the pavement.	145
Fig. 3.99—The apparent thickness measurement for the pavement.	146
Fig. 4.1—Photograph taken at Site 1 (US 63) showing operator, push-cart, high-frequency 1.5 GHz GPR antenna (in white plastic shell on pavement surface) and GSSI SIR-3000 control unit (top of cart). The 400 MHz data (discussed in Section 5) were acquired using the same set-up (lower-frequency 400 MHz antenna was placed in the white plastic shell). The acquired GPR data are displayed in real time on the control unit screen. At some project-level test sites, core locations were selected, in part, on the basis of the real-time interpretation of the acquired high-frequency GPR data.	147
Fig. 4.2—A GPR antenna emits a short duration pulse (approx. one wavelength in duration) of radio wave frequency electromagnetic (EM) radiation at regular intervals as it is moved across the paved surface. EM radiation is emitted like light from a flashlight. The GPR pulse propagates into the subsurface with a velocity (V) that is a function of the speed of light in a vacuum (c) and the dielectric permittivity (ε) of the material through which it is passing. If the downward propagating pulse encounters an interface across which there is a change in electrical properties (dielectric permittivity; often associated with moisture content in non-metals), some of the incident radiation will be transmitted and some will be reflected back to the antenna. The GPR antenna records both the arrival time (two-way travel time; TWTT) and the magnitude of these reflected pulses. If the velocity with which the GPR pulse travels is known (or can be reliably estimated), the depth to the reflector can be estimated.....	148
Fig. 4.3—Example plan view map of a project-level site. At each project-level site, high-frequency (1.5 GHz) GPR data were acquired five parallel traverses (six traverses at Sites 7 and 8) spaced 2 ft intervals (1.5 ft at Site 7). Low-frequency GPR data were acquired along traverse 3 only. All GPR data (low-frequency and high-frequency) were acquired at each project-level site in less than four hours. Lane closures were required.....	151
Fig. 4.4— Cross-sectional example of high-frequency (1.5 GHz) GPR data (Site 1; US 63). A constant GPR-pulse velocity (selected for each site based on the correlation between a “typical” core and the corresponding GPR data) was used to transform reflection travel times to reflector depths. The depths to each reflector, particularly on GPR data acquired at sites where pavement condition varied or where different pavement	

materials were used, are therefore “apparent” rather than “absolute”. The interpreted bases of upper and lower bituminous mix (BM) layers are marked in red and the green, respectively; the interpreted base of the portland cement concrete (PCC) layer is marked in yellow. The horizontal axis is in units of feet; the vertical axis is in units of inches. 154

Fig. 4.5–Photograph of US 63 (Site 1). GPR traverses 1-5 (left to right) are marked (Fig. 4.7).. 155

Fig. 4.6–Typical Site 1 cores consisted of three layers: approx. 1.5 in. of upper BM; approx. 2 in. of underlying BM; and approx. 8.5 in. of basal PCC. At core locations 1, 2, 4, and 7 the BM/PCC contact was debonded; at the other five core locations (3, 5, 6 and 8) the BM/PCC contact was not debonded. Debonded core 7 (above right) is the only core that showed visual evidence of chemical degradation (note staining of PCC). Core locations were selected on the basis of the preliminary on-site visual interpretation of the acquired GPR data. Edge of pavement (hand written notes in core photographs) refers to the edge of the driving lane. The edge of the driving lane was 10 ft from the edge of the paved shoulder (Fig. 4.5 and Fig. 4.7). 155

Fig. 4.7–Plan view map of US 63 (Site 1) showing locations of GPR traverses 1-5. High-frequency (1.5 GHz antenna) GPR data were acquired along all five traverses; low-frequency (400 MHz antenna) data GPR data were acquired along traverse 3 only. Solid black lines represent the driving lane boundaries. Lane width was 12 ft. Core locations are marked as black circles. PSPA locations are marked as blue circles. MASW locations are marked as red crosses. Traverse 1 was 2 ft from the edge of driving lane boundary (12 feet from edge of the paved shoulder; Fig. 4.5). 156

Fig. 4.8–Plan view showing GPR-estimated “apparent” depth to the base of: A) the upper layer of BM (BM1). Horizontal solid black lines represent locations of the GPR traverses ; B) the lower layer of BM (BM2); and C) the base PCC. GPR data were processed using a dielectric permittivity of 8.0. Vertical and horizontal axes are distance in feet. The vertical bars on Fig. 4.8C correspond to joint locations. 157

Fig. 4.9–Plan view showing base map with superposed GPR interpretations: A) amplitude of GPR signal reflected from the base of the top layer of BM. Horizontal solid black lines represent locations of the GPR traverses; B) amplitude of GPR signal reflected from the base of the lower layer of BM; and C) amplitude of GPR signal reflection from the base of the PCC. Vertical and horizontal axes are distance in feet. 158

Fig. 4.10–Photograph of site the project-level segment US54 (Site 2). 160

Fig. 4.11–Plan view map of US 54 (Site 2) showing locations of GPR traverses 1-5. High-frequency (1.5 GHz antenna) GPR data were acquired along all five traverses; low-frequency (400 MHz antenna) data GPR data were acquired along traverse 3 only. Solid black lines represent the driving lane boundaries. Lane width was 11 ft. Core locations (10) are marked as black circles. PSPA locations are marked as blue circles. MASW locations are marked as red crosses. Traverse 1 was 2 ft from the edge of driving lane boundary. Core locations are marked as black circles. PSPA locations are marked as blue circles. MASW locations are marked as red crosses. 162

Fig. 4.12–Representative example of Site 2 high-frequency (1.5 GHz) GPR profile (GPR profile 3, stations 560-660) showing tie with core 5 (at station 600; Fig. 4.11). Reflections from the multiple stripped interfaces and the base of the BM can be

identified. Variations in the apparent depth to the base of the BM are attributed to both lateral changes in the actual thickness of the BM and to lateral changes in the physical and chemical condition of the BM. The horizontal axis is in units of feet; the vertical axis is in units of inches..... 164

Fig. 4.13–Base map showing variations in the apparent thickness of the bituminous mix (BM). Thickness values are apparent and are based on the dielectric permittivity of 8.0. Traverse 1 (0 ft mark on map) was located 2 ft from the edge of the driving lane. 165

Fig. 4.14–GPR amplitude map of reflection from base bituminous mix (BM). Areas highlighted in orange, red and blue (<-34 NdB) indicate evidence of deterioration (stripping). Vertical and horizontal axes distances are in units of feet. 165

Fig. 4.15–Photograph of site the project-level segment Rte 179 (Site 3). 166

Fig. 4.16–Plan view map of MO 179 (Site 3) showing locations of GPR traverses 1-5. High-frequency (1.5 GHz antenna) GPR data were acquired along all five traverses; low-frequency (400 MHz antenna) data GPR data were acquired along traverse 3 only. Solid black lines represent the driving lane boundaries. Lane width was 12 ft. Core locations (10) are marked as black circles. PSPA locations are marked as blue circles. MASW locations are marked as red crosses. Traverse 1 was 2 feet from the edge of the driving lane. Core locations are marked as black circles. PSPA locations are marked as blue circles. MASW locations are marked as red crosses. All 10 cores were described as moderately to highly stripped. Cores 5-10 were described as debonded. 168

Fig. 4.17–Example of Site 3 GPR profile (GPR profile 3, stations 820-1000) showing correspondence to core 8 (at station 868; Fig. 4.16). Yellow lines represents the base of BM. The horizontal axis is in units of feet; the vertical axis is in units of inches. 169

Fig. 4.18– Base map with superposed apparent depth to base bituminous mix (BM) based on the GPR data. Depth values are apparent and are based on the dielectric permittivity of 7.5. Traverse 1 (0 ft mark on map) was located 1 ft (2 ft in Fig. 4.11) away from the outer edge of the driving lane..... 170

Fig. 4.19–Base map with superposed GPR amplitude values from the base BM. All 10 cores were described as moderately to highly stripped. Cores 5-10 were described as debonded. Areas of anomalously low amplitude probably represent areas where the BM is severely degraded..... 170

Fig. 4.20–Photograph of site the project-level segment HWY AT (Section 4). Photograph was taken looking west..... 172

Fig. 4.21–Plan view map of HWY AT (Site 4) showing locations of GPR traverses 1-5. High-frequency (1.5 GHz antenna) GPR data were acquired along all five traverses; low-frequency (400 MHz antenna) data GPR data were acquired along traverse 3 only. Solid black lines represent the driving lane boundaries. Lane width was 12 ft. Core locations (10) are marked as black circles. PSPA locations are marked as blue circles. MASW locations are marked as red crosses. Traverse 1 was 2 ft from the edge of the driving lane. Core locations are marked as black circles. PSPA locations are marked as blue circles. MASW locations are marked as red crosses. The BM in all nine cores is described as stripped (low to moderate) and debonded at one or more levels. 173

Fig. 4.22–Representative example of Site 4 GPR profile (GPR profile 1, stations 0-25). Core 1 encountered 15.25 in. of BM; the other cores encountered variable thicknesses of

BM over PCC. The horizontal axis is in units of feet; the vertical axis is in units of inches.	175
Fig. 4.23—Depth values are apparent and are based on the dielectric permittivity of 7.5. Traverse 1 (0 ft mark on map) was located 1 ft (2 ft in Fig. 4.11) away from the outer edge of the driving lane. Upper Map shows GPR-estimated “apparent” depth to the base of the BM; Lower map shows GPR-estimated “apparent” depth to the base of the PCC. As noted in Table 4.4, GPR-estimated depths to the base of the BM and PCC and the corresponding core depths differ significantly at several core locations. The lack of correlation is attributed to the poor condition of the asphalt layer and partial recovery during coring.	176
Fig. 4.24—A) Base map with superposed GPR amplitude values from the bottom bituminous mix (BM) layer base; B) reflection amplitude GPR signal from the base of the concrete layer (PCC) base. Area highlighted in blue at the stations 5-18 is the excavation (see Figure 4.22). Based on the GPR and core data areas with weak bonded and debonded BM layers are present throughout the entire 1000 ft pavement section. Amplitude values lower than -34 NdB indicate poor condition of the pavement. All cores (1 to 10) confirmed the debonding and the stripping within the asphalt layer. Vertical and horizontal axes are distance in units of feet. Horizontal to vertical scale ratio is 1:30.	177
Fig. 4.25—Photograph of site the project-level segment I-55 Pemiscot County (Site 5). Photograph was taken looking south.	179
Fig. 4.26—Plan view map of I-55 Pemiscot Co. (Site 5) showing locations of GPR traverses 1-5. High-frequency (1.5 GHz antenna) GPR data were acquired along all five traverses; low-frequency (400 MHz antenna) data GPR data were acquired along traverse 3 only. Solid black lines represent the driving lane boundaries. Lane width was 12 ft. Core locations (10) are marked as black circles. PSPA locations are marked as blue circles. MASW locations are marked as red crosses. Traverse 1 was 1 ft from the edge of the driving lane. Core locations are marked as black circles. PSPA locations are marked as blue circles. MASW locations are marked as red crosses. The PCC/BM interface (upper interface) in cores 3, 5, 6, 7, and 8 (Fig. 4.26) is described as debonded; stripping in core 1 is described as moderate; stripping in all other cores is described as low.	181
Fig. 4.27—Example of GPR section (GPR profile 5, stations 240-310) showing imaged features: base of the top concrete layer, asphalt layer, bottom concrete layer, and slab joints. The horizontal axis is in units of feet; the vertical axis is in units of inches.	182
Fig. 4.28—Base map with superposed GPR amplitude values from the PCC/BM interface. Vertical and horizontal axes are distance in units of feet. Horizontal to vertical scale ratio is 1:30. Traverse 1 was located 1 ft away from the edge of the driving lane. Horizontal dashed lines represent locations of the GPR traverses. Vertical dashed lines represent locations of the mapped slab joints in the upper PCC layer; notice the amplitude changes near the joints.	183
Fig. 4.29—Base map with superposed GPR estimated “apparent” depth values from the PCC/BM interface. Vertical and horizontal axes are distance in feet. Horizontal to vertical scale ratio is 1:30. Traverse 1 was located 1 ft away from the edge of the driving lane. Dielectric constant of 7.5 was used to convert reflection times to reflector	

depths. Variations in the apparent depth to the base PCC is attributed mostly to variations in the actual depth to this interface. Horizontal dashed lines represent locations of the GPR traverses. Vertical dashed lines represent locations of the mapped slab joints in the upper PCC layer; notice the apparent depth changes near the joints. 183

Fig. 4.30–Photograph of site the project-level segment I-55 Perry County (Section 6). Photograph was taken looking north. 185

Fig. 4.31–Plan view map of I-55 Perry Co. (Site 6) showing locations of GPR traverses 1-5. High-frequency (1.5 GHz antenna) GPR data were acquired along all five traverses; low-frequency (400 MHz antenna) data GPR data were acquired along traverse 3 only. Solid black lines represent the driving lane boundaries. Lane width was 12 ft. Core locations (9) are marked as black circles. PSPA locations are marked as blue circles. MASW locations are marked as red crosses. Traverse 1 was 1 ft from the edge of the driving lane. The PCC in the eight cores is described as good quality..... 187

Fig. 4.32–Base map with superposed GPR estimated “apparent” depth values for base PCC. Vertical and horizontal axes are distance in feet. Traverse 1 was located 1 ft from the edge of the driving lane. A dielectric permittivity of 8.0 was used to convert reflection times to reflector depths. Patched areas were with no reinforcing steel were found at stations 440-450, 550-580, 760-775, 830-840, 950-962 on all the GPR traverses and at stations 630-640 at the GPR traverse 5. Variations in the apparent depth to the base BM is attributed mostly to variations in the actual depth to this interface. The cross-hatched areas represent locations where the reflection from the base PCC is polarity-reversed. These probably represent areas where void space underlies the PCC. Black solid lines represent locations of the joints..... 188

Fig. 4.33–A base map with superposed GPR amplitude values from the base PCC. The cross-hatched areas represent locations where the reflection from the base PCC is polarity-reversed. These probably represent areas where void space underlies the PCC. Black solid lines represent locations of the joints. 189

Fig. 4.34–A) Segment of representative Site 6 GPR profile (GPR profile 3, stations 766-800) showing GPR image of base of concrete layer, a patched area; and B) Segment of representative Site 6 GPR profile (GPR profile 3, stations 17-52) showing a polarity reversal at the base PCC reflector that could be indicative of a void space. The horizontal axis is in units of feet; the vertical axis is in units of inches. 190

Fig. 4.35–Core 5 location at Site 6. During coring it was noted that the water seeping through the slab transverse and edge joints, which probably caused fine material pumping out, and as a result, forming voids beneath the PCC layer.. 191

Fig. 4.36–Photograph of site the project-level segment HWY U (Section 7). Photograph was taken looking north. 192

Fig. 4.37–Plan view map showing locations of the GPR traverses and the cores at the project-level Site 7 (HWY U). A total six GPR profiles (each 1000 ft long) were acquired along parallel traverses spaced at 1.5-ft intervals. High-frequency (1.5GHz antenna) data GPR data were acquired along all six traverses (spaced at 1.5 ftintervals), low-frequency (400 MHz antenna) data GPR data were acquired along Traverse 3 only. Solid black lines represent the lane boundaries. The total lane width was 10 ft. Core

locations are marked as black circles. PSPA locations are marked as blue circles. MASW locations are marked as red crosses. Only partial cores were recovered at most core locations.....	192
Fig. 4.38—An example of a GPR segment (GPR profile 3, stations 380-470) with some imaged features is shown: base of the top asphalt layer, the base of the top debonded asphalt layer (reflection not present everywhere along the 1000-ft pavement section) and a culvert (stations 448-464). The horizontal axis is in units of feet; the vertical axis is in units of inches.....	194
Fig. 4.39—A base map showing variations in the apparent thickness of the bituminous mix (BM). Thickness values are apparent and are based on the dielectric permittivity of 10.0. Traverse 1 (0 ft mark on map) was located 1.5 ft from the edge of the driving lane.....	195
Fig. 4.40—A base map with superposed GPR amplitude values from the bottom asphalt layer base. Areas highlighted in orange, red, and blue (<-34 NdB) indicate overall poor pavement condition. All cores (1 to 8) confirmed presence of deteriorated asphalt and debonding where two layers of asphalt recovered from the core. Traverse 1 was located 1.5 ft away from the pavement edge.	196
Fig. 4.41—Photograph of site the project-level segment I-35 (Section 8). Photograph was taken looking north.....	198
Fig. 4.42—Plan view map showing locations of the GPR traverses and the cores at the project-level segment I-35 (Section 8). A total of 6 GPR profiles 1000 ft long were acquired along parallel traverses spaced at 2 ft intervals. High-frequency (1.5GHz antenna) data GPR data were acquired along five traverses, low-frequency (400 MHz antenna) data GPR data were acquired along Traverse 3 only. Solid black lines represent the lane boundaries, total lane width was 12 ft. Core locations are marked as black circles. PSPA locations are marked as blue circles. MASW locations are marked as red crosses. Stripping in all eight cores is described as low to moderate. The BM is described as debonded in all cores, except core 1. The upper PCC/BM interface of core 1 is described as bonded.	199
Fig. 4.43—Example of GPR section (GPR profile 3, stations 790-890) showing imaged features: the BM layer and reinforcing mesh. The horizontal axis is in units of feet; the vertical axis is in units of inches.....	200
Fig. 4.44—A) Base map showing variations in the apparent thickness of the upper layer of PCC; and B) variations in the amplitude of the reflection from the base PCC. Thickness values are apparent and are based on the dielectric permittivity of 8.0. Traverse 1 (0 ft mark on map) was located 2 ft from the edge of the driving lane.....	201
Fig. 5.1—Photograph showing the push-cart and low-frequency 400 MHz GPR antenna (red box on pavement surface) and GSSI SIR-3000 control unit (top of cart).	205
Fig. 5.2—Example of GPR data (Site 1; US 63; stations 920-1000). A) Section of 400 MHz GPR profile acquired along traverse 3. B) Section of 1.5 GHz GPR profile acquired along same section of traverse 3. GPR data were processed using a dielectric permittivity of 8.0. As illustrated, the low-frequency GPR antenna was unable to image the base of the upper BM layer, the base of the lower BM layer and/or the base of PCC layer. Also, the low-frequency antenna was unable to image the subsurface beneath the	

reinforcing mesh probably due to the close spacing of the mesh wires and related interference effects. The horizontal axis is in units of feet; the vertical axis is in units of inches. 206

Fig. 5.3—Example of GPR data (Site 2; US 54; stations 930-1000). A) Section of 400 MHz GPR profile acquired along traverse 3. B) Section of 1.5 GHz GPR profile acquired along traverse 3. Dielectric permittivity is 8.0. Yellow solid line represents base of the BM layer, dashed yellow line represents estimated base of the BM. The red line represents a reflection from a lower pavement layer. However, the specific nature of the lower interface could not be independently verified due to absence of the core data (at a depth of approx. 20 in.). The horizontal axis is in units of feet; the vertical axis is in units of inches..... 207

Fig. 5.4—Example of GPR data (Site 3; Rte 179; stations 820-1000). A) Section of 400 MHz GPR profile acquired along traverse 3. B) Section of 1.5 GHz GPR profile acquired along same section of traverse 3. GPR data were processed using a dielectric permittivity of 7.5. As illustrated, the low-frequency GPR antenna was able to detect debonding between the upper and the middle BM layers, and to image the base of the BM (lower) layer. The low-frequency antenna was unable to image the pavement beneath the BM layers. Yellow solid line represents base of the BM layer. Red solid line represents possible debonded BM layers. The horizontal axis is in units of feet; the vertical axis is in units of inches..... 208

Fig. 5.5—Example of GPR data (Site 4; MO 179; stations 0-100). A) Section of 400 MHz GPR profile acquired along traverse 3. B) Section of 1.5 GHz GPR profile acquired along traverse 3. GPR data were processed using a dielectric permittivity of 7.5. As illustrated, the low-frequency GPR antenna was able to image the base of the PCC layer, reinforcing mesh embedded in the PCC layer and possible utilities. The low-frequency GPR antenna was not able continuously image the BM layer base and was not able to confidently image any features below the PCC base, except possible utilities. Yellow solid line represents base of the PCC layer. Red solid line represents interpreted base of the BM layer. The horizontal axis is in units of feet; the vertical axis is in units of inches..... 209

Fig. 5.6—Example of GPR data (Site 5; I-55, Pemiscot County; stations 0-100). A) Section of 400 MHz GPR profile acquired along traverse 3. B) Section of 1.5 GHz GPR profile acquired along the same section of traverse 3. GPR data were processed using a dielectric permittivity of 8.0. As illustrated, the low-frequency GPR antenna was able to image the base of the PCC layer, reinforcing mesh embedded in the PCC layer and possible utilities. The low-frequency GPR antenna was not able to continuously image the BM layer base and was not able to confidently image any features below the PCC base. Yellow solid line represents base of the upper PCC layer. Red solid line represents the base of the lower layer of PCC. The horizontal axis is in units of feet; the vertical axis is in units of inches. 210

Fig. 5.7—Example of GPR data (Site 6; I-55 Perry County; stations 0-100). Some of the imaged features are shown in the low-frequency GPR data (A) and the high-frequency GPR data (B). The low-frequency GPR antenna did not image any base, subbase or subgrade layers. GPR data were processed using a dielectric permittivity of 8.0. Yellow

solid line represents base of the PCC layer. The horizontal axis is in units of feet; the vertical axis is in units of inches.....	211
Fig. 5.8—Example of GPR data (Site 7; HWY U; stations 360-460). Some of the imaged features are shown in the low-frequency GPR data (A) and the high-frequency GPR data (B). The low-frequency GPR antenna was able to image a layer beneath pavement which is most likely the top subgrade, however, the interpretation couldn't not be confirmed or verified due to lack of the core data. GPR data were processed using a dielectric permittivity of 10.0. Yellow solid line represents base of the upper PCC layer. Red solid line represents possible top of subgrade, however, the interpretation could not be verified due to lack of the core data. The horizontal axis is in units of feet; the vertical axis is in units of inches.....	212
Fig. 5.9—Example of GPR data (Site 8; I-35; stations 410-500). Some of the imaged features are shown in the low-frequency GPR data (A) and the high-frequency GPR data (B). The low-frequency GPR antenna did not image any base, subbase or subgrade layers. GPR data were processed using a dielectric permittivity of 8.0. Yellow solid line represents base of the upper PCC layer. The horizontal axis is in units of feet; the vertical axis is in units of inches.....	213
Fig. 6.1—Example interpreted ERT profile (Site 1) with elevation control. Distances and depths are in units of feet. Resistivity is in units of ohm-m. Intact rock (as per the superposed interpretation) is characterized by resistivity values in excess of 1500 ohm-m; weathered rock by values between 75 and 1500 ohm-m; and soil mostly by values less than 100 ohm-m. The soil/rock contact corresponds (approx.) to the 75 ohm-m contour interval.....	217
Fig. 6.2—Example active MASW data were acquired using a 24-channel engineering seismograph, 24 low-frequency (4.5 Hz) vertically-polarized geophones spaced at 1.5 ft and a sledge hammer source. MASW raw seismic field data, the corresponding dispersion curve and the corresponding 1-D shear-wave velocity profile (depths are in units of feet) are displayed. During processing, the raw seismic field data are transformed into a dispersion curve (phase velocity vs. frequency). The dispersion curve is transformed into a 1-D shear-wave velocity profile (inversion curve).	218
Fig. 6.3—Example 2-D MASW shear-wave profile (Site 1). Horizontal and vertical scales are in units of feet. During processing, each of the 41 MASW field records acquired at each project-level site was transformed into dispersion data (Rayleigh-wave velocity vs. frequency format; standard, established mathematical process that does not require any interactive input from the interpreter; Fig. 6.2). The dispersion data were analyzed qualitatively (processor input was required), and optimum phase velocities were selected (dispersion curve; Fig. 6.2). Each dispersion curve was inverted without any qualitative input from the interpreter and transformed into a 1-D shear-wave velocity profile. The forty-one (41) 1-D shear-wave velocity profiles generated at 25 ft intervals along each project-level roadway were used to generate 2D shear-wave profiles that extended to depths in excess of 40 ft.	220
Fig. 6.4—Example project-level site layout. ERT data were acquired at each project-level site along a 1000 ft traverse in the DOT ROW (Figs. 6.1 and 6.5). The start and end of each ERT traverse were consistent with the start and end of the corresponding GPR	

traverses. Active MASW data were acquired at 41 stations (every 25 ft from the 0 ft mark to the 1000 ft mark) along GPR traverse 3 (GPR traverses 1-5 are identified at the left of the figure). A 1-D shear-wave velocity profile was generated for each MASW station (Fig. 6.2). The forty-one (41) 1-D shear-wave velocity profiles generated for each project-level site were combined together (placed side-by-side) to generate a 2-D shear-wave velocity profile (Figs. 6.3 and 6.5). The datum on each ERT profile (acquired in DOT ROW) is generally 1-2 ft lower than the datum on the corresponding 2-D MASW shear-wave velocity profile (acquired on paved roadway). The separation between each MASW traverse and the corresponding ERT traverse was typically 20 to 30 ft. This separation can explain many of the minor differences between the ERT and MASW interpretations as subsurface conditions can vary significantly over short distances, especially in karst terrain. 221

Fig. 6.5—Example project-level site layout (Site 1). ERT data were acquired at each project-level site along a 1000 ft traverse in the DOT ROW. The start/end of each ERT traverse was consistent with the start/end of the corresponding GPR traverses. MASW data were acquired at 41 stations (every 25 ft from the 0 ft mark to the 1000 ft mark) along GPR traverse 3 (Fig. 6.4). The separation between each MASW traverse and the corresponding ERT traverse was typically 20 to 30 ft. This separation can explain many of the minor differences between the ERT and MASW interpretations as subsurface conditions can vary significantly over short distances, especially in karst terrain..... 222

Fig. 6.6—ERT data were acquired at each project-level site using an AGI SuperSting R8/IP resistivity system and a dipole-dipole array. Electrodes were spaced at 5 ft intervals. The intent was to image the subsurface to depths on the order of 40 ft. 223

Fig. 6.7—Active MASW data were acquired at each project-level site using a 24-channel engineering seismograph and 24 low-frequency (4.5 Hz) geophones spaced at 1.5 ft intervals. The intent was to image the subsurface to depths on the order of 40 ft. 224

Fig. 6.8—Example interpreted Site 1 ERT profile without elevation control. The datum is the ground surface in the DOT ROW (approx. 1-2 ft below pavement surface). Distances and depths are in units of feet. Resistivity is in units of ohm-m. Interpreted top of rock is shown by the white line. The iteration error was 12%. This error value is typical of good quality ERT data acquired in karst terrain. The term “good quality” refers to the extent to which the acquired ERT field data and the output ERT profile correlate. ERT data quality usually decreases as the complexity (3-D) of the subsurface increases. 225

Fig. 6.9—Site 1 basic MASW data (station 300 ft): MASW field record, corresponding dispersion curve and 1-D shear-wave velocity profile. Interpreted top of weathered rock (1000 ft/sec) is at a depth of approx. 7 ft. This depth correlates well with the ERT-estimated depth to the top of rock at station 300 ft (Fig. 6.8). MASW data quality is excellent. 226

Fig. 6.10—Site 1: Example interpreted 2-D MASW shear-wave velocity profile with elevation control. Elevation control cannot be applied using the software provided by the MASW manufacturer (Kansas Geological Survey). Datum on the 2-D MASW profile corresponds to the top of pavement (approx. 1-2 ft above ERT datum). Distances and depths are in units of feet. Velocities are in units of ft/sec. 227

Fig. 6.11—Example interpreted Site 2 ERT profile without elevation control. Elevation control was not applied in order to facilitate comparison to the Site 2 MASW data (Fig. 6.12 and 6.13). The datum is the ground surface in the DOT ROW (approx. 1-2 ft below pavement surface). Distances and depths are in units of feet. Resistivity is in units of ohm-m. The iteration error was 28.2%. This high error value is typical of poor-fair quality ERT data acquired in karst terrain. The term “poor-fair quality” refers to the extent to which the acquired ERT field data and the output ERT profile correlate. The locations of interpreted solution-widened joints are shown by thick vertical red lines. 228

Fig. 6.12—Site 2 basic MASW data (station 400 ft): dispersion curve and corresponding 1-D shear-wave velocity profile. Interpreted top of rock (1000 ft/s) is at a depth of approx. 14 ft. MASW data are excellent quality. 229

Fig. 6.13—Site 2: Example interpreted 2-D MASW shear-wave velocity profile. Elevation control cannot be applied using the software provided by the MASW manufacturer (Kansas Geological Survey). The datum on the 2-D MASW profile corresponds to the top of pavement (approx. 1-2 ft above ERT datum). Distances and depths are in units of feet. Velocities are in units of ft/sec..... 230

Fig. 6.14—Example interpreted Site 3 ERT profile without elevation control. Elevation control was not applied in order to facilitate comparison to the Site 3 MASW data (Fig. 6.15 and 6.16). The datum is the ground surface in the DOT ROW (approx. 1-2 ft below pavement surface). Distances and depths are in units of feet. Resistivity is in units of ohm-m. The iteration error was 16.2%. This error value is typical of fair-good quality ERT data acquired in karst terrain. The term “fair-good quality,” in this sense, refers to the extent to which the acquired ERT field data and the output ERT profile correlate. The locations of interpreted solution-widened joints are shown by thick vertical red lines..... 231

Fig. 6.15—Site 3 basic MASW data (station 625 ft): dispersion curve and corresponding 1-D shear-wave velocity profile (inversion curve). Interpreted top of rock (1000 ft/sec) is at a depth of approx. 22 ft. Data quality is excellent..... 232

Fig. 6.16—Site 3: Example interpreted 2-D MASW shear-wave velocity profile with elevation control. Elevation control cannot be applied using the software provided by the MASW manufacturer (Kansas Geological Survey). The 0 ft mark on the 2-D MASW profile corresponds to the top of pavement (approx. 1-2 ft above ERT datum). Distances and depths are in units of feet. Velocities are in units of ft/sec..... 233

Fig. 6.17—Example interpreted Site 4 ERT profile without elevation control. Elevation control was not applied in order to facilitate comparison to the Site 4 MASW data (Fig. 6.18 and 6.19). The datum is the ground surface in the DOT ROW (approx. 1-2 ft below pavement surface). Distances and depths are in units of feet. Resistivity is in units of ohm-m. The iteration error was 6.2%. This error value is typical of excellent quality ERT data acquired in karst terrain. The term “excellent quality,” in this sense, refers to the extent to which the acquired ERT field data and the output ERT profile correlate. The locations of interpreted solution-widened joints are shown by thick vertical red lines..... 234

Fig. 6.18–Site 4 basic MASW data (station 875 ft): dispersion curve and corresponding 1-D shear-wave velocity profile (inversion curve). Interpreted top of rock (1000 ft/sec) is at a depth of approx. 11.5 ft. Data quality is excellent..... 235

Fig. 6.19–Site 4: Example interpreted 2-D MASW shear-wave velocity profile with elevation control. Elevation control cannot be applied using the software provided by the MASW manufacturer (Kansas Geological Survey). The 0-ft mark on the 2-D MASW profile corresponds to the top of pavement (approx. 1-2 ft above ERT datum). The MASW data were acquired using a 1.5 ft geophone spacing. Distances and depths are in units of feet. Velocities are in units of ft/sec..... 236

Fig. 6.20–Example interpreted Site 5 ERT profile without elevation control. Elevation control was not applied in order to facilitate comparison to the Site 5 MASW data (Fig. 6.21 and 6.22). The datum is the ground surface in the DOT ROW (approx. 1-2 ft below pavement surface). Distances and depths are in units of feet. Resistivity is in units of ohm-m. The iteration error was 3.9%. This error value is typical of excellent quality ERT data acquired in karst terrain. The term “excellent quality,” in this sense, refers to the extent to which the acquired ERT field data and the output ERT profile correlate. The location of a possible fault is shown by the thick vertical red line. 237

Fig. 6.21–Site 5 basic MASW data (station 25 ft): dispersion curve and corresponding 1-D shear-wave velocity profile. Interpreted top of dense soil (3000 ft/sec) is at a depth of 23.5 ft. Data quality is excellent. 238

Fig. 6.22–Site 5: Example interpreted 2-D MASW shear-wave velocity profile with elevation control. Elevation control cannot be applied using the software provided by the MASW manufacturer (Kansas Geological Survey). The 0 ft mark on the 2-D MASW profile corresponds to the top of pavement (approx. 1-2 ft above ERT datum). The MASW data were acquired using a 1.5 ft geophone spacing. Distances and depths are in units of feet. Velocities are in units of ft/sec..... 239

Fig. 6.23–Example interpreted Site 6 ERT profile without elevation control. Elevation control was not applied in order to facilitate comparison to the Site 6 MASW data (Fig. 6.24 and 6.25). The datum is the ground surface in the DOT ROW (approx. 1-2 ft below pavement surface). ERT data were acquired using a 5 ft electrode spacing. Distances and depths are in units of feet. Resistivity is in units of ohm-m. The locations of interpreted solution-widened joints are shown by thick vertical red lines..... 240

Fig. 6.24–Site 6 basic MASW data (station 75): dispersion curve and corresponding 1-D shear-wave velocity profile. Interpreted top of rock (1000 ft/s) is at a depth of approx. 22 ft. Data quality is excellent..... 241

Fig. 6.25–Site 6: Example interpreted 2-D MASW shear-wave velocity profile with elevation control. Elevation control cannot be applied using the software provided by the MASW manufacturer (Kansas Geological Survey). The 0 ft mark on the 2-D MASW profile corresponds to the top of pavement (approx. 1-2 ft above ERT datum). The MASW data were acquired using a 1.5 ft geophone spacing. Distances and depths are in units of feet. Velocities are in units of ft/sec..... 242

Fig. 6.26–Example interpreted Site 7 ERT profile without elevation control. Elevation control was not applied in order to facilitate comparison to the Site 7 MASW data (Fig. 6.27 and 6.28). The datum is to the ground surface in the DOT ROW (approx. 1-2 ft

below pavement surface). ERT data were acquired using a 5 ft electrode spacing. Distances and depths are in units of feet. Resistivity is in units of ohm-m. The iteration error was 3.2%. This error value is typical of excellent quality ERT data acquired in karst terrain. The term “excellent quality,” in this sense, refers to the extent to which the acquired ERT field data and the output ERT profile correlate. The locations of interpreted solution-widened joints are shown by thick vertical red lines. 243

Fig. 6.27–Site 7 basic MASW data (station 675): raw record, corresponding dispersion curve and corresponding 1-D shear-wave velocity profile (inversion curve). Interpreted top of rock (1000 ft/sec) is at a depth of approx. 8.5 ft. Data quality is excellent..... 244

Fig. 6.28–Site 7: Example interpreted 2-D MASW shear-wave velocity profile with elevation control. Elevation control cannot be applied using the software provided by the MASW manufacturer (Kansas Geological Survey). The 0 ft mark on the 2-D MASW profile corresponds to the top of pavement (approx. 1-2 ft above ERT datum). The MASW data were acquired using a 1.5 ft geophone spacing. Distances and depths are in units of feet. Velocities are in units of ft/sec..... 245

Fig. 6.29–Example interpreted Site 8 ERT profile without elevation control. Elevation control was not applied in order to facilitate comparison to the Site 8 MASW data (Fig. 6.30 and 6.31). The datum is the ground surface in the DOT ROW (approx. 1-2 ft below pavement surface). Distances and depths are in units of feet. Resistivity is in units of ohm-m. The iteration error was 8.3%. This error value is typical of good-excellent quality ERT data acquired in karst terrain. The term “good-excellent quality,” in this sense, refers to the extent to which the acquired ERT field data and the output ERT profile correlate. The locations of interpreted solution-widened joints are shown by thick vertical red lines. 246

Fig. 6.30–Site 8 basic MASW data (station 675 ft): raw record, corresponding dispersion curve and corresponding 1-D shear-wave velocity profile (inversion curve). Interpreted top of rock (1000 ft/s) is at a depth of approx. 9 ft. MASW data quality is excellent. 247

Fig. 6.31–Site 8: Example interpreted 2-D MASW shear-wave velocity profile with elevation control. Elevation control cannot be applied using the software provided by the MASW manufacturer (Kansas Geological Survey). The 0 ft mark on the 2-D MASW profile corresponds to the top of pavement (approx. 1-2 ft above ERT datum). The MASW data were acquired using a 1.5 ft geophone spacing. Distances and depths are in units of feet. Velocities are in units of ft/sec..... 248

Fig. 7.1– Photograph of the Falling Weight Deflectometer (FWD) manufactured by Dynatest and operated by the Missouri Department of Transportation (MoDOT). 251

Fig. 7.2–Photograph of the first generation Rolling Dynamic Deflectometer (RDD) used in this project. 252

Fig. 7.3–Rolling Dynamic Deflectometer (RDD) loading and measurement configuration..... 254

Fig. 7.4–Photo of falling weight deflectometer (FWD) equipment in operation at Site 1 (US 63). 256

Fig. 7.5–FWD sensor arrangement and set-up for testing load transfer at a joint (entering slab)..... 256

Fig. 7.6–Example of processed RDD data showing the deflection values from the three rolling sensors plotted vs. distance over a length of about 1.5 miles 260

Fig. 7.7–Examples of load transfer evaluation using the RDD, showing (a) good load transfer and (b) poor load transfer at a joint.	260
Fig. 7.8–Illustration of calculation of load transfer efficiency (LTE) from RDD data (from Lee et al., 2004).	260
Fig. 7.9–Illustration of mid-slab support conditions evaluated from RDD data.	261
Fig. 7.10–Example deflection basin from RDD data.	262
Fig. 7.11–Example of reflection crack observed at Site 1 (US 63) during RDD testing.	263
Fig. 7.12–RDD data over the full 1.5 mile extent on US 63 with the 1000 ft test section shaded.	263
Fig. 7.13–RDD data over the 1000-ft test section on US 63.	263
Fig. 7.14–Histogram of W3 displacement measured on the (a) 1000 ft section and the (b) 1.5 mile section.	264
Fig. 7.15–Comparison of center slab deflections obtained from the RDD and the FWD at Site 1, US 63.	265
Fig. 7.16–Comparison of joint deflections obtained from the RDD and the FWD at Site 1, US 63.	265
Fig. 7.17–Deflection difference (W1-W3) between Sensors 1 and 3 over 1000 ft test section at Site 1.	266
Fig. 7.18–Comparison of LTE at joints obtained from the RDD and the FWD at Site 1, US 63. Note: RDD measurements were performed approx. 14 months after the FWD measurements.	266
Fig. 7.19–Photograph of the RDD in operation at US 54.	267
Fig. 7.20–RDD data over the full 0.65 mile extent on US 54 with the 1000 ft test section shaded.	268
Fig. 7.21–RDD data over the 1000 ft test section on US 54.	268
Fig. 7.22–Histogram of W3 displacement measured on the (a) 1000 ft section and the (b) 1.5 mile section.	268
Fig. 7.23–Comparison of deflection profiles obtained from the first receiver of RDD and FWD measurements normalized to a load of 10 kips. Note RDD testing was performed after placement of a 2.75 in. asphalt overlay.	269
Fig. 7.24–Comparison of deflection profiles normalized by the maximum values obtained from the first receiver of RDD and FWD measurements showing the similarity in recorded trends over the 1000 ft section. Note RDD testing was performed after placement of a 2.75 in. asphalt overlay.	270
Fig. 7.25–Subgrade modulus estimated using the Hogg model from FWD data collected at Site 2 (US 54).	270
Fig. 7.26–Composite stiffness estimated using the AREA model from FWD data collected at Site 2 (US 54).	271
Fig. 7.27–Surface layer modulus estimated using the AREA model from FWD data collected at Site 2 (US 54). Note estimates were only made where nearby core control of surface layer thickness was available.	271
Fig. 7.28–Photograph of pavement surface at Site 3 during RDD testing showing extensive longitudinal and transverse cracking in the asphalt layer.	272
Fig. 7.29–RDD data over the 1000-ft test section on HWY 179.	273

Fig. 7.30–Histogram of W3 displacement measured on the 1000 ft section at Site 3 (HWY 179).	273
Fig. 7.31–Comparison of deflection profiles obtained from the first receiver of RDD and FWD measurements normalized to a load of 10 kips.	274
Fig. 7.32–Subgrade modulus estimated using the Hogg model from FWD data collected at Site 3 (HWY 179).	274
Fig. 7.33–Composite stiffness estimated using the AREA model from FWD data collected at Site 3 (HWY 179).	274
Fig. 7.34–Surface layer modulus estimated using the AREA model from FWD data collected at Site 3 (HWY 179). Estimates were only made where nearby core control of surface layer thickness was available.	275
Fig. 7.35–Deflection profile obtained from the first receiver of FWD measurements normalized to a load of 10 kips.	275
Fig. 7.36–Subgrade modulus estimated using the Hogg model from FWD data collected at Site 4 (HWY AT).	276
Fig. 7.37–Composite stiffness estimated using the AREA model from FWD data collected at Site 4 (HWY AT).	276
Fig. 7.38–RDD data over the full 2.0 mile extent on I-55 Pemiscot County with the 1000 ft test section shaded.	277
Fig. 7.39–RDD data over the 1000 ft test section on I-55 Pemiscot County.	277
Fig. 7.40– Histogram of W3 displacement measured on the (a) 1000 ft section and the (b) 1.5 mile section.	278
Fig. 7.41–RDD data over the 500 ft section where location of joints is clear.	279
Fig. 7.42–RDD data over 500 ft length of 1000 ft test section showing difficulty identifying individual joints.	279
Fig. 7.43–RDD data over 500 ft length of 1000 ft test section showing difficulty locating joints.	279
Fig. 7.44–Joint LTE measured using entering and leaving FWD deflections at every third joint.	280
Fig. 7.45–Deflection profile obtained from the first receiver of FWD measurements normalized to a load of 10 kips.	281
Fig. 7.46–Subgrade modulus estimated using the Hogg model from FWD data collected at Site 7 (HWY U).	281
Fig. 7.47–Composite stiffness estimated using the AREA model from FWD data collected at Site 7 (HWY U).	281
Fig. 7.48–Photographs of 1000 ft test section on I-35NB showing (a) repair of cracked slabs (b) replacement of slabs.	283
Fig. 7.49–RDD data over the full 2.0 mile extent on I-35 Northbound near Daviess County with the 1000 ft test section shaded.	283
Fig. 7.50–RDD data over the 1000 ft test section on I-35 Northbound near Daviess County.	284
Fig. 7.51–Histogram of W3 displacement measured on the (a) 1000 ft section and the (b) 2.0 mile section of I-35 NB.	284
Fig. 7.52–Comparison of joint deflections from FWD testing with deflection profile from RDD measurements at Site 8.	285

Fig. 7.53–Comparison of joint LTE measured with the FWD and the RDD at Site 8. 285

Fig. 7.54–Photograph of section on I-35SB showing the good quality of pavement. 286

Fig. 7.55–RDD data over the full 1.6 mile extent on I-35 Southbound site..... 287

Fig. 7.56–Histogram of W3 displacement measured on the 1.6 mile section of I-35 SB. 287

Fig. 7.57–Example deflection profiles at two locations showing unusual features in the profile, namely (a) downward spikes in the W3 profile, and (b) higher deflections on W2 than W1. 288

Fig. 8.1–Map showing network-level Site 9 (I-70). The test segment of I-70 extended from mile marker 84.2 to mile marker 20.8 and extended across three counties (Jackson, Saline and Lafayette). GPR data were acquired in the west-bound driving lane only. 290

Fig. 8.2–Map showing network-level Site10 (MO 465). The test segment of MO 465 (Taney County only) extended from the intersection with HWY 76 to the intersection with US 65. GPR data were acquired in all four lanes (two north-bound; two south-bound)..... 291

Fig. 8.3–Two higher-frequency (2.0 GHz) GPR antennae were mounted to the front of the truck. 292

Fig. 8.4–The lower-frequency (400 MHz) GPR antenna was mounted to the back of the truck. 292

Fig. 8.5–Distance measuring instrument (DMI) mounted on the truck wheel. 293

Fig. 8.6–Schematic drawing of survey system design (not to scale). 293

Fig. 8.7–Schematic showing relative locations of the network-level Site 9 (segment of I-70) GPR traverses. Solid black lines represent the boundaries of west-bound driving lane. Mile marker 51 (MM 51) is shown for illustration purposes. The test segment of I-70 extended from mile marker 84.2 to mile marker 20.8 and extended across three counties (Jackson, Saline and Lafayette); GPR data were acquired in the west-bound driving lane only..... 295

Fig. 8.8–Example of GPR data: Three parallel non-interpreted GPR profiles are presented. Two 2.0 GHz profiles and one 400 MHz GPR profile. A dielectric permittivity of 6.5 was used to convert reflection times to reflector depths. The horizontal axis is in units of feet; the vertical axis is in units of inches. 296

Fig. 8.9–Two segments of Site 9 network GPR data acquired in proximity to core 01: A) high-frequency GPR data acquired with 2.0 GHz air-launched antenna (one of two channels is shown); B) low-frequency GPR data acquired with 400 GHz antenna. Core 01 is superposed on the GPR data. A dielectric permittivity of 8.0 was used to convert reflection times to reflector depths. The horizontal axis is in units of feet; the vertical axis is in units of inches..... 300

Fig. 8.10–Two segments of Site 9 network GPR data acquired in proximity to core 02: A) high-frequency GPR data acquired with 2.0 GHz air-launched antenna (one of two channels is shown); B) low-frequency GPR data acquired with 400 GHz antenna. Core 02 is superposed on the GPR data. A dielectric permittivity of 8.0 was used to convert reflection times to reflector depths. The horizontal axis is in units of feet; the vertical axis is in units of inches..... 301

Fig. 8.11–Two segments of Site 9 network GPR data acquired in proximity to core 03: A) high-frequency GPR data acquired with 2.0 GHz air-launched antenna (one of two

channels is shown); B) low-frequency GPR data acquired with 400 GHz antenna. Core 03 is superposed on the GPR data. A dielectric permittivity of 8.0 was used to convert reflection times to reflector depths. The horizontal axis is in units of feet; the vertical axis is in units of inches.....	302
Fig. 8.12—Two segments of Site 9 network GPR data acquired in proximity to core 04: A) high-frequency GPR data acquired with 2.0 GHz air-launched antenna (one of two channels is shown); B) low-frequency GPR data acquired with 400 GHz antenna. Core 04 is superposed on the GPR data. A dielectric permittivity of 8.0 was used to convert reflection times to reflector depths. The horizontal axis is in units of feet; the vertical axis is in units of inches.....	303
Fig. 8.13—Two segments of Site 9 network GPR data acquired in proximity to core 05: A) high-frequency GPR data acquired with 2.0 GHz air-launched antenna (one of two channels is shown); B) low-frequency GPR data acquired with 400 GHz antenna. Core 05 is superposed on the GPR data. A dielectric permittivity of 8.0 was used to convert reflection times to reflector depths. The horizontal axis is in units of feet; the vertical axis is in units of inches.....	304
Fig. 8.14—Two segments of Site 9 network GPR data acquired in proximity to core 06: A) high-frequency GPR data acquired with 2.0 GHz air-launched antenna (one of two channels is shown); B) low-frequency GPR data acquired with 400 GHz antenna. Core 06 is superposed on the GPR data. A dielectric permittivity of 8.0 was used to convert reflection times to reflector depths. The horizontal axis is in units of feet; the vertical axis is in units of inches.....	305
Fig. 8.15—Two segments of Site 9 network GPR data acquired in proximity to core 07: A) high-frequency GPR data acquired with 2.0 GHz air-launched antenna (one of two channels is shown); B) low-frequency GPR data acquired with 400 GHz antenna. Core 07 is superposed on the GPR data. A dielectric permittivity of 8.0 was used to convert reflection times to reflector depths. The horizontal axis is in units of feet; the vertical axis is in units of inches.....	306
Fig. 8.16—Two segments of Site 9 network GPR data acquired in proximity to core 08: A) high-frequency GPR data acquired with 2.0 GHz air-launched antenna (one of two channels is shown); B) low-frequency GPR data acquired with 400 GHz antenna. Core 08 is superposed on the GPR data. A dielectric permittivity of 8.0 was used to convert reflection times to reflector depths. The horizontal axis is in units of feet; the vertical axis is in units of inches.....	307
Fig. 8.17—Two segments of Site 9 network GPR data acquired in proximity to core 09: A) high-frequency GPR data acquired with 2.0 GHz air-launched antenna (one of two channels is shown); B) low-frequency GPR data acquired with 400 GHz antenna. Core 09 is superposed on the GPR data. A dielectric permittivity of 8.0 was used to convert reflection times to reflector depths. The horizontal axis is in units of feet; the vertical axis is in units of inches.....	308
Fig. 8.18—Schematic showing locations of the GPR traverses along network-level Site 10 (MO 465). Solid black lines represent the boundaries of west -bound driving lane. Comparable GPR data were also acquired in east-bound lanes. Drawing is not to scale....	310
Fig. 8.19—Network-level Site 10 core 07 (Table 8.2).....	312

Fig. 8.20—Segment of network-level high-frequency GPR data (in proximity to network-level Site 10 Core 01; Core 01 is shown acquired using the high-frequency 2.0 GHz air-launched antenna (one of two channels is shown). A dielectric permittivity of 6.5 was used to convert reflection times to reflector depths. The horizontal axis is in units of feet; the vertical axis is in units of inches. 313

Fig. 8.21—Segment of network-level high-frequency GPR data (in proximity to network-level Site 10 Core 02; Core 02 is shown) acquired using the high-frequency 2.0 GHz air-launched antenna (one of two channels is shown). A dielectric permittivity of 6.5 was used to convert reflection times to reflector depths. The horizontal axis is in units of feet; the vertical axis is in units of inches. 314

Fig. 8.22—Segment of network-level high-frequency GPR data (in proximity to network-level Site 10 Core 03; Core 03 is shown) acquired using the high-frequency 2.0 GHz air-launched antenna (one of two channels is shown) at Site 10. A dielectric permittivity of 6.5 was used to convert reflection times to reflector depths. The horizontal axis is in units of feet; the vertical axis is in units of inches..... 315

Fig. 8.23—Segment of network-level high-frequency GPR data (in proximity to network-level Site 10 Core 04; Core 04 is shown) acquired using the high-frequency 2.0 GHz air-launched antenna (one of two channels is shown) at Site 10. A dielectric permittivity of 6.5 was used to convert reflection times to reflector depths. The horizontal axis is in units of feet; the vertical axis is in units of inches..... 316

Fig. 8.24—Segment of network-level high-frequency GPR data (in proximity to network-level Site 10 Core 05; Core 05 is shown) acquired using the high-frequency 2.0 GHz air-launched antenna (one of two channels is shown) at Site 10. A dielectric permittivity of 6.5 was used to convert reflection times to reflector depths. The horizontal axis is in units of feet; the vertical axis is in units of inches..... 317

Fig. 8.25—Segment of network-level high-frequency GPR data (in proximity to network-level Site 10 Core 06; Core 06 is shown) acquired using the high-frequency 2.0 GHz air-launched antenna (one of two channels is shown) at Site 10. A dielectric permittivity of 6.5 was used to convert reflection times to reflector depths. The horizontal axis is in units of feet; the vertical axis is in units of inches..... 318

Fig. 8.26—Segment of network-level high-frequency GPR data (in proximity to network-level Site 10 Core 07; Core 07 is shown) acquired using the high-frequency 2.0 GHz air-launched antenna (one of two channels is shown) at Site 10. A dielectric permittivity of 6.5 was used to convert reflection times to reflector depths. The horizontal axis is in units of feet; the vertical axis is in units of inches..... 319

LIST OF TABLES

	Page
Table 1.1–Summary of non-invasive technologies assessed as part of Task 4	1
Table 1.2–Links to report sections.....	5
Table 2.1–Background information about eight project-level sites (see Fig. 2.1).....	6
Table 2.2–Background information about two network-level sites (see Figs. 2.2 and 2.3).	6
Table 2.3–Summary of investigation dates and weather conditions of the pavement sites investigated.....	9
Table 2.4–Summary of RDD and FWD investigation dates and weather conditions of the pavement sites investigated	10
Table 2.5–Summary of project-level pavement site defects observed.....	11
Table 2.6–US 63 (project-level Site 1) core summary.	28
Table 2.7–US 54 (project-level Site 2) core summary.	31
Table 2.8–MO 179 (project-level Site 3) core summary.....	34
Table 2.9–HWY AT (project-level Site 4) core summary.....	37
Table 2.10–I-55 Pemiscot County (project-level Site 5) core summary.	40
Table 2.11–I-55 Perry County (project-level Site 6) core summary.	42
Table 2.12–HWY U (project-level Site 7) core summary.	44
Table 2.13–I-35 (project-level Site 8) core summary.....	47
Table 2.14–I-70 (network-level Site 9) core summary.	49
Table 2.15–MO 465 (network-level Site 10) core summary.....	51
Table 3.1–Typical elastic modulus of 28 day PCC (Source: 2011, Russel W. Lenz, Pavement Design Guide; Typical Values of Young’s Elastic Modulus and Poisson’s Ratio for Pavement Materials, Cornell Local Roads Program).	60
Table 3.2–Typical elastic modulus of asphalt concrete (AC; bituminous mix (BM)) (Source: 2012, Gudmarsson, Laboratory Seismic Testing of Asphalt Concrete; Typical Values of Young’s Elastic Modulus and Poisson’s Ratio for Pavement Materials, Cornell Local Roads Program).....	60
Table 4.1–Core depths and GPR apparent depths to base of pavement layers at Site 1.	159
Table 4.2–Core depths and GPR apparent depths to base of pavement layers at Site 2.	163
Table 4.3–Core depths and GPR apparent depths to base of pavement layers at Site 3. Differences between the actual and apparent thicknesses are also noted. All of the ten cores were described as moderately to highly stripped. Cores 5-10 were described as debonded.....	163
Table 4.4–Core depths and GPR apparent depths to base of pavement layers at Site 4. Differences between the actual and apparent thicknesses are also noted. The BM in all nine cores is described as stripped (low to moderate) and debonded at one or more levels.	178
Table 4.5–Core thicknesses and GPR apparent thicknesses of the PCC layer at Site 4. Differences between the actual and apparent thicknesses are due to incomplete recovery of BM in cores and average dielectric permittivity (7.5) used at the site. Actual dielectric permittivity varies for BM and PCC layers.....	178

Table 4.6–Core depths and GPR apparent depths to base of BM layer at Site 5. Differences between the actual and apparent thicknesses are also noted. The PCC/BM interface (upper interface) in cores 3, 5, 6, 7, and 8 is described as debonded; the BM/PCC interface (lower interface) in all cores is described as debonded. Stripping in core 1 is described as moderate; stripping in all other cores is described as low.....	184
Table 4.7–Core depths and GPR apparent depths to base of BM layer at Site 6. Differences between the actual and apparent thicknesses are also noted. The PCC in all cores is described as being in good condition.	186
Table 4.8–Core depths and GPR apparent depths to base of BM layer at Site 7. Differences between the actual and apparent thicknesses are due mostly to incomplete core recovery.	197
Table 4.9–Core depths and GPR apparent depths to base of BM layer at Site 8. Differences between the actual and apparent thicknesses are also noted. The PCC in all cores is described as being in good condition.	202
Table 7.1–Summary of RDD and FWD investigation dates and weather conditions of the pavement sites investigated.	255
Table 7.2–RDD testing summary.	258
Table 7.3–W3 deflection statistics for the 1.5 mile and 1000 ft section of US 63.	264
Table 7.4–W3 deflection statistics for the 0.65 mile and 1000 ft section of US 54.	269
Table 7.5–W3 deflection statistics for 1000 ft section of HWY 179.....	273
Table 7.6–W3 deflection statistics for the 2.0 mile and 1000 ft section of I-55 in Pemiscot County.....	278
Table 7.7–W3 deflection statistics for the 2.0 mile and 1000 ft section of I-35 NB near Daviess County.....	284
Table 7.8–W3 deflection statistics for the 1.6 mile section of I-35 SB.....	287
Table 8.1–Site 9 (I-70) core locations. The description is based on the visual assessment only, no lab testing was conducted.	297
Table 8.2–Site 10 (MO 465) core locations. The description is based on the visual assessment only, no laboratory testing was conducted.	311
Table 9.1–Positive outcomes from the eight project-level site investigations.	325
Table 9.2–Positive outcomes from the two network-level site investigations.	328
Table A.1–Applications to assessment of bituminous mix (BM) pavements (USW: ultrasonic surface wave; IE: impact echo; HF-GC-GPR: high-frequency ground-coupled ground penetrating radar; LF-GC-GPR: low-frequency ground-coupled ground penetrating radar; HF-AL-GPR: high-frequency air-launched ground penetrating radar; FWD: falling weight deflectometer; RRD: rolling wheel deflectometer; ERT: electrical resistivity tomography; MASW: multi-channel analyses of surface waves). D–Direct Measurement/Primary Application; d–Direct Measurement/Non-primary Application; I–Indirect Measurement/Primary Application; i–Indirect Measurement/Non-primary Application.	332
Table A.2–Applications to assessment of portland cement concrete (PCC) pavements (USW: ultrasonic surface wave; IE: impact echo; HF-GC-GPR: high-frequency ground-coupled ground penetrating radar; LF-GC-GPR: low-frequency ground-coupled ground penetrating radar; HF-AL-GPR: high-frequency air-launched ground penetrating radar;	

FWD: falling weight deflectometer; RRD: rolling wheel deflectometer; ERT: electrical resistivity tomography; MASW: multi-channel analyses of surface waves). D–Direct Measurement/Primary Application; d–Direct Measurement/Non-primary Application; I–Indirect Measurement/Primary Application; i–Indirect Measurement/Non-primary Application.	333	
Table A.3–Applications to assessment of base and subbase (USW: ultrasonic surface wave; IE: impact echo; HF-GC-GPR: high-frequency ground-coupled ground penetrating radar; LF-GC-GPR: low-frequency ground-coupled ground penetrating radar; HF-AL-GPR: high-frequency air-launched ground penetrating radar; FWD: falling weight deflectometer; RRD: rolling wheel deflectometer; ERT: electrical resistivity tomography; MASW: multi-channel analyses of surface waves). D–Direct Measurement/Primary Application; d–Direct Measurement/Non-primary Application; I–Indirect Measurement/Primary Application; i–Indirect Measurement/Non-primary Application.	334	
Table A.4–Applications to assessment of soil and rock (USW: ultrasonic surface wave; IE: impact echo; HF-GC-GPR: high-frequency ground-coupled ground penetrating radar; LF-GC-GPR: low-frequency ground-coupled ground penetrating radar; HF-AL-GPR: high-frequency air-launched ground penetrating radar; FWD: falling weight deflectometer; RRD: rolling wheel deflectometer; ERT: electrical resistivity tomography; MASW: multi-channel analyses of surface waves). D – Direct Measurement/Primary Application; d – Direct Measurement/Non-primary application; I – Indirect Measurement/Primary Application; i – Indirect Measurement/Non-primary application.	335	
Table A.5–Ultrasonic surface wave (USW)	336	
Table A.6–Impact echo (IE)	337	
Table A.7–High-frequency ground-coupled GPR	338	
Table A.8–Low-frequency ground-coupled GPR340		344
Table A.9–Electrical resistivity tomography (ERT)		344
Table A.10–Multi-channel analyses of surface waves (MASW)	347	
Table A.11–Falling weight deflectometer (FWD)	349	
Table A.12–Rolling dynamic deflectometer (RDD)	351	
Table A.13–High-frequency air-launched GPR	356	

1 INTRODUCTION

1.1 Objectives

The objective of Task 4 was to thoroughly assess the cost-effectiveness and utility of the non-invasive technologies identified in Task 3 (Table 1.1) as applicable to MoDOT roadways. The intent was to develop a guidance document focused on the utility and cost-effectiveness of project-applicable and network-applicable non-invasive imaging technologies. The optimal utilization of appropriate non-invasive imaging technologies will result in more accurate pavement assessments at significantly reduced costs. Specific objectives included:

- Assessment of the utility and cost-effectiveness of the tested network-applicable non-invasive imaging tools based, in large part, on the analyses of data acquired along two designated roadways;
- Assessment of the utility and cost-effectiveness of the tested project-applicable non-invasive imaging tools based, in large part, on the analyses of data acquired along eight designated roadways; and
- Development of a comprehensive guidance document including a matrix of which cost-effective site assessment technologies are applicable, how to employ them, and what site condition data can be obtained.

Table 1.1–Summary of non-invasive technologies assessed as part of Task 4

Non-invasive Imaging Technology	Tested on Project-level Roadways	Tested on Network-level Roadways
Ultrasonic Surface Waves (USW)	Yes	No
Impact Echo (IE)	Yes	No
Ground-coupled Ground Penetrating Radar (GPR) (400 MHz and 1500 MHz)	Yes	No
Electrical Resistivity Tomography (ERT)	Yes	No
Multichannel Analyses of Surface Waves (MASW)	Yes	No
Falling Weight Deflectometer (FWD)	Yes	No
Rolling Dynamic Deflectometer (RDD)	Yes	No
Air-launched Ground Penetrating Radar (GPR)	No	Yes

1.2 Justification

To rapidly and cost-effectively assess the condition of new and existing pavements, various non-invasive in-situ data must be collected and interpreted. The extent and level of data needed depends on the type of pavement condition information sought (distress, structural capacity, or surface characteristics) and influences the type of assessment conducted (network-level or project-level).

As discussed in Section 1.1, the objective of Task 4 was to thoroughly assess, in part through network-level and project-level field studies, the non-invasive imaging technologies identified and selected in Task 3 as applicable to MoDOT roadways (Table 1.1). The intent was to develop a guidance document focused on the utility and cost-effectiveness of identified project-applicable and network-applicable non-invasive imaging technologies. The guidance document is focused on when, where and how to use each tool. The data acquired during the comprehensive test phase of Task 4 were used to evaluate the utility, cost-effectiveness, user-friendliness, accuracy, reliability, reproducibility and limitations of each technology.

The optimal utilization of appropriate non-invasive technologies will result in more accurate pavement assessments and significantly reduced costs. The tools that were tested in this study can be applied to new pavements for quality control and quality assurance purposes, and can also be used to assess existing pavements. The tools that were tested will generate information about thicknesses, moisture content, and elastic modulus of pavement. Information can also be generated about the thickness, elastic modulus, and moisture content of the soil.

1.3 Scope of Work

The scope of work for this task was to select both network-level and project-level sites (Section 2.1) that are generally representative of the different pavement conditions within the state of Missouri. Comprehensive characterizations of these sites were then performed using the state-of-the-art non-invasive practices identified in Task 3 as applicable to MoDOT roadways. Core control and auger samples were collected at each site for calibration and verification purposes.

The scope of work included five subtasks, Sub-task 4.A, Sub-task 4.B, Sub-task 4.C, Sub-task 4.D, and Sub-task 4.E. Each of these tasks is described below.

Sub-task 4.A: This sub-task had four components. Components 1 and 2 were the selection of roadways suitable for the acquisition of the network-applicable and project-applicable non-invasive imaging data identified in Task 3, respectively, and the procurement of existing ground truth. Components 3 and 4 were the design of optimal field data acquisition procedures and the coring program. MoDOT was responsible for the acquisition of cores.

Sub-task 4.A.1: This sub-task was the selection of the two 60 mile-long roadways along which demonstration network-applicable non-invasive imaging data were acquired.

Sub-task 4.A.2: This sub-task was the selection of the eight 1000 foot-long roadways along which demonstration project-applicable non-invasive imaging data were acquired.

Sub-task 4.A.3: This sub-task was the design of the field procedures (protocol and acquisition parameters) for the acquisition of the network-applicable non-invasive imaging data set and the design of the supplemental coring program. Lane closures were not necessary for the acquisition of network-level non-invasive imaging data set.

Sub-task 4.A.4: This sub-task was the design of the field procedures (protocol and acquisition parameters) for the acquisition of the project-applicable non-invasive data sets and the design of the supplemental coring program.

Sub-task 4.B: This sub-task had four components. Components 1 and 2 were the scheduling of field work, including the acquisition of the non-invasive imaging data.

Sub-task 4.B.1: This sub-task was the scheduling of the acquisition of the network-applicable non-invasive imaging data. Lane closures were not necessary.

Sub-task 4.B.2: This sub-task was the scheduling of the acquisition of the project-applicable non-invasive data. As part of the project-level testing program, the project team collaborated with personnel from the University of Texas at Austin to utilize a Rolling Dynamic Deflectometer (RDD) to collect continuous profiles of pavement deflection.

Sub-task 4.B.3: This sub-task was the acquisition of the network-applicable non-invasive imaging data.

Sub-task 4.B.4: This sub-task was the acquisition of the project-applicable non-invasive data.

Sub-task 4.C: This sub-task had four components. Components 1 and 2 were the processing of the acquired non-invasive data. Components 3 and 4 were the analyses of all available relevant ARAN data and available ground truth including core control, construction histories, maintenance histories, etc.

Sub-task 4.C.1: This sub-task was the processing of the network-applicable non-invasive data. This task involved the design and implementation of quality control and quality assurance procedures to ensure imaging data were correctly processed and accurately positioned.

Sub-task 4.C.2: This sub-task was the processing of the project-applicable non-invasive data. This task involved the design and implementation of quality control and quality assurance procedures to ensure data were correctly processed and accurately positioned.

Sub-task 4.C.3: This sub-task was the analyses of all available relevant ground truth including core control, construction histories, maintenance histories, etc., along the two 60 mile-long network-level roadways. It was anticipated that core control would be acquired at each site. These data were used to constrain the interpretation of the acquired network-applicable non-invasive imaging data and to verify the reasonableness of the same.

Sub-task 4.C.4: This sub-task was the analyses of all available relevant ARAN data and ground truth including core control, construction histories, maintenance histories, etc., along the eight roadway segments on which project-applicable non-invasive imaging data were acquired. It was anticipated that core control would be acquired at each site. These data were

to constrain the interpretation of the acquired project-applicable non-invasive imaging data and verify the reasonableness of the same.

Sub-task 4.D: This sub-task was the interpretation of the non-invasive imaging data. The interpretation of each set of non-invasive data was constrained by ground truth and by the interpretations of all other acquired sets of non-invasive imaging data. The primary objective was to collect as much site condition information as possible.

Sub-task 4.D.1: This sub-task was the interpretation of the network-applicable non-invasive imaging data. The interpretation of each set of non-invasive imaging data was constrained by ground truth. The primary objective was to collect as much site condition information as possible. It was anticipated that the output would include information about pavement thickness and base/subgrade moisture content. A secondary objective was to assess the accuracy of the interpretations and the various factors that affect the reliability of interpretations.

Sub-task 4.D.2: This sub-task was the interpretation of the project-applicable non-invasive data. The interpretation of each set of non-invasive imaging data was constrained by ground truth and by the interpretations of all other acquired sets of non-invasive imaging data. The primary objective was to collect as much site condition information as possible. It was anticipated that the output would include information about pavement thickness, pavement/base/subgrade elastic moduli, base and subgrade moisture content, base thickness, subgrade clay content, and depth to top of rock. A secondary objective was to assess the accuracy of the interpretations and the various factors that affect the reliability of the interpretations.

Sub-task 4.E: This sub-task was the development of a comprehensive guidance document including a matrix on which site assessment technologies are applicable, where to employ them, when to employ them, how to employ them, and what site condition data can be obtained. Topics addressed include: parameters measured, optimum acquisition parameters, optimum processing parameters, sampling interval, crew size, equipment costs, software costs, vehicle requirements, estimated daily cost, volume of data acquired per day, ease of data acquisition, ease of data processing, ease of data interpretation, reproducibility of interpretations, reliability of interpretations and cost-effectiveness, and recommendations for improvements to current site investigation and testing practices that can help achieve cost savings for MoDOT projects. This information was intended to provide the basis and data to establish the value of different non-invasive imaging technologies in various conditions so that MoDOT can use the most effective means available to characterize future sites.

1.4 Organization of the Report

An overview of the project-level and network-level sites investigated is presented in Section 2. Sections 3-7 include the results of the project-level and network-level investigations conducted in this study. Section 8 summarizes the findings. The Guidance Document is included as a stand-alone appendix in Appendix A. [Appendix B](#) details the core and auger samples.

1.5 Links to Report Sections on Individual Pavement Sections

Electronic links to specific sections in this report pertaining to individual pavement sections are included below as hyperlinks in Table 1.2.

Table 1.2–Links to report sections

Pavement Section	Visual Assessment Results	Cores	USW Results	IE Results	High Frequency GPR Results	Low Frequency GPR Results	ERT Results	MASW Results	FWD and RDD Results
US 63 Phelps County (Site 1)	2.3.1.1	2.4.1.1	3.3.1.1	3.3.1.2	4.3.1	5.3.1	6.4.1.1	6.4.1.2	7.4.1
US 54 Camden County (Site 2)	2.3.1.2	2.4.1.2	3.3.2.1	3.3.2.2	4.3.2	5.3.2	6.4.2.1	6.4.2.2	7.4.2
MO 179 Cole County (Site 3)	2.3.1.3	2.4.1.3	3.3.3.1	3.3.3.2	4.3.3	5.3.3	6.4.3.1	6.4.3.2	7.4.3
HWY AT Franklin County (Site 4)	2.3.1.4	2.4.1.4	3.3.4.1	3.3.4.2	4.3.4	5.3.4	6.4.4.1	6.4.4.2	7.4.4
I-55 Pemiscot County (Site 5)	2.3.1.5	2.4.1.5	3.3.5.1	3.3.5.2	4.3.5	5.3.5	6.4.5.1	6.4.5.2	7.4.5
I-55 Perry County (Site 6)	2.3.1.6	2.4.1.6	3.3.6.1	3.3.6.2	4.3.6	5.3.6	6.4.6.1	6.4.6.2	7.4.6
HWY U Dent County (Site 7)	2.3.1.7	2.4.1.7	3.3.7.1	3.3.7.2	4.3.7	5.3.7	6.4.7.1	6.4.7.2	7.4.7
I-35 Jackson County (Site 8)	2.3.1.8	2.4.1.8	3.3.8.1	3.3.8.2	4.3.8	5.3.8	6.4.8.1	6.4.8.2	7.4.8
I-70 WB (Site 9)	2.3.2.1	2.4.2.1	-	-	8.3.1	-	-	-	-
MO 465 Branson (Site 10)	2.3.2.2	2.4.2.2	-	-	8.3.2	-	-	-	-

2 DESCRIPTION OF PROJECT- AND NETWORK-LEVEL ROADWAYS

2.1 Project- and Network-Level Roadways: Survey Objectives

2.1.1 Project-Level Sites

The project-level sites and survey objectives were selected by the project team and MoDOT. Non-invasive imaging data and core control were acquired along eight project-level roadway sites. Each tested segment of project-level roadway was 1000 ft in length. Non-invasive imaging data were collected in one lane only. Lane closures were required. Table 2.1 summarizes the survey objectives of each of the eight project-level sites. Fig. 2.1 shows the location of the project-level sites.

Table 2.1–Background information about eight project-level sites (see Fig. 2.1)

Project Location	Survey Objective(s)
US 63 Phelps County (Site 1)	Estimate pavement thickness and assess roadway condition
US 54 Camden County (Site 2)	Detect deep (>6 in.) stripping layer and assess roadway condition
Rte 179 Cole County (Site 3)	Detect debonding and assess roadway condition
HWY AT Franklin County (Site 4)	Detect shallow (<6 in.) stripping layer and assess roadway condition
I-55 Pemiscot County (Site 5)	Assess an unbonded concrete overlay (no flaws anticipated)
I-55 Perry County (Site 6)	Assess pavement joint condition
HWY U Dent County (Site 7)	Assess a poor-condition asphalt roadway
I-35 Jackson County (Site 8)	Assess an unbonded concrete overlay (flaws are anticipated)

2.1.2 Network-Level Sites

The network-level sites and survey objectives were selected by the project team and MoDOT. Non-invasive imaging data and core control were acquired along two network-level roadways. Table 2.2 summarizes the survey objectives for both network-level investigations. Fig. 2.2 and Fig. 2.3 show the locations of the network-level sites. The locations of the network-level sites are also shown in Fig. 2.1.

Table 2.2–Background information about two network-level sites (see Figs. 2.2 and 2.3)

Project Location	Survey Objective(s)
I -70 MM84.2-MM20.8, driving lane, WB, survey extended across three counties (Jackson, Saline and Lafayette) (Site 9)	Estimate pavement layer thicknesses and assess roadway condition
MO 465 (between HWY 76 and US 65, both lanes, NB and SB) is located in Taney County (Site 10)	Estimate pavement layer thicknesses and assess roadway condition



Fig. 2.2—Map showing network-level Site 9 (I-70). GPR data were acquired in the west-bound driving lane.



Fig. 2.3—Map showing network-level Site 10 (MO 465). GPR data were acquired in all four lanes (two north-bound; two south-bound).

2.2 Project- and Network-Level Roadways: Investigation Dates and Weather Conditions

The dates and weather conditions for the geophysical field investigations and coring data acquisition for all the sites are presented in Table 2.3. RDD and some FWD data were collected on different dates due to scheduling issues and technical problems. Table 2.4 summarizes the RDD and FWD investigation dates and weather conditions.

Table 2.3–Summary of investigation dates and weather conditions of the pavement sites investigated

Pavement Site	Date of Investigation	Weather Conditions	Coring Date	Weather Conditions
US 63 (Site 1)	10/29-30/2012	27-55° F, absence of rain	11/01/2012	51-68° F, absence of rain
US 54 (Site 2)	11/12-13/2012	27-70° F, absence of rain	12/12/2012	19-52° F, absence of rain
MO 179 (Site 3)	12/03-05/2012	30-66° F, absence of rain	12/11/2012	16-43° F, absence of rain
HWY AT (Site 4)	07/25-26/2013	56-83° F, absence of rain	08/05/2013	67-91° F, absence of rain
I-55 Pemiscot County (Site 5)	07/31/2013	72-86° F, absence of rain	08/29/2013	72-94° F, absence of rain
I-55 Perry (Site 6)	09/23/2013	45-75° F, absence of rain	09/24/2013	50-81° F, absence of rain
HWY U (Site 7)	03/13-14/2013	25-67° F, absence of rain	05/05/2013	40-54° F, rain
I-35 (Site 8)	08/06/2013	70-89° F, absence of rain	08/07/2013	71-90° F, absence of rain
US 63 (Site 1) (2 nd survey)	02/13/2014	20-49° F, absence of rain	N/A	N/A
I-55 Pemiscot County (Site 5) (2 nd survey)	04/18/2014	50-73° F, absence of rain	N/A	N/A
I-55 Perry (Site 6) (2 nd survey)	04/17/2014	39-68° F, absence of rain	N/A	N/A
I-70 WB (Site 9)	07/01/2013	61-83° F, absence of rain	04/08/2014	44-60° F, absence of rain
MO 465 Branson (Site 10)	09/19/2013	69-90° F, absence of rain	12/02/2013	41-64° F, absence of rain

Table 2.4–Summary of RDD and FWD investigation dates and weather conditions of the pavement sites investigated

Pavement Site	Date of RDD Investigation	Weather Conditions	Date of FWD Investigation	Weather Conditions
US 63 North of Rolla (Site 1)	12/11/2013	28-35° F, sunny	10/30/2012	33-46° F, no rain
US 54 Camden County (Site 2)	11/19/2013	50-56° F, sunny	11/14/2012	37-42° F, no rain
MO 179 Jefferson City (Site 3)	12/10/2013	36-38° F, sunny	12/04/2012	26-29° F, cloudy, rain
HWY AT (Site 4)	N/A	N/A	08/05/2013	71-74° F, no rain
I-55 Pemiscot County (Site 5)	12/12/2013	28-35° F, sunny	4/30/2014	49-53° F, no rain
I-55 Perry County (Site 6)	N/A	N/A	09/24/2013	51-71° F, no rain
HWY U (Site 7)	N/A	N/A	05/02/2013	57-65° F, no rain
I-35 (Site 8)	11/18/2013	38-45° F, sunny	05/28/2014	84-87° F, no rain
I-35 Daviess County (RDD Only)	11/18/2013	42-45° F, sunny	N/A	N/A

2.3 Project- and Network-Level Roadways: Visual Assessments

2.3.1 Project-Level Sites

A comprehensive visual assessment of the paved surface was conducted by the research team at each project-level site. Mapped defects included cracking (block, alligator, transverse and longitudinal), rutting, distortions, raveling, and patches. A tabular summary of the types of defects observed at each of the project-level pavement sites is presented in Table 2.5. Numerical and qualitative PASER (Pavement Surface Evaluation and Rating) rating for each of the project-level pavement sites are noted in Table 2.5.

Table 2.5–Summary of project-level pavement site defects observed.

Pavement Site	Type of Defect Observed in Pavement Site								PASER Rating Excellent (9, 10), Very Good (8), Good (7, 6), Fair (4, 5), Poor (3), Very Poor (2), Failed (1).
	Cracking				Rutting	Distortions	Raveling	Patches	
	Block	Alligator	Transverse	Longitudinal					
US 63 (Site 1)									9
US 54 (Site 2)	x	x	x	x	x	x	x	x	4, 5
MO 179 (Site 3)	x		x	x	x	x			6
HWY AT (Site 4)		x	x	x	x			x	7
I-55 Pemiscot County (Site 5)			x	x					8
I-55 Perry (Site 6)			x	x					8
HWY U (Site 7)	x	x	x	x	x	x	x	x	3
I-35 (Site 8)	x		x	x				x	7

2.3.1.1 Project-Level Site 1 (US 63)

No visual defects were documented during the investigation of Site 1. A layer of bituminous mix (approx. 3.5 in.) had recently been overlaid on the pavement surface. Hence, the site appeared to be in excellent condition with a PASER rating of 9. The condition of the site is shown in Fig. 2.4.



Fig. 2.4—Photograph of US 63 (Site 1). The pavement was observed to be in excellent condition with no visible surface defects.

2.3.1.2 Project-Level Site 2 (US 54)

Site 2 was considered to be in fair condition with a PASER rating of between 4 and 5. Common defects observed in the pavement included cracking (block, alligator, transverse and longitudinal), rutting, distortions, and patches. Photographs of Site 2 are shown in Fig. 2.5 and Fig. 2.6.

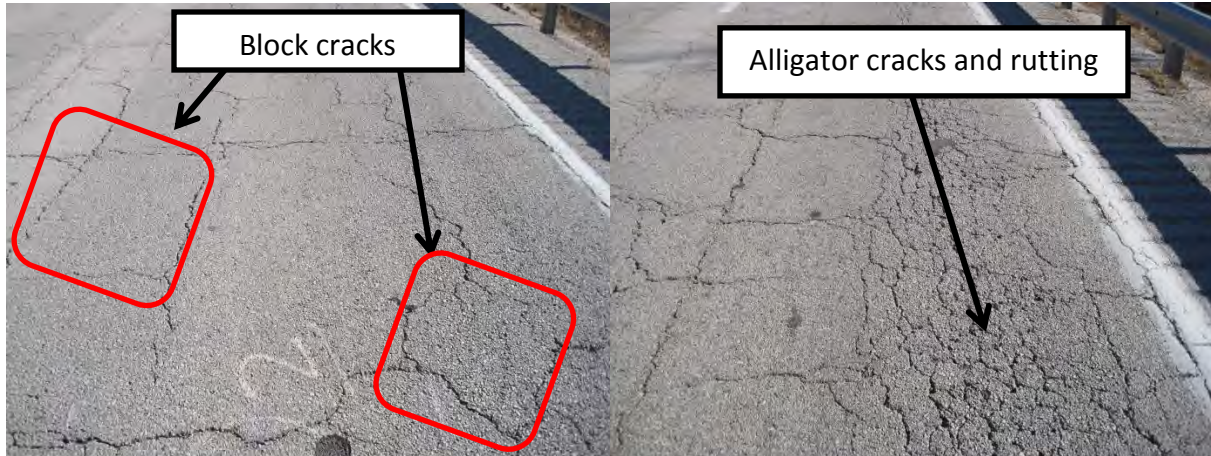


Fig. 2.5—Photograph of US 54 (Site 2). The pavement appeared to be in fair condition with block crack, alligator cracks and rutting observed on the surface.

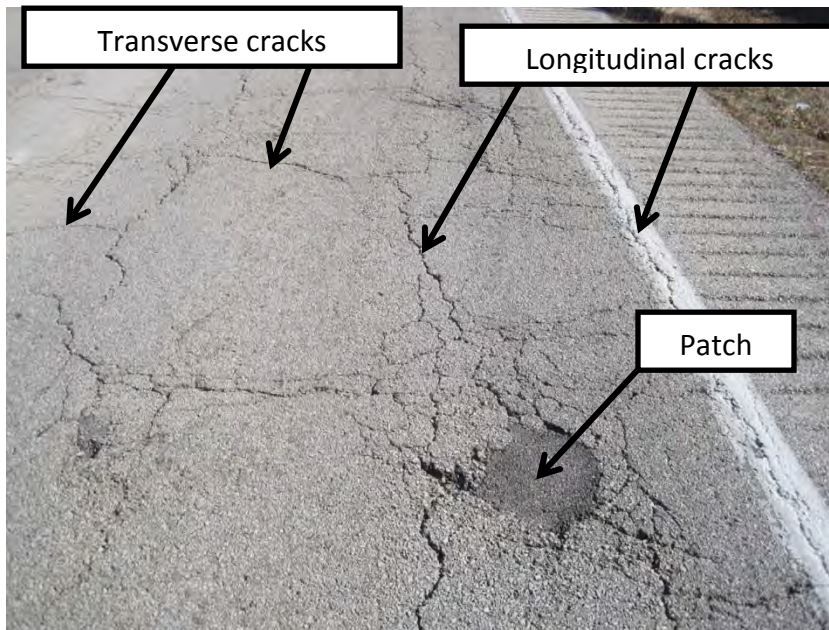


Fig. 2.6—Photograph of US 54 (Site 2). The pavement was observed to be in fair condition with evidence of patches as well as longitudinal and transverse cracks on the surface.

2.3.1.3 Project-Level Site 3 (MO 179)

Site 3 was investigated at night. A thorough visual inspection of the site as seen in Fig. 2.7 indicated that the pavement was in good condition with a PASER rating of 6. Some common defects observed in the pavement included cracks (longitudinal, transverse, and block) and rutting. A photograph of Site 3 is shown in Fig. 2.7.

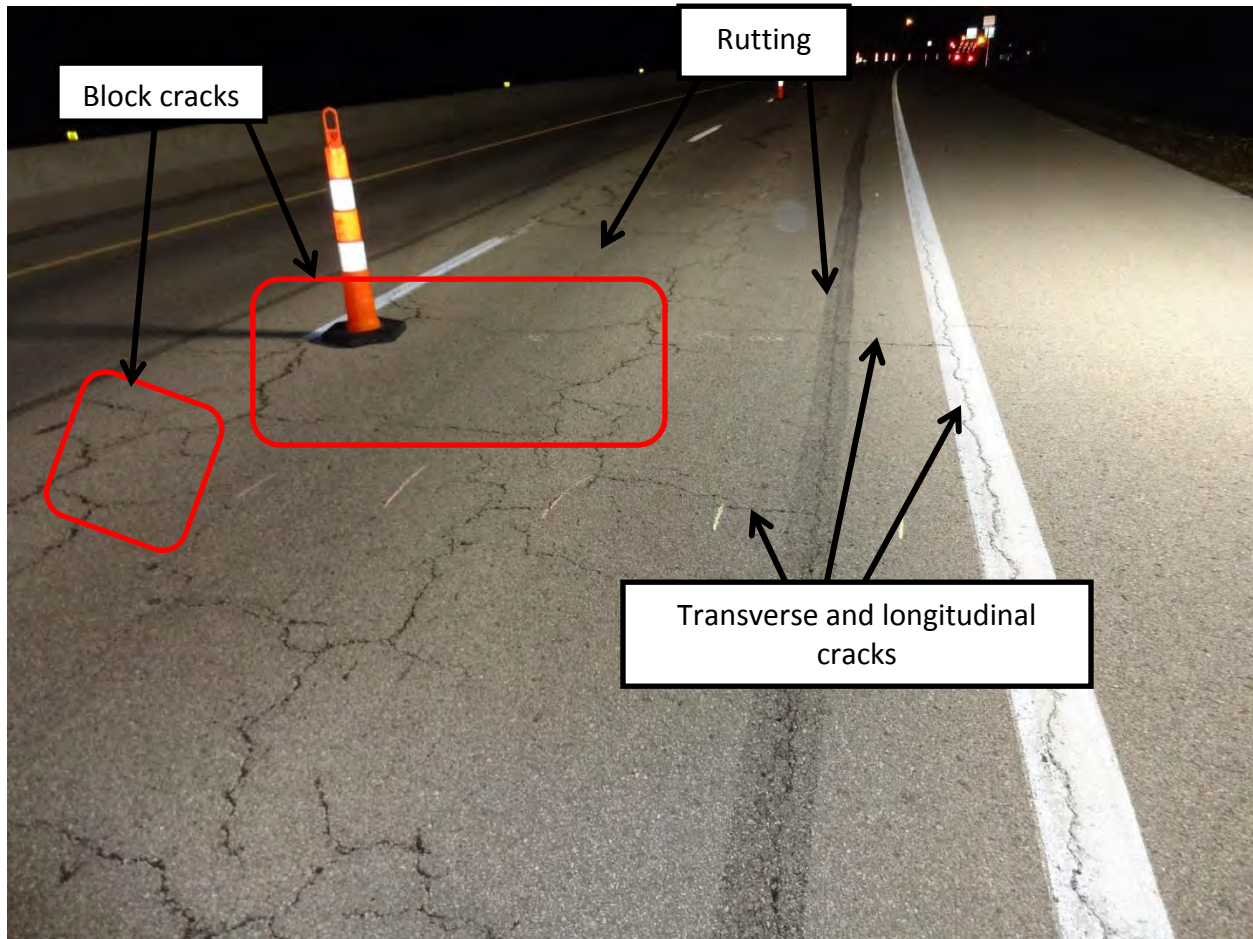


Fig. 2.7—Photograph showing typical condition of the MO 179 (Site 3) pavement site at the time of field investigation.

2.3.1.4 Project-Level Site 4 (HWY AT)

Site 4 was observed to be in good condition with a PASER rating of 7 as seen in Fig. 2.8. Some evidence of deterioration such as cracking, slight distortion, and patches were observed. A photograph of a typical patch observed is shown in Fig. 2.9.

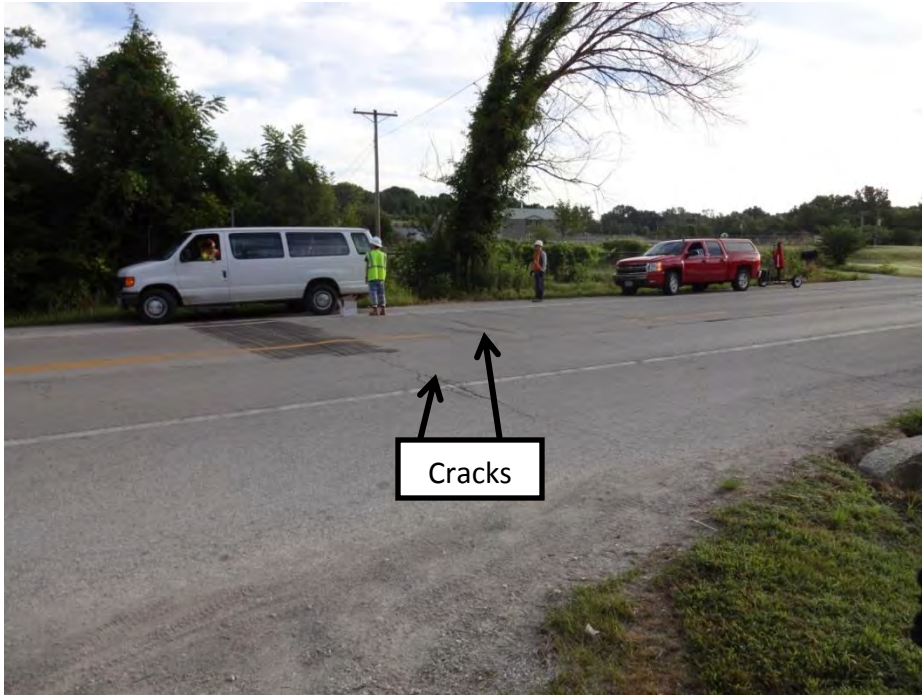


Fig. 2.8—Photograph of HWY AT (Site 4) pavement. Cracks were visible on the pavement surface.

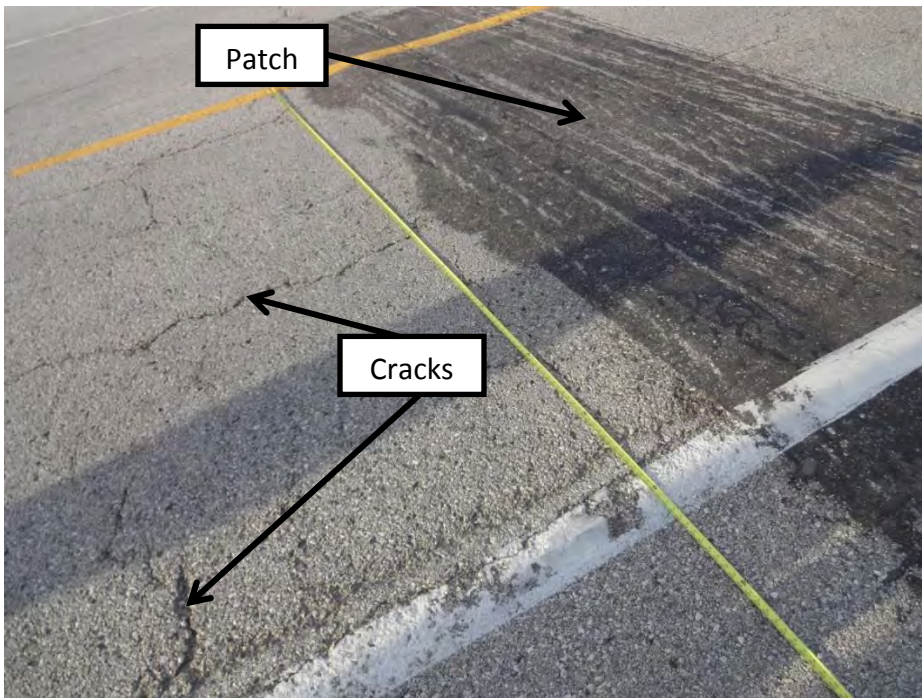


Fig. 2.9—Photograph showing cracks and patch observed on the HWY AT (Site 4) pavement surface.

2.3.1.5 Project-Level Site 5 (I-55 Pemiscot County)

A visual inspection of the concrete pavement at Site 5 showed no evidence of surface defects. Site 5 was given a PASER rating of 9, indicating very good condition. The condition of the site is depicted in Fig. 2.10.



Fig. 2.10—Photograph of I-55 Pemiscot County (Site 5) pavement.

2.3.1.6 Project-Level Site 6 (I-55 Perry County)

Concrete pavement Site 6 showed little visible evidence of deterioration. A few longitudinal and transverse cracks and patches were observed in scattered locations around the site. The site was given a PASER rating of 8 denoting very good condition. The general condition of the Site 6 pavement is shown in Fig. 2.11.



Fig. 2.11—Photograph of I-55 Perry County (Site 6). The pavement appeared to be in very good condition with few cracks on the surface.

2.3.1.7 Project-Level Site 7 (HWY U)

The asphalt pavement was observed to be in poor condition with a PASER rating of 3. The pavement showed evidence of multiple closely spaced longitudinal and transverse cracks, raveling, alligator cracks, and distortions. The condition of the pavement is shown in Fig. 2.12.



Fig. 2.12—Cracks, rutting, and patches observed on the pavement surface at HWY U (Site 7).

2.3.1.8 Project-Level Site 8 (I-35)

Visual assessment of Site 8 indicated that the pavement was in good condition with PASER rating of 7. A few patches and cracks (longitudinal and traverse) were observed at the site. The condition of the pavement is shown in Fig. 2.13 and Fig. 2.14.



Fig. 2.13–I-35 (Site 8) showing evidence of cracks and patches on the pavement surface.



Fig. 2.14–I-35 (Site 8) showing evidence of cracks on the pavement surface.

2.3.2 Network-Level Sites

While data were being acquired with the air-launched GPR (Section 8), video of the pavement surface was continuously recorded and later used for visual assessment purposes.

Approximately sixty miles of video coverage were recorded for each network-level site. The intent was to rate the pavement surface condition as Good, Fair, or Poor based on the level of deterioration observed on the surface of the pavements. Both network-level pavement surfaces were judged to be in Good condition with relatively few cracks or patches. The bridge deck surfaces along these paved roadways, in contrast, showed signs of deterioration including cracks and many patches.

2.3.2.1 Network-Level Site 9 (I-70)

The pavement surface is predominantly composite bituminous mix (BM) over PCC with few sections of portland cement concrete (PCC). The pavement surface along network-level Site 9 appeared (visually) to be in good condition as evidenced by Fig. 2.15 through Fig. 2.20. However, the network-level Site 9 bridge decks showed signs of cracks and patches (Fig. 2.16 through Fig. 2.17).



Fig. 2.15—Typical section of the network-level Site 9 (I-70) pavement. This paved surface was judged to be in good condition.



Fig. 2.16—Photograph of section of network-level Site 9 (I-70) showing cracked and patched surface of a bridge deck.



Fig. 2.17—Photograph of section of network-level Site 9 (I-70) showing patched pavement near bridge.



Fig. 2.18—Photograph of section of network-level Site 9 (I-70) showing transition from PCC to bituminous mix.



Fig. 2.19—Photograph section of network-level Site 9 (I-70) showing cracks and patches on bridge deck.



Fig. 2.20—Photograph of section of network-level Site 9 (I-70) showing pavement that was recently treated.

2.3.2.2 Network-Level Site 10 (MO 465)

Site 10 is paved with full-depth BM (AC; asphaltic concrete). Recorded video indicated that the pavement is in good condition as shown in Fig. 2.21. In places, minor surface defects were observed, such as minor longitudinal cracks and rutting (Fig. 2.23). Fig. 2.22 and Fig. 2.24 show sections of the network-level 10 Site that were recently treated. In general, by visual assessment, the network-level site 10 pavement surface was considered to be in good condition.



Fig. 2.21—MO 465 (network-level Site 10) pavement in good condition.



Fig. 2.22—Photograph of segment of network-level Site 10 (MO 465) bridge with recently applied treatment.



Fig. 2.23— Section of network-level Site 10 (MO 465) pavement with evidence of cracks and rutting.



Fig. 2.24—Recently treated segment of MO 465 (network-level Site 10).

2.4 Project- and Network-Level Roadways: Core Assessments

Cores and auger samples were acquired at each site investigated in this project to serve as ground truth for the various non-destructive test methods. Sections 2.4.1 and 2.4.2 summarize the core results for each project-level and network-level pavement site, respectively. Complete documentation of the core and auger sample information is provided in [Appendix B](#), including an assessment of bond between different pavement layers; degree of stripping in BM layers; granular base gradation and Atterberg limits; subgrade gradation and Atterberg limits, unified soil classification, and moisture content; depth of borings; and blow counts.

2.4.1 Project-Level Sites

Eight to ten cores and auger samples were extracted from each project-level site. Where possible, locations of cores were selected based on visual inspection and field GPR data and/or USW data. Cores were extracted from areas both where the pavement appeared to be in good condition and from areas where the pavement appeared to be deteriorated. Cores were 4 in. diameter and were drilled to the base of pavement where possible. Then, auger samples were collected from the same locations. After the core locations were marked by the research team, all cores and auger samples were extracted by MoDOT personnel. The cores holes were investigated after the cores were removed, and then the cores and auger samples were individually labeled, bagged, and transported to Missouri S&T for further testing and documentation and testing.

2.4.1.1 Project-Level Site 1 (US 63)

Eight cores/auger samples were extracted from project-level Site 1. Fig. 2.25 shows photographs of the cores. Fig. 2.26 shows photographs of the BM layers that were split to evaluate the degree of stripping. Table 2.6 summarizes the core length, surface material, number of pieces, bond conditions between layers, and stripping of BM layers.



Fig. 2.25—Photographs of cores extracted at US 63 (project-level Site 1).

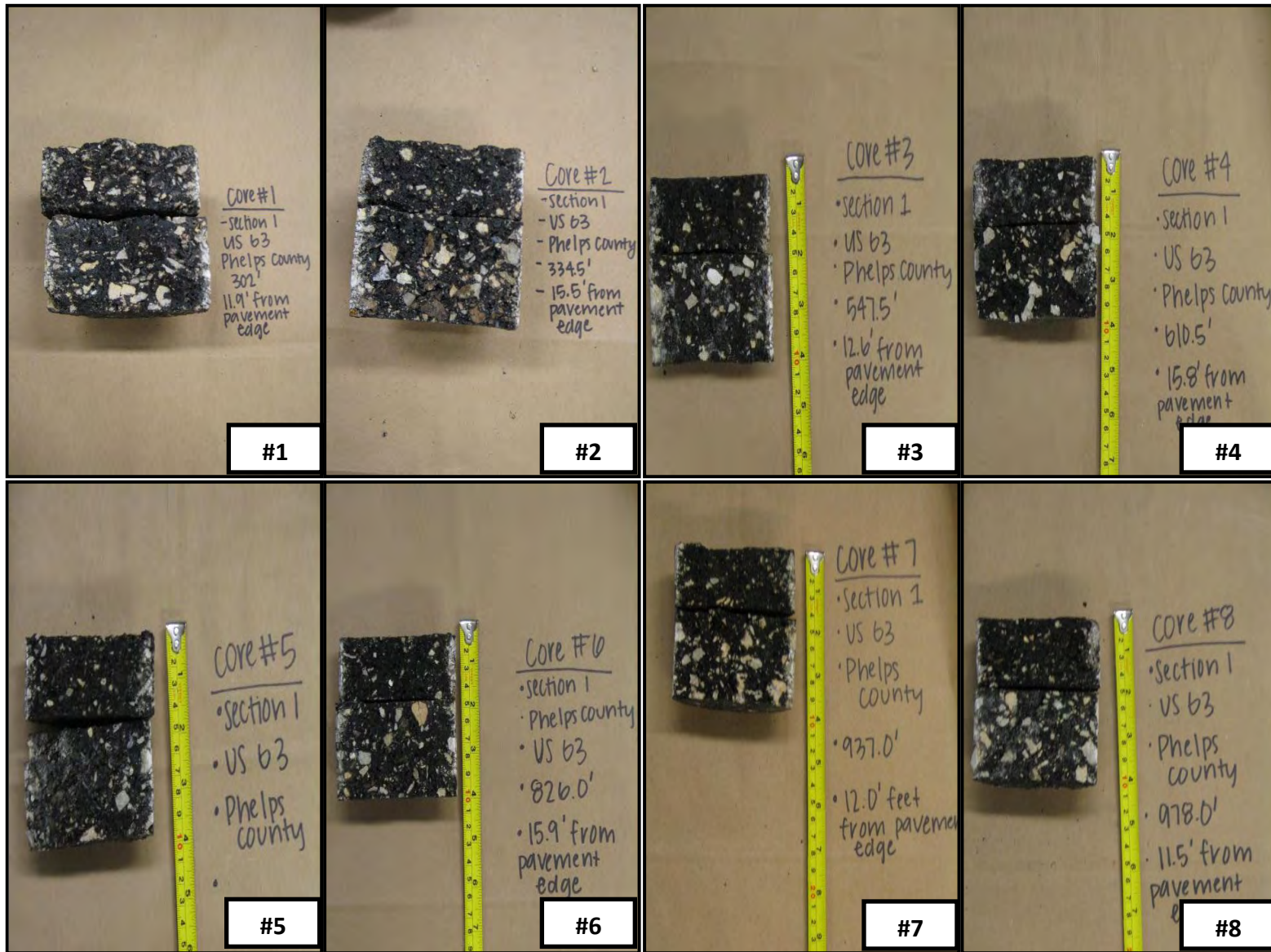


Fig. 2.26—Photographs of US 63 (project-level Site 1) cores split to evaluate degree of stripping.

Table 2.6–US 63 (project-level Site 1) core summary

Core	1	2	3	4	5	6	7	8
Total Length (nearest 0.25 in.)	11.25	11.75	11.5	12.375	11.25	12.5	11.5	11.5
Surface (Asphalt: A, Concrete: C)	A	A	A	A	A	A	A	A
Number of Pieces	1	1	1	2	1	1	2	1
#1 Length (in.) and Failure Mode ¹	11.25 No failure	11.75 No failure	11.5 No failure	3.375 PRE	11.25 No failure	12.5 No failure	3.375 PRE	11.5 No failure
#2 Length (in.) and Failure Mode ¹	N/A	N/A	N/A	No failure	N/A	N/A	8.125 No failure	N/A
#3 Length (in.) and Failure mode ¹	N/A	N/A	N/A	N/A	N/A	N/A	N/A	N/A
Stripping (Low, Moderate, High)	None	None	None	None	None	None	None	None
Other Comments	No missing material. Pieces fit together	No missing material. Pieces fit together	2 nd asphalt layer weakly bonded to concrete	2 nd asphalt layer separated from concrete	No missing material. Pieces fit together	No missing material. Pieces fit together	2 nd asphalt layer separated from concrete	No missing material. Pieces fit together

¹Preexisting Rupture (PRE)

2.4.1.2 Project-Level Site 2 (US 54)

Ten cores were extracted from project-level Site 2. Fig. 2.27 shows photographs of the cores. Fig. 2.28 shows photographs of the asphalt layers that were split to evaluate the degree of stripping. Table 2.7 summarizes the core length, surface material, number of pieces, bond conditions between layers, and stripping of BM layers.



Fig. 2.27—Photographs of cores extracted at US 54 (project-level Site 2).

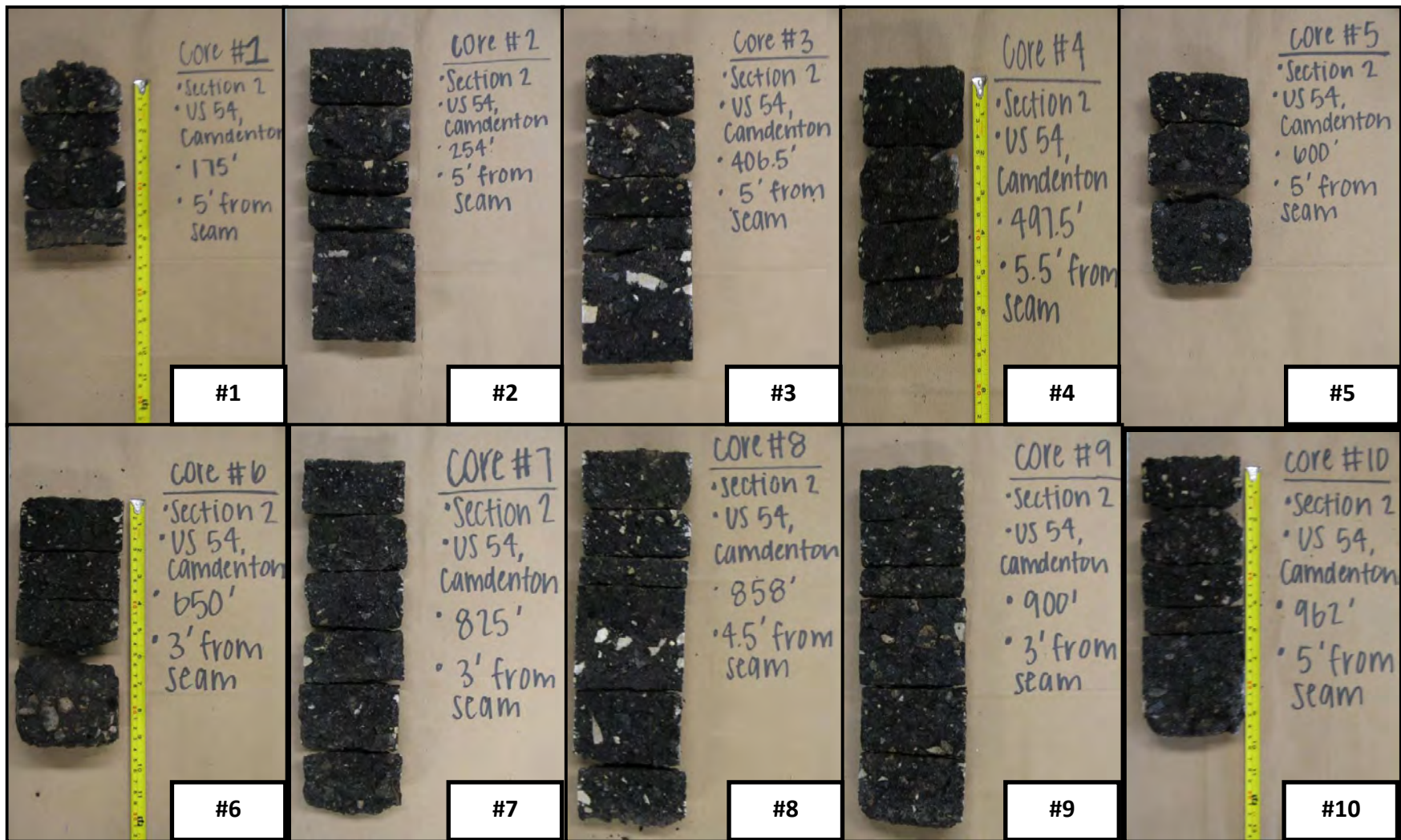


Fig. 2.28—Photographs of US 54 (project-level Site 2) cores split to evaluate degree of stripping.

Table 2.7–US 54 (project-level Site 2) core summary

Core	1	2	3	4	5	6	7	8	9	10
Total Length (nearest 0.25 in.)	8.5	10.5	11	11.25	9.5	4.75	11.25	11	11.5	8.25
Surface (Asphalt: A, Concrete: C)	A	A	A	A	A	A	A	A	A	A
Number of Pieces	4	3	3	3	3	2	2	2	3	3
#1 Length (in.) and Failure Mode ¹	1 PRE	2 PRE	1.75 PRE	1.75 PRE	1.75 PRE	1.75 PRE	9.25 IDC	1.5 PRE	1.75 PRE	1.5 PRE
#2 Length (in.) and Failure Mode ¹	1 PRE	1.5 PRE	2 PRE	1.25 PRE	2 PRE	3	N/A	9.5	5.5 PRE	1.25 PRE
#3 Length (in.) and Failure mode ¹	1.25 PRE	7	7.25	8.25	5.75	N/A	N/A	N/A	2.25	5.5
#4 Length (in.) and Failure Mode ¹	5.25	N/A	N/A	N/A	N/A	3 PRE	9.25	11	7.5	8.625
Stripping (Low, Moderate, High)	Low to moderate	Low to moderate	Low to moderate	Low	Low	Low	Low	Low	Low	Low
Other Comments	All asphalt layers are separated	Asphalt layers 1 and 2 are separated	Asphalt layer 2 is separated	Asphalt layers 1 and 2 are separated	Asphalt layers 1 and 2 are separated	Asphalt layer 1 is separated	Asphalt layer 1 is separated	Asphalt layer 1 is separated	Asphalt layers 1 and 4 are separated	Asphalt layers 1 and 2 are separated

¹Preexisting Rupture (PRE)

2.4.1.3 Project-Level Site 3 (MO 179)

Ten cores were extracted from project-level Site 3. Fig. 2.29 shows photographs of the cores. Fig. 2.30 shows photographs of the asphalt layers that were split to evaluate the degree of stripping. Table 2.8 summarizes the core length, surface material, number of pieces, bond conditions between layers, and stripping of BM layers.



Fig. 2.29—Photographs of cores extracted at MO 179 (project-level Site 3).

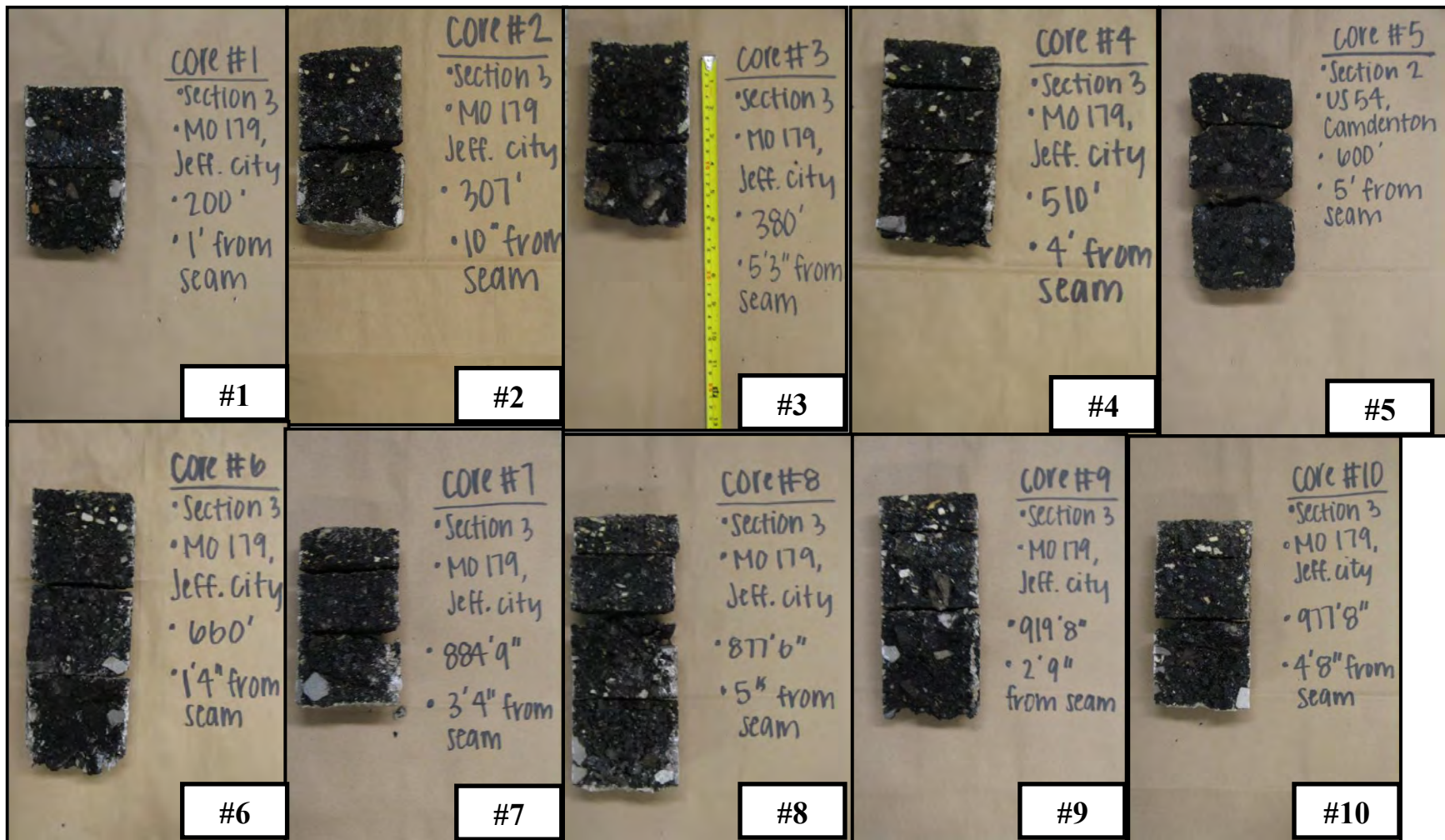


Fig. 2.30—Photographs of MO 179 (project-level Site 3) cores split to evaluate degree of stripping.

Table 2.8–MO 179 (project-level Site 3) core summary

Core	1	2	3	4	5	6	7	8	9	10
Total Length (nearest 0.25 in.)	11.25	11.5	11.5	12.25	12.25	12.25	12.5	12.25	12	11.875
Surface (Asphalt: A, Concrete: C)	A	A	A	A	A	A	A	A	A	A
Number of Pieces	1	1	1	1	2	3	2	2	2	2
#1 Length (in.) and Failure Mode ¹	11.25 No failure	11.5 No failure	11.5 No failure	12.25 No failure	6 PRE	3.25 PRE	3.25 PRE	1.25 PRE	6.25	3.25 PRE
#2 Length (in.) and Failure Mode ¹	N/A	N/A	N/A	N/A	6.25	3 PRE	9.25	11	5.75	8.625
#3 Length (in.) and Failure mode ¹	N/A	N/A	N/A	N/A	N/A	6 IDC	N/A	N/A	N/A	N/A
Stripping (Low, Moderate, High)	Low, High	Low, High	Low, Moderate	Low, High	Low, High	Low, High	Low, High	Low, High	Low, High	Low, High
Other Comments	No missing material. Pieces fit together	Asphalt layer 2 is separated	Asphalt layers 1 and 2 are separated	Asphalt layer 2 is separated	Asphalt layer 1 is separated	Asphalt layer 2 is separated	Asphalt layer 2 is separated			

¹Preexisting Rupture (PRE)

2.4.1.4 Project-Level Site 4 (HWY AT)

Nine cores were extracted from project-level Site 4. Fig. 2.31 shows photographs of the cores. Fig. 2.32 shows photographs of the asphalt layers that were split to evaluate the degree of stripping. Table 2.9 summarizes the core length, surface material, number of pieces, bond conditions between layers, and stripping of BM layers.



Fig. 2.31—Photographs of cores extracted at HWY AT (project-level Site 4).



Fig. 2.32—Photographs of HWY AT (project-level Site 4) cores split to evaluate degree of stripping.

Table 2.9–HWY AT (project-level Site 4) core summary

Core	1	2	3	4	5	6	7	8	9
Total Length (nearest 0.25 in.)	15.25	10.5	9.25	9.25	7	8.75	8.5	11	9
Surface (Asphalt: A, Concrete: C)	A	A	A	A	A	A	A	A	A
Number of Pieces	4	3	3	2	2	3	4	2	3
#1 Length (in.) and Failure Mode ¹	1.25 PRE	1.5 PRE	3 PRE	3.25 PRE	1 PRE	1.5 PRE	1.5 PRE	4 PRE	1.5 PRE
#2 Length (in.) and Failure Mode ¹	3.5 PRE	3 PRE	6.5	6	6	1.25 PRE	1PRE	7	1.5 PRE
#3 Length (in.) and Failure mode ¹	6 PRE	6	N/A	N/A	N/A	6	6	N/A	6
#4 Length (in.) and Failure mode ¹	4.5	N/A	N/A	N/A	N/A	N/A	N/A	N/A	N/A
Stripping (Low, Moderate, High)	Low, Moderate	Low	Low, Severe	Low, Severe	Severe	Low	Low, moderate, severe	Low	Low, Moderate
Other Comments	All asphalt layers are separated	All layers are separated	All layers are separated; asphalt layer 2 disintegrated	Top asphalt layer is separated from concrete	Top asphalt layer is separated from concrete	All layers are separated	All layers are separated	Asphalt layer 1 is weak bonded. Asphalt layer 2 is separated	All layers are separated

¹Preexisting Rupture (PRE)

2.4.1.5 Project-Level Site 5 (I-55 Pemiscot County)

Eight cores were extracted from project-level Site 5. Fig. 2.33 shows photographs of the cores. Fig. 2.26 shows photographs of the asphalt layers that were split to evaluate the degree of stripping. Table 2.10 summarizes the core length, surface material, number of pieces, bond conditions between layers, and stripping of BM layers.

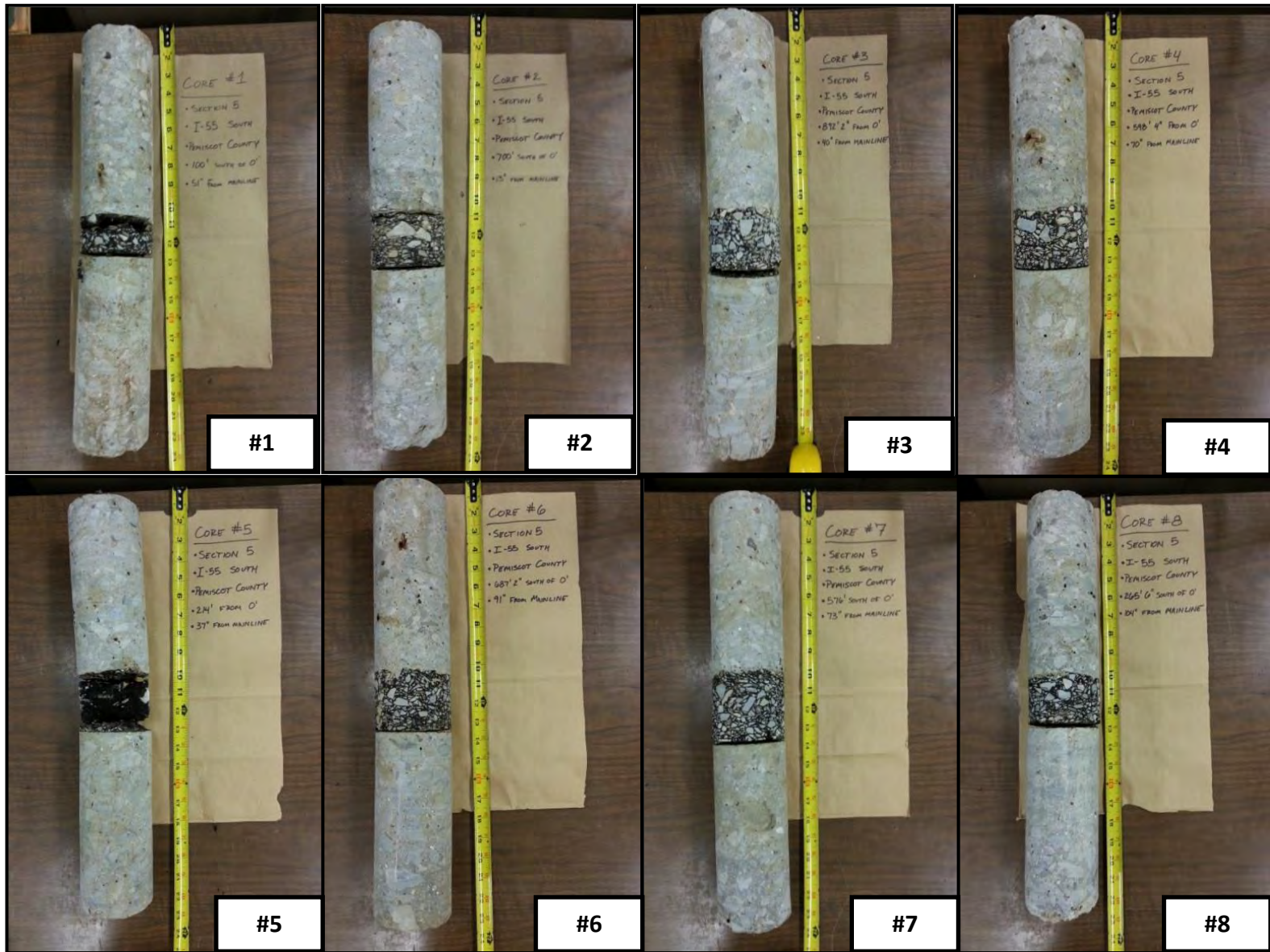


Fig. 2.33—Photographs of cores extracted at I-55 Pemiscot County (project-level Site 5).

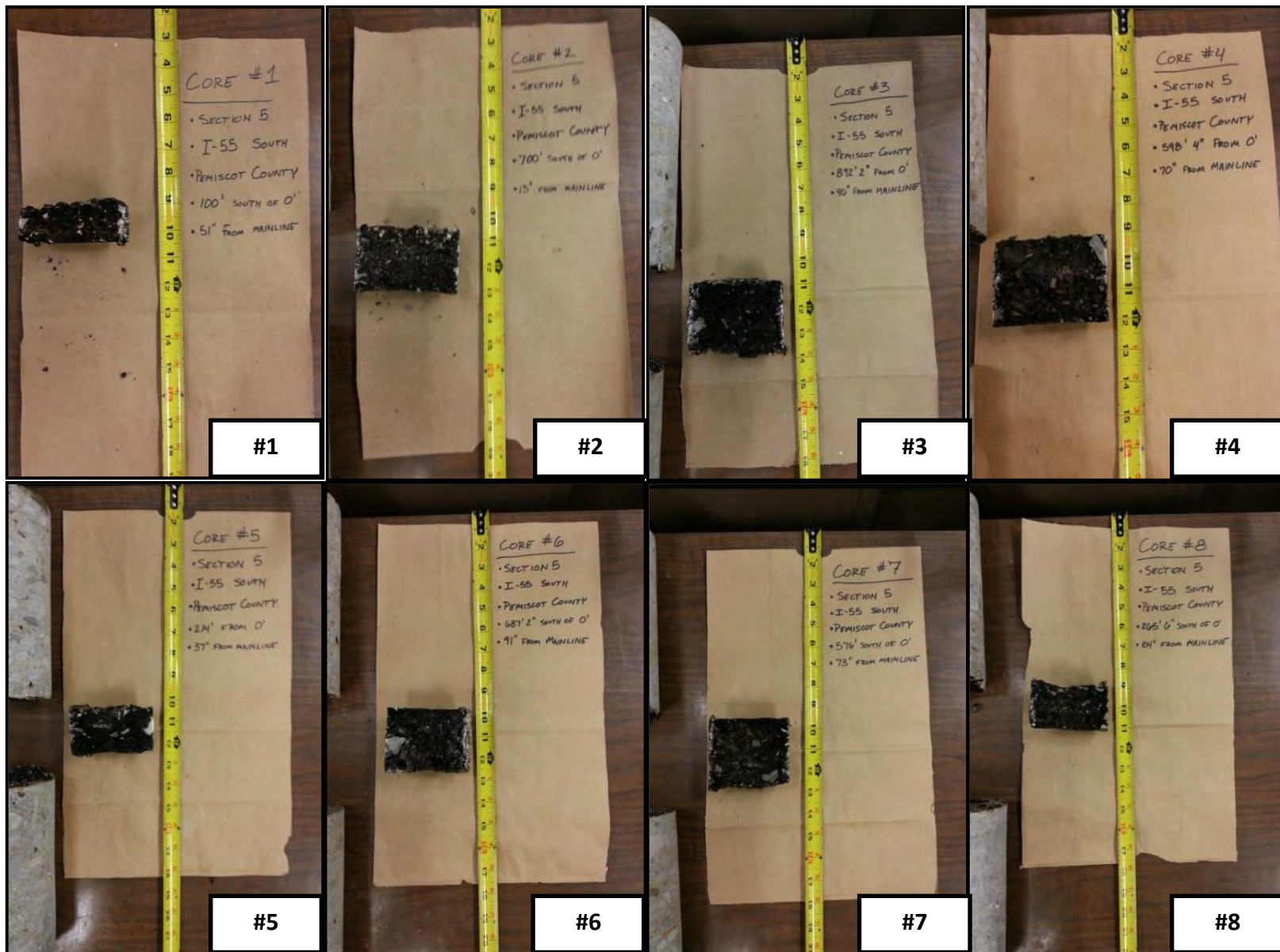


Fig. 2.34—Photographs of I-55 Pemiscot County (project-level Site 5) cores split to evaluate degree of stripping.

Table 2.10–I-55 Pemiscot County (project-level Site 5) core summary

Core	1	2	3	4	5	6	7	8
Total Length (nearest 0.25 in.)	19	20.50	21	20	18.5	20	20.5	20
Surface (Asphalt: A, Concrete: C)	C	C	C	C	C	C	C	C
Number of Pieces	3	3	2	2	2	2	2	2
#1 Length (in.) and Failure Mode ¹	9 PRE	9 PRE	12 PRE	11 PRE	10 PRE	11.5 PRE	11.5 PRE	11 PRE
#2 Length (in.) and Failure Mode ¹	1 PRE	2.5PRE	9	9	8.5	8.5	9	9
#3 Length (in.) and Failure mode ¹	9	9	N/A	N/A	N/A	N/A	N/A	N/A
Stripping (Low, Moderate, High)	Moderate	Low	Low	Low	Low	Low	Low	Low
Other Comments	All layers are separated	All layers are separated	Layer 2 is separated	Layer 1 is weak bonded. Layer 2 is separated	Layer 2 is separated	Layer 2 is separated	Layer 2 is separated	Layer 2 is separated

¹Preexisting Rupture (PRE)

2.4.1.6 Project-Level Site 6 (I-55 Perry County)

Nine cores were extracted from project-level Site 6. Fig. 2.31 shows photographs of the cores. Table 2.11 summarizes the core length, surface material, and number of pieces.

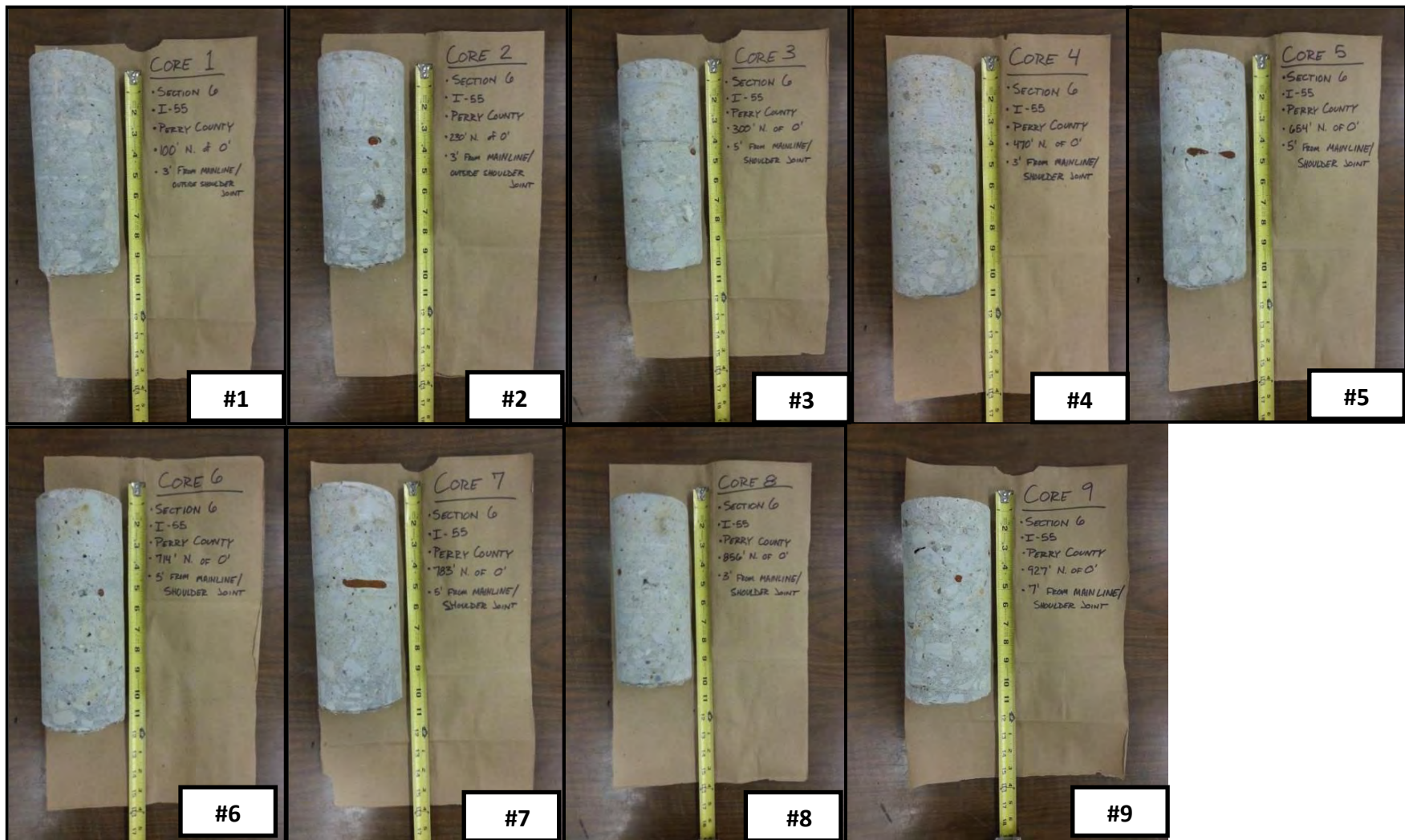


Fig. 2.35—Photographs of cores extracted at I-55 Perry County (project-level Site 6).

Table 2.11–I-55 Perry County (project-level Site 6) core summary

Core	1	2	3	4	5	6	7	8	9
Total Length (nearest 0.25 in.)	9	8	8.5	9	9	9	8.5	8	8.75
Surface (Asphalt: A, Concrete: C)	C	C	C	C	C	C	C	C	C
Number of Pieces	1	1	1	1	1	1	1	1	1
#1 Length (in.) and Failure Mode	9 No failure	8 No failure	8.5 No failure	9 No failure	9 No failure	9 No failure	8.5 No failure	8 No failure	8.75 No failure
Other Comments	One whole piece; no failure								

2.4.1.7 Project-Level Site 7 (HWY U)

Eight cores were extracted from project-level Site 7. Fig. 2.36 shows photographs of the cores. The core samples at this location were too small to evaluate the degree of stripping. Table 2.12 summarizes the core length, surface material, number of pieces, bond conditions between layers, and stripping of BM layers.

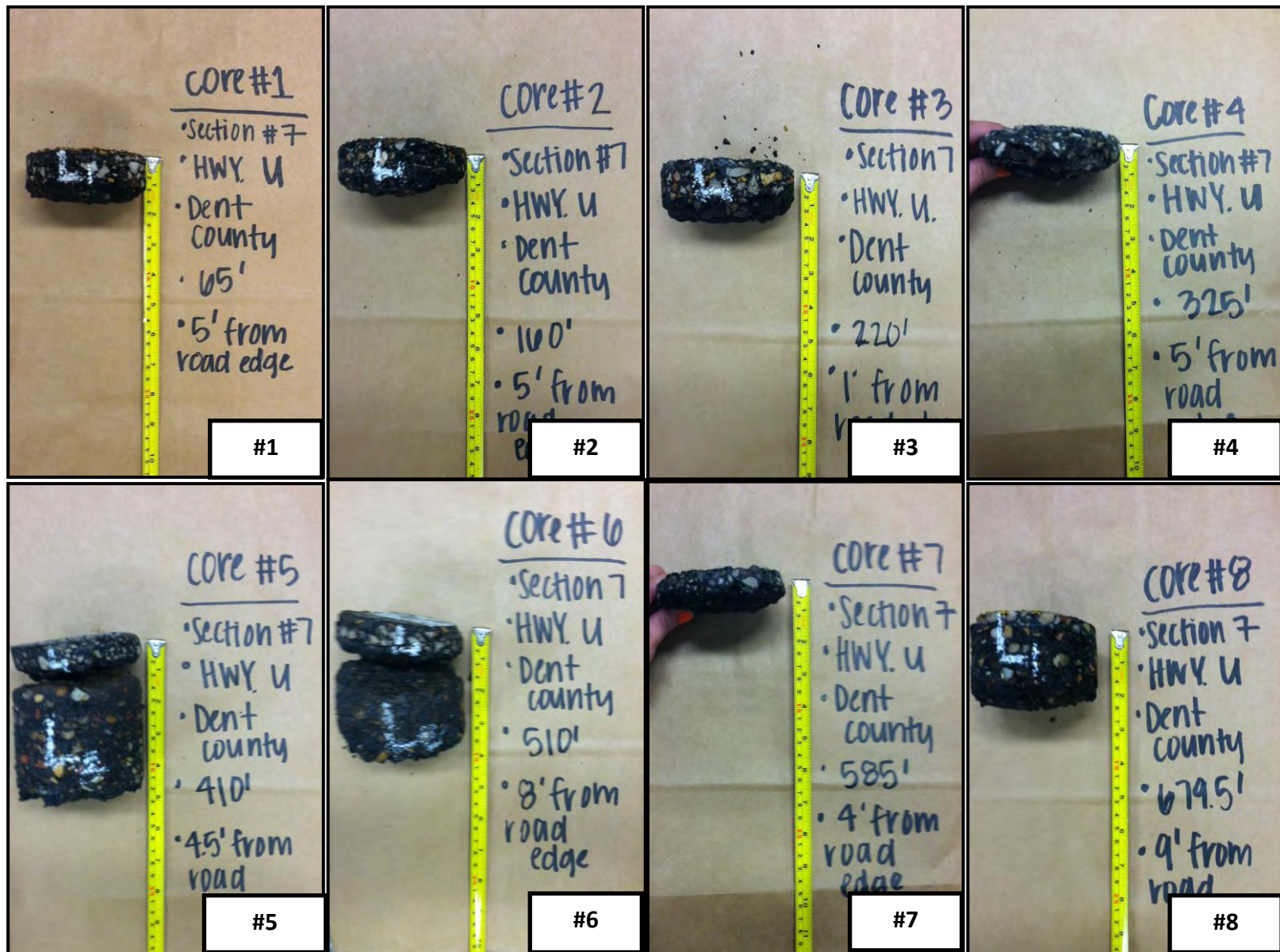


Fig. 2.36—Photographs of cores extracted at HWY U (project-level Site 7).

Table 2.12–HWY U (project-level Site 7) core summary

Core	1	2	3	4	5	6	7	8
Total Length (nearest 0.25 in.)	1	1	1	0.25	4	2.5	0.25	2
Surface (Asphalt: A, Concrete: C)	A	A	A	A	A	A	A	A
Number of Pieces	1	1	1	1	2	2	1	1
#1 Length (in.) and Failure Mode ¹	1 No failure	1 No failure	1 No failure	0.25 No failure	1	0.75	.25 No failure	2 No failure
#2 Length (in.) and Failure Mode ¹	N/A	N/A	N/A	N/A	3	1.75	N/A	N/A
#3 Length (in.) and Failure mode ¹	N/A	N/A	N/A	N/A	N/A	N/A	N/A	N/A
Stripping (Low, Moderate, High)	(not tested ²)	(not tested ²)	(not tested ²)	(not tested ²)				
Other Comments	None	None	None	None	Asphalt layer 1 is separated	Asphalt layer 1 is separated	None	None

¹Preexisting Rupture (PRE)

²Not tested due to limited sample size

2.4.1.8 Project-Level Site 8 (I-35)

Eight cores were extracted from project-level Site 8. Fig. 2.37 shows photographs of the cores. Fig. 2.38 shows photographs of the asphalt layers that were split to evaluate the degree of stripping. Table 2.13 summarizes the core length, surface material, number of pieces, bond conditions between layers, and stripping of BM layers.

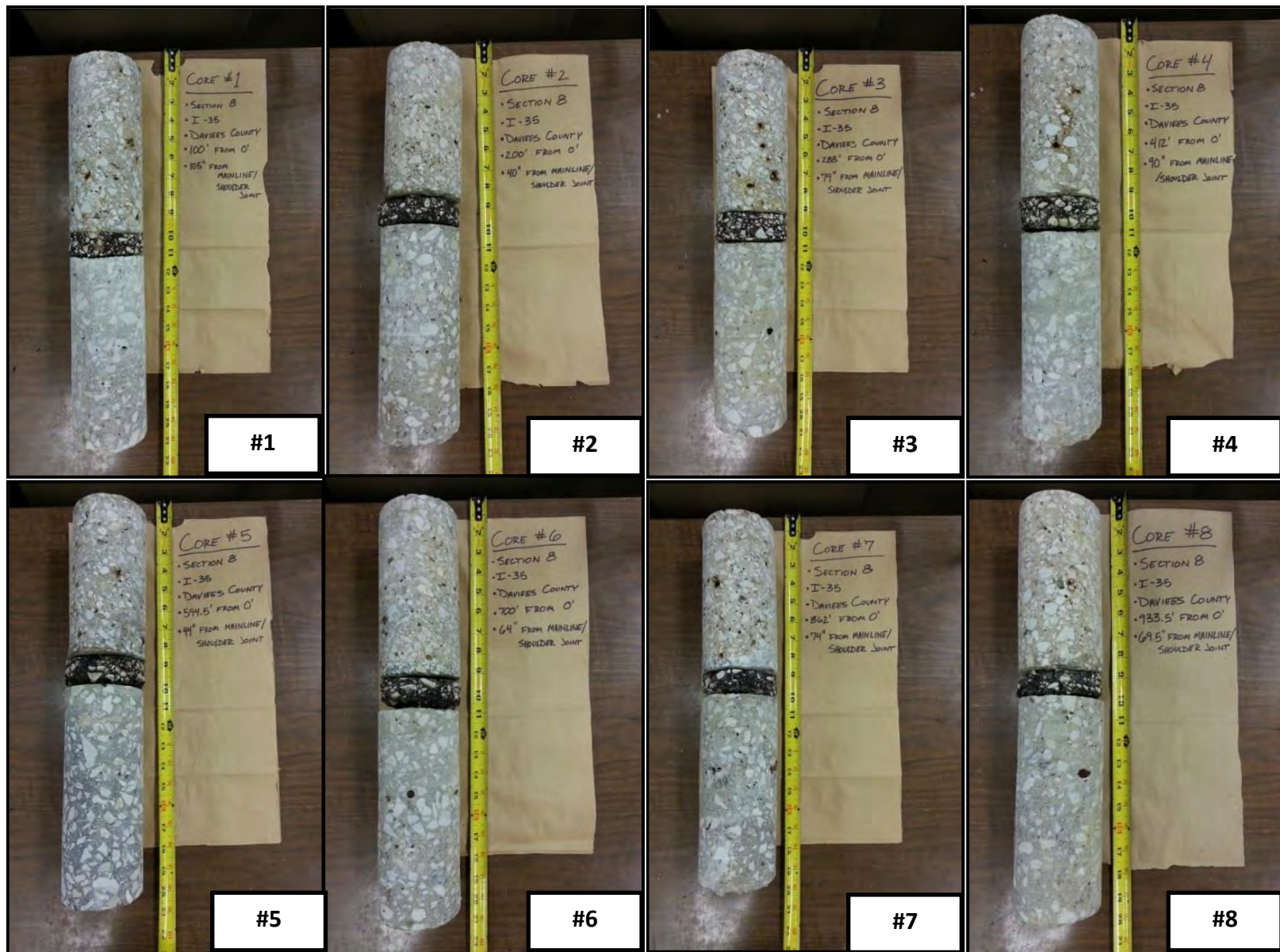


Fig. 2.37—Photographs of cores extracted at I-35 (project-level Site 8).

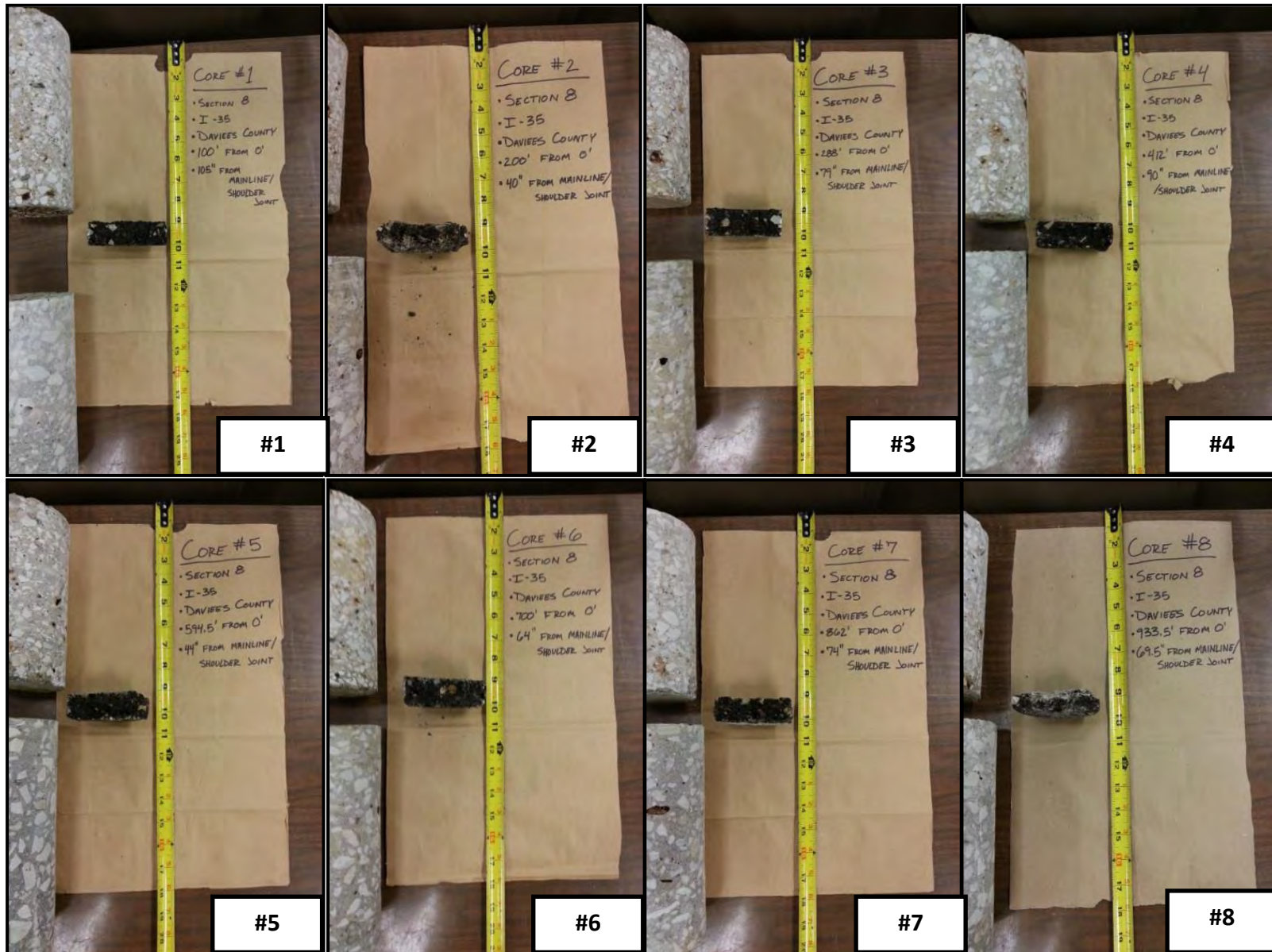


Fig. 2.38—Photographs of I-35 (project-level Site 8) cores split to evaluate degree of stripping.

Table 2.13–I-35 (project-level Site 8) core summary

Core	1	2	3	4	5	6	7	8
Total Length (nearest 0.25 in.)	17.5	17	17.5	17.75	17	17.75	17.25	16.75
Surface (Asphalt: A, Concrete: C)	C	C	C	C	C	C	C	C
Number of Pieces	2	3	3	3	3	3	3	3
#1 Length (in.) and Failure Mode ¹	9 PRE	7 PRE	7.5 PRE	7.5 PRE	7 PRE	7.5 PRE	7.25 PRE	7 PRE
#2 Length (in.) and Failure Mode ¹	8.5	1PRE	1PRE	1.25 PRE	1PRE	1.5 PRE	1PRE	1 PRE
#3 Length (in.) and Failure mode ¹	N/A	9	9	9	9	8.75	9	8.75
Stripping (Low, Moderate, High)	Low	Low	Low	Moderate	Low	Low	Low	Moderate
Other Comments	Layer 2 is separated	All layers are separated	All layers are separated	All layers are separated	All layers are separated	All layers are separated	All layers are separated	All layers are separated

¹Preexisting Rupture (PRE)

2.4.2 Network-Level Sites

Seven to nine cores and auger samples were extracted from each network-level site. Where possible, locations of cores were selected based on visual inspection and field GPR data. Cores were extracted from areas both where the pavement appeared to be in good condition and from areas where the pavement appeared to be deteriorated. Cores were 4 in. diameter and were drilled to the base of pavement where possible. Then, auger samples were collected from the same locations. After the core locations were marked by the research team, all cores and auger samples were extracted by MoDOT personnel. The cores holes were investigated after the cores were removed, and then the cores and auger samples were individually labeled, bagged, and transported to Missouri S&T for further testing and documentation and testing. Stripping of BM layers was not evaluated in network-level cores.

2.4.2.1 Network-Level Site 9 (I-70)

Nine cores were extracted from network-level Site 9. Fig. 2.39 shows photographs of the cores. Table 2.14 summarizes the core length, surface material, number of pieces, and bond conditions between layers.

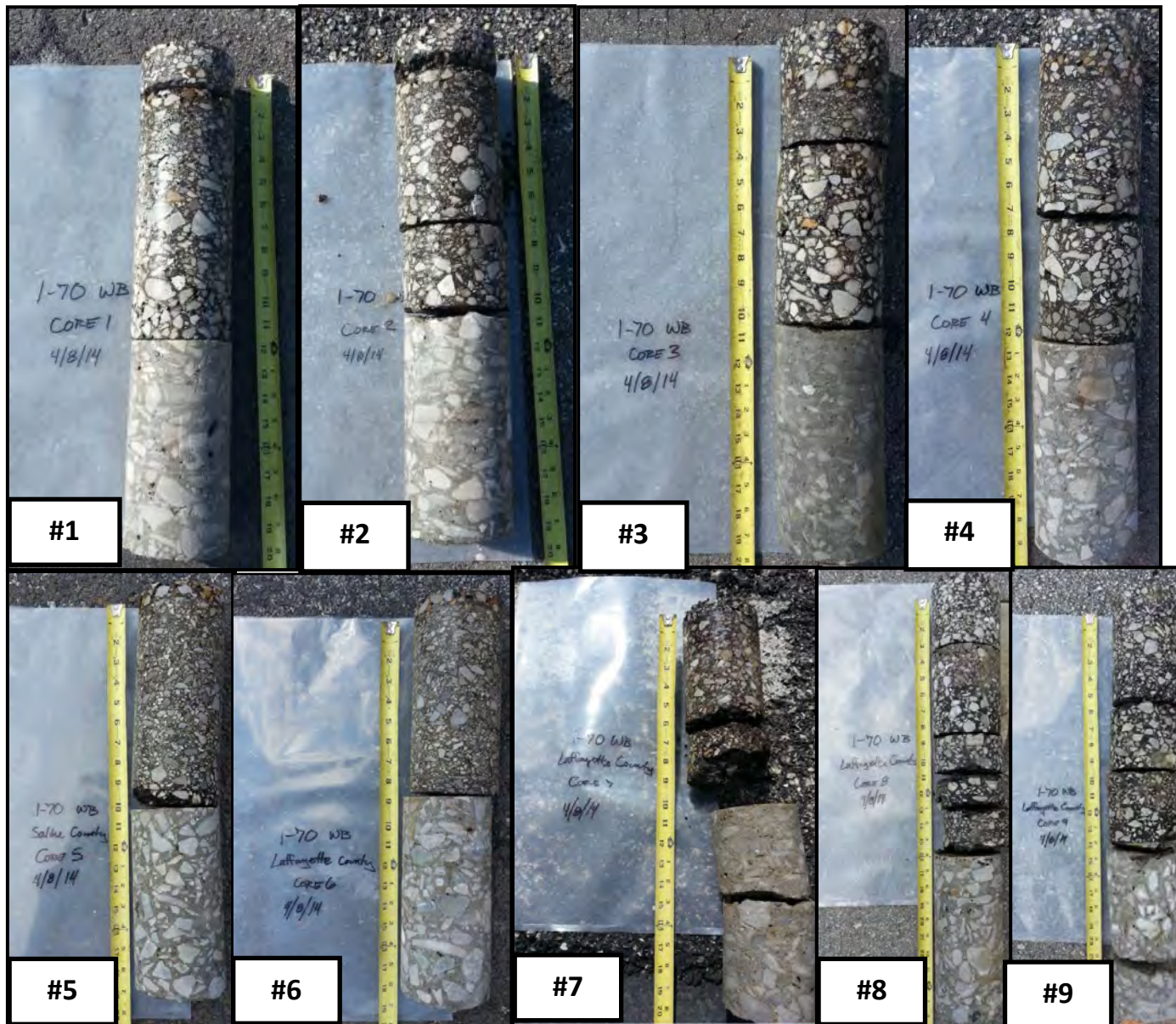


Fig. 2.39—Photographs of cores extracted at I-70 (network-level Site 9).

Table 2.14–I-70 (network-level Site 9) core summary

Core	1	2	3	4	5	6	7	8	9
Total Length (nearest 0.25 in.)	20	19	20	21	18.75	18	19.5	25.5	24
Surface (Asphalt: A, Concrete: C)	A	A	A	A	A	A	A	A	A
Number of Pieces	2	3	2	2	2	2	2	3	3
#1 Length (in.) and Failure Mode ¹	1.5 PRE	1 PRE	11 PRE	7 PRE	10 PRE	8.5 PRE	10 PRE	10.5 PRE	9.5 PRE
#2 Length (in.) and Failure Mode ¹	18.5	9.5 PRE	9	14	8.75	9.5	9.5	2 PRE	4.5 PRE
#3 Length (in.) and Failure Mode	N/A	8.5 IDC	N/A	N/A	N/A	N/A	N/A	13	10
Other Comments	Asphalt layer 1 is separated	Top and bottom layers are separated	Asphalt layer separated from concrete	Asphalt layer 1 is separated	Asphalt layer separated from concrete	Asphalt layer separated from concrete	Asphalt layer separated from concrete	Two asphalt layers are separated	Two asphalt layers are separated

¹Preexisting Rupture (PRE)

2.4.2.2 Network-Level Site 10 (MO 465)

Seven cores were extracted from network-level Site 10. Fig. 2.40 shows photographs of the cores. Table 2.15 summarizes the core length, surface material, number of pieces, and bond conditions between layers.

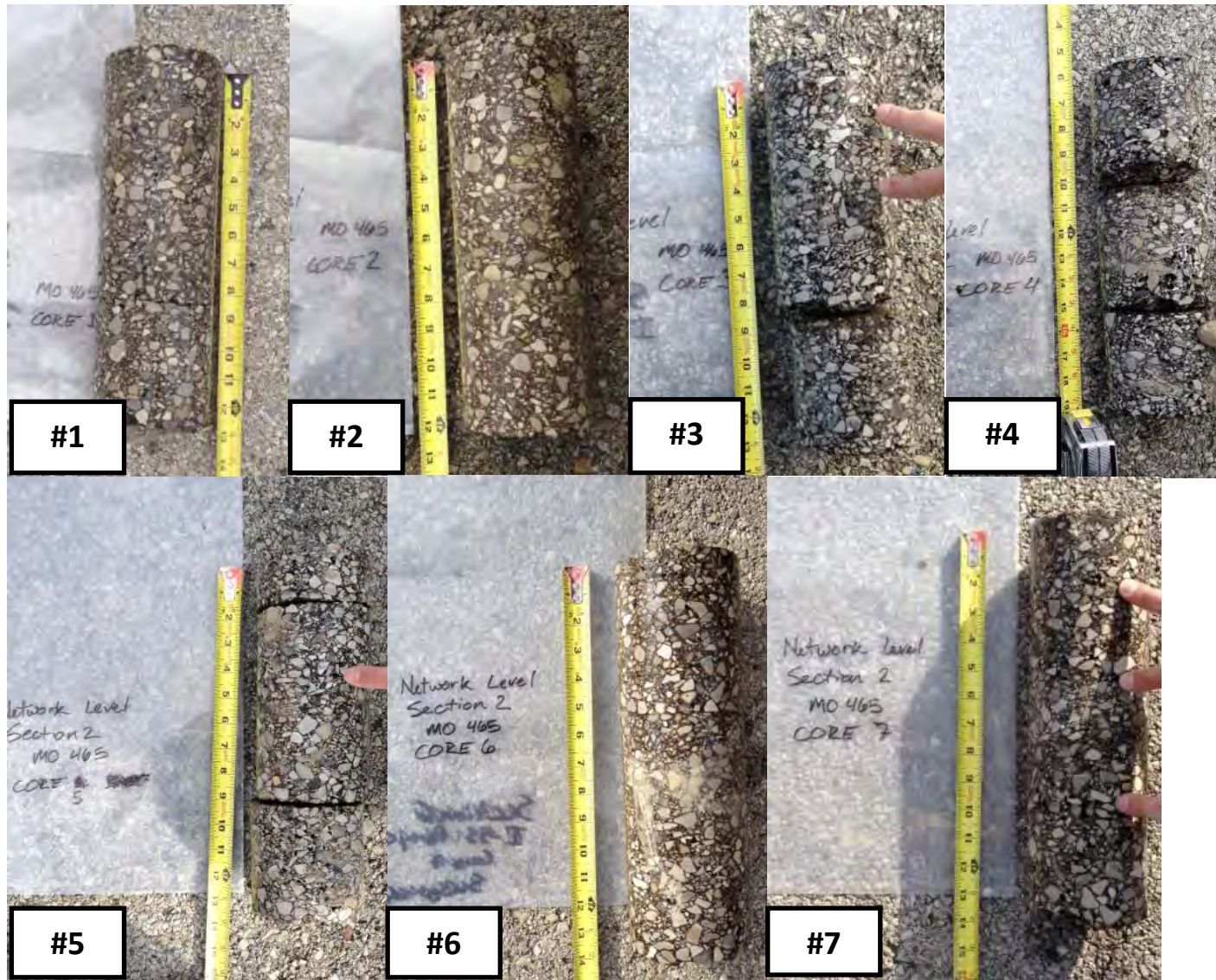


Fig. 2.40—Photographs of cores extracted at MO 465 (network-level Site 10).

Table 2.15—MO 465 (network-level Site 10) core summary

Core	1	2	3	4	5	6	7
Total Length (nearest 0.25 in.)	12.5	12.25	13	13	13	13.75	13.75
Surface (Asphalt: A, Concrete: C)	A	A	A	A	A	A	A
Number of Pieces	1	1	2	3	1	1	1
#1 Length (in.) and Failure Mode ¹	12.5 No failure	12.25	8.5 PRE	3 PRE	13 No failure	13.75 No failure	13.75 No failure
#2 Length (in.) and Failure Mode	N/A	N/A	13	5 PRE	N/A	N/A	N/A
#3 Length (in.) and Failure Mode	N/A	N/A	N/A	5	N/A	N/A	N/A
Other Comments	One whole piece; no failure	One whole piece; no failure	Asphalt layer 1 is separated	Asphalt layers 1,2,3 are separated	One whole piece; no failure	One whole piece; no failure	One whole piece; no failure

¹Preexisting Rupture (PRE)

3 PROJECT-LEVEL ULTRASONIC SURFACE WAVE AND IMPACT ECHO INVESTIGATIONS

3.1 Introduction

At each project-level site, ultrasonic surface wave and impact echo data were acquired using a portable seismic property analyzer (PSPA; Fig. 3.1) tool. The PSPA tool is an integrated ultrasonic seismic device designed to measure the elastic modulus and thickness of pavement and to locate flaws (Nazarian, 1997). The PSPA consists of a high-frequency impact source and two vertically-polarized receiver transducers (near and far) packaged into a portable system for performing and analyzing seismic tests in the field (Baker, 1995). The PSPA data acquisition box is connected to a laptop computer that controls the PSPA tool and automatically analyzes the acoustic signals recorded by each receiver transducer.

Each time the high-frequency acoustic source is discharged, ultrasonic surface waves (USW; more specifically, Rayleigh waves) and compressional waves are generated. The ultrasonic surface wave (USW) data are used to generate a 1-D plot of dynamic elastic modulus (Young's modulus) vs. depth for that test location. Reverberating compressional wave (impact echo; IE) data are used to identify flaws (e.g. debonding and delaminations) and/or to estimate the thickness of the pavement and/or pavement layers (Gucunski, 2008).

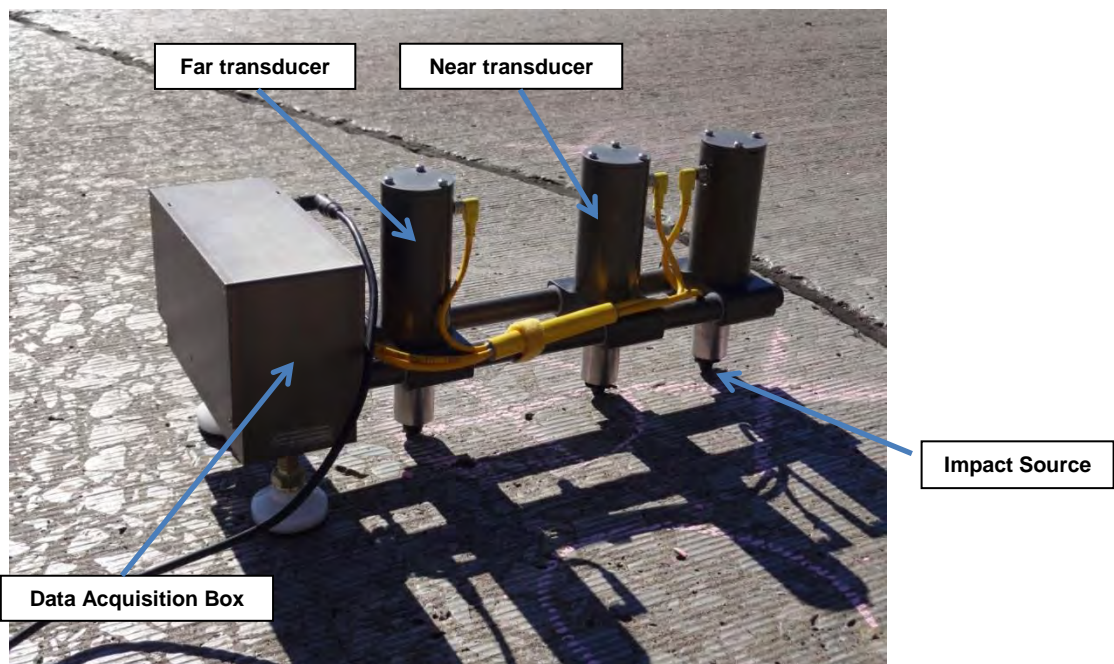


Fig. 3.1—Photograph of the portable seismic property analyzer (PSPA). The PSPA is a portable system consisting of a data acquisition box, a high-frequency acoustic impact source and two vertically-polarized receiver transducers. The PSPA is connected to a laptop computer that controls the PSPA and automatically stores, processes and interprets the acoustic signals (surface wave and compressional wave) recorded by the receiver transducers. A transducer spacing of either 4 in. or 6 in. is normally employed.

3.2 PSPA Data Acquisition, Processing and Interpretation

3.2.1 PSPA Data Acquisition

PSPA pavement data are normally acquired at discrete locations and on a pre-designed grid (Fig. 3.2; 2 ft x 100 ft grid spacing). It normally takes less than 30 seconds to acquire data at each test location. Denser location spacing provides for more control, but at an increased cost.

The operator inputs several parameters to aid in the automated analyses of the acquired PSPA acoustic data. More specifically, the operator can input:

- Type of material (one only)
 - Portland cement concrete (PCC): Density 150 pcf, Poisson's ratio: 0.18
 - Asphalt concrete (AC): Density 135 pcf, Poisson's ratio: 0.3
- Pavement condition (only for PCC: Fresh, Cured)
 - Density and Poisson's ratio values listed above will change slightly
- Pavement condition (Good, Fair, Poor)
 - Density and Poisson's ratio values listed above will change slightly
- Air temperature (only for AC: Hot, Mild, Cold)
 - Density and Poisson's ratio values listed above will change slightly
- Estimated pavement thickness

In Fig. 3.2, the test grid employed for each project-level pavement section is shown. As shown, five PSPA data sets were acquired every 100 ft. PSPA data were acquired along the GPR traverses and in one lane only. PSPA data were not acquired along the network-level roadways.

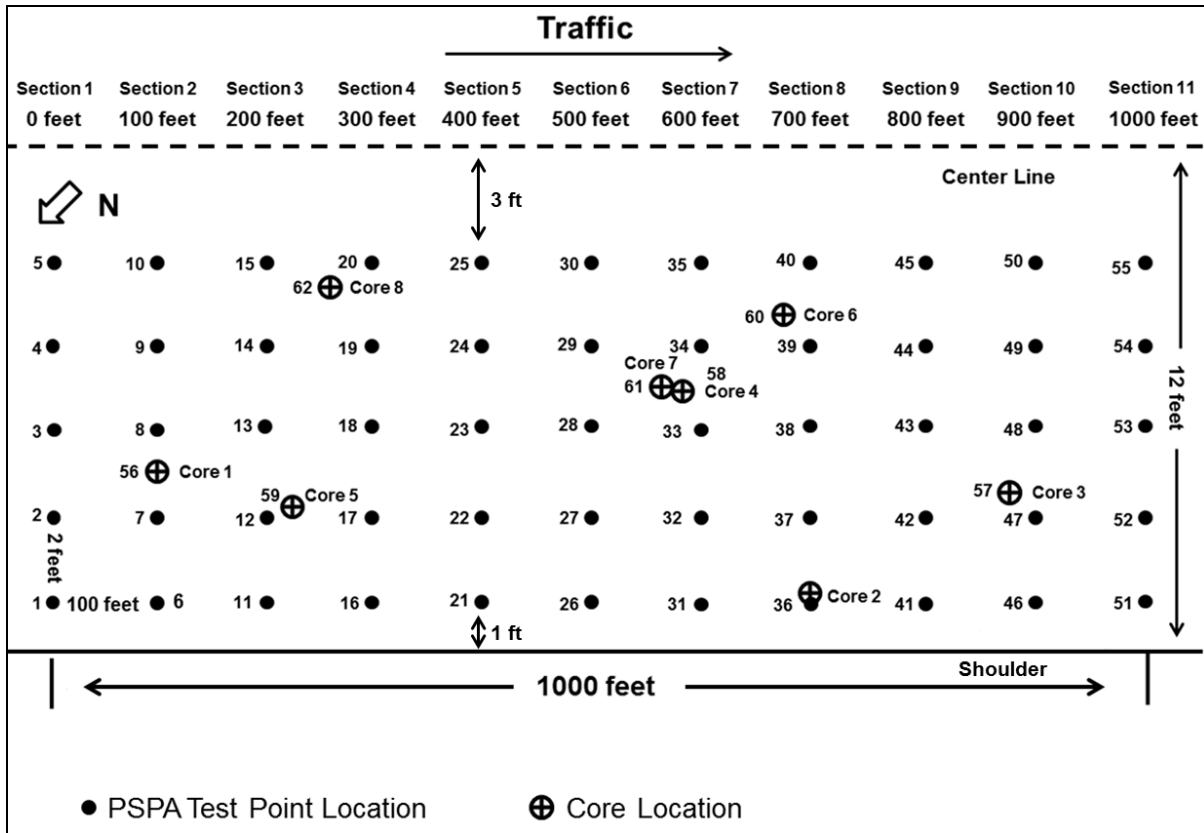


Fig. 3.2–Not-to-scale sketch showing PSPA test grid (2 ft x 100 ft) employed for each project-level Sites 1-6 and 8 (a 1.5 ft x 100 ft grid was employed at Site 7). As shown, five PSPA data sets (e.g. 1-5, 6-10, etc.) were acquired every 100 ft along each project-level pavement section. In total, 55 PSPA data sets were acquired for each project-level investigation except Sites 7 and 8 (where 66 PSPA data sets were acquired). All PSPA data sets were acquired along a GPR traverse (see Section 4 of this report). The spacing (1 ft in figure) between the outermost PSPA test locations and the edge of pavement varied from site to site. Core locations also varied from site to site.

3.2.2 PSPA Data Processing and Interpretation

3.2.2.1 Ultrasonic Surface Wave Data Analyses

Each recorded PSPA acoustic data set consists in part of superposed ultrasonic surface wave data (USW) and ultrasonic reverberating compressional wave data (Fig. 3.3). The USW wave (Rayleigh wave) data acquired at each PSPA test location were automatically transformed (using the PSPA manufacturer’s software) into a 1-D plot of dynamic elastic modulus (Young’s modulus) vs. depth (Fig. 3.4). The compressional wave data, as is discussed in Section 3.2.2.2 of this report, was used (ideally) to estimate thickness of pavement layers and/or to detect horizontal flaws (e.g. debonding and delaminations) within the pavement.

The acquisition of USW data is relatively straightforward. The PSPA instrument is placed (well-coupled) on the pavement surface, and the source is discharged (Fig. 3.1 and Fig. 3.3).

The PSPA manufacturer’s software automatically identifies, processes and interprets the surface wave (Rayleigh wave) energy recorded by both receiver transducers and calculates the phase velocities with which the different frequencies travel. The acquired USW surface wave data are automatically transformed into a 1-D plot of dynamic elastic modulus that extends from 2 in. to approximately 7 in. or from 3 in. to approximately 11 in. (thickness direction), depending on whether a 4 in. or 6 in. receiver transducer spacing is utilized (Fig. 3.3).

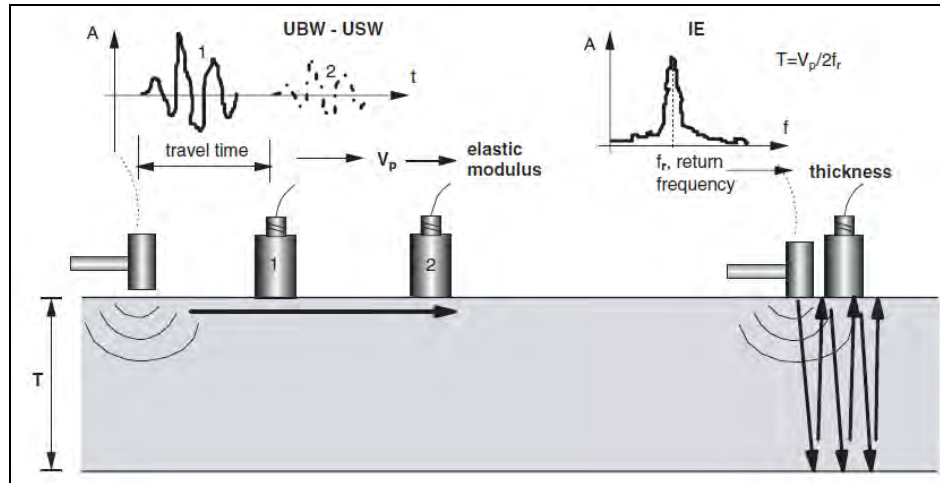


Fig. 3.3–The PSPA tool records both ultrasonic surface wave (UBW-USW caption) and reverberating compressional wave (IE caption) data. The ultrasonic surface wave (USW) data acquired at each test location were automatically transformed into a 1-D plot of elastic modulus. The reverberating compressional wave (IE; impact echo) data were used to estimate pavement layer thicknesses and/or to detect horizontal flaws (Gucunski et al., 2008). Receiver transducer spacing can be set at either 4 in. or 6 in.

The automated transformation of the acquired USW phase velocity data into a 1-D plot of elastic modulus vs. depth (Fig. 3.3) is relatively straightforward, but is based on several assumptions. The PSPA USW tool also suffers from some limitations. More specifically:

1. The automatic PSPA USW software assumes a constant and standard value of Poisson’s ratio depending on the operator-input pavement type, pavement condition and air temperature (AC only). This assumption (constant value of Poisson’s ratio) allows the measured “average” surface wave velocity (over depth range tested) to be transformed into a corresponding average compressional-wave velocity using Eq. 3.1 (Baker, 1995):

$$V_p = (1.13 - 0.16\nu) V_R \sqrt{\frac{1 - \nu}{0.5 - \nu}} \quad \text{Eq. 3.1}$$

where:

V_p = Average compressional wave (P-wave) velocity over depth range tested

V_R = Average surface wave (Rayleigh wave) velocity over depth range tested

ν = PSPA standard Poisson’s ratio for pavement type

This limitation is probably most significant when a pavement, over the tested depth range, is comprised of different materials (AC over PCC, for example). In this case, the operator-input pavement type is normally that of the uppermost layer (AC in this case). The average surface wave velocity over the depth range tested will therefore not represent that of either the AC or the PCC. The assigned average compressional wave (P-wave) velocity will therefore also be inaccurate.

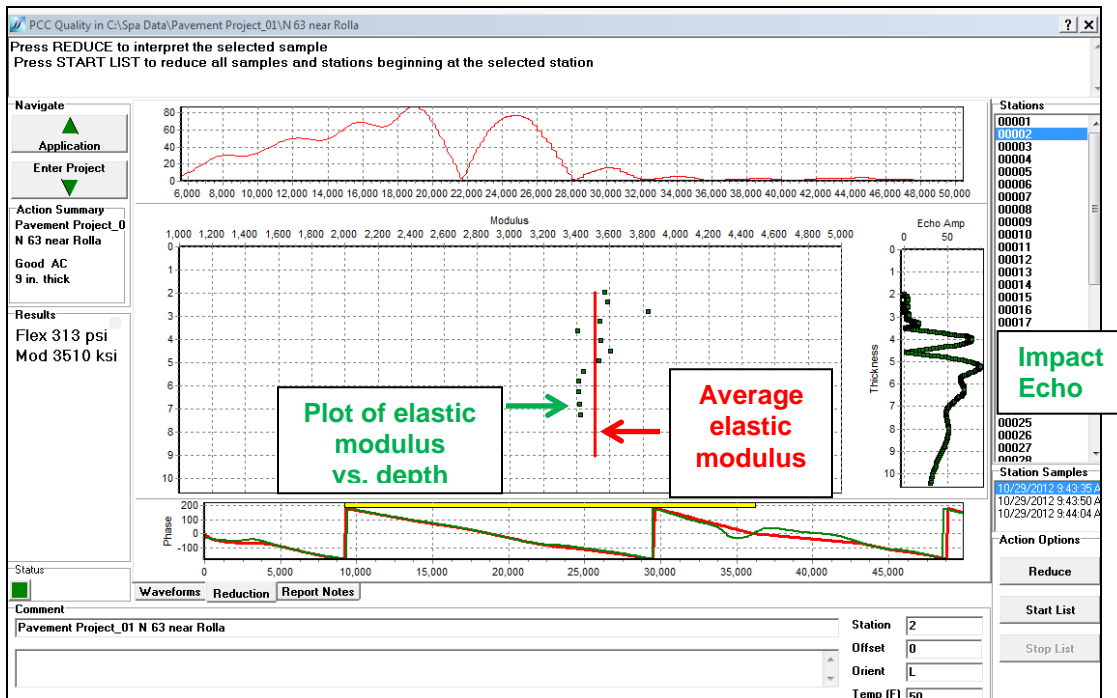


Fig. 3.4—Example automated output for a single example PSPA test location. Calculated elastic moduli (ksi) are plotted over the depth range tested (2 in. - approx. 7 in.); the average elastic modulus over this depth range is also plotted. The plotted elastic moduli range from 3405 ksi to 3825 ksi; the average elastic modulus is 3510 ksi. The reflector depths (4.0 in. and 5.3 in.) corresponding to the peaks on the “Echo Amp” plot ideally represent either pavement layer thicknesses or the depth to flaws (debonding or delaminations) within the pavement. In this case, 4.0 in. depth corresponds to the thickness of the overlying asphalt concrete. The 5.3 in. depth does not correspond to either a pavement layer or a known defect. Rather, it is thought to be caused by the flexural wave propagating within the upper asphalt concrete layer.

2. The automatic PSPA USW software assumes a constant and standard value of density depending on the operator-input pavement type (AC or PCC), pavement condition and air temperature (AC only). This assumption (constant density) allows the surface wave phase velocity data to be transformed into a 1-D layered elastic modulus vs. depth model. Equation 3.2 can be used to calculate the elastic modulus (E; Young’s modulus) of uniform pavement [Baker, 1995]:

$$E = 2\rho[(1.13 - 0.16\nu)V_R]^2(1 + \nu) \quad \text{Eq. 3.2}$$

where:

V_R = surface wave (Rayleigh wave) velocity

ρ = PSPA standard density for operator-input of pavement type

ν = PSPA standard Poisson's ratio for pavement type

In this case, the operator-input pavement type is normally that of the uppermost layer; the output elastic modulus values for the lower layer are therefor referred to as "apparent" elastic modulus. This limitation is probably most significant when a pavement, over the tested depth range, is comprised of different materials (AC over PCC for example). In this case, the assigned elastic modulus values will only be reliable for the AC section of the pavement. The modulus values assigned to the underlying concrete are referred to as "apparent" modulus values.

3. The output plot of elastic modulus vs. depth (Fig. 3.3) extends from either approximately 2 in. to 7 in. or from approximately 3 in. to 11 in. depending upon the operator-set separation between the two receiver transducers (either 4 in. or 6 in.; Fig. 3.1). Modulus values cannot be obtained for depths shallower than 2 in. or for depths greater than approximately 11 in.
4. The output average elastic modulus assigned to each test location is based on the average elastic modulus over the depth range tested (either approx. 2-7 in. or approx. 3-11 in.; Fig. 3.4). This assigned value of average elastic modulus will not be accurate (in an absolute sense) if the depth range tested extends across different materials (AC over PCC for example).

3.2.2.2 Impact Echo Data Analyses

Each recorded PSPA acoustic data set consists of superposed ultrasonic surface wave data and ultrasonic reverberating compressional wave data (Impact Echo; IE). The IE data acquired at each PSPA test location were automatically transformed (using the PSPA manufacturer's software) into estimated reflector depths (Figs. 3.3, 3.4 and 3.5).

The acquisition of PSPA IE data is relatively straightforward. The PSPA instrument is placed (well-coupled) on the pavement surface, and the source is discharged (Fig. 3.1 and Fig. 3.3). The PSPA manufacturer's software automatically identifies, processes and interprets the frequencies of reverberating compressional wave energy recorded by the near receiver transducer (Fig. 3.1 and Fig. 3.3) and calculates the depths to the corresponding reflectors. Ideally, reflectors correspond to pavement layers (including base pavement) and/or to near-horizontal flaws within the pavement.

If the pavement is uniform and devoid of flaws, the primary reflector should be the base of the pavement. Because of a significant contrast between the rigidity of pavement and rigidity of the underlying granular base or subgrade material, much of the down-going compressional wave is reflected from the bottom of intact pavement (rather than transmitted into the

base/subgrade; Fig. 3.3 and Fig. 3.5). Similarly, most of the up-going reflected compressional wave is reflected from the pavement/air interface. As a consequence, essentially entrapped reflected compressional wave energy reverberates between the top and base of intact pavement.

If the pavement is layered and comprised of different materials with contrasting rigidities (AC over PCC for example) compressional wave energy can reverberate within the top layer (AC in this case). If a horizontal flaw (e.g delamination) is present, acoustic energy can also reverberate between the pavement surface and the flaw (Fig. 3.3).

The automated transformation of the acquired IE data into reflector depths (Fig. 3.4) is based on several assumptions. The PSPA IE tool suffers from some limitations. More specifically:

1. Ideally, the frequency of the reverberating reflection from the base of pavement, called the return frequency (f), can be identified in the response spectrum of the recorded signal (Fig. 3.3; Baker, 1995). Ideally, the depth of the reflector, in this case the thickness of the pavement (T), can be calculated using the following expression (where V_p is the average compressional-wave velocity as determined for that specific PSPA test location during USW data analyses).

$$T = V_p/2f \quad \text{Eq. 3.3}$$

Note that the calculated pavement thickness (T) will be inaccurate if the average compressional wave velocity (calculated during analyses of USW data) is inaccurate.

2. If the pavement is delaminated or debonded, down-going compressional wave energy will be partially reflected from the horizontal flaw (Fig. 3.5). Ideally, if a flaw is present in the pavement, the amplitude spectrum will be characterized by a second peak frequency (f_d). Ideally, the depth of the reflector, in this case the depth to the flaw (T_f), can be obtained using the following expression.

$$T_f = V_p/2f_d \quad \text{Eq. 3.4}$$

Note that the second peak frequency can also be generated by a second interface within layered pavement. Again, depth estimates will only be as reliable as the average compressional wave velocity (from the USW data analysis) for that PSPA test location.

3. For impact-echo data analysis, the PSPA instrument cannot obtain usable data if the pavement thickness or the depth to the flaw (internal reflector) is less than half the spacing between the two transducers (Fig. 3.1; Baker, 1995). Furthermore, the PSPA instrument needs to be properly coupled in the pavement in order to obtain high quality test results.

4. There are three major vibration modes present in the impact-echo (IE) data recorded using the PSPA instrument: the IE resonance mode, the USW mode and the flexural vibration resonance mode. In the case of debonded or layered pavement, the PSPA manufacturer's software can incorrectly identify flexural vibration resonance modes as the dominant peak frequency and use this frequency to estimate the pavement thickness (Sansalone and Streett, 1997).
5. When impact-echo data are acquired on layered and/or debonded pavement, the flexural mode (pavement layer and/or debonded layer) can dominate the transient response and obscure the IE resonance mode. In this case, the depth to the layer/defect cannot be accurately estimated based on the software identified dominant peak frequency.

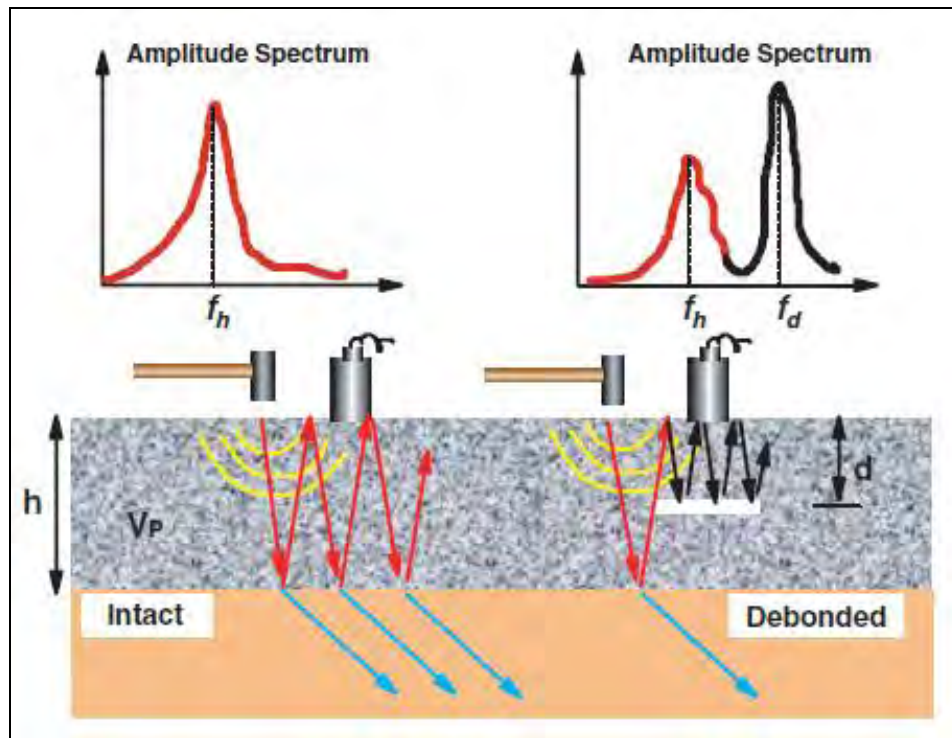


Fig. 3.5—The “ideal” amplitude spectrum for intact and layered/debonded concrete pavement (Source: 2007, Celaya et al). “ f_h ” is the resonance frequency of the reverberating compressional wave energy reflected from the base of pavement; “ f_d ” is the resonance frequency of the reverberating compressional wave energy reflected from the flaw within the pavement.

3.2.3 Typical Elastic Modulus of Asphalt Concrete (AC; Bituminous Mix (BM)) and Portland Cement Concrete (PCC))

Typical values of elastic modulus (Young's modulus) for PCC are listed in Table 3.1. The modulus of good quality PCC is 5000 ksi or above, the modulus of fair quality PCC is between 4000 to 5000 ksi, the modulus of poor quality PCC is between 3000 to 4000 ksi and the modulus of severely deteriorated quality concrete is less than 3000 ksi. Typical elastic modulus for asphalt

concrete (bituminous mix; BM) is listed in Table 3.2. The elastic modulus of AC decreases as temperature increases.

Table 3.1–Typical elastic modulus of 28 day PCC (Source: 2011, Russel W. Lenz, Pavement Design Guide; Typical Values of Young’s Elastic Modulus and Poisson’s Ratio for Pavement Materials, Cornell Local Roads Program).

Concrete Quality	Good	Fair	Poor	Severely Deteriorated
28-day Concrete Elastic Modulus (ksi)	≥ 5000	4000-5000	3000-4000	≤ 3000

Table 3.2–Typical elastic modulus of asphalt concrete (AC; bituminous mix (BM)) (Source: 2012, Gudmarsson, Laboratory Seismic Testing of Asphalt Concrete; Typical Values of Young’s Elastic Modulus and Poisson’s Ratio for Pavement Materials, Cornell Local Roads Program).

Asphalt Concrete Quality	Good	Fair	Poor	Severely Deteriorated
Elastic Modulus (ksi), 32 °F	≥ 4000	3000-4000	2000-3000	≤ 2000
Elastic Modulus (ksi), 50 °F	≥ 3000	2000-3000	1000-2000	≤ 1000
Elastic Modulus (ksi), 70 °F	≥ 2000	1000-2000	500-1000	≤ 500
Elastic Modulus (ksi), 77 °F	≥ 1000	500-1000	300-500	≤ 300

3.3 Project-Level PSPA Data: USW and IE

3.3.1 Project-Level Site 1 (US 63)

Project-level Site 1 is located along the north-bound lane of highway US 63 near Rolla, MO (Fig. 3.6). The pavement consists of approximately 3.5 in. of bituminous mix (BM) overlay over an existing 8 in. PCC layer. The surface of the BM displayed no visible evidence of surface cracks. The average air temperature during field data acquisition at the test site was 38 °F.

Fifty-five (55) PSPA data sets and eight (8) cores were acquired at test Site 1 (Fig. 3.2 and Fig. 3.7). The PSPA data were acquired using a 4 in. transducer spacing. Hence, the USW modulus plot extends from a depth of 2 in. to a depth of approximately 7 in. (Fig. 3.8). PSPA data were not acquired in immediate proximity to all core locations.

3.3.1.1 Ultrasonic Surface Wave Data

In this report, the project-level pavement Site 1 USW elastic modulus data are presented in 1-D plot format and in 2-D plot format.

PSPA USW data acquired in proximity to core locations 01, 04 and 07 (Fig. 3.7) are presented in 1-D plot format to illustrate the utility and limitations of the PSPA tool. Core 01 and the corresponding PSPA elastic modulus plot are shown in Fig. 3.8. Core 01 consisted of 3 layers (two overlying BM layers and underlying PCC). There was no evidence of debonding or stripping in core 01, nor was there any evidence of chemical or physical degradation of the PCC.

The elastic modulus plot of Fig. 3.8 can be divided into two layers based on the type of pavement: overlying bituminous mix (BM) and underlying PCC (Fig. 3.8). The average elastic modulus of the two overlying BM layers is 3520 ksi indicating the asphalt concrete is fair quality (Table 3.2). It should be remembered that the temperature at the time of testing was relatively low (38 °F), hence resulting in relatively high moduli.

The “apparent” average modulus of underlying PCC layer in Core 01 is 3250 ksi. The plotted elastic modulus values for the PCC are referred to as “apparent” as these elastic modulus values were calculated using the PSPA standard values of density and Poisson’s ratio for BM. The average “apparent” elastic modulus for entire 5 in. tested section of pavement is 3358 ksi (Fig. 3.8). The “apparent” average elastic moduli for the PCC layer and for entire tested section of pavement are not accurate in an absolute sense, but can be used to assess PCC and “overall” pavement quality, respectively, in a relative sense.



Fig. 3.6—Photograph of PSPA tool placed on pavement at project-level Site 1 (US 63 N). Core 04 and the corresponding PSPA elastic modulus plot are shown in Fig. 3.9. The BM/PCC interface was debonded. However, there was no evidence of physical or chemical degradation of the underlying PCC.

The average elastic modulus of the BM in core 04 is 3195 ksi indicating the BM is fair quality (Table 3.2). However, the elastic modulus of the BM is slightly less than 3100 ksi near the debonded BM/PCC interface. The apparent average modulus of underlying concrete layer is 3386 ksi. The average modulus of entire 5 in. tested section of BM and PCC is 3313 ksi.

Core 07 and the corresponding PSPA elastic modulus plot are shown in Fig. 3.10. The BM/PCC interface was debonded. Additionally, the PCC exhibited staining from causes that were undetermined. The average elastic modulus of the BM in core 07 is 3200 ksi indicating the BM is fair quality (Table 3.2). However, the elastic modulus of the asphalt concrete is slightly less than 3100 ksi near the debonded BM/PCC interface. The apparent average modulus of PCC layer in Core 07 is 2654 ksi. This average apparent modulus is much lower than the corresponding values for cores 01 and 04. The average modulus of entire 5 in. tested section of asphalt concrete and concrete pavement is 2864 ksi. This value is also anomalously low compared to cores 01 and 04.

Analyses of cores 01, 04 and 07 and the corresponding elastic modulus plots indicates that the elastic modulus of the BM immediately above the BM/PCC contact is slightly lower where the BM and PCC are debonded. These results suggest the PSPA USW tool may be useful for detecting debonded PCC under BM overlay. The acoustic interface between the BM and PCC cannot be confidently identified on the modulus plots, presumably because there is not a uniformly statistically significant difference between the modulus of the BM and the apparent modulus of the underlying PCC.

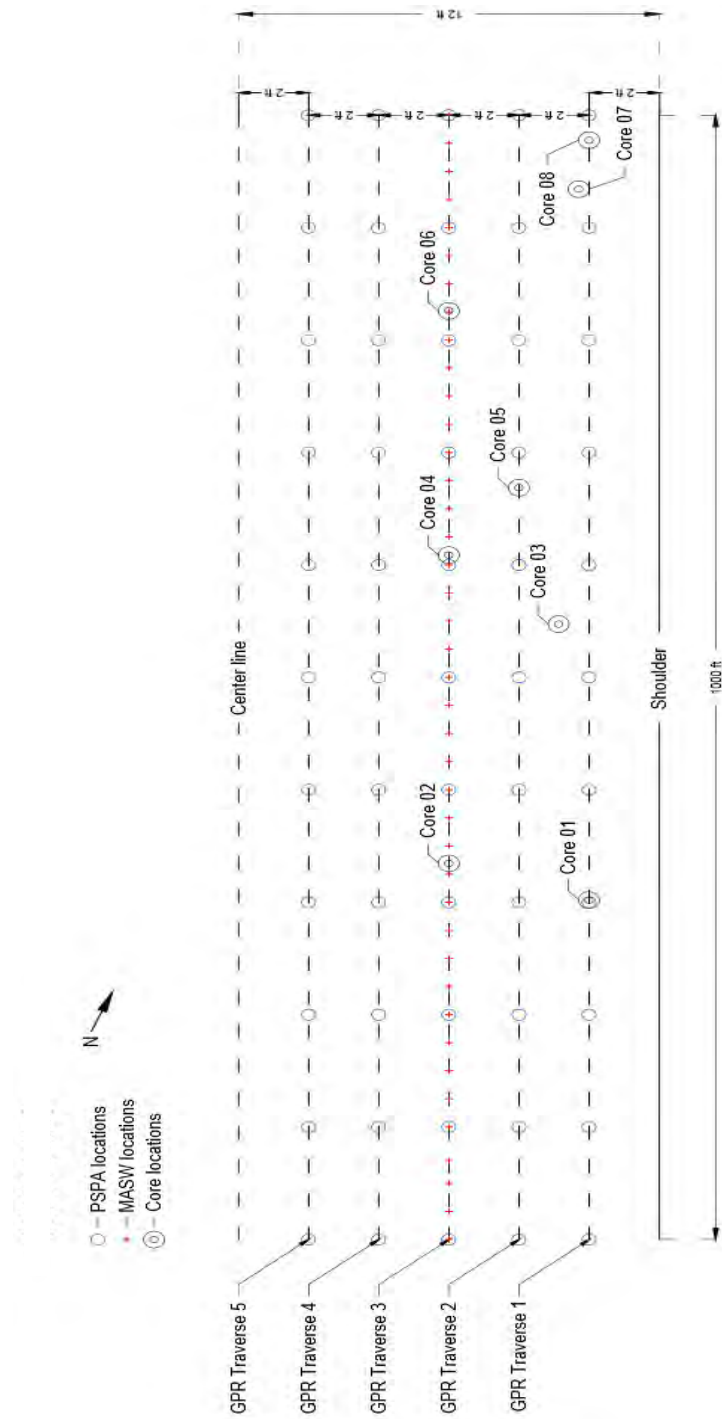


Fig. 3.7–Base map for project-level Site 1 showing PSPA test locations and core locations. PSPA data were acquired at 100 ft intervals along each GPR traverse. GPR traverse 1 was located 2 ft from the outer edge of the driving lane (shoulder). Only cores 1 and 4 were located within 10 ft of a PSPA location.

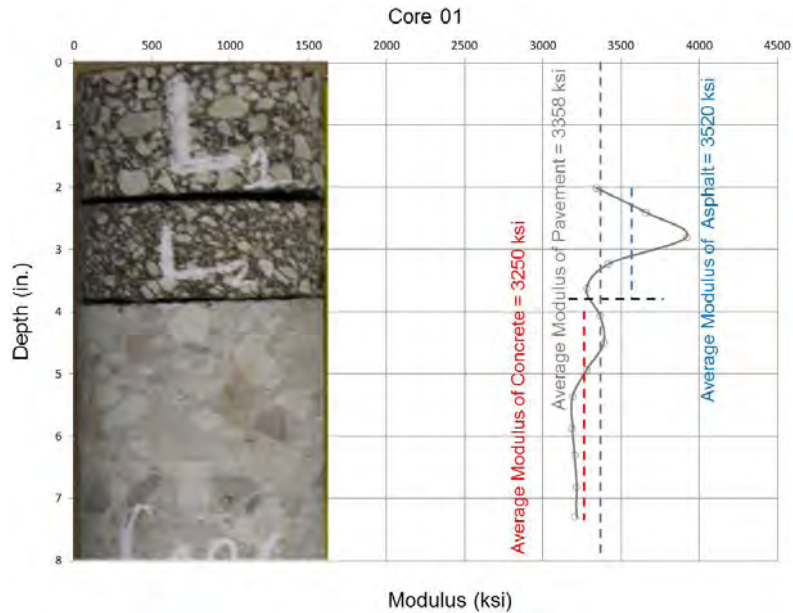


Fig. 3.8—Elastic modulus plot generated from PSPA USW data acquired in immediate proximity to core 01 (Fig. 3.7). The pavement consists of two BM layers over an existing PCC layer. No visible evidence of debonding or stripping was observed in core 01. The elastic modulus of the BM is consistently greater than 3200 ksi, even in proximity to the BM/PCC interface. The acoustic interface between the BM and PCC cannot be confidently identified. The apparent average elastic modulus of the PCC is 3250 ksi.

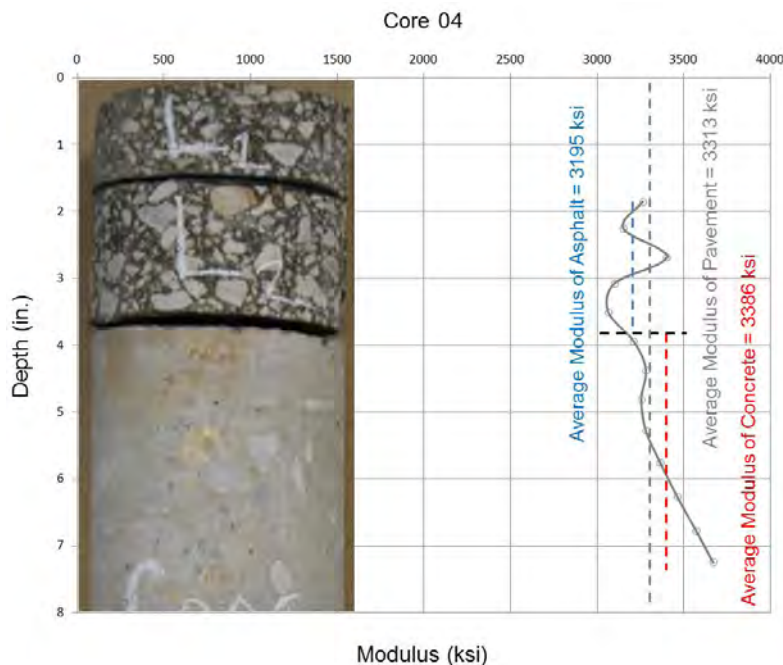


Fig. 3.9—Elastic modulus plot generated from PSPA USW data acquired in immediate proximity to core 04 (Fig. 3.7). The BM/PCC contact was debonded, however there was no evidence of chemical or physical degradation of the PCC. The elastic modulus of the BM is slightly less than 3100 ksi near the BM/PCC interface. The acoustic interface between the BM and PCC cannot be confidently identified. The apparent average elastic modulus of the PCC is 3386 ksi.

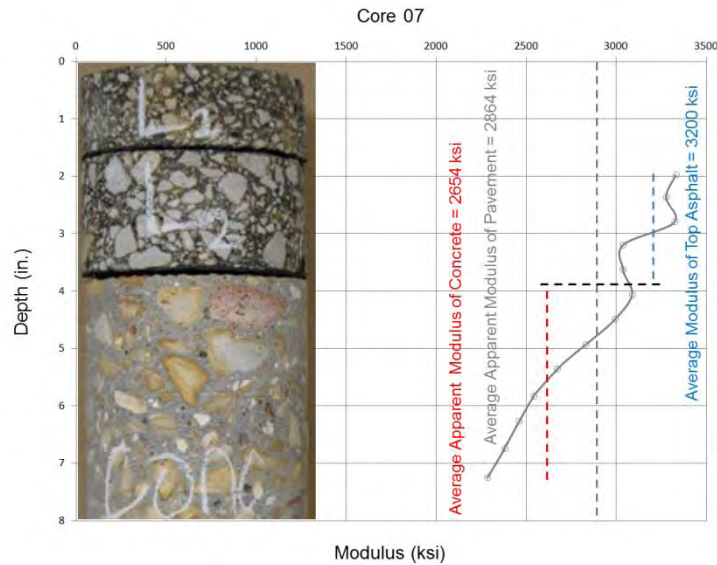


Fig. 3.10—Elastic modulus plot generated from PSPA USW data acquired about 30 ft from core 07 (Fig. 3.7). The pavement consists of two BM layers over an existing PCC layer. The interface between the second layer of BM and PCC was debonded. The elastic modulus of the BM is slightly less than 3100 ksi near the BM/PCC interface. The acoustic interface between the BM and PCC cannot be confidently identified. The apparent average elastic modulus of the PCC is 2654. This value is anomalously low compared to the PSPA data acquired at core locations 01 and 04. The core 07 PCC appears to be physically and chemically degraded.

PSPA USW data are presented in 2-D cross-sectional format to provide information about lateral and vertical variations in pavement quality. The elastic modulus data acquired at Site 1 are displayed in cross-section format in Fig. 3.11 to 3.15. Each cross-section is presented in two sections (upper and lower) based on the material difference: overlying BM and underlying PCC. The cross-sections depicting the elastic modulus for BM (depths of 2 in. to 3.7 in.) are shown as Fig. 3.11 and Fig. 3.12. The cross-sections depicting the “apparent” elastic modulus for concrete (depths of 4 to 7.2 in.) are shown as Figs. 3.13 - 3.15.

The location of core 01 is shown in Fig. 3.11. This core was not debonded or stripped, and the elastic modulus of the BM concrete at this location is consistently greater than 3200 ksi. The apparent modulus of the concrete is also consistently greater than 3200 ksi (Fig. 3.13).

The location of core 04 is shown in Fig. 3.12. This core was debonded, and the elastic modulus of the BM at this location is slightly less than 3100 ksi near the base of the asphalt. The apparent modulus of the concrete is consistently greater than 3200 ksi.

The elastic modulus of the BM is consistently below the 3100 ksi near the BM/PCC interface of the cross-sections acquired at stations 600, 700, 800 and 900 ft (Fig. 3.7 and Fig. 3.12). The elastic modulus of the BM is consistently below the 3100 ksi level at almost all depths on the cross-section acquired at station 1000.

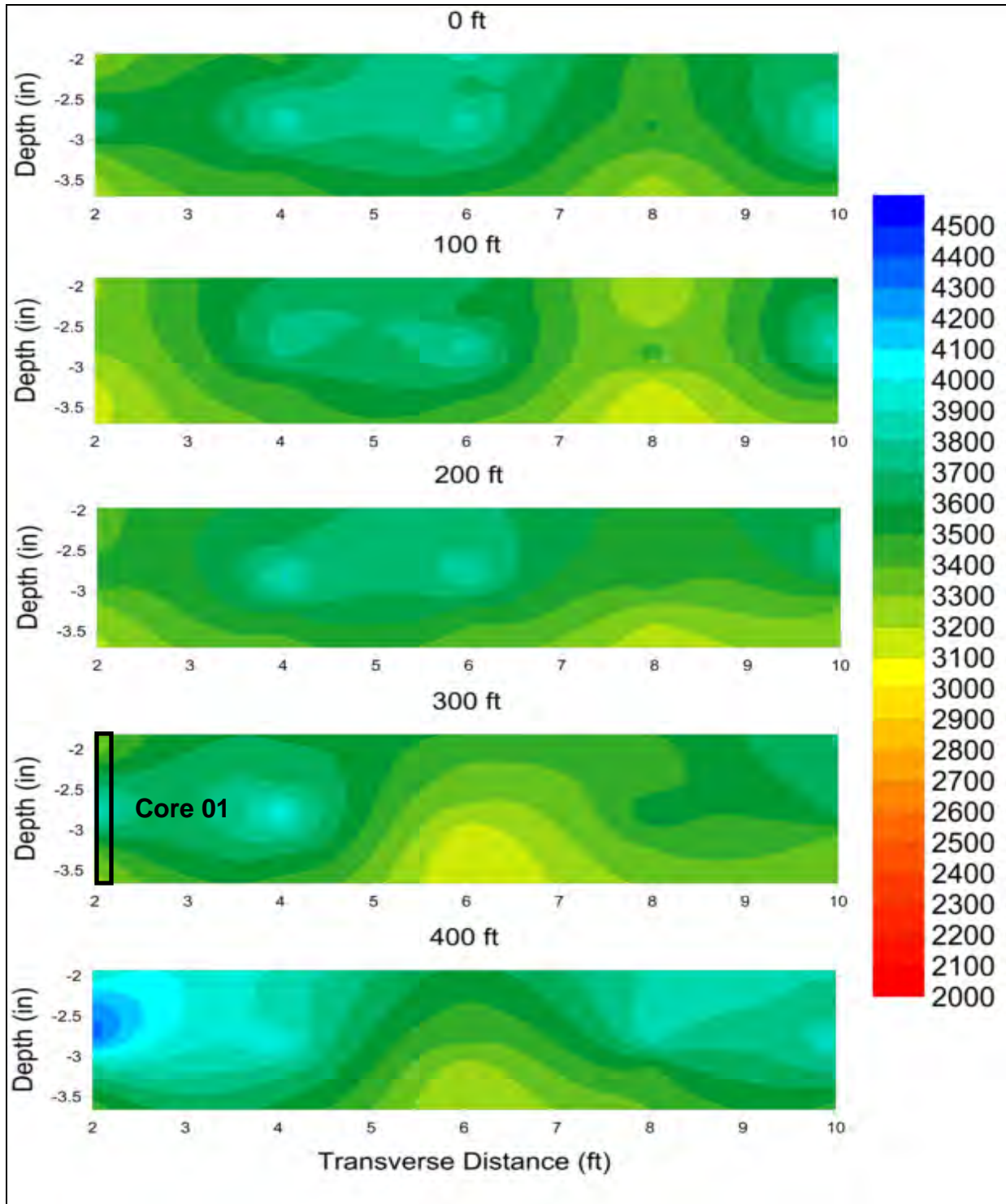


Fig. 3.11—Cross-sections depicting variations in the elastic modulus (ksi) for BM for PSPA USW data acquired at the 0 ft to 400 ft intervals along the GPR traverses. The five PSPA USW data sets in each cross-section were acquired at 2 ft intervals starting 2 ft from the edge of pavement (Fig. 3.7). Depth of investigation extends from 2 in. to approx. 3.7 in.

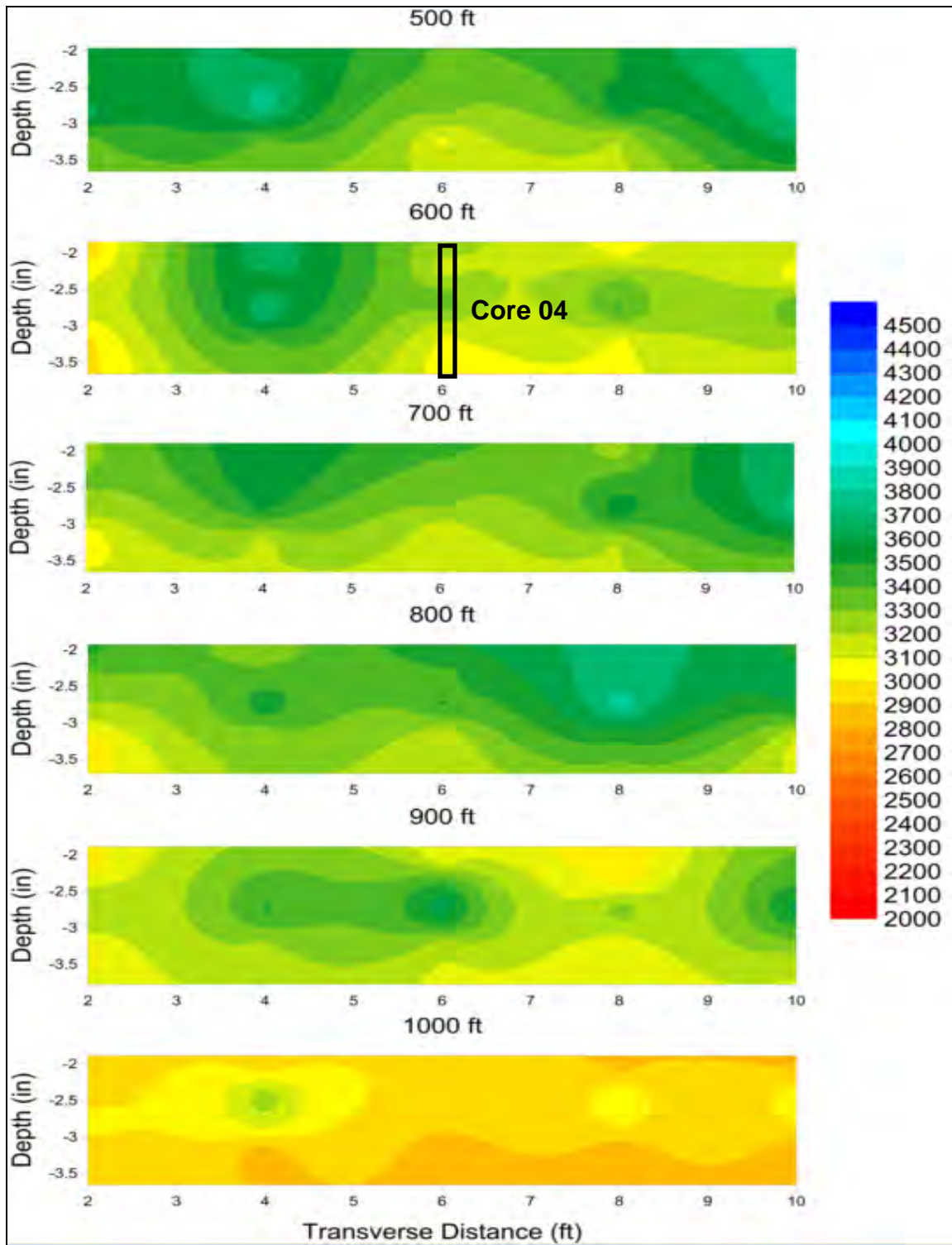


Fig. 3.12—Cross-sections depicting variations in the elastic modulus (ksi) for BM for PSPA USW data acquired at the 500 ft to 1000 ft intervals along the GPR traverses.

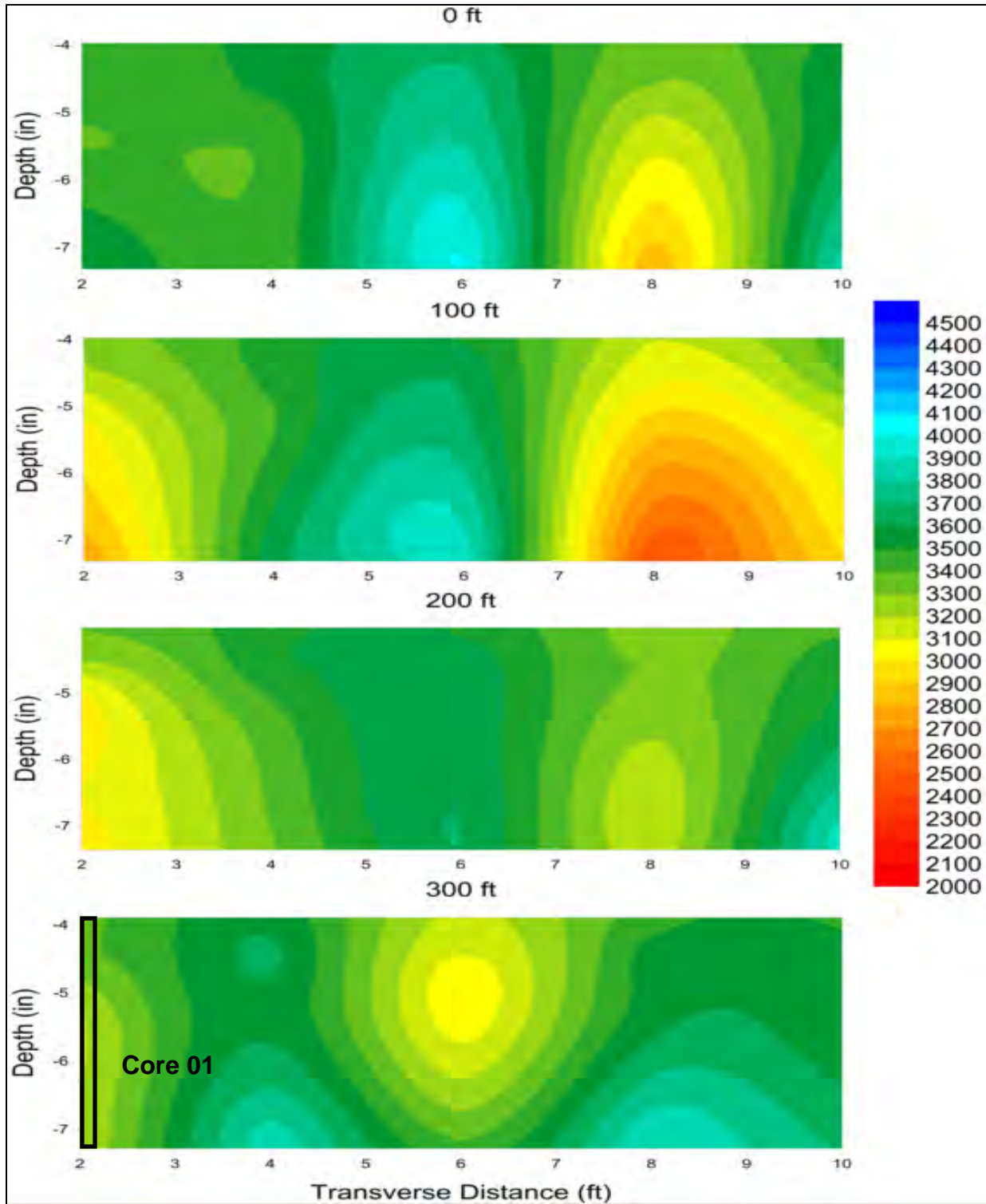


Fig. 3.13—Cross-sections depicting variations in the elastic modulus (ksi) for concrete for PSPA USW data acquired at the 0 ft to 300 ft intervals along the GPR traverses. The five PSPA USW data sets in each cross-section were acquired at 2 ft intervals starting 2 ft from the edge of pavement (Fig. 3.7). Depth of investigation extends from 4 in. to approx. 7.2 in.

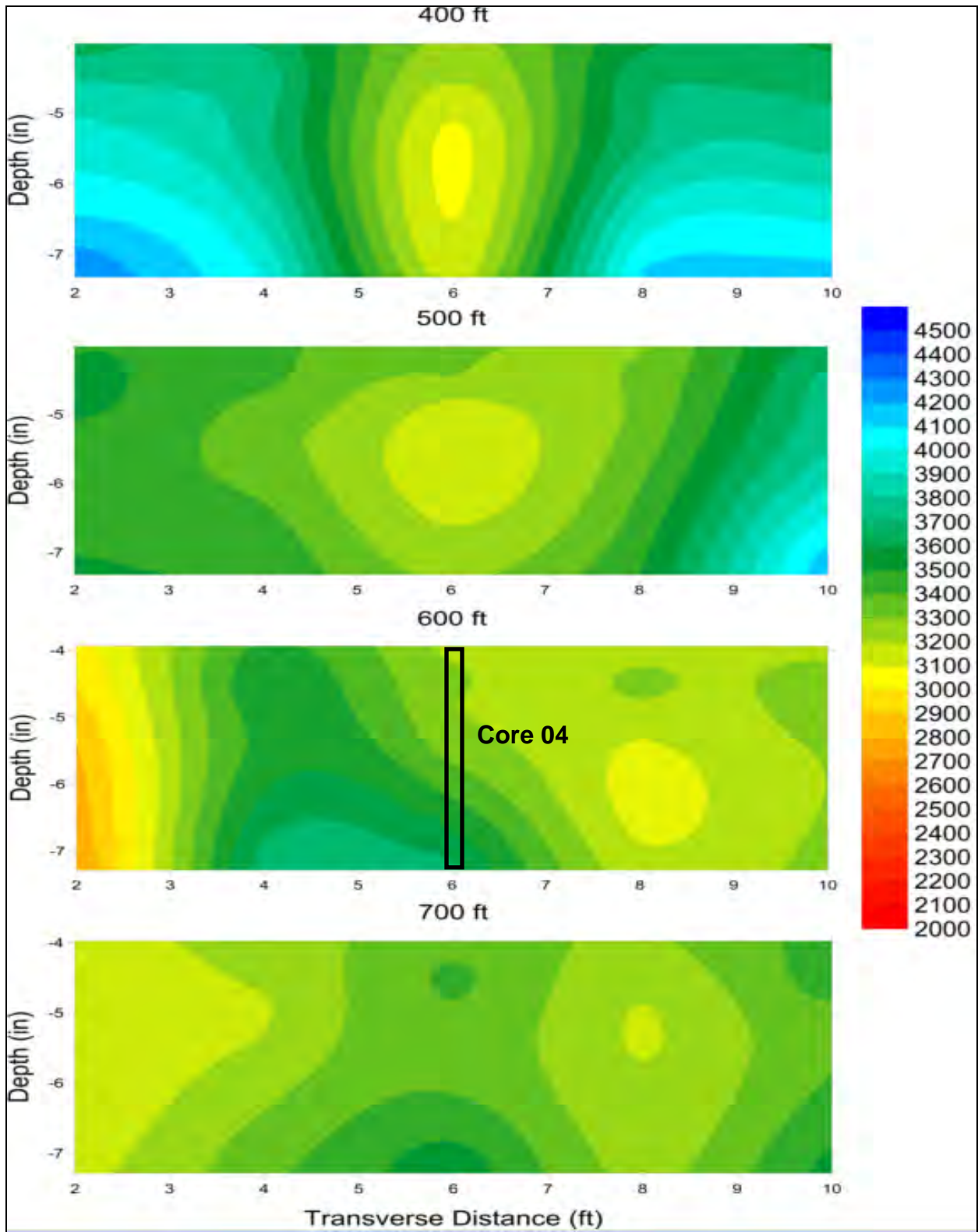


Fig. 3.14–Cross-sections depicting variations in the elastic modulus (ksi) for concrete for PSPA USW data acquired at the 400 ft to 700 ft intervals along the GPR traverses.

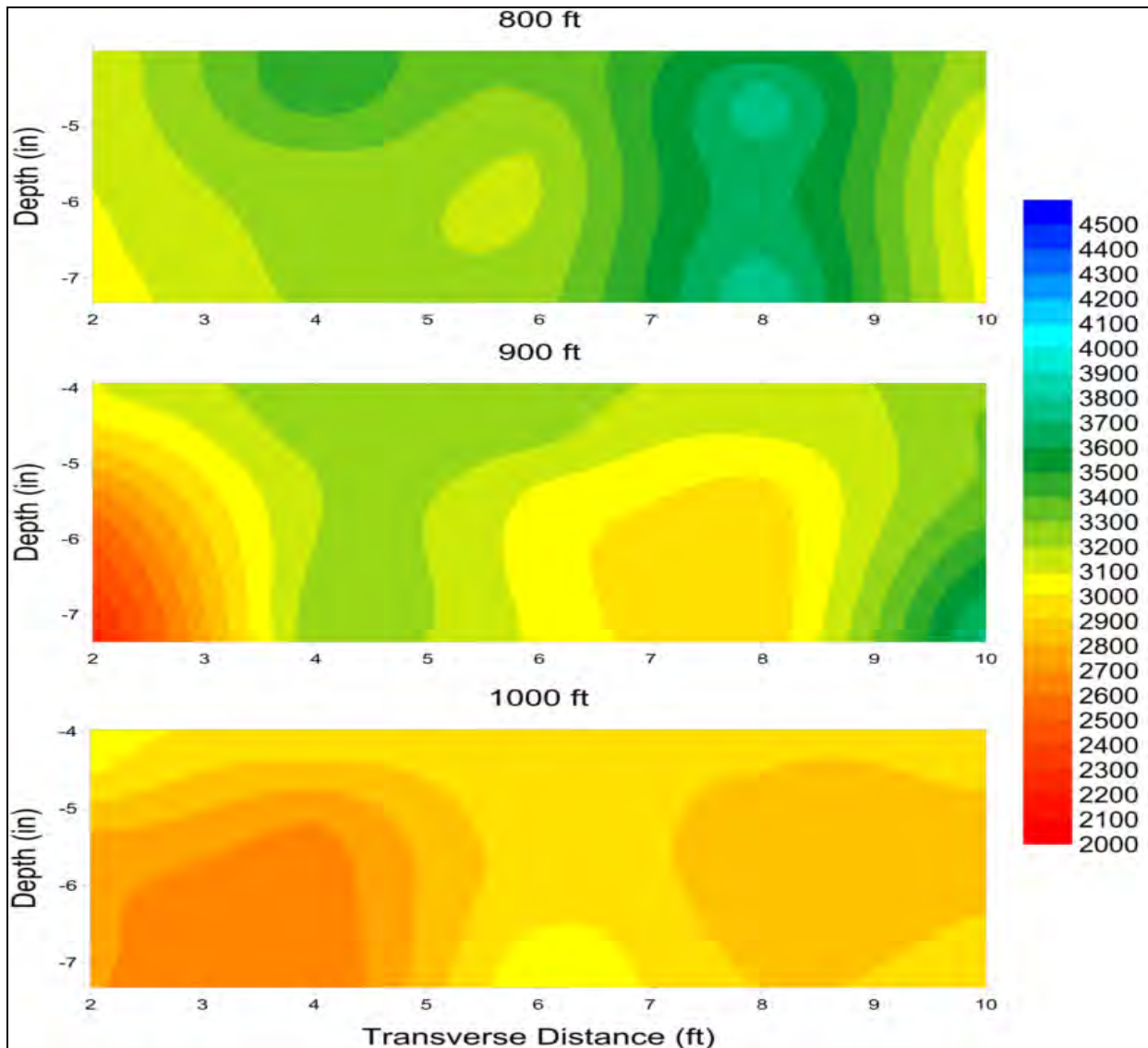


Fig. 3.15—Cross-sections depicting variations in the elastic modulus (ksi) for concrete for PSPA USW data acquired at the 800 ft to 1000 ft intervals along the GPR traverses

The apparent elastic modulus of the PCC is anomalously low at almost all depths near the outer edges of the cross-sections on the cross-sections acquired at stations 900 and 1000 ft (Fig. 3.15). This observation is consistent with the PSPA data acquired in proximity to core 07 and the visual assessment of core 07. The average modulus of the PCC at core 07 is anomalously low compared to the PSPA data acquired at core locations 01 and 04.

The average elastic modulus along each GPR transverse for the entire tested section pavement (2 in. to 7.2 in.) was calculated and plotted in Fig. 3.16. It is interesting to note that the average elastic modulus of the pavement is statistically lowest in those areas where vehicles tires are most commonly in contact with the roadway (2 ft and 8 ft from the outer edge of pavement).

Statistical Analysis Diagram

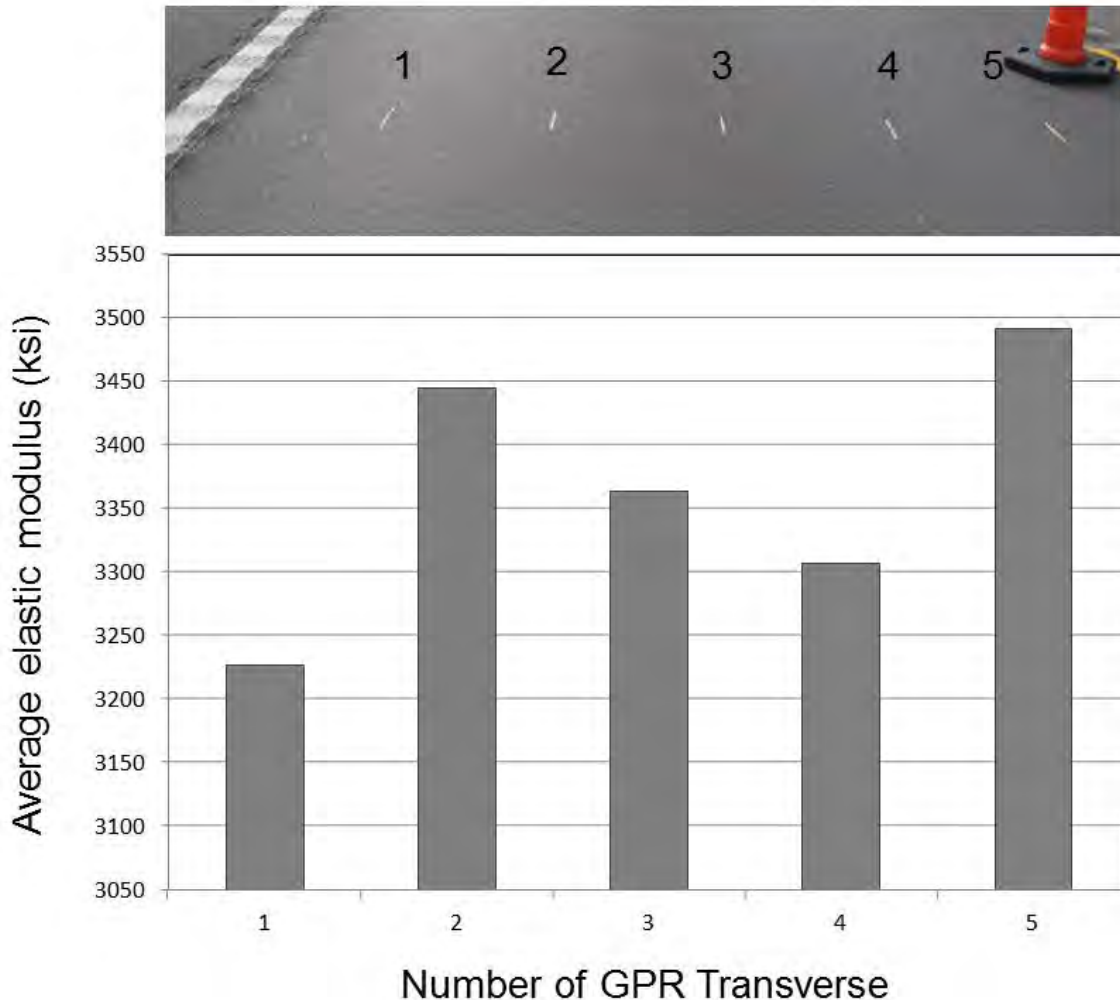


Fig. 3.16—Plot of the average elastic modulus (over depth range of 2 to 7.2 in.) along each GPR transverse. The GPR traverses are spaced at 2 ft intervals. GPR traverse 1 is 2 ft from the outer edge of the pavement.

3.3.1.2 Impact Echo Data

IE data were acquired at each Site 1 PSPA test location (Fig. 3.7). The PSPA IE software automatically analyzed the amplitude spectrum of the acoustic data recorded by the near receiver transducer at each test location and identified relative peak amplitudes on the amplitude spectra. These peak frequencies (Fig. 3.5) were interpreted as resonant frequencies. The depths to the corresponding reflectors were calculated using Eq. 3.3 (Section 3.2.2.2).

The PSPA software consistently identified two peak frequencies (higher and lower) on the IE data acquired at Site 1. The calculated depth to the shallower reflector (corresponding to the higher peak frequency) is consistently about 4 in. (Fig. 3.17). This reflector is believed to be the BM/PCC interface (at an actual depth of approximately 3.5 in.).

The slight, but consistent, overestimation (approximately 0.4 in.) of the depth to the BM/PCC interface is attributed to the fact that the compressional wave velocity used in Eq. 3.3 was calculated using Eq. 3.1 (Section 3.2.2.1). The compressional wave velocity (V_p) calculated using Eq. 3.1 is a function of the average surface wave velocity (V_R) of the upper approx. 7 in. of pavement. Additionally, the Poisson's ratio of asphalt was used to calculate V_p .

The calculated depth to the deeper reflector (corresponding to the lower peak frequency) was consistently about 5.2 in. (Fig. 3.18). The depth to the PSPA IE identified deeper reflector does not correlate to any known pavement interface. This resonant frequency is therefore attributed to noise (possibly the flexural wave propagating through the BM layer).

A peak frequency corresponding to reverberations originating from the base of the pavement (at a depth of 11.5 in.) was not identified by the PSPA IE software.

In summary, the PSPA IE tool appeared to be able to estimate the thickness of the BM with a reasonable degree of reliability and consistency. However, the tool also appears to have identified a false reflector and was unable to identify the reflector from the base of the pavement.

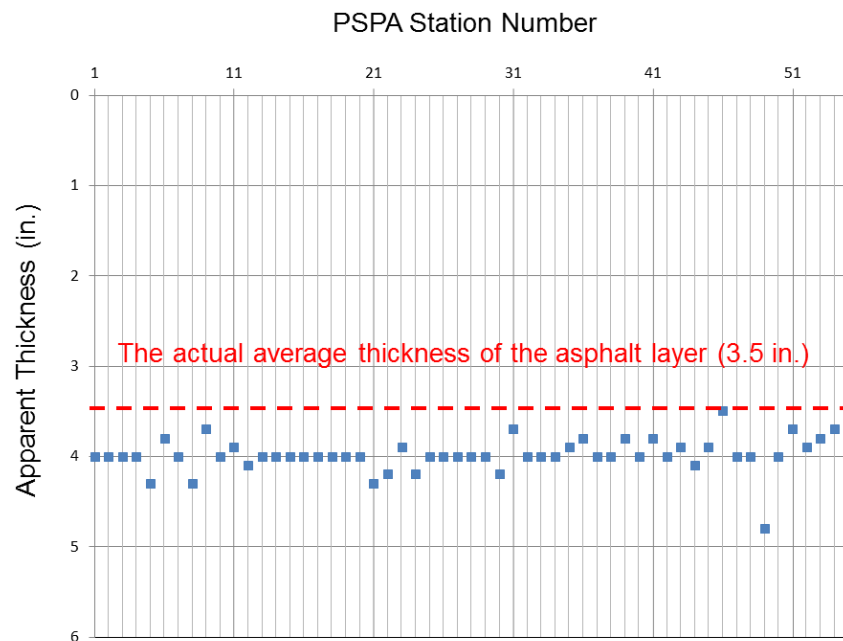


Fig. 3.17—The PSPA IE calculated depth to shallowest identified reflector is plotted for all PSPA test locations (Fig. 3.7). The average calculated depth to this reflector (approx. 4 in.) measurement agrees well with the actual thickness (approx. 3.5 in.) of the BM layer.

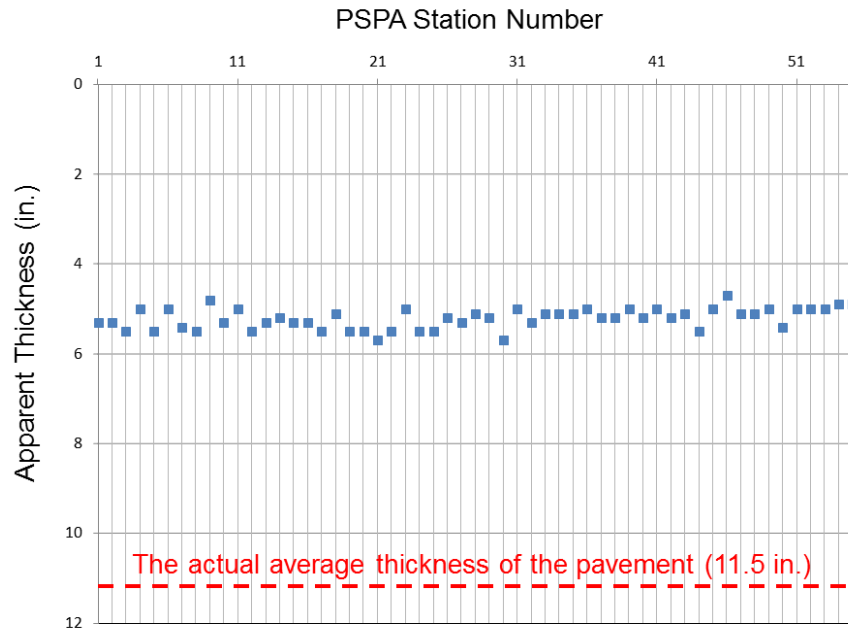


Fig. 3.18–The calculated depth to the deeper reflector (corresponding to the lower peak frequency) was consistently about 5.2 in. (Fig. 3.17). The depth to the PSPA IE identified deeper reflector does not correlate to any known pavement interface. This resonant frequency is therefore attributed to noise (possibly the flexural wave propagating through the asphalt layer).

3.3.2 Project-Level Site 2 (US 54)

Project-level Site 2 is located along highway US 54 in Camden County, Missouri (Fig. 3.19). The test pavement consisted of approximately 11 in. of BM. There was visible evidence of surface cracks. The average air temperature during field data acquisition at the test site was 36 °F.

Fifty-five (55) PSPA data sets and ten (10) cores were acquired at test Site 2 (Fig. 3.2 and Fig. 3.20). The PSPA data were acquired using a 4 in. transducer spacing. Hence, the USW modulus plot extends from a depth of 2 in. to a depth of approximately 7 in. (Fig. 3.8). PSPA data were not acquired in immediate proximity to all core locations.

3.3.2.1 Ultrasonic Surface Wave Data

In this report, the project-level pavement Site 2 PSPA USW elastic modulus data are presented in 1-D plot format and in 2-D plot format.

PSPA USW data acquired in proximity to core locations 03, 04, 05, and 09 (Fig. 3.20) are presented to illustrate the utility and limitations of the PSPA tool. Cores 03, 04, 05 and 09 and the corresponding PSPA elastic modulus plot are shown as Fig. 3.21-Fig. 3.24, respectively. All of the four retrieved cores were stripped and debonded at multiple depths (Fig. 3.21-Fig. 3.24). The PSPA USW average elastic modulus for cores 03, 04, 05 and 06 were 1058 ksi, 1914 ksi, 1368 ksi and 1858 ksi respectively. These average elastic modulus values are consistent with severely deteriorated BM (at an air temperature of 32 °F; Table 3.2). These results suggest the PSPA USW is a useful tool for assessing the condition of BM.



Fig. 3.19—Photograph of PSPA tool placed on pavement at project-level Site 2 (US 54).

PSPA USW data are presented in 2-D cross-sectional format to provide information about lateral and vertical variations in pavement quality. The elastic modulus data acquired at Site 2 are displayed in cross-section format in Figs. 3.25 – 3.28. As shown on these figures, the tested section of BM (2 in. to approximately 7.2 in.) is characterized mostly by elastic modulus values between 1000 ksi and 3000 ksi indicating most of the tested section of BM paved roadway is poor quality or severely deteriorated. These results suggest the PSPA USW is a useful tool for assessing the condition of BM.

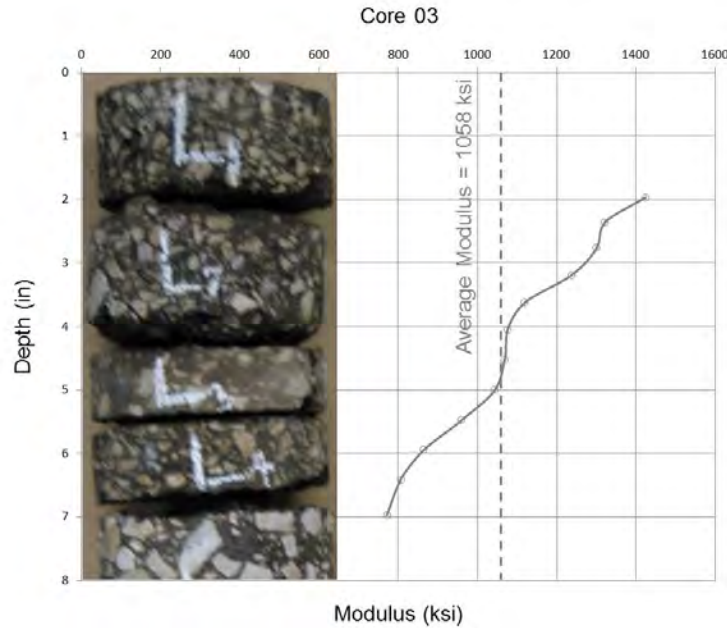


Fig. 3.21—Elastic modulus plot generated from PSPA USW data acquired in immediate proximity to stripped and debonded core 03 (Fig. 3.20). The pavement consists of approximately 11 in. of BM. The PSPA USW average elastic modulus for core 03 is 1058 ksi indicating the BM is severely deteriorated BM (at an air temperature of 32 °F; Table 3.2).

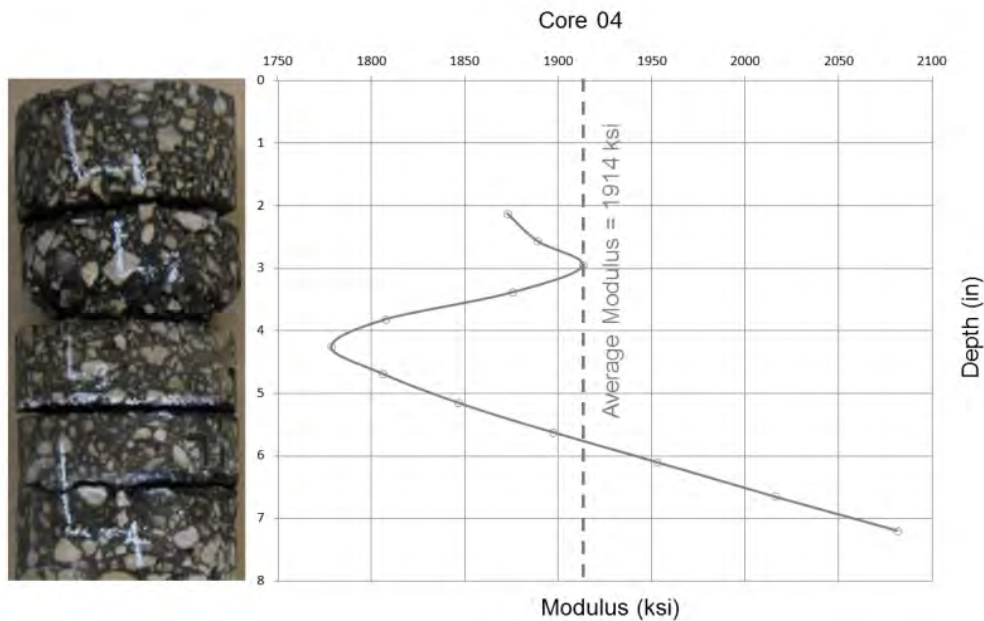


Fig. 3.22—Elastic modulus plot generated from PSPA USW data acquired in immediate proximity to stripped and debonded core 04 (Fig. 3.20). The PSPA USW average elastic modulus for core 04 is 1914 ksi indicating the BM is severely deteriorated BM (at an air temperature of 32 °F; Table 3.2).

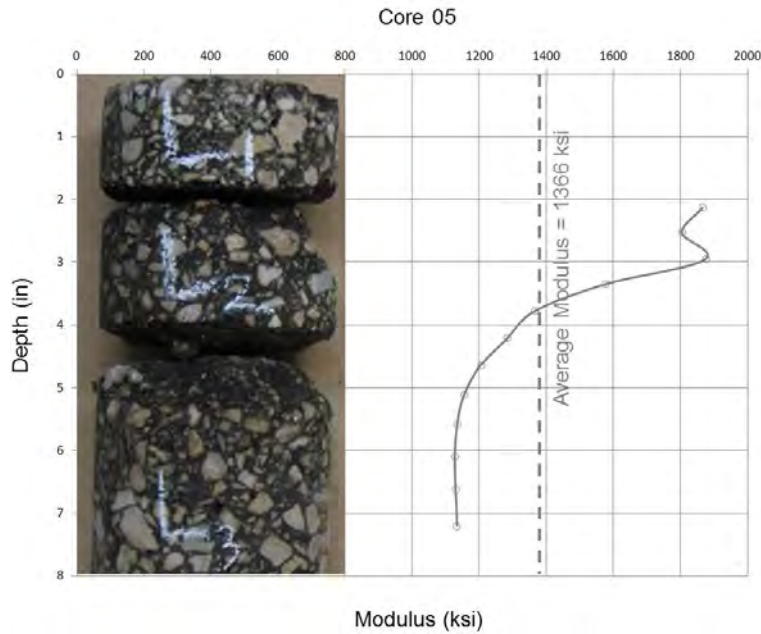


Fig. 3.23—Elastic modulus plot generated from PSPA USW data acquired in immediate proximity to stripped and debonded core 05 (Fig. 3.20). The PSPA USW average elastic modulus for core 05 is 1366 ksi indicating the BM is severely deteriorated BM (at an air temperature of 32 °F; Table 3.2).

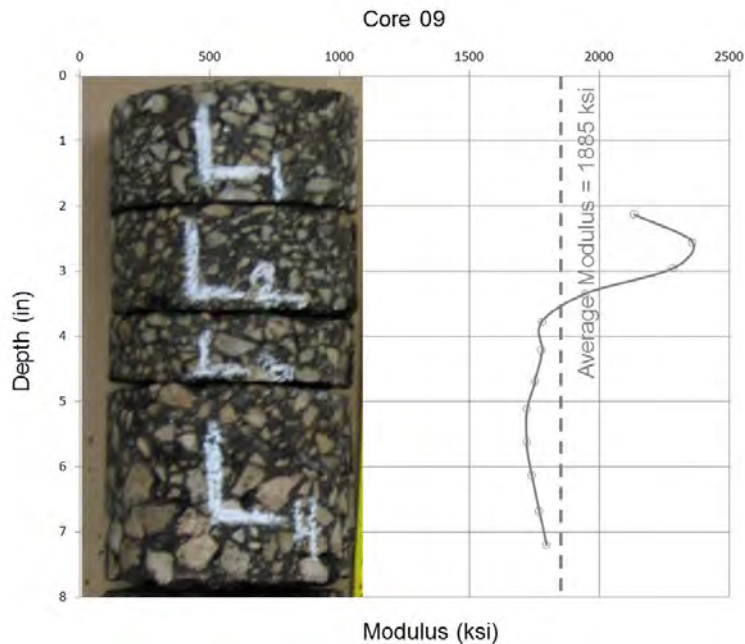


Fig. 3.24—Elastic modulus plot generated from PSPA USW data acquired in immediate proximity to stripped and debonded core 09 (Fig. 3.20). The PSPA USW average elastic modulus for core 09 is 1858 ksi indicating the BM is severely deteriorated BM (at an air temperature of 32 °F; Table 3.2).

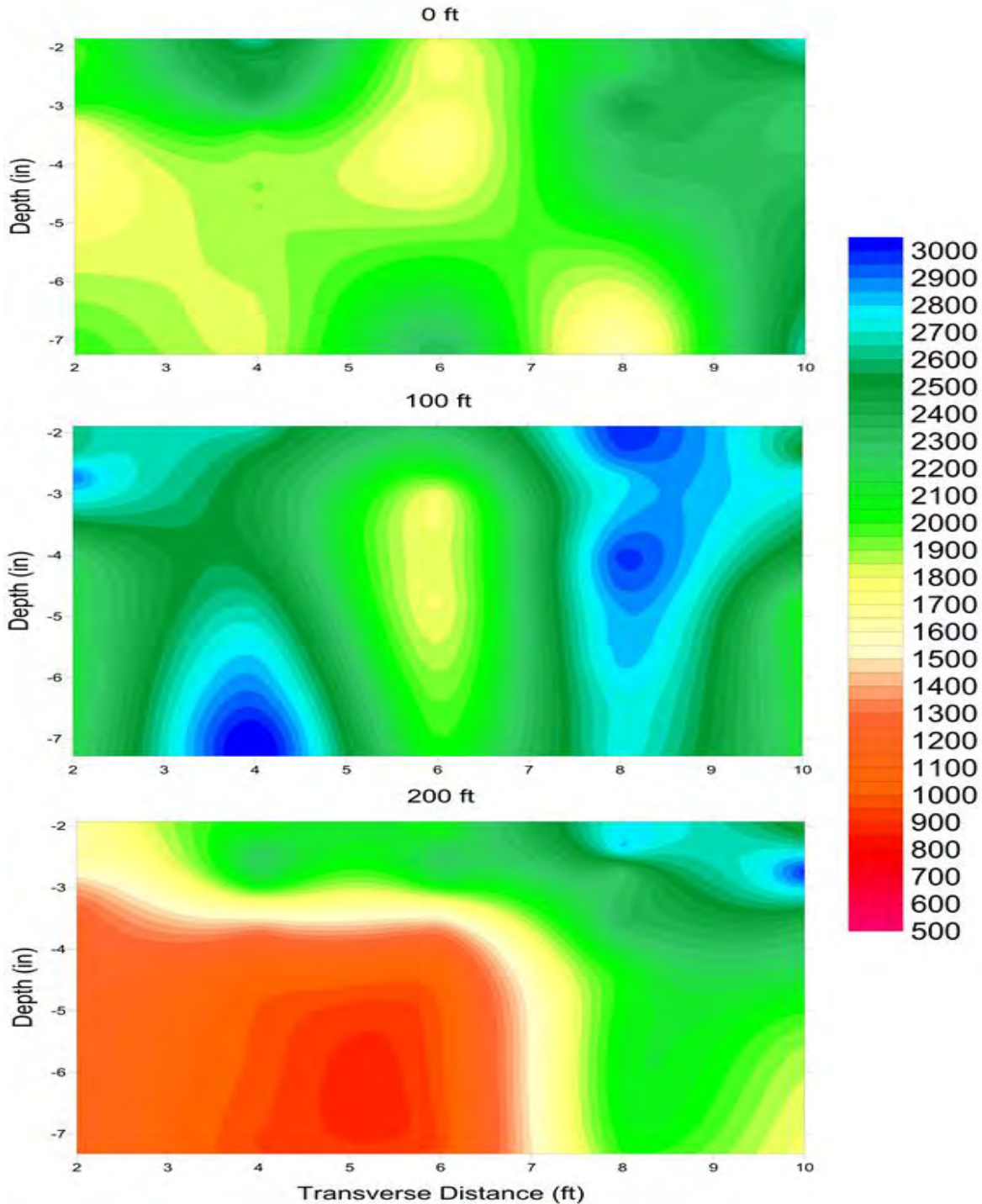


Fig. 3.25—Cross-sections depicting variations in the PSPA USW elastic modulus (ksi) of the BM at the 0 ft, 100 ft, and 200 ft intervals along the GPR traverses. The five PSPA USW data sets in each cross-section were acquired at 2 ft intervals starting 2 ft from the edge of pavement (Fig. 3.20). Depth of investigation extends from 2 in. to approx. 7.2 in.

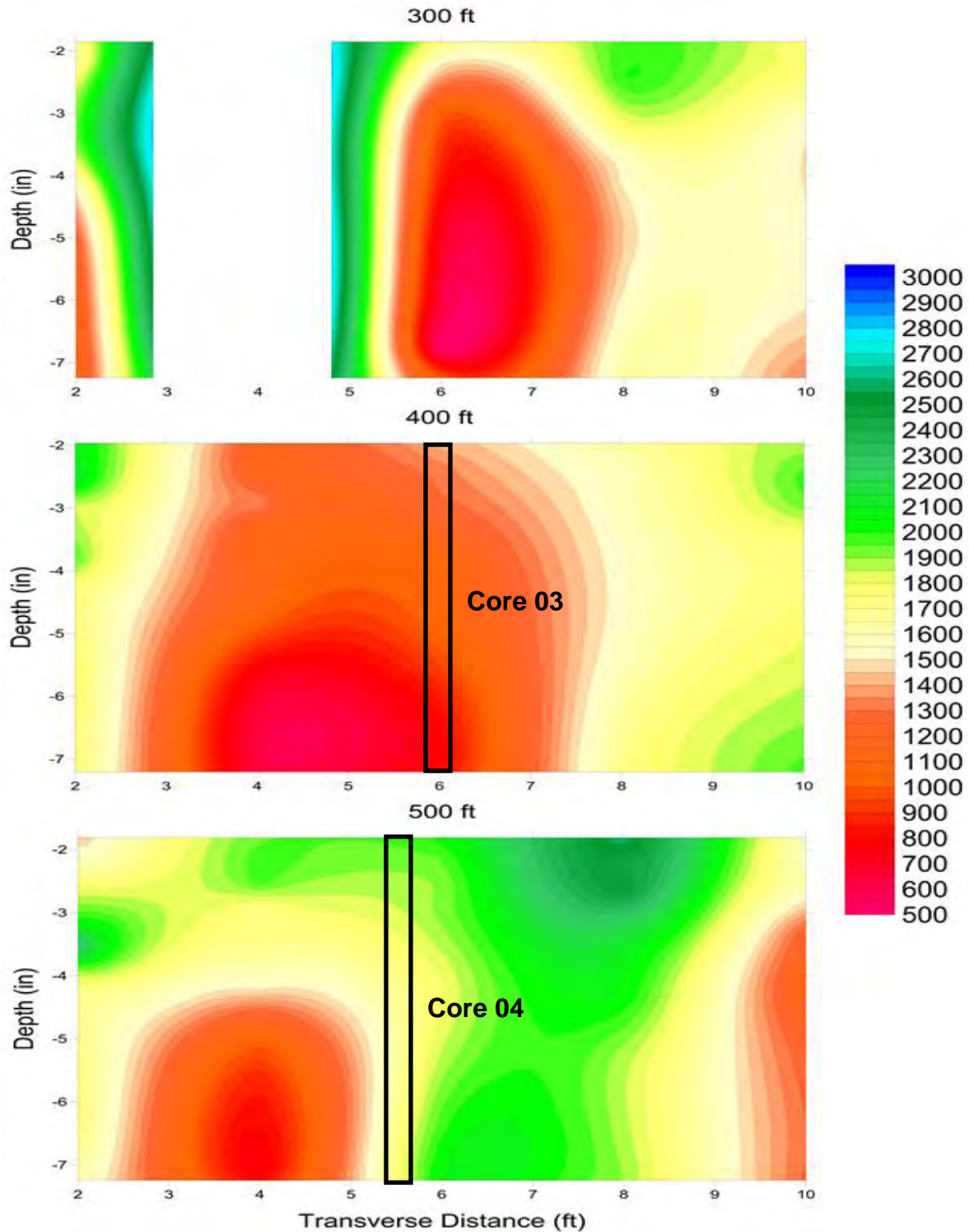


Fig. 3.26—Cross-sections depicting variations in the PSPA USW elastic modulus (ksi) of the BM at the 300 ft, 400 ft, and 500 ft intervals along the GPR traverses. PSPA data could not be acquired at the 4 ft mark on the 300 ft profile because of the deteriorated nature of the paved surface.

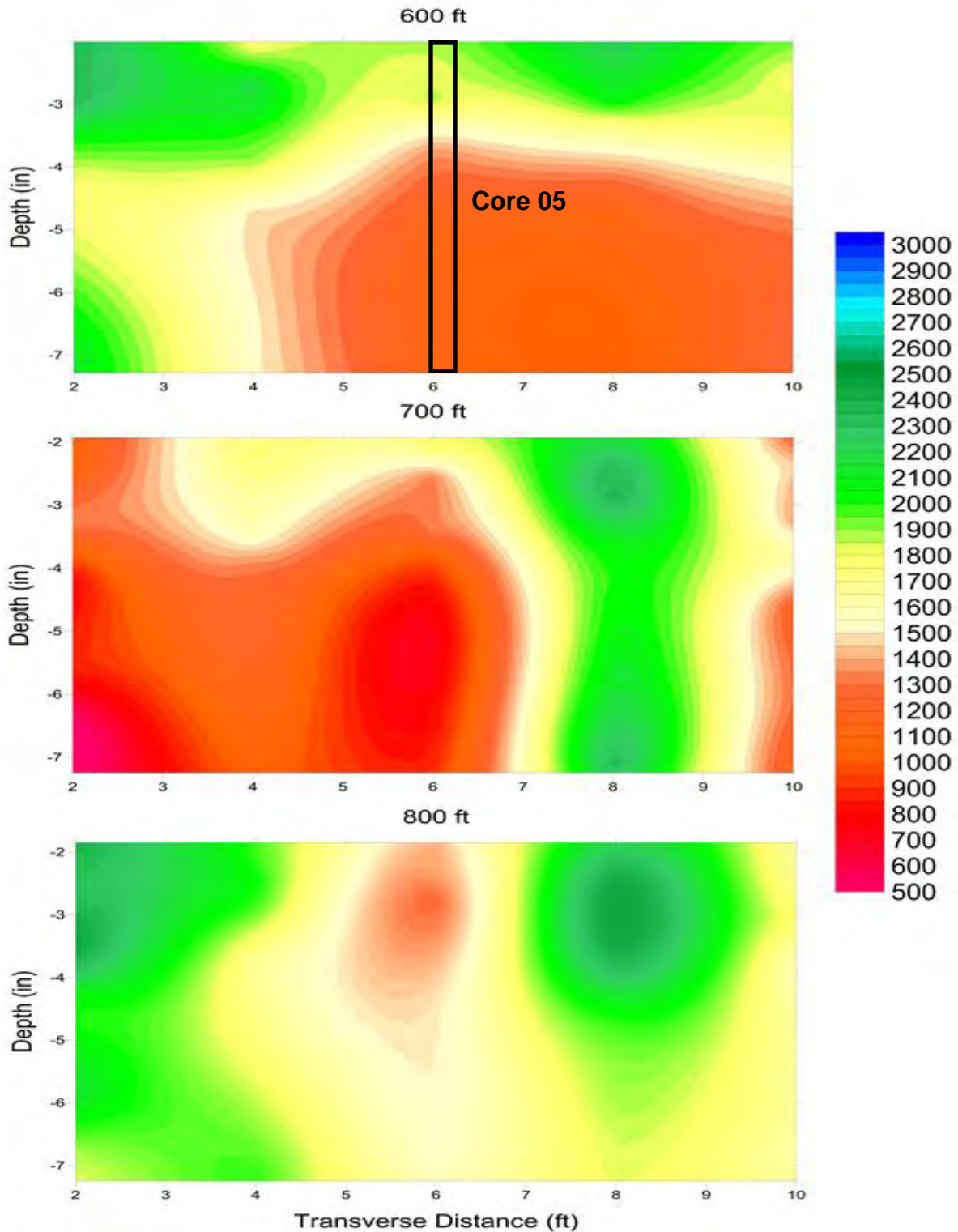


Fig. 3.27—Cross-sections depicting variations in the PSPA USW elastic modulus (ksi) of the BM at the 600 ft, 700 ft, and 800 ft intervals along the GPR traverses.

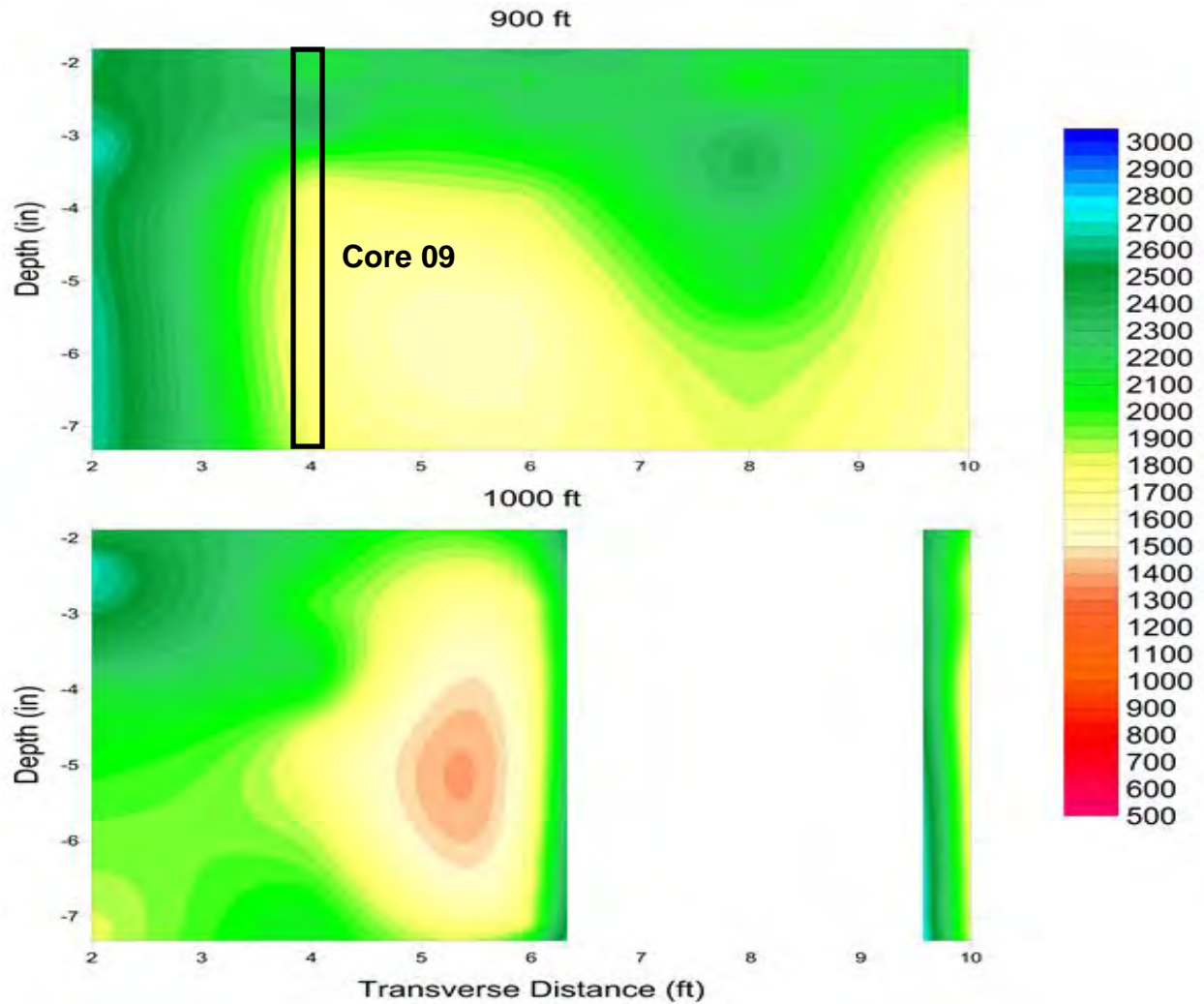


Fig. 3.28—Cross-sections depicting variations in the PSPA USW elastic modulus (ksi) of the BM at the 900 ft and 1000 ft intervals along the GPR traverses. PSPA data could not be acquired at the 8 ft mark on the 1000 ft profile because of the deteriorated nature of the paved surface.

The average elastic modulus along each GPR transverse for the entire tested section pavement (2 in. to 7.2 in.) was calculated and plotted in Fig. 3.29. The average elastic modulus along each GPR traverse is less than 2000 ksi (with the exception of traverse 4 which is characterized by an average modulus slightly greater than 2000 ksi). These modulus values are consistent with the assessment that the BM pavement is poor quality to severely deteriorated.

Statistical Analysis Diagram

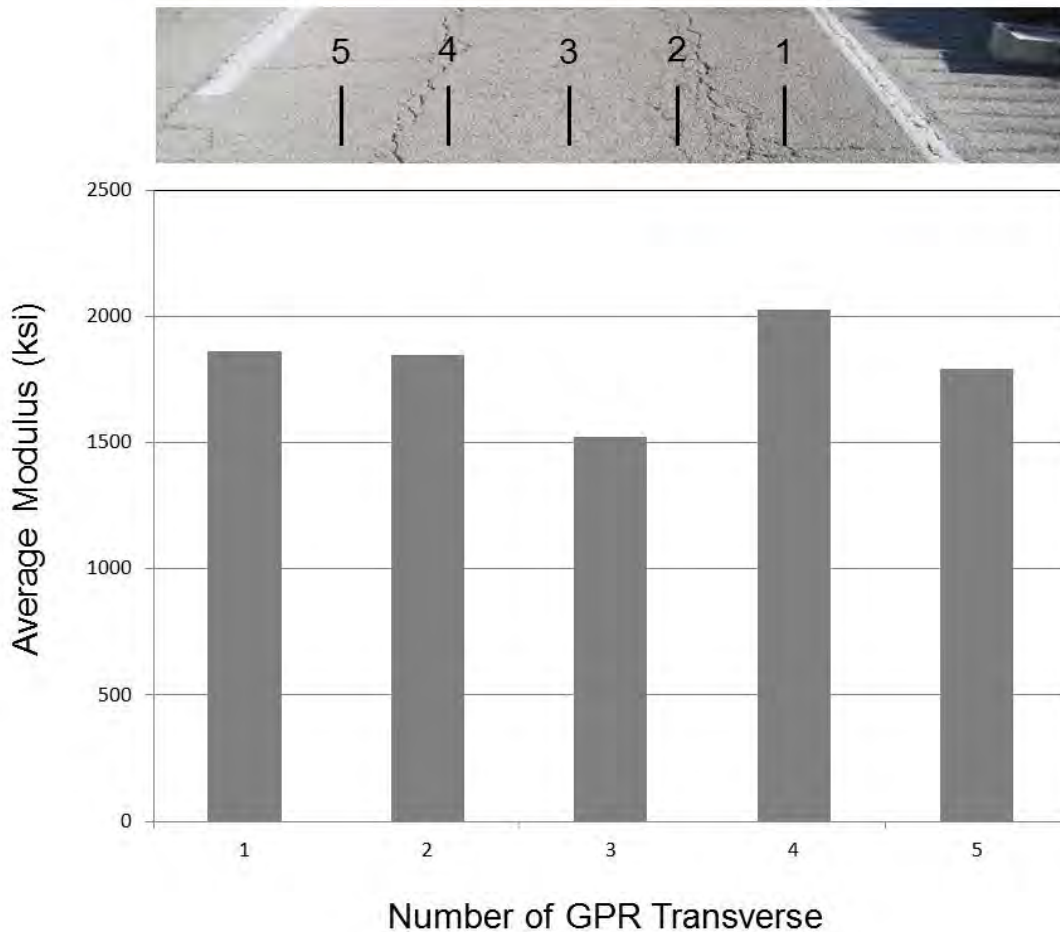


Fig. 3.29—Plot of the average elastic modulus (over depth range of 2 to 7.2 in.) along each GPR transverse. The GPR traverses are spaced at 2 ft intervals. GPR traverse 1 is 2 ft from the outer edge of the pavement.

3.3.2.2 Impact Echo Data

IE data were acquired at each Site 2 PSPA test location (Fig. 3.20). The PSPA IE software automatically analyzed the amplitude spectrum of the acoustic data recorded by the near receiver transducer at each test location and identified a single peak on each amplitude spectra. These peak frequencies (Fig. 3.5) were interpreted as resonant frequencies. The depths to the corresponding reflectors were calculated using Eq. 3.3 (Section 3.2.2.2).

The PSPA software consistently identified a single peak frequency on the IE data acquired at Site 2. The PSPA output calculated depth to the corresponding reflector varied from 2 in. to 7 in. (Fig. 3.30). These reflectors are believed to be flaws within the BM.

The compressional wave velocity used in Eq. 3.3 was calculated using Eq. 3.1 (Section 3.2.2.1). The compressional wave velocity (V_p) calculated using Eq. 3.1 is a function of the average surface wave velocity (V_R) of the upper approx. 7.2 in. of BM pavement.

The wide variation in calculated reflector depths is probably due to variations in the depths to the respective flaws. However, it could also be caused, in part, by the fact that compressional waves travel along near-vertical paths, whereas the Rayleigh waves propagate laterally through the anisotropic pavement. Hence, Eq. 3.1 might not generate highly reliable compressional wave velocities at some PSPA test locations due to the presence of vertical cracks, for example.

In summary, the PSPA IE tool was unable to estimate the thickness of the BM pavement with a reasonable degree of reliability and consistency. However, the tool might have been able to identify the approximate depths to the shallowest significant flaw at each location.

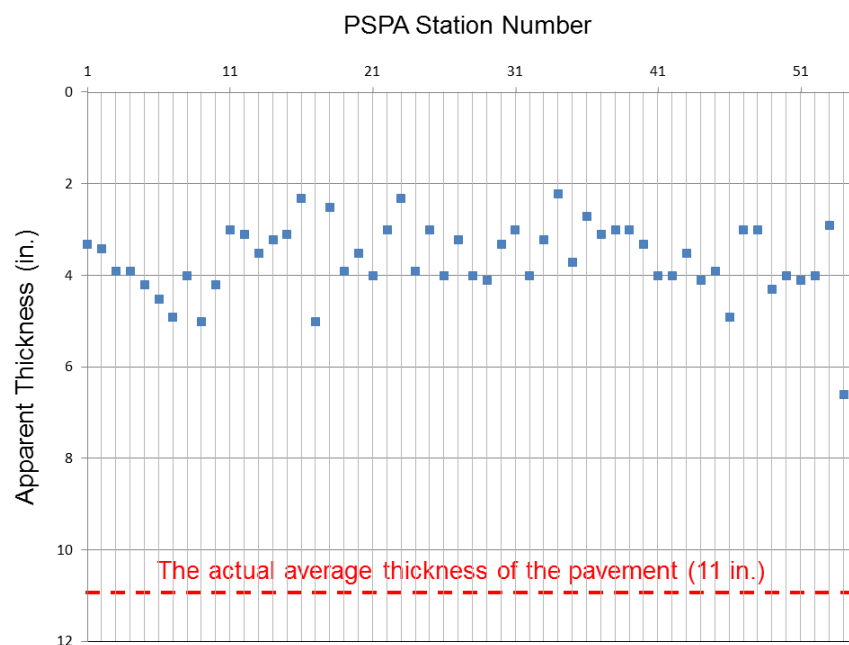


Fig. 3.30–The PSPA IE calculated depth to shallowest identified reflector is plotted for all PSPA test locations (Fig. 3.20).

3.3.3 Project-Level Site 3 (MO 179)

Project-level Site 3 is located along the north-bound lane of MO 179 near Jefferson City, Missouri (Fig. 3.31). The pavement consisted of approximately 12 in. of BM. There was visible evidence of surface cracks. The average air temperature during field data acquisition at the test site was 43 °F.

Fifty-five (55) PSPA data sets and ten (10) cores were acquired at Site 3 (Fig. 3.2 and Fig. 3.32). The PSPA data were acquired using a 4 in. transducer spacing. Hence, the USW modulus plot extends from a depth of 2 in. to a depth of approximately 7 in. (Fig. 3.8). PSPA data were not acquired in immediate proximity to all core locations.



Fig. 3.31—Photograph of PSPA tool placed on pavement at project-level Site 3 (MO 179).

3.3.3.1 Ultrasonic Surface Wave Data

In this report, the project-level pavement Site 3 PSPA USW elastic modulus data are presented in 1-D plot format and in 2-D plot format.

Cores 01, 02, 04 and 07 and the corresponding PSPA elastic modulus plots are shown as Figs. 3.33-3.36, respectively. Cores 01, 02 and 04 were not debonded and are characterized by a PSPA USW average elastic modulus of 3022 ksi, 3147 ksi and 3582 ksi, respectively. These average elastic modulus values are consistent with fair quality BM (at air temperatures of 32-50 °F; Table 3.2).

Core 07 was debonded at a depth of about 4 in. and is characterized by a PSPA USW average elastic modulus of 2522 ksi, which corresponds to poor quality BM at air temperatures of 32-50 °F (Table 3.2). As shown in Fig. 3.36, the elastic modulus of the pavement in proximity to core 04 decreases abruptly at a depth of 4 in.

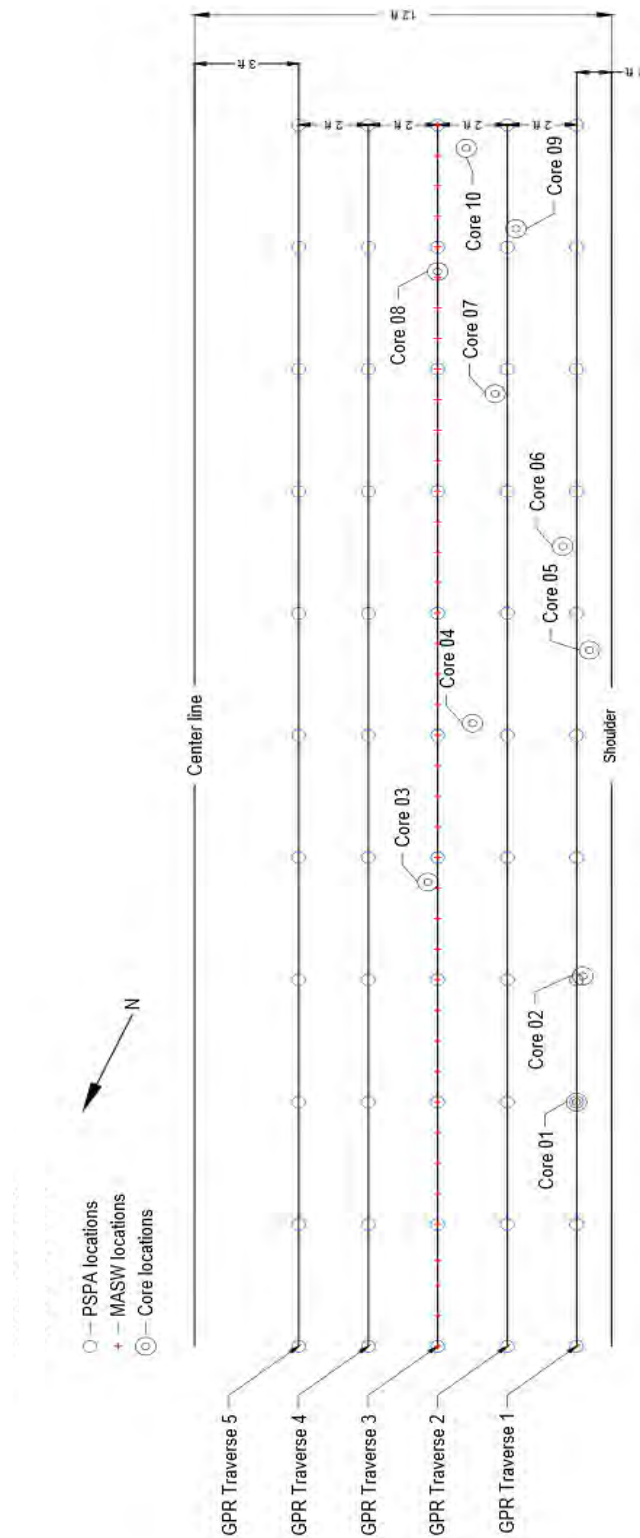


Fig. 3.32—Base map for project-level Site 3 showing PSPA test locations and core locations. PSPA data were acquired at 100 ft intervals along each GPR traverse. GPR traverse 1 was located 1 ft from the outer edge of the paved driving lane (shoulder). Only cores 01 and 02 are located within 20 ft of a PSPA location.

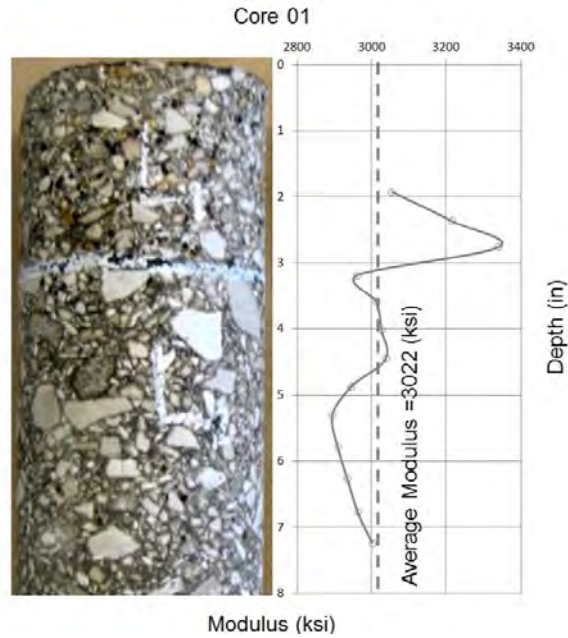


Fig. 3.33—Elastic modulus plot generated from PSPA USW data acquired in immediate proximity to intact core 01 (Fig. 3.32). The pavement consists of approx. 12 in. of BM. The PSPA USW average elastic modulus for core 01 is 3022 ksi indicating the BM is fair quality (at air temperatures of 32-50 °F; Table 3.2).

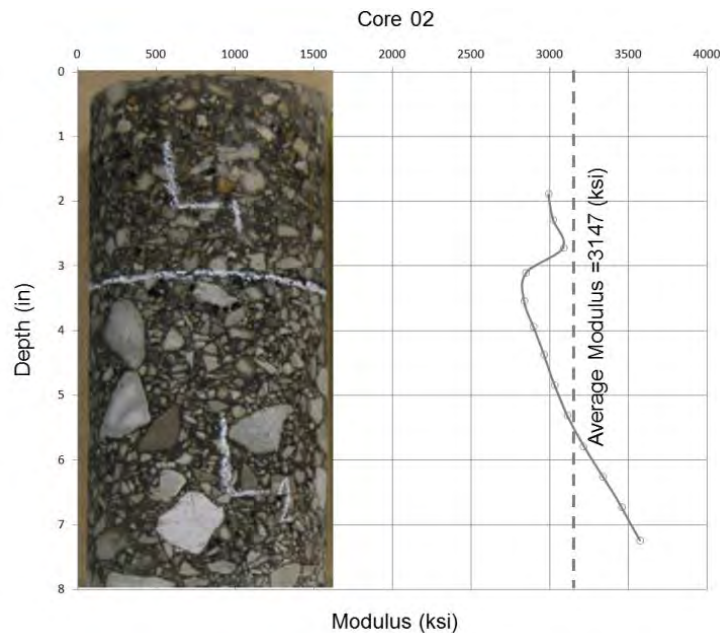


Fig. 3.34—Elastic modulus plot generated from PSPA USW data acquired in immediate proximity to intact core 02 (Fig. 3.32). The pavement consists of approx. 12 in. of BM. The PSPA USW average elastic modulus for core 01 is 3147 ksi indicating the BM is fair quality (at air temperatures of 32-50 °F; Table 3.2).

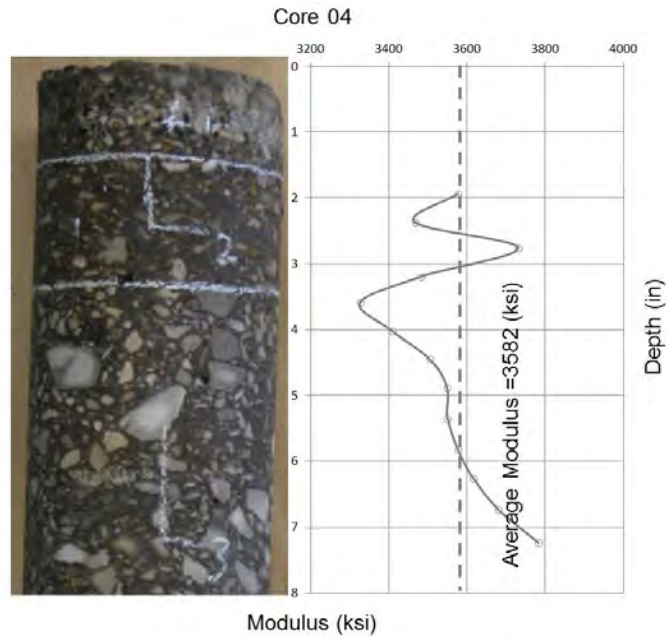


Fig. 3.35—Elastic modulus plot generated from PSPA USW data acquired within 12 ft of intact core 04 (Fig. 3.32). The pavement consists of approx. 12 in. of BM. The PSPA USW average elastic modulus for core 04 is 3582 ksi indicating the BM is fair quality (at air temperatures of 32-50 °F; Table 3.2). Core 04 was located about 12 ft from the PSPA location.

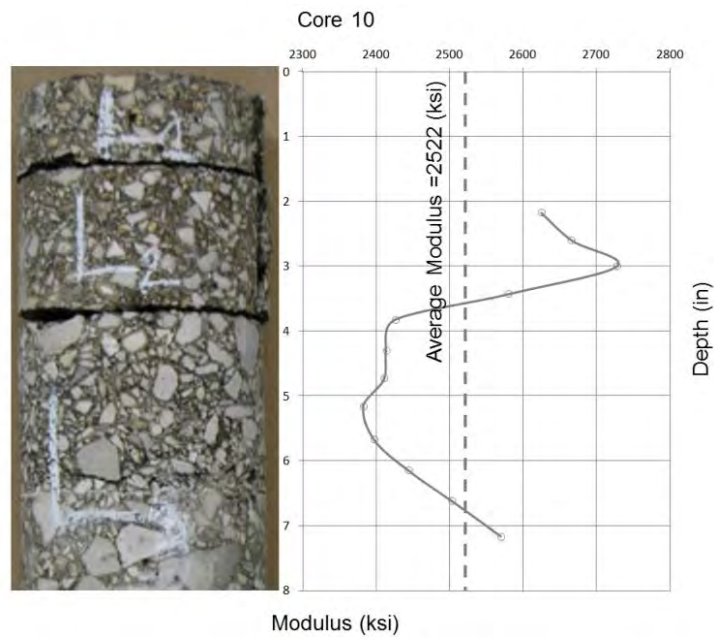


Fig. 3.36—Elastic modulus plot generated from PSPA USW data acquired within 20 ft of core 07 (Fig. 3.32). This core was debonded at a depth of approx. 4 in. (weak bonded at a depth of 1.5 in.) The PSPA USW average elastic modulus for core 04 is 2522 ksi indicating the BM is poor quality (at air temperatures of 32-50 °F; Table 3.2). Note that the elastic modulus of the pavement decreases abruptly at a depth of 4 in.

The elastic modulus data acquired at Site 3 is displayed in cross-section format in Figs. 3.37-3.40. As shown on these figures, the tested section of BM (2 in. to approximately 7.2 in.) is characterized by elastic modulus values between 1000 ksi and 4500 ksi indicating most of the quality of the tested section of BM roadway is highly variable (severely deteriorated to good).

The acquired core control is consistent with elastic modulus data. More specifically: 1) the PSPA elastic modulus curve acquired closest to the location of debonded core 03 (Fig. 3.32; within 20 ft) is characterized by values between 2500 ksi and 3000 ksi, which indicates fair quality BM; 2) the elastic modulus values acquired closest (within 20 ft) to the location of core 05 which is debonded at a depth of 6.5 in. decrease rapidly at depths below 6 in. (Fig. 3.32); 3) the elastic modulus curve acquired near (within 20 ft) the location of core 08 which is debonded at a depth of 1.25 in. (Fig. 3.32) is characterized by values between 2500 ksi and 3000 ksi at depths above 5 in. and elastic modulus values between 3000 ksi and 3900 ksi at depths below 5 in. which indicates fair quality; and 6) the elastic modulus curve acquired near (within 20 ft) the location of core 10 which is debonded at a depth of 3.5 in. (Fig. 3.32) are characterized by values between 2200 ksi and 2900 ksi, which indicates fair quality. These results suggest the PSPA USW is a useful tool for assessing the condition of BM.

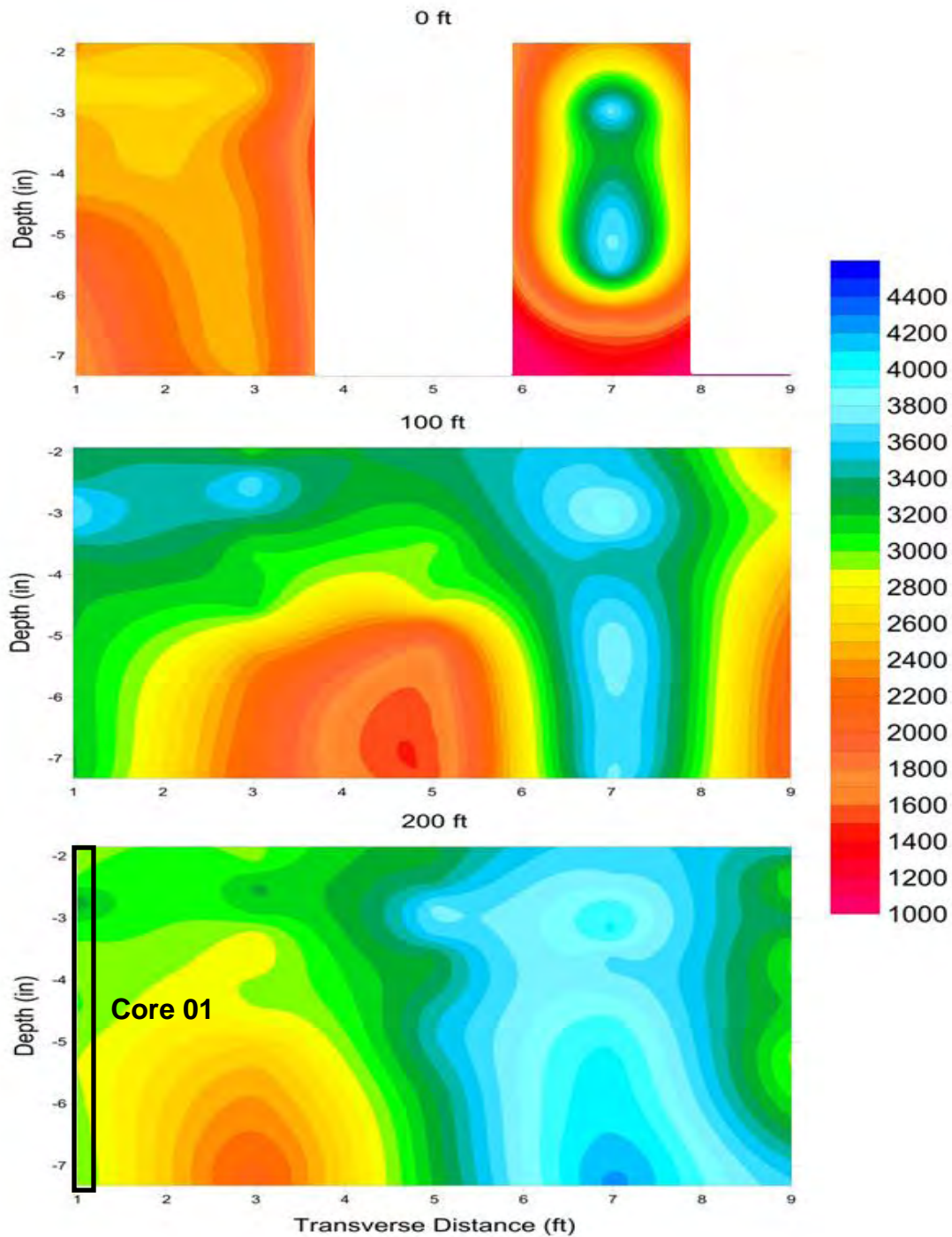


Fig. 3.37—Cross-sections depicting variations in the PSPA USW elastic modulus (ksi) of the BM at the 0 ft, 100 ft, and 200 ft intervals along the GPR traverses. The five PSPA USW data sets in each cross-section were acquired at 2 ft intervals starting 1 ft from the edge of pavement. PSPA data could not be acquired at the 5 ft and 9 ft marks on the 0 ft traverse because of the deteriorated nature of the paved surface.

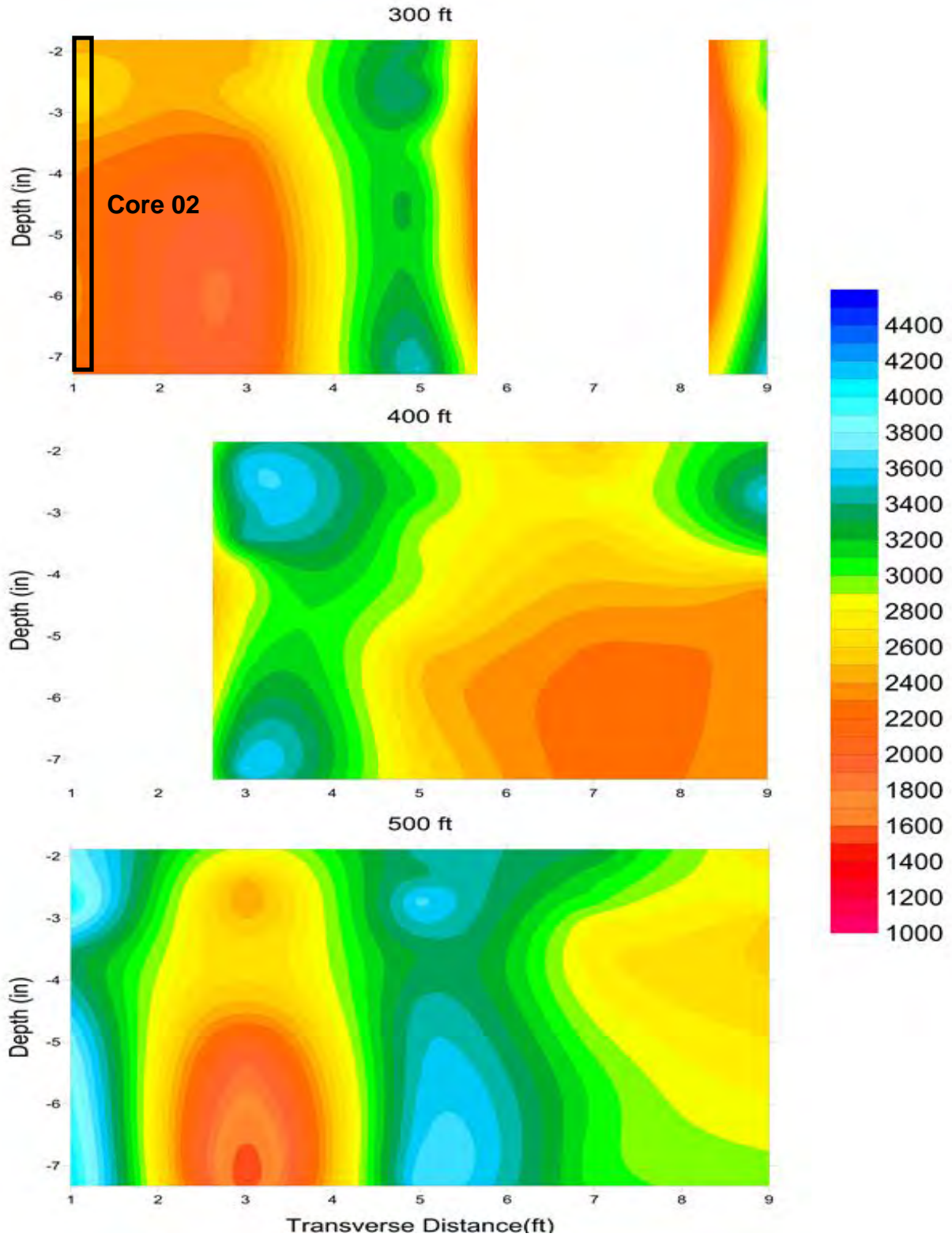


Fig. 3.38—Cross-sections depicting variations in the PSPA USW elastic modulus (ksi) of the BM at the 300 ft, 400 ft, and 500 ft intervals along the GPR traverses. PSPA data could not be acquired at several test locations because of the deteriorated nature of the paved surface.

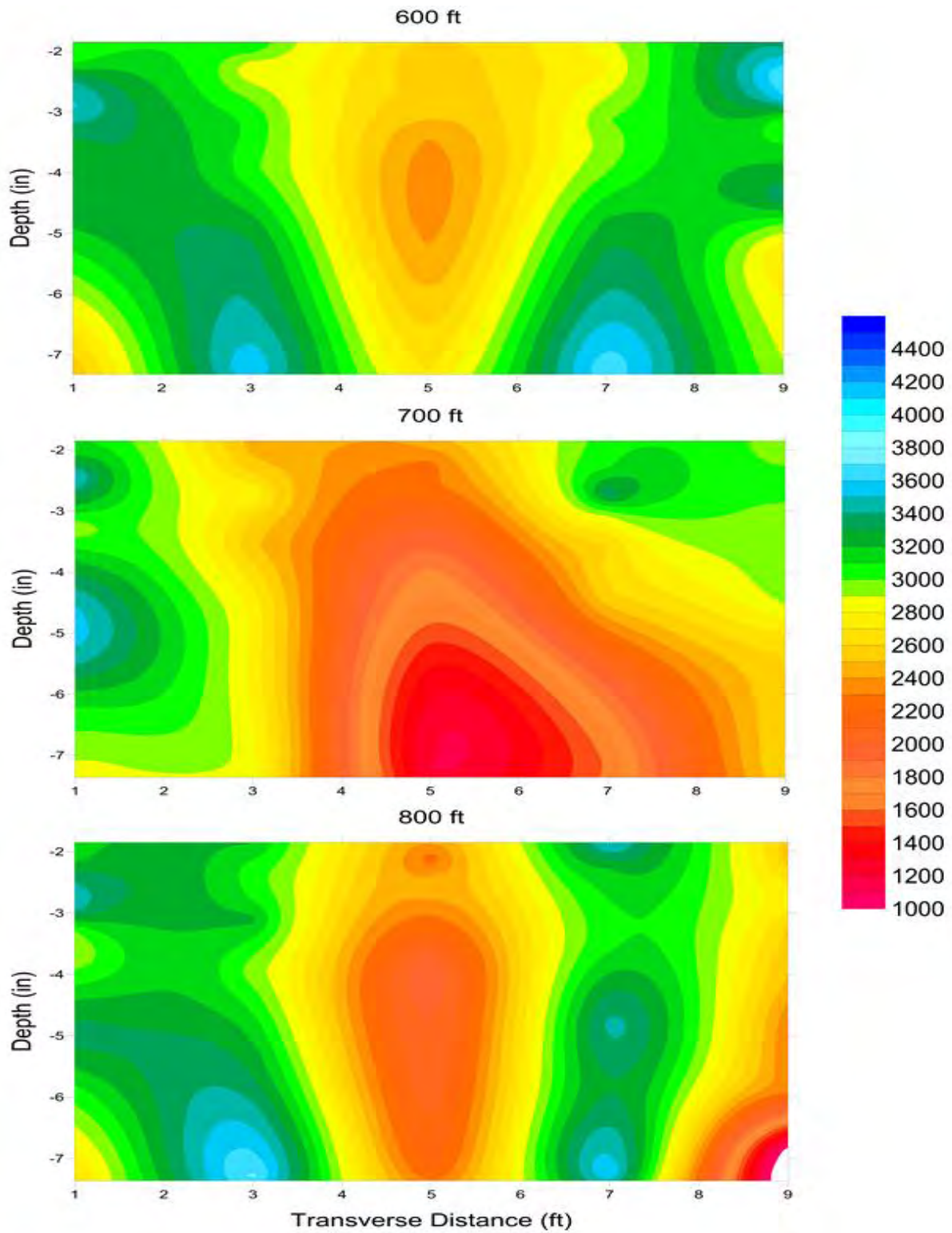


Fig. 3.39—Cross-sections depicting variations in the PSPA USW elastic modulus (ksi) of the BM at the 600 ft, 700 ft, and 800 ft intervals along the GPR traverses.

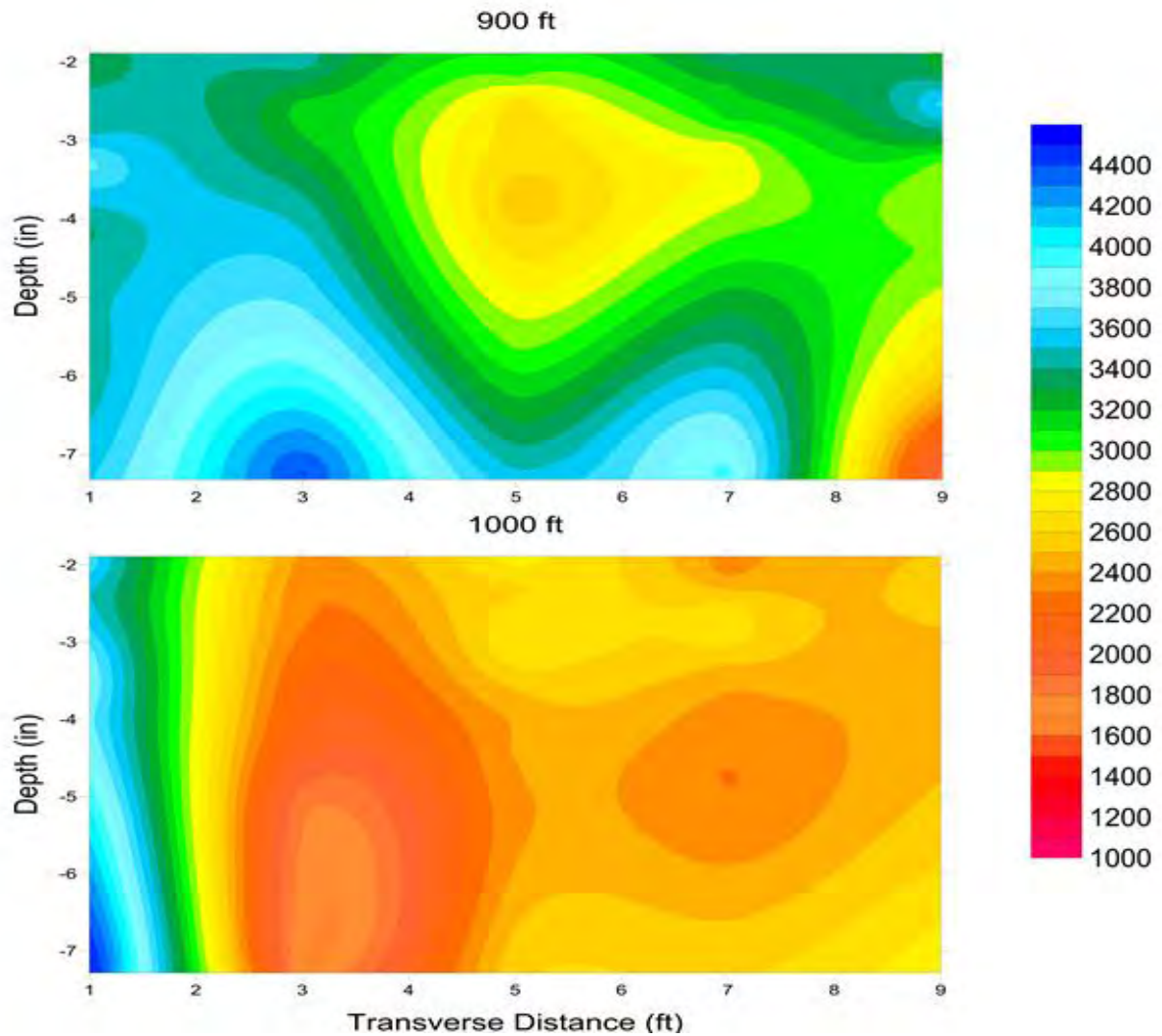


Fig. 3.40—Cross-sections depicting variations in the PSPA USW elastic modulus (ksi) of the BM at the 900 ft and 1000 ft intervals along the GPR traverses.

The average elastic modulus along each GPR transverse for the entire tested section pavement (2 in. to 7.2 in.) was calculated and plotted as Fig. 3.41. The average elastic modulus of the pavement is statistically lowest in those areas where vehicles tires are most commonly in contact with the roadway (3-5 ft and 9 ft from the outer edge of pavement).

Statistical Analysis Diagram

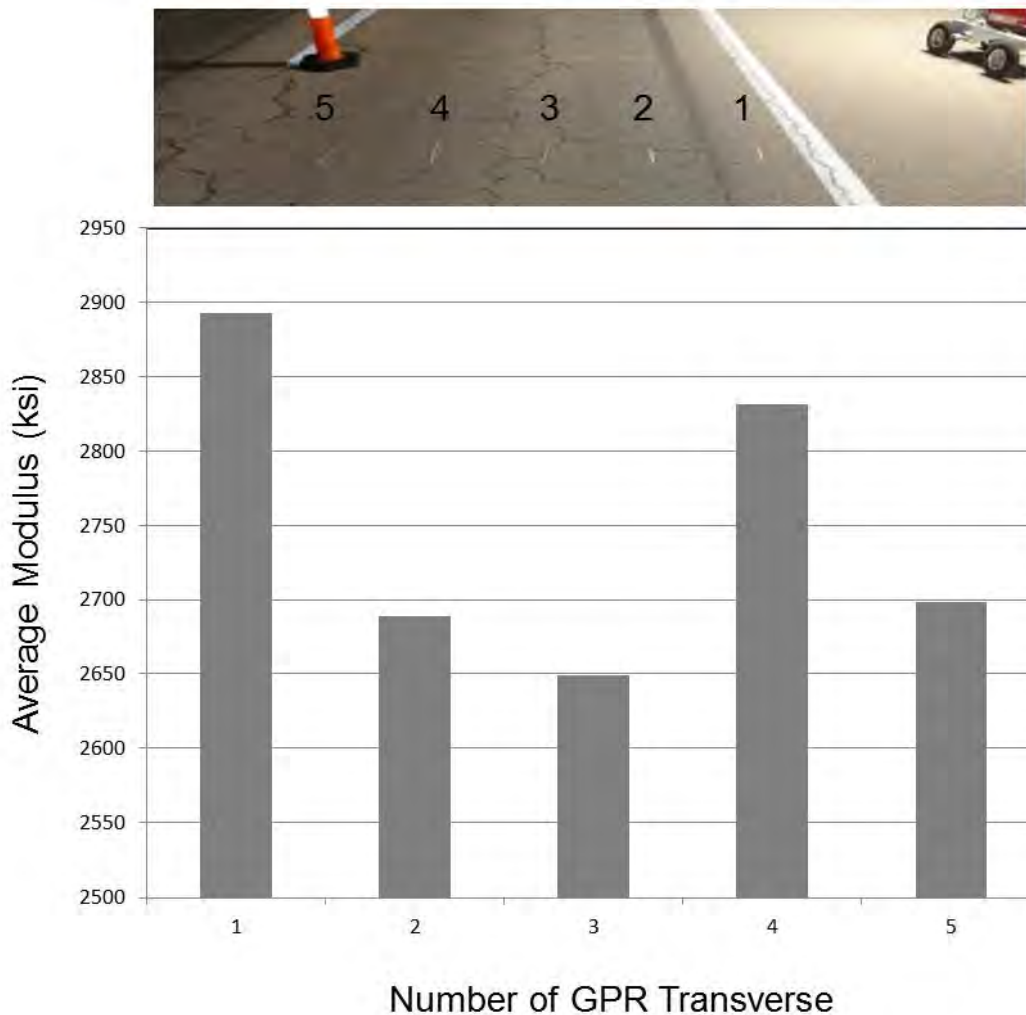


Fig. 3.41—Plot of the average elastic modulus (over depth range of 2 in. to 7.2 in.) along each GPR transverse. The GPR traverses are spaced at 2 ft intervals. GPR traverse 1 is 1 ft from the outer edge of the pavement.

3.3.3.2 Impact Echo Data

IE data were acquired at each Site 3 PSPA test location (Fig. 3.32). The PSPA IE software automatically analyzed the amplitude spectrum of the acoustic data recorded by the near receiver transducer at each test location and identified a single peak on each amplitude spectra. These peak frequencies (Fig. 3.5) were interpreted as resonant frequencies. The depths to the corresponding reflectors were calculated using Eq. 3.3 (Section 3.2.2.2).

The PSPA software consistently identified a single peak frequency on the IE data acquired at Site 3. The PSPA output calculated depth to the corresponding reflector varied from 2 in. to 6 in. (Fig. 3.42). These reflectors could be flaws (debonded interfaces; zones of significant stripping) within the BM.

The compressional wave velocity used in Eq. 3.3 was calculated using Eq. 3.1 (Section 3.2.2.1). The compressional wave velocity (V_p) calculated using Eq. 3.1 is a function of the average surface wave velocity (V_R) of the upper approx. 7.2 in. of pavement.

The wide variation in calculated reflector depths could be due to variations in the depths to the respective flaws. However, it could also be caused, in part, by the fact that compressional waves travel along near-vertical paths, whereas the Rayleigh waves propagate laterally through the anisotropic pavement.

In summary, the PSPA IE tool was unable to estimate the thickness of the asphalt with a reasonable degree of reliability and consistency. However, the PSPA IE tool might have been able to identify the depths to the shallowest flaw (debonded interface or zone of significant stripping) at each PSPA test location.

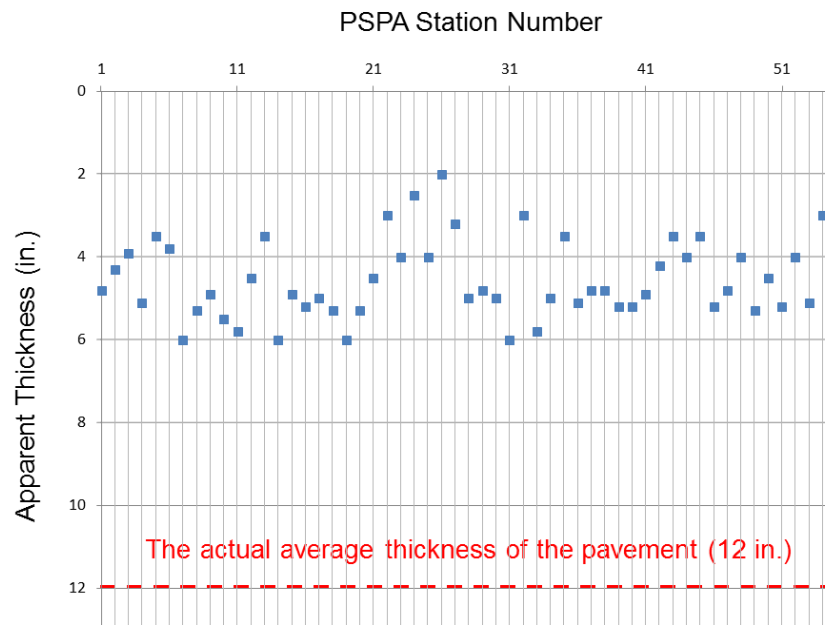


Fig. 3.42—The PSPA IE calculated depth to shallowest identified reflector is plotted for all PSPA test locations (Fig. 3.32).

3.3.4 Project-Level Site 4 (HWY AT)

Project-level Site 4 is located along HWY AT in Franklin County, near Missouri US 63 (Fig. 3.43). The pavement consisted of AC overlay (variable thickness) over 6 in. of PCC. The top BM layer displayed visible evidence of surface cracks. The average air temperature during field data acquisition at the test site was 70 °F.

Sixty-six (66) PSPA data sets and nine (9) cores were acquired at Site 4 (Fig. 3.44). The PSPA data were acquired using a 6 in. transducer spacing. Hence, the USW modulus plots

extend from a depth of 3 in. to a depth of approximately 11 in. (Fig. 3.45). PSPA data were not acquired in immediate proximity to all core locations.



Fig. 3.43—Photograph of PSPA tool placed on pavement at project-level Site 4 (HWY AT).

3.3.4.1 Ultrasonic Surface Wave Data

In this report, the project-level pavement Site 4 PSPA USW elastic modulus data are presented in 1-D plot format and in 2-D plot format.

PSPA data acquired in proximity to core locations 01, 02, 07, and 09 (Fig. 3.44) are presented in 1-D plot format to illustrate the utility and limitations of the PSPA tool. Stripped core 01 and the corresponding PSPA elastic modulus plot are shown in Fig. 3.45. The average elastic modulus of the BM is 1160 ksi which corresponds to fair quality at 70 °F (Table 3.2).

Debonded and stripped core 01 and the corresponding PSPA elastic modulus plot are shown in 5. The core is comprised of approximately 14 in. of BM. The average elastic modulus of the PCC is 729 ksi which corresponds to poor quality at 70 °F (Table 3.2). The average “apparent” elastic modulus of the PCC is 609 ksi. This extremely low “apparent” average elastic modulus means the PCC is severely deteriorated (Table 3.1).

Debonded and stripped core 02 and the corresponding PSPA elastic modulus plot are shown in Fig. 3.46. The core is comprised of approximately 8 in. of BM overlay and 6 in. of underlying PCC. The average elastic modulus of the BM is 729 ksi which corresponds to poor quality at 70 °F (Table 3.2). The average “apparent” elastic modulus of the PCC is 609 ksi. This extremely low “apparent” average elastic modulus means the PCC is severely deteriorated (Table 3.1).

Debonded and stripped core 07 and the corresponding PSPA elastic modulus plot are shown in Fig. 3.47. The core is comprised of approximately 7 in. of BM overlay and 6 in. of underlying PCC. The average elastic modulus of the BM is 885 ksi which corresponds to poor quality at 70 °F (Table 3.2). The average “apparent” elastic modulus of the PCC is 702 ksi. This

extremely low “apparent” average elastic modulus means the PCC is severely deteriorated (Table 3.1).

Debonded and stripped core 09 and the corresponding PSPA elastic modulus plot are shown in Fig. 3.48. The core is comprised of approximately 4 in. of BM overlay and 6 in. of underling PCC. The average elastic modulus of the BM is 507 ksi, which corresponds to poor (almost severely deteriorated) quality at 70 °F (Table 3.2). The average “apparent” elastic modulus of the PCC is 594 ksi. This extremely low “apparent” average elastic modulus means the PCC is severely deteriorated (Table 3.1).

The elastic modulus data acquired at Site 4 is displayed in cross-section format in Fig. 3.49-3.52. As shown in Fig. 3.45-3.48, the thickness of the BM overlay is highly variable. Therefore, while most the elastic modulus values presented in Fig. 3.49-3.52 are those of BM overlay, some of the values (especially at greater depths) are “apparent” elastic modulus values for the underlying PCC. The elastic modulus values displayed in Figs. 3.49-3.52 are herein referred to as elastic modulus because the depth to the BM/PCC contact is known at only a few core locations.

The acquired core control is consistent with elastic modulus data. More specifically: 1) the location of debonded and stripped core 01 (Fig. 3.49) is characterized by an average elastic modulus value of less than 1000 ksi, which indicates poor quality; 2) the elastic modulus at the locations of debonded and stripped core 03 and 04 (Fig. 3.50) are characterized by average elastic modulus values of less than 1000 ksi, which indicates poor quality; 3) the elastic moduli near the locations of debonded and stripped cores 08 and 09 (Figure 44) are characterized by average elastic modulus values less than 1000 ksi which indicates poor quality.

The acoustic interface between the BM and PCC cannot be confidently identified on the modulus plots, presumably because there is not a uniformly statistically significant difference between the modulus of the BM and the apparent modulus of the underlying PCC. However, the study results suggest the PSPA USW is a useful tool for assessing the condition of BM.

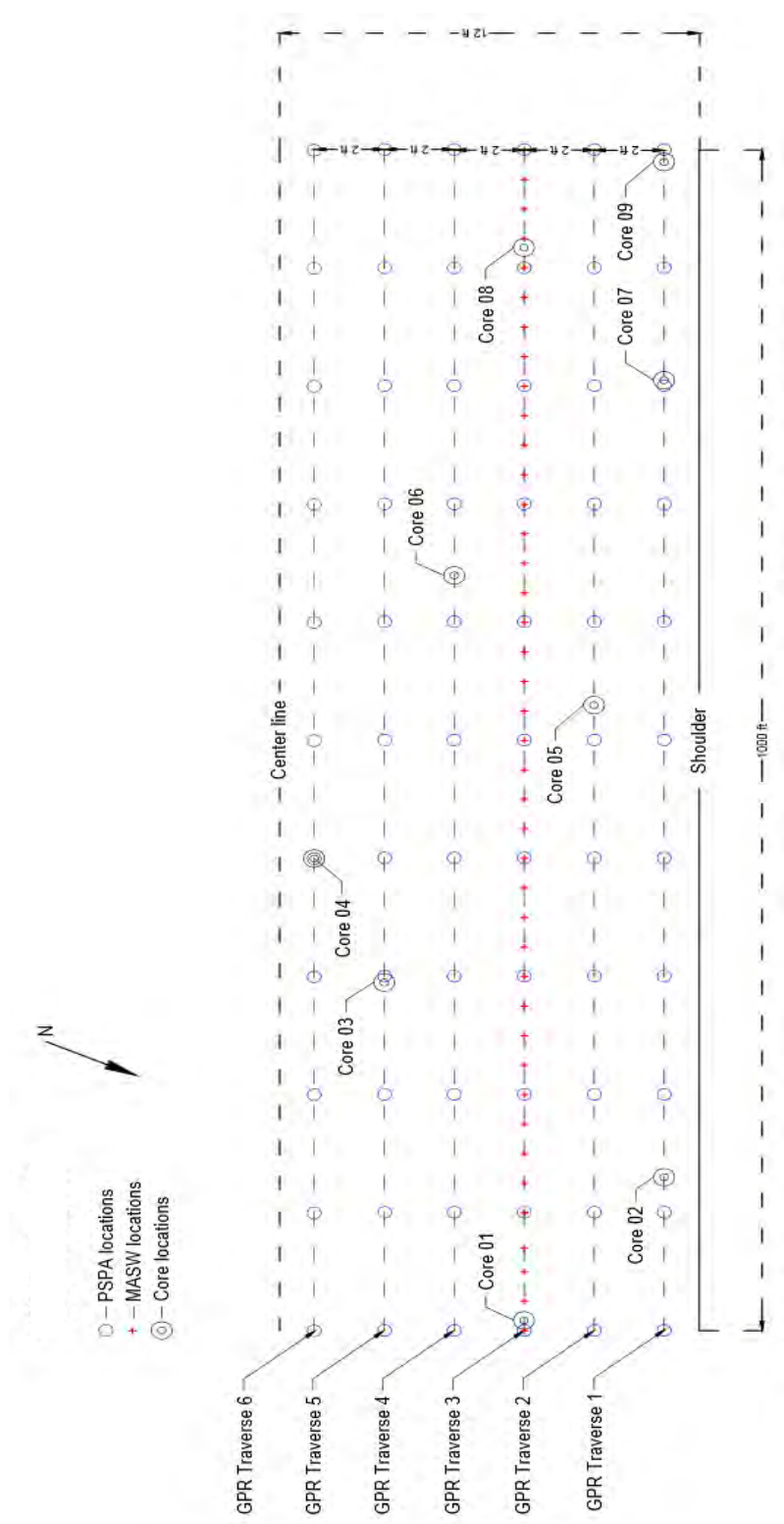


Fig. 3.44—Base map for project-level Site 4 showing PSPA test locations and core locations. PSPA data were acquired at 100 ft intervals along each GPR traverse. GPR traverse 1 was located 1 ft from the outer edge of the paved driving lane (shoulder). Only cores 01, 03, 04, and 07 are located within 5 ft of a PSPA location.

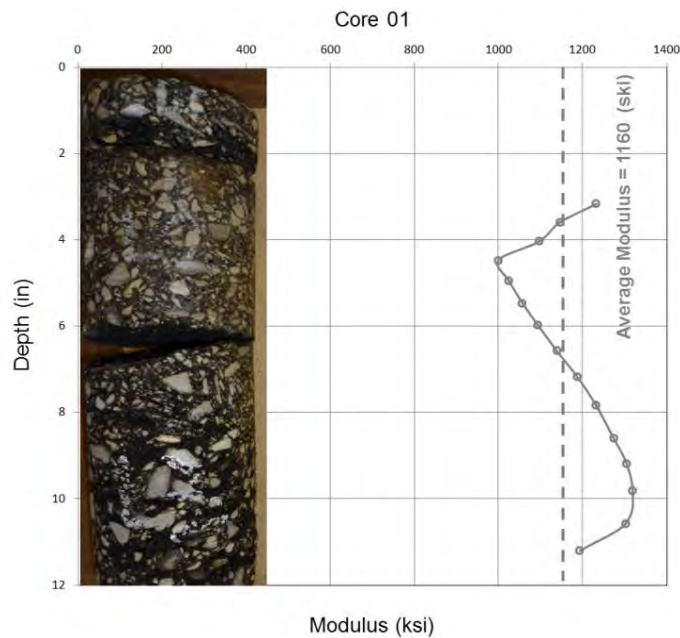


Fig. 3.45—Elastic modulus plot generated from PSPA USW data acquired in immediate proximity to stripped core 01 (Fig. 3.44). The PSPA USW average elastic modulus for core 01 is 1160 ksi indicating the BM is fair quality (at an air temperature of 70 °F, Table 3.2).

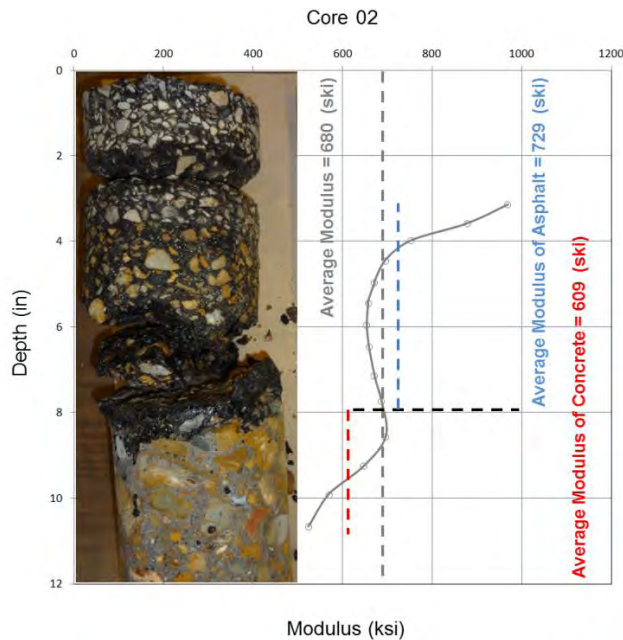


Fig. 3.46—Elastic modulus plot generated from PSPA USW data acquired within 25 ft of debonded and stripped core 02 (Fig. 3.44). The core is comprised of approx. 8 in. of BM overlay and 6 in. of underlying PCC. The average elastic modulus of the BM is 729 ksi which corresponds to poor quality at 70 °F (Table 3.2). The average “apparent” elastic modulus of the PCC is 609 ksi. This extremely low “apparent” average elastic modulus means the PCC is severely deteriorated (Table 3.1).

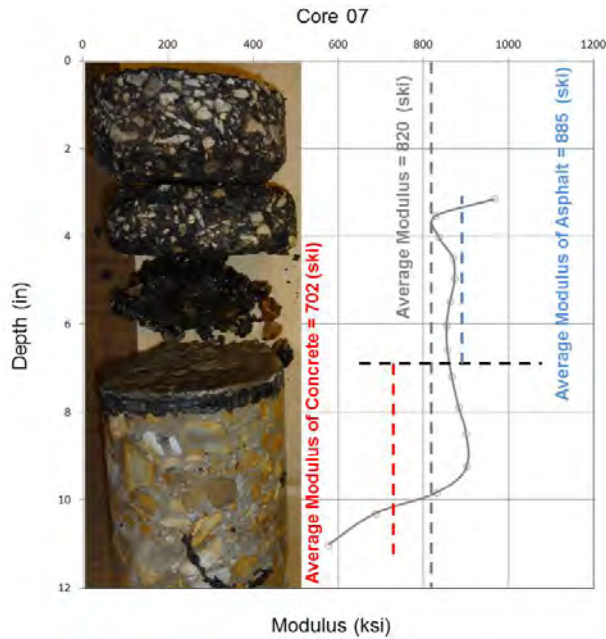


Fig. 3.47—Elastic modulus plot generated from PSPA USW data acquired in immediate proximity to debonded and stripped core 07 (Fig. 3.44). The core is comprised of approx. 7 in. of BM overlay and 6 in. of underlying PCC. The average elastic modulus of the BM is 885 ksi which corresponds to poor quality at 70 °F (Table 3.2). The average “apparent” elastic modulus of the PCC is 702 ksi. This extremely low “apparent” average elastic modulus means the PCC is severely deteriorated (Table 3.1).

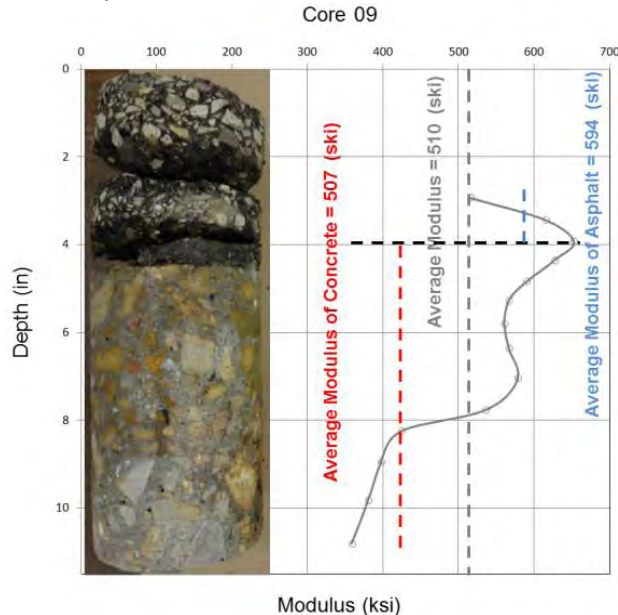


Fig. 3.48—Elastic modulus plot generated from PSPA USW data acquired in immediate proximity to debonded and stripped core 09 (Fig. 3.44). The core is comprised of approx. 4 in. of BM overlay and 6 in. of underlying PCC. The average elastic modulus of the BM is 594 ksi which corresponds to poor quality at 70 °F (Table 3.2). The average “apparent” elastic modulus of the PCC is 507 ksi. This extremely low “apparent” average elastic modulus means the PCC is severely deteriorated (Table 3.1).

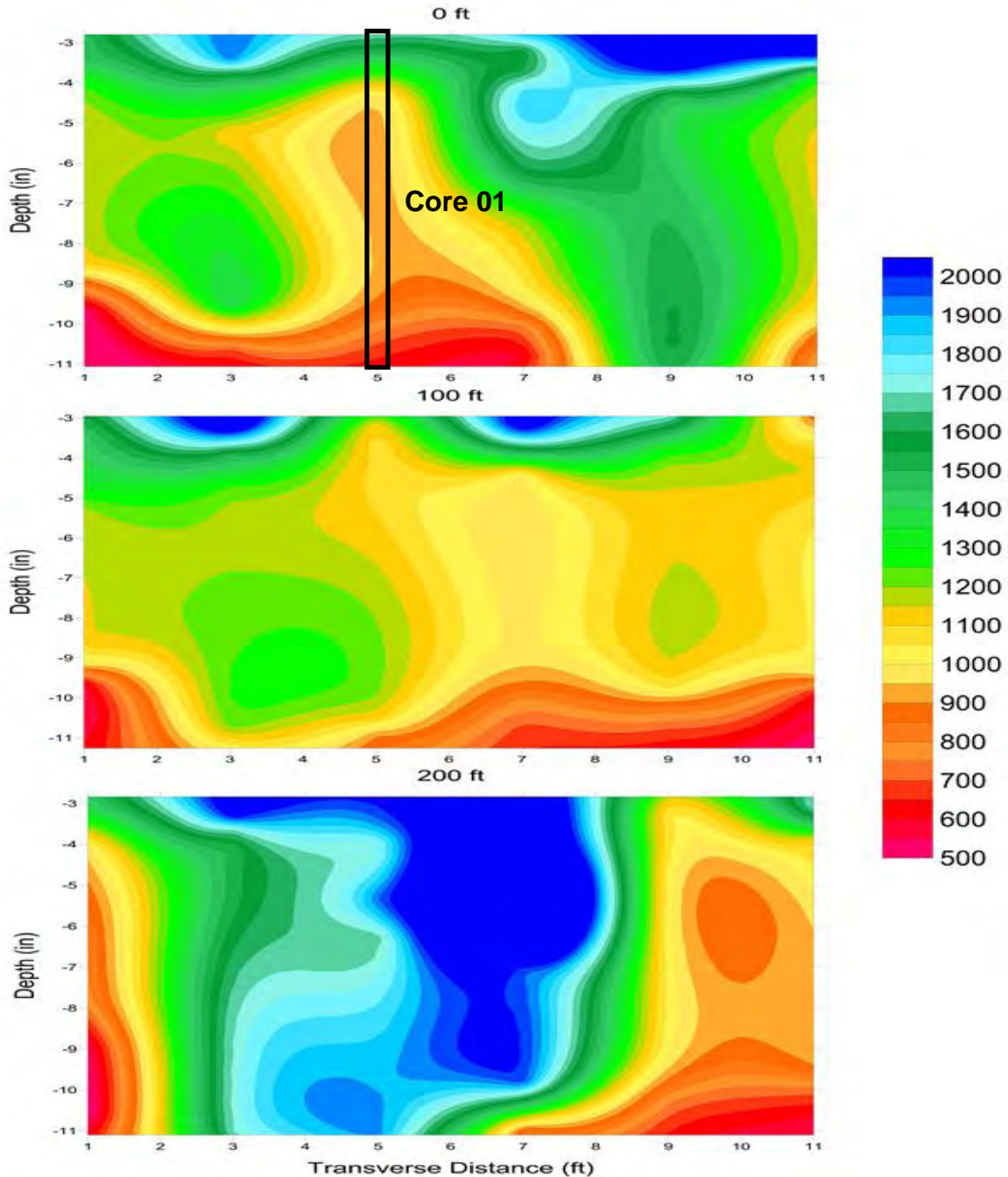


Fig. 3.49—Cross-sections depicting variations in the PSPA USW elastic modulus (ksi) of the pavement at the 0 ft, 100 ft, and 200 ft intervals along the GPR traverses. The six PSPA USW data sets in each cross-section were acquired at 2 ft intervals starting 1 ft from the edge of pavement. The pavement at Site 4 is comprised of BM of variable thickness and underlying PCC. Inasmuch as the thickness of the BM is unknown at most PSPA test locations, no attempt has been made to differentiate the elastic modulus values of the overlying AC from the “apparent” elastic modulus of the underlying PCC.

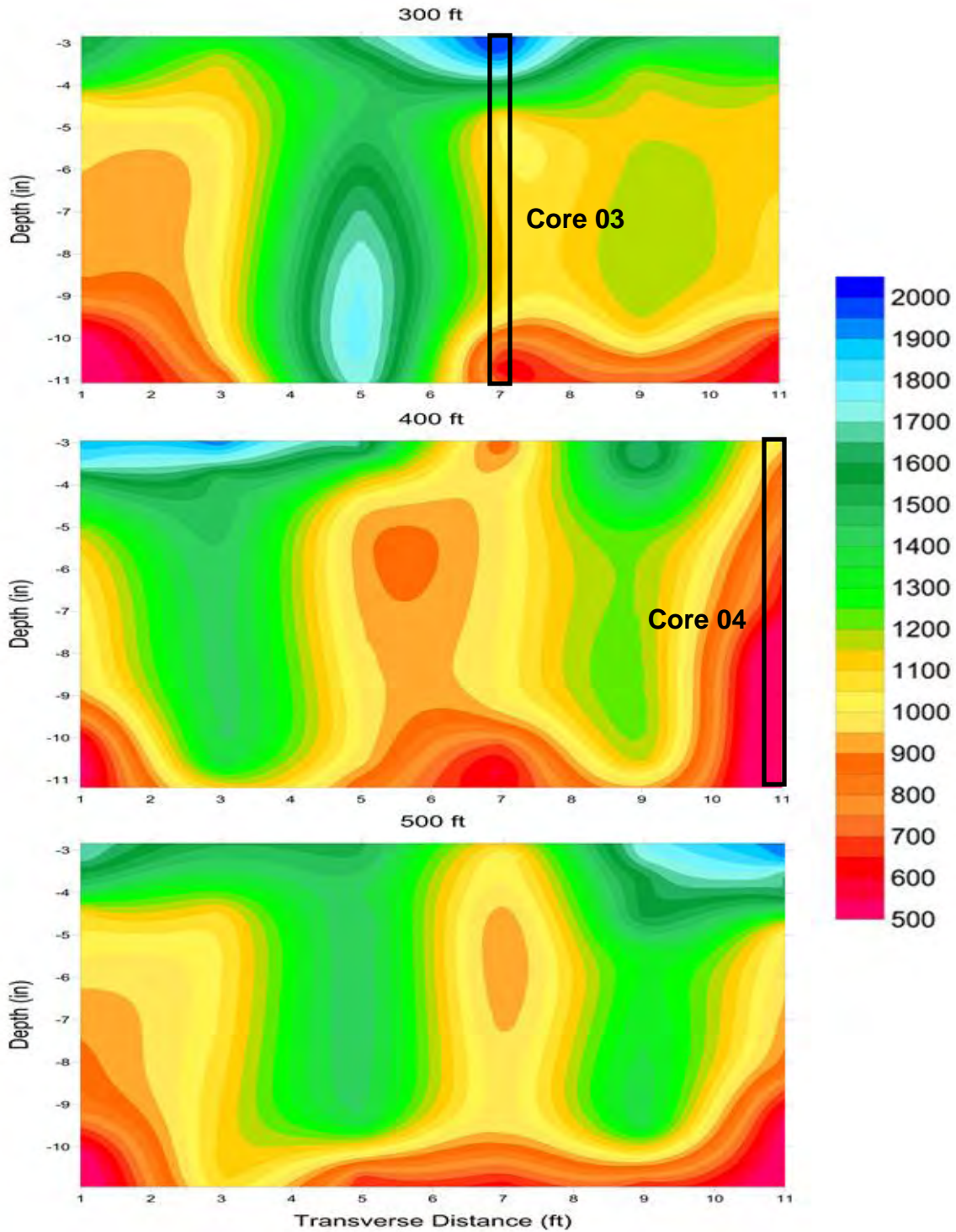


Fig. 3.50—Cross-sections depicting variations in the PSPA USW elastic modulus (ksi) of the pavement at the 300 ft, 400 ft, and 500 ft intervals along the GPR traverses. No attempt has been made to differentiate the elastic modulus values of the overlying BM from the “apparent” elastic modulus of the underlying PCC.

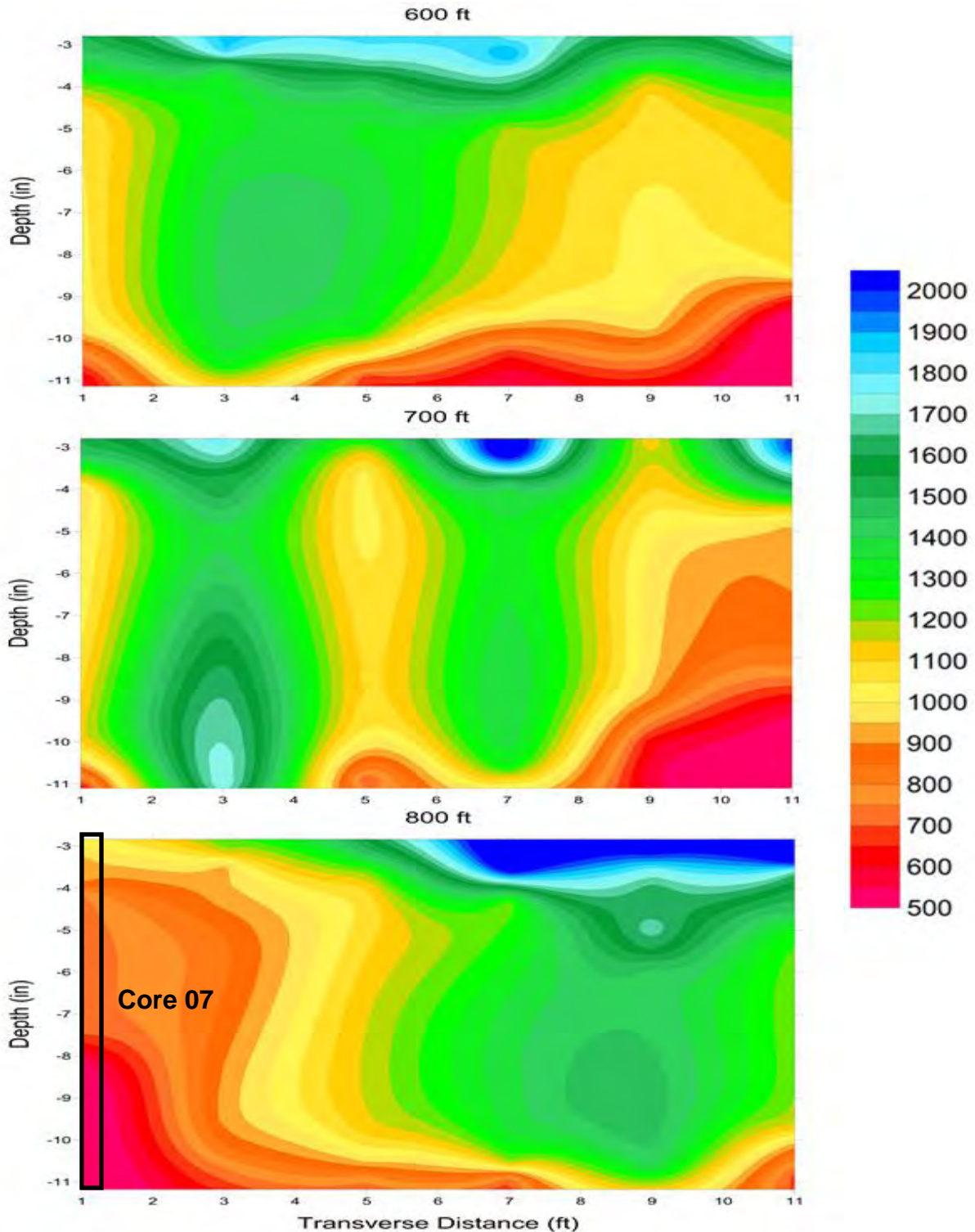


Fig. 3.51—Cross-sections depicting variations in the PSPA USW elastic modulus (ksi) of the pavement at the 600 ft, 700 ft, and 800 ft intervals along the GPR traverses. No attempt has been made to differentiate the elastic modulus values of the overlying BM from the “apparent” elastic modulus of the underlying PCC.

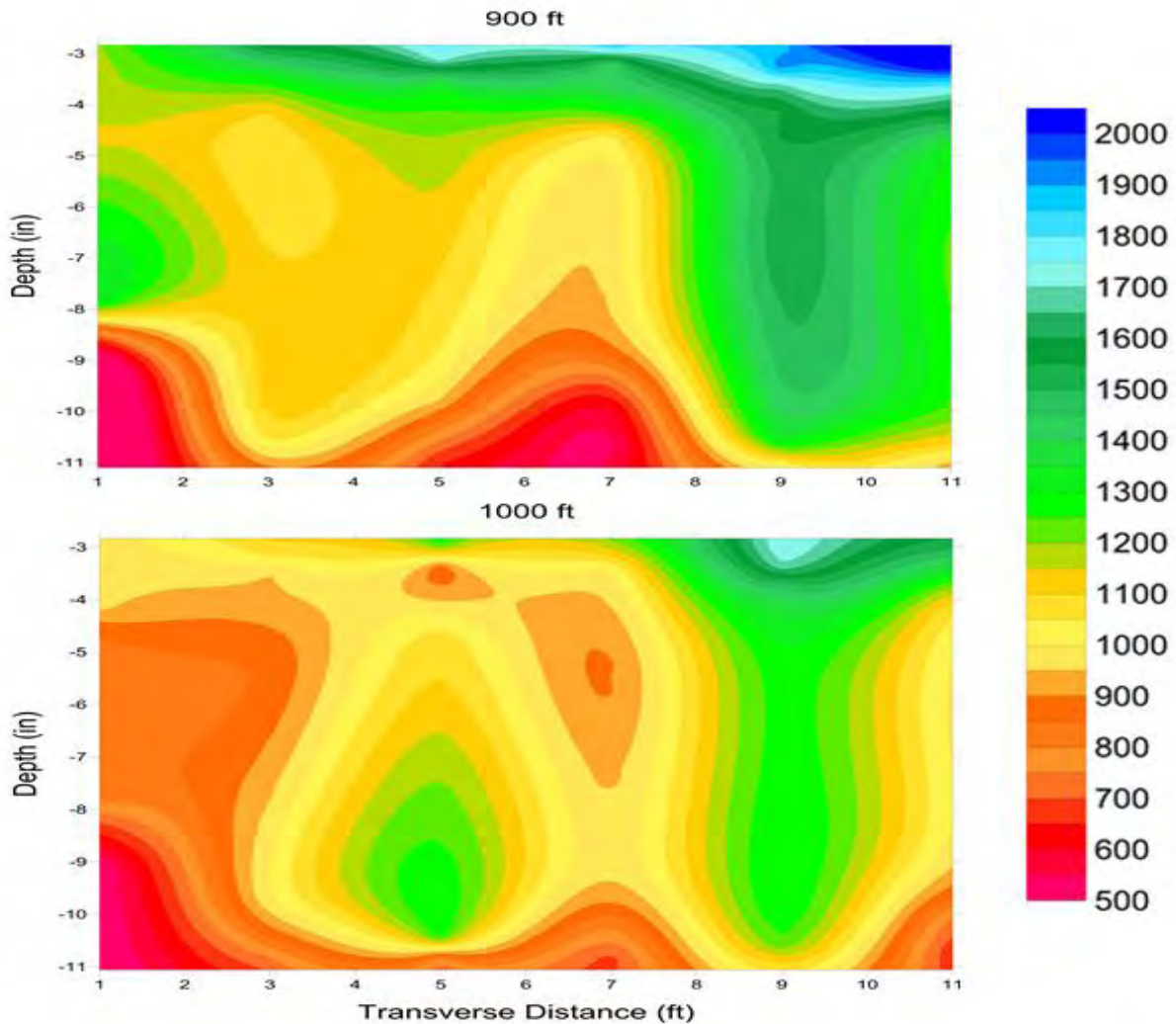


Fig. 3.52—Cross-sections depicting variations in the PSPA USW elastic modulus (ksi) of the pavement at the 300 ft, 400 ft, and 500 ft intervals along the GPR traverses. No attempt has been made to differentiate the elastic modulus values of the overlying BM from the “apparent” elastic modulus of the underlying PCC.

The average elastic modulus along each GPR transverse for the entire tested section pavement (3 in. to 11 in.) was calculated and plotted in Fig. 3.53. The average elastic modulus of the pavement does not appear to be statistically lowest in those areas where vehicles tires are most commonly in contact with the roadway.

Statistical Analysis Diagram

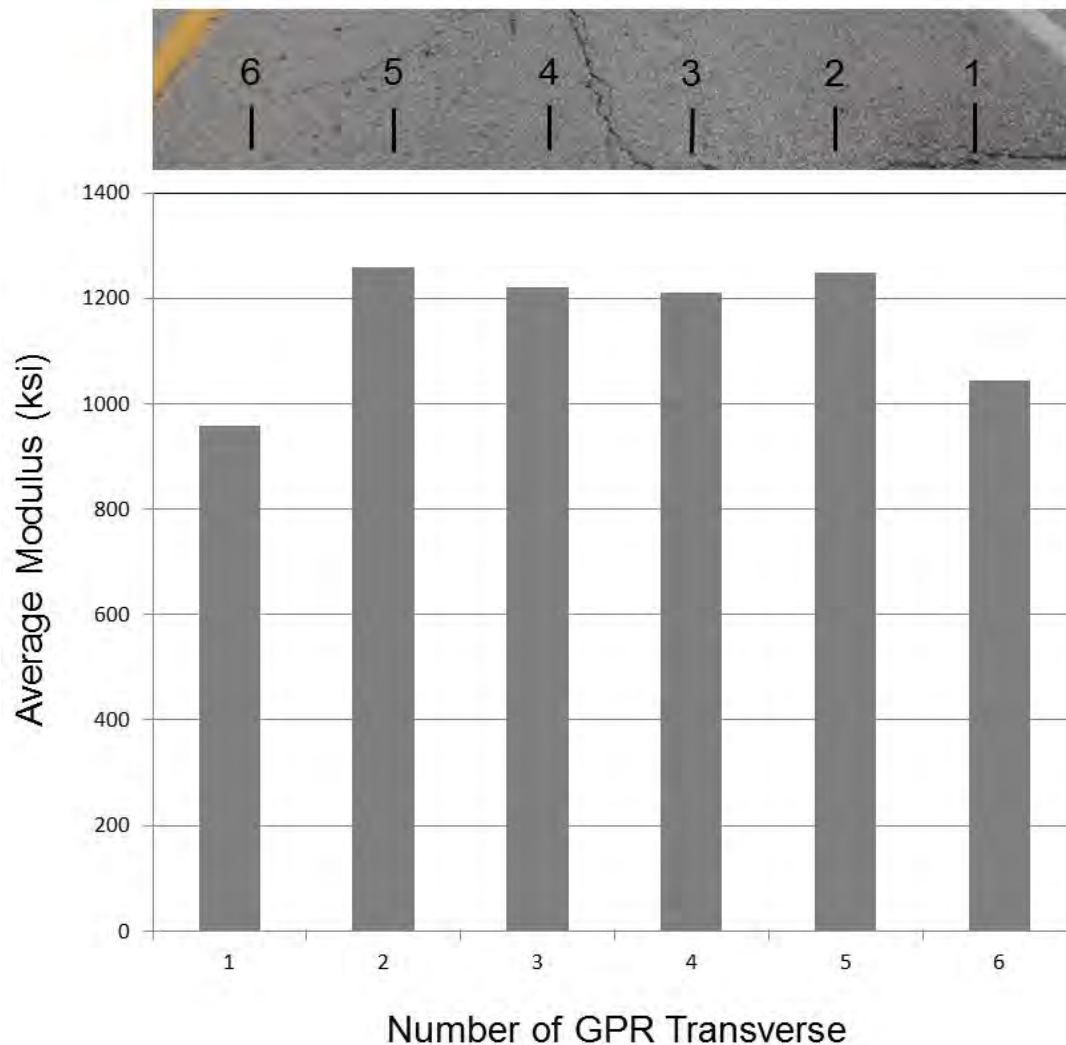


Fig. 3.53—Plot of the average elastic modulus (over depth range of 3 in. to 11 in.) along each GPR transverse. The GPR traverses are spaced at 2 ft intervals. GPR traverse 1 is 1 ft from the outer edge of the pavement.

3.3.4.2 Impact Echo Data

IE data were acquired at each Site 4 PSPA test location (Fig. 3.44). The PSPA IE software automatically analyzed the amplitude spectrum of the acoustic data recorded by the near receiver transducer at each test location and identified a single peak on each amplitude spectra. These peak frequencies (Fig. 3.5) were interpreted as resonant frequencies. The depths to the corresponding reflectors were calculated using Eq. 3.3 (Section 3.3.1.2).

The PSPA software consistently identified a single peak frequency on the IE data acquired at Site 4. The PSPA output calculated depth to the corresponding reflector varied from 12 in. to 15 in. (Figure 42). This reflector probably represents the base of pavement.

The compressional wave velocity used in Eq. 3.3 was calculated using Eq. 3.1 (Section 3.3.1.1). The compressional wave velocity (V_p) calculated using Eq. 3.1 is a function of the average surface wave velocity (V_R) of the upper approx. 11 in. of pavement.

The wide variation in calculated reflector depths can be attributed, in part, to the fact that compressional waves travel along near-vertical paths, whereas the Rayleigh waves propagate laterally through the anisotropic pavement. Also, the compressional wave velocity (as per Eq. 3.1) was calculated on the assumption the entire paved section is BM.

In summary, the PSPA IE tool was unable to accurately estimate the thickness of either the BM or entire paved section with a reasonable degree of reliability and consistency.

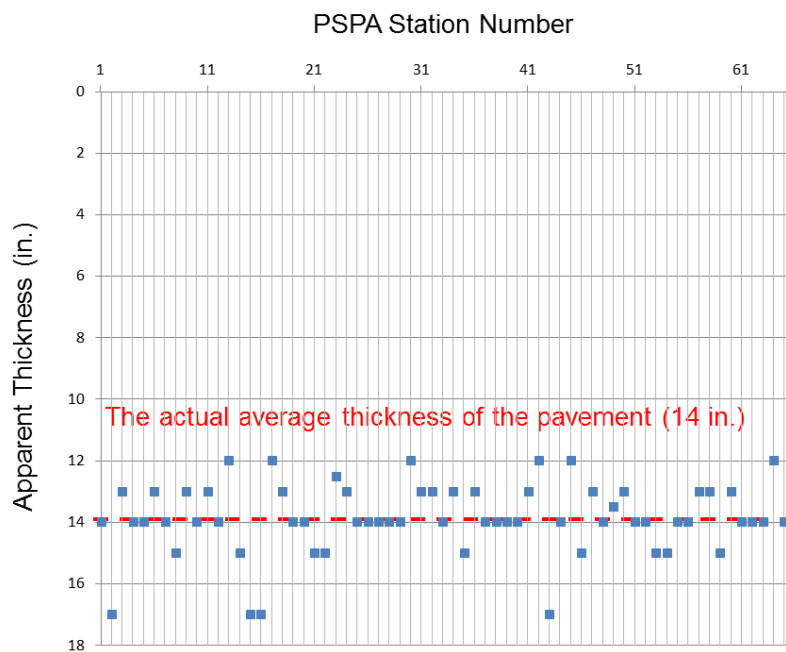


Fig. 3.54–The apparent thickness measurements for the pavement.

3.3.5 Project-Level Site 5 (I-55 Pemiscot Co.)

Project-level Site 5 is located along the north bound lane of interstate I-55 in southeast Missouri (Fig. 3.55). The tested pavement consists of 8.5 in. of PCC overlay above an 8.75 in. thick PCC layer. An approximately 2.5 in. thick layer of BM is embedded between the two PCC layers. The top PCC layer displayed no visible evidence of surface cracks. The average air temperature during field data acquisition at the test site was 77 °F.

Fifty-five (55) PSPA data sets and eight (8) cores were acquired at Site 5 (Fig. 3.2 and Fig. 3.56). The PSPA data were acquired using a 6 in. transducer spacing. Hence, the USW modulus plot extends from a depth of 3 in. to a depth of approximately 11 in. (Fig. 3.8). PSPA data were not acquired in immediate proximity to all core locations.



Fig. 3.55—Photograph of PSPA tool placed on pavement at project-level Site 5 (I-55 N).

3.3.5.1 Ultrasonic Surface Wave Data

In this report, the project-level pavement Site 5 PSPA USW elastic modulus data are presented in 1-D plot format and in 2-D plot format.

PSPA data acquired in proximity to core locations 01, 02, 06 and 08 (Fig. 3.56) are presented in 1-D format to illustrate the utility and limitations of the PSPA tool. Core 01 and the corresponding PSPA elastic modulus plot are shown in Fig. 3.57. Core 01 consists of 8.5 in. of PCC overlay above an 8.75 in. thick PCC layer. A 2.5 in. thick layer of BM is embedded between the two PCC layers. The upper layer of PCC and the underlying AC were debonded. The upper layer of PCC showed visible evidence of physical degradation. The elastic modulus plot of tested depth corresponding to core 01 (Fig. 3.57) can be divided into two layers based on the type of pavement: overlying BM and underlying PCC. The average elastic modulus of the overlying PCC layers is 4200 ksi indicating concrete is fair quality (Table 3.2). Note that the elastic modulus of the concrete decreases significantly at the debonded PCC/BM acoustic interface. The average “apparent” elastic modulus of the underlying BM layers is 2649 ksi indicating the BM is good quality (Table 3.2), but poorer quality than the BM at core locations 04 and 07.

The elastic modulus plot of tested depth corresponding to core 02 (Fig. 3.58) can be divided into two layers based on the type of pavement: overlying PCC and underlying BM. The

average elastic modulus of the overlying PCC layers is 4545 ksi indicating concrete is fair quality (Table 3.2). Note that the elastic modulus of the concrete decreases significantly immediately above the debonded PCC/BM interface. The average “apparent” elastic modulus of the underlying BM layers is 3171 ksi indicating the BM is good quality (Table 3.2). (It should be noted that “apparent” elastic modulus values for BM are calculated here based on properties for PCC, which explains the magnitude of this value.)

The elastic modulus plot of tested depth corresponding to core 06 (Fig. 3.59) can be divided into two layers based on the type of pavement: overlying PCC and underlying BM. The average elastic modulus of the overlying PCC layers is 5454 ksi indicating concrete is good quality (Table 3.2). The average “apparent” elastic modulus of the underlying BM layers is 4933 ksi indicating the BM is also good quality (Table 3.2).

The elastic modulus plot of tested depth corresponding to core 08 (Fig. 3.60) can be divided into two layers based on the type of pavement: overlying PCC and underlying BM. The average elastic modulus of the overlying PCC layers is 5570 ksi indicating concrete is good quality (Table 3.2). The average “apparent” elastic modulus of the underlying BM layers is 4783 ksi indicating the BM is also good quality (Table 3.2).

The elastic modulus data acquired at Site 5 are displayed in 2-D cross-sectional format in Fig. 3.61-3.66. Each cross-section is presented in two sections (upper and lower) based on the material difference: overlying PCC and underlying BM. The cross-sections depicting the elastic modulus for PCC (depths of 2 to 8.5 in.) are shown as Fig. 3.61-3.64. The cross-sections depicting the “apparent” elastic modulus for concrete (depth of 8.5 to 11 in.) are shown as Fig. 3.65-3.67.

The location of core 03 is shown in Fig. 3.64 and Fig. 3.67. This core was not debonded at the PCC/BM interface. The elastic modulus of the PCC (Fig. 3.61) varies between 5200 ksi and 6200 ksi indicating the PCC is good quality. The apparent modulus of the BM (Fig. 3.65) varies is at this location varies between 3600 ksi and 4800 ksi indicating the BM is also good quality.

The location of core 04 is shown in Fig. 3.63 and Fig. 3.66. This core was debonded at the PCC/BM interface. The elastic modulus of the PCC (Fig. 3.63) varies between 4000 ksi and 4700 ksi indicating the PCC is fair quality. The apparent modulus of the BM (Fig. 3.66) varies is at this location varies between 2400 ksi and 4400 ksi indicating the BM is fair quality.

The location of core 05 is shown in Fig. 3.65. This core was not debonded at the PCC/BM interface. The elastic modulus of the PCC (Fig. 3.61) varies between 5400 ksi and 5900 ksi indicating the PCC is good quality. The apparent modulus of the BM (Fig. 3.65) varies is at this location varies between 5100 ksi and 5600 ksi indicating the BM is also good quality.

In summary, the test results demonstrate that the PSPA USW was a useful tool at site 05 for assessing the condition of the PCC and underling BM.

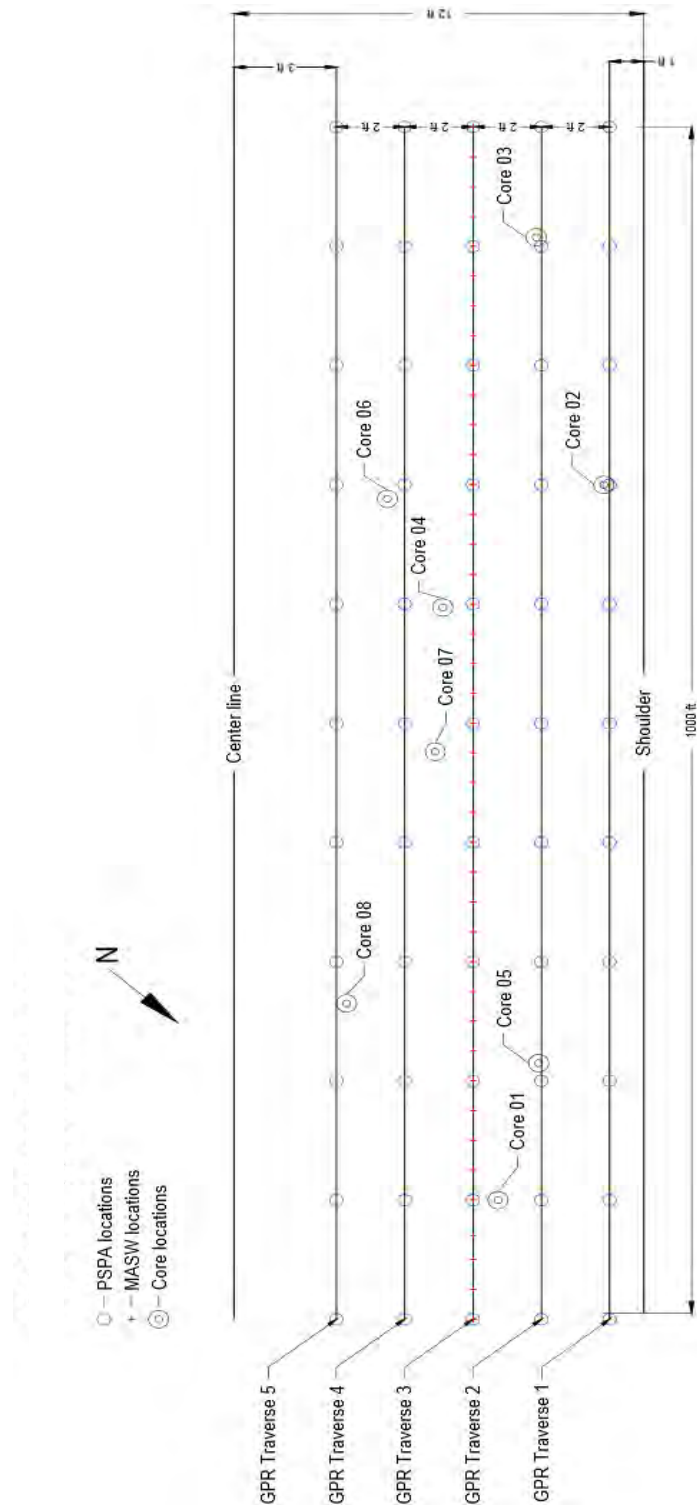


Fig. 3.56—Base map for project-level Site 5 showing PSPA test locations and core locations. PSPA data were acquired at 100 ft intervals along each GPR traverse. GPR traverse 1 was located 1 foot from the outer edge of the paved driving lane (shoulder). Only cores 01, 02, 03 and 04 are located within 5 ft of a PSPA location.

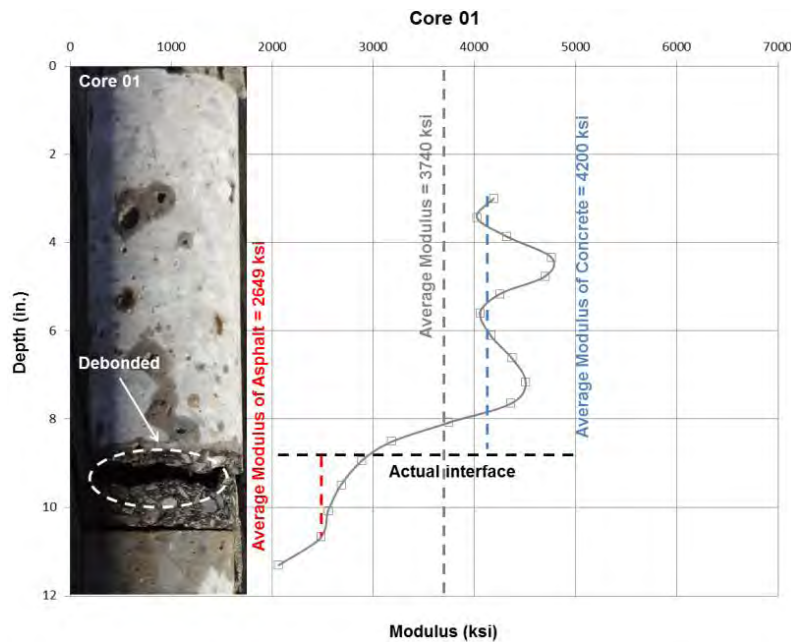


Fig. 3.57—Elastic modulus plot generated from PSPA USW data acquired in immediate proximity to debonding core 01 (Fig. 3.56). The tested pavement consists of 8.5 in. of PCC overlay above an 8.75 in. thick PCC layer. A 2.5 in. thick layer of asphalt (BM) is embedded between the two PCC layers. The upper layer of PCC and the underlying BM were debonded. The upper layer of PCC showed visible evidence of physical degradation.

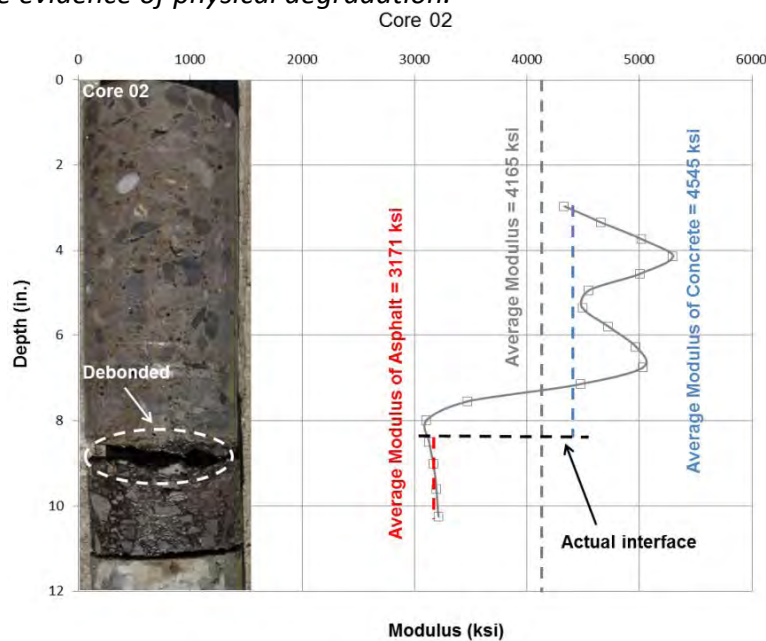


Fig. 3.58—Elastic modulus plot generated from PSPA USW data acquired in immediate proximity to stripped and debonded core 02 (Fig. 3.56). The tested pavement consists of 8.5 in. of overlay above an 8.75 in. thick PCC layer. A 2.5 in. thick layer of asphalt is embedded between the two PCC layers. The upper layer of PCC and the underlying AC were debonded. The upper layer of PCC showed visible evidence of physical degradation.

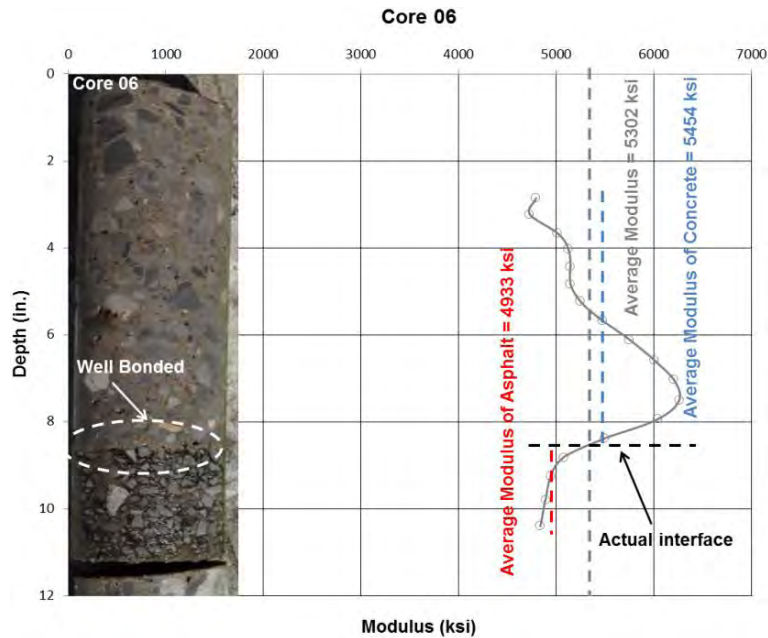


Fig. 3.59—Elastic modulus plot generated from PSPA USW data acquired in immediate proximity to intact core 06 (Fig. 3.56). The tested pavement consists of 8.5 in. of PCC overlay above an 8.75 in. thick PCC layer. A 2.5 in. thick layer of asphalt (BM) is embedded between the two PCC layers. No visible evidence of debonding was observed in core 06.

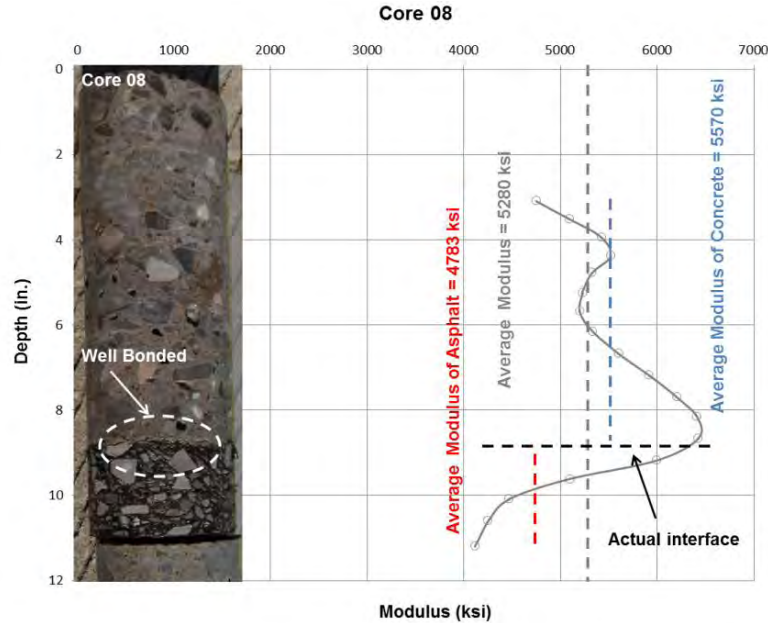


Fig. 3.60—Elastic modulus plot generated from PSPA USW data acquired in immediate proximity to intact core 08 (Fig. 3.56). The tested pavement consists of 8.5 in. of overlay above an 8.75 in. thick PCC layer. A 2.5 in. thick layer of asphalt (BM) is embedded between the two PCC layers. No visible evidence of debonding was observed in core 08.

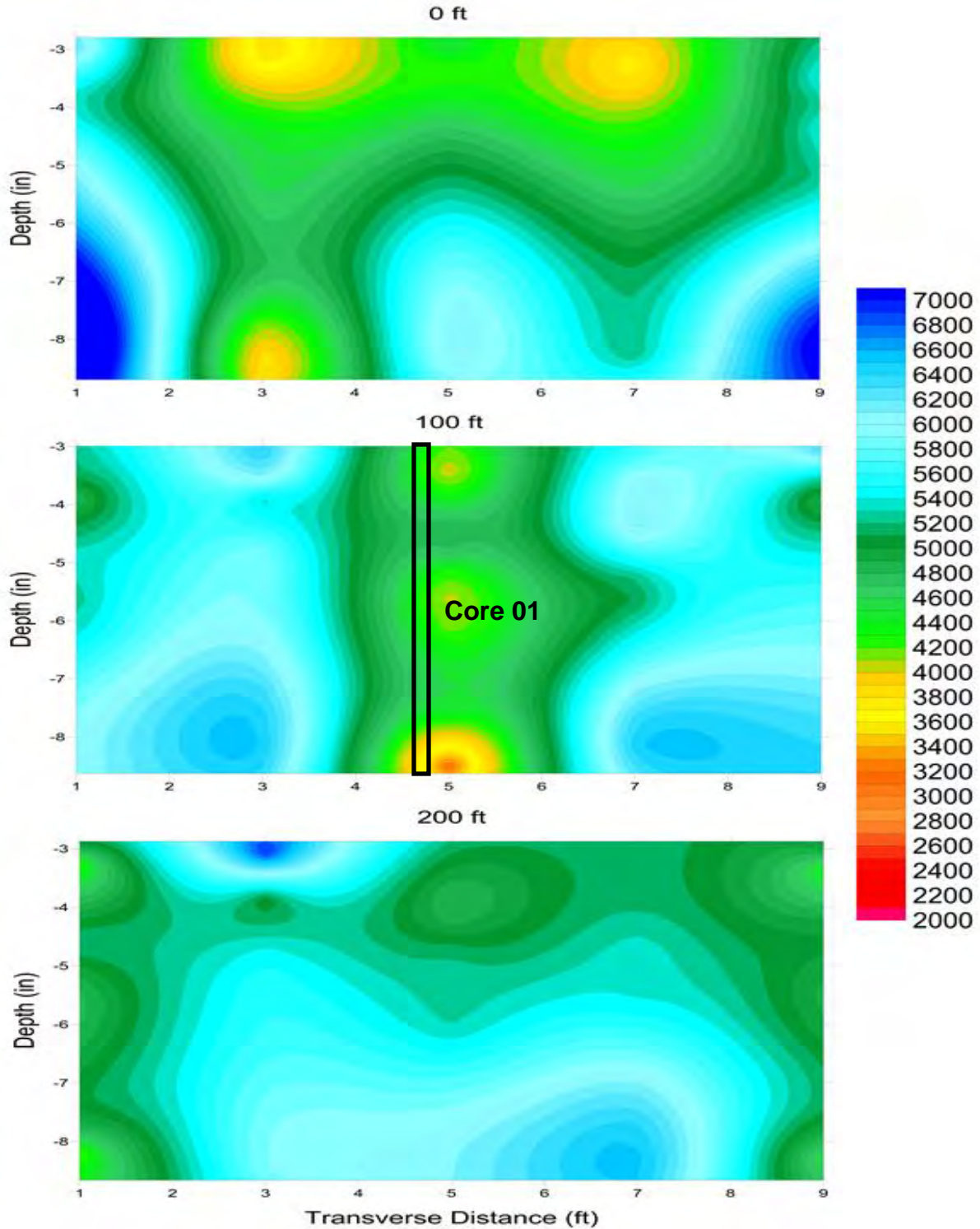


Fig. 3.61—Cross-sections depicting variations in the elastic modulus (ksi) for PCC for PSPA USW data acquired at the 0 ft, 100 ft, and 200 ft intervals along the GPR traverses. The five PSPA USW data sets in each cross-section were acquired at 2 ft intervals starting 1 ft from the edge of pavement (Fig. 3.56). Depth of investigation extends from 2 in. to 8.5 in.

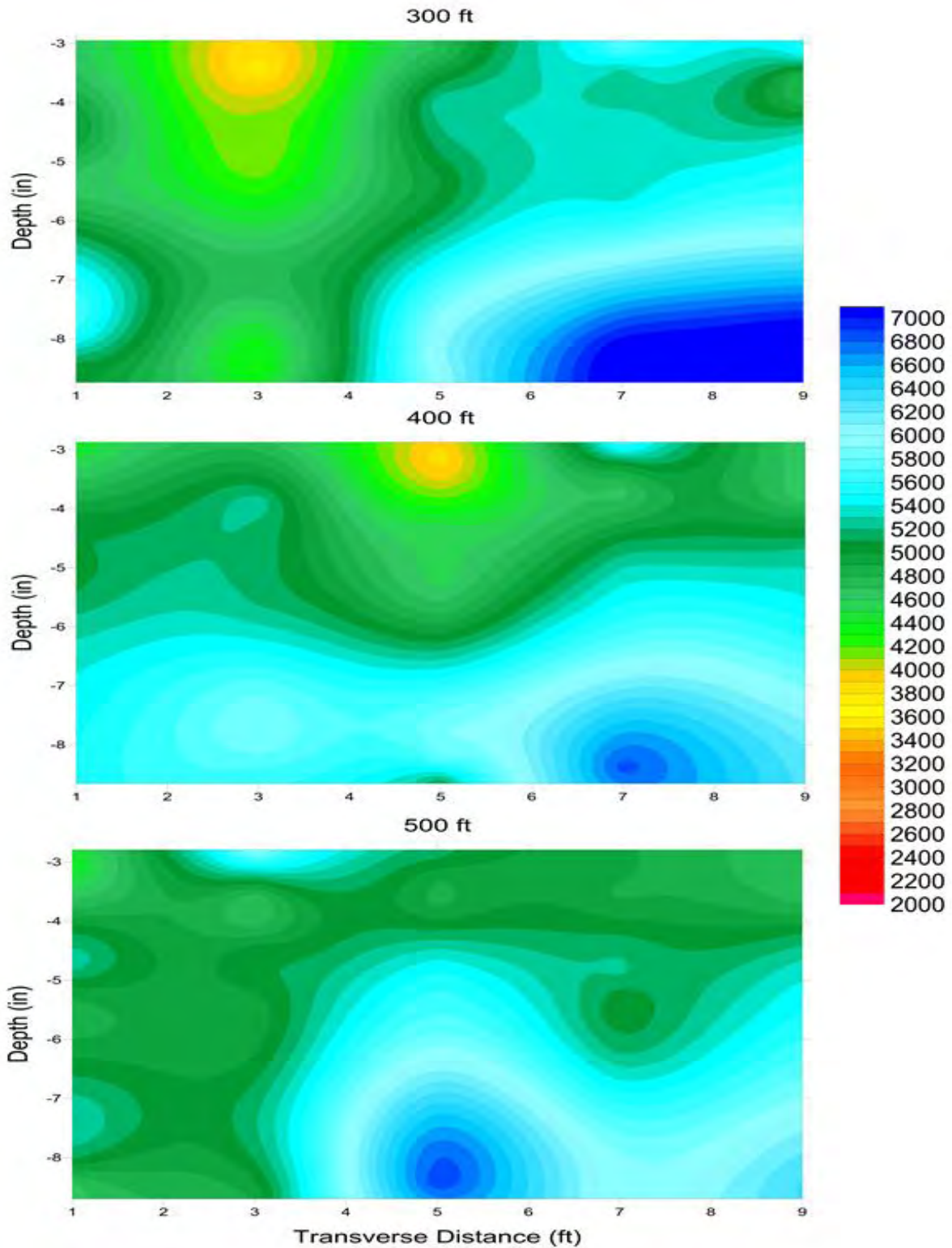


Fig. 3.62—Cross-sections depicting variations in the elastic modulus (ksi) for PCC for PSPA USW data acquired at the 300 ft, 400 ft, and 500 ft intervals along the GPR traverses.

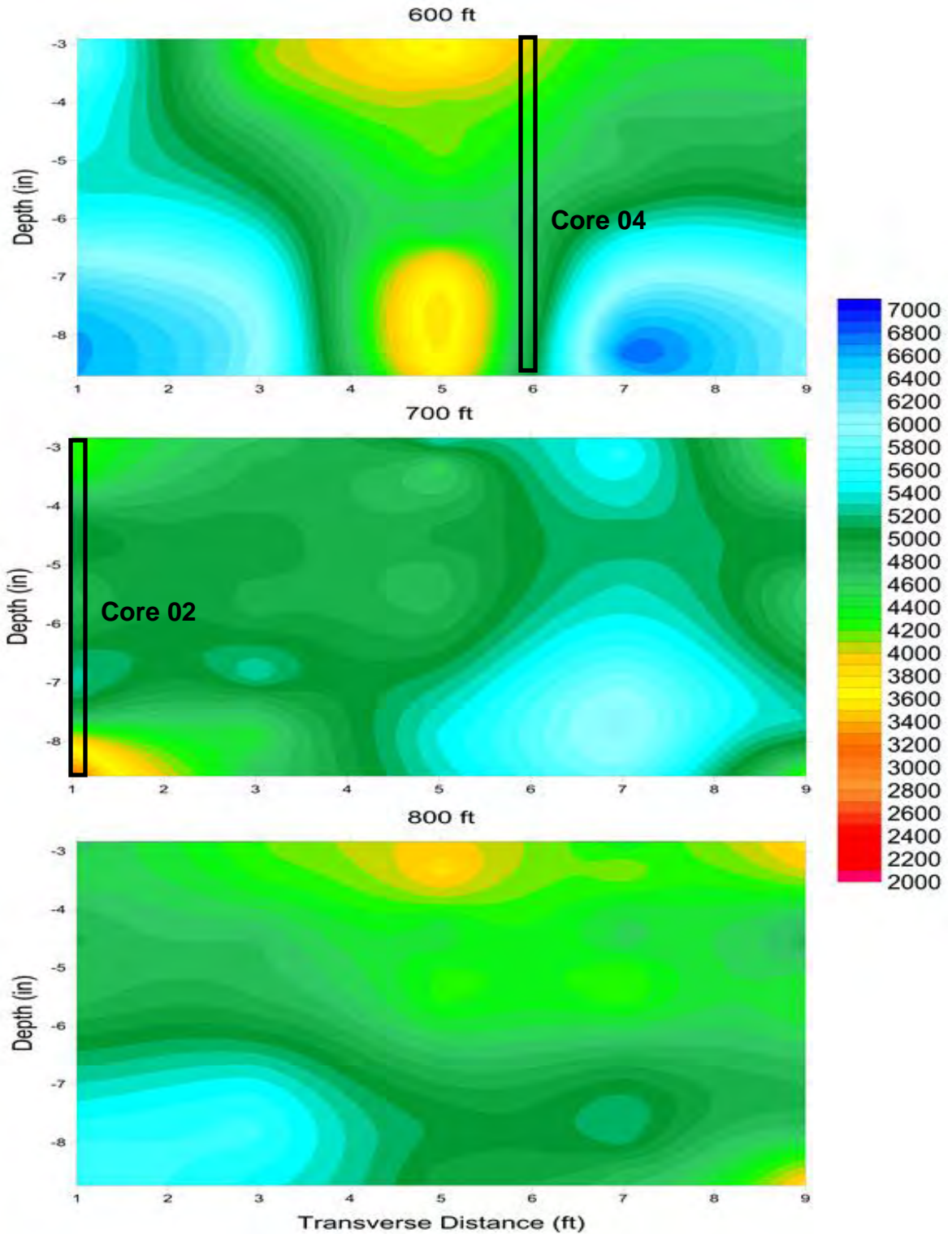


Fig. 3.63—Cross-sections depicting variations in the elastic modulus (ksi) for PCC for PSPA USW data acquired at the 600 ft, 700 ft, and 800 ft intervals along the GPR traverses.

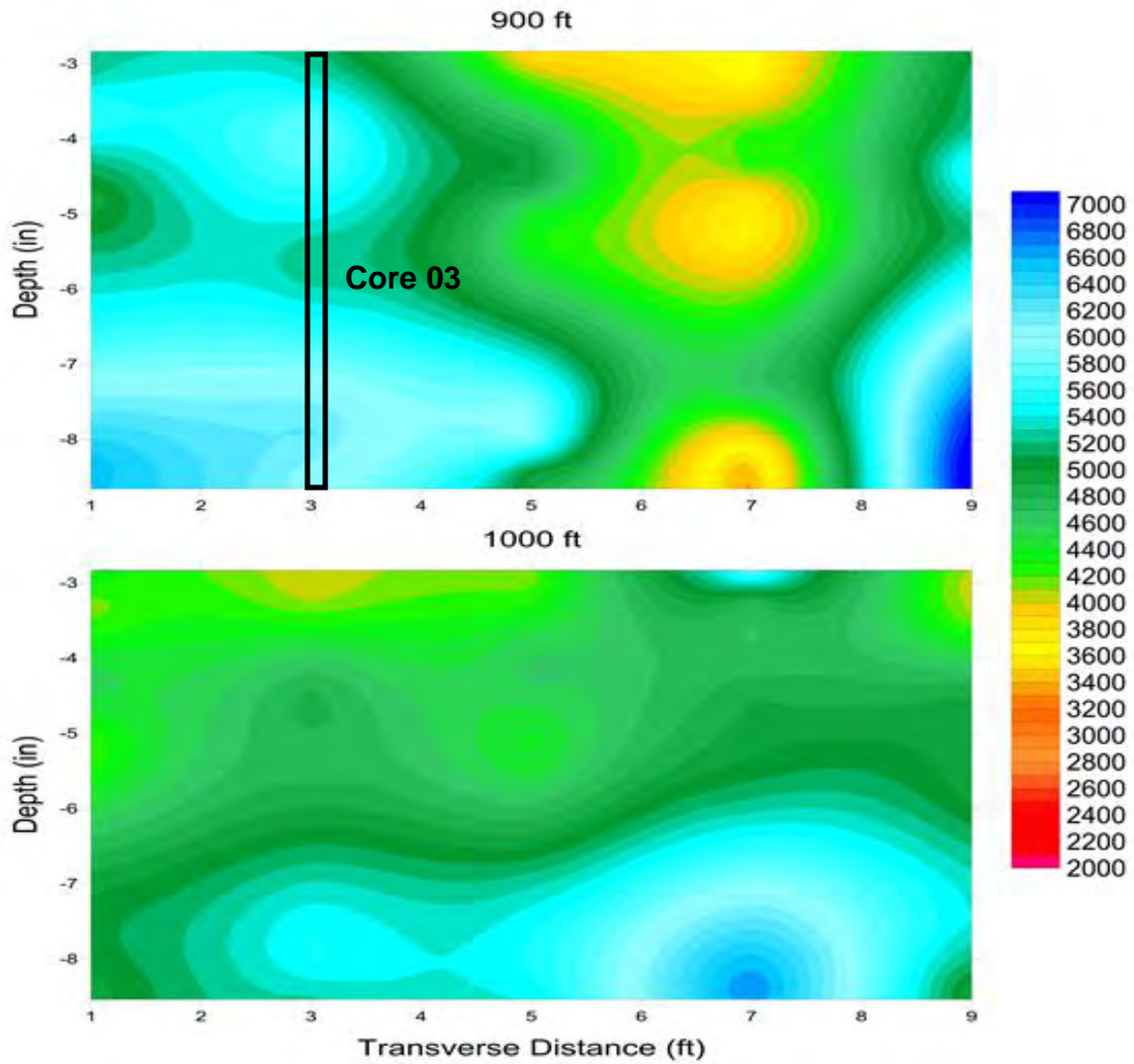


Fig. 3.64—Cross-sections depicting variations in the elastic modulus (ksi) for PCC for PSPA USW data acquired at the 900 ft and 1000 ft intervals along the GPR traverses.

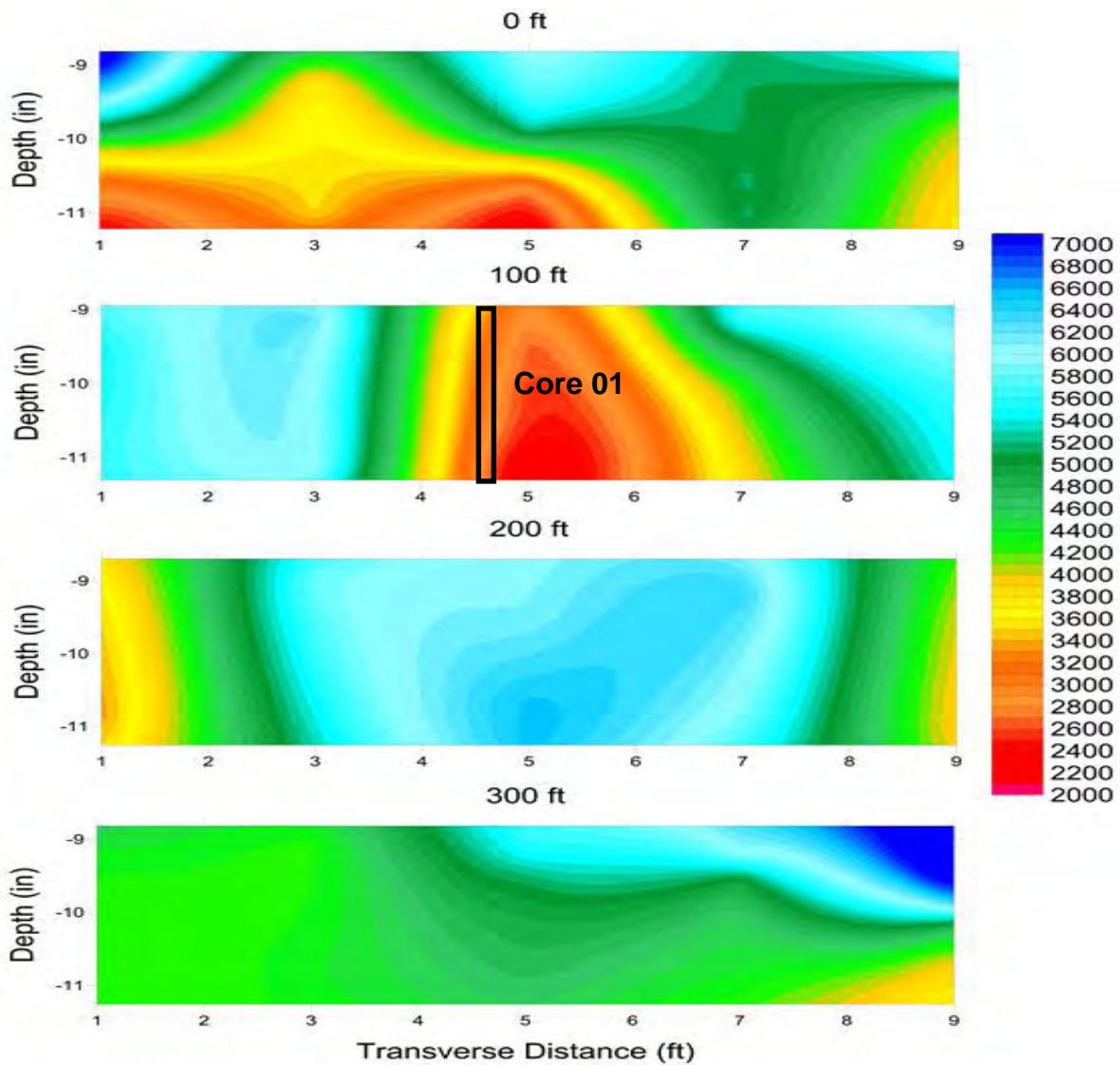


Fig. 3.65—Cross-sections depicting variations in the apparent elastic modulus (ksi) of BM for PSPA USW data acquired at the 0 ft, 100 ft, 200 ft, and 300 ft intervals along the GPR traverses. Depth of investigation extends from 8.5 in. to 11 in.

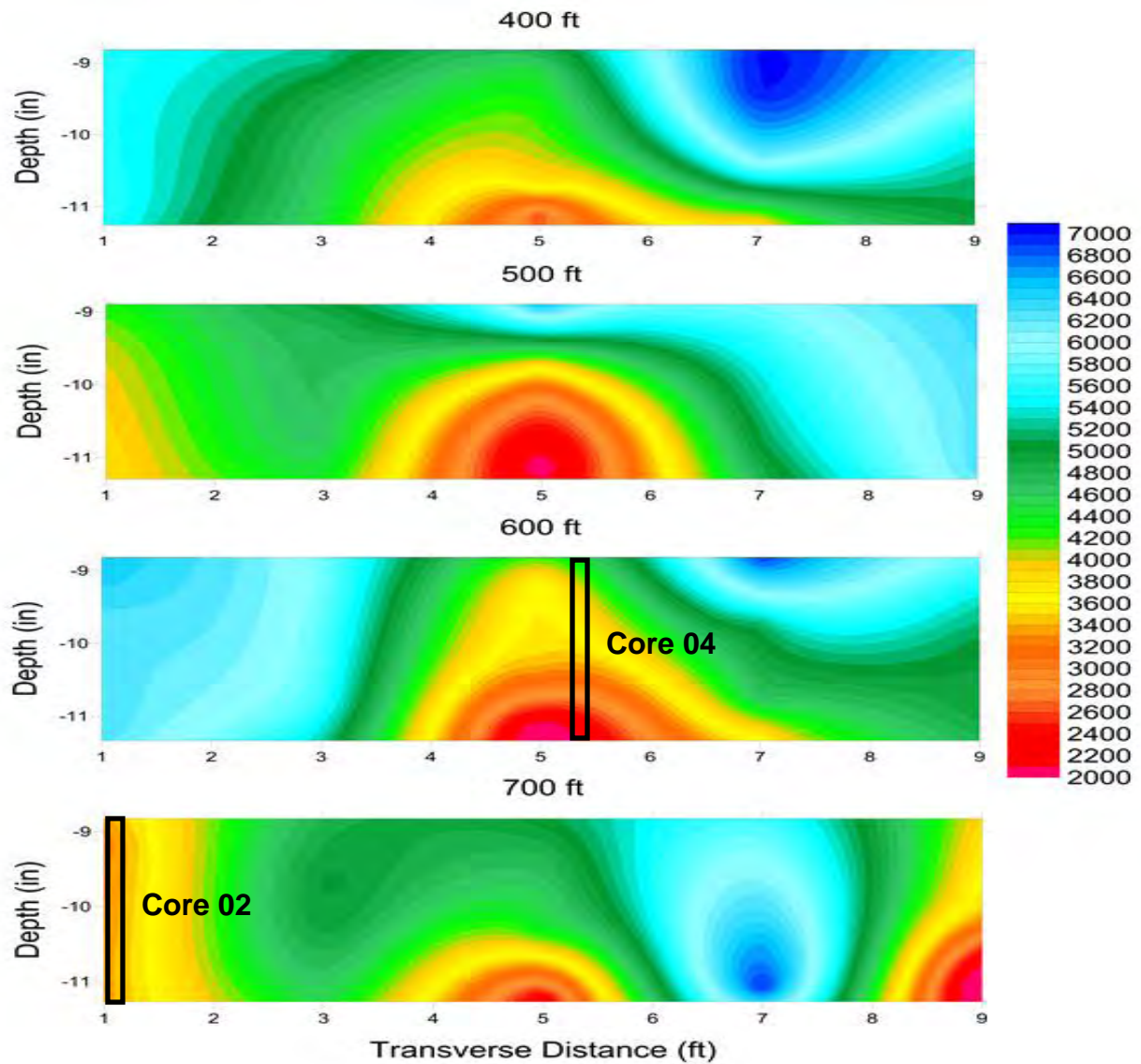


Fig. 3.66—Cross-sections depicting variations in the apparent elastic modulus (ksi) of BM for PSPA USW data acquired at the 400 ft, 500 ft, 600 ft, and 700 ft intervals along the GPR traverses. Depth of investigation extends from 8.5 in. to 11 in.

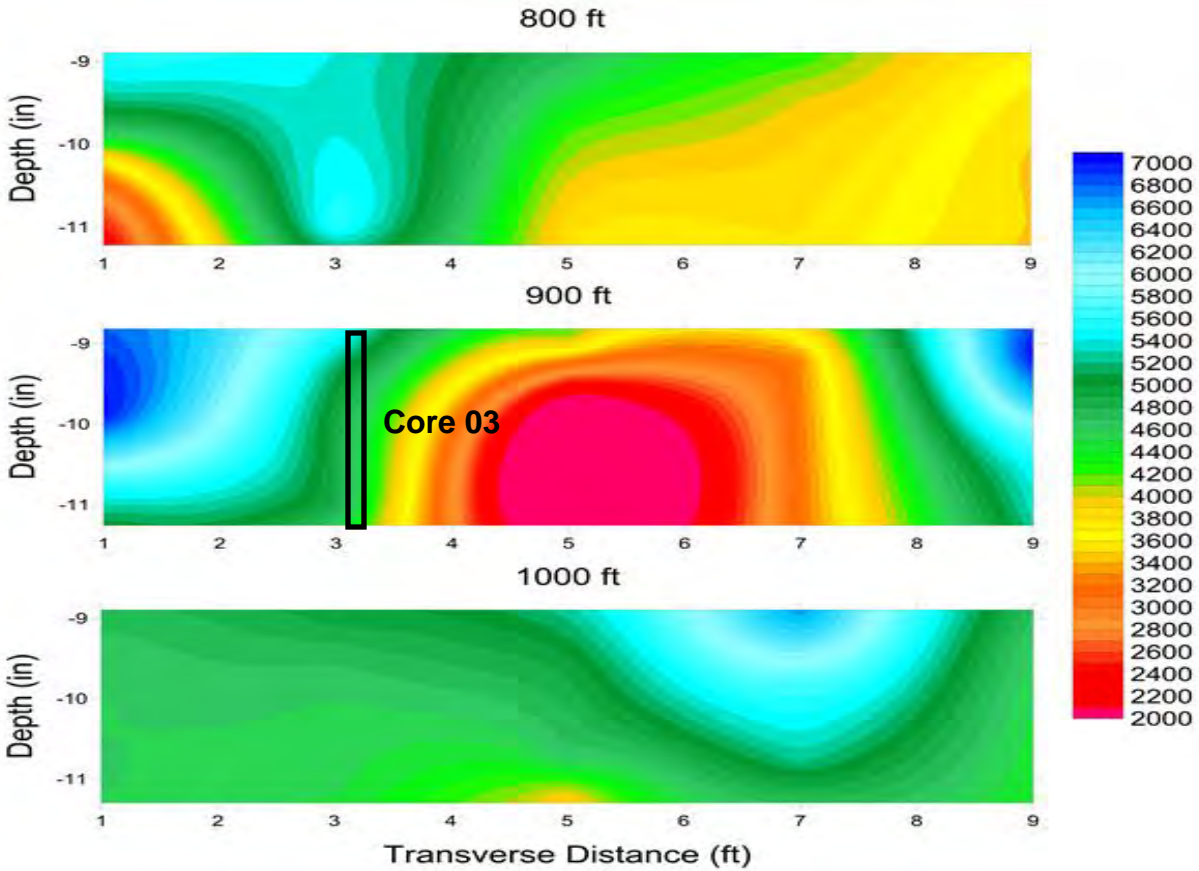


Fig. 3.67—Cross-sections depicting variations in the apparent elastic modulus (ksi) of BM for PSPA USW data acquired at the 800 ft, 900 ft, and 1000 ft intervals along the GPR traverses. Depth of investigation extends from 8.5 in. to 11 in.

The average elastic modulus along each GPR transverse for the entire tested section pavement (3 in. to 11 in.) was calculated and plotted in Fig. 3.68. The average elastic modulus of the pavement does not appear to be statistically lowest in those areas where vehicles tires are most commonly in contact with the roadway.

Statistical Analysis Diagram

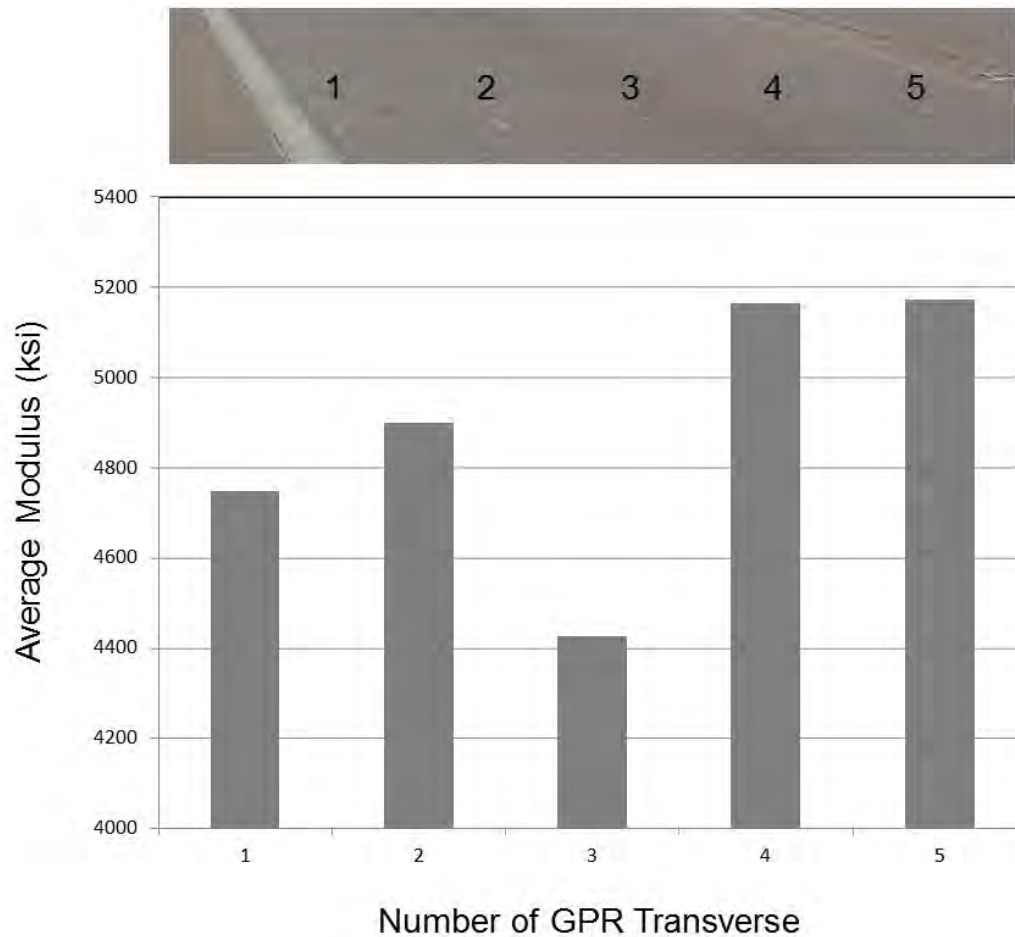


Fig. 3.68—Plot of the average elastic modulus (over depth range of 3 in. to 11 in.) along each GPR transverse. The GPR transverses are spaced at 2 ft intervals. GPR traverse 1 is 1 ft from the outer edge of the pavement.

3.3.5.2 Impact Echo Data

IE data were acquired at each Site 5 PSPA test location (Fig. 3.56). The PSPA IE software automatically analyzed the amplitude spectrum of the acoustic data recorded by the near receiver transducer at each test location and identified a single peak on each amplitude spectra. These peak frequencies (Fig. 3.5) were interpreted as resonant frequencies. The depths to the corresponding reflectors were calculated using Eq. 3.3 (Section 3.2.2.2).

The PSPA software consistently identified a single peak frequency on the IE data acquired at Site 5. The PSPA output calculated depth to the corresponding reflector averaged about 5 in. and varied from 4 in. to 7 in. (Fig. 3.69). This reflector, if real, probably corresponds to the PCC/BM interface at a depth of 8.5 in.

The compressional wave velocity used in Eq. 3.3 was calculated using Eq. 3.1 (Section 3.2.2.1). The compressional wave velocity (V_p) calculated using Eq. 3.1 is a function of the average surface wave velocity (V_R) of the upper 11 in. of pavement. The difference between the calculated reflector depth and the actual depth to the PCC/BM interface can be attributed, in part, to the fact that compressional wave velocity was based on the average surface wave velocity of both PCC and BM.

In summary, the PSPA IE tool was unable to accurately estimate the thickness of either the BM or entire paved section with a reasonable degree of reliability and consistency.

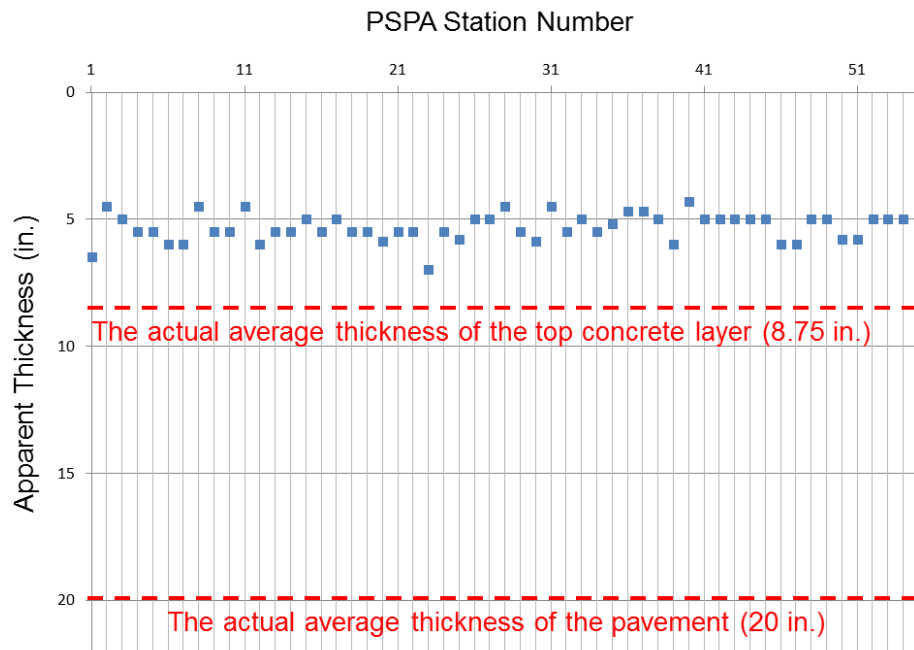


Fig. 3.69—The PSPA IE calculated depth to identified reflector is plotted for all PSPA test locations (Fig. 3.56). The average calculated depth to this reflector (approx. 5 in.) measurement does not agree well with the actual thickness (approx. 8.75 in.) of the PCC layer.

3.3.6 Project-Level Site 6 (I-55 Perry County)

Project-level Site 6 is located along the south-bound lane of interstate I-55 in Perry County, Missouri (Fig. 3.70). The pavement consists of 9 in. of PCC. The PCC layer displayed no visible evidence of surface cracks. The average air temperature during field data acquisition at the test site was 38 °F.

Fifty-five (55) PSPA data sets and nine (9) cores were acquired at Site 6 (Fig. 3.2 and Fig. 3.71). The PSPA data were acquired using a 6 in. transducer spacing. Hence, the USW modulus plot extends from a depth of 3 in. to a depth of approximately 9 in. (Fig. 3.72). PSPA data were not acquired in immediate proximity to all core locations.



Fig. 3.70–Photograph of PSPA tool placed on pavement at project-level Site 6 (I-55 S).

3.3.6.1 Ultrasonic Surface Wave Data

In this report, the project-level pavement Site 6 PSPA USW elastic modulus data are presented in 1-D plot format and in 2-D plot format.

PSPA data acquired in proximity to core locations 01 and 03 (Fig. 3.71) are presented to illustrate the utility and limitations of the PSPA tool. Intact core 01 and the corresponding PSPA elastic modulus plot are shown in Fig. 3.72. Small pits are visible. The core, with an average elastic modulus of 5973 ksi is classified as good quality (Table 3.2).

Intact core 03 and the corresponding PSPA elastic modulus plot are shown in Fig. 3.73. Small pits are visible. The core, with an average elastic modulus of 5897 ksi is classified as good quality (Table 3.2).

The elastic modulus data acquired at Site 6 is displayed in 2-D cross-section format in Figs. 3.74-3.77. As shown on these figures, the tested section of PCC (4 in. to approximately 9 in.) is characterized mostly by elastic modulus values above 5000 ksi indicating the PCC is good quality.

At a few PSPA test locations (Figs. 3.74-3.77), the elastic modulus values drop to values as low as 3500 ksi, indicating that localized degradation could be occurring. However, none of these PSPA anomalies were cored.

The PSPA elastic modulus data are consistent with core control as all nine (9) cores appear to be good quality.

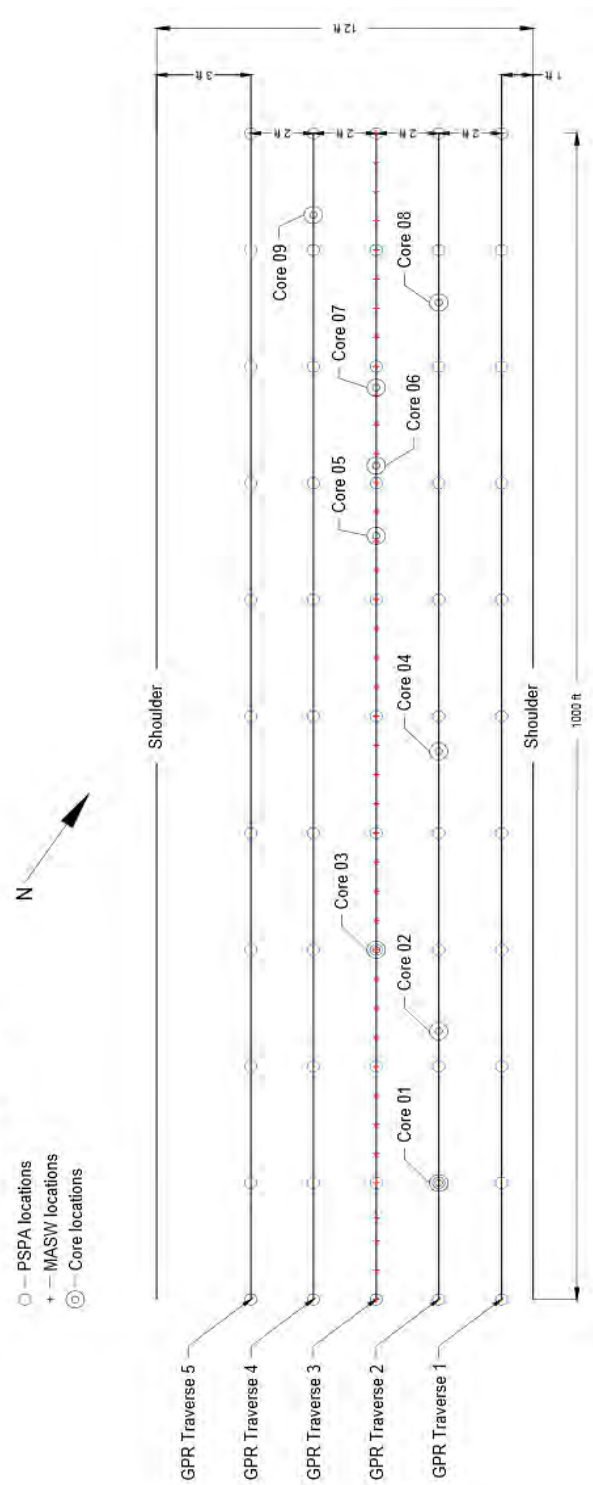


Fig. 3.71—Base map for project-level Site 6 showing PSPA test locations and core locations. PSPA data were acquired at 100 ft intervals along each GPR traverse. GPR traverse 1 was located 1 ft from the outer edge of the paved driving lane (shoulder). Only cores 01 and 03 are located within 5 ft of a PSPA location.

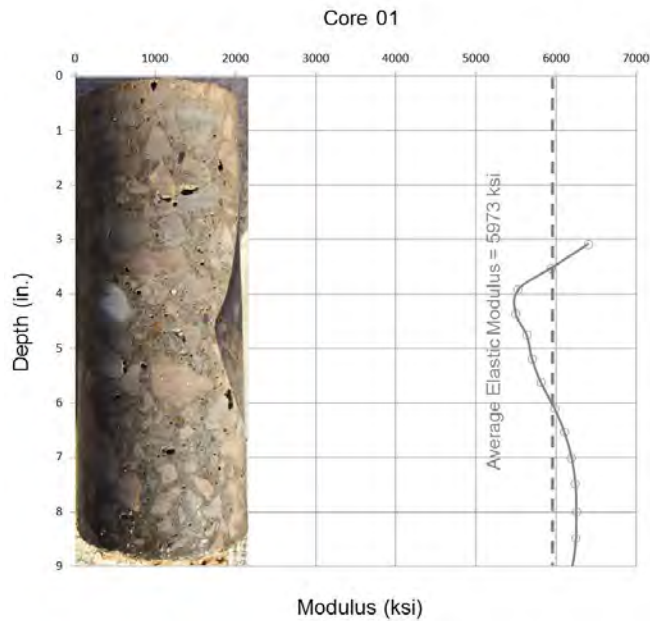


Fig. 3.72—Elastic modulus plot generated from PSPA USW data acquired in immediate proximity to intact PCC core 01 (Fig. 3.71). Small pits are visible. The core, with an average elastic modulus of 5973 ksi is classified as good quality (Table 3.2).

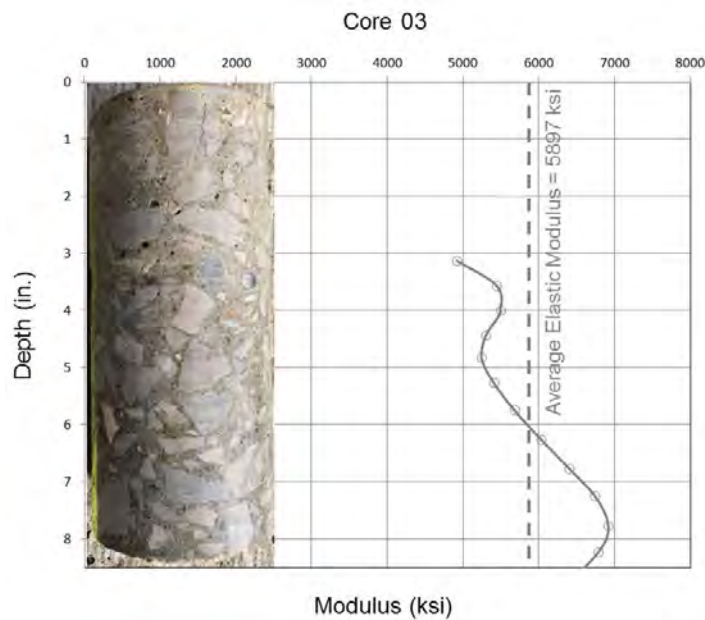


Fig. 3.73—Elastic modulus plot generated from PSPA USW data acquired in immediate proximity to intact PCC core 03 (Fig. 3.71). Small pits are visible. The core, with an average elastic modulus of 5897 ksi is classified as good quality (Table 3.2).

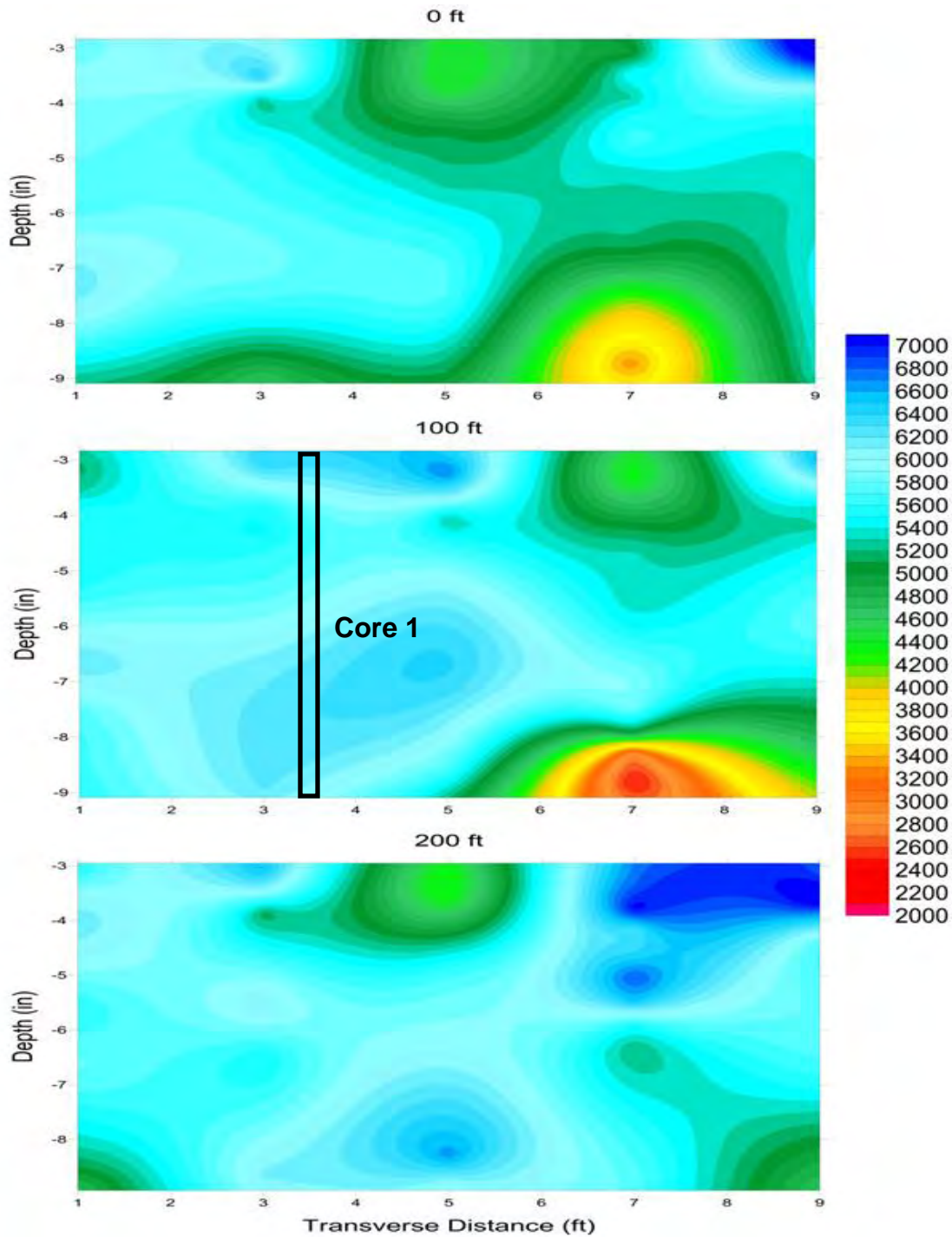


Fig. 3.74—Cross-sections depicting variations in the elastic modulus (ksi) for concrete for PSPA USW data acquired at the 0 ft, 100 ft, and 200 ft intervals along the GPR traverses. The five PSPA USW data sets in each cross-section were acquired at 2 ft intervals starting 1 ft from the edge of pavement (Fig. 3.71). Depth of investigation extends from 4 in. to 9 in.

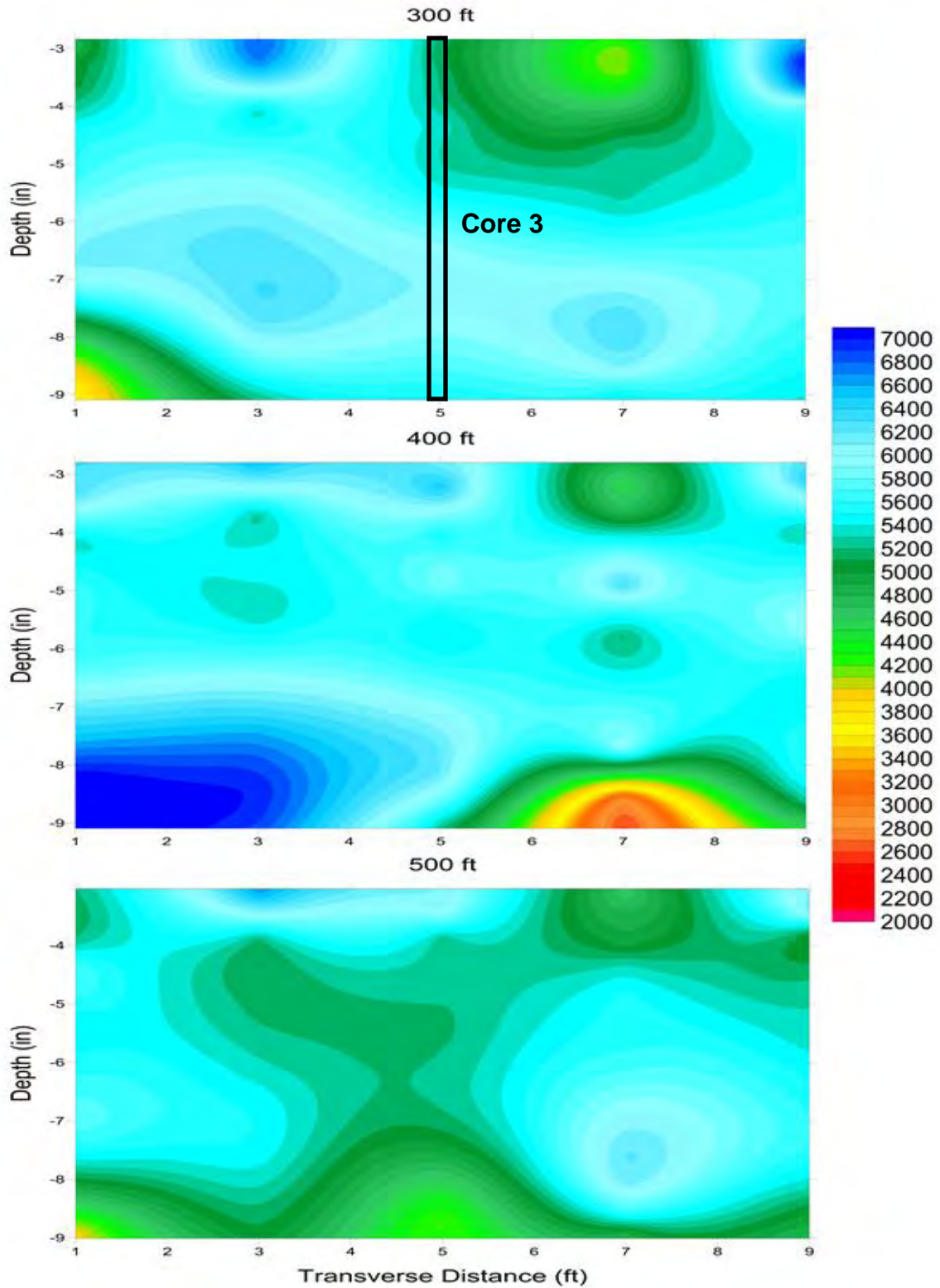


Fig. 3.75—Cross-sections depicting variations in the elastic modulus (ksi) for concrete for PSPA USW data acquired at the 300 ft, 400 ft, and 500 ft intervals along the GPR traverses.

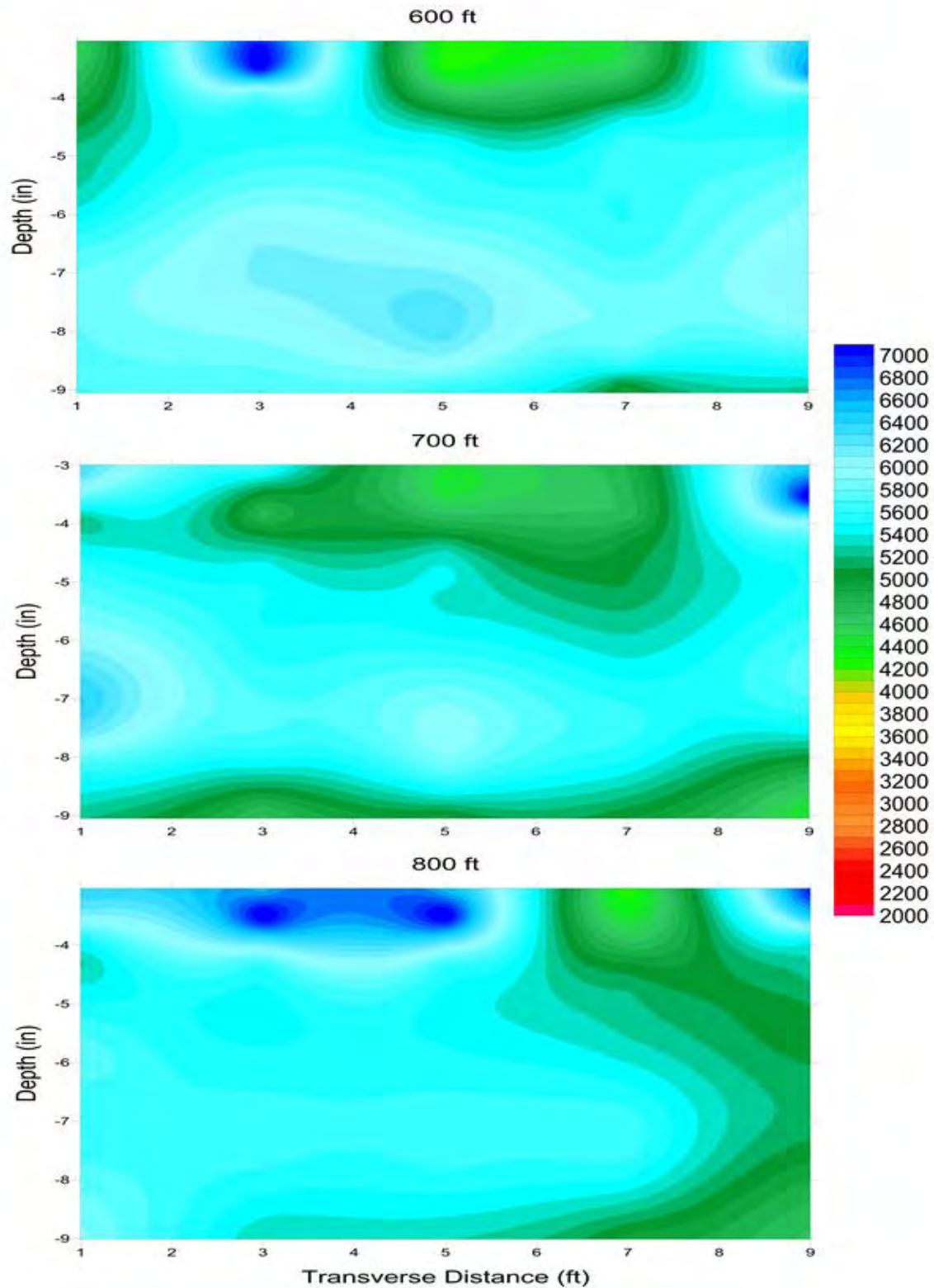


Fig. 3.76—Cross-sections depicting variations in the elastic modulus (ksi) for concrete for PSPA USW data acquired at the 600 ft, 700 ft, and 800 ft intervals along the GPR traverses.

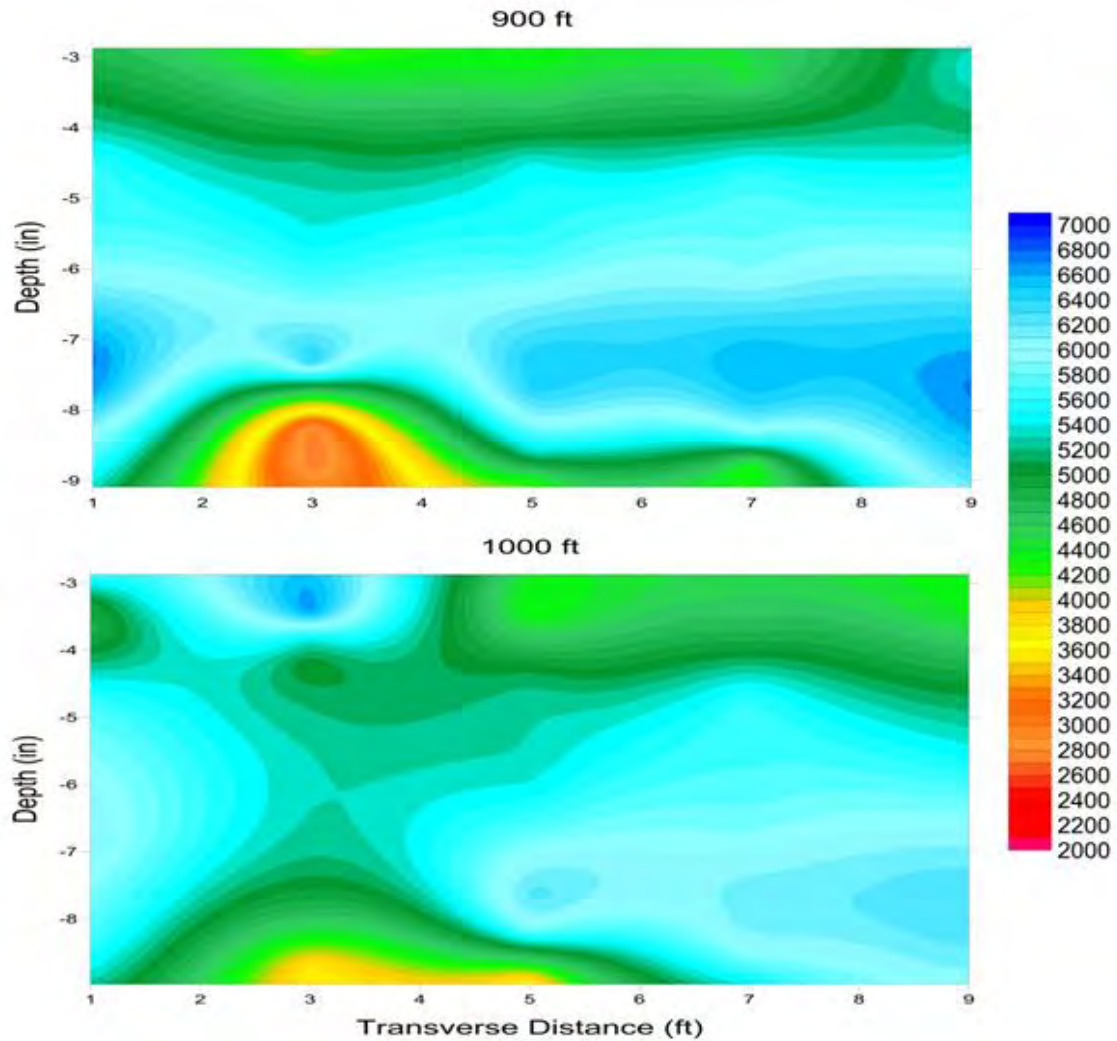


Fig. 3.77—Cross-sections depicting variations in the elastic modulus (ksi) for concrete for PSPA USW data acquired at the 600 ft, 700 ft, and 800 ft intervals along the GPR traverses.

The average elastic modulus along each GPR transverse for the entire tested section pavement (3 in. to 9 in.) was calculated and plotted in Fig. 3.78. The average moduli of the PCC does not seem to be statistically lowest in those areas where vehicles tires are most commonly in contact with the roadway.

Statistical Analysis Diagram

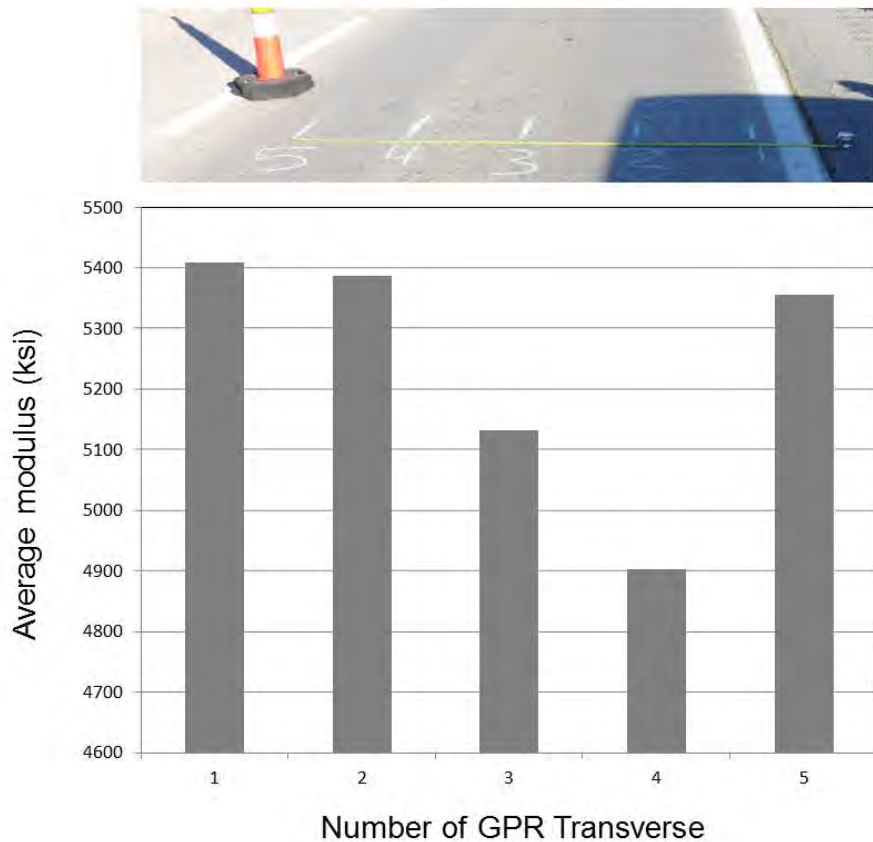


Fig. 3.78—Plot of the average elastic modulus (over depth range of 3 in. to 9 in.) along each GPR transverse. The GPR traverses are spaced at 2 ft intervals. GPR traverse 1 is 1 ft from the outer edge of the pavement.

3.3.6.2 Impact Echo Data

IE data were acquired at each Site 6 PSPA test location (Fig. 3.71). The PSPA IE software automatically analyzed the amplitude spectrum of the acoustic data recorded by the near receiver transducer at each test location and identified a single peak on each amplitude spectra. These peak frequencies (Fig. 3.5) were interpreted as resonant frequencies. The depths to the corresponding reflectors were calculated using Eq. 3.3 (Section 3.2.2.2).

The PSPA software consistently identified a single peak frequency on the IE data acquired at Site 6. The PSPA output calculated depth to the corresponding reflector varied from 4.2 in. to 7 in. and averaged approximately 5.9 in. (Fig. 3.79). As neither layers nor flaws in the PCC pavement, this thickness can only be assumed to be an inaccurate estimate of the pavement thickness.

The compressional wave velocity used in Eq. 3.3 was calculated using Eq. 3.1 (Section 3.2.2.1). The compressional wave velocity (V_p) calculated using Eq. 3.1 is a function of the average surface wave velocity (V_R) of the upper approx. 9 in. of PCC.

In summary, the PSPA IE tool was unable to estimate the thickness of the concrete with a reasonable degree of reliability and consistency.

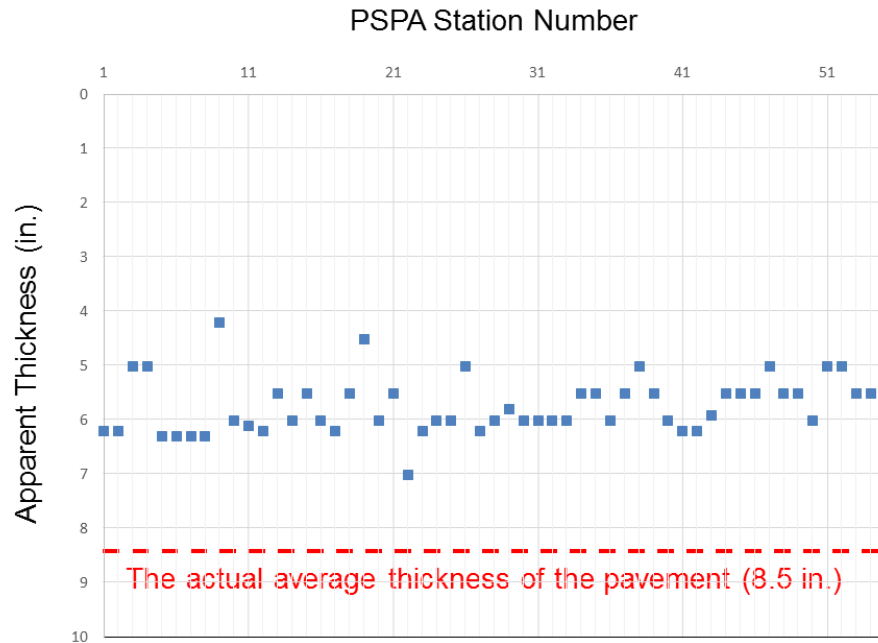


Fig. 3.79—The PSPA IE calculated depth to identified reflector is plotted for all PSPA test locations (Fig. 3.71). The average calculated depth to this reflector (approx. 5.9 in.) measurement does not agree well with the actual thickness (approx. 8.5 in.) of the PCC layer.

3.3.7 Project-Level Site 7 (HWY U)

Project-level Site 7 is located along HWY U in Dent County, Missouri (Fig. 3.80). The pavement consisted of approximately 4 in. of BM overlay. The BM surface displayed visible evidence of surface cracks. The average air temperature during field data acquisition at the test site was 34 °F.

Sixty-six (66) PSPA data sets and eight (8) cores were acquired at Site 7 (Fig. 3.2 and Fig. 3.81). The PSPA data were acquired using a 4 in. transducer spacing. Hence, the USW modulus plot extends from a depth of 2 in. to a depth of approximately 7 in. (Fig. 3.82). PSPA data were not acquired in immediate proximity to all core locations. GPR control and available core control indicates the BM layer is approximately 4 in. thick. Hence the USW modulus plots (2 in. to approximately 7 in.) extend well below the base of the BM layer.

As shown in Fig. 3.84 and Fig. 3.87, reliable PSPA data could not be acquired at multiple locations because of severe surface cracking. Where necessary and possible, the PSPA locations

were shifted by up to 1 ft, so that data could be acquired as close as possible to the planned test locations (Fig. 3.81).



Fig. 3.80—Photograph of PSPA tool placed on pavement at project-level Site 7 (HWY U).

3.3.7.1 Ultrasonic Surface Wave Data

In this report, the project-level pavement Site 7 PSPA USW elastic modulus data are presented in 1-D plot format and in 2-D plot format.

PSPA data acquired in proximity to core locations 01 and 05 (Fig.3.81) are presented to illustrate the utility and limitations of the PSPA tool. Stripped core 01 and the corresponding PSPA elastic modulus plot are shown in Fig. 3.82. Only 1 in. of core 01 was recovered. The BM (estimated thickness of 4 in.), with an average elastic modulus of 717 ksi, is classified as severely deteriorated (Table 3.2).

Stripped core 05 and the corresponding PSPA elastic modulus plot are shown in Fig. 3.83. Only 4 in. of core 05 was recovered. The core 05, with an average elastic modulus of 589 ksi is classified as severely deteriorated (Table 3.2).

The elastic modulus data acquired at Site 7 is displayed in 2-D cross-sectional format in Figs. 3.84-3.87. The tested section of BM (2 in. to approximately 4 in.) on all of the 2-D cross-sections is characterized by elastic modulus values below 2000 ksi (mostly below 1000 ksi) indicating the BM is severely deteriorated. The PSPA USW elastic modulus plots are consistent with core control. All of the retrieved partial cores were stripped. As previously noted, GPR control and available core control indicates the BM layer is approximately 4 in thick. Hence the USW modulus plots (2 in. to approximately 7 in.) extend well below the base of the BM layer.

The average elastic modulus along each GPR transverse for the entire tested section pavement (2 in. to 4 in.) was calculated and plotted in Fig. 3.88. The average elastic modulus of the pavement is statistically lowest in the central section of the lane.

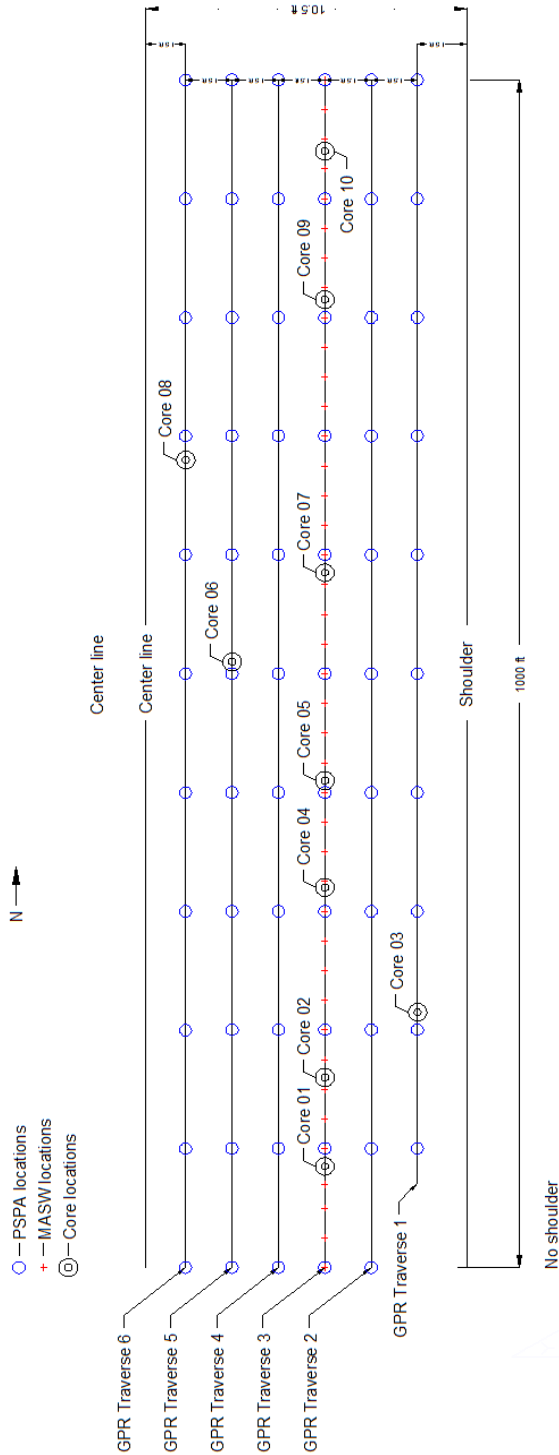


Fig. 3.81–Base map for project-level Site 7 showing PSPA test locations and core locations. PSPA data were acquired at 100 ft intervals along each GPR traverse. GPR traverse 1 was located 1.5 ft from the outer edge of the paved driving lane (shoulder). Reliable PSPA data could not be acquired at several locations because of severe surface cracking. Where necessary and possible, the PSPA locations were shifted by up to 1 ft, so that data could be acquired as close as possible to the planned test locations. Only cores 05 and 08 are located within 5 ft of a PSPA location.

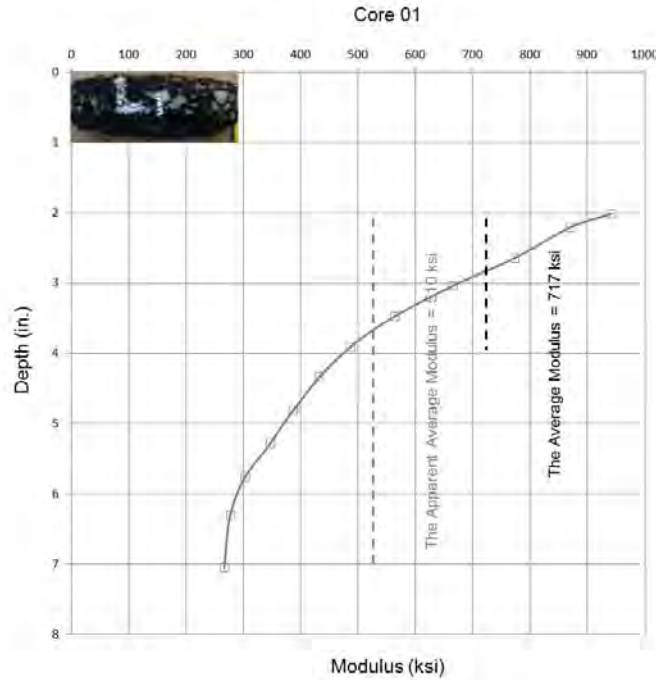


Fig. 3.82—Elastic modulus plot generated from PSPA USW data acquired in immediate proximity to stripped core 01 (Fig. 3.81). Only 1 in. of core was recovered.

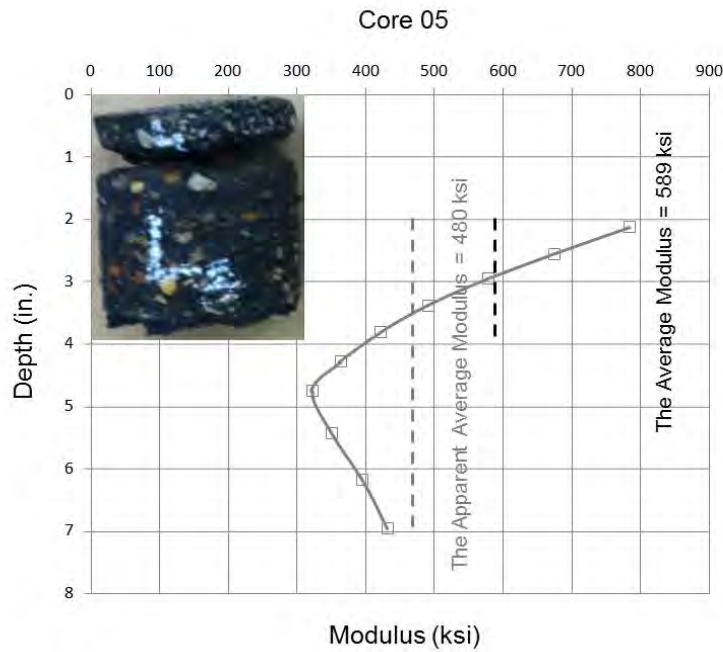


Fig. 3.83—Elastic modulus plot generated from PSPA USW data acquired in immediate proximity to stripped core 05 (Fig. 3.81). Only 4 in. of core was recovered.

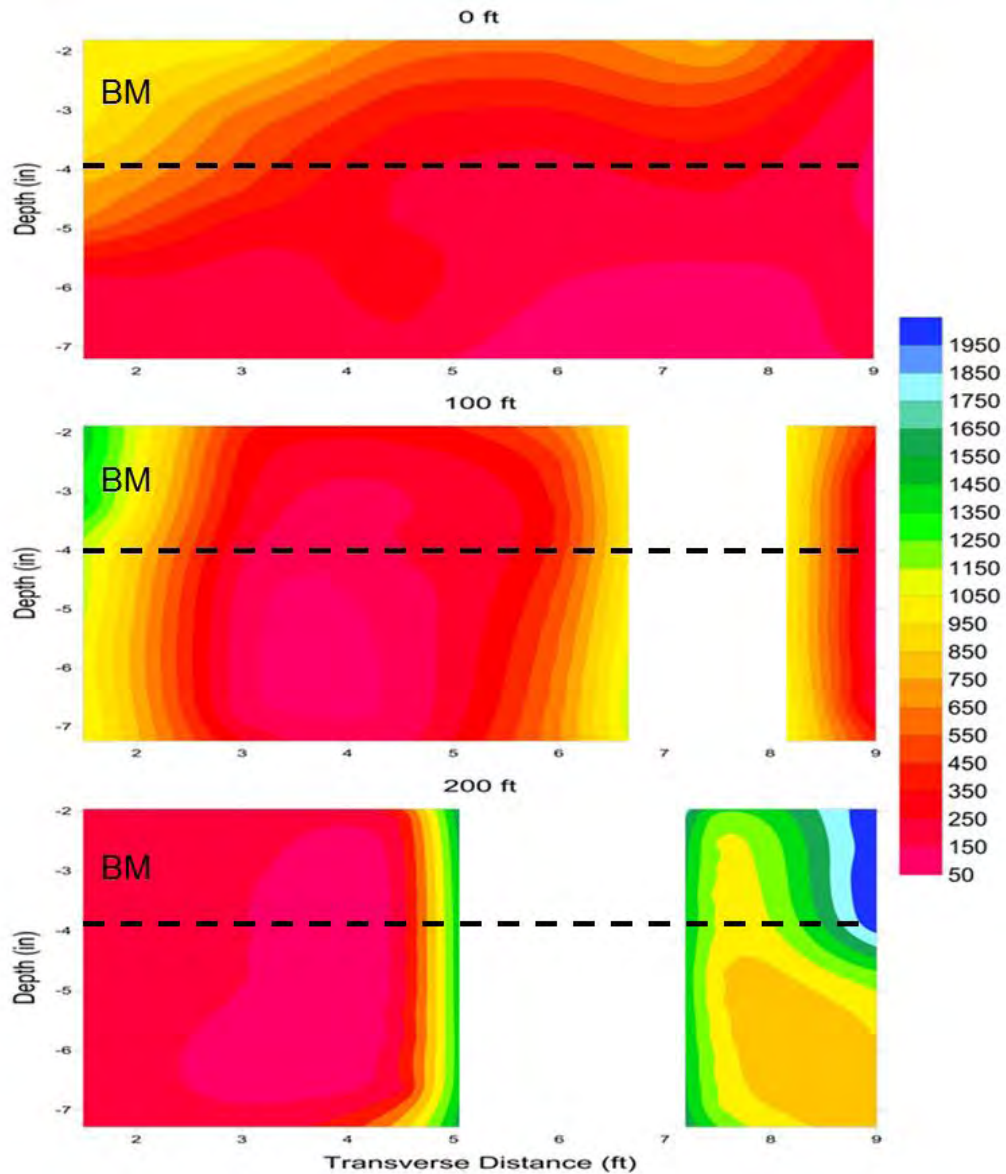


Fig. 3.84—Cross-sections depicting variations in the elastic modulus (ksi) for BM and for PSPA USW data acquired at the 0 ft, 100 ft, and 200 ft intervals along the GPR traverses. The six PSPA USW data sets in each cross-section were acquired at 2 ft intervals starting 1 ft from the edge of pavement (Fig. 3.81). Reliable PSPA data could not be acquired at several locations because of severe surface cracking. Where necessary and possible, the PSPA locations were shifted by up to 1 ft, so that data could be acquired as close as possible to the planned test locations.

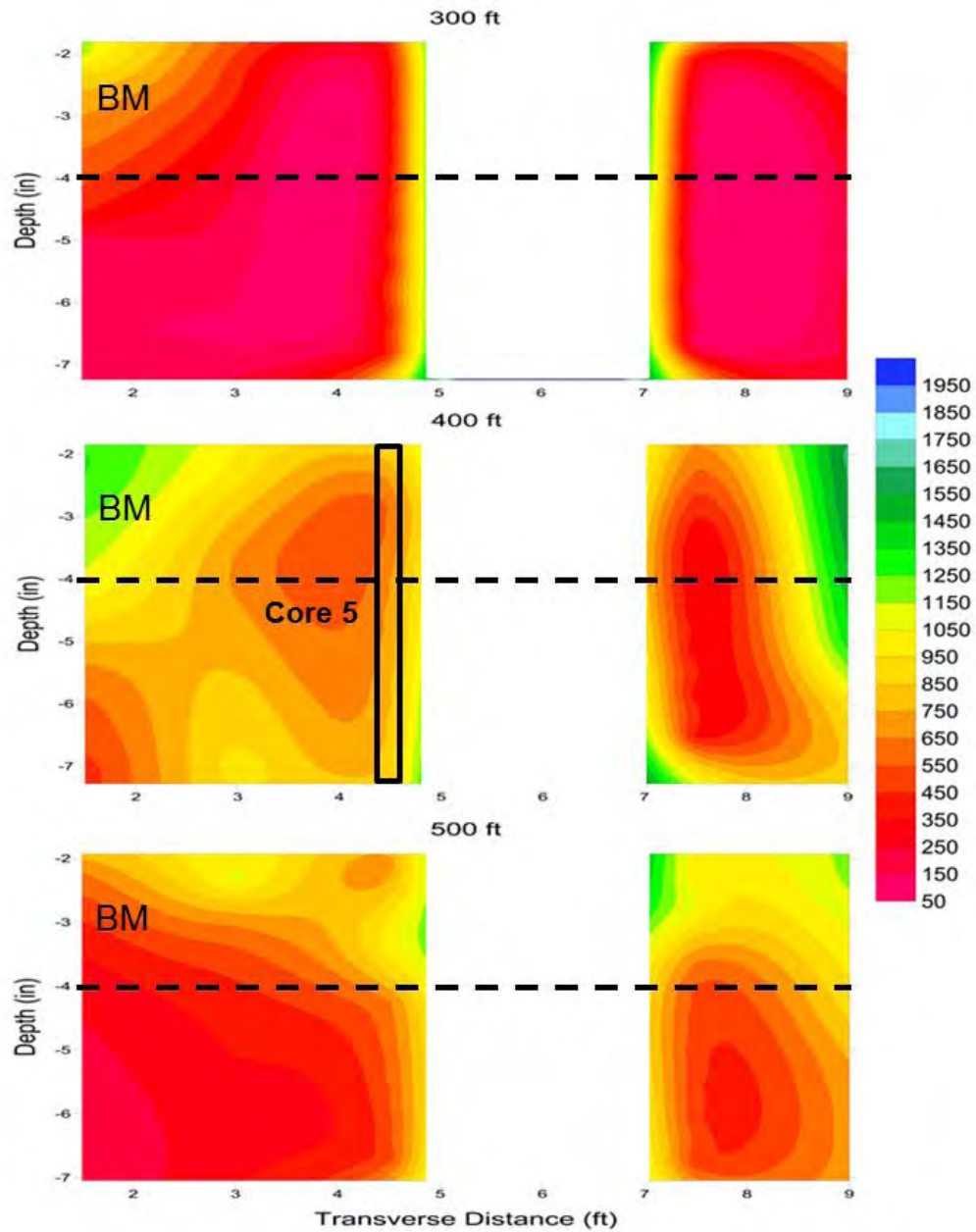


Fig. 3.85—Cross-sections depicting variations in the elastic modulus (ksi) for asphalt (BM) for PSPA USW data acquired at the 300 ft, 400 ft, and 500 ft intervals along the GPR traverses.

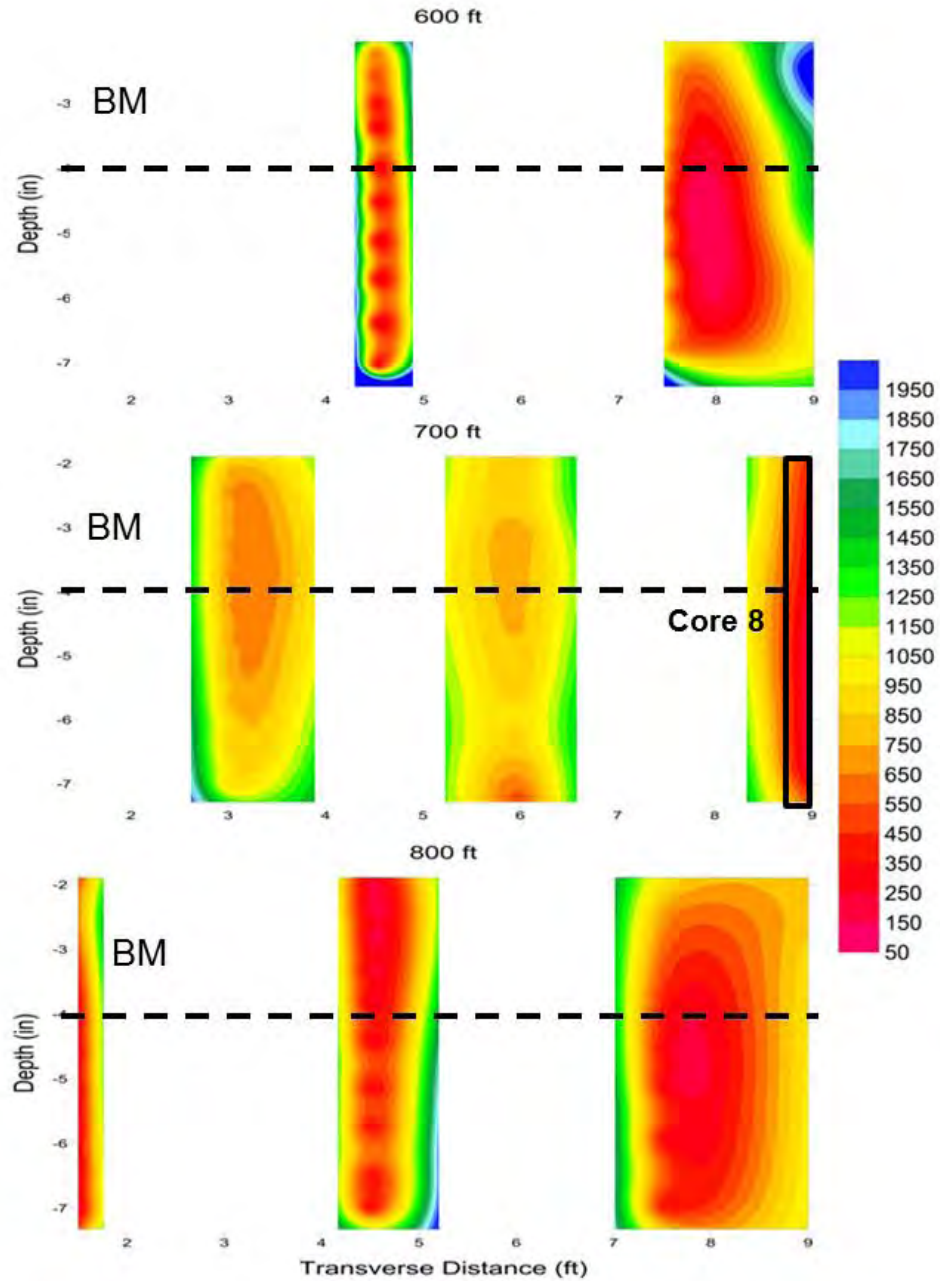


Fig. 3.86—Cross-sections depicting variations in the elastic modulus (ksi) for asphalt (BM) for PSPA USW data acquired at the 600 ft, 700 ft, and 800 ft intervals along the GPR traverses. PSPA data could not be acquired at several test locations because of the deteriorated nature of the paved surface.

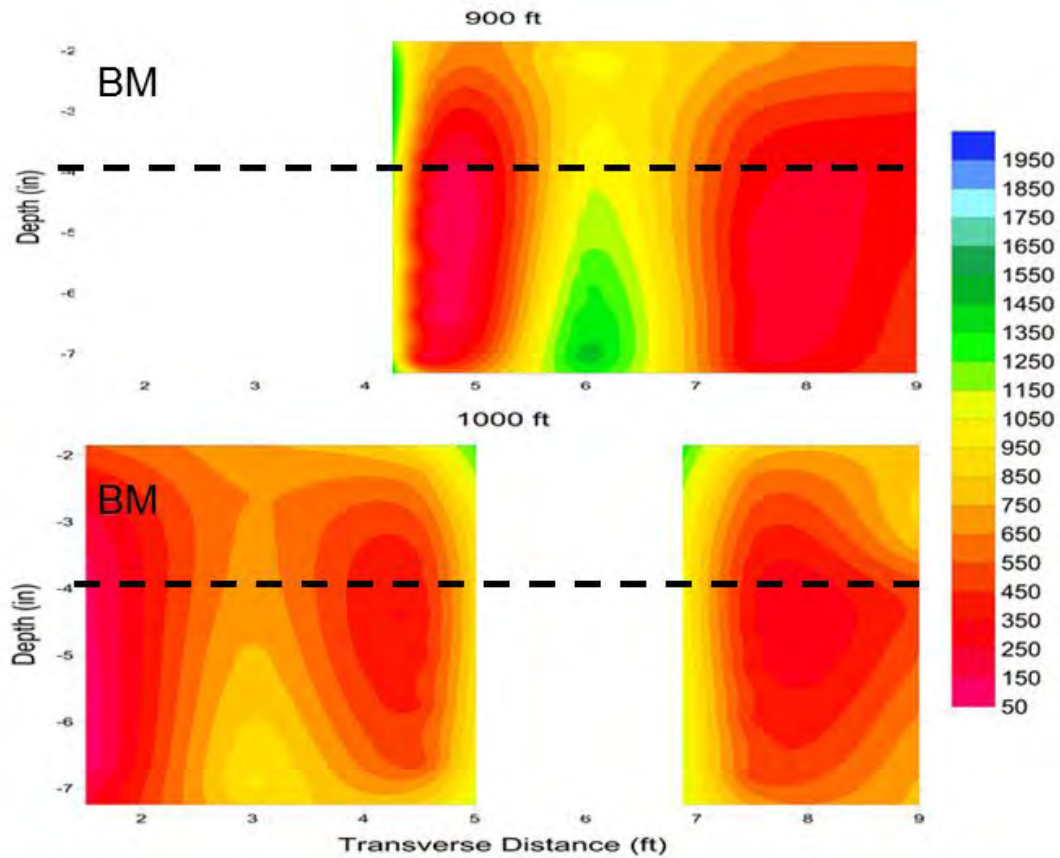


Fig. 3.87—Cross-sections depicting variations in the elastic modulus (ksi) for asphalt (BM) for PSPA USW data acquired at the 900 ft and 1000 ft intervals along the GPR traverses. PSPA data could not be acquired at several test locations because of the deteriorated nature of the paved surface.

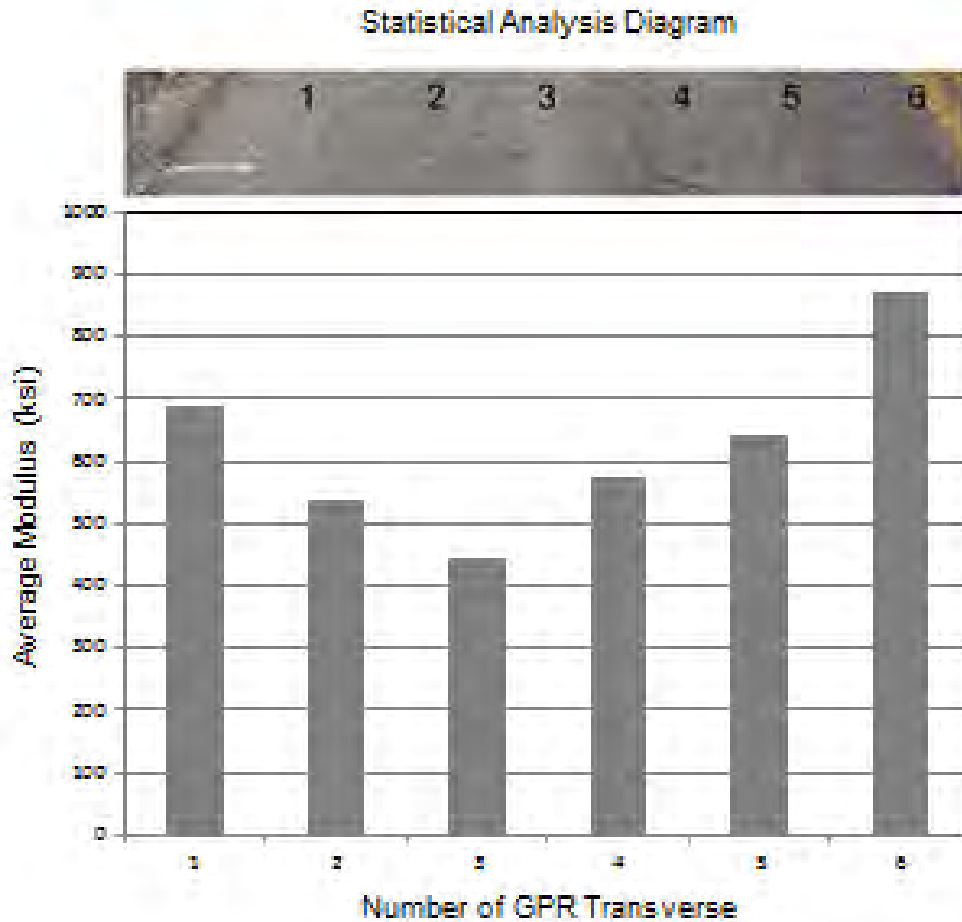


Fig. 3.88—Plot of the average elastic modulus (over depth range of 2 in. to 7.2 in.) along each GPR transverse. The GPR traverses are spaced at 1.5 ft intervals. GPR traverse 1 is 1.5 ft from the outer edge of the pavement.

3.3.7.2 Impact Echo Data

IE data were acquired at each Site 7 PSPA test location (Fig. 3.81). The PSPA IE software automatically analyzed the amplitude spectrum of the acoustic data recorded by the near receiver transducer at each test location and identified a single peak on each amplitude spectra. These peak frequencies (Fig. 3.5) were interpreted as resonant frequencies. The depths to the corresponding reflectors were calculated using Eq. 3.3 (Section 3.2.2.2).

The PSPA software consistently identified a single peak frequency on the IE data acquired at Site 7. The PSPA output calculated depth to the corresponding reflector varied significantly from 2 in. to 14 in. (Fig. 3.89), with many values clustered between depths of 2 in. and 4 in. The values clustered between 2 in. and 4 in. could represent reflections from the base of the BM layer or from flaws within the BM layer.

The compressional wave velocity used in Eq. 3.3 was calculated using Eq. 3.1 (Section 3.2.2.1). The compressional wave velocities (V_p) calculated using Eq. 3.1 are a function of the

average surface wave velocity (V_R) of the upper approx. 7 in. of BM and underlying lower-velocity base. The compressional wave velocity is probably too low. This could account for the cluster of depth estimates between 2 in. and 4 in.

In summary, the PSPA IE tool was unable to estimate the thickness of the BM with a reasonable degree of reliability and consistency.

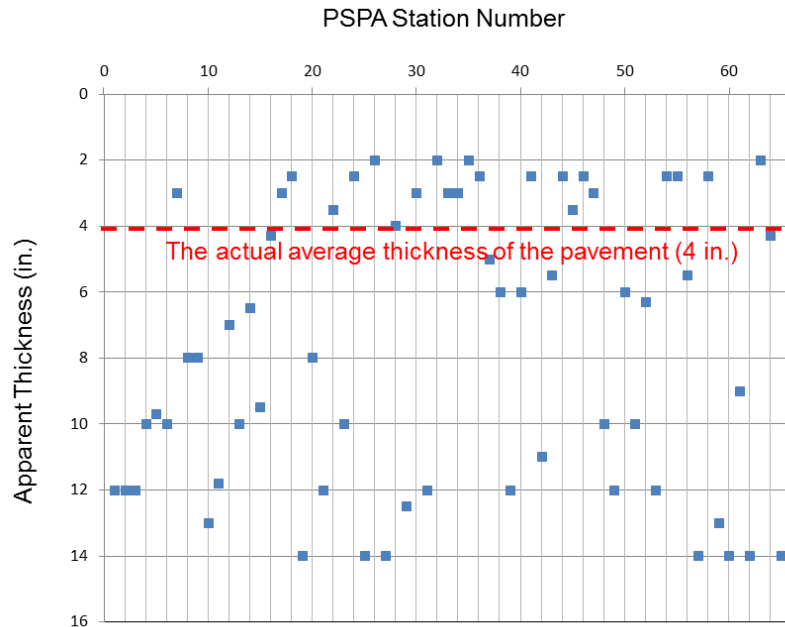


Fig. 3.89—The calculated depth to the identified reflector varied significantly. The values clustered between 2 in. and 4 in. could represent reflections from the base of the BM layer or from flaws within the BM layer.

3.3.8 Project-Level Site 8 (I-35)

Project-level Site 8 is located along the north-bound lane of interstate I-35 near Daviess County, Missouri (Fig. 3.90). The tested pavement consists of approximately 7 in. of PCC overlay above a 9 in. thick PCC layer. A 1 in. thick layer of BM is embedded between the two PCC layers. The top PCC layer displayed visible evidence of surface cracks. The average air temperature during field data acquisition at the test site was 80 °F.

Fifty-five (55) PSPA data sets and eight (8) cores were acquired at Site 8 (Fig. 3.2 and Fig. 3.91). The PSPA data were acquired using a 6 in. transducer spacing. Hence, the USW modulus plot extends from a depth of 3 in. to a depth of approximately 11 in. (Fig. 3.92). PSPA data were not acquired in immediate proximity to all core locations.

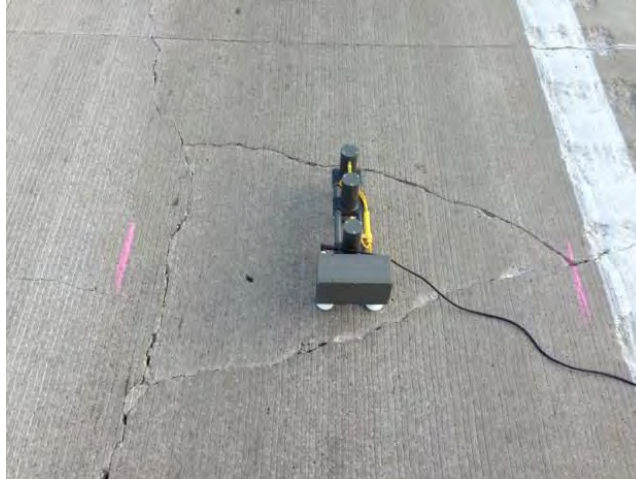


Fig. 3.90—Photograph of PSPA tool placed on pavement at project-level Site 8 (I-35 N).

3.3.8.1 Ultrasonic Surface Wave Data

In this report, the project-level pavement Site 8 PSPA USW elastic modulus data are presented in 1-D plot format and in 2-D plot format.

PSPA data acquired in proximity to core locations 01 and 02 (Fig. 3.91) are presented to illustrate the utility and limitations of the PSPA tool. Core 01 and the corresponding PSPA elastic modulus plot are shown in Fig. 3.92. Core 01 consists of 8 in. of PCC overlay above a 9 in. thick PCC layer. A 1 in. thick layer of BM is embedded between the two PCC layers. The upper layer of PCC and the underlying BM were not debonded and the the BM was not stripped. The elastic modulus plot corresponding to core 01 (Fig. 3.92) can be divided into three layers based on the type of pavement: Upper PCC, BM and lower PCC. The average elastic modulus of the upper PCC layer is 5205 ksi indicating concrete is good quality (Table 3.2). The average “apparent” elastic modulus of the underlying BM layer is 5906 ksi indicating the BM is also good quality (Table 3.2). (It should be noted that “apparent” elastic modulus values for BM are calculated here based on properties for PCC, which explains the magnitude of this value.) The average “apparent” elastic modulus of the lower PCC layer is 4600 ksi indicating the PCC is probably fair quality (Table 3.2).

The elastic modulus plot corresponding to debonded core 02 (Fig. 3.93) can also be divided into two layers based on the type of pavement. The average elastic modulus of the overlying PCC layer is 4495 ksi indicating concrete is fair quality (Table 3.2). Note that the elastic modulus of the concrete decreases significantly immediately above the debonded PCC/BM interface. The average “apparent” elastic modulus of the underlying BM layers is 4070 ksi indicating the BM is probably good quality (Table 3.2). The average “apparent” elastic modulus of the lower PCC layer is 3450 ksi indicating the lower PCC is probably poor quality (Table 3.2).

The elastic modulus data generated for the upper layer of PCC at Site 8 are displayed in 2-D cross-sectional format in Figs. 3.94-3.97. The 2-D plots of elastic modulus correlate well with proximal cores. Core 03 and 04 were bonded and are characterized by average PCC elastic modulus values of about 4500 ksi (fair quality) and 5000 ksi (marginally good quality). Note

that PSPA data could not be acquired at several PSPA test locations because of the presence of surface cracks.

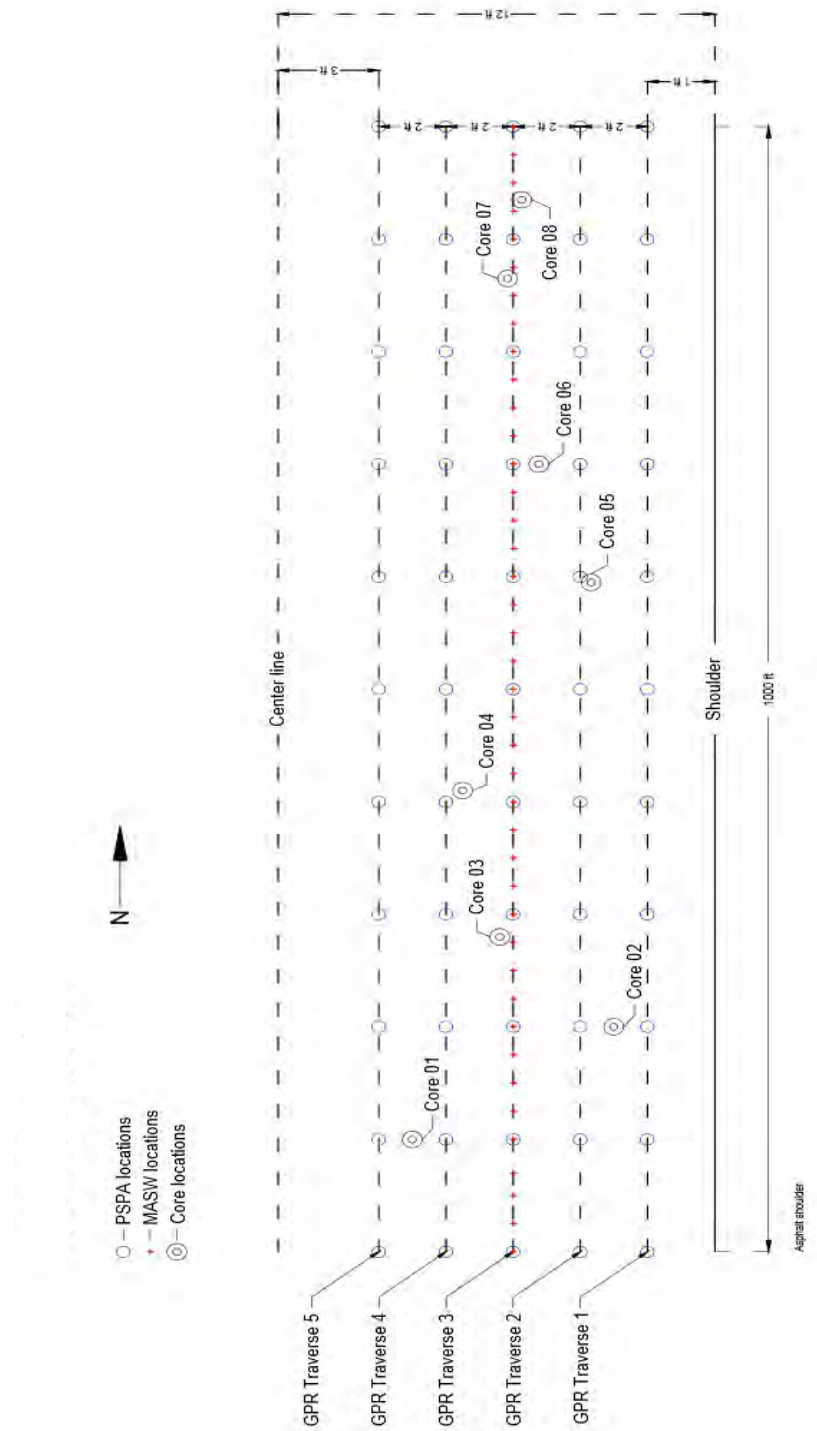


Fig. 3.91—Base map for project-level Site 8 showing PSPA test locations and core locations. PSPA data were acquired at 100 ft intervals along each GPR traverse. GPR traverse 1 was located 1 ft from the outer edge of the paved driving lane (shoulder). Only cores 01,02,05 and 06 are located within 5 ft of a PSPA location.

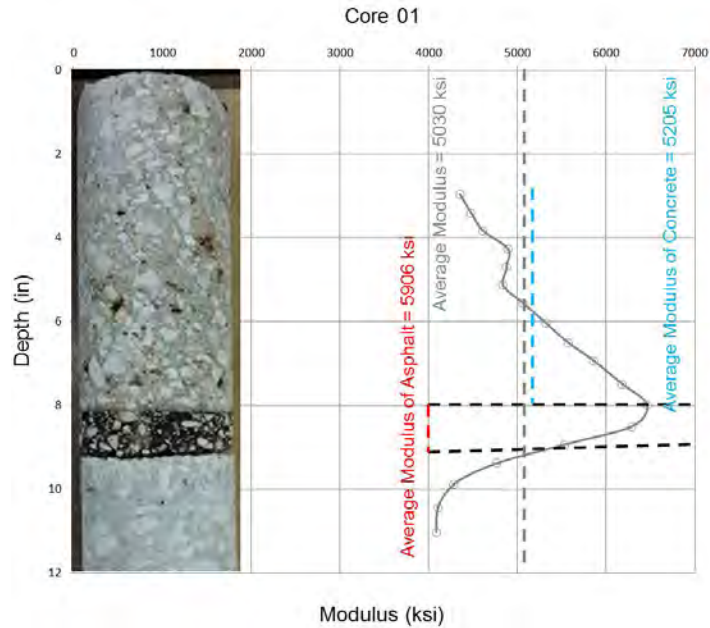


Fig. 3.92—Elastic modulus plot generated from PSPA USW data acquired in immediate proximity to intact core 01 (Fig. 3.91). The tested pavement consists of approx. 7 in. of PCC overlay above a 9 in. thick PCC layer. A 1 in. thick layer of BM is embedded between the two PCC layers. There was no evidence of debonding or stripping in core 01.

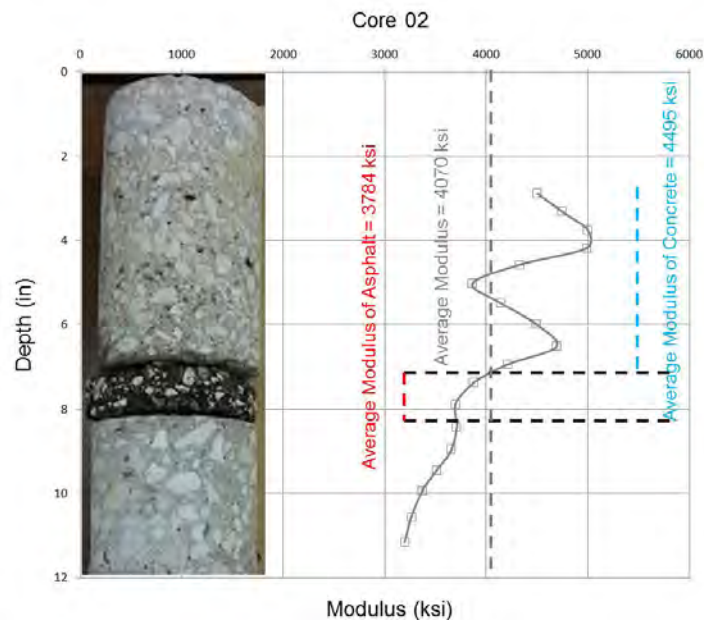


Fig. 3.93—Elastic modulus plot generated from PSPA USW data acquired in immediate proximity to debonded core 02 (Fig. 3.91). The tested pavement consists of approx. 7 in. of PCC bonded overlay above a 9 in. thick PCC layer. A 1 in. thick layer of BM is embedded between the two PCC layers. Core 02 was debonded at PCC/BM interface with the depth of 7 in.

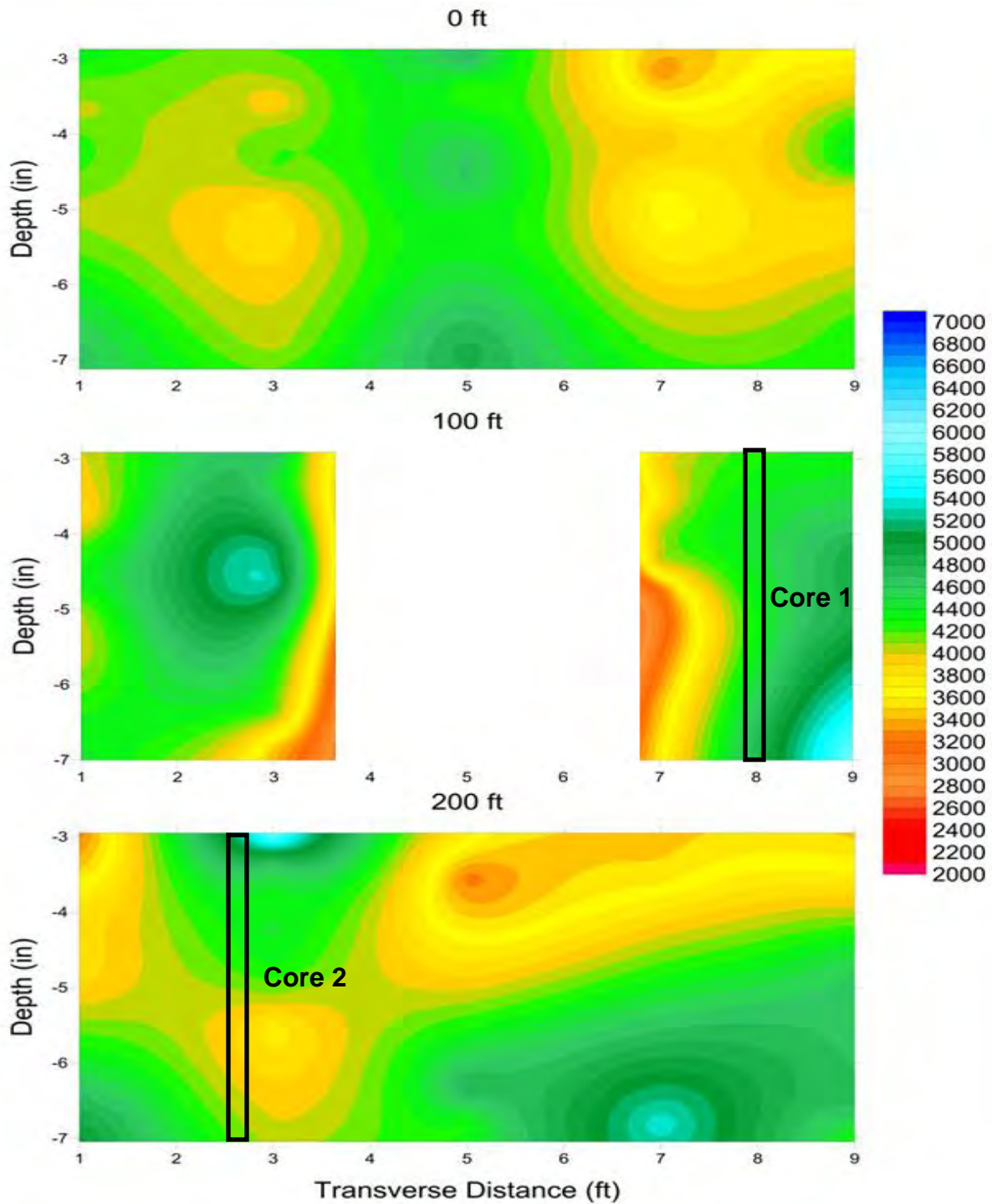


Fig. 3.94– Cross-sections depicting variations in the elastic modulus (ksi) for upper layer of PCC for PSPA USW data acquired at the 0 ft, 100 ft, and 200 ft intervals along the GPR traverses. The five PSPA USW data sets in each cross-section were acquired at 2 ft intervals starting 1 ft from the edge of pavement (Fig. 3.91). Depth of investigation extends from 3 in. to 7 in. PSPA data could not be acquired at several test locations because of the deteriorated nature of the paved surface.

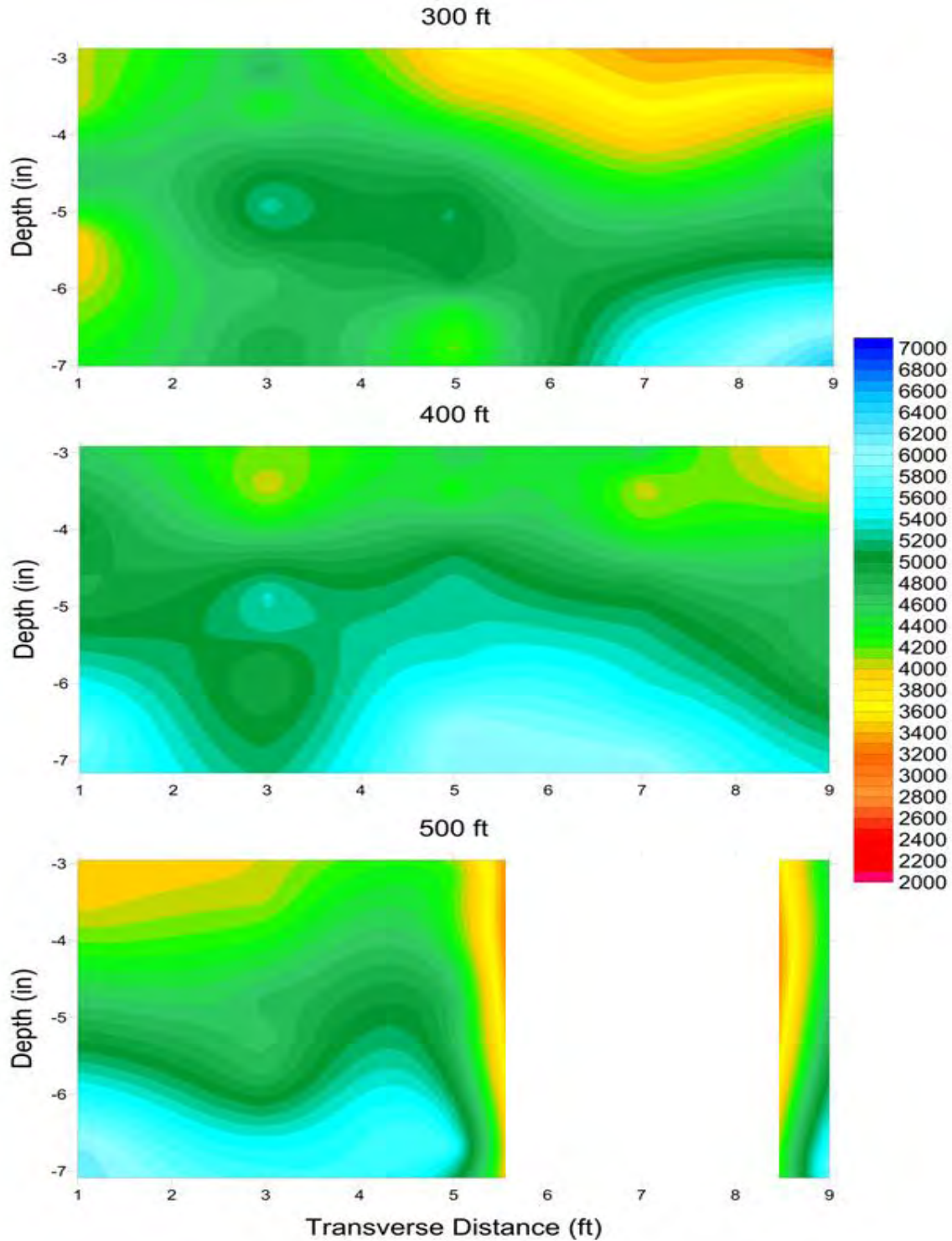


Fig. 3.95—Cross-sections depicting variations in the elastic modulus (ksi) for concrete for PSPA USW data acquired at the 300 ft, 400 ft, and 500 ft intervals along the GPR traverses. PSPA data could not be acquired at several test locations because of the deteriorated nature of the paved surface.

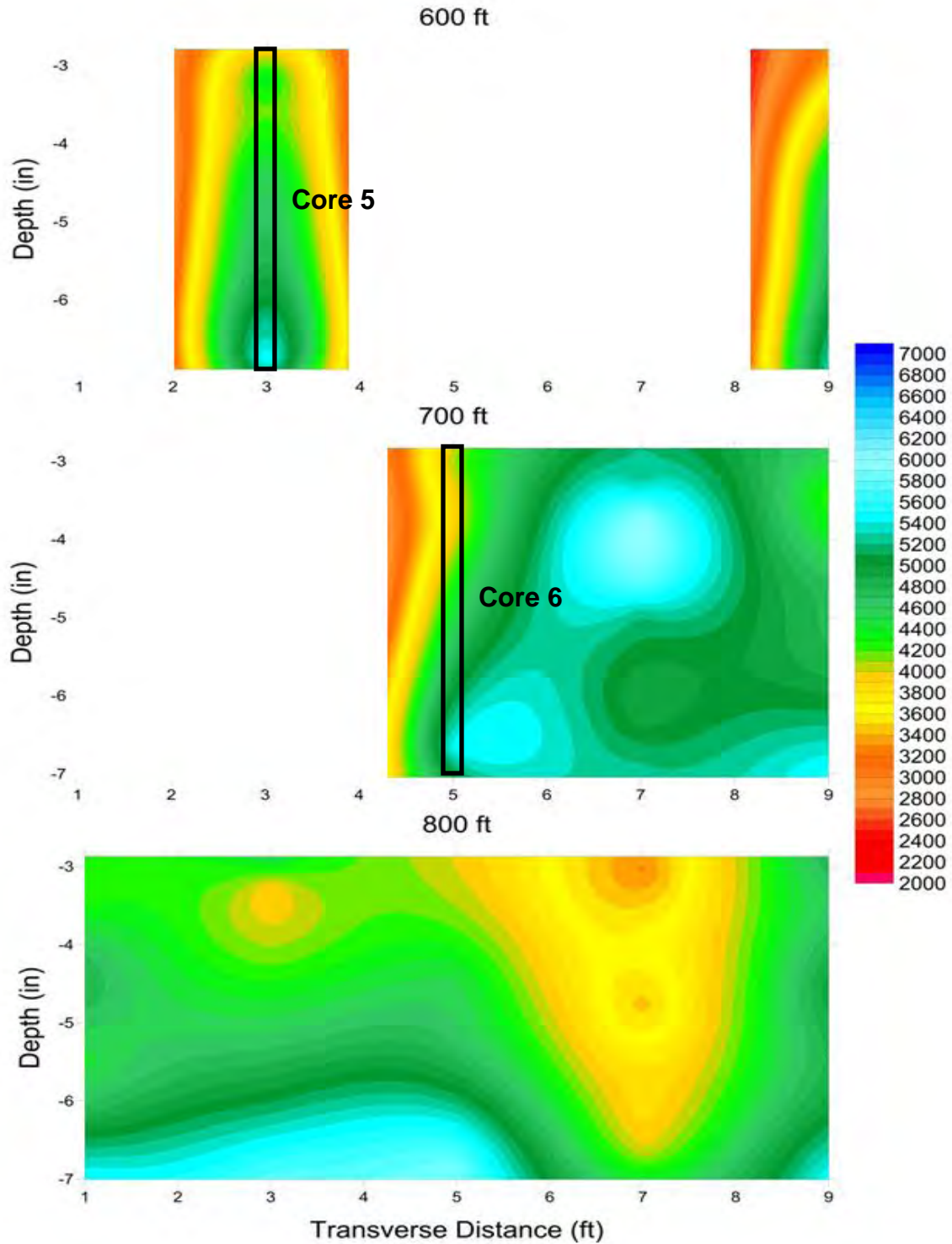


Fig. 3.96—Cross-sections depicting variations in the elastic modulus (ksi) for concrete for PSPA USW data acquired at the 600 ft, 700 ft, and 800 ft intervals along the GPR traverses. PSPA data could not be acquired at several test locations because of the deteriorated nature of the paved surface.

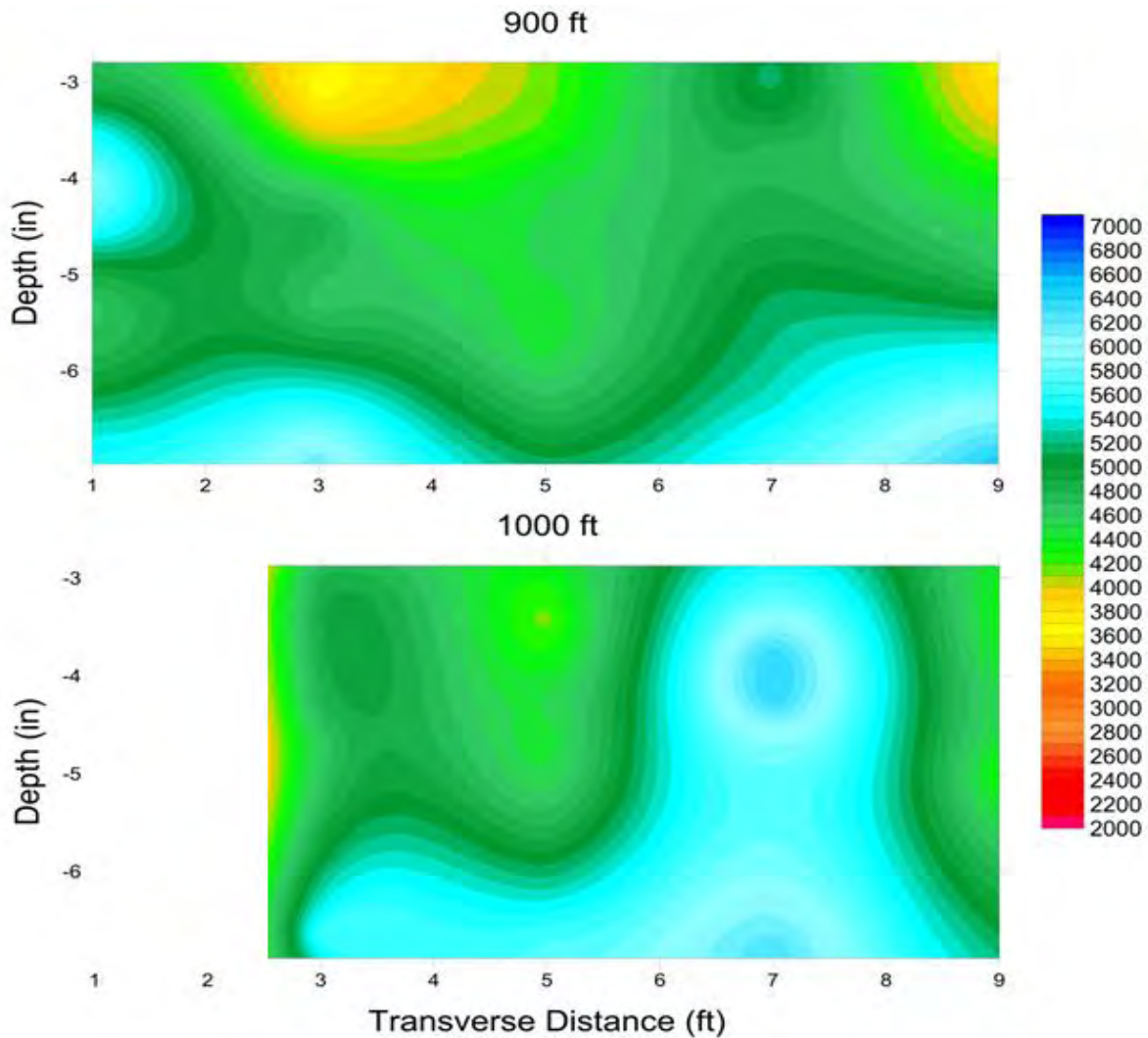


Fig. 3.97—Cross-sections depicting variations in the elastic modulus (ksi) for concrete for PSPA USW data acquired at the 900 ft and 1000 ft intervals along the GPR traverses. PSPA data could not be acquired at several test locations because of the deteriorated nature of the paved surface.

The average elastic modulus along each GPR transverse for the entire tested section pavement (3 in. to 11 in.) was calculated and plotted in Fig. 3.98. The average elastic modulus of the pavement does not appear to be statistically lowest in those areas where vehicles tires are most commonly in contact with the roadway.

Statistical Analysis Diagram

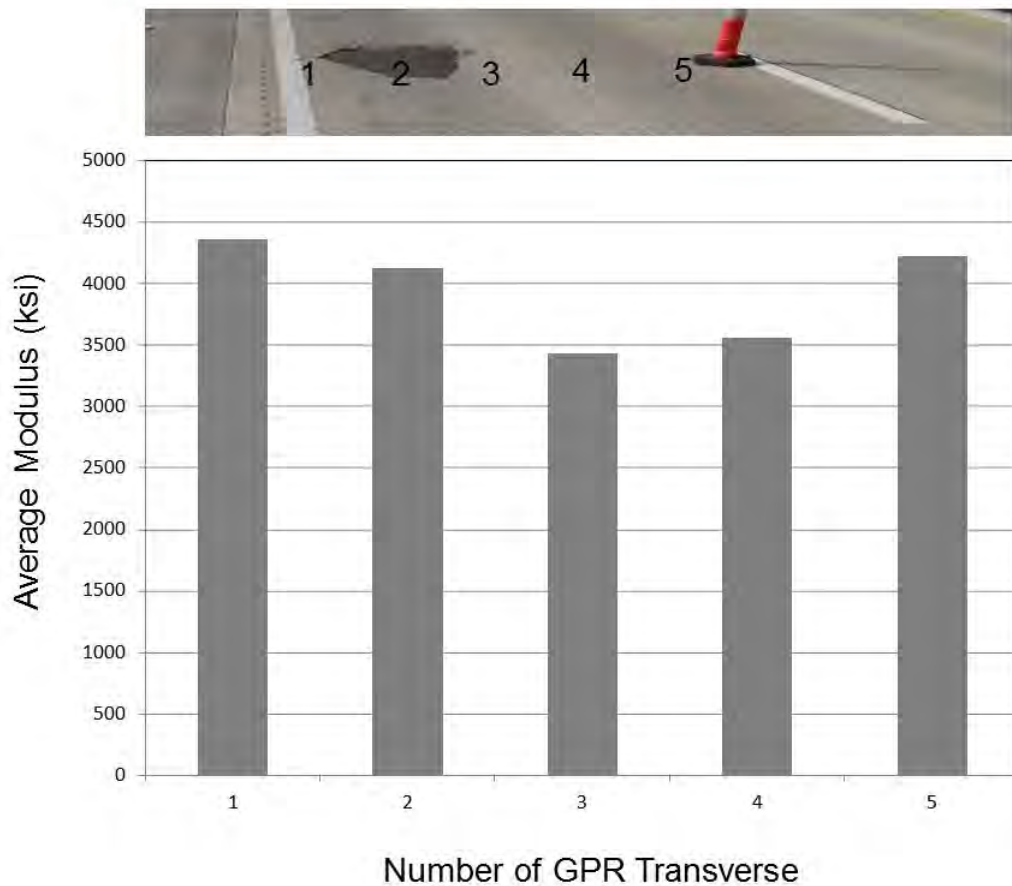


Fig. 3.98—Plot of the average elastic modulus (over depth range of 3 in. to 11 in.) along each GPR transverse. The GPR traverses are spaced at 2 ft intervals. GPR traverse 1 is 1 ft from the outer edge of the pavement.

3.3.8.2 Impact Echo Data

IE data were acquired at each Site 8 PSPA test location (Fig. 3.91). The PSPA IE software automatically analyzed the amplitude spectrum of the acoustic data recorded by the near receiver transducer at each test location and identified a single peak on each amplitude spectra. These peak frequencies (Fig. 3.5) were interpreted as resonant frequencies. The depths to the corresponding reflectors were calculated using Eq. 3.3 (Section 3.2.2.2).

The PSPA software consistently identified a single peak frequency on the IE data acquired at Site 8. The PSPA output calculated depth to the corresponding reflector varied from 3 in. to 14 in. and averaged about 5.5 in. (Fig. 3.99). The depth to the PSPA IE identified reflector correlates somewhat with the PCC/BM interface.

The compressional wave velocity used in Eq. 3.3 was calculated using Eq. 3.1 (Section 3.2.2.1). The compressional wave velocity (V_p) calculated using Eq. 3.1 is a function of the average surface wave velocity (V_R) of the upper approx. 11 in. of pavement (7 in. of PCC, 1 in. of

BM and 3 in. of PCC). The compressional wave velocity used for depth estimation purposes is probably lower than the actual compressional wave velocity of the upper layer of PCC. Hence the thickness of this layer is underestimated.

In summary, the PSPA IE tool was unable to accurately estimate the thickness of the pavement with a reasonable degree of reliability and consistency.

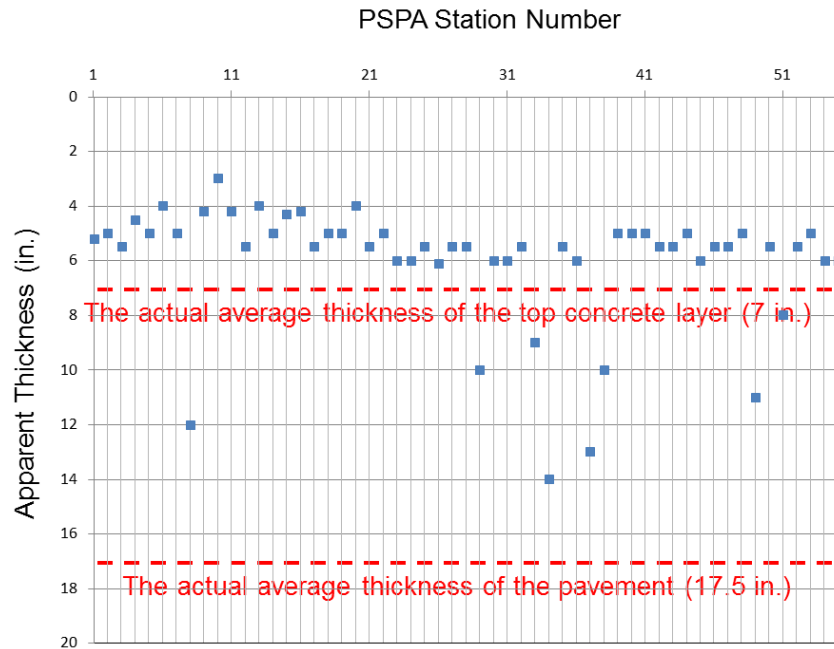


Fig. 3.99–The apparent thickness measurement for the pavement.

3.4 Concluding Remarks

Based on the correlations between core control and the acquired PSPA USW data the following conclusions are reached:

1. The elastic modulus values of the uppermost layer of pavement (BM or PCC) as determined in-situ using the PSPA USW tool are consistent with the visual assessment core control.
2. The “apparent” elastic modulus values of underlying layers of pavement (BM or PCC) as determined in-situ using the PSPA USW tool are consistent with the visual assessment core control.
3. The PSPA IE tool was not able to consistently generate reliable estimates of pavement layer thicknesses.
4. The PSPA IE tool was not able to consistently generate reliable estimates of the depths to flaws within the pavement layers. Indeed, at several sites and at multiple locations, the PSPA IE tool output depths to apparently non-existent reflectors.

4 PROJECT-LEVEL HIGH-FREQUENCY GROUND PENETRATING RADAR INVESTIGATIONS

4.1 Introduction

High-frequency ground-coupled ground penetrating radar (GPR) data are most commonly acquired using an antenna in monostatic-mode (transmitter/receiver housed in single case). However, in some situations (for example where velocity control is desired and/or to enhance the amplitude of specific reflections) high-frequency ground-coupled GPR data are acquired using two antennae in bistatic-mode (transmitter/receiver housed in separate cases). For Task 4 investigation purposes, pavement GPR data were acquired using single cart-mounted high-frequency (1.5 GHz) antenna operated in monostatic-mode (Fig. 4.1).



Fig. 4.1—Photograph taken at Site 1 (US 63) showing operator, push-cart, high-frequency 1.5 GHz GPR antenna (in white plastic shell on pavement surface) and GSSI SIR-3000 control unit (top of cart). The 400 MHz data (discussed in Section 5) were acquired using the same set-up (lower-frequency 400 MHz antenna was placed in the white plastic shell). The acquired GPR data are displayed in real time on the control unit screen. At some project-level test sites, core locations were selected, in part, on the basis of the real-time interpretation of the acquired high-frequency GPR data.

In this investigation, ground-coupled pavement GPR data were acquired at low speeds (walking speed; typically three to five miles per hour) using both a relatively high-frequency antenna (1.5 GHz; 1500 MHz) and a relatively low-frequency (400 MHz) antenna. A single cart-mounted antenna was employed (Fig. 4.1). The high-frequency GPR data are presented and discussed in Section 4.3 of this report; the low-frequency antenna data are presented and discussed in Section 5.3.

As the GPR antennae was moved along a traverse across the pavement, a short burst (GPR pulse; little more than one wavelength in duration) of band-limited electromagnetic radiation was emitted at predetermined distance intervals (48 scans per foot for 1.5 GHz antenna and 24 scans per foot for 400 MHz antenna) (Fig. 4.2).

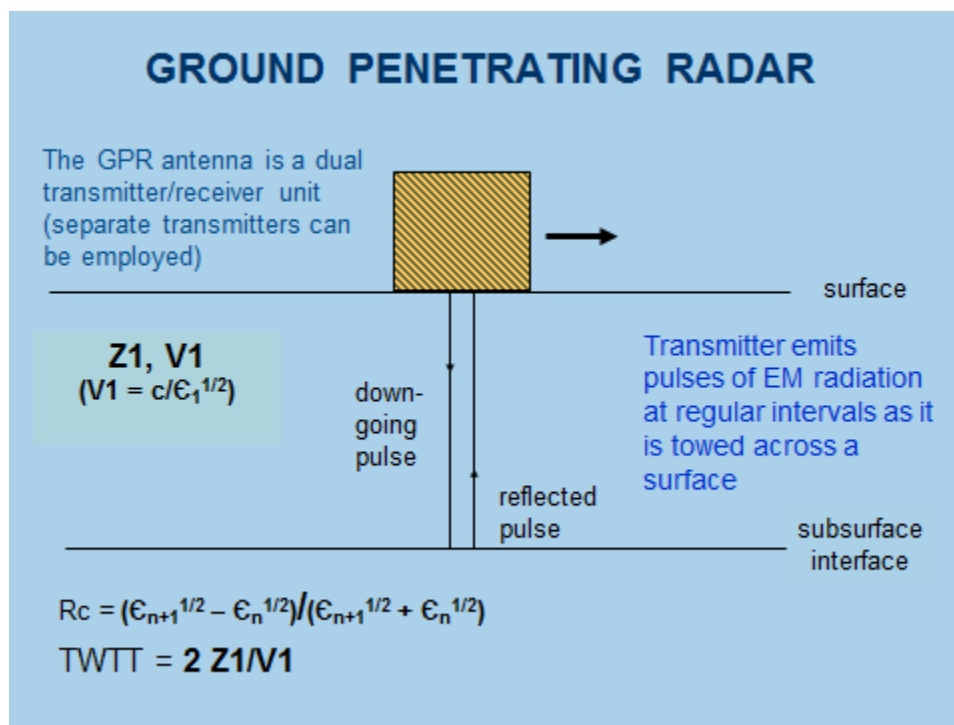


Fig. 4.2—A GPR antenna emits a short duration pulse (approx. one wavelength in duration) of radio wave frequency electromagnetic (EM) radiation at regular intervals as it is moved across the paved surface. EM radiation is emitted like light from a flashlight. The GPR pulse propagates into the subsurface with a velocity (V) that is a function of the speed of light in a vacuum (c) and the dielectric permittivity (ε) of the material through which it is passing. If the downward propagating pulse encounters an interface across which there is a change in electrical properties (dielectric permittivity; often associated with moisture content in non-metals), some of the incident radiation will be transmitted and some will be reflected back to the antenna. The GPR antenna records both the arrival time (two-way travel time; TWTT) and the magnitude of these reflected pulses. If the velocity with which the GPR pulse travels is known (or can be reliably estimated), the depth to the reflector can be estimated.

The GPR pulse propagates away from the shielded transmitter coil in the antenna and into the pavement (like visible light emanating from a flashlight). When the GPR pulse is incident on an interface separating materials with different electrical properties (dielectric permittivity), some of the incident energy is reflected back towards the receiver coil housed in the antenna. Typical pavement reflectors include the tops and bases of bituminous mix (BM) layers, the tops and bases of portland cement concrete (PCC) layers, embedded reinforcing steel and/or wire mesh, and (for lower-frequency antennae) the tops and bases of other underlying pavement layers.

The arrival times and the magnitudes of all reflected GPR energy (within a preset time window) are recorded as a single trace each time a pulse is discharged. The time window is set such that reflections can be recorded from the base of the lowermost target. Higher-frequency antenna can normally be used to image the bases of BM and PCC layers. Lower-frequency antenna can normally be used to image the tops and bases underlying pavement layers (and in certain instances, native soil layers and top of rock). If the materials through which the signals pass and the distance to the objects causing the reflections are the same, *variations* in arrival times and magnitudes of the GPR reflected energy are usually attributed to the presence of degradation, or the conditions favorable for the development of degradation. In particular, amplitudes lower than the maximum reflection amplitude, and travel times longer than the minimum travel time are usually associated with regions of degradation.

Pavement GPR data are normally acquired with the objective of mapping variations in the amplitude of the reflections from the pavement layers and variations in the apparent thickness of the pavement layers. In areas where the shallow bituminous mix (BM) and/or portland cement concrete (PCC) are deteriorated, the GPR images of underlying reflectors are generally characterized by anomalously low amplitudes and relatively high apparent embedment depths. Saline moisture in deteriorated BM and PCC increases signal attenuation and decreases GPR pulse velocity. If there is no moisture within the deteriorated pavement, these characteristic signatures may not be present. Accordingly, moist pavement conditions are more favorable than hot, dry conditions.

This interpretive approach normally works very well if the pavement layers are uniformly thick. However, if the layer thicknesses vary, care must be taken not to misinterpret the effects of variable apparent thickness and associated variations in amplitude as indicative of changes in the condition of the pavement.

4.2 Overview of Project-Level High-Frequency GPR Investigations

Ground penetrating radar (GPR) data were acquired at eight (8) project-level roadways (Sites 1-8, respectively) using a GSSI SIR-3000 system and two different push-cart mounted ground-coupled GSSI antennae (400 MHz and 1.5 GHz) (Fig. 4.1). The 1.5 GHz antenna generated higher-resolution images that extended to a depth of not more than 18 in. The 400 MHz ground coupled antenna generated much lower-resolution images that extended to depths of multiple feet.

Ground-coupled GPR data were acquired with the objective of assessing the utility and cost-effectiveness of the both the high-frequency (1.5 GHz) and low-frequency (400 MHz) GPR tools for pavement investigations.

High-frequency and low-frequency ground-coupled GPR data were acquired at each of the following eight project-level sites:

- Project-level Site US 63 (Site 1)
- Project-level Site US 54 (Site 2)
- Project-level Site Rte 179 (Site 3)
- Project-level Site HWY AT (Site 4)
- Project-level Site I-55 (Pemiscot Co., Site 5)
- Project-level Site I-55 (Perry Co., Site 6)
- Project-level Site HWY U (Site 7)
- Project-level Site I-35 (Site 8)

At each project-level test site, high-frequency 1.5 GHz GPR data were acquired along five parallel traverses (six traverses at Sites 7 and 8) spaced 2 ft intervals (1.5 ft at Site 7) (Fig. 4.1 and Fig. 4.3). At each project-level pavement site, low-frequency GPR data were acquired along traverse 3 only (Fig. 4.3). All GPR data (low-frequency and high-frequency) were acquired at each project-level site in less than four hours. Lane closures were required.

High-frequency (1.5 GHz) GPR data were acquired using sampling rates of 512 samples/scan and 48 scans/ft, but processed using 24 scans/ft. Low-frequency (400 MHz) GPR data were acquired using sampling rates of 512 samples/scan and 24 scans/ft, but processed using 12 scans/ft. The GPR data were processed using GSSI RADAN 6 and RADAN 7 processing software. Initial processing steps included:

1. Time-to-depth conversion (reflection time to reflector depth). A **constant velocity** (selected for each site based on the correlation between a “typical” core and the corresponding GPR data) was used to transform reflection travel times to apparent reflector depths. To facilitate comparisons, the same dielectric permittivity was used for both the high-frequency and low-frequency GPR profiles. The term “apparent” is used because a constant velocity is used to transform “reflection arrival time” to “reflector depth”. For example, in areas where the pavement is deteriorated, the **constant velocity** may be greater than the actual GPR pulse velocity. Hence, layer depths in these areas may be overestimated. Conversely, in areas where the pavement is in excellent condition, layer depths may be underestimated.
2. Time-zero correction and filtering to eliminate noise and improve image for visual interpretation.
3. Mapping (“picking”) of the variable apparent depths and amplitudes of the reflections from base of the identifiable BM and/or PCC layers.

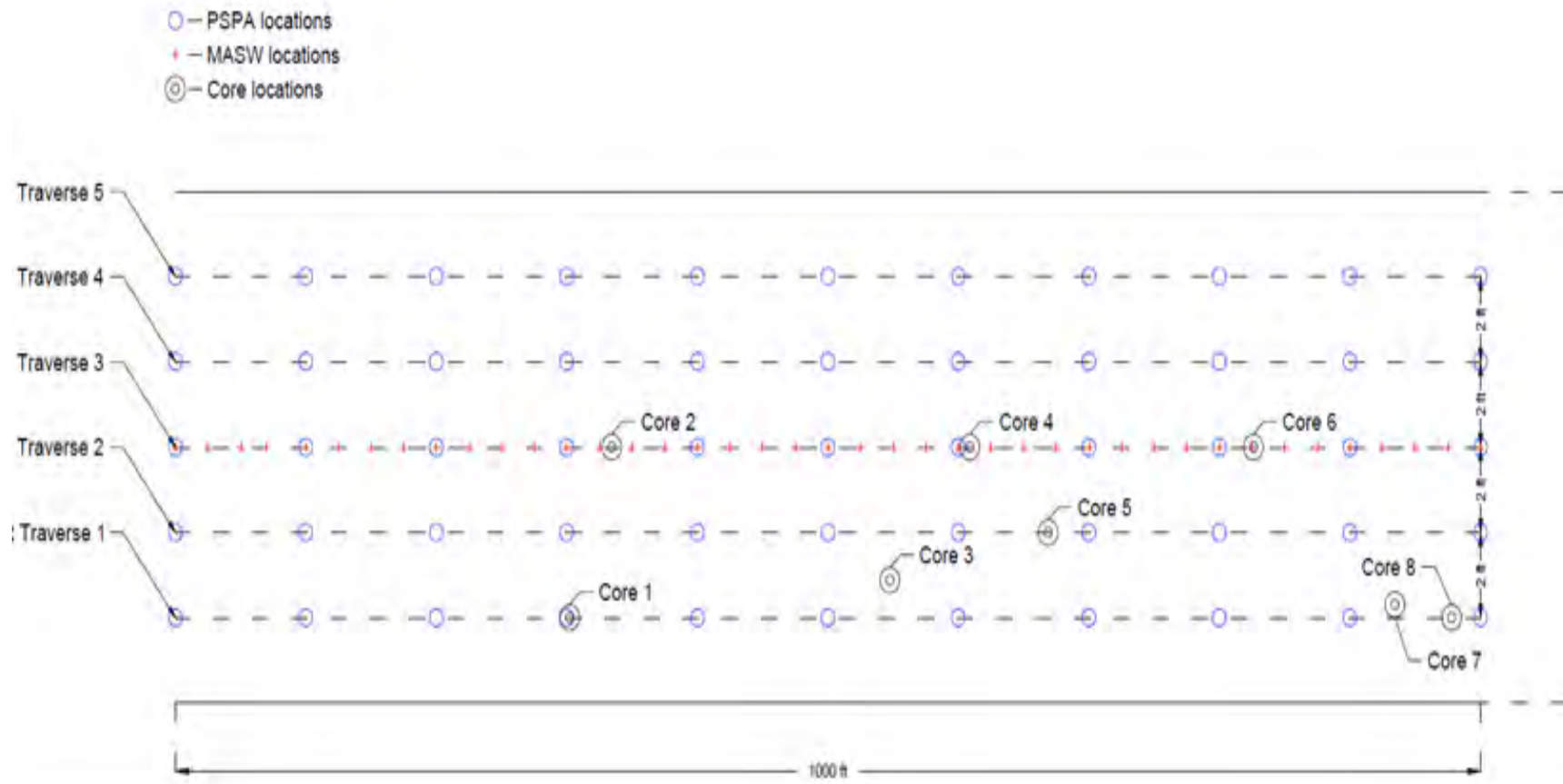


Fig. 4.3—Example plan view map of a project-level site. At each project-level site, high-frequency (1.5 GHz) GPR data were acquired five parallel traverses (six traverses at Sites 7 and 8) spaced 2 ft intervals (1.5 ft at Site 7). Low-frequency GPR data were acquired along traverse 3 only. All GPR data (low-frequency and high-frequency) were acquired at each project-level site in less than four hours. Lane closures were required.

The initial output of processing was an Excel spreadsheet that included reflection amplitudes (in units of normalized decibels, NdB) and two-way travel times (in units of nanoseconds, ns) for each mapped pavement layer. Post-processing steps included combining the Excel spreadsheet information from individual GPR profiles into one Excel file with assigned coordinates for each GPR profile.

The final processing step was the generation of contour maps plotted on the top surface of the pavement depicting variations in the reflection amplitude from the base of each mapped pavement layer using the software program Surfer (by Golden Software). It should be noted that it was necessary to interpolate between control points on adjacent GPR profiles (across 2 ft intervals in most instances). Also, many of the cores were not acquired exactly on GPR traverses. This could explain why the GPR interpretations do not always correlate exactly with the acquired core control.

Each GPR profile was visually assessed and interpreted. Example GPR data (GPR profile 1, stations 904-992) are shown in Fig. 4.4. Imaged features include embedded steel reinforcement (e.g. welded wire mesh), concrete slab joints, and base of the BM and the PCC layers.

In Section 4.3 of this report, the high-frequency (1.5 GHz) project-level GPR data are presented. In Section 5, the low-frequency (400 MHz) project-level GPR data are presented.

4.3 Project-Level High-Frequency GPR (1.5 GHz) Data

4.3.1 Project-Level Site 1 (US 63)

Project-level pavement Site 1 (US 63) is located north of Rolla, Missouri (Figs. 4.5- 4.7). The pavement at Site 1 consists of two layers of bituminous mix (BM) over portland cement concrete (PCC) (Fig. 4.6). Typical Site 1 pavement layer thicknesses (based on core control) are as follows: upper BM: 1.5 in.; middle BM: 2.0 in.; lower PCC: 8.5 in. (Fig. 4.6).

High-frequency (1.5 GHz) GPR data were acquired in the north-bound lane of US 63 along five parallel traverses spaced at 2 ft intervals (Fig. 4.5 and Fig. 4.7). The acquisition parameters employed were 512 samples/scan and 48 scans/ft. A dielectric permittivity of 8.0 was used to convert reflection times to reflector depths. All the Site 1 GPR data (low-frequency and high-frequency) were acquired in less than four hours.

The objectives of the high-frequency GPR investigation at Site 1 were to two-fold. The first objective was to determine the approximate thicknesses of the BM and PCC layers within the paved roadway. The second objective was to identify areas of possible pavement degradation. A representative segment of a Site 1 GPR profile is shown as Fig. 4.4.

The profiles were used to generate 2D contour maps of the apparent depth to various features. In Fig. 4.8, the following apparent depth maps are presented (a constant velocity was used to transform reflection times to reflector depths; dielectric permittivity of 8.0):

1. Apparent depth to base of the first BM layer;
2. Apparent depth to base of the second BM layer;
3. Apparent depth to base of the PCC layer.

In Table 4.1, the core depths to each of the pavement layers are compared to the GPR-estimated depths to each of the corresponding pavement layers. As noted in Table 4.1, all twenty-four GPR-estimated base pavement layer depths (with two exceptions) and corresponding core depths differ by 10% or less. The differences (of up to 10%) can be attributed to: a) slight variations in the thicknesses of both the higher velocity BM layers and the lower velocity PCC layer; b) slight changes in the physical and chemical properties of the BM and PCC; and c) the use of a constant GPR pulse velocity. With respect to bonded and debonded cores (Fig. 4.6) there does not appear to be a statistical correlation between the core thicknesses and GPR-estimated thicknesses. However, at one core location there appears to be a possible correlation between the core and GPR-estimated thicknesses and the visual appearance of the PCC. More specifically, core 7 (Fig. 4.6) is the only core that shows visual evidence of chemical degradation. The GPR-estimated depth to the base of the PCC is 2.6% greater than the corresponding core depth. At all other core locations, the core depths to the base of the PCC are the same or greater than GPR-estimated depth. The most logical explanation is that GPR pulse velocity of the PCC segment of core 7 is slightly lower than that of the PCC at the other cores. Because a uniform velocity was used to convert all GPR reflection times to reflector depths, the GPR-estimated thickness at the core 7 location is therefore anomalously high.

The profiles were also used to generate 2D contour maps of the reflection amplitudes to various features. In Fig. 4.9, the following reflection amplitude maps are presented:

1. Amplitude of the GPR reflection from the base of the top layer of BM layer;
2. Amplitude of GPR reflection from the base of the bottom layer of BM layer;
3. Amplitude GPR reflection from the base of the concrete (PCC) reinforced with reinforcing mesh layer.

The amplitudes of the reflections from the base of the upper layer of BM and the base of the lower layer of BM at all core locations are relatively uniform. This is consistent with the core control that indicates these layers are not stripped or otherwise degraded at any of the core locations. However, it should be noted that cores were not acquired in areas where the amplitudes of these reflectors are anomalously low. The lack of stripping was expected because the overlay was only about one month old.

The amplitudes of the reflections from the base of the PCC at all core locations are relatively uniform, with the exception of core 4 and core 7. The anomalously low amplitude of the PCC reflection at core location 4 can be attributed to the fact that this core was acquired immediately adjacent to a joint (where reflection amplitudes and arrival times are difficult to map with confidence). The anomalously low amplitude of the PCC reflection at core location 7 is consistent with the concept that the GPR signal would be attenuated anomalously rapidly as it passed through degraded PCC.

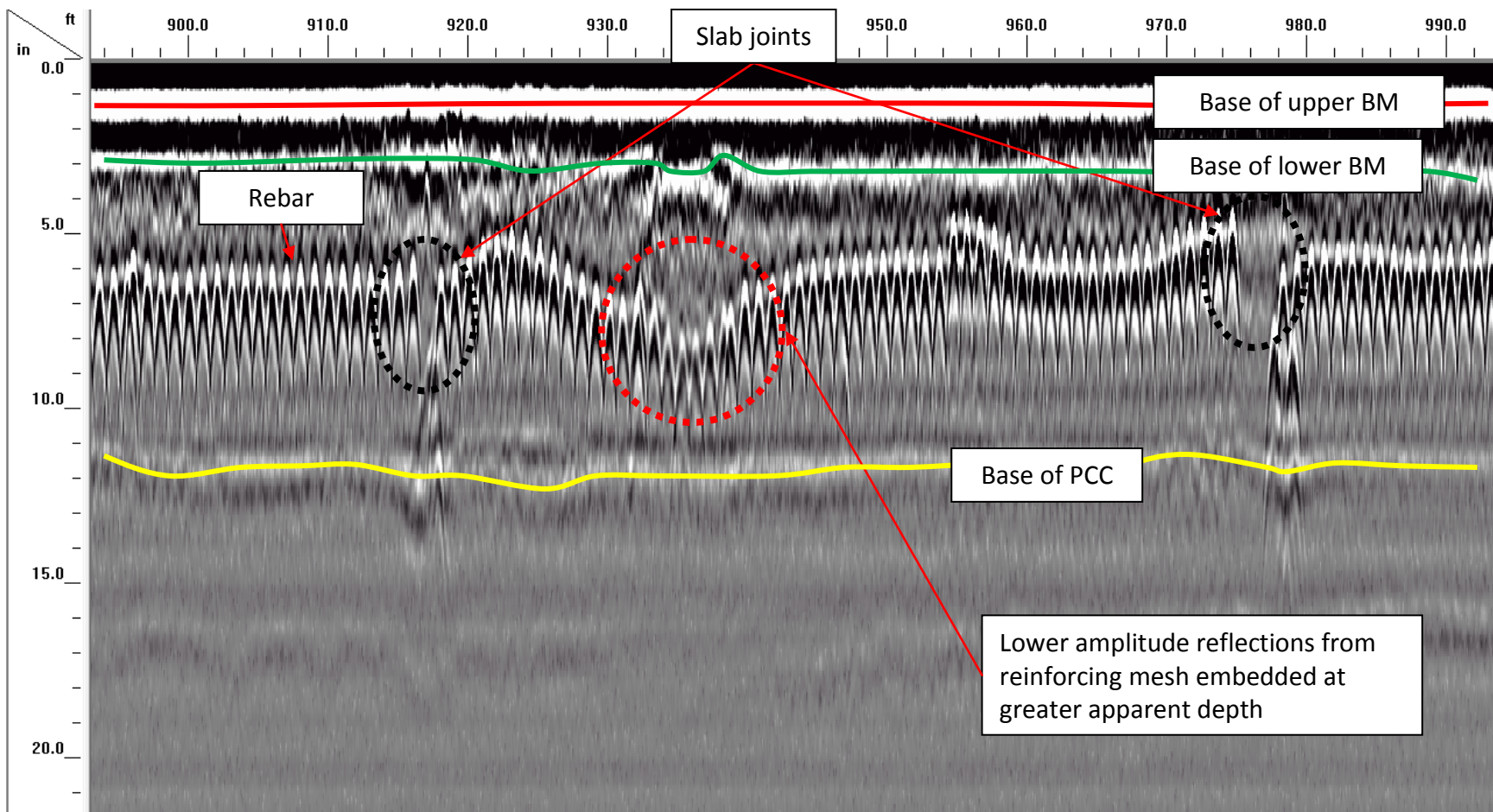


Fig. 4.4—Cross-sectional example of high-frequency (1.5 GHz) GPR data (Site 1; US 63). A constant GPR-pulse velocity (selected for each site based on the correlation between a “typical” core and the corresponding GPR data) was used to transform reflection travel times to reflector depths. The depths to each reflector, particularly on GPR data acquired at sites where pavement condition varied or where different pavement materials were used, are therefore “apparent” rather than “absolute”. The interpreted bases of upper and lower bituminous mix (BM) layers are marked in red and the green, respectively; the interpreted base of the portland cement concrete (PCC) layer is marked in yellow. The horizontal axis is in units of feet; the vertical axis is in units of inches.



Fig. 4.5—Photograph of US 63 (Site 1). GPR traverses 1-5 (left to right) are marked (Fig. 4.7)



Fig. 4.6—Typical Site 1 cores consisted of three layers: approx. 1.5 in. of upper BM; approx. 2 in. of underlying BM; and approx. 8.5 in. of basal PCC. At core locations 1, 2, 4, and 7 the BM/PCC contact was debonded; at the other five core locations (3, 5, 6 and 8) the BM/PCC contact was not debonded. Debonded core 7 (above right) is the only core that showed visual evidence of chemical degradation (note staining of PCC). Core locations were selected on the basis of the preliminary on-site visual interpretation of the acquired GPR data. Edge of pavement (hand written notes in core photographs) refers to the edge of the driving lane. The edge of the driving lane was 10 ft from the edge of the paved shoulder (Fig. 4.5 and Fig. 4.7).

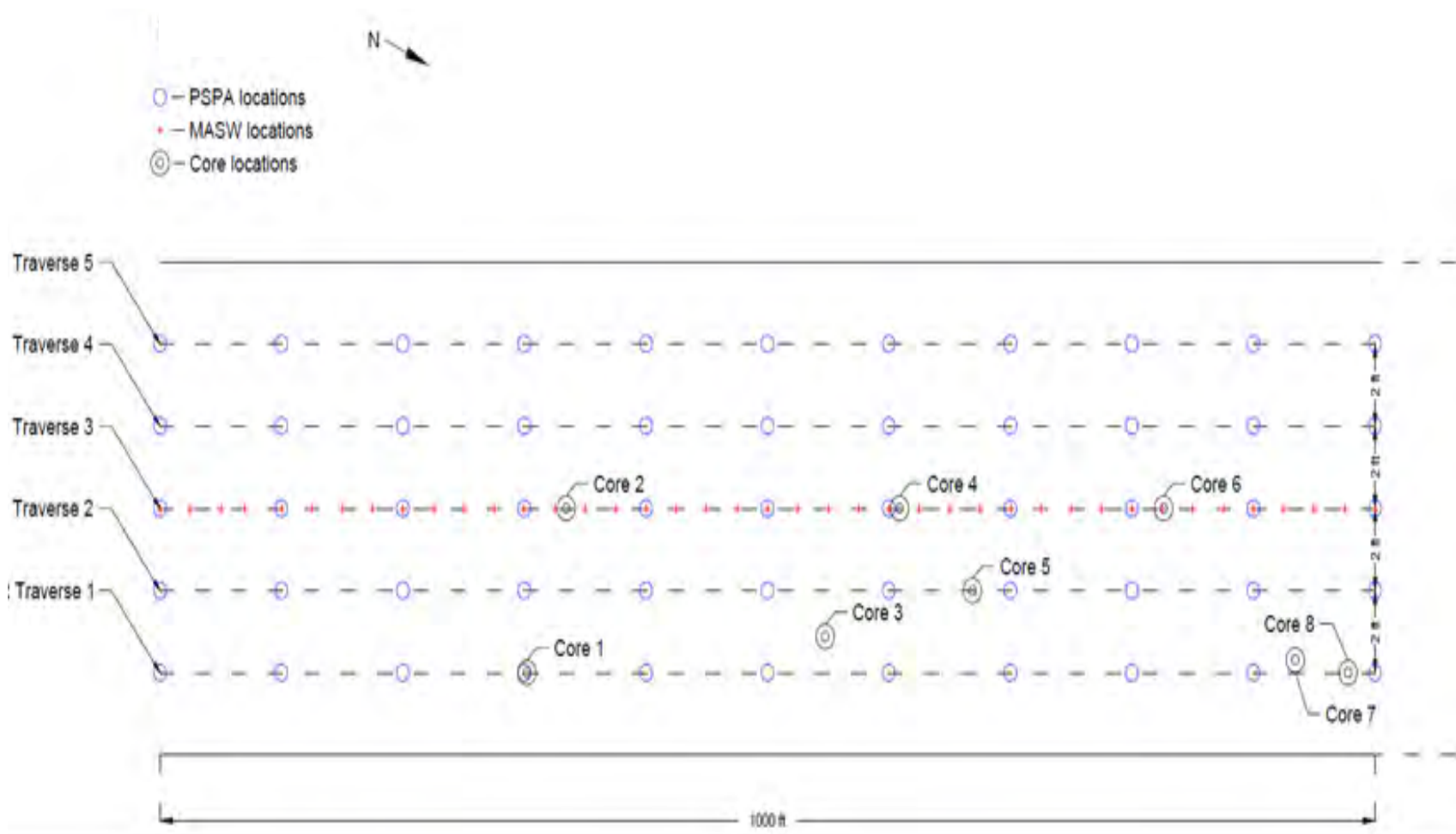


Fig. 4.7—Plan view map of US 63 (Site 1) showing locations of GPR traverses 1-5. High-frequency (1.5 GHz antenna) GPR data were acquired along all five traverses; low-frequency (400 MHz antenna) data GPR data were acquired along traverse 3 only. Solid black lines represent the driving lane boundaries. Lane width was 12 ft. Core locations are marked as black circles. PSPA locations are marked as blue circles. MASW locations are marked as red crosses. Traverse 1 was 2 ft from the edge of driving lane boundary (12 feet from edge of the paved shoulder; Fig. 4.5).

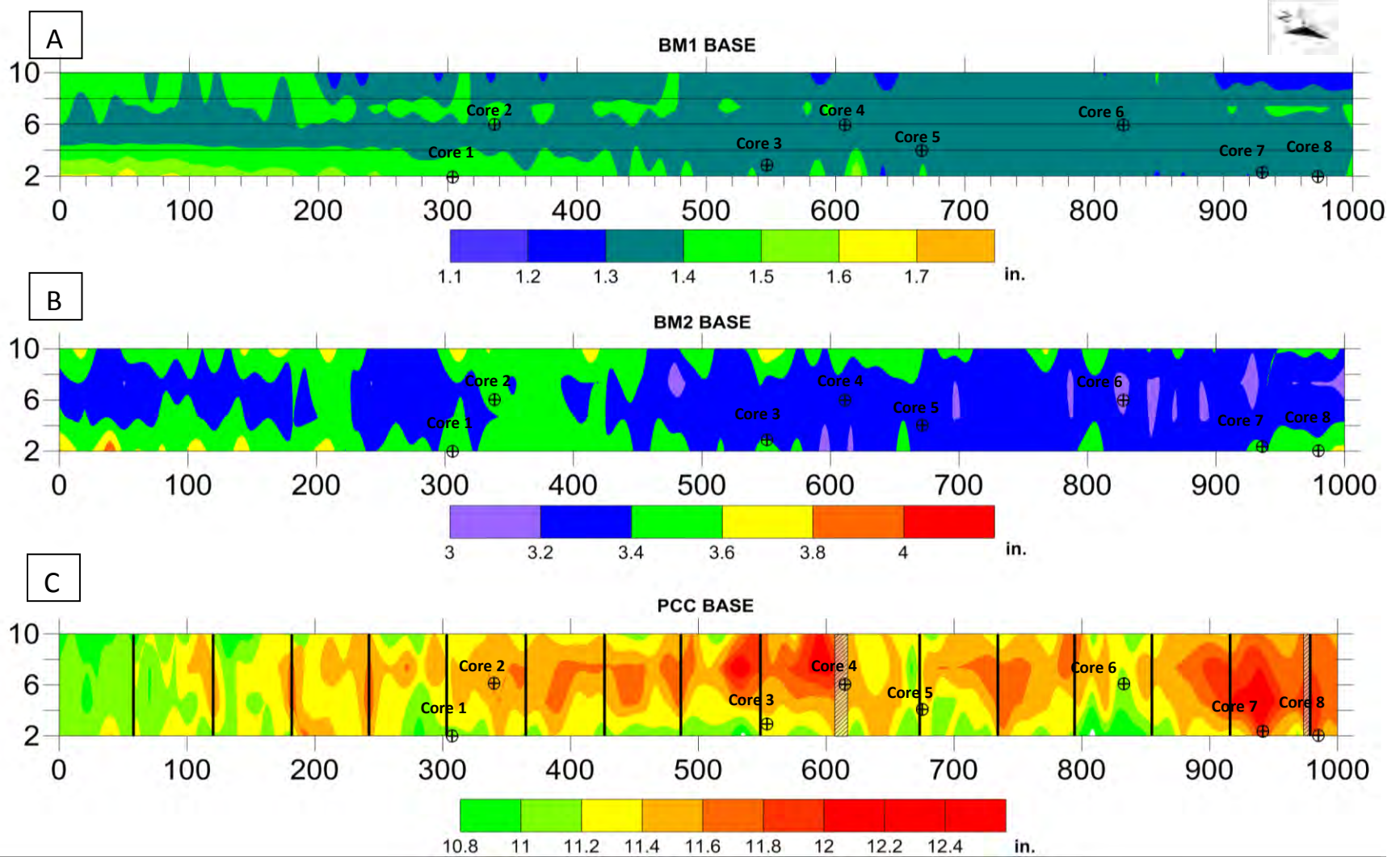


Fig. 4.8—Plan view showing GPR-estimated “apparent” depth to the base of: A) the upper layer of BM (BM1). Horizontal solid black lines represent locations of the GPR traverses ; B) the lower layer of BM (BM2); and C) the base PCC. GPR data were processed using a dielectric permittivity of 8.0. Vertical and horizontal axes are distance in feet. The vertical bars on Fig. 4.8C correspond to joint locations.

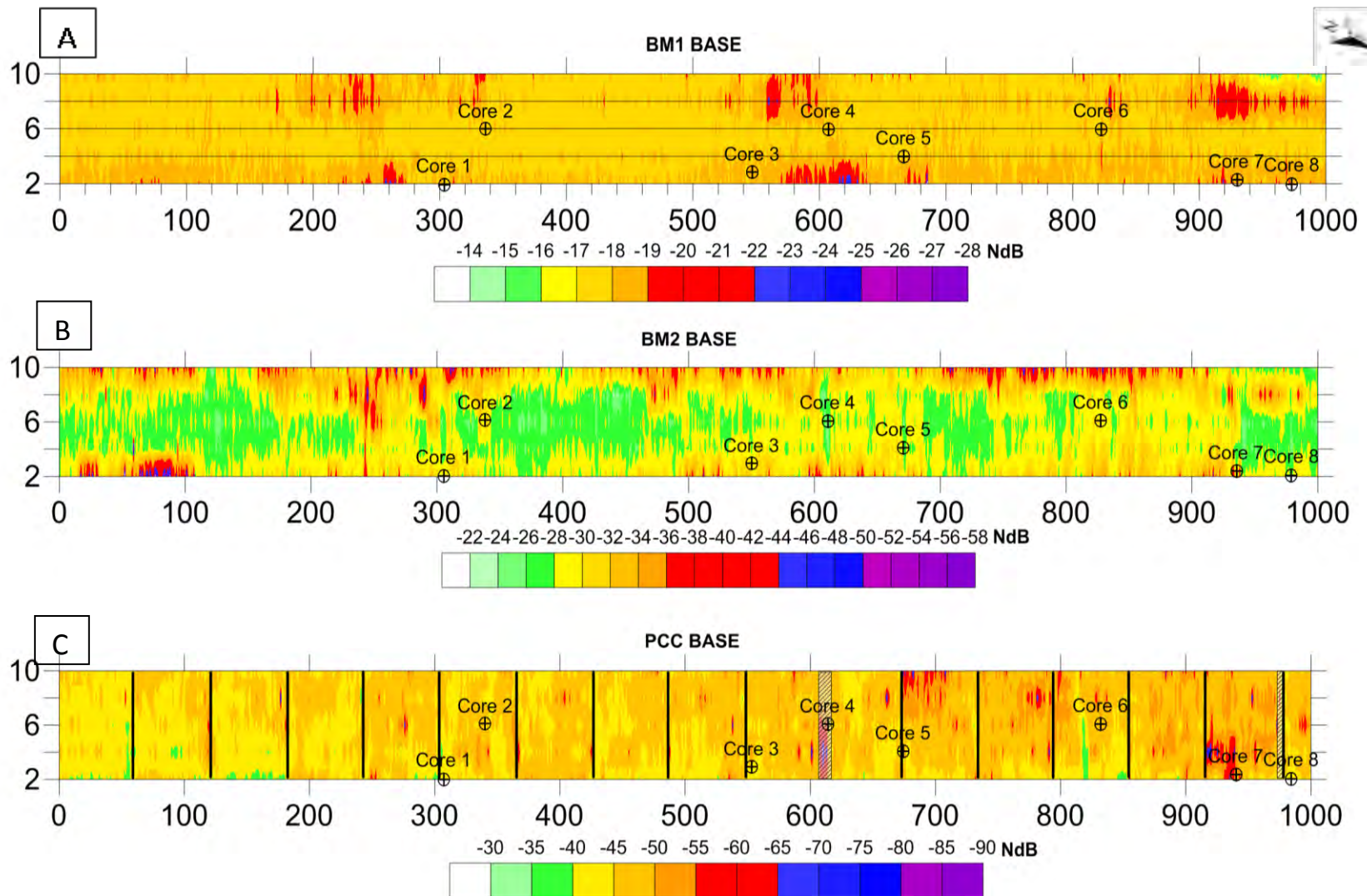


Fig. 4.9—Plan view showing base map with superposed GPR interpretations: A) amplitude of GPR signal reflected from the base of the top layer of BM. Horizontal solid black lines represent locations of the GPR traverses; B) amplitude of GPR signal reflected from the base of the lower layer of BM; and C) amplitude of GPR signal reflection from the base of the PCC. Vertical and horizontal axes are distance in feet.

Table 4.1–Core depths and GPR apparent depths to base of pavement layers at Site 1

Core #	1	2	3	4	5	6	7	8
BM1 (Core) depth, in.	1.5	1.5	1.375	1.375	1.375	1.375	1.375	1.5
BM1 (GPR) depth, in.	1.4	1.4	1.3	1.3	1.3	1.3	1.3	1.3
Correlation*,%	93.3	93.3	94.5	94.5	94.5	94.5	94.5	86.7
BM2 (Core) depth, in.	3.5	3.5	3.3	3.3	3.3	3.3	3.3	3.5
BM2 (GPR) depth, in.	3.4	3.4	3.4	3.2	3.2	3	3.4	3.4
Correlation*,%	97.1	97.1	103.0	97.0	97.0	90.9	103.0	97.1
PCC (Core) depth, in.	11.3	11.75	11.5	12.375	11.25	12.5	11.5	11.5
PCC (GPR) depth, in.	11	11.4	11.2	12	11.2	11.1	11.8	11.5
Correlation*,%	97.8	97.0	97.4	97.0	99.6	88.8	102.6	100.0

*Correlation is calculated based on the following formula: [Depth based on GPR data]/[Depth based on core control]*100. Correlation values below 100% typically indicate use of an overestimated dielectric permittivity (relative permittivity); correlation values above 100% typically indicate the dielectric permittivity (relative permittivity) used was underestimated. Values highlighted in red show correlation values below 90% and/or above 110%.

The GPR tool could also be used to map joints and the location and depth of embedded reinforcing mesh.

Analyses of the acquired GPR data and core control suggest that the GPR tool could not be used at Site 1 to detect areas where BM/BM and/or BM/PCC interfaces are debonded. However, the GPR tool could be used to estimate pavement layer thicknesses to within $\pm 3\%$ accuracy (except at core location 6) and the location of mesh.

4.3.2 Project-Level Site 2 (US 54)

Project-level pavement Site 2 (US 54) is located approximately 2 miles west of Camdenton, Missouri. The pavement at Site 2 consists of approximately 12 in. thick of full depth bituminous mix (BM) (Figs. 4.10, 4.11, 4.12). Locations of the GPR traverses and cores are shown in Fig. 4.11.

High-frequency (1.5 GHz) GPR data were acquired in the east-bound lane of US 54 along five parallel traverses spaced at 2 ft intervals (Fig. 4.11 and Fig. 4.12). The acquisition parameters employed were 512 samples/scan and 48 scans/ft. A dielectric permittivity 8.0 was used to convert reflection times to reflector depths. All the Site 3 GPR data (low-frequency and high-frequency) were acquired in less than four hours.

The objectives of the high-frequency GPR investigation at Site 2 were to detect stripping and debonding within the BM and to estimate the thickness of the BM. Stripping in all ten cores was described as low to moderate. Debonding was observed at all ten core locations.



Fig. 4.10—Photograph of site the project-level segment US54 (Site 2).

A representative core and corresponding representative segment of a Site 2 GPR profile is shown in Fig. 4.12. Note that reflections originating from debonded interfaces are imaged on the representative GPR profile. Reflections from stripped zones could not be differentiated from reflections from debonded interfaces on the high-frequency GPR profiles.

In Fig. 4.13, a map depicting the apparent depth (based on interpretation of GPR data) to the base of the BM is presented. (A dielectric permittivity of 8.0 was used to convert reflection times to depths.) Note that the apparent depth to the base of the BM varies significantly. The observed variations in apparent thickness are mostly attributed to actual variations in the thickness of the BM and to variations in the condition of the BM. A comparison

of core thicknesses to GPR-estimated thicknesses is presented in Table 4.2. GPR-estimated depths (with four exceptions) and corresponding core depths differ by 10% or less.

The differences (of up to 220%) can be attributed to: a) slight variations in the thicknesses of both the higher velocity BM layers; b) slight changes in the physical and chemical properties of the BM layers; and c) the use of a constant GPR pulse velocity; d) incomplete core recovery (especially cores 1, 6 and 10).

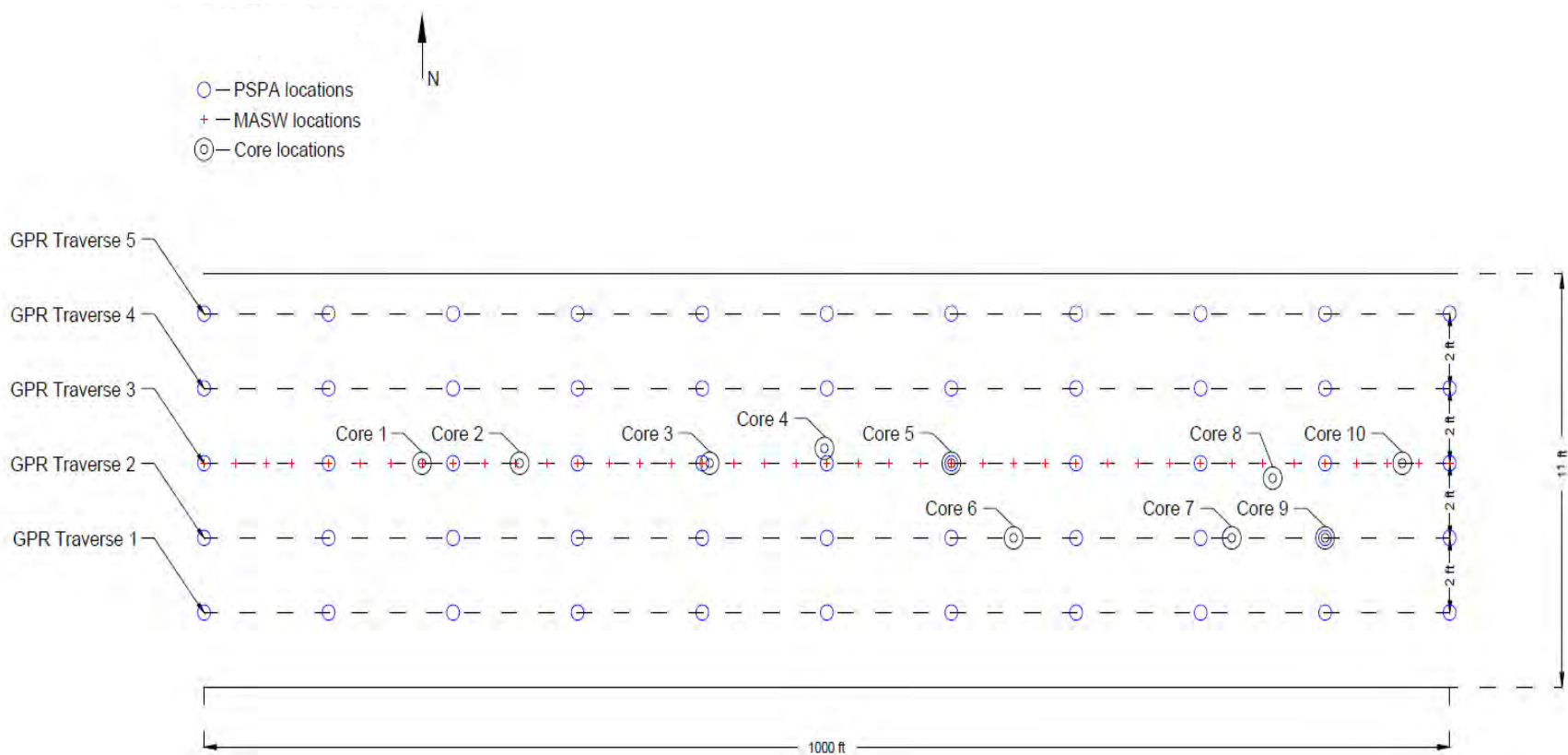


Fig. 4.11—Plan view map of US 54 (Site 2) showing locations of GPR traverses 1-5. High-frequency (1.5 GHz antenna) GPR data were acquired along all five traverses; low-frequency (400 MHz antenna) data GPR data were acquired along traverse 3 only. Solid black lines represent the driving lane boundaries. Lane width was 11 ft. Core locations (10) are marked as black circles. PSPA locations are marked as blue circles. MASW locations are marked as red crosses. Traverse 1 was 2 ft from the edge of driving lane boundary. Core locations are marked as black circles. PSPA locations are marked as blue circles. MASW locations are marked as red crosses.

Table 4.2–Core depths and GPR apparent depths to base of pavement layers at Site 2

Core #	1	2	3	4	5	6	7	8	9	10
BM (Core) depth, in.	8.5	10.5	11	11.25	9.5	4.75	11.25	11	11.25	8.25
BM (GPR) depth, in.	11	10.5	10.5	11	10.5	10	11	10.5	10.5	11
Correlation*,%	129.4	100.0	95.5	97.8	110.5	210.5	97.8	95.5	93.3	133.3

*Correlation is calculated based on the following formula: [Depth based on GPR data]/[Depth based on core control]*100. Correlation values below 100% typically indicate use of an overestimated dielectric permittivity (relative permittivity); correlation values above 100% typically indicate the dielectric permittivity (relative permittivity) used was underestimated. However, at site 2, the high positive values (in red) were recorded at locations where incomplete cores were extracted. Values highlighted in red show correlation values above 110%.

Differences between the actual and apparent thicknesses are also noted. Core depths and GPR apparent depths correlate well except for cores 1, 5, 6 and 10. The cores at these four locations were incomplete and/or not fully extracted.

In Fig. 4.14, a reflection amplitude map of the base of the BM is presented. As shown, the amplitudes of the reflections from the base of the BM are low and vary significantly. This is consistent with the core control that indicates the BM is both stripped and debonded at multiple depths. The degree of correlation between Fig. 4.13 and Fig. 4.14 is not overly high. This suggests that variations in apparent thickness of the BM are due to both real variations in BM thickness and variations in BM condition.

Analyses of the acquired GPR data and core control suggest that the GPR tool could be used at Site 2 to detect areas where stripping/debonding was present and to map the base of the BM. The generated apparent depth and amplitude maps indicate overall poor condition of the pavement, however, the presence of stripping and debonding in some areas can be confidently identified most readily based on the visual assessment individual GPR profiles.

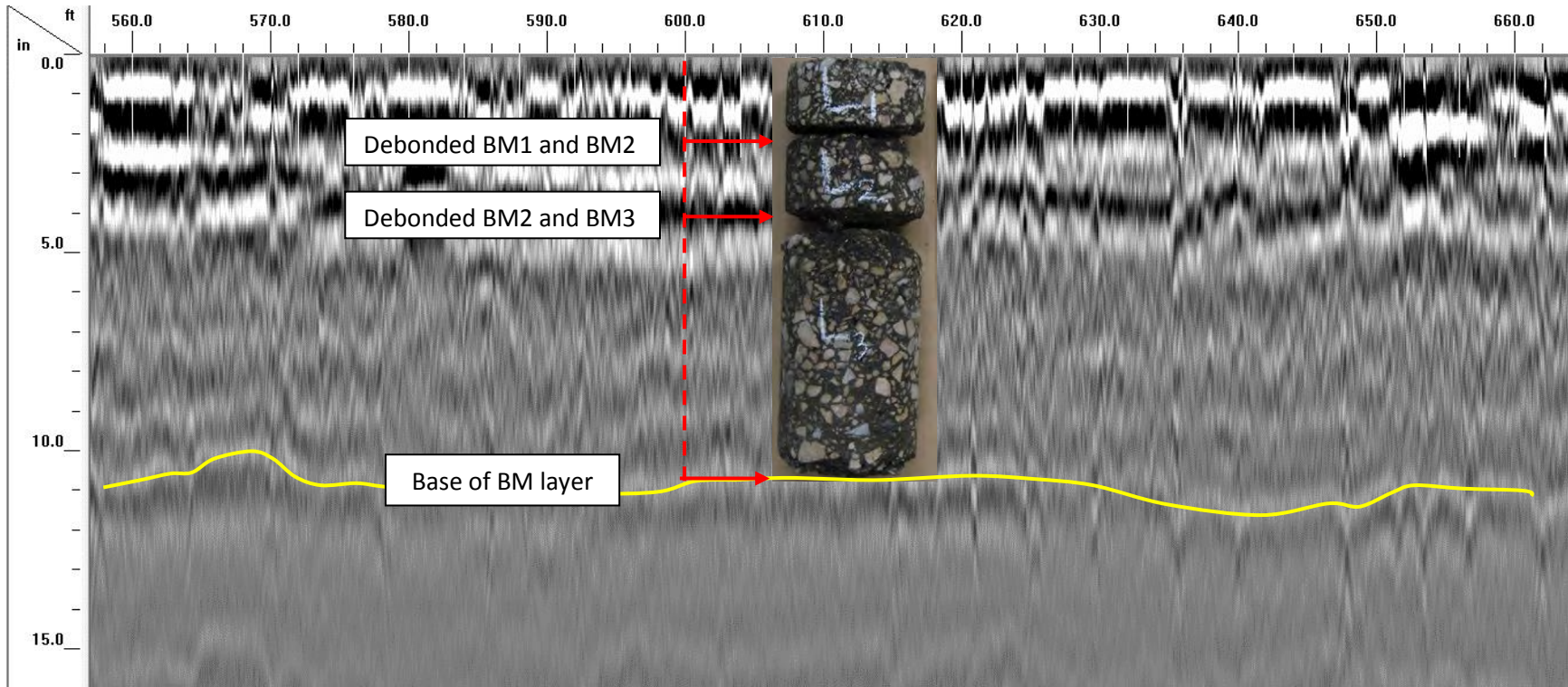


Fig. 4.12—Representative example of Site 2 high-frequency (1.5 GHz) GPR profile (GPR profile 3, stations 560-660) showing tie with core 5 (at station 600; Fig. 4.11). Reflections from the multiple stripped interfaces and the base of the BM can be identified. Variations in the apparent depth to the base of the BM are attributed to both lateral changes in the actual thickness of the BM and to lateral changes in the physical and chemical condition of the BM. The horizontal axis is in units of feet; the vertical axis is in units of inches.

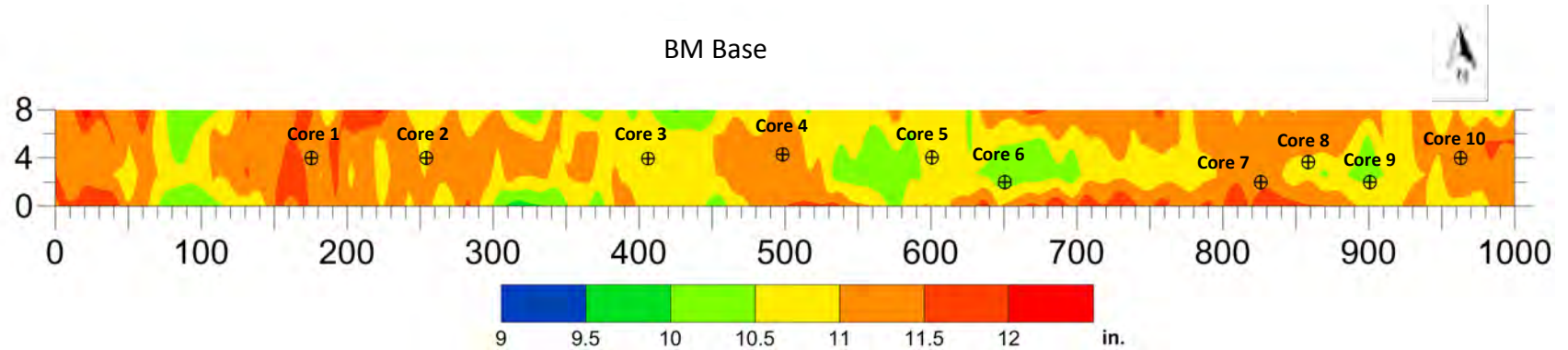


Fig. 4.13—Base map showing variations in the apparent thickness of the bituminous mix (BM). Thickness values are apparent and are based on the dielectric permittivity of 8.0. Traverse 1 (0 ft mark on map) was located 2 ft from the edge of the driving lane.

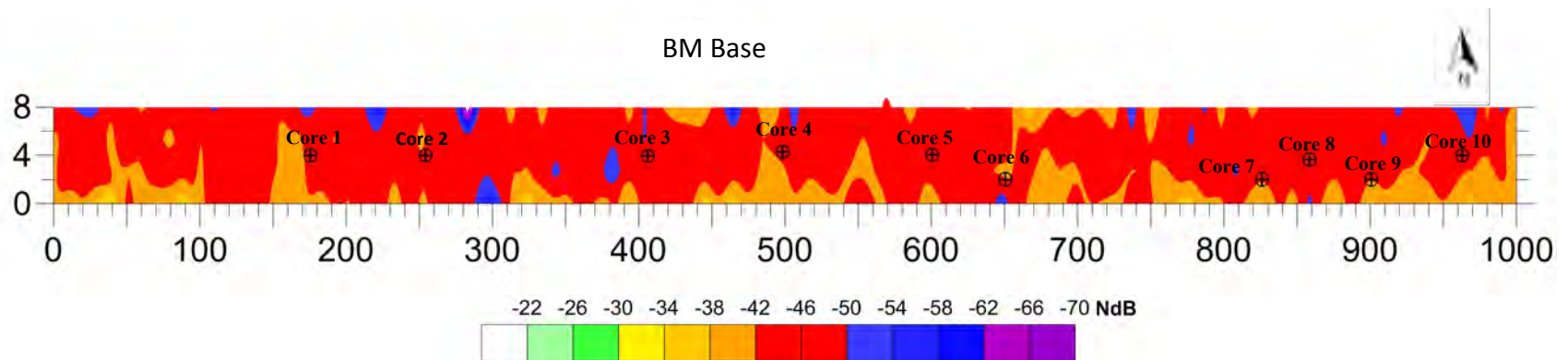


Fig. 4.14—GPR amplitude map of reflection from base bituminous mix (BM). Areas highlighted in orange, red and blue (<-34 NdB) indicate evidence of deterioration (stripping). Vertical and horizontal axes distances are in units of feet.

4.3.3 Project-Level Site 3 (MO 179)

The project-level pavement Site 3 (MO 179) is located approximately 4 miles west of Jefferson City, Missouri (Figs. 4.15, 4.16, 14.17). The investigation was conducted during the night due to the MoDOT safety policies. Typical Site 3 pavement consists of approximately 12.25 in. thick full depth bituminous mix (BM) (Fig. 4.15).

High-frequency (1.5 GHz) GPR data were acquired in the south-bound driving lane of MO 179 along five parallel traverses spaced at 2 ft intervals (Fig. 4.16). The acquisition parameters employed were 512 samples/scan and 48 scans/ft. A dielectric permittivity 7.5 was used to convert reflection times to reflector depths. All the Site 3 GPR data (low-frequency and high-frequency) were acquired in less than four hours. A map showing locations of the traverses and cores is shown in Fig. 4.16.

The objective of the high-frequency GPR investigation at Site 3 was to detect stripping and/or debonding within the BM. All 10 cores were described as moderately to highly stripped. Cores 5-10 were described as debonded.



Fig. 4.15—Photograph of site the project-level segment Rte 179 (Site 3).

A representative core and corresponding representative segment of a Site 3 GPR profile are shown in Fig. 4.17. The reflection from the base of the BM is shown. In Fig. 4.18, a map depicting the apparent depth to the base BM is presented. Note that the apparent depth to the base of the BM varies significantly. The observed variations in apparent thickness are attributed to actual variations in the thickness of the BM and to variations in the condition of the BM. A comparison of core thicknesses to GPR-estimated thicknesses is presented in Table 4.3. All GPR-estimated depths and corresponding core depths differ by less than 7%.

The differences (of up to 7%) can be attributed to: a) slight variations in the thicknesses of both the higher velocity BM layers; b) slight changes in the physical and chemical properties of the BM layers; and c) the use of a constant GPR pulse velocity.

Table 4.3–Core depths and GPR apparent depths to base of pavement layers at Site 3. Differences between the actual and apparent thicknesses are also noted. All of the ten cores were described as moderately to highly stripped. Cores 5-10 were described as debonded

Core #	1	2	3	4	5	6	7	8	9	10
BM (Core) depth, in.	11.3	11.5	11.5	12.25	12.25	12.25	12.25	12.25	12	11.875
BM (GPR) depth, in.	11	11.5	12	11.5	12.5	12.5	12.5	12.5	12	12.5
Correlation*, %	97.8	100.0	104.3	93.9	102.0	102.0	102.0	102.0	100.0	105.3

*Correlation is calculated based on the following formula: [Depth based on GPR data]/[Depth based on core control]*100. Correlation values below 100% typically indicate overestimated dielectric permittivity (relative permittivity); correlation values above 100% typically indicate the dielectric constant (relative permittivity) used was underestimated.

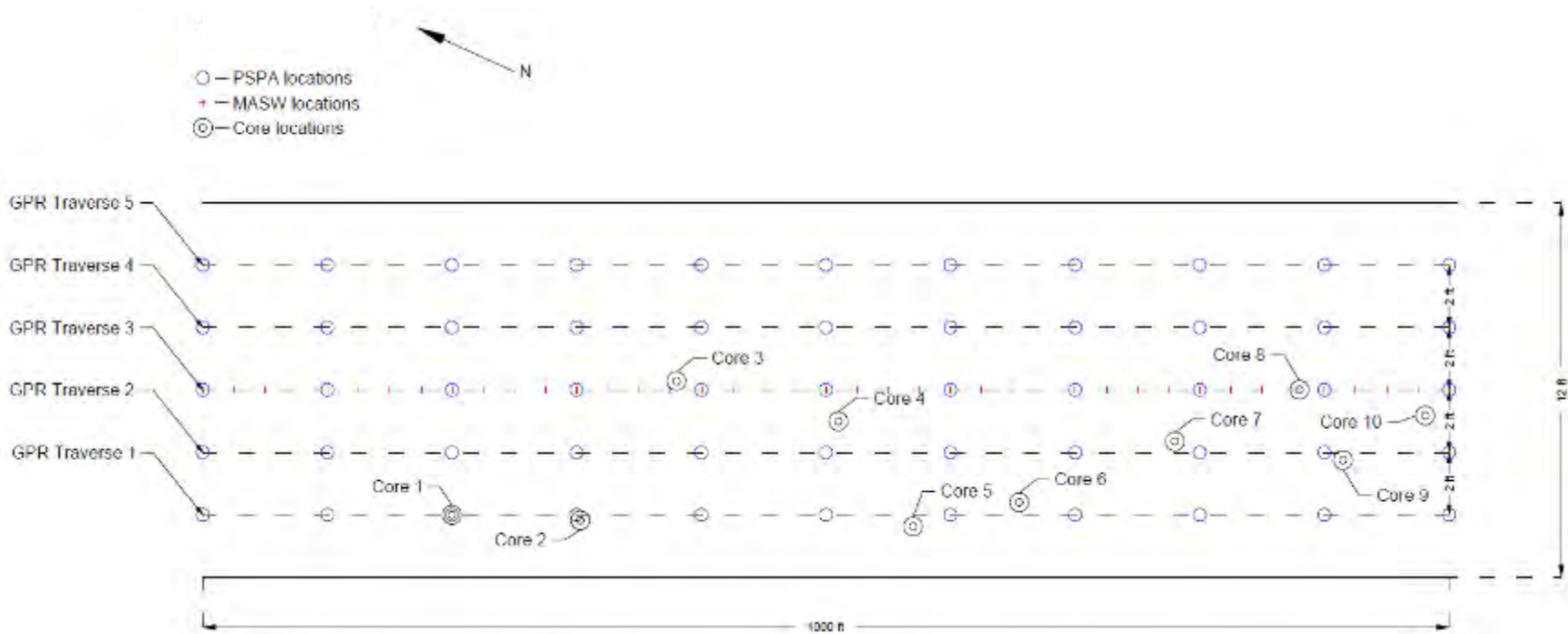


Fig. 4.16—Plan view map of MO 179 (Site 3) showing locations of GPR traverses 1-5. High-frequency (1.5 GHz antenna) GPR data were acquired along all five traverses; low-frequency (400 MHz antenna) data GPR data were acquired along traverse 3 only. Solid black lines represent the driving lane boundaries. Lane width was 12 ft. Core locations (10) are marked as black circles. PSPA locations are marked as blue circles. MASW locations are marked as red crosses. Traverse 1 was 2 feet from the edge of the driving lane. Core locations are marked as black circles. PSPA locations are marked as blue circles. MASW locations are marked as red crosses. All 10 cores were described as moderately to highly stripped. Cores 5-10 were described as debonded.

In Fig. 4.19, a reflection amplitude map for the reflection from the base of the BM is presented. As shown, the amplitudes of the reflection from the base of the BM are consistently between -30 and -42 NdB at all core locations. Elsewhere on the base map, the amplitude of the reflection is as low as -58 NdB. These areas of lower reflection amplitude could represent areas where the BM is more extensively degraded than at any of the core locations.

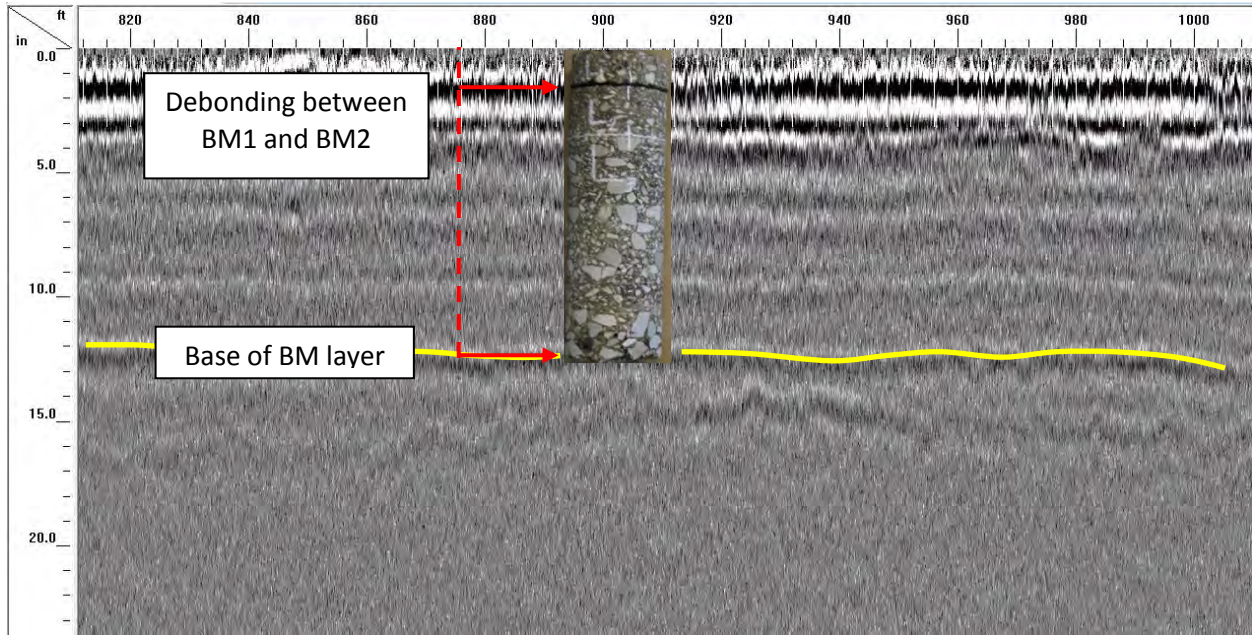


Fig. 4.17—Example of Site 3 GPR profile (GPR profile 3, stations 820-1000) showing correspondence to core 8 (at station 868; Fig. 4.16). Yellow lines represents the base of BM. The horizontal axis is in units of feet; the vertical axis is in units of inches.

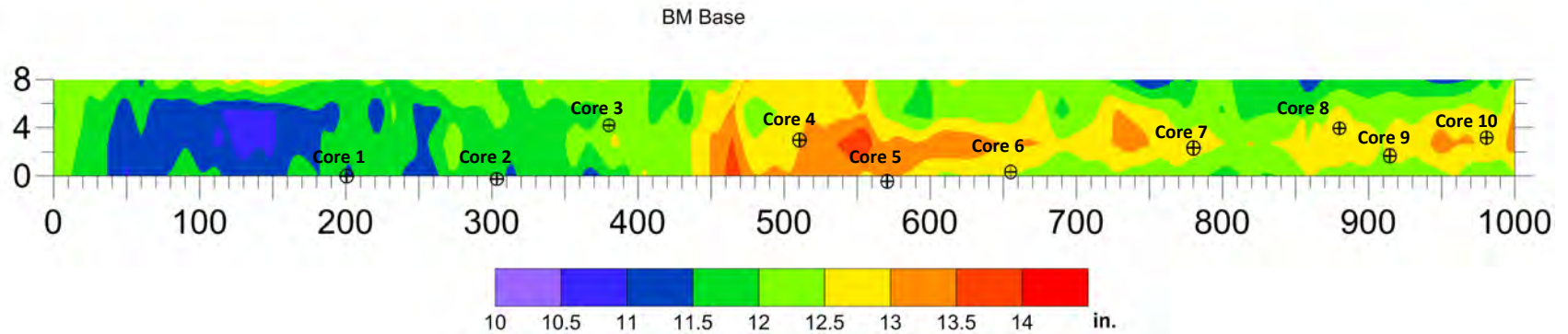


Fig. 4.18– Base map with superposed apparent depth to base bituminous mix (BM) based on the GPR data. Depth values are apparent and are based on the dielectric permittivity of 7.5. Traverse 1 (0 ft mark on map) was located 1 ft (2 ft in Fig. 4.11) away from the outer edge of the driving lane.

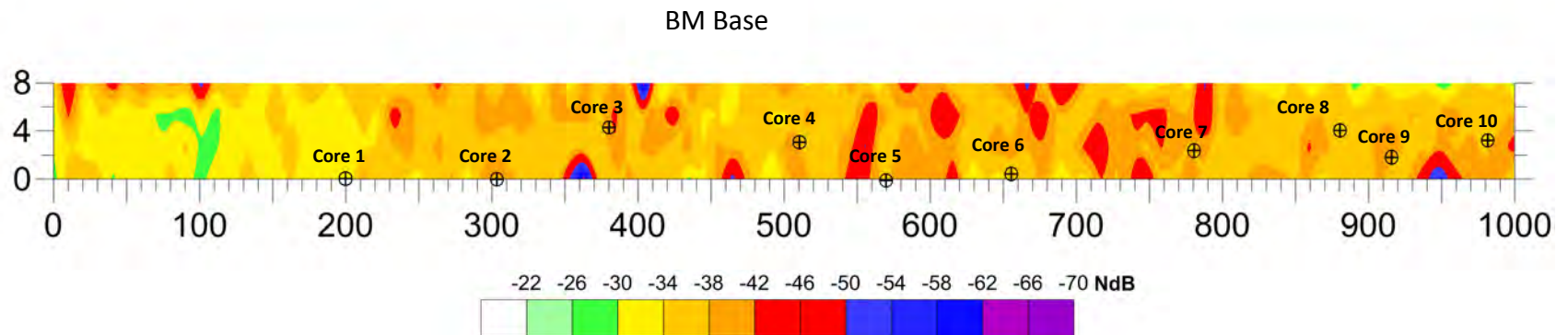


Fig. 4.19–Base map with superposed GPR amplitude values from the base BM. All 10 cores were described as moderately to highly stripped. Cores 5-10 were described as debonded. Areas of anomalously low amplitude probably represent areas where the BM is severely degraded.

Analyses of the acquired GPR data and core control suggest that the GPR tool could be used at Site 3 to detect areas where stripping/debonding was present and to map the base of the BM. The generated apparent depth and amplitude maps indicate overall poor to fair condition of the pavement, however, the presence of stripping and debonding in some areas can be confidently identified most readily based on the visual assessment of individual GPR profiles.

4.3.4 Project-Level Site 4 (HWY AT)

Project-level pavement Site 4 (HWY AT) is located approximately 7 miles east of Union, Missouri (Fig. 4.20). The pavement was variable depth BM over PCC. (Fig. 4.6).

High-frequency (1.5 GHz) GPR data were acquired in the south-bound lane along parallel traverses spaced at 2 ft intervals (Fig. 4.21). The acquisition parameters employed were 512 samples/scan and 48 scans/ft. A dielectric permittivity 7.5 was used to convert reflection times to reflector depths. All the Site 4 GPR data (low-frequency and high-frequency) were acquired in less than four hours.

The objectives of the GPR investigation at this site was to detect shallow stripping within the BM and debonding within the BM and between the BM and underlying PCC. The pavement was variable depth BM over PCC. The total thickness of BM and PCC encountered at the core locations varied from 7 in. (core 7) to 15.25 in. (core 1).

In Fig. 4.22, a section of a representative GPR profile from Site 4 is shown. As noted, the pavement between the 5 ft and 16 ft marks consisted of full-depth (approximately 15.25 in.) of BM. Elsewhere on the GPR profile, approximately 5 in. of BM is interpreted to overlie approximately 7 in. of PCC. The BM in all nine cores is described as stripped (low to moderate) and debonded at one or more levels. The PSPA USW data acquired at the HWY AT site indicate the PCC is severely deteriorated (Section 3).

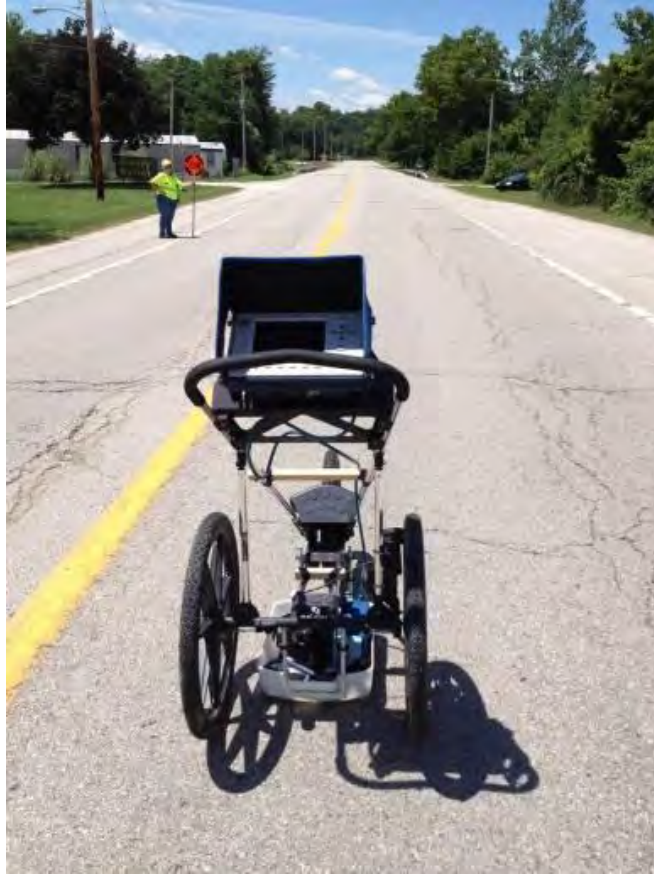


Fig. 4.20—Photograph of site the project-level segment HWY AT (Section 4). Photograph was taken looking west.

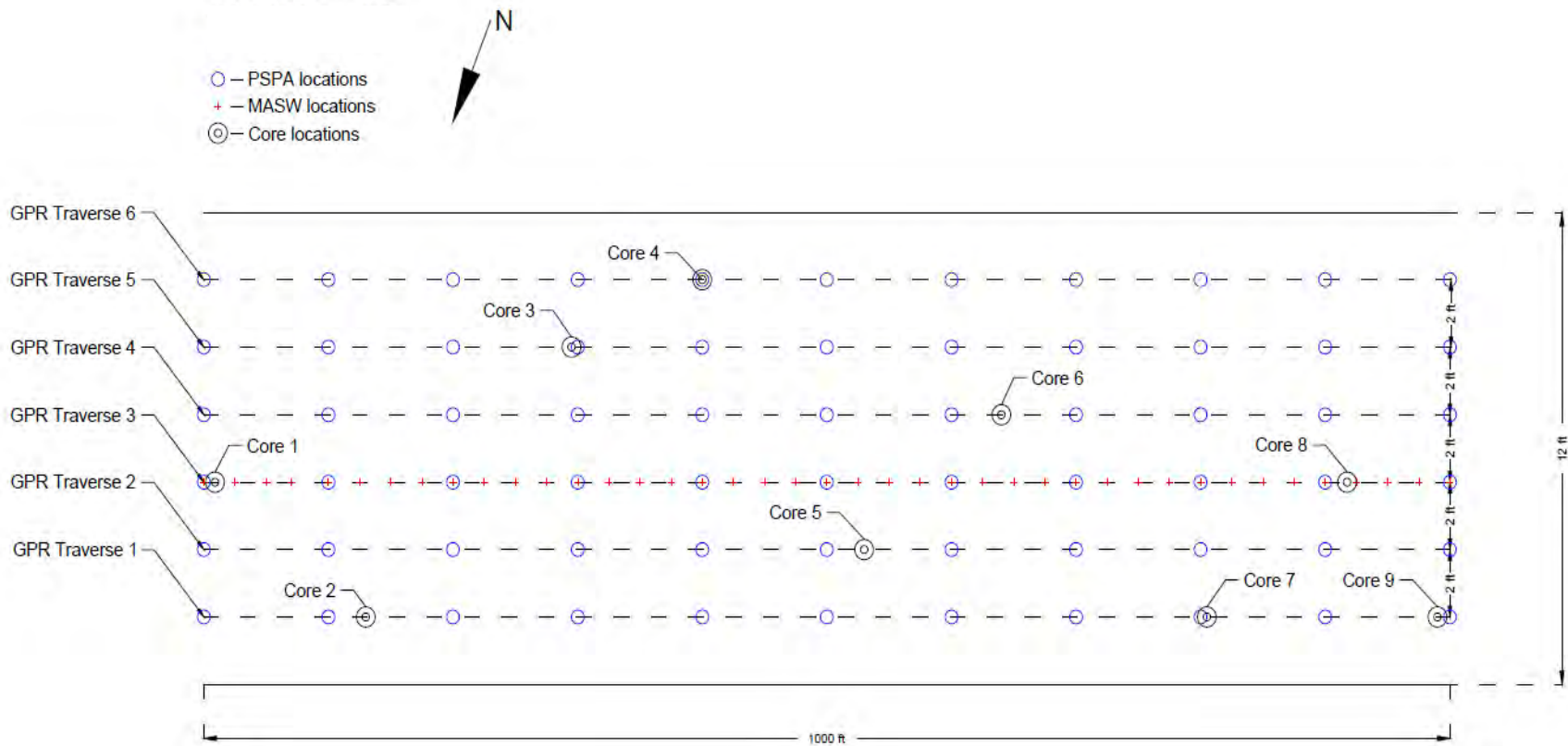


Fig. 4.21—Plan view map of HWY AT (Site 4) showing locations of GPR traverses 1-5. High-frequency (1.5 GHz antenna) GPR data were acquired along all five traverses; low-frequency (400 MHz antenna) data GPR data were acquired along traverse 3 only. Solid black lines represent the driving lane boundaries. Lane width was 12 ft. Core locations (10) are marked as black circles. PSPA locations are marked as blue circles. MASW locations are marked as red crosses. Traverse 1 was 2 ft from the edge of the driving lane. Core locations are marked as black circles. PSPA locations are marked as blue circles. MASW locations are marked as red crosses. The BM in all nine cores is described as stripped (low to moderate) and debonded at one or more levels.

In Fig. 4.23 a depth map for the reflection from the base of the BM is presented. The BM in all nine cores is described as stripped (low to moderate) and debonded at one or more levels. As shown, the GPR apparent depths vary from 3.75 to 4.75 in. (except in proximity to core 1). Variations in the apparent depth to the base of the BM are attributed to real changes in the thickness of the BM and to changes in the condition of the BM. The core depths of the BM and the corresponding GPR depths (Table 4.4) do not agree well at many locations for several reasons: a) complete BM cores were not recovered at all locations; b) at other locations BM thicknesses were difficult to estimate because of the poor condition of the cores; and c) the condition of the BM varied causing the GPR pulse velocity to vary.

Fig. 4.23 also shows a depth map for the reflection from the base of the PCC is presented. As shown, the GPR apparent depths vary from 9.75 to 12.75 in. (except in proximity to core 1). Variations in the apparent depth to the base of the PCC are attributed mostly to real changes in the thickness of the PCC and changes in the condition of the PCC. The core thicknesses of the PCC and the corresponding GPR depths (Table 4.5) do not agree well at many locations for several reasons: a) complete cores (BM only) were not recovered at all locations; b) at other locations BM thicknesses were difficult to estimate because of the poor condition of the cores; c) the condition of the BM varied causing the GPR pulse velocity to vary; and d) average dielectric permittivity of 7.5 was used; actual values differ for BM and PCC layers.

In Fig. 4.24, an amplitude map for the reflection from the base of the BM is presented. The BM in all nine cores is described as stripped (low to moderate) and debonded at one or more levels. As a result, the amplitudes of the reflection from the base of the BM are low and consistent (between -26 and -42 NdB) at all core locations, except core 1. At the core 1 location, the amplitude of the BM reflection is as low -54 NdB. The anomalously low amplitude can be attributed to the fact that full-depth BM (15.25 in.) was encountered in core 1 (debonded at multiple depths).

Fig. 4.24 also presents an amplitude map for the reflection from the base of the PCC. As shown, the amplitudes of the reflection from the base of the BM are low and consistent (between -32 and -48 NdB) at all core locations (except core 1 where PCC is not present). This could be attributed, in part, to the fact that the thickness of the BM layer varies significantly in the study area. Also, the condition of the PCC varies.

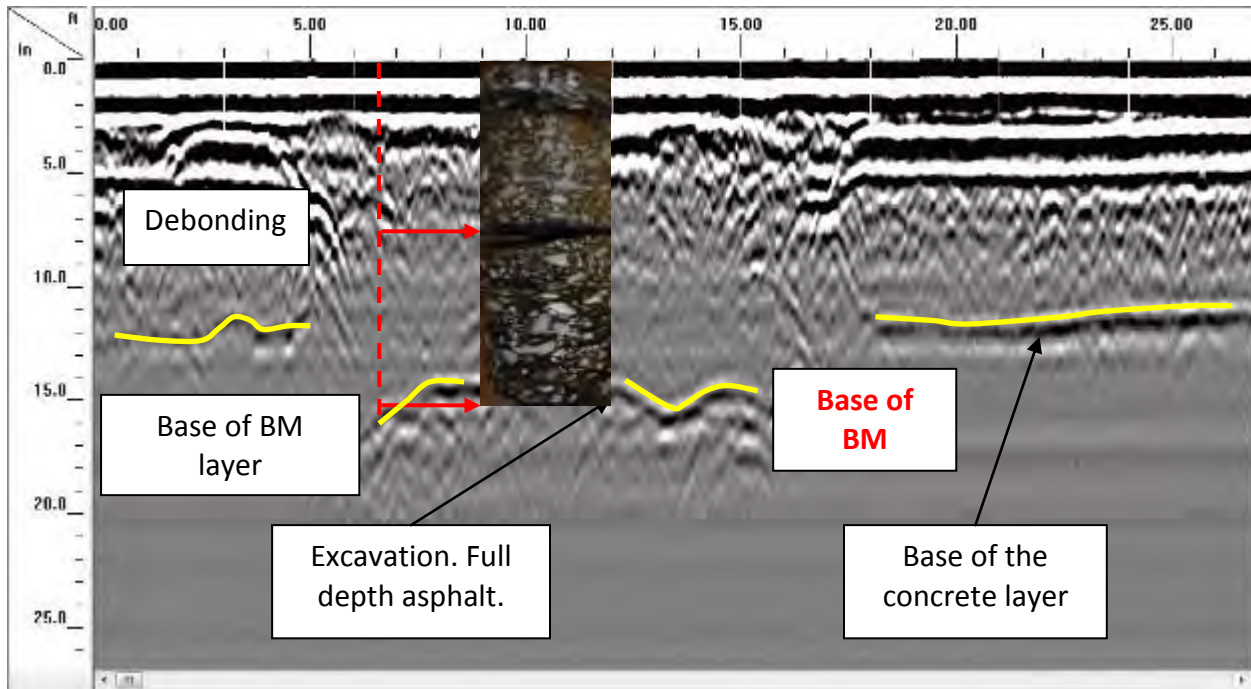


Fig. 4.22—Representative example of Site 4 GPR profile (GPR profile 1, stations 0-25). Core 1 encountered 15.25 in. of BM; the other cores encountered variable thicknesses of BM over PCC. The horizontal axis is in units of feet; the vertical axis is in units of inches.

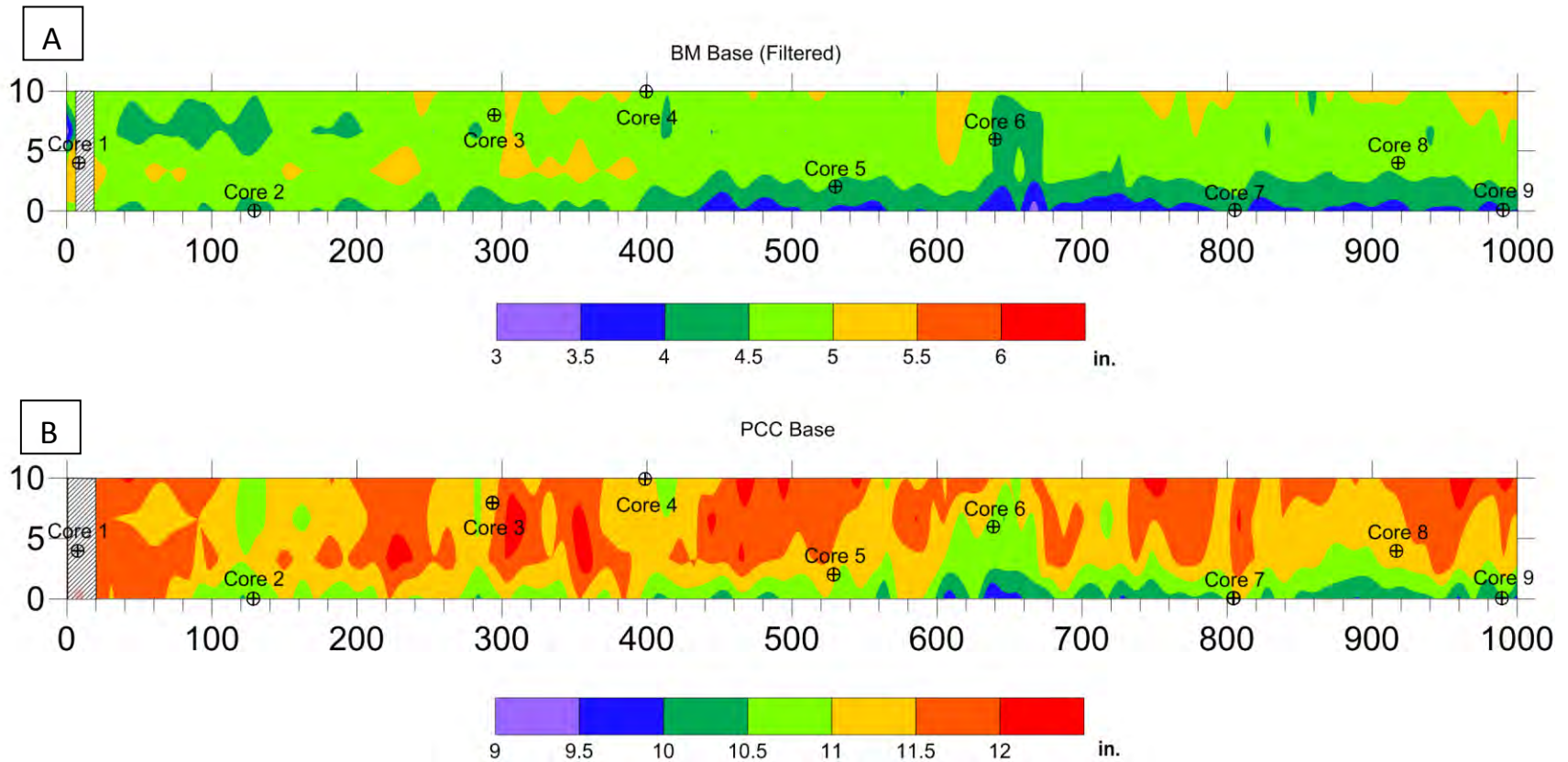


Fig. 4.23—Depth values are apparent and are based on the dielectric permittivity of 7.5. Traverse 1 (0 ft mark on map) was located 1 ft (2 ft in Fig. 4.11) away from the outer edge of the driving lane. Upper Map shows GPR-estimated “apparent” depth to the base of the BM; Lower map shows GPR-estimated “apparent” depth to the base of the PCC. As noted in Table 4.4, GPR-estimated depths to the base of the BM and PCC and the corresponding core depths differ significantly at several core locations. The lack of correlation is attributed to the poor condition of the asphalt layer and partial recovery during coring.

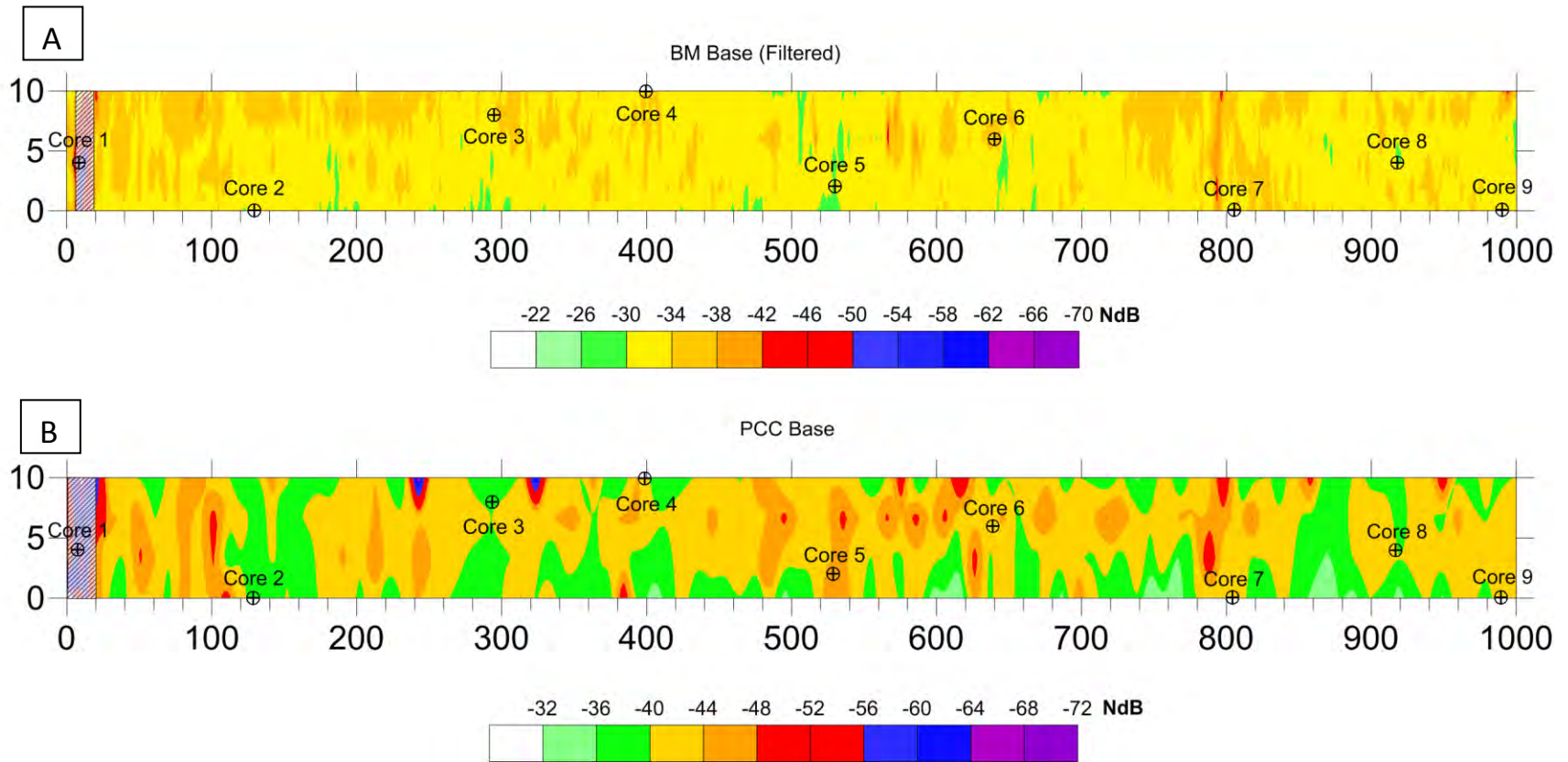


Fig. 4.24—A) Base map with superposed GPR amplitude values from the bottom bituminous mix (BM) layer base; B) reflection amplitude GPR signal from the base of the concrete layer (PCC) base. Area highlighted in blue at the stations 5-18 is the excavation (see Figure 4.22). Based on the GPR and core data areas with weak bonded and debonded BM layers are present throughout the entire 1000 ft pavement section. Amplitude values lower than -34 NdB indicate poor condition of the pavement. All cores (1 to 10) confirmed the debonding and the stripping within the asphalt layer. Vertical and horizontal axes are distance in units of feet. Horizontal to vertical scale ratio is 1:30.

Table 4.4–Core depths and GPR apparent depths to base of pavement layers at Site 4. Differences between the actual and apparent thicknesses are also noted. The BM in all nine cores is described as stripped (low to moderate) and debonded at one or more levels

Core #	1	2	3	4	5	6	7	8	9
BM (Core) depth, in.	15.3	4.5	3+	3.25	1	2.75	2.5+	4	3
BM (GPR) depth, in.	15	4	4.5	4.5	4	4	4	4.5	4
Correlation*, %	98.4	88.9	150.0	138.5	400.0	145.5	160.0	112.5	133.3
Base PCC (Core) depth, in.	NA	10.5	9.5	9.25	7	8.75	8.5	11	9
PCC (GPR)	NA	10.5	11	11	11	10.5	10.5	11	10
Correlation*, %	NA	100.0	115.8	118.9	157.1	120.0	123.5	100.0	111.1

Table 4.5–Core thicknesses and GPR apparent thicknesses of the PCC layer at Site 4. Differences between the actual and apparent thicknesses are due to incomplete recovery of BM in cores and average dielectric permittivity (7.5) used at the site. Actual dielectric permittivity varies for BM and PCC layers

Core #	1	2	3	4	5	6	7	8	9
PCC (Core) thickness, in.	NA	6.0	6.5	6.0	6.0	6.0	6.0	7.0	6.0
PCC (GPR) thickness, in.	NA	6.5	6.5	6.5	7.0	6.5	6.5	6.5	6.0
Correlation*, %	NA	108.3	100.0	108.3	116.7	108.3	108.3	92.9	100.0

*Correlation is calculated based on the following formula: [Depth based on GPR data]/[Depth based on core control]*100. Correlation values below 100% typically indicate overestimated dielectric permittivity (relative permittivity); correlation values above 100% typically indicate the dielectric permittivity (relative permittivity) used was underestimated. Values highlighted in red show correlation values above 110%.

Analyses of the acquired GPR data and core control suggest that the GPR tool could be used at Site 4 to detect areas where stripping/debonding was present and to map the base of the BM and PCC. The generated apparent depth and amplitude maps indicate overall fair condition of the pavement, however, the presence of stripping and debonding in some areas can be confidently identified most readily based on the visual assessment of individual GPR profiles.

4.3.5 Project-Level Site 5 (I-55 Pemiscot Co.)

Project-level pavement Site 5 (I-55 Pemiscot Co.) is located approximately 13 miles south from Hayti, Missouri. (Fig. 4.25). GPR data were acquired in the south-bound lane along parallel traverses spaced at 2 ft intervals (Fig. 4.26). All of the GPR data, including low-frequency data, were acquired in four hours.

The pavement at Site 5 consists of an upper layer of PCC (approximately 12 in.), an intervening layer of BM (approximately 2.2 in.) and a basal layer of PCC (approximately 10 in.). The objective of the GPR investigation was to evaluate an unbonded PCC overlay without apparent problems. The acquisition parameters employed were 512 samples/scan and 48 scans/ft. A dielectric permittivity of 7.5 was used to convert reflection times to depths. In Fig. 4.27, a section of a representative GPR profile from Site 5 is shown.



Fig. 4.25—Photograph of site the project-level segment I-55 Pemiscot County (Site 5). Photograph was taken looking south.

In Fig. 4.28 an apparent depth map for the reflection from the base of the PCC is presented. The PCC/BM interface (upper interface) in cores 3, 5, 6, 7 and 8 (Fig. 4.28) is described as unbonded; the BM/PCC interface (lower interface) in all cores is described as unbonded. Stripping in core 1 is described as moderate; stripping in all other cores is described as low. It should be noted that non-bonding at the PCC/BM or BM/PCC interface is not considered to be problematic for a pavement of this type, however, the utility of the GPR tool to detect this type of distress was evaluated here. As shown in Fig. 4.28, the GPR apparent depths of PCC base vary from 8.0 to 9.0 in. Variations in the apparent depth to the base of the PCC are attributed to: a) real changes in the thicknesses of the upper PCC; and b) changes in the conditions of the upper PCC. The core depths of the BM and the corresponding GPR depths (Table 4.6) agree well at five of the eight core locations suggesting that the changes in the actual thicknesses of the upper PCC layer are the primary cause of the plotted variations in the apparent thickness of the upper PCC layer.

In Fig. 4.29, an amplitude map for the reflection from the PCC/BM interface is presented. As shown, the amplitudes of the reflection from the base of the BM vary between -

36 and -56 NdB (at core locations). There does not appear to be a correlation between the amplitude of this reflection, the apparent depth to the base of the upper PCC, and the core depths and conditions. These results suggest that the GPR tool could not be used to differentiate: a) moderately stripped BM from low stripped BM; and b) debonded PCC/BM from bonded PCC/BM at Site 5.

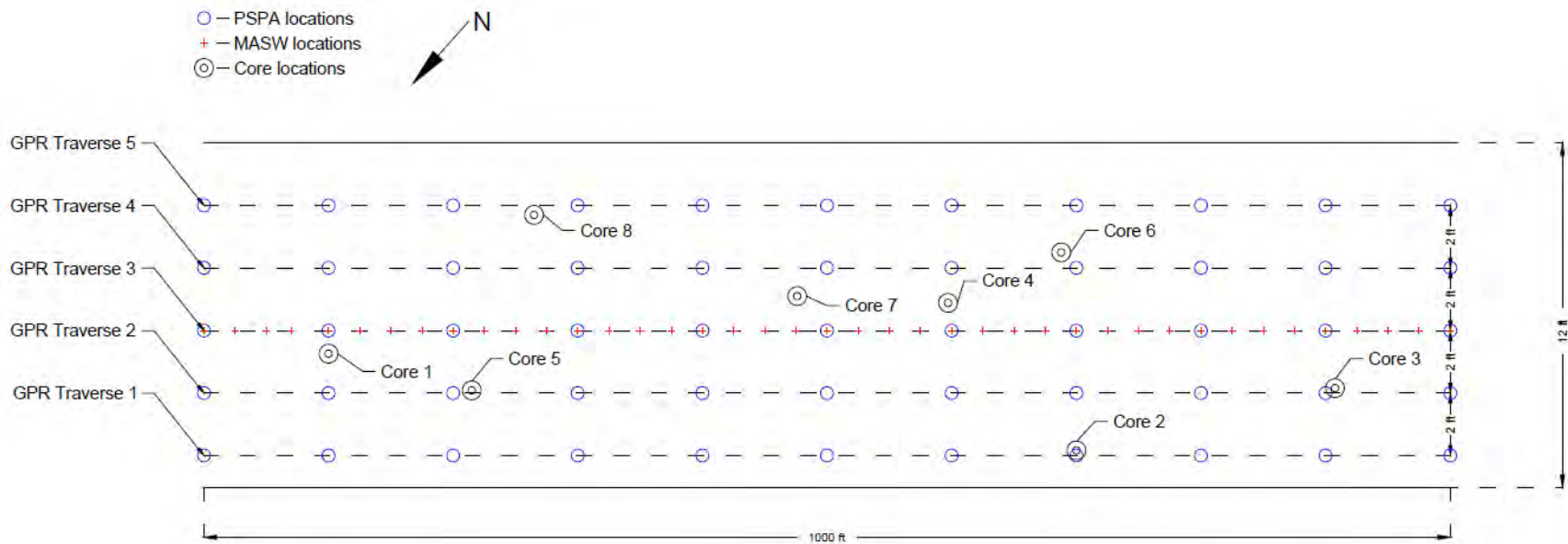


Fig. 4.26—Plan view map of I-55 Pemiscot Co. (Site 5) showing locations of GPR traverses 1-5. High-frequency (1.5 GHz antenna) GPR data were acquired along all five traverses; low-frequency (400 MHz antenna) data GPR data were acquired along traverse 3 only. Solid black lines represent the driving lane boundaries. Lane width was 12 ft. Core locations (10) are marked as black circles. PSPA locations are marked as blue circles. MASW locations are marked as red crosses. Traverse 1 was 1 ft from the edge of the driving lane. Core locations are marked as black circles. PSPA locations are marked as blue circles. MASW locations are marked as red crosses. The PCC/BM interface (upper interface) in cores 3, 5, 6, 7, and 8 (Fig. 4.26) is described as debonded; stripping in core 1 is described as moderate; stripping in all other cores is described as low.

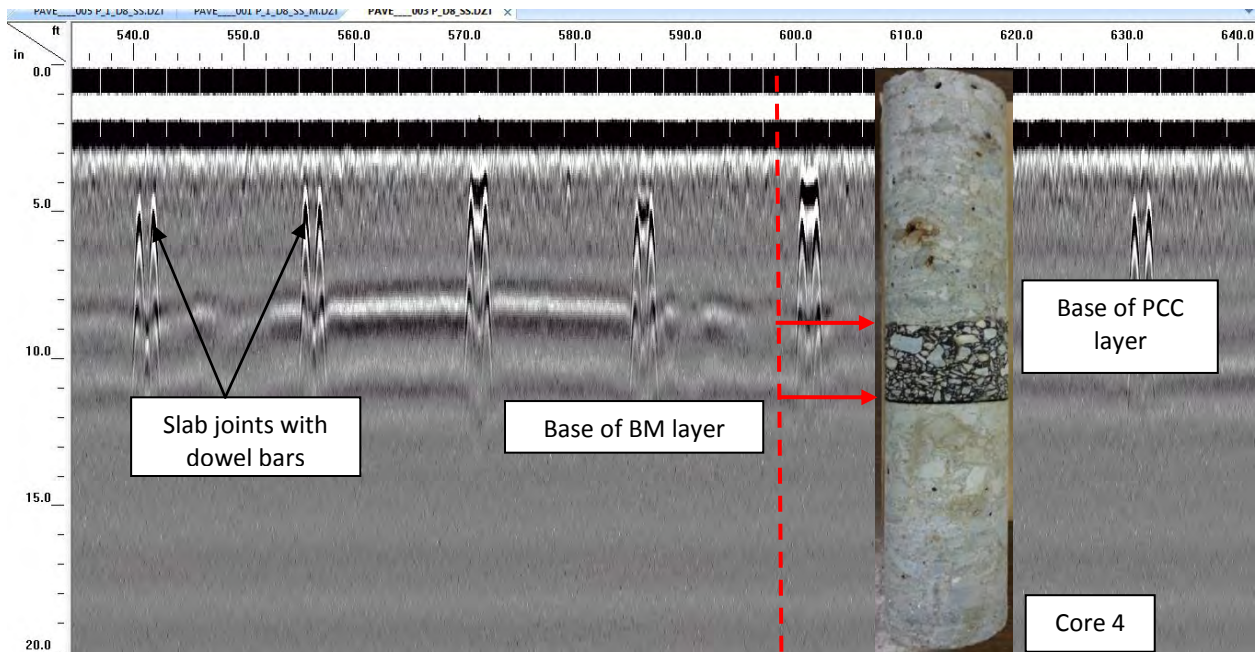


Fig. 4.27—Example of GPR section (GPR profile 5, stations 240-310) showing imaged features: base of the top concrete layer, asphalt layer, bottom concrete layer, and slab joints. The horizontal axis is in units of feet; the vertical axis is in units of inches

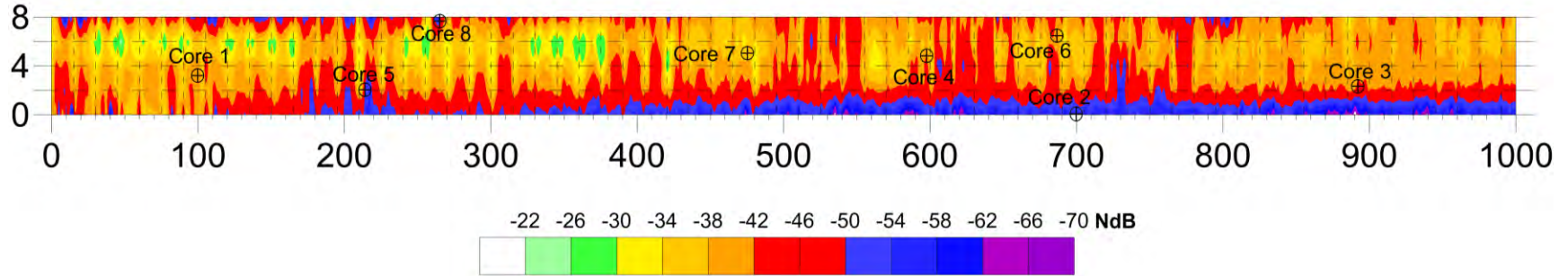


Fig. 4.28—Base map with superposed GPR amplitude values from the PCC/BM interface. Vertical and horizontal axes are distance in units of feet. Horizontal to vertical scale ratio is 1:30. Traverse 1 was located 1 ft away from the edge of the driving lane. Horizontal dashed lines represent locations of the GPR traverses. Vertical dashed lines represent locations of the mapped slab joints in the upper PCC layer; notice the amplitude changes near the joints.

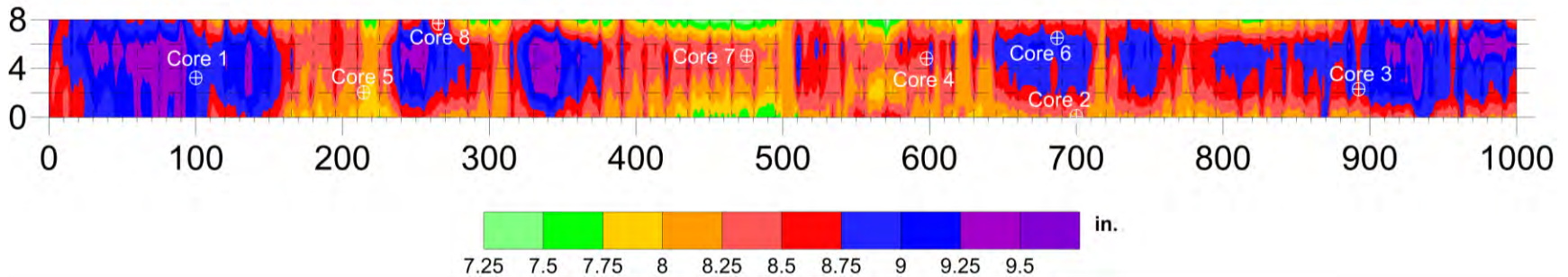


Fig. 4.29—Base map with superposed GPR estimated “apparent” depth values from the PCC/BM interface. Vertical and horizontal axes are distance in feet. Horizontal to vertical scale ratio is 1:30. Traverse 1 was located 1 ft away from the edge of the driving lane. Dielectric constant of 7.5 was used to convert reflection times to reflector depths. Variations in the apparent depth to the base PCC is attributed mostly to variations in the actual depth to this interface. Horizontal dashed lines represent locations of the GPR traverses. Vertical dashed lines represent locations of the mapped slab joints in the upper PCC layer; notice the apparent depth changes near the joints.

Table 4.6–Core depths and GPR apparent depths to base of BM layer at Site 5. Differences between the actual and apparent thicknesses are also noted. The PCC/BM interface (upper interface) in cores 3, 5, 6, 7, and 8 is described as debonded; the BM/PCC interface (lower interface) in all cores is described as debonded. Stripping in core 1 is described as moderate; stripping in all other cores is described as low.

Core #	1	2	3	4	5	6	7	8
BM (Core) depth, in.	9.0	9.0	9.0	8.5	8.0	9.0	8.5	8.5
BM (GPR) depth, in.	9.0	8.2	8.6	8.5	8.0	8.9	8.4	8.5
Correlation*, %	100.0	91.1	95.6	100.0	100.0	98.9	98.8	100.0

*Correlation is calculated based on the following formula: [Depth based on GPR data]/[Depth based on core control]*100. Correlation values below 100% typically indicate overestimated dielectric permittivity (relative permittivity); correlation values above 100% typically indicate the dielectric permittivity (relative permittivity) used was underestimated. Values highlighted in red show correlation values below 90% and/or above 110%.

Analyses of the acquired GPR data and core control suggest that the GPR tool could not be used at Site 5 to differentiate moderately stripped BM from low stripped BM and debonded BM from bonded BM. However, the GPR tool can be used to evaluate overall condition of the pavement and map joints in the upper PCC layer and determine the BM thickness.

4.3.6 Project-Level Site 6 (I-55 Perry Co.)

The project-level Site 6 (I-55 Perry County; Fig. 4.30) is located approximately 8 miles north of Perryville, Missouri. The pavement at this site is comprised of approximately 9-11 in. of full-depth PCC. The objective of the GPR investigation at this site was to evaluate the condition of PCC pavement with problems at the joints.

The GPR data were acquired in the north-bound driving lane along parallel traverses spaced at 2 ft intervals. All of the GPR control (high-frequency and low-frequency) was acquired in four hours. Lane closures were required. The acquisition parameters employed were 512 samples/scan and 48 scans/ft. A map showing locations of the traverses and cores is shown in Fig. 4.31.



Fig. 4.30—Photograph of site the project-level segment I-55 Perry County (Section 6). Photograph was taken looking north.

In Fig. 4.32 an apparent depth map for the reflection from the base of the PCC is presented. The PCC in all cores is described as in good condition. The core depths and the corresponding GPR depths (Table 4.7) agree well at all eight core locations suggesting that the changes in the actual thicknesses of the PCC layer are the primary cause of the plotted variations in the apparent thickness of the PCC layer. In the cross-hatched areas on Fig. 4.32, the reflection from the base of the PCC is polarity-reversed. This polarity reversal is attributed to the presence of void space immediately beneath the PCC.

Fig. 4.33 presents a reflection amplitude map from the base of the PCC layer. Based on the GPR and core data the condition of the pavement appears to be fairly uniform, except where the pavement was patched. Patched areas were found at stations 440-450, 550-580, 760-775, 830-840, 950-962 on all the GPR traverses and at stations 630-640 at the GPR traverse 5. In the cross-hatched areas on Fig. 4.32, the reflection from the base of the PCC is polarity-reversed. This polarity reversal is attributed to the presence of void space beneath the PCC layer as a result of pumping. During coring it was noted that the water is seeping through the slab transverse and edge joints (Fig. 4.36).

Table 4.7–Core depths and GPR apparent depths to base of BM layer at Site 6. Differences between the actual and apparent thicknesses are also noted. The PCC in all cores is described as being in good condition

Core #	1	2	3	4	5	6	7	8	9
PCC (Core) depth, in.	9	8	8.5	9	9	9	8.5	8	8.75
PCC (GPR) depth, in.	8.75	8.5	8.75	8.75	9.25	9	8.75	8.5	9
Correlation*,%	97.2	106.3	102.9	97.2	102.8	100.0	102.9	106.3	102.9

*Correlation is calculated based on the following formula: [Depth based on GPR data]/[Depth based on core control]*100. Correlation values below 100% typically indicate overestimated dielectric permittivity (relative permittivity); correlation values above 100% typically indicate the dielectric permittivity (relative permittivity) used was underestimated.

Analyses of the acquired GPR data and core control suggest that the GPR tool could be used at Site 6 to detect areas where voids beneath the PCC layer are present. The generated apparent depth and amplitude maps indicate overall fairly uniform condition of the pavement, however, the presence of the problematic areas with voids beneath the pavement in some areas can be confidently identified most readily based on the visual assessment individual GPR profiles.

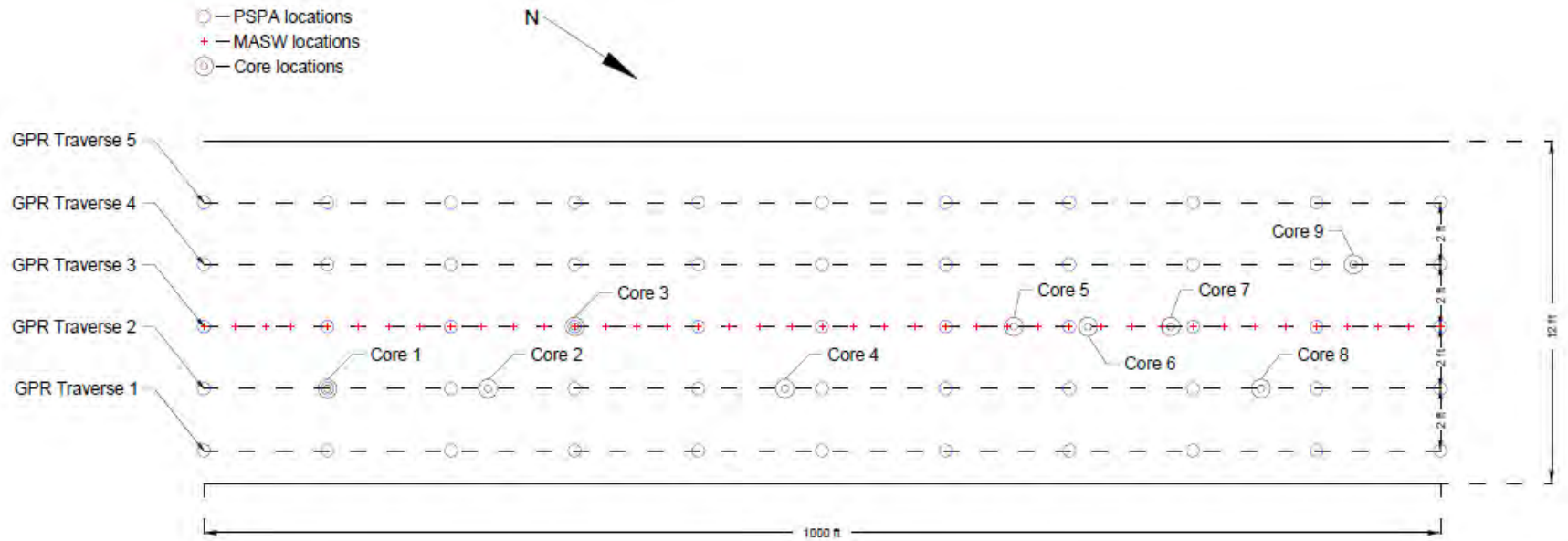


Fig. 4.31—Plan view map of I-55 Perry Co. (Site 6) showing locations of GPR traverses 1-5. High-frequency (1.5 GHz antenna) GPR data were acquired along all five traverses; low-frequency (400 MHz antenna) data GPR data were acquired along traverse 3 only. Solid black lines represent the driving lane boundaries. Lane width was 12 ft. Core locations (9) are marked as black circles. PSPA locations are marked as blue circles. MASW locations are marked as red crosses. Traverse 1 was 1 ft from the edge of the driving lane. The PCC in the eight cores is described as good quality.

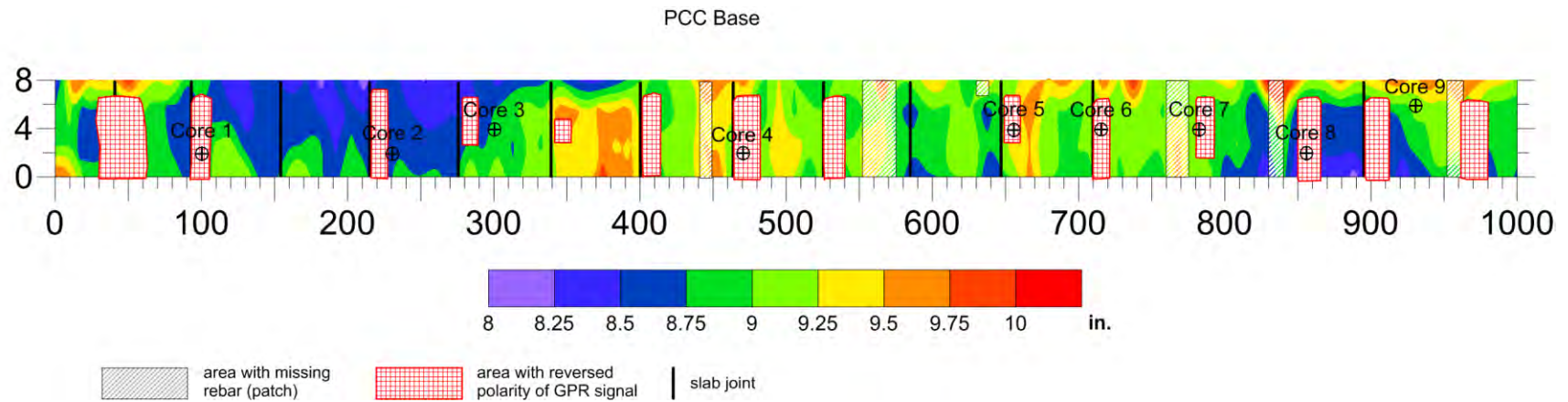


Fig. 4.32—Base map with superposed GPR estimated “apparent” depth values for base PCC. Vertical and horizontal axes are distance in feet. Traverse 1 was located 1 ft from the edge of the driving lane. A dielectric permittivity of 8.0 was used to convert reflection times to reflector depths. Patched areas were with no reinforcing steel were found at stations 440-450, 550-580, 760-775, 830-840, 950-962 on all the GPR traverses and at stations 630-640 at the GPR traverse 5. Variations in the apparent depth to the base BM is attributed mostly to variations in the actual depth to this interface. The cross-hatched areas represent locations where the reflection from the base PCC is polarity-reversed. These probably represent areas where void space underlies the PCC. Black solid lines represent locations of the joints.

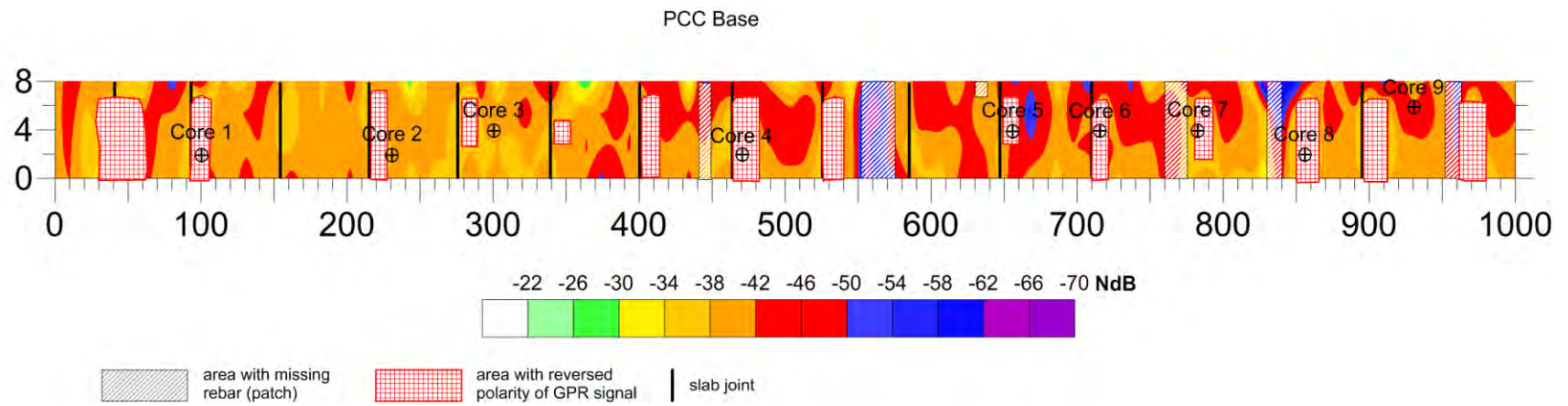


Fig. 4.33—A base map with superposed GPR amplitude values from the base PCC. The cross-hatched areas represent locations where the reflection from the base PCC is polarity-reversed. These probably represents areas where void space underlies the PCC. Black solid lines represent locations of the joints.

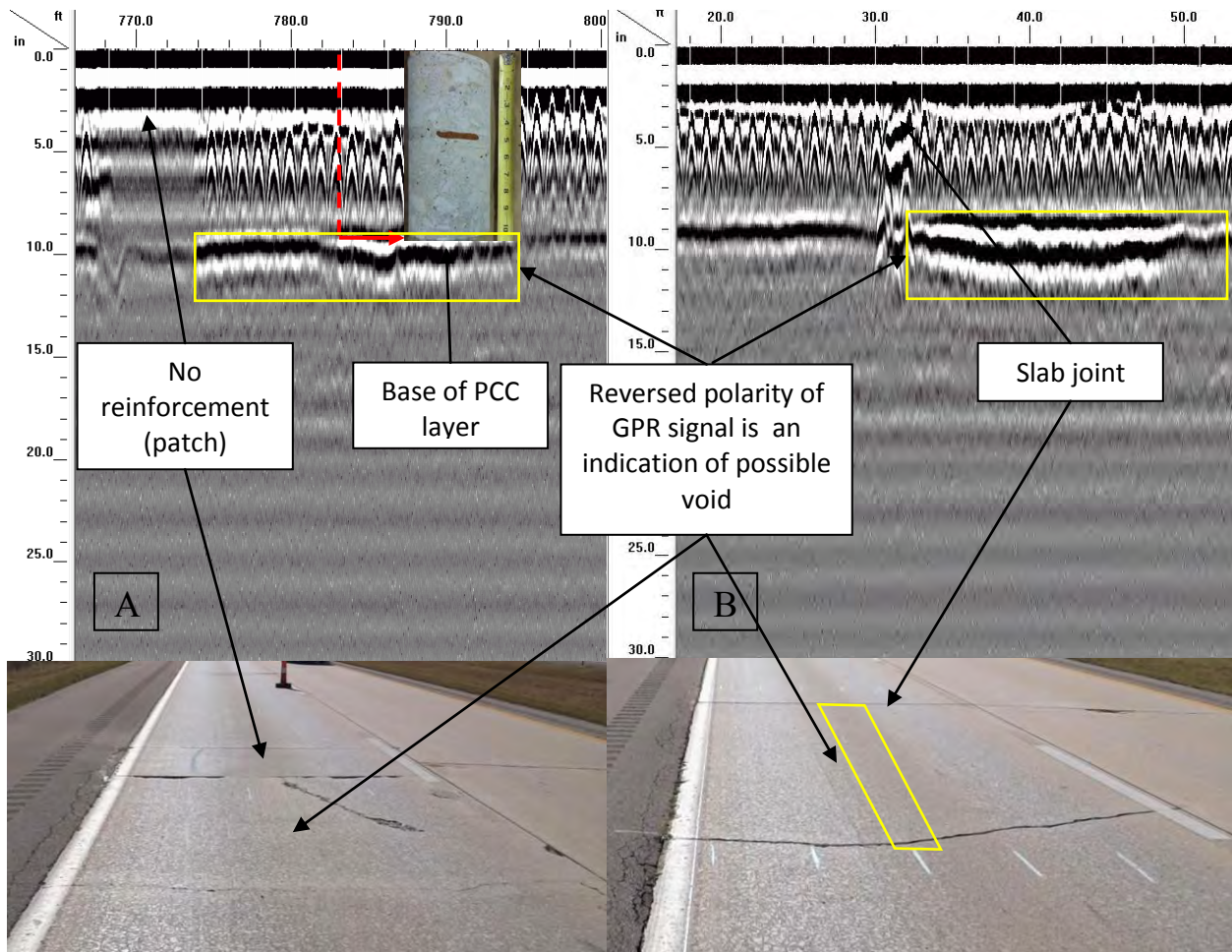


Fig. 4.34—A) Segment of representative Site 6 GPR profile (GPR profile 3, stations 766-800) showing GPR image of base of concrete layer, a patched area; and B) Segment of representative Site 6 GPR profile (GPR profile 3, stations 17-52) showing a polarity reversal at the base PCC reflector that could be indicative of a void space. The horizontal axis is in units of feet; the vertical axis is in units of inches.



Fig. 4.35—Core 5 location at Site 6. During coring it was noted that the water seeping through the slab transverse and edge joints, which probably caused fine material pumping out, and as a result, forming voids beneath the PCC layer.

4.3.7 Project-Level Site 7 (HWY U)

Project-level pavement Site 7 HWY U (Fig. 4.36) is located approximately 6 miles north of Salem, Missouri. The goal of the GPR investigation at Site 7 was to evaluate a poor quality BM road. Type of the pavement was full depth BM. The GPR data were acquired on the top surface of the south-bound lane along six parallel traverses spaced at 1.5 ft intervals. General view of the pavement section HWY U is shown in Fig. 4.36.

The acquisition parameters employed were 512 samples/scan and 48 scans/ft. The dielectric permittivity was set to 10.0 after correlation with the core data. Map locations of the traverses and cores locations is shown as Fig. 4.37. Only partial cores were acquired at most core locations. A representative core and corresponding representative segment of a Site 3 GPR profile is shown in Fig. 4.38. The reflection from the base of the BM is shown.



Fig. 4.36—Photograph of site the project-level segment HWY U (Section 7). Photograph was taken looking north.

In Fig. 4.39, a map depicting the apparent depth of the base BM is presented. Note that the apparent depth to the base of the BM varies significantly. The observed variations in apparent thickness are attributed to actual variations in the thickness of the BM and to variations in the condition of the BM.

In Fig. 4.40, a reflection amplitude map for the base of the BM is presented. As shown, the amplitudes of the reflection from the base of the BM are low and vary significantly. This is consistent with the core control that indicates the BM is stripped at multiple depths in many areas. The correlation between Fig. 4.39 and Fig. 4.40 is not convincing. This suggests that variations in apparent thickness of the BM are due to both actual variations in BM thickness and variations in BM condition.

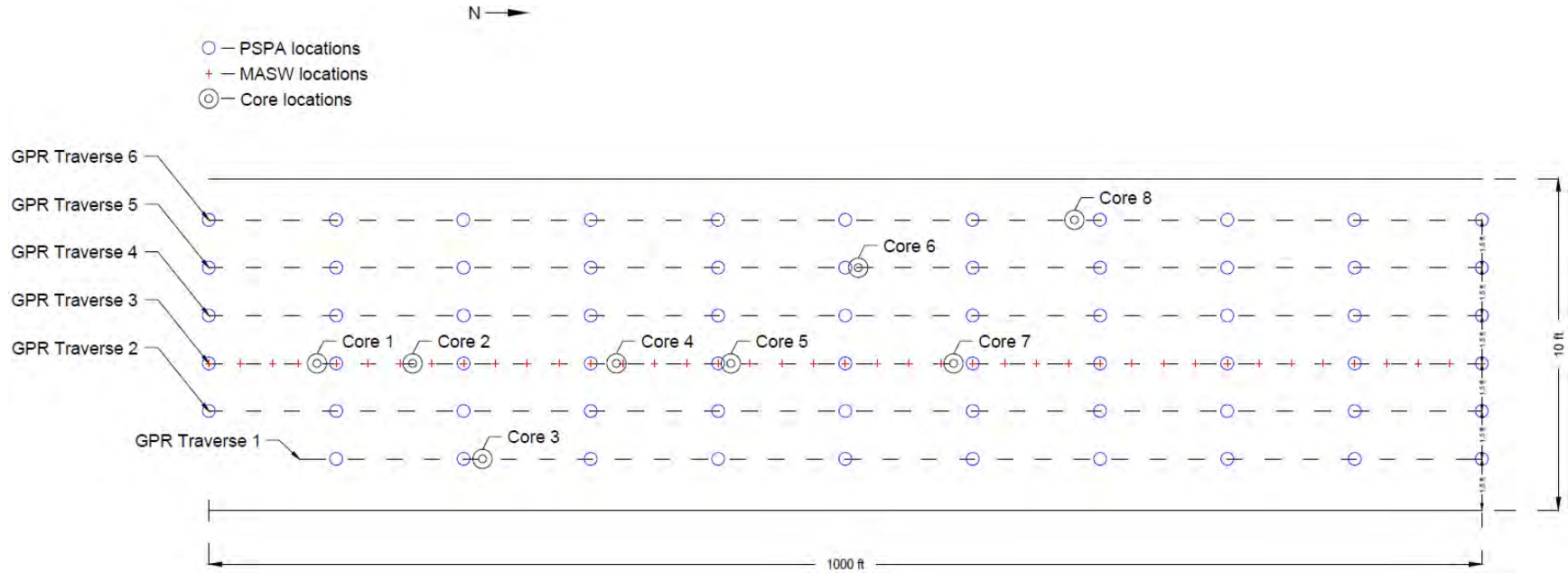


Fig. 4.37—Plan view map showing locations of the GPR traverses and the cores at the project-level Site 7 (HWY U). A total six GPR profiles (each 1000 ft long) were acquired along parallel traverses spaced at 1.5-ft intervals. High-frequency (1.5GHz antenna) data GPR data were acquired along all six traverses (spaced at 1.5 ft intervals), low-frequency (400 MHz antenna) data GPR data were acquired along Traverse 3 only. Solid black lines represent the lane boundaries. The total lane width was 10 ft. Core locations are marked as black circles. PSPA locations are marked as blue circles. MASW locations are marked as red crosses. Only partial cores were recovered at most core locations.

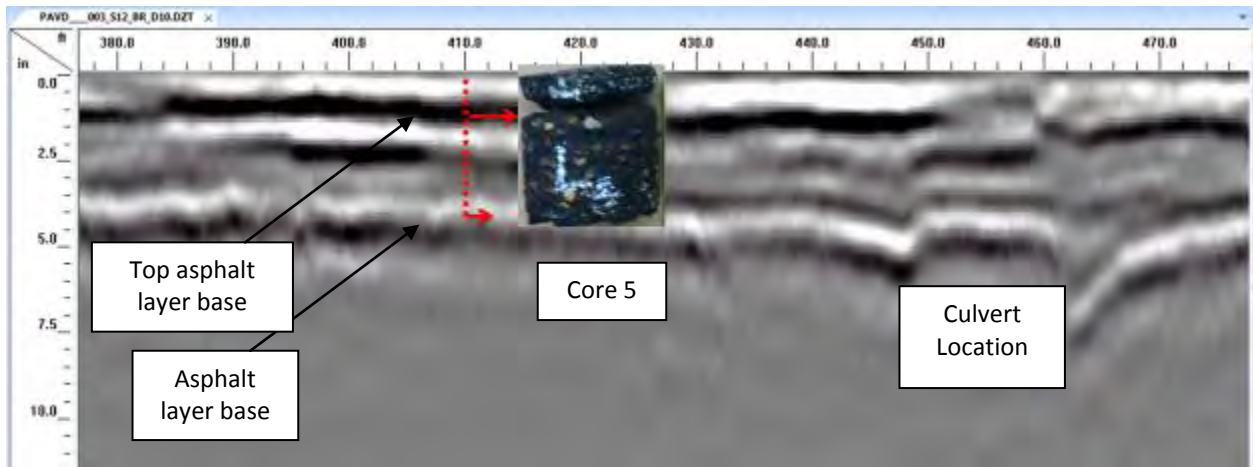


Fig. 4.38—An example of a GPR segment (GPR profile 3, stations 380-470) with some imaged features is shown: base of the top asphalt layer, the base of the top debonded asphalt layer (reflection not present everywhere along the 1000-ft pavement section) and a culvert (stations 448-464). The horizontal axis is in units of feet; the vertical axis is in units of inches.

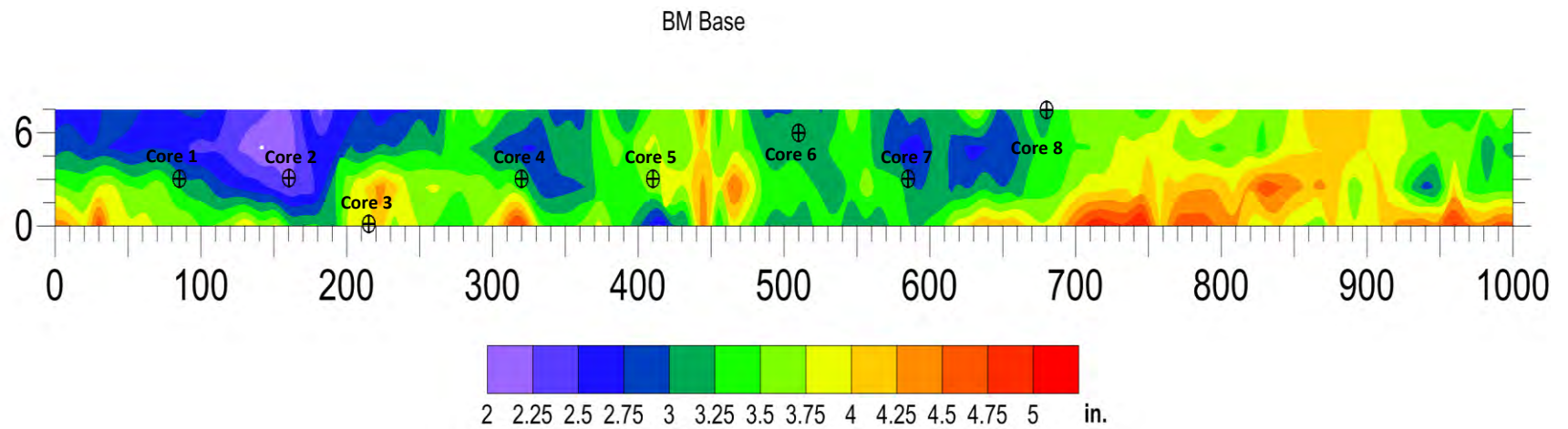


Fig. 4.39—A base map showing variations in the apparent thickness of the bituminous mix (BM). Thickness values are apparent and are based on the dielectric permittivity of 10.0. Traverse 1 (0 ft mark on map) was located 1.5 ft from the edge of the driving lane.

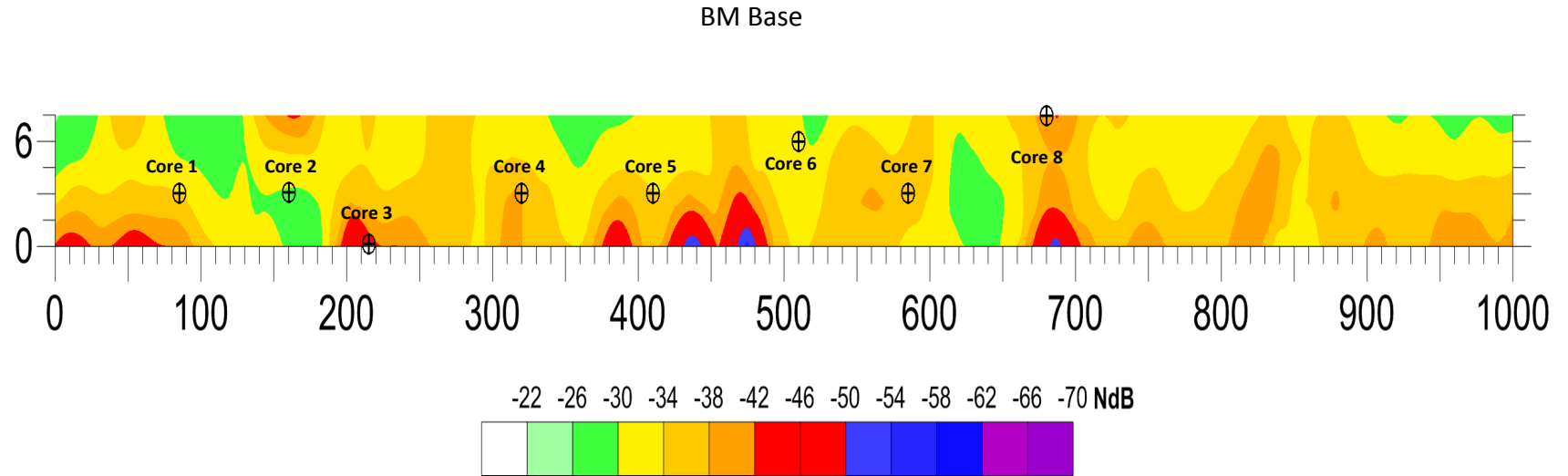


Fig. 4.40—A base map with superposed GPR amplitude values from the bottom asphalt layer base. Areas highlighted in orange, red, and blue (<-34 NdB) indicate overall poor pavement condition. All cores (1 to 8) confirmed presence of deteriorated asphalt and debonding where two layers of asphalt recovered from the core. Traverse 1 was located 1.5 ft away from the pavement edge.

Table 4.8—Core depths and GPR apparent depths to base of BM layer at Site 7. Differences between the actual and apparent thicknesses are due mostly to incomplete core recovery.

Core #	1	2	3	4	5	6	7	8
PCC (Core) depth, in.	1	1	1	0.25	4	2.5	0.25	2
PCC (GPR) depth, in.	3	2	3.75	3.25	3.5	3	3	3
Correlation*, %	300.0	200.0	375.0	1300.0	87.5	120.0	1200.0	150.0

*Correlation is calculated based on the following formula: [Depth based on GPR data]/[Depth based on core control]*100. Correlation values below 100% typically indicate overestimated dielectric permittivity (relative permittivity); correlation values above 100% typically indicate the dielectric permittivity (relative permittivity) used was underestimated. Values highlighted in red show correlation values below 90% and/or above 110%.

Analyses of the acquired GPR data and core control suggest that the GPR tool was effectively used at Site 7 to evaluate a poor quality BM road. However, stripped and debonded layers could be confidently identified most readily based on the visual assessment of individual GPR profiles.

4.3.8 Project-Level Site 8 (I-35)

Project-level pavement Site 8 (I-35) is located about 20 miles north of Cameron, Missouri. (Fig. 4.41). GPR data were acquired in the south-bound lane along parallel traverses spaced at 2 ft intervals (Fig. 4.42). All of the GPR data, including low-frequency data, were acquired in four hours.

The pavement at Site 8 consists of an upper layer of PCC (approximately 7 in), an intervening layer of BM (approximately 1 in.) and a basal layer of PCC (approximately 9 in.). The objective of the GPR investigation was to evaluate an unbonded PCC overlay with apparent problems.

The acquisition parameters employed were 512 samples/scan and 48 scans/ft. A dielectric permittivity of 8 was used to convert reflection times to depths. In Fig. 4.43, a section of a representative GPR profile from Site 7 in shown. Stripping in all eight cores is described as low to moderate. The BM is described as debonded in all cores, except core 1. The upper PCC/BM interface of core 1 is described as bonded. It should be noted that debonding at the PCC/BM or BM/PCC interface is not considered to be problematic for a pavement of this type, however, the utility of the GPR tool to detect this type of distress was evaluated here.



Fig. 4.41—Photograph of site the project-level segment I-35 (Section 8). Photograph was taken looking north.

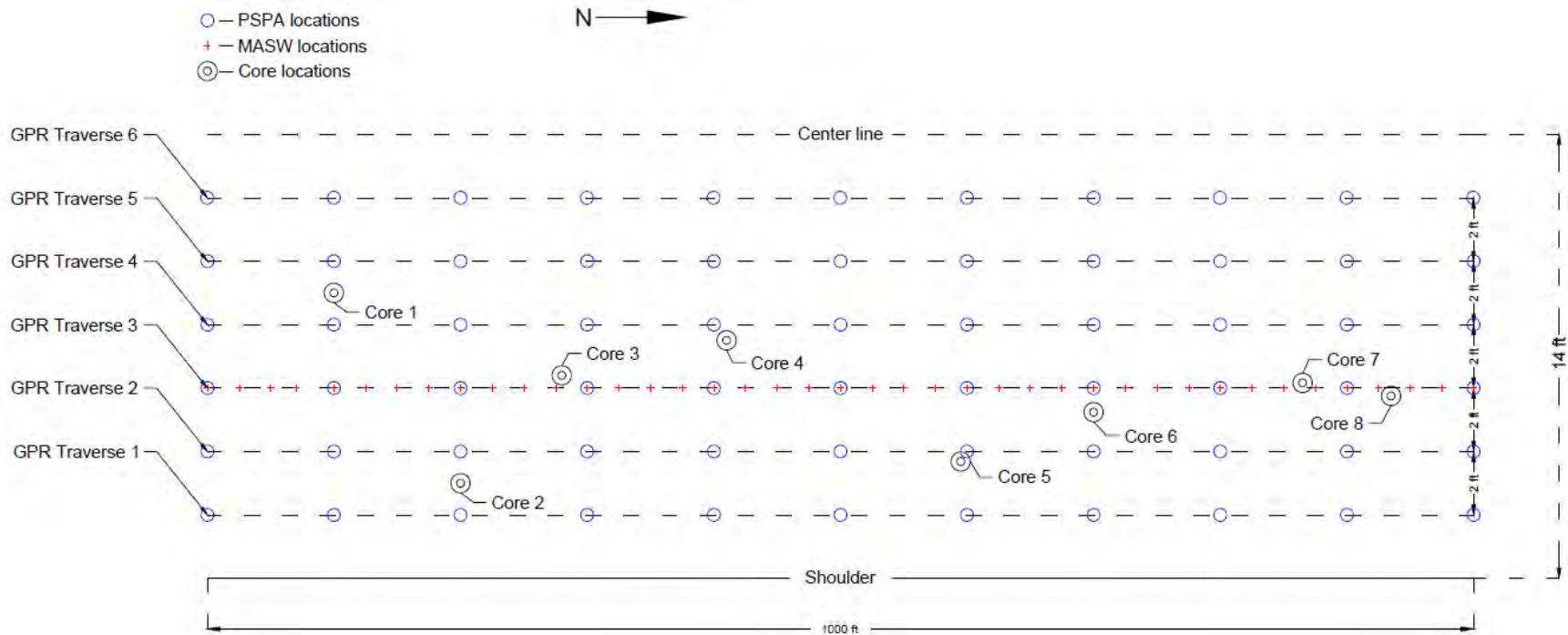


Fig. 4.42—Plan view map showing locations of the GPR traverses and the cores at the project-level segment I-35 (Section 8). A total of 6 GPR profiles 1000 ft long were acquired along parallel traverses spaced at 2 ft intervals. High-frequency (1.5GHz antenna) data GPR data were acquired along five traverses, low-frequency (400 MHz antenna) data GPR data were acquired along Traverse 3 only. Solid black lines represent the lane boundaries, total lane width was 12 ft. Core locations are marked as black circles. PSPA locations are marked as blue circles. MASW locations are marked as red crosses. Stripping in all eight cores is described as low to moderate. The BM is described as debonded in all cores, except core 1. The upper PCC/BM interface of core 1 is described as bonded.

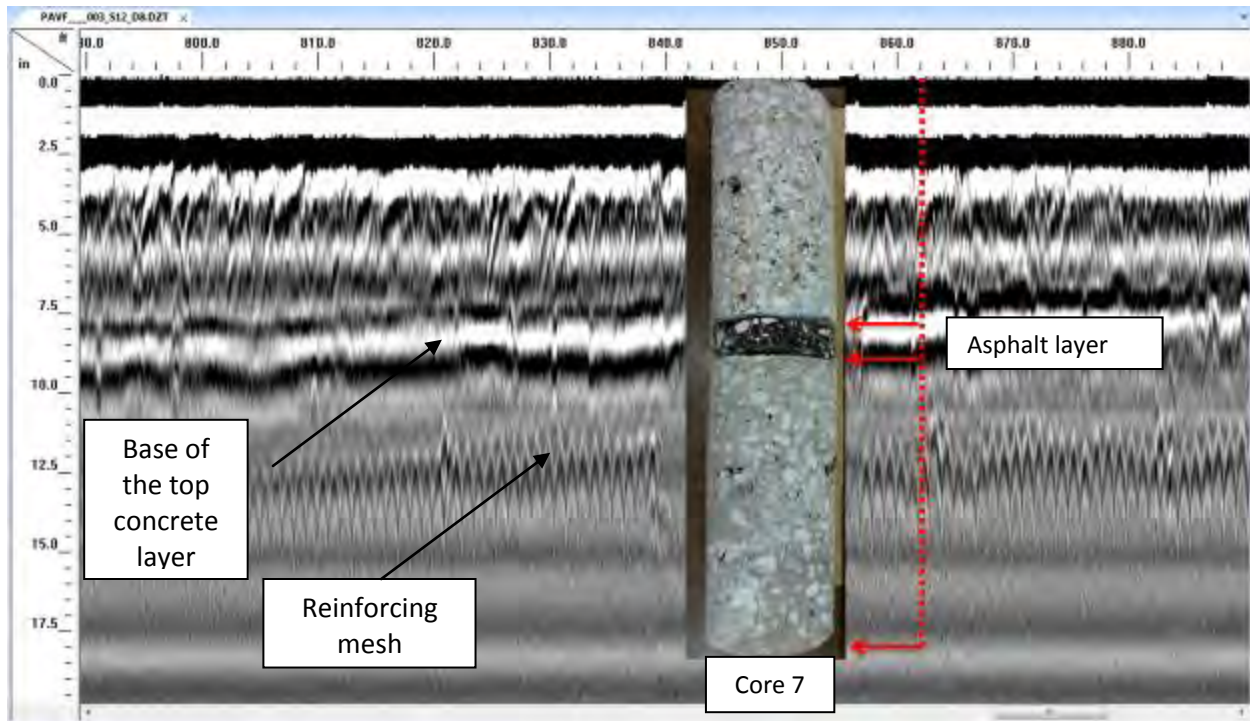


Fig. 4.43—Example of GPR section (GPR profile 3, stations 790-890) showing imaged features: the BM layer and reinforcing mesh. The horizontal axis is in units of feet; the vertical axis is in units of inches.

In Fig. 4.44, the following maps are presented: A) Apparent depth to base of the base upper layer of PCC (top BM); and B) Amplitude of the GPR reflection from the base of the top layer of PCC. Analyses of the GPR data indicate that there are no anomalous amplitude variations at the PCC/BM interface.

In Table 4.9, the core depths to the base upper layer of PCC are compared to the GPR-estimated depths to each of the pavement layers. As noted in Table 4.9, all GPR-estimated thicknesses and corresponding core depths differ by 8% or less. Differences can be attributed to: a) slight variations in the thicknesses of the PCC layer; and b) slight changes in the physical and chemical properties of the PCC.

The amplitudes of the reflections from the base of the upper layer of PCC at all core locations are relatively uniform, except for core location 1 (only core described as bonded) where slightly lower amplitudes were recorded.

Analyses of the acquired GPR data and core control suggests that the GPR tool could not be used at Site 7 to detect areas where PCC/BM and/or BM/PCC interface is debonded. However, the GPR tool could also be used to estimate pavement layer thicknesses to within 10%. Imaging of the lower PCC base layer was not possible, probably due to the GPR signal attenuation from the PCC/BM, BM/PCC interfaces and reinforcing mesh.

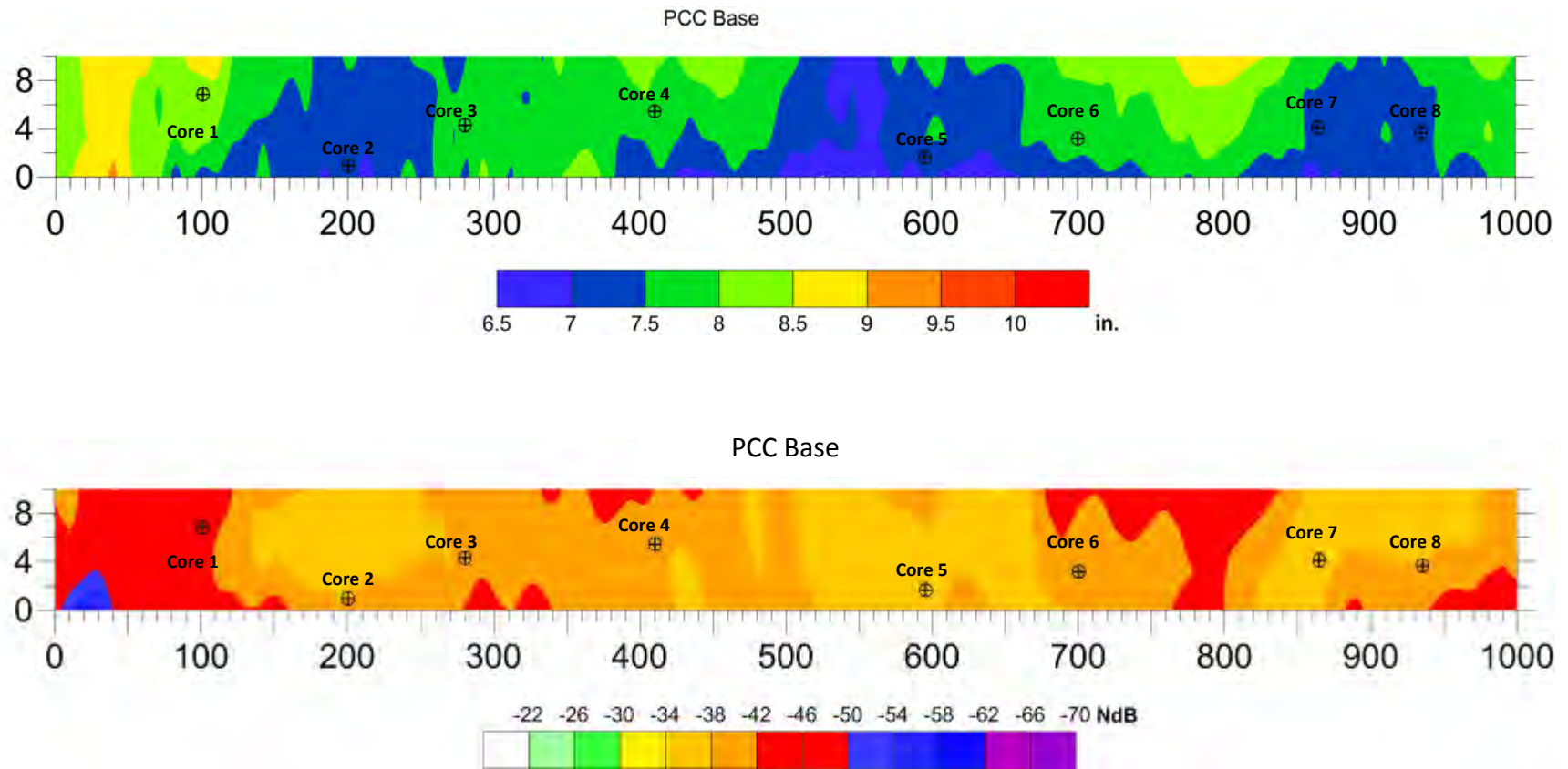


Fig. 4.44–A) Base map showing variations in the apparent thickness of the upper layer of PCC; and B) variations in the amplitude of the reflection from the base PCC. Thickness values are apparent and are based on the dielectric permittivity of 8.0. Traverse 1 (0 ft mark on map) was located 2 ft from the edge of the driving lane.

Table 4.9—Core depths and GPR apparent depths to base of BM layer at Site 8. Differences between the actual and apparent thicknesses are also noted. The PCC in all cores is described as being in good condition

Core #	1	2	3	4	5	6	7	8
PCC (Core) depth, in.	8	7	7.5	7.5	7	7.5	7.25	7
PCC (GPR) depth, in.	8	7	7.5	7.5	6.5	7.5	7.5	7
Correlation*,%	100.0	100.0	100.0	100.0	92.9	100.0	103.4	100.0

*Correlation is calculated based on the following formula: [Depth based on core information]/[Depth based on GPR information]*100. Correlation values below 100% typically indicate overestimated dielectric permittivity (relative permittivity); correlation values above 100% typically indicate the dielectric permittivity (relative permittivity) used was underestimated. Values highlighted in red show correlation values below 90% and/or above 110%.

Analyses of the acquired GPR data and core control suggest that the GPR tool could be used at Site 8 to detect thicknesses of the upper PCC and BM layers, and image the reinforcing mesh in the lower PCC layer. However debonding could not be confidently identified in the GPR data.

4.4 Concluding Remarks

High-frequency GPR data were acquired at eight 1000-ft long pavement section with a general goal to evaluate utility of the GPR tool. The acquired GPR data and control suggest the GPR tool can be used to estimate the thickness of the BM and PCC (to within 10% or better depending on the condition of the pavement), to image joints and reinforcing mesh, and to identify voids beneath PCC. The tool could also be used to identify debonded and/or stripped zones within BM. If core control is available, the GPR tool can also be used to estimate the condition of both PCC and BM.

The objectives of the high-frequency GPR investigation at Site 1 (US 63) were to determine the approximate thicknesses of the layers within the paved roadway and to identify areas of possible pavement degradation. Analyses of the acquired GPR data and core control suggest that the GPR tool could be used to estimate pavement layer thicknesses to within 10% accuracy, however, it could not be used to detect areas where BM/BM and/or BM/PCC interfaces are debonded. Also, the GPR tool was able to image joints and reinforcing mesh.

The objectives of the high-frequency GPR investigation at Site 2 (US 54) was to detect stripping and debonding, and to map the base of the BM. Analyses of the acquired GPR data and core control suggest that the GPR tool could be used to detect areas where stripping/debonding was present and to map the base of the BM. The generated apparent depth and amplitude maps indicate overall poor condition of the pavement. The presence of stripping and debonding is identified most readily based on the visual assessment individual GPR profiles.

The objective of the high-frequency GPR investigation at Site 3 (MO 179) was to detect stripping and/or debonding within the BM. Analyses of the acquired GPR data and core control suggest that the GPR tool could be used at Site 3 to detect areas where stripping/debonding was present and to map the base of the BM. The generated apparent depth and amplitude maps indicate overall fair condition of the pavement. The presence of stripping and debonding is identified most readily based on the visual assessment of individual GPR profiles.

The objectives of the GPR investigation at Site 4 (HWY AT) was to detect shallow stripping (less than 6 in. deep) and debonding. Analyses of the acquired GPR data and core control suggest that the GPR tool could be used at Site 4 to detect areas where stripping/debonding was present and to map the base of the BM and PCC. The generated apparent depth and amplitude maps indicate overall fair condition of the pavement. The presence of stripping and debonding is identified most readily based on the visual assessment of individual GPR profiles.

The objective of the GPR investigation at Site 5 (I-55 Pemiscot County) was to evaluate an unbonded PCC overlay without apparent problems. Analyses of the acquired GPR data and core control suggest that the GPR tool could be used at this site to differentiate moderately stripped BM from low stripped BM and debonded BM from bonded BM.

The objective of the GPR investigation at Site 6 (I-55 Perry County) was to evaluate the condition of PCC pavement with problems at the joints. Analyses of the acquired GPR data and core control suggest that the GPR tool could be used to detect areas where voids beneath the PCC layer are present. The generated apparent depth and amplitude maps indicate overall fairly uniform condition of the pavement. The presence of the problematic areas with voids beneath the pavement can be identified most readily based on the visual assessment individual GPR profiles.

The goal of the GPR investigation at Site 7 (HWY U) was to evaluate a poor quality BM road. Analyses of the acquired GPR data and core control suggest that the GPR tool could not be effectively used at this site to evaluate a poor quality BM road. Poor correlation between apparent thicknesses from the GPR data and thicknesses from core control are due to due actual variations in BM thickness and variations in BM condition, also due to the partial recovery of the cores. The presence of stripping and debonding is identified most readily based on the visual assessment of individual GPR profiles.

The objective of the GPR investigation at Site 8 (I-35) was to evaluate an unbonded PCC overlay with apparent problems. Analyses of the acquired GPR data and core control suggest that the GPR tool could be used at Site 8 to map the thicknesses of the upper PCC and BM layers, and to image the reinforcing mesh in the lower PCC layer. However, debonding could not be confidently identified on the GPR data.

5 PROJECT-LEVEL LOW-FREQUENCY GROUND PENETRATING RADAR INVESTIGATIONS

5.1 Introduction

Low-frequency ground-coupled ground penetrating radar (GPR) data are most commonly acquired using an antenna in monostatic-mode (transmitter/receiver housed in single case). However, in some situations (for example where velocity control is desired and/or to enhance the amplitude of specific reflections) low-frequency ground-coupled GPR data are acquired using two antennae in bistatic-mode (transmitter/receiver housed in separate cases). For Task 4 investigation purposes, pavement data were acquired using single cart-mounted low-frequency (400 MHz) GPR antenna operated in monostatic-mode (Fig. 4.1).

5.2 Overview of Project-Level Low-Frequency GPR Investigations

Low-frequency (400 MHz; Fig. 5.1) GPR data were acquired using sampling rates of 512 samples/scan and 24 scans/ft, but processed using 12 scans per ft. The GPR data were processed using GSSI RADAN 6 and RADAN 7 processing software. Initial processing steps included:

1. Time-to-depth conversion (reflection time to reflector depth). It is important to note that a **constant velocity** (selected for each site based on the correlation between a “typical” core and the corresponding GPR data) was used to transform reflection travel times to apparent reflector depths. The term “apparent” is used because a constant velocity is used to transform “reflection arrival time” to “reflector depth”. In areas where the pavement is deteriorated, the **constant velocity** will normally be greater than the actual velocity. Hence, layer thicknesses/depths in these areas will be “overestimated”. Conversely, in areas where the pavement is in excellent condition, layer thicknesses/depths may be underestimated.
2. Time-zero correction and filtering to eliminate noise and improve image for visual interpretation.
3. Mapping (“picking”) of the variable apparent depths and amplitudes of the reflections from base of the identifiable BM and/or PCC layers.

The initial output of processing was an Excel spreadsheet that included reflection amplitudes (in units of normalized decibels, NdB) and two-way travel times (in units of nanoseconds, ns) for each mapped pavement layer. Post-processing steps included combining the Excel spreadsheet information from individual GPR profiles into one Excel file with assigned coordinates for each GPR profile.

It should be noted that the low-frequency (400 MHz) data were acquired at each site only along a GPR traverse 3. Most of the cores were not acquired on GPR traverse 3.



Fig. 5.1—Photograph showing the push-cart and low-frequency 400 MHz GPR antenna (red box on pavement surface) and GSSI SIR-3000 control unit (top of cart).

5.3 Project-Level Low-Frequency GPR (400 MHz) Data

5.3.1 Project-Level Site 1 (US 63)

The project-level pavement Site 1 (US 63) is located north of Rolla, Missouri. The pavement at Site 1 consists of two layers of bituminous mix (BM) over portland cement concrete PCC (Fig. 4.6). Typical Site 1 pavement layer thicknesses are estimated as follows: upper BM: 1.5 in.; middle BM: 2.0 in.; lower PCC: 8.5 in. (Fig. 4.6).

The goal of investigation was to assess the utility and ability of the low-frequency GPR antenna to image the base, subbase, grade and subgrade layers where present at this site. Low-frequency GPR data were acquired in the north-bound lane of US 63 along traverse 3 (Fig. 4.7). The acquisition parameters employed were 512 samples/scan and 24 scans/ft. A dielectric permittivity of 8.0 was used to convert reflection times to depths.

In Fig. 5.2 GPR images generated along a segment of GPR traverse 3 (Site 1) are shown. The upper profile was generated using the lower-frequency 400 MHz antenna and a dielectric permittivity of 8.0 (estimated for base); the lower profile was generated using the higher-frequency 1.5 GHz antenna and a dielectric permittivity of 8.0 (see Section 4.3.1 of this report). As illustrated, the low-frequency GPR antenna was unable to image beneath the layer of reinforcing mesh, due to the close spacing of the mesh wires. Note that the diffractions from the mesh effectively mask any reflections above an apparent depth of 25 in. (including the base PCC).

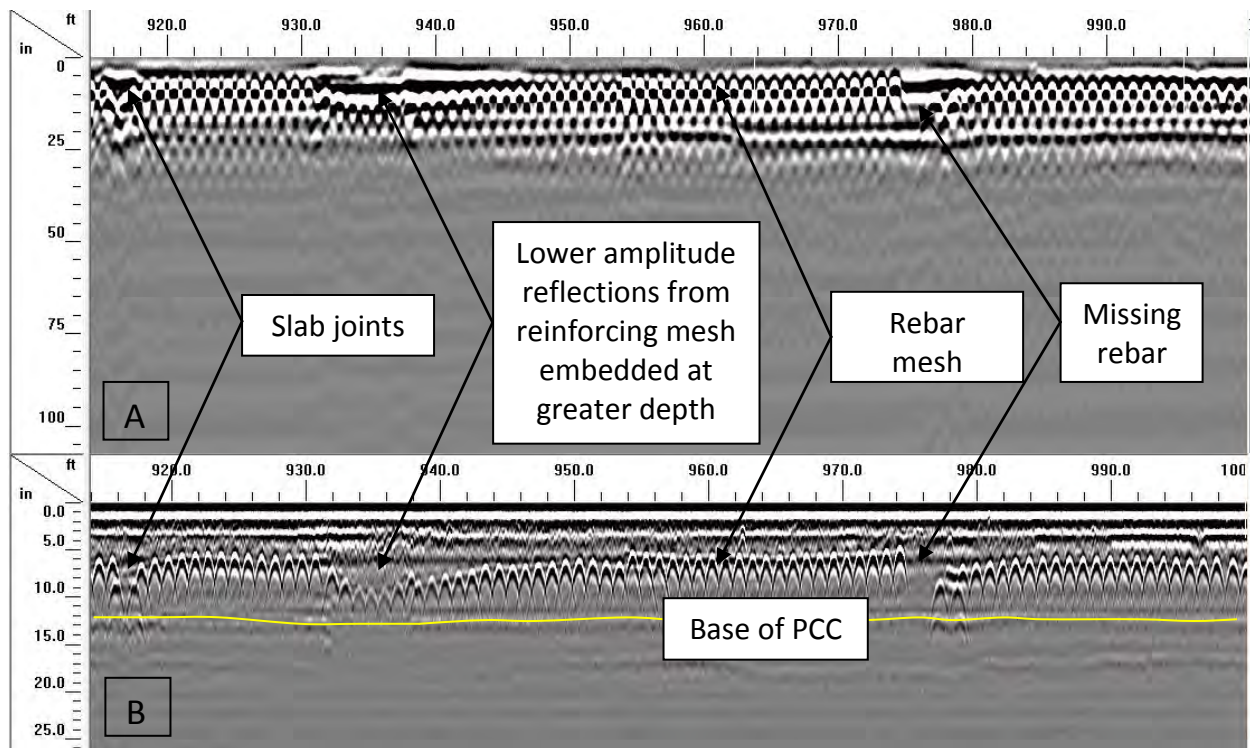


Fig. 5.2—Example of GPR data (Site 1; US 63; stations 920-1000). A) Section of 400 MHz GPR profile acquired along traverse 3. B) Section of 1.5 GHz GPR profile acquired along same section of traverse 3. GPR data were processed using a dielectric permittivity of 8.0. As illustrated, the low-frequency GPR antenna was unable to image the base of the upper BM layer, the base of the lower BM layer and/or the base of PCC layer. Also, the low-frequency antenna was unable to image the subsurface beneath the reinforcing mesh probably due to the close spacing of the mesh wires and related interference effects. The horizontal axis is in units of feet; the vertical axis is in units of inches.

5.3.2 Project-Level Site 2 (US 54)

The project-level pavement section US 54 (Section 2) is located about 5 miles west of Camdenton, Missouri. The goal of investigation was to assess the utility of the low-frequency GPR antenna at this site.

In Fig. 5.3, the upper profile was generated using the lower-frequency 400 MHz antenna and a dielectric permittivity of 8.0 (estimated for base); the lower profile was generated using the higher-frequency 1.5 GHz antenna and a dielectric permittivity of 8.0 (see Section 4.3.2 of this report). As illustrated, the low-frequency GPR antenna was unable to image beneath the layer of reinforcing mesh due to the close spacing of the mesh wires.

The low-frequency GPR antenna was able to image reflectors (if any) at depths greater than those imaged using the high-frequency antenna (approx. 20 in.). The base of the BM layer and a pavement interface at a greater depth (approx. 20 in.) were imaged. The exact nature of

the lower interface could not be independently verified due to lack of the core data at a depth of 20 in., but it is assumed that this interface was probably the top of the subgrade.

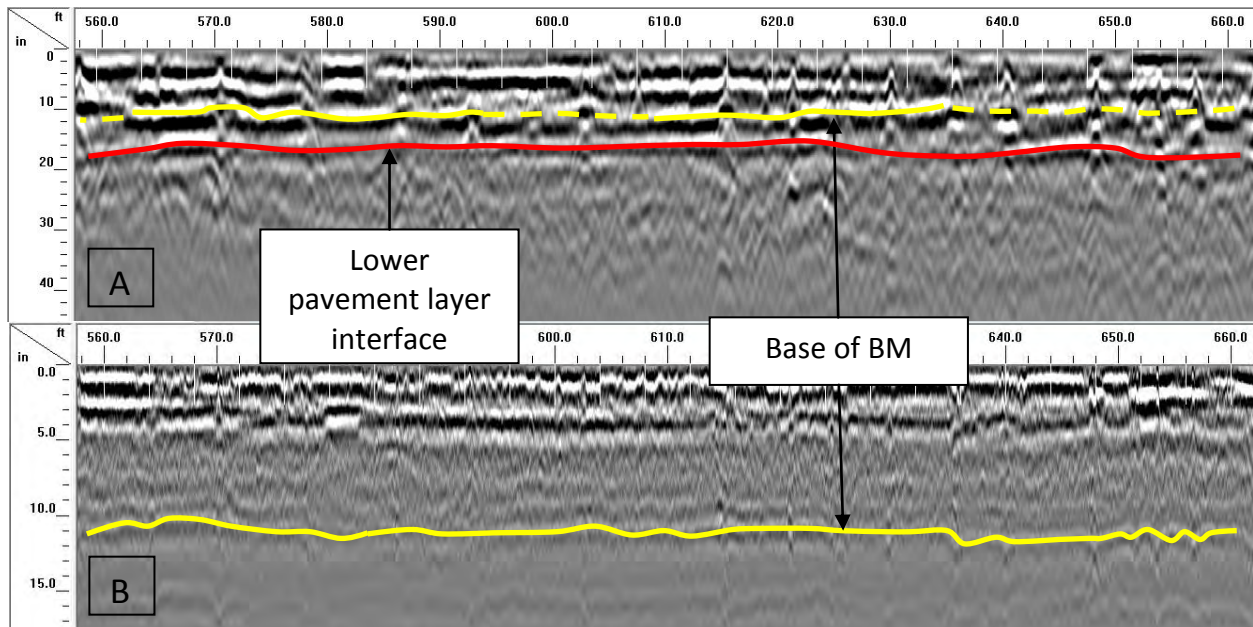


Fig. 5.3—Example of GPR data (Site 2; US 54; stations 930-1000). A) Section of 400 MHz GPR profile acquired along traverse 3. B) Section of 1.5 GHz GPR profile acquired along traverse 3. Dielectric permittivity is 8.0. Yellow solid line represents base of the BM layer, dashed yellow line represents estimated base of the BM. The red line represents a reflection from a lower pavement layer. However, the specific nature of the lower interface could not be independently verified due to absence of the core data (at a depth of approx. 20 in.). The horizontal axis is in units of feet; the vertical axis is in units of inches.

5.3.3 Project-Level Site 3 (MO 179)

The project-level pavement Site 3 (MO 179) is located approximately 4 miles west of Jefferson City, Missouri. The pavement at Site 3 consists of approximately 12.5 in. thick full depth bituminous mix (BM) (Fig. 4.15).

The goal of investigation was to assess the utility and ability of the low-frequency GPR antenna to image the base, subbase, grade and subgrade layers where present at this site. Low-frequency GPR data were acquired in the south-bound lane along traverse 3 (Fig. 4.16). The acquisition parameters employed were 512 samples/scan and 24 scans/ft. A dielectric permittivity 7.5 was used to convert reflection times to reflector depths.

The more subtle features (debonded interfaces) imaged using the high-frequency antenna could not be identified as confidently on the GPR data acquired with the low-frequency antenna, most likely due to the lower resolution of the antenna (Fig. 5.4). The GPR data acquired with the low-frequency antenna was not useful for mapping pavement layers (if any) beneath the base of the BM.

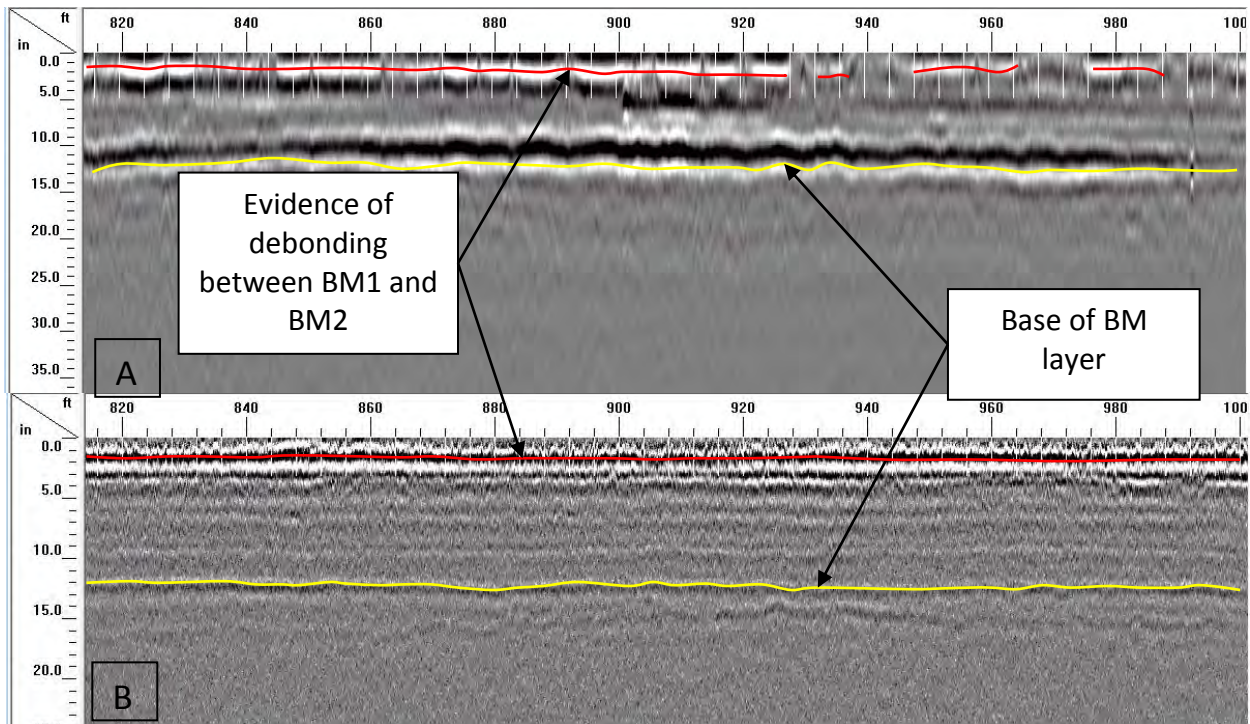


Fig. 5.4—Example of GPR data (Site 3; MO 179; stations 820-1000). A) Section of 400 MHz GPR profile acquired along traverse 3. B) Section of 1.5 GHz GPR profile acquired along same section of traverse 3. GPR data were processed using a dielectric permittivity of 7.5. As illustrated, the low-frequency GPR antenna was able to detect debonding between the upper and the middle BM layers, and to image the base of the BM (lower) layer. The low-frequency antenna was unable to image the pavement beneath the BM layers. Yellow solid line represents base of the BM layer. Red solid line represents possible debonded BM layers. The horizontal axis is in units of feet; the vertical axis is in units of inches.

5.3.4 Project-Level Site 4 (HWY AT)

The project-level pavement Site 4 (HWY AT) is located approximately 7 miles east of Union, MO. Low-frequency GPR data were acquired in the south-bound lane along traverse 3 (Fig. 4.21). The pavement was variable depth BM over PCC. The total thickness of BM and PCC retrieved at the core locations varied from 7 in. (core 7) to 15.25 in. (core 1).

The goal of the ground penetrating radar (GPR) investigation using a low-frequency antenna at this site was to assess the possibility of the GPR system to image the base, subbase, grade and subgrade layers where present. Low-frequency GPR data were acquired in the south-bound lane along traverse 3 (Fig. 4.21). The acquisition parameters employed were 512 samples/scan and 24 scans/ft. A dielectric permittivity of 7.5 was used to convert reflection times to depths. In Fig. 5.5, a section of a representative GPR profile from Site 4 is shown.

Some of the more subtle features imaged with the high-frequency antenna could not be confidently identified on the GPR data acquired with the low-frequency antenna, most likely due to the lower resolution of the antenna (Fig. 5.5). However, base of the PCC layer and base

of the BM layer in places could be mapped using the low frequency antenna. Also, a possible utility line was imaged. The data acquired with the low-frequency antenna was not useful for determining base, subbase or subgrade layers.

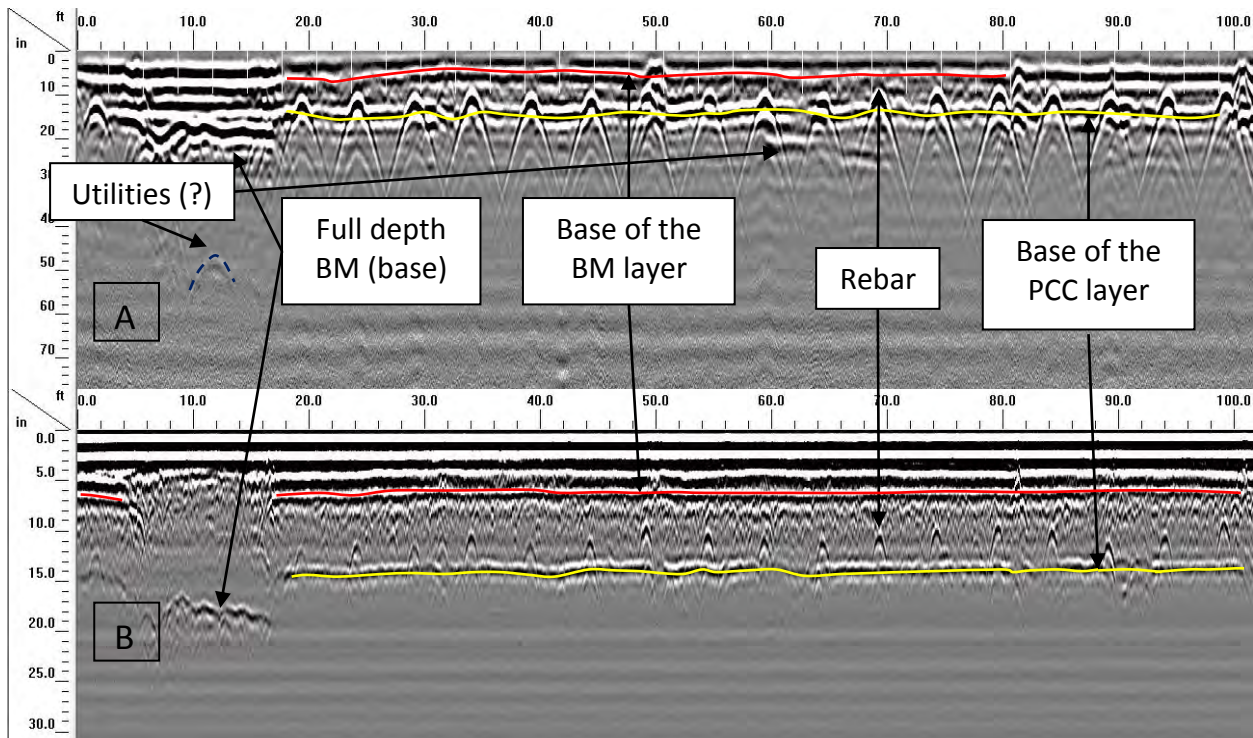


Fig. 5.5—Example of GPR data (Site 4; MO 179; stations 0-100). A) Section of 400 MHz GPR profile acquired along traverse 3. B) Section of 1.5 GHz GPR profile acquired along traverse 3. GPR data were processed using a dielectric permittivity of 7.5. As illustrated, the low-frequency GPR antenna was able to image the base of the PCC layer, reinforcing mesh embedded in the PCC layer and possible utilities. The low-frequency GPR antenna was not able continuously image the BM layer base and was not able to confidently image any features below the PCC base, except possible utilities. Yellow solid line represents base of the PCC layer. Red solid line represents interpreted base of the BM layer. The horizontal axis is in units of feet; the vertical axis is in units of inches.

5.3.5 Project-Level Site 5 (I-55 Pemiscot County)

Project-level pavement Site 5 (I-55 Pemiscot Co.) is located approximately 13 miles south from Hayti, Missouri. The pavement at Site 5 consists of an upper layer of PCC (approximately 12 in.), an intervening layer of BM (approximately 2.2 in.) and a basal layer of PCC (approximately 10 in.) (Fig. 4.25).

The goal of investigation was to assess the utility and ability of the low-frequency GPR antenna to image the base, subbase, grade and subgrade layers where present at this site. Low-frequency GPR data were acquired in the south-bound lane along traverse 3 (Fig. 4.26). The acquisition parameters employed were 512 samples/scan and 24 scans/ft. A dielectric permittivity 8.0 was used to convert reflection times to reflector depths.

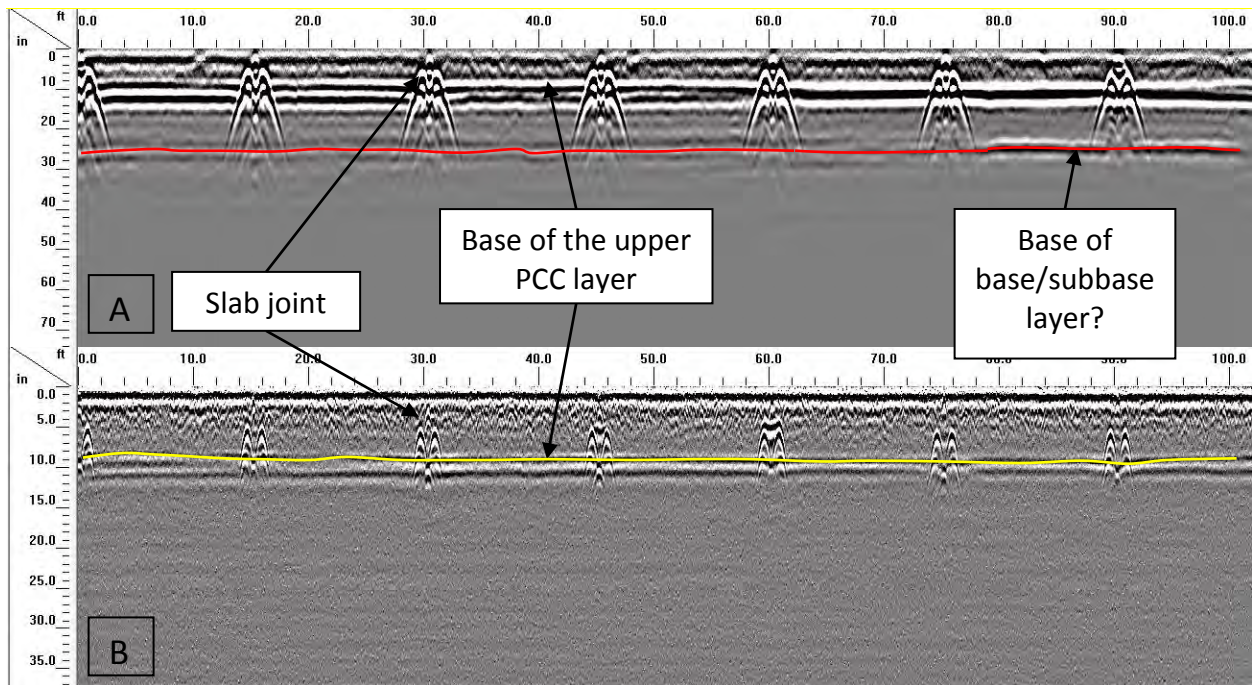


Fig. 5.6—Example of GPR data (Site 5; I-55, Pemiscot County; stations 0-100). A) Section of 400 MHz GPR profile acquired along traverse 3. B) Section of 1.5 GHz GPR profile acquired along the same section of traverse 3. GPR data were processed using a dielectric permittivity of 8.0. As illustrated, the low-frequency GPR antenna was able to image the base of the PCC layer, reinforcing mesh embedded in the PCC layer and possible utilities. The low-frequency GPR antenna was not able to continuously image the BM layer base and was not able to confidently image any features below the PCC base. Yellow solid line represents base of the upper PCC layer. Red solid line represents the base of the lower layer of PCC. The horizontal axis is in units of feet; the vertical axis is in units of inches.

The low-frequency GPR antenna was able to image the subsurface to a greater depth than the high-frequency antenna (30 in. vs. 12 in. accordingly). Base of the upper PCC layer and the base of the lower layer of PCC were imaged.

5.3.6 Project-Level Site 6 (I-55 Perry County)

The project-level pavement section I-55 Perry County (Section 6) was located about 8 miles north of Perryville, Missouri. The goal of the ground penetrating radar (GPR) investigation using a low-frequency antenna at this site was to assess the possibility of the GPR system with a low-frequency antenna to image the base, subbase and subgrade layers where present.

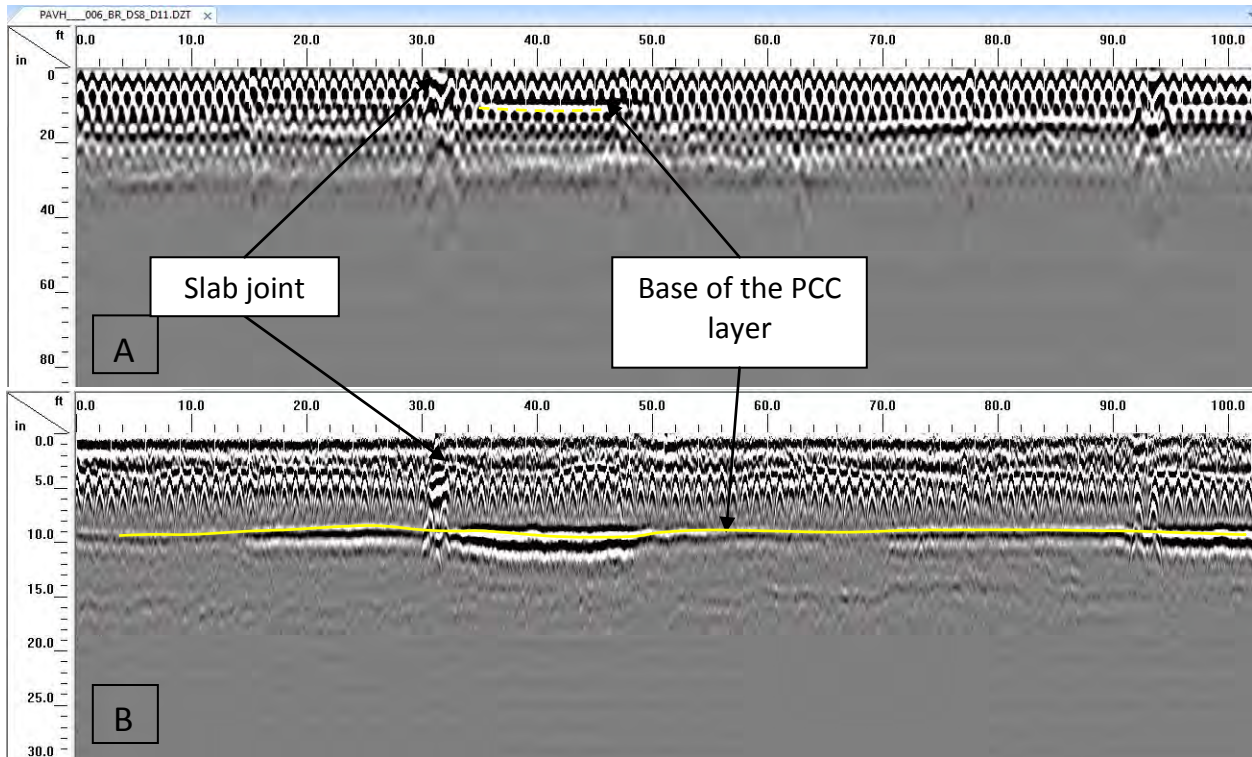


Fig. 5.7—Example of GPR data (Site 6; I-55 Perry County; stations 0-100). Some of the imaged features are shown in the low-frequency GPR data (A) and the high-frequency GPR data (B). The low-frequency GPR antenna did not image any base, subbase or subgrade layers. GPR data were processed using a dielectric permittivity of 8.0. Yellow solid line represents base of the PCC layer. The horizontal axis is in units of feet; the vertical axis is in units of inches.

The low-frequency GPR antenna was able to image the subsurface to a greater depth than the high-frequency antenna (32 in. vs. 17 in. accordingly). Base of the PCC layer was not confidently mapped using the low-frequency antenna, most likely due to the close spacing of the reinforcing mesh and associated interference effects.

5.3.7 Project-Level Site 7 (HWY U)

The project-level pavement section HWY U (Section 7) was located about 6 miles north of Salem, Missouri. The goal of the ground penetrating radar (GPR) investigation using a low-frequency antenna at this site was to assess the possibility of the GPR system with a low-frequency antenna to image the base, subbase, and subgrade layers where present.

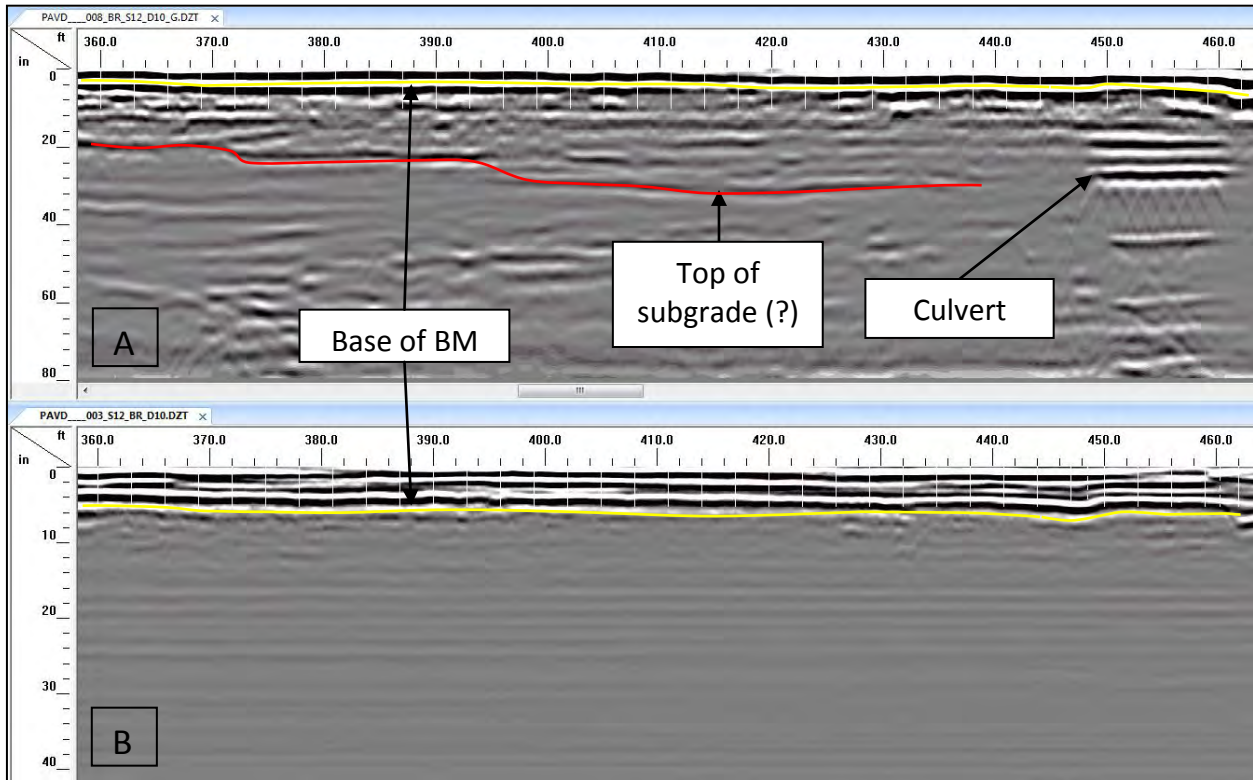


Fig. 5.8—Example of GPR data (Site 7; HWY U; stations 360-460). Some of the imaged features are shown in the low-frequency GPR data (A) and the high-frequency GPR data (B). The low-frequency GPR antenna was able to image a layer beneath pavement which is most likely the top subgrade, however, the interpretation couldn't not be confirmed or verified due to lack of the core data. GPR data were processed using a dielectric permittivity of 10.0. Yellow solid line represents base of the upper PCC layer. Red solid line represents possible top of subgrade, however, the interpretation could not be verified due to lack of the core data. The horizontal axis is in units of feet; the vertical axis is in units of inches.

The low-frequency GPR antenna was able to image the subsurface to a greater depth than the high-frequency antenna (80 in. vs. 10 in. accordingly). Base of the BM layer and a layer at a greater depth, which is most likely the top of subgrade, were imaged, however, the interpretation could not be verified due to lack of the core data. Also, a culvert was imaged.

5.3.8 Project-Level Site 8 (I-35)

The project-level pavement section I-35 (Section 8) was located about 20 miles north of Cameron, Missouri. The goal of the ground penetrating radar (GPR) investigation using a low-frequency antenna at this site was to assess the possibility of the GPR system with a low-frequency antenna to image the base, subbase, and subgrade layers where present.

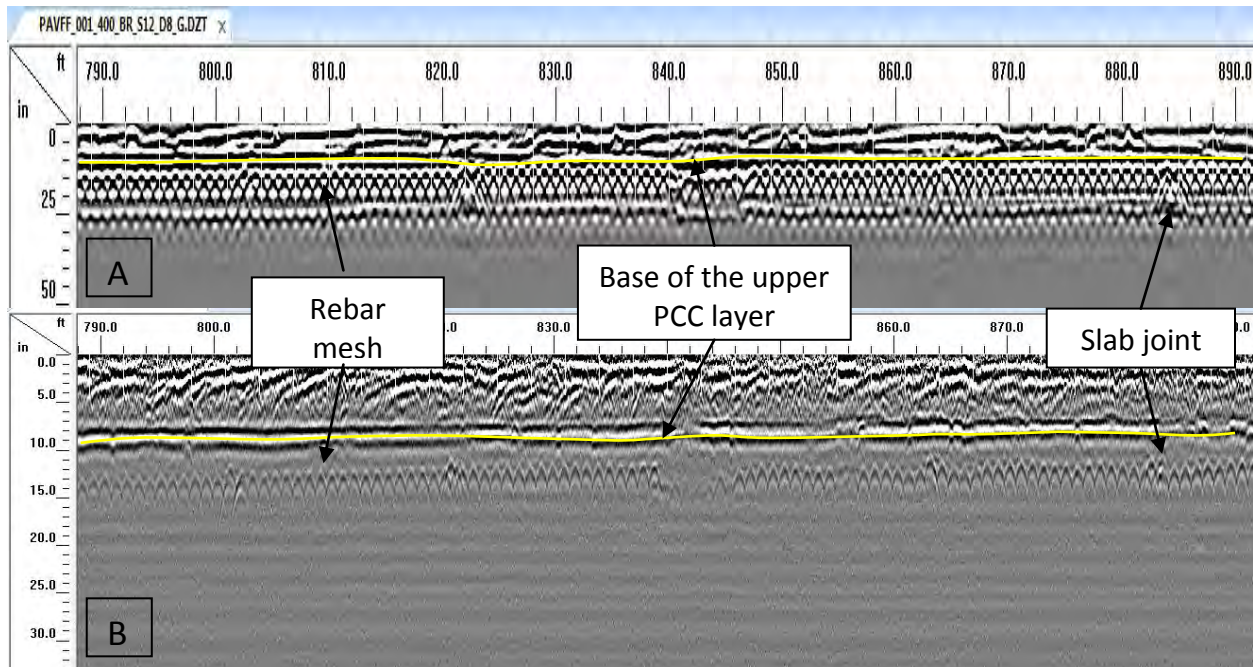


Fig. 5.9—Example of GPR data (Site 8; I-35; stations 410-500). Some of the imaged features are shown in the low-frequency GPR data (A) and the high-frequency GPR data (B). The low-frequency GPR antenna did not image any base, subbase, or subgrade layers. GPR data were processed using a dielectric permittivity of 8.0. Yellow solid line represents base of the upper PCC layer. The horizontal axis is in units of feet; the vertical axis is in units of inches.

The low-frequency GPR antenna was able to image the subsurface to a greater depth than the high-frequency antenna (30 in. vs. 16 in. accordingly). Base of the upper PCC layer, joints and reinforcing mesh were imaged with both antennas. However, the low-frequency GPR antenna was unable to confidently image beneath the layer of mesh, most likely due to the close spacing of the mesh wires.

5.4 Concluding Remarks

Low-frequency GPR data were acquired at eight 1000-ft long pavement sections along one traverse with a general goal to assess the utility and ability of the low-frequency GPR antenna to image base, subbase, and subgrade layers and any other features if present at a site. The acquired low-frequency GPR data suggest the GPR tool can be used to image the subsurface at a greater depth, compared to the high-frequency antenna. However, the low-frequency antenna was not useful at the sites with reinforced PCC layers (Sites 1, 6 and 8) because of the

signal attenuation and reflection from the reinforcing mesh, and possibly because of the site specific conditions (high concentration moisture and clayey soils). Also, the low-frequency antenna was not useful to map the base of BM layers at all sites, except Sites 3, 4 and 7, but was able to image the base of PCC layers at Sites 4, 5 and 8. The tool likely mapped the top of the subgrade at Site 2 and Site 7, however, the interpretations could not be verified because lack of the core data below base BM. Features such as utility lines and a culvert were imaged with low-frequency antenna at Site 4 and 7, respectively.

At Site 1 (US 63) the low-frequency GPR antenna was unable to confidently image base of the BM and PCC layers, because of the low antenna resolution, or subsurface beneath the layer of rebar, most likely due to the close spacing of the mesh wires.

At Site 2 (US 54) the low-frequency GPR antenna was able to image the subsurface to a greater depth than the high-frequency antenna (40 in. vs. 15 in. accordingly). The base of the BM layer and a layer at a greater depth, which is most likely the top of the subgrade, were imaged, however, the interpretation could not be verified due to lack of the core data.

At Site 3 (MO 179) the features imaged with the high-frequency antenna could not be confidently identified in the data acquired with the low-frequency antenna, most likely due to the lower resolution of the antenna. Unfortunately, the data acquired with the low-frequency antenna was not useful for determining base, subbase, or subgrade layers.

At Site 4 (HWY AT) the features imaged with the high-frequency antenna could not be confidently identified in the data acquired with the low-frequency antenna, most likely due to the lower resolution of the antenna. However, the base of the PCC layer and base of the BM layer in places could be mapped using the low-frequency antenna. Also, a possible utility line was imaged. The data acquired with the low-frequency antenna were not useful for determining base, subbase, or subgrade layers.

At Site 5 (I-55, Pemiscot County) the low-frequency GPR antenna was able to image the subsurface to a greater depth than the high-frequency antenna (30 in. vs. 12 in. accordingly). The base of the upper and lower PCC layers were imaged.

At Site 6 (I-55, Perry County) the low-frequency GPR antenna was able to image the subsurface to a greater depth than the high-frequency antenna. However, the base of the PCC layer was not confidently mapped using the low-frequency antenna, most likely due to the close spacing of the mesh wires.

At Site 7 (HWY U) the low-frequency GPR antenna was able to image the subsurface to a greater depth than the high-frequency antenna. The base of the BM layer and a layer at a greater depth, which is most likely the top subgrade, were imaged, however, the interpretation could not be verified due to lack of the core data. Also, a culvert cover was imaged.

At Site 8 (I-35) the low-frequency GPR antenna was able to image the subsurface to a greater depth than the high-frequency antenna. The base of the upper PCC layer, joints and reinforcing mesh were imaged with both antennas. However, the low-frequency GPR antenna was unable to confidently image beneath the layer of mesh, most likely due to the close spacing of the mesh wires.

6 SURFACE WAVE AND ELECTRICAL RESISTIVITY TOMOGRAPHY INVESTIGATIONS

6.1 Introduction

6.1.1 Electrical Resistivity Tomography (ERT)

Electrical resistivity tomography (ERT) data are normally acquired with the objective of generating two-dimensional (2-D) resistivity profiles of the subsurface (Fig. 6.1). If correlations can be established between resistivity and lithology, a 2-D resistivity profile can be effectively transformed into a 2-D geologic image (interpretation) of the subsurface. The geologic interpretations are based on the assumption that variations in the resistivity of the subsurface reflect corresponding changes in lithology (and moisture content). Geologic interpretations are generally reliable, especially if ground truth is available to constrain and/or verify interpretations.

Generally, intact rock is characterized by high resistivity values; weathered rock is characterized by intermediate resistivity values; soil is characterized by low to intermediate resistivity values; and clays are characterized by very low resistivity values (Fig. 6.1). The ERT image of the subsurface will vary seasonally as the moisture content of the soil and/or rock changes. Soil and rock resistivity values increase as moisture content decreases.

An interpreted 2-D ERT profile can be of significant utility to those engaged in highway construction and/or maintenance. Interpretations of interest include, but are not limited to, the mapping/identification of the following:

- depth to top of rock
- variations in rock quality
- variations in rock lithology
- pattern, placement and density of solution-widened joints
- pattern, placement, density and offset of faults
- locations of air-filled voids
- locations of water- and clay-filled vugs in karst terrain
- top of water table
- distribution of dry soil
- distribution of moist soil
- distribution of sandy-silty soil
- distribution of clayey soil
- seepage flow pathways

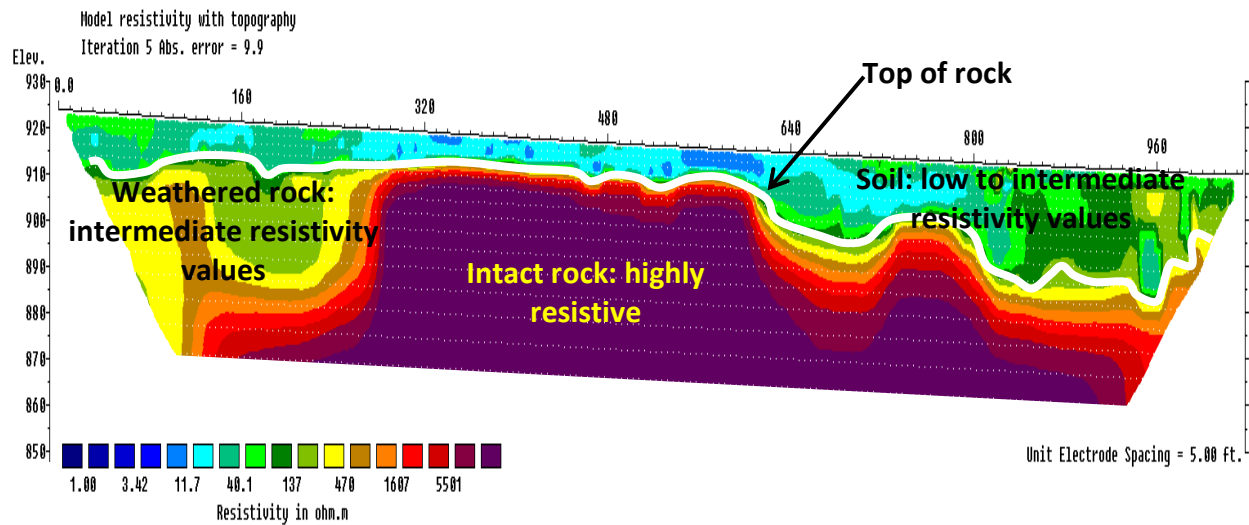


Fig. 6.1—Example interpreted ERT profile (Site 1) with elevation control. Distances and depths are in units of feet. Resistivity is in units of ohm-m. Intact rock (as per the superposed interpretation) is characterized by resistivity values in excess of 1500 ohm-m; weathered rock by values between 75 and 1500 ohm-m; and soil mostly by values less than 100 ohm-m. The soil/rock contact corresponds (approx.) to the 75 ohm-m contour interval.

6.1.2 Multi-Channel Analyses of Surface Wave (MASW)

Active multi-channel analyses of surface wave (MASW) data (Fig. 6.2) are normally acquired with the objective of generating one-dimensional (1-D) shear-wave velocity profiles of the subsurface often with superposed geologic interpretations. 2-D shear-wave velocity profiles can also be created by generating 1-D shear-wave velocity profiles at multiple pre-determined locations along a traverse, placing these 1-D profiles side-by-side, and contouring (Fig. 6.3).

An interpreted 2-D MASW profile can be of significant utility to those engaged in highway construction and/or maintenance. Interpretations of interest include, but are not limited to, the mapping/ identification of the following:

- depth to top of rock
- variations in soil and rock rigidity
- variations in soil and rock lithology

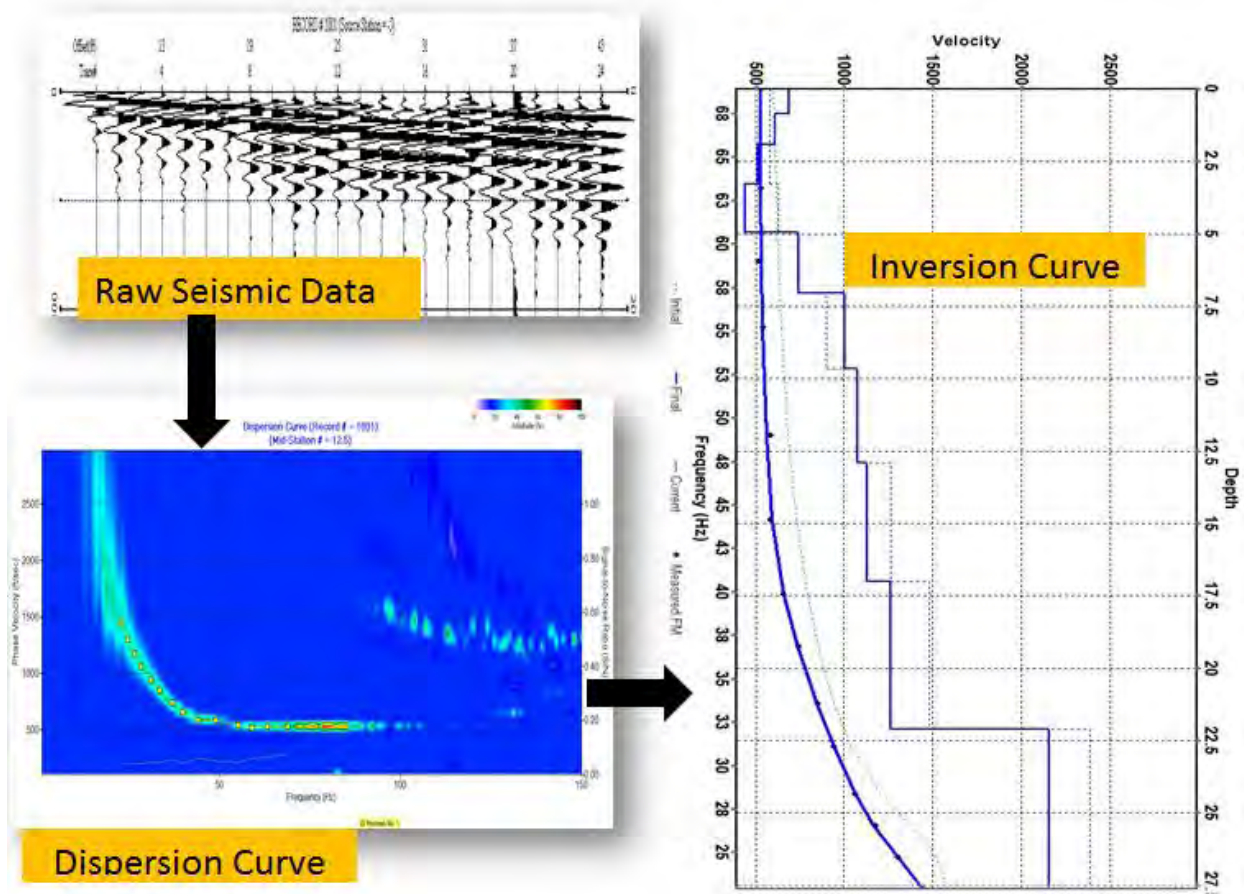


Fig. 6.2—Example active MASW data were acquired using a 24-channel engineering seismograph, 24 low-frequency (4.5 Hz) vertically-polarized geophones spaced at 1.5 ft and a sledge hammer source. MASW raw seismic field data, the corresponding dispersion curve, and the corresponding 1-D shear-wave velocity profile (depths are in units of feet) are displayed. During processing, the raw seismic field data are transformed into a dispersion curve (phase velocity vs.. frequency). The dispersion curve is transformed into a 1-D shear-wave velocity profile (inversion curve).

6.2 Overview of Project-Level ERT and MASW Investigations

Electrical resistivity tomography (ERT) and multi-channel analyses of surface wave (MASW) data were acquired at the following eight (8) project-level roadways (Sites 1-8):

- Project-level Site US 63 (Site 1)
- Project-level Site US 54 (Site 2)
- Project-level Site Rte 179 (Site 3)
- Project-level Site HWY AT (Site 4)
- Project-level Site I-55 (Pemiscot Co., Site 5)
- Project-level Site I-55 (Perry Co., Site 6)
- Project-level Site HWY U (Site 7)
- Project-level Site I-35 (Site 8)

The ERT field data were acquired in the DOT right of way (ROW) (Figs. 6.4, 6.5, and 6.6) at each project-level site using an AGI SuperSting R8/IP resistivity system and 68 electrodes spaced at 5 ft intervals (dipole-dipole array). (Note, in this report, the term ROW refers to the unpaved land that is alongside the pavement.) The output at each project-level site was a 1000 ft long 2-D resistivity image of the subsurface (ERT profile) with superposed geologic interpretations (Fig. 6.1). The geologic interpretations are based on the assumption that measured variations in the resistivity of the subsurface reflect corresponding changes in lithology. Interpretations are generally reliable, especially if ground truth is available to constrain and/or verify interpretations. Unfortunately, boring control was not available for any of the eight project-level sites for which ERT control was acquired. The interpretations of the acquired project-level ERT profiles are therefore based on the investigators' experience and available MASW shear-wave velocity control (also acquired as part of this investigation).

MASW field data were acquired at 41 locations (Fig. 6.4) along each project-level roadway using an engineering seismograph and twenty-four low-frequency (4.5 Hz) vertical geophones spaced at 1.5 ft (Fig. 6.7). Acoustic energy was generated at an offset (distance to nearest geophone) of 10 ft using a 12 lb sledge hammer and metal plate. The final output at each project-level site was a 1000 ft 2-D shear-wave velocity profile of the subsurface (MASW profile) with superposed geologic interpretations (Fig. 6.3). The geologic interpretations are based on the assumption that measured variations in the acoustic properties of the subsurface at a specific study site reflect corresponding changes in lithology content. Interpretations are generally reliable, especially if ground truth is available to constrain and/or verify interpretations. Unfortunately, boring control was not available for the eight project-level sites for which MASW control was acquired. As a consequence, the interpretations of the acquired MASW data are based on the author's experience and available ERT control (also acquired as part of this investigation).

The separation between each MASW traverse and the corresponding ERT traverse was typically 20 to 30 ft (center of lane to DOT ROW). This separation can explain many of the minor differences between the ERT and MASW interpretations as subsurface conditions can vary significantly over short distances in karst terrain. Also, the paved surfaces on which the MASW data were acquired were elevated (typically by multiple feet) relative to the DOT ROWs in which the ERT data were acquired.

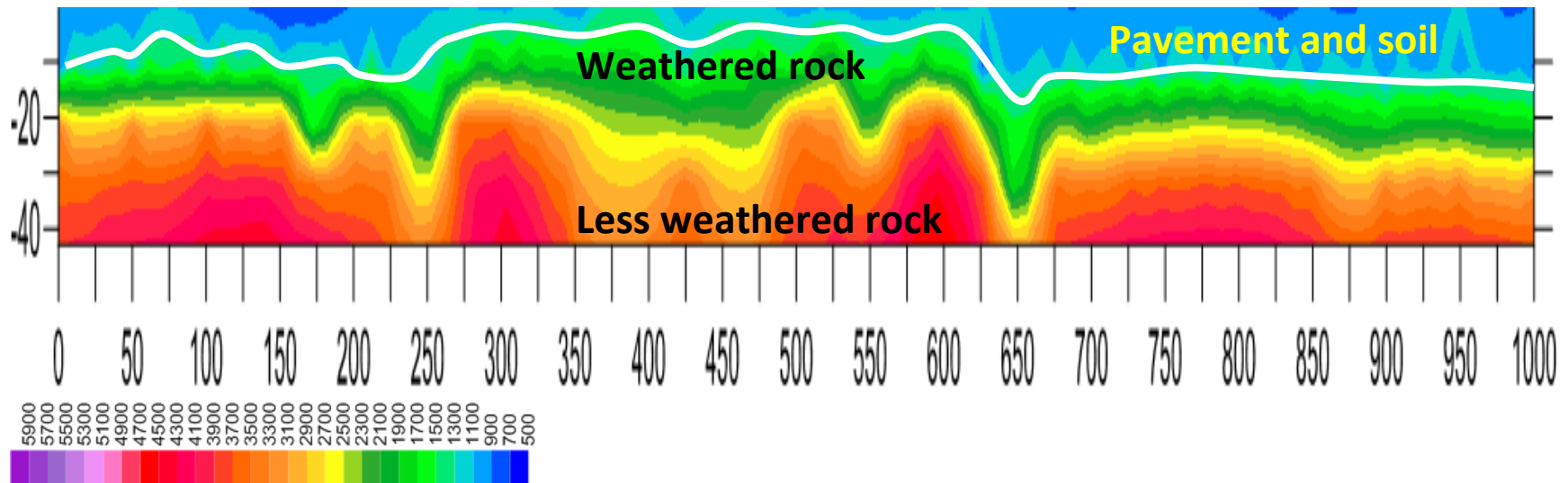


Fig. 6.3—Example 2-D MASW shear-wave profile (Site 1). Horizontal and vertical scales are in units of feet. During processing, each of the 41 MASW field records acquired at each project-level site was transformed into dispersion data (Rayleigh-wave velocity vs. frequency format; standard, established mathematical process that does not require any interactive input from the interpreter; Fig. 6.2). The dispersion data were analyzed qualitatively (processor input was required), and optimum phase velocities were selected (dispersion curve; Fig. 6.2). Each dispersion curve was inverted without any qualitative input from the interpreter and transformed into a 1-D shear-wave velocity profile. The forty-one (41) 1-D shear-wave velocity profiles generated at 25 ft intervals along each project-level roadway were used to generate 2D shear-wave profiles that extended to depths in excess of 40 ft.

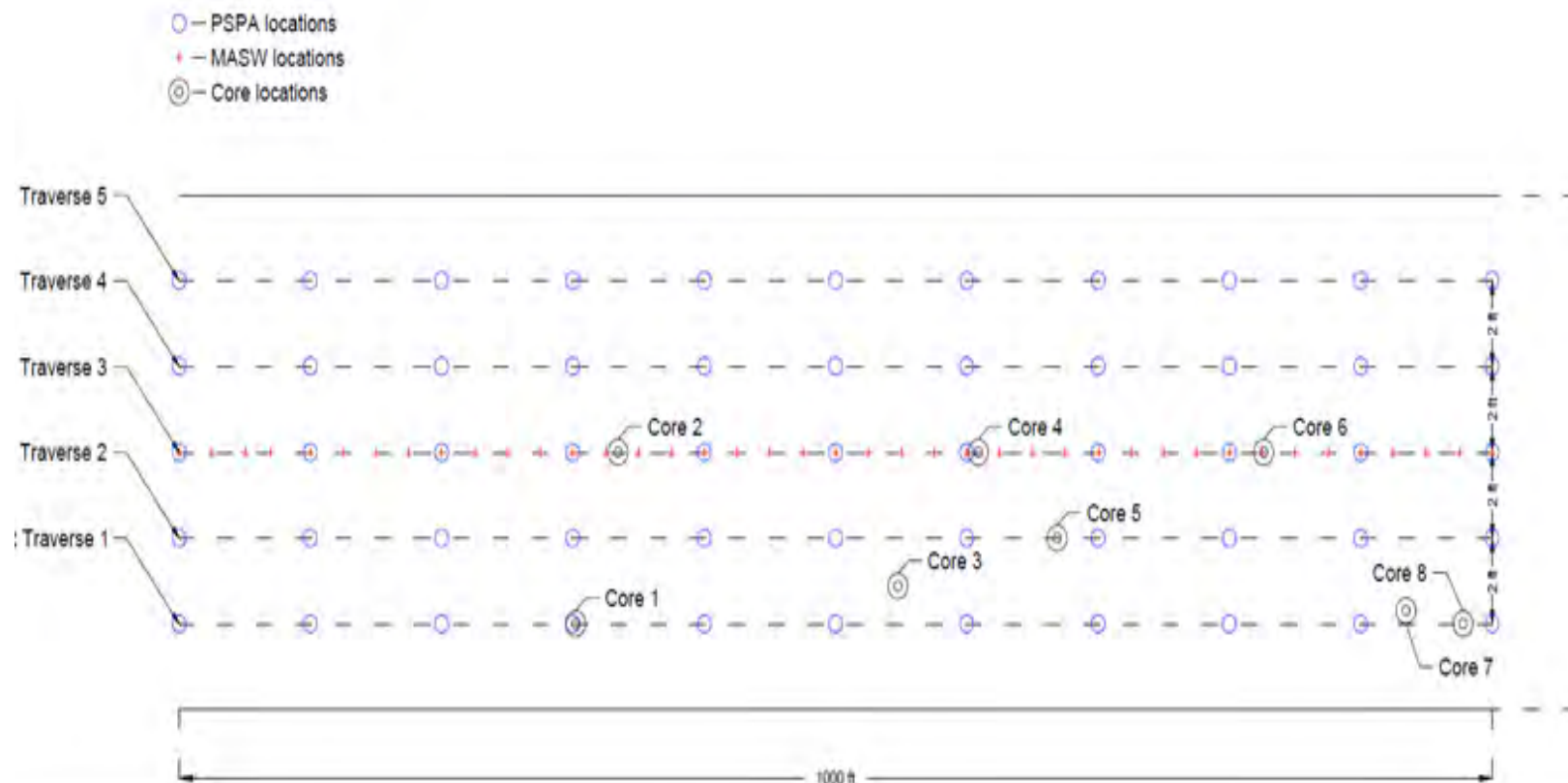


Fig. 6.4—Example project-level site layout. ERT data were acquired at each project-level site along a 1000 ft traverse in the DOT ROW (Figs. 6.1 and 6.5). The start and end of each ERT traverse were consistent with the start and end of the corresponding GPR traverses. Active MASW data were acquired at 41 stations (every 25 ft from the 0 ft mark to the 1000 ft mark) along GPR traverse 3 (GPR traverses 1-5 are identified at the left of the figure). A 1-D shear-wave velocity profile was generated for each MASW station (Fig. 6.2). The forty-one (41) 1-D shear-wave velocity profiles generated for each project-level site were combined together (placed side-by-side) to generate a 2-D shear-wave velocity profile (Figs. 6.3 and 6.5). The datum on each ERT profile (acquired in DOT ROW) is generally 1-2 ft lower than the datum on the corresponding 2-D MASW shear-wave velocity profile (acquired on paved roadway). The separation between each MASW traverse and the corresponding ERT traverse was typically 20 to 30 ft. This separation can explain many of the minor differences between the ERT and MASW interpretations as subsurface conditions can vary significantly over short distances, especially in karst terrain.

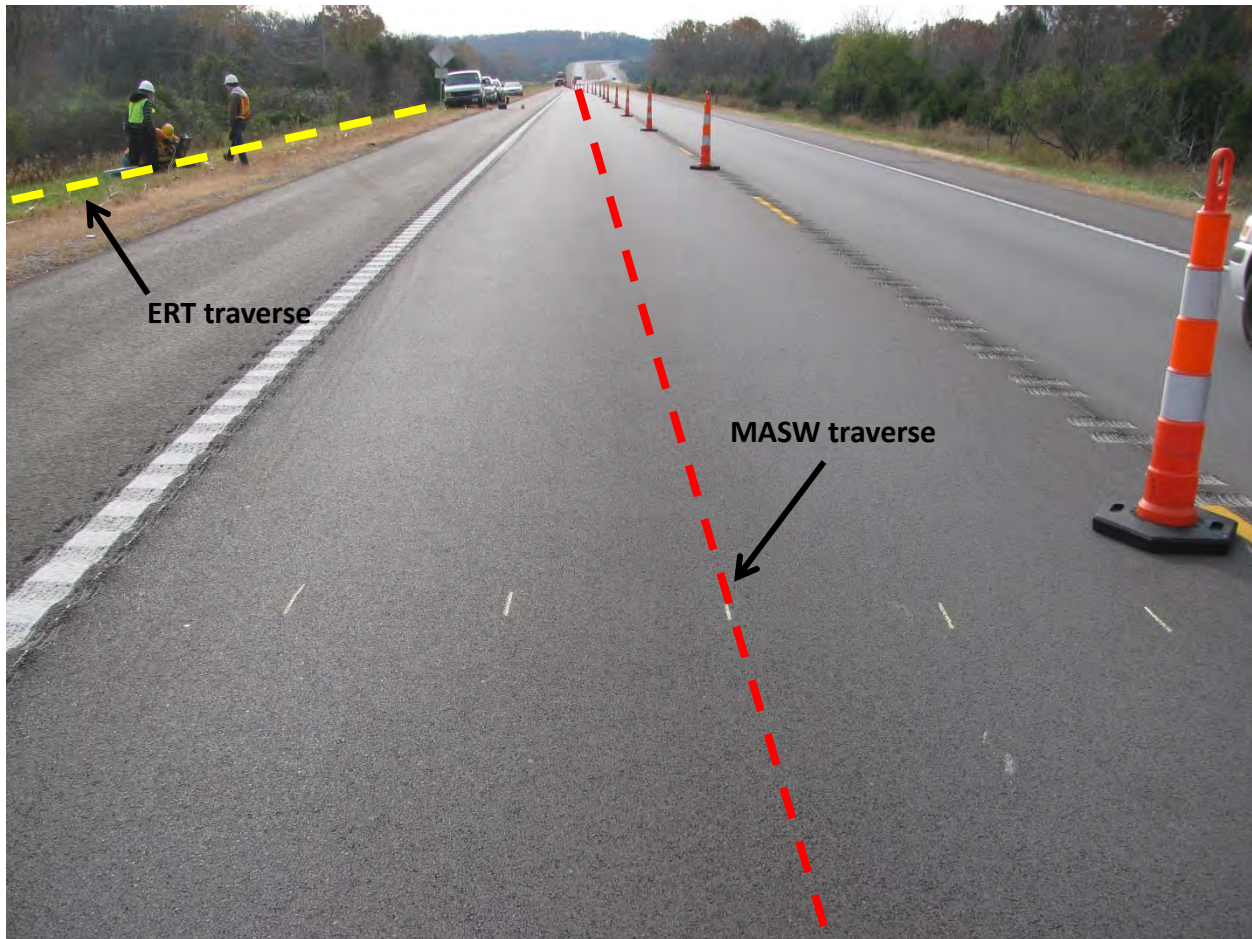


Fig. 6.5—Example project-level site layout (Site 1). ERT data were acquired at each project-level site along a 1000 ft traverse in the DOT ROW. The start/end of each ERT traverse was consistent with the start/end of the corresponding GPR traverses. MASW data were acquired at 41 stations (every 25 ft from the 0 ft mark to the 1000 ft mark) along GPR traverse 3 (Fig. 6.4). The separation between each MASW traverse and the corresponding ERT traverse was typically 20 to 30 ft. This separation can explain many of the minor differences between the ERT and MASW interpretations as subsurface conditions can vary significantly over short distances, especially in karst terrain.

6.3 Overview of Data Acquisition, Processing, and Interpretation

6.3.1 Electrical Resistivity Tomography (ERT)

An array of interconnected electrodes (68 for this investigation) is coupled to the ground surface at uniform predetermined intervals (5 ft for this investigation) along a designated traverse and to the control unit (Fig. 6.6). At any instant in time, one pair of electrodes is used to induce current (I) into the ground while a second pair of electrodes is used to measure potential differences (ΔV). The control unit automatically acquires apparent resistivity data (ρ_a) by using all possible combinations of electrode pairs (depending upon type of array employed) as both current electrodes and voltmeter electrodes. Each recorded potential difference is used to calculate a value of resistance (R ; $R = \Delta V/I$) and then a value of apparent resistivity (ρ_a ;

$\rho_a = KR$, where K is a geometric factor based on the separations between the relevant electrodes).

Raw data (calculated apparent resistivity ρ_a) are downloaded from the control unit for further processing. Processing software provides for automated or manual editing to remove individual data values that appear to be anomalous and therefore unreliable. Processing software also automatically inverts the apparent resistivity data and generates an optimum resistivity image of the subsurface. Usually, the inversion of the apparent resistivity data does not require interactive input from the interpreter. However, some processing parameters can be interactively changed to enhance the output.

The output is 2-D electrical resistivity image of the subsurface (Fig. 6.1). An estimate of the extent to which the output 2-D image correlates with the input apparent resistivity data is provided as a percent error. At each project-level site, ERT data were acquired using a 5 ft electrode spacing. Five feet is therefore one estimate of the ERT lateral resolution.



Fig. 6.6—ERT data were acquired at each project-level site using an AGI SuperSting R8/IP resistivity system and a dipole-dipole array. Electrodes were spaced at 5 ft intervals. The intent was to image the subsurface to depths on the order of 40 ft.

6.3.2 Multi-Channel Analyses of Surface Wave (MASW)

A linear array of geophones (24 geophones spaced at 1.5 ft intervals; Fig. 6.7) and an engineering seismograph were used to record active Rayleigh (surface) wave data. The array of geophones was centered at predetermined station locations (every 25 ft) along each project-level roadway. Active Rayleigh wave data sets were generated using a sledge hammer and striking plate (source discharged off the end of the geophone array). When the active source is discharged, the seismograph is triggered and field data are recorded (typically for one second or less). Stacking will improve the signal-to-noise ratio.

Each MASW field record was transformed into dispersion data (Rayleigh-wave velocity vs. frequency format; standard, established mathematical process that does not require any interactive input from the interpreter). The dispersion data are analyzed qualitatively (processor input is required) and optimum phase velocities are selected (dispersion curve). The dispersion curve is usually inverted without any qualitative input from the interpreter and transformed into a 1-D shear-wave velocity profile (Fig. 6.2). By convention, the 1-D shear-wave velocity profile is assumed to represent the velocity of the subsurface at the mid-point of the array (stations every 25 ft). In reality, the 1-D velocity profile represents (more-or-less) the average shear-wave velocity along the entire length of the array.



Fig. 6.7—Active MASW data were acquired at each project-level site using a 24-channel engineering seismograph and 24 low-frequency (4.5 Hz) geophones spaced at 1.5 ft intervals. The intent was to image the subsurface to depths on the order of 40 ft.

The forty-one 1-D shear-wave velocity profiles generated for each site were combined to create a 2-D shear-wave velocity profile. Each 2-D profile was 1000 ft in length. These 2-D profiles depict both lateral and vertical variations in the shear-wave velocity and can be transformed into 2-D geologic profiles. The 2-D geologic profiles are normally very reliable, especially if ground truth is available. These 2-D geologic profiles constitute the final deliverable. As noted, the 1-D velocity profile represents (more-or-less) the average shear-wave velocity along the entire length of the array. MASW lateral resolution at each site is therefore on the order of 34.5 ft.

6.4 Project-Level ERT and MASW Data

6.4.1 Project-Level Site 1 (US 63)

6.4.1.1 Electrical Resistivity Tomography Data

An interpreted version of the 2-D ERT profile generated for Site 1 is shown in Fig. 6.8. Boring control was not available to constrain the geologic interpretations. Elevation control was not applied in order to facilitate comparison with the corresponding 2-D MASW profile (Figs. 6.9 and 6.10). At Site 1, intact rock (as per interpretation) is characterized by resistivity values in excess of 2000 ohm-m; weathered rock by values between 75 and 1500 ohm-m; and soil mostly by values less than 100 ohm-m (with moist clayey soils being characterized by resistivity values less than approximately 10 ohm-m). The soil/rock contact corresponds (approx.) to the 75 ohm-m contour interval (Fig. 6.8).

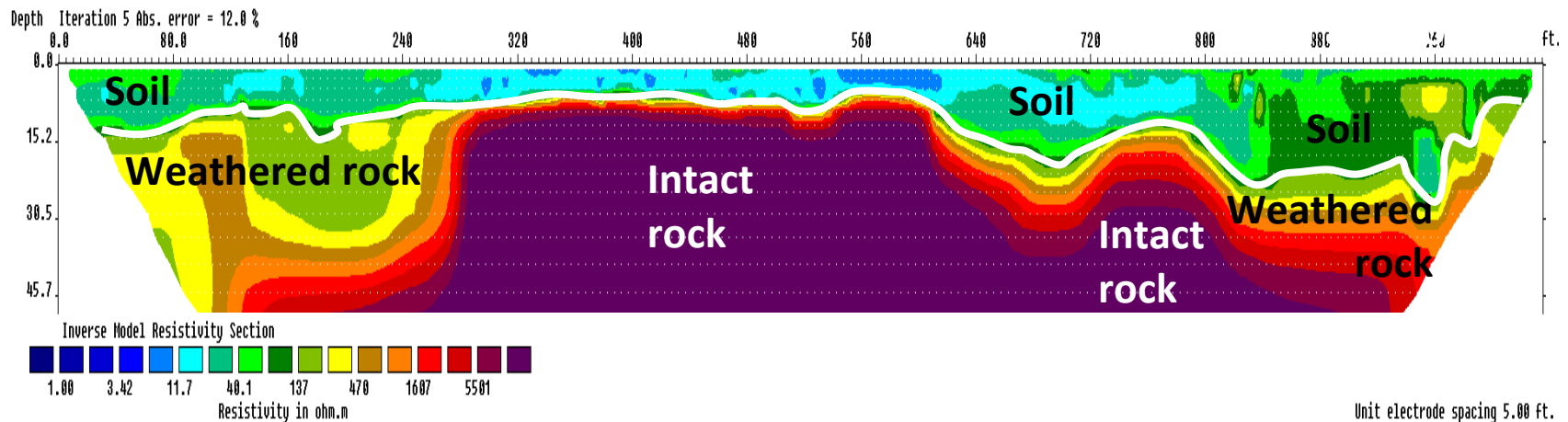


Fig. 6.8—Example interpreted Site 1 ERT profile without elevation control. The datum is the ground surface in the DOT ROW (approx. 1-2 ft below pavement surface). Distances and depths are in units of feet. Resistivity is in units of ohm-m. Interpreted top of rock is shown by the white line. The iteration error was 12%. This error value is typical of good quality ERT data acquired in karst terrain. The term “good quality” refers to the extent to which the acquired ERT field data and the output ERT profile correlate. ERT data quality usually decreases as the complexity (3-D) of the subsurface increases.

6.4.1.2 Multi-Channel Surface Wave Analyses Data

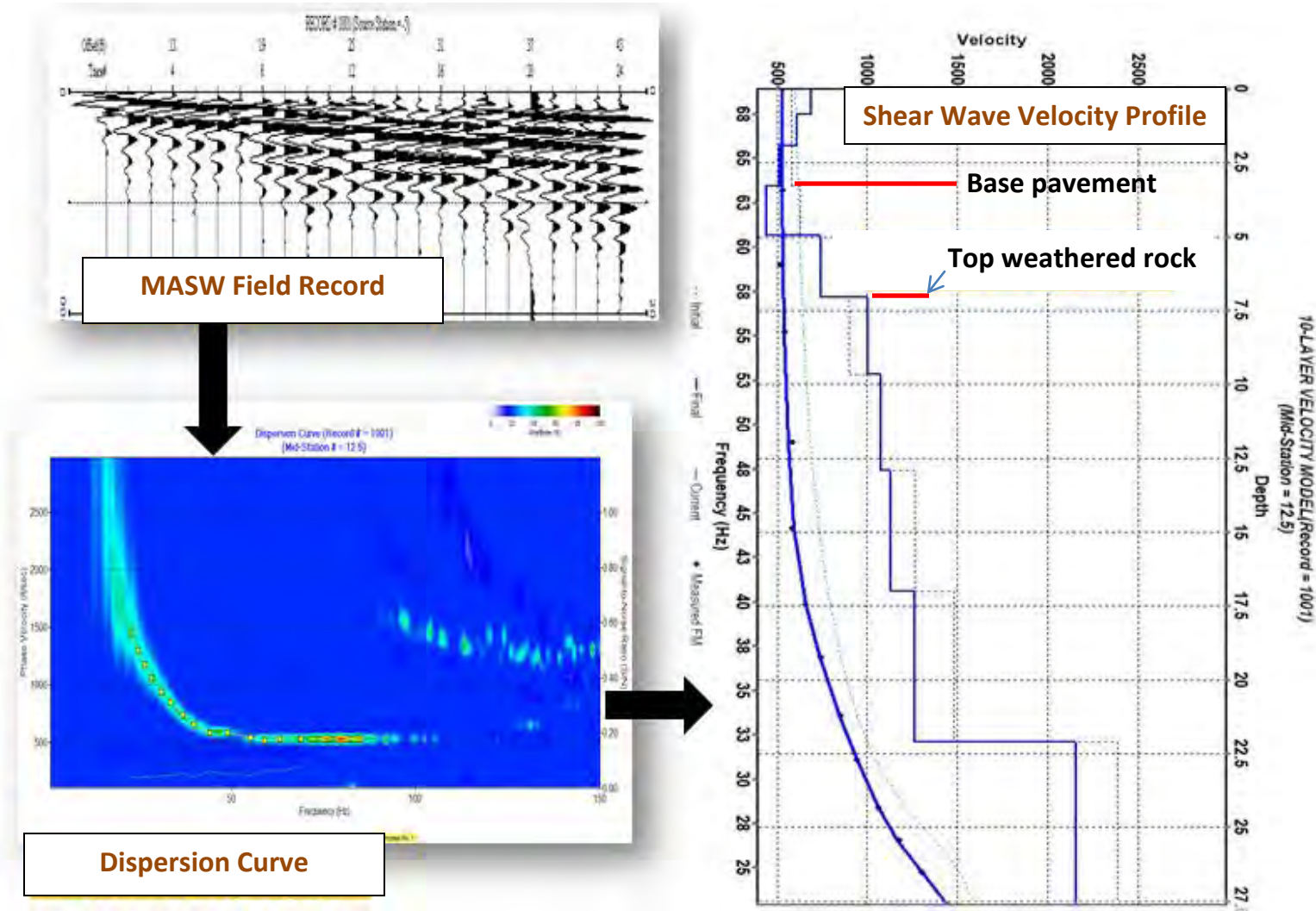


Fig. 6.9—Site 1 basic MASW data (station 300 ft): MASW field record, corresponding dispersion curve and 1-D shear-wave velocity profile. Interpreted top of weathered rock (1000 ft/sec) is at a depth of approx. 7 ft. This depth correlates well with the ERT-estimated depth to the top of rock at station 300 ft (Fig. 6.8). MASW data quality is excellent.

A representative 1-D shear-wave velocity profile from Site 1 is shown in Fig. 6.9. The interpreted top of weathered rock (shear-wave velocity >1000 ft/sec) is at a depth of 7 ft. This depth estimate is consistent with the interpreted ERT profile (Fig. 6.8).

An interpreted version of the 2-D MASW profile generated for Site 1 is shown in Fig. 6.10. Boring control was not available to constrain the geologic interpretations. At Site 1, the top of weathered rock (as per interpretation) is characterized by velocities greater than 1000 ft/sec. Pavement and soil are characterized by velocities less than 1000 ft/sec. A comparison of Fig. 6.8 and Fig. 6.10 indicate that the ERT and MASW data compare rather favorably. The ERT data are more definitive and almost certainly slightly more reliable (recall that spatial resolution provided the 1-D shear-wave velocity profile is significantly less than that provided by the ERT profile).

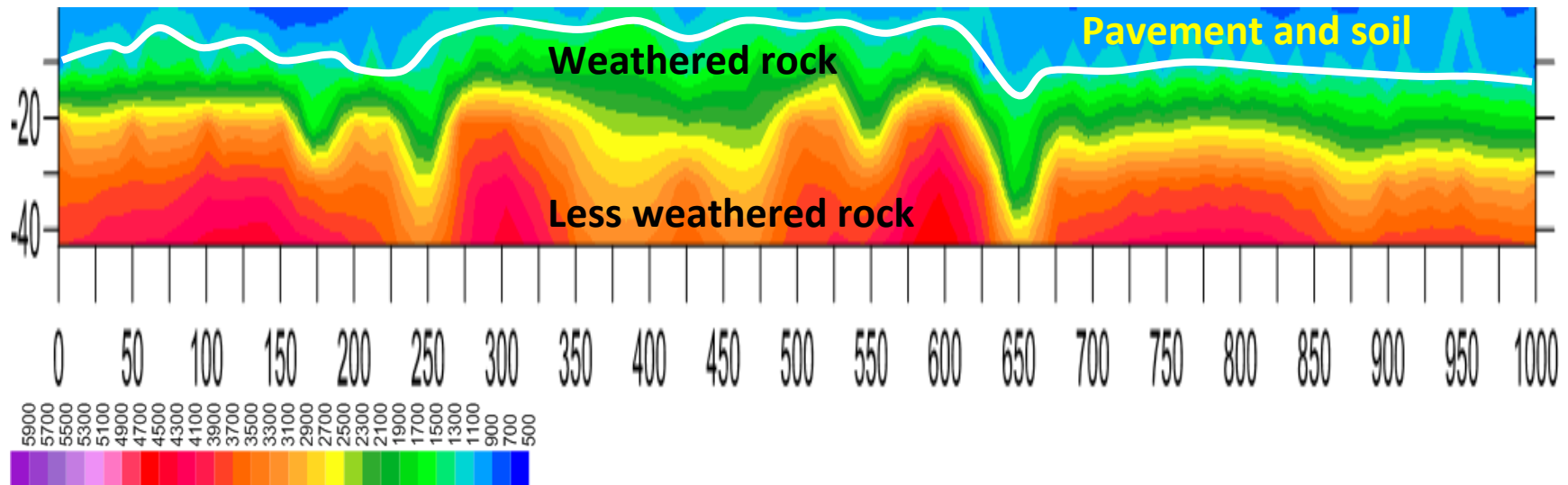


Fig. 6.10—Site 1: Example interpreted 2-D MASW shear-wave velocity profile with elevation control. Elevation control cannot be applied using the software provided by the MASW manufacturer (Kansas Geological Survey). Datum on the 2-D MASW profile corresponds to the top of pavement (approx. 1-2 ft above ERT datum). Distances and depths are in units of feet. Velocities are in units of ft/sec.

6.4.2 Project-Level Site 2 (US 54)

6.4.2.1 Electrical Resistivity Tomography Data

An interpreted version of the 2-D ERT profile generated for Site 2 is shown in Fig. 6.11. At Site 2, intact/dry rock (as per interpretation) is characterized by resistivity values in excess of 1500 ohm-m and weathered rock by values between 50 and 1500 ohm-m. The soils at Site 2 are characterized by a broad range of resistivity values. Moist clayey soils are characterized by resistivity values less than about 20 ohm-m; dry fill, in places, is characterized by resistivity values in excess of 1000 ohm-m. Indeed, where dry fill and soil overly rock, the contact between the layers cannot be differentiated.

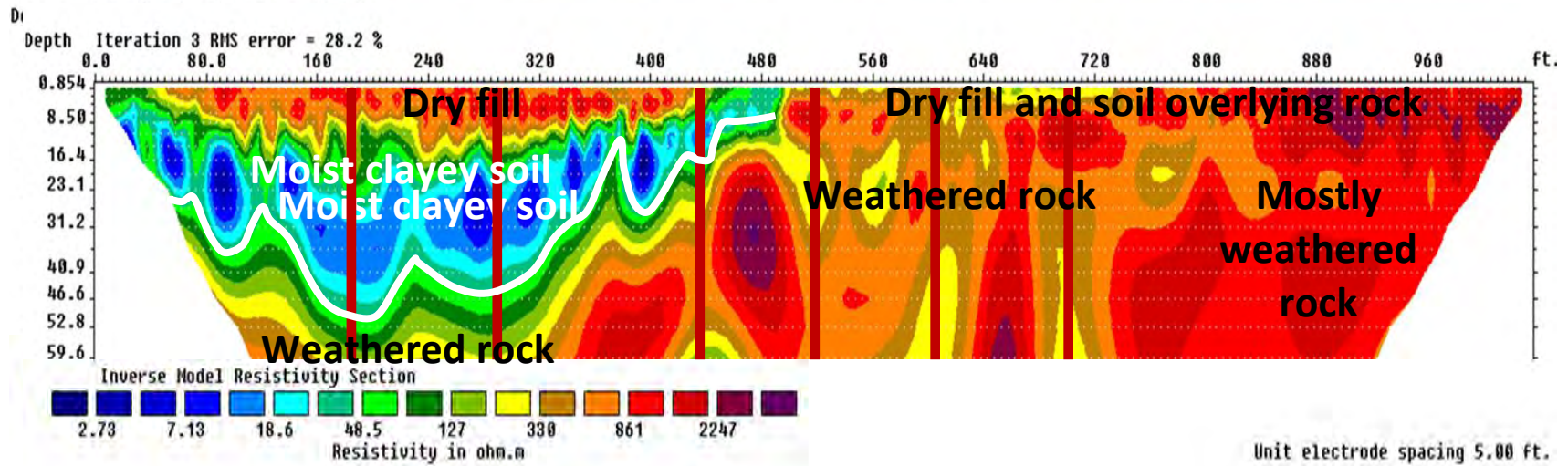


Fig. 6.11—Example interpreted Site 2 ERT profile without elevation control. Elevation control was not applied in order to facilitate comparison to the Site 2 MASW data (Figs. 6.12 and 6.13). The datum is the ground surface in the DOT ROW (approx. 1-2 ft below pavement surface). Distances and depths are in units of feet. Resistivity is in units of ohm-m. The iteration error was 28.2%. This high error value is typical of poor-fair quality ERT data acquired in karst terrain. The term “poor-fair quality” refers to the extent to which the acquired ERT field data and the output ERT profile correlate. The locations of interpreted solution-widened joints are shown by thick vertical red lines.

6.4.2.2 Multi-Channel Surface Wave Analyses Data

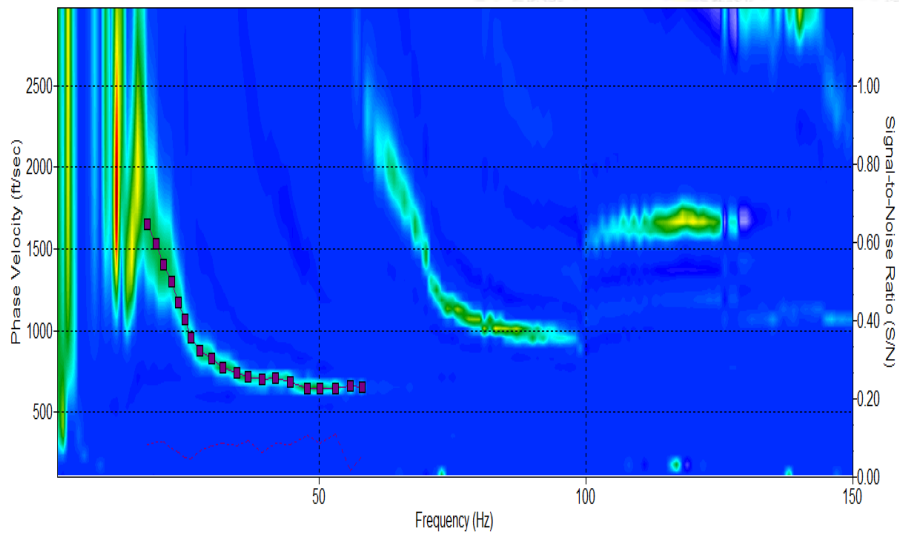
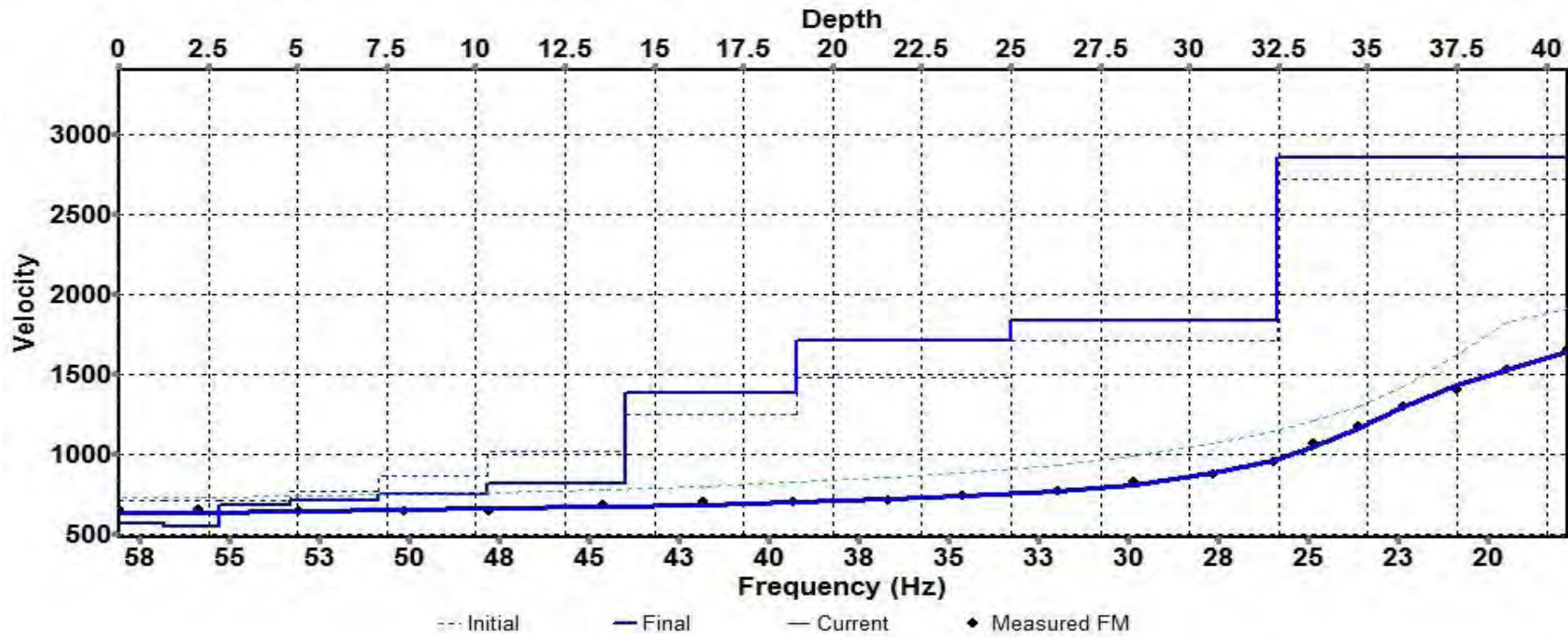


Fig. 6.12—Site 2 basic MASW data (station 400 ft): dispersion curve and corresponding 1-D shear-wave velocity profile. Interpreted top of rock (1000 ft/s) is at a depth of approx. 14 ft. MASW data are excellent quality.

A representative 1-D shear-wave velocity profile from Site 2 is shown in Fig. 6.12. The interpreted top of weathered rock (shear-wave velocity >1000 ft/sec) is at a depth of 14 ft. This depth estimate is reasonably consistent with the interpreted ERT profile (Fig. 6.11) where the depth to interpreted top of rock is seen to vary (in proximity to station 300) from 14 ft to 27 ft.

An interpreted version of the 2-D MASW profile generated for Site 2 is shown as Fig. 6.13. Boring control was not available to constrain the geologic interpretations. At Site 2, the top of weathered rock (as per interpretation) is characterized by velocities greater than 1000 ft/sec. Pavement and soil are characterized by velocities less than 1000 ft/sec. A comparison Fig. 6.11 and Fig. 6.13 indicate that the ERT and MASW data compare rather favorably. The ERT data are more definitive and almost certainly slightly more reliable.

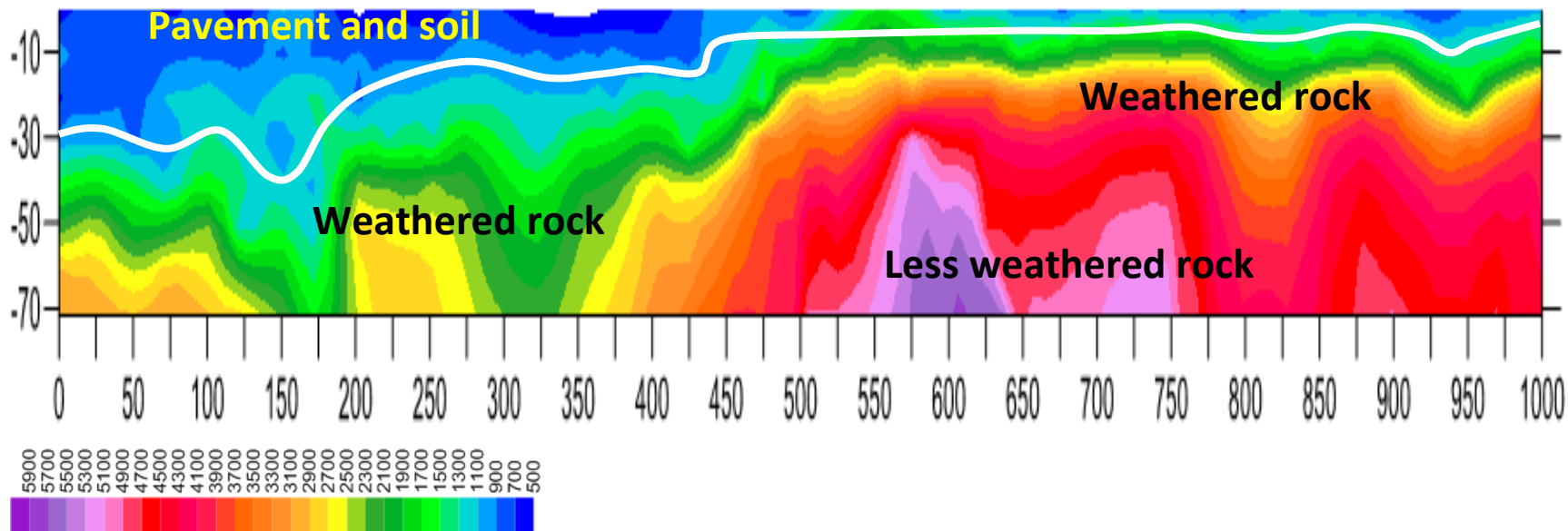


Fig. 6.13—Site 2: Example interpreted 2-D MASW shear-wave velocity profile. Elevation control cannot be applied using the software provided by the MASW manufacturer (Kansas Geological Survey). The datum on the 2-D MASW profile corresponds to the top of pavement (approx. 1-2 ft above ERT datum). Distances and depths are in units of feet. Velocities are in units of ft/sec.

6.4.3 Project-Level Site 3 (MO 179)

6.4.3.1 Electrical Resistivity Tomography Data

An interpreted version of the 2-D ERT profile generated for Site 3 is shown as Fig. 6.14. At Site 3, intact/dry rock (as per interpretation) is characterized by resistivity values in excess of 1500 ohm-m and weathered rock by values between 50 and 1500 ohm-m. The soils at Site 3 are characterized by a broad range of resistivity values. Moist clayey soils are characterized by resistivity values less than about 20 ohm-m; dry fill and soil, in places, is characterized by resistivity values in excess of 1000 ohm-m. Indeed, where dry fill or dry soil overly rock, the contact between the two layers cannot be differentiated.

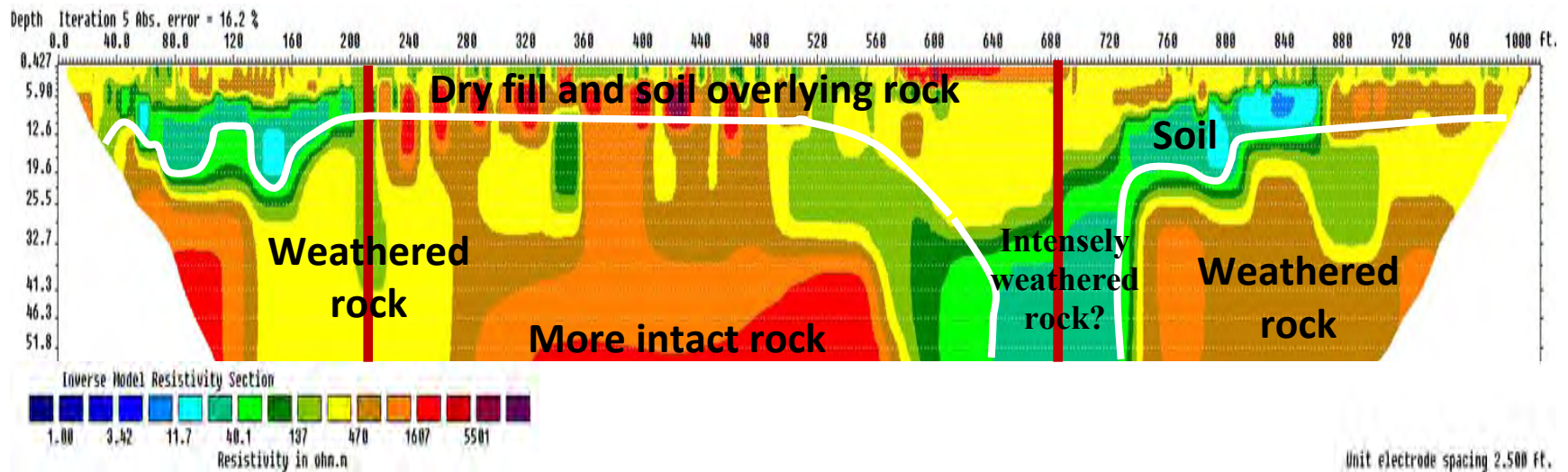


Fig. 6.14—Example interpreted Site 3 ERT profile without elevation control. Elevation control was not applied in order to facilitate comparison to the Site 3 MASW data (Figs. 6.15 and 6.16). The datum is the ground surface in the DOT ROW (approx. 1-2 ft below pavement surface). Distances and depths are in units of feet. Resistivity is in units of ohm-m. The iteration error was 16.2%. This error value is typical of fair-good quality ERT data acquired in karst terrain. The term “fair-good quality,” in this sense, refers to the extent to which the acquired ERT field data and the output ERT profile correlate. The locations of interpreted solution-widened joints are shown by thick vertical red lines.

6.4.3.2 Multi-Channel Surface Wave Analyses Data

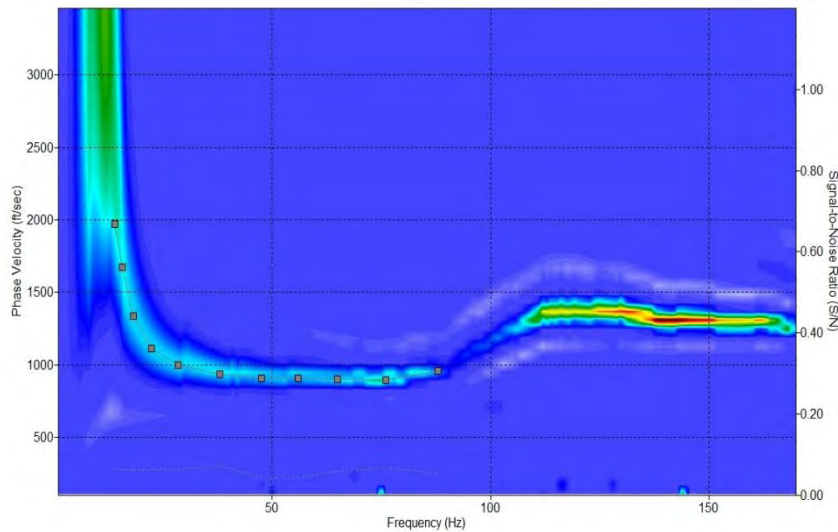
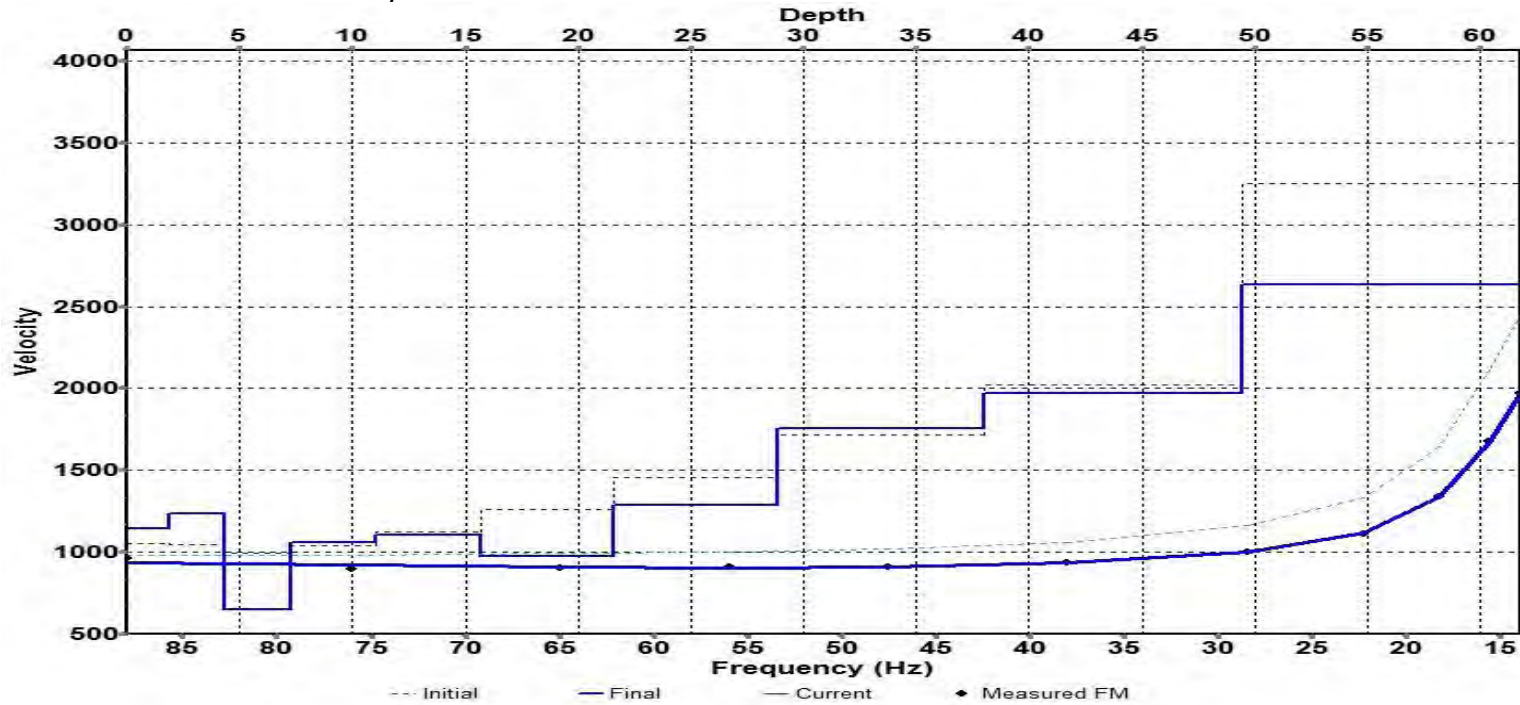


Fig. 6.15—Site 3 basic MASW data (station 625 ft): dispersion curve and corresponding 1-D shear-wave velocity profile (inversion curve). Interpreted top of rock (1000 ft/sec) is at a depth of approx. 22 ft. Data quality is excellent.

A representative 1-D shear-wave velocity profile from Site 3 is shown in Fig. 6.15. The interpreted top of weathered rock (shear-wave velocity >1000 ft/sec) is at a depth of 22 ft. This depth estimate is reasonably consistent with the interpreted ERT profile (Fig. 6.14) where the depth to interpreted top of rock is seen to vary (in proximity to station 300) from 19 ft to 25 ft.

An interpreted version of the 2-D MASW profile generated for Site 3 is shown in Fig. 6.16. Boring control was not available to constrain the geologic interpretations. At Site 3, the top of weathered rock (as per interpretation) is characterized by velocities greater than 1000 ft/sec. Pavement and soil are characterized by velocities less than 1000 ft/sec. A comparison of Fig. 6.14 and Fig. 6.16 indicate that the ERT and MASW data compare rather favorably. The ERT data are more definitive and almost certainly slightly more reliable.

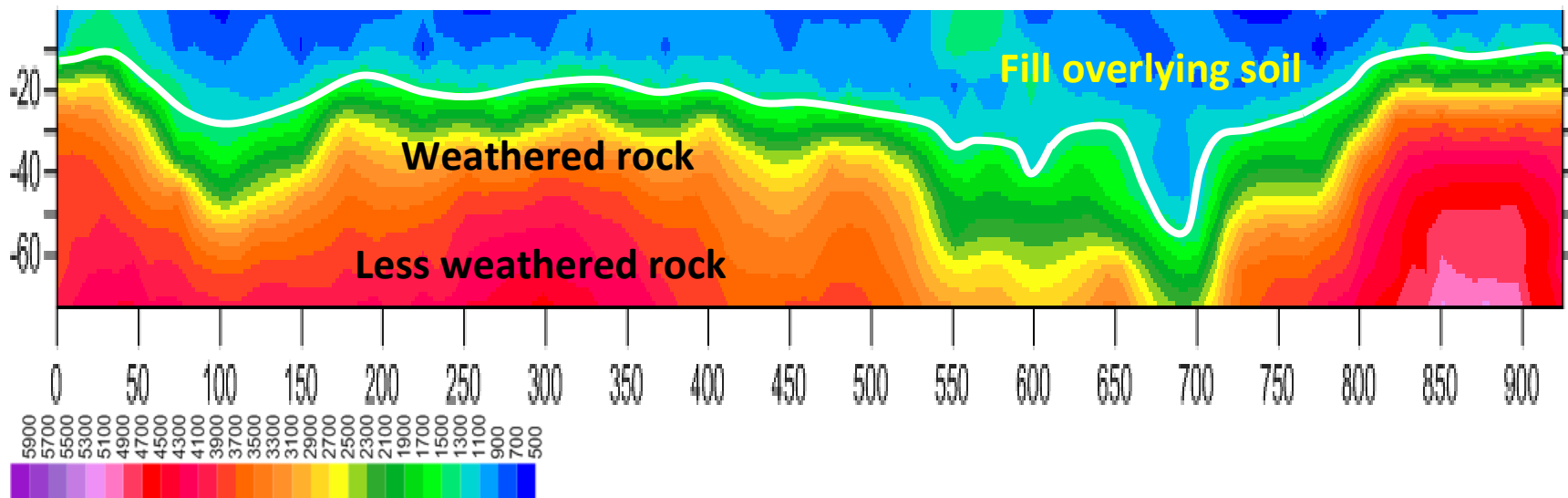


Fig. 6.16–Site 3: Example interpreted 2-D MASW shear-wave velocity profile with elevation control. Elevation control cannot be applied using the software provided by the MASW manufacturer (Kansas Geological Survey). The 0 ft mark on the 2-D MASW profile corresponds to the top of pavement (approx. 1-2 ft above ERT datum). Distances and depths are in units of feet. Velocities are in units of ft/sec.

6.4.4 Project-Level Site 4 (HWY AT)

6.4.4.1 Electrical Resistivity Tomography Data

An interpreted version of the 2-D ERT profile generated for Site 4 is shown in Fig. 6.17. At Site 4, intact/dry rock (as per interpretation) is characterized by resistivity values in excess of 1500 ohm-m and weathered rock by values between 35 and 1500 ohm-m. The soils at Site 4 are characterized by a broad range of resistivity values. Moist clayey soils are characterized by resistivity values less than about 20 ohm-m; dry fill, in places, is characterized by resistivity values in excess of 500 ohm-m.

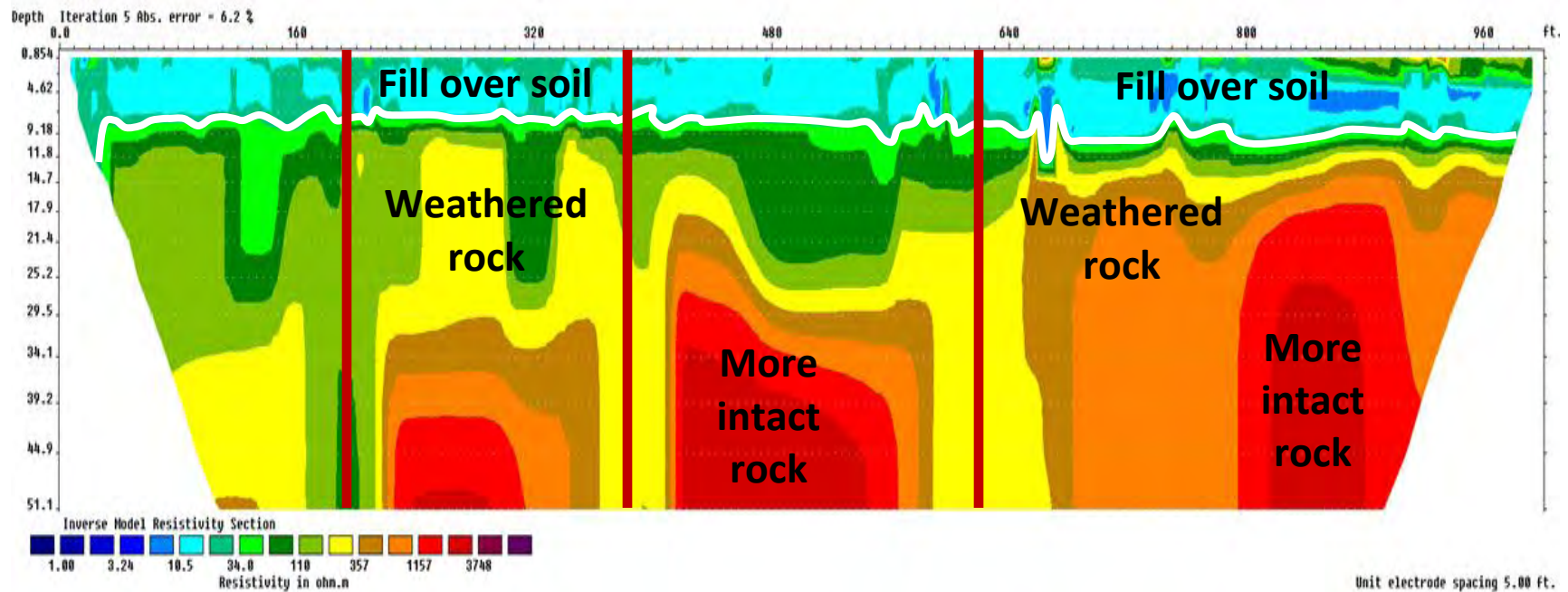


Fig. 6.17—Example interpreted Site 4 ERT profile without elevation control. Elevation control was not applied in order to facilitate comparison to the Site 4 MASW data (Figs. 6.18 and 6.19). The datum is the ground surface in the DOT ROW (approx. 1-2 ft below pavement surface). Distances and depths are in units of feet. Resistivity is in units of ohm-m. The iteration error was 6.2%. This error value is typical of excellent quality ERT data acquired in karst terrain. The term “excellent quality,” in this sense, refers to the extent to which the acquired ERT field data and the output ERT profile correlate. The locations of interpreted solution-widened joints are shown by thick vertical red lines.

6.4.4.2 Multi-Channel Surface Wave Analyses Data

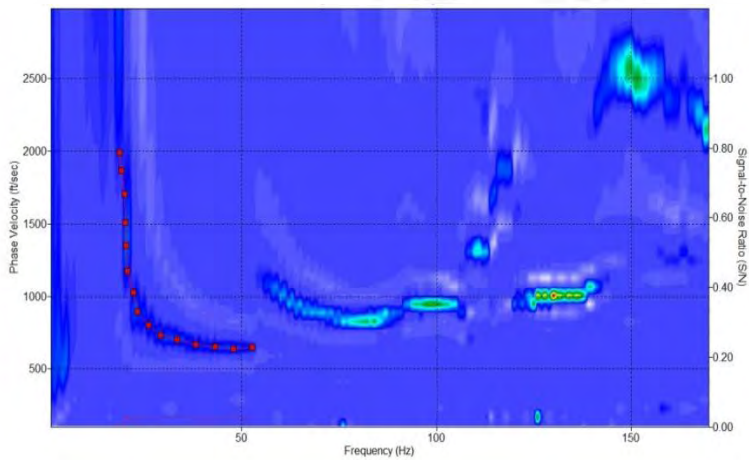
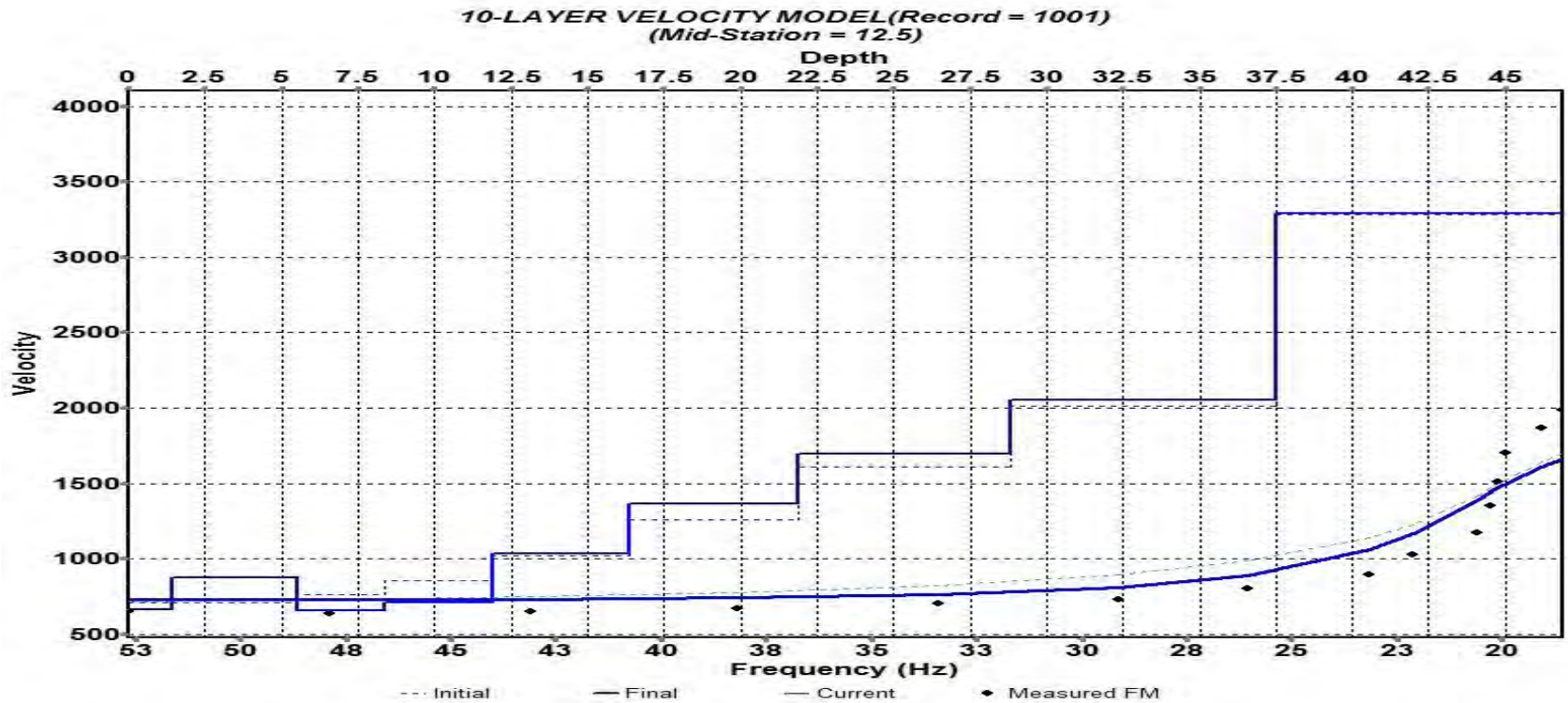


Fig. 6.18—Site 4 basic MASW data (station 875 ft): dispersion curve and corresponding 1-D shear-wave velocity profile (inversion curve). Interpreted top of rock (1000 ft/sec) is at a depth of approx. 11.5 ft. Data quality is excellent.

A representative 1-D shear-wave velocity profile from Site 4 is shown in Fig. 6.18. The interpreted top of weathered rock (shear-wave velocity >1000 ft/sec) is at a depth of 11.5 ft. This depth estimate is reasonably consistent with the interpreted ERT profile (Fig. 6.17) where the depth to interpreted top of rock is approximately 8 ft.

An interpreted version of the 2-D MASW profile generated for Site 4 is shown in Fig. 6.19. Boring control was not available to constrain the geologic interpretations. At Site 4, the top of weathered rock (as per interpretation) is characterized by velocities greater than 1000 ft/sec. Pavement and soil are characterized by velocities less than 1000 ft/sec. A comparison of Fig. 6.17 and Fig. 6.19 indicate that the ERT and MASW data compare rather favorably. The ERT data are more definitive and almost certainly slightly more reliable.

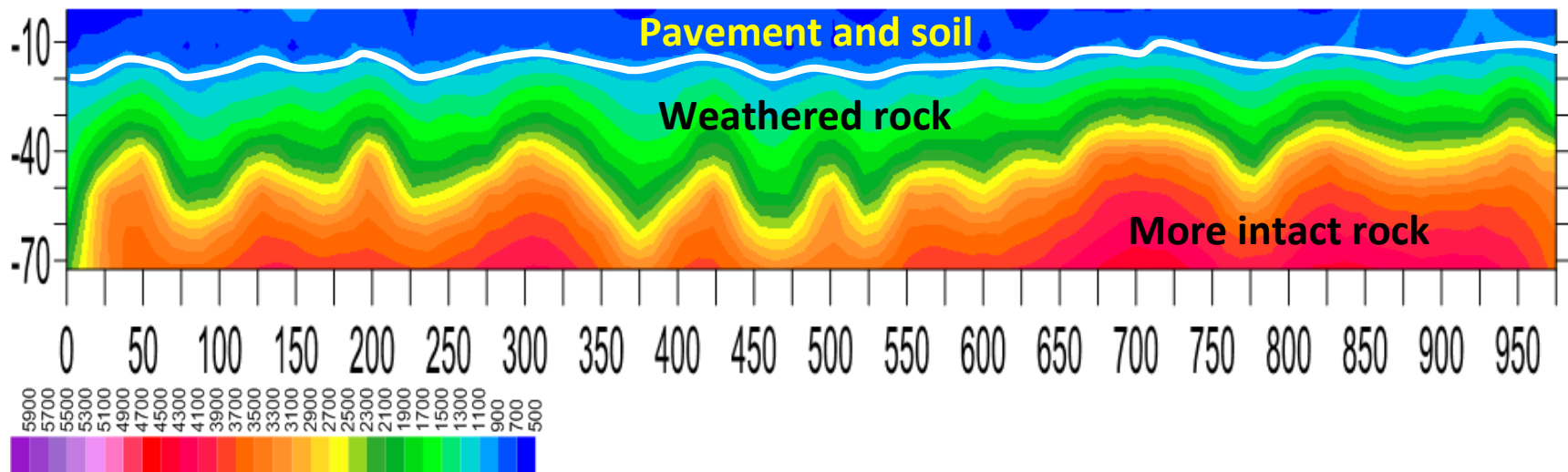


Fig. 6.19—Site 4: Example interpreted 2-D MASW shear-wave velocity profile with elevation control. Elevation control cannot be applied using the software provided by the MASW manufacturer (Kansas Geological Survey). The 0-ft mark on the 2-D MASW profile corresponds to the top of pavement (approx. 1-2 ft above ERT datum). The MASW data were acquired using a 1.5 ft geophone spacing. Distances and depths are in units of feet. Velocities are in units of ft/sec.

6.4.5 Project-Level Site 5 (I-55 Pemiscot County)

6.4.5.1 Electrical Resistivity Tomography Data

An interpreted version of the 2-D ERT profile generated for Site 5 is shown in Fig. 6.20. The soil at Site 5 can be divided into three layers on the basis of resistivity: a thin (approximately 5 ft) upper layer of dry fill (resistivity values greater than 75 ohm-m); an intermediate layer (approximately 5 ft to 25 ft) of less dense soil characterized by resistivity values between 10 and 50 ohm-m; and an underlying layer (depths > 25 ft) of denser soil characterized by resistivity values greater than 50 ohm-m. At station 950, a zone clayey soil of unknown origin and a possible fault are highlighted on the interpreted ERT profile.

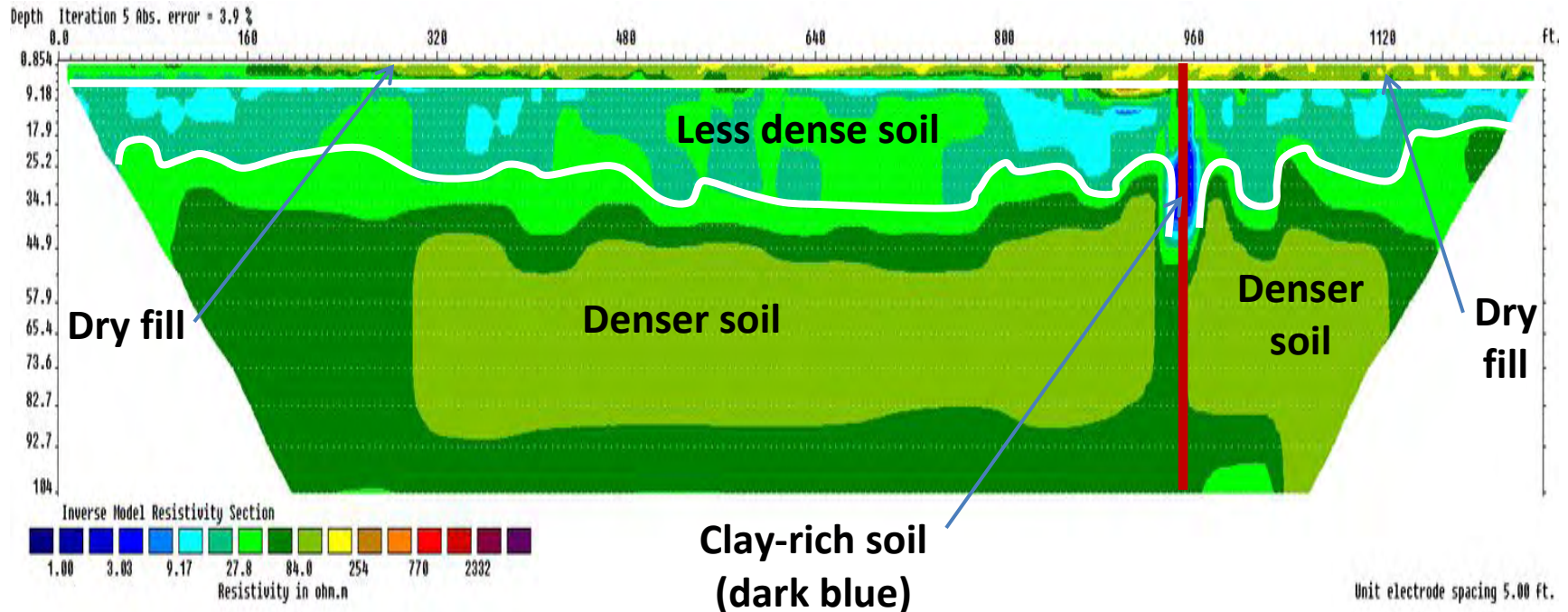


Fig. 6.20—Example interpreted Site 5 ERT profile without elevation control. Elevation control was not applied in order to facilitate comparison to the Site 5 MASW data (Fig. 6.21 and 6.22). The datum is the ground surface in the DOT ROW (approx. 1-2 ft below pavement surface). Distances and depths are in units of feet. Resistivity is in units of ohm-m. The iteration error was 3.9%. This error value is typical of excellent quality ERT data acquired in karst terrain. The term “excellent quality,” in this sense, refers to the extent to which the acquired ERT field data and the output ERT profile correlate. The location of a possible fault is shown by the thick vertical red line.

6.4.5.2 Multi-Channel Surface Wave Analyses Data

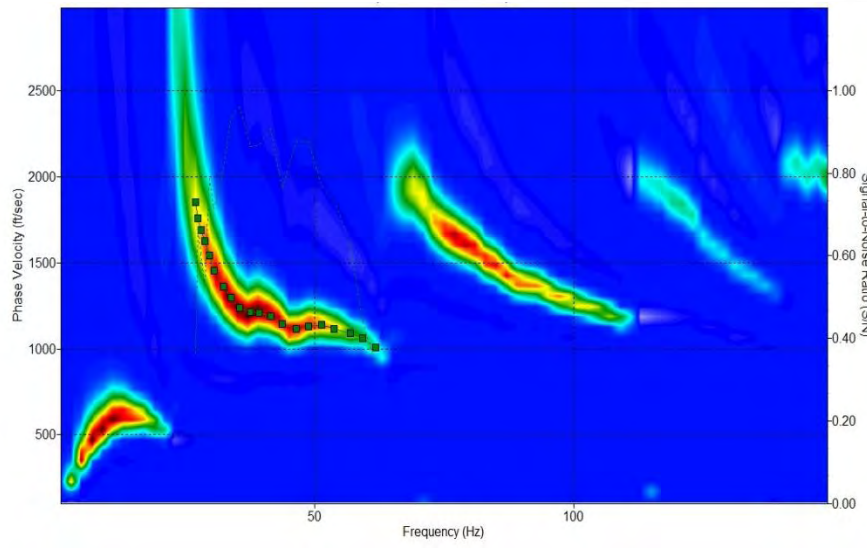
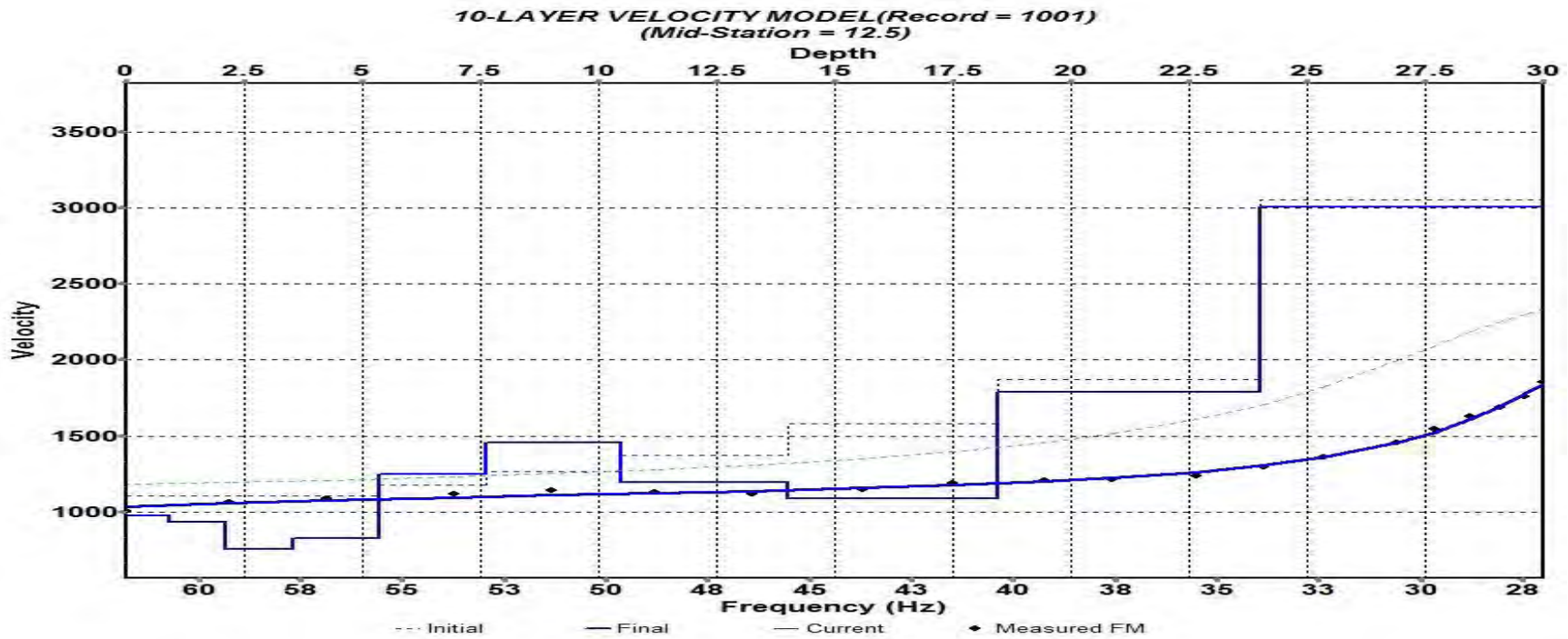


Fig. 6.21—Site 5 basic MASW data (station 25 ft): dispersion curve and corresponding 1-D shear-wave velocity profile. Interpreted top of dense soil (3000 ft/sec) is at a depth of 23.5 ft. Data quality is excellent.

A representative 1-D shear-wave velocity profile from Site 5 is shown in Fig. 6.21. The interpreted top of dense soil (shear-wave velocity >1000 ft/sec) is at a depth of 23.5 ft. This depth estimate is consistent with the interpreted ERT profile (Fig. 6.20) where the depth to interpreted top of dense soil is about 20 ft.

An interpreted version of the 2-D MASW profile generated for Site 5 is shown in Fig. 6.22. Boring control was not available to constrain the geologic interpretations. At Site 4, the top of dense soil (as per interpretation) is characterized by velocities greater than 1000 ft/sec. Pavement and shallow soils are characterized by velocities less than 1000 ft/sec. A comparison of Fig. 6.20 and Fig. 6.22 indicate that the ERT and MASW data compare rather favorably. The ERT data are more definitive and almost certainly slightly more reliable.

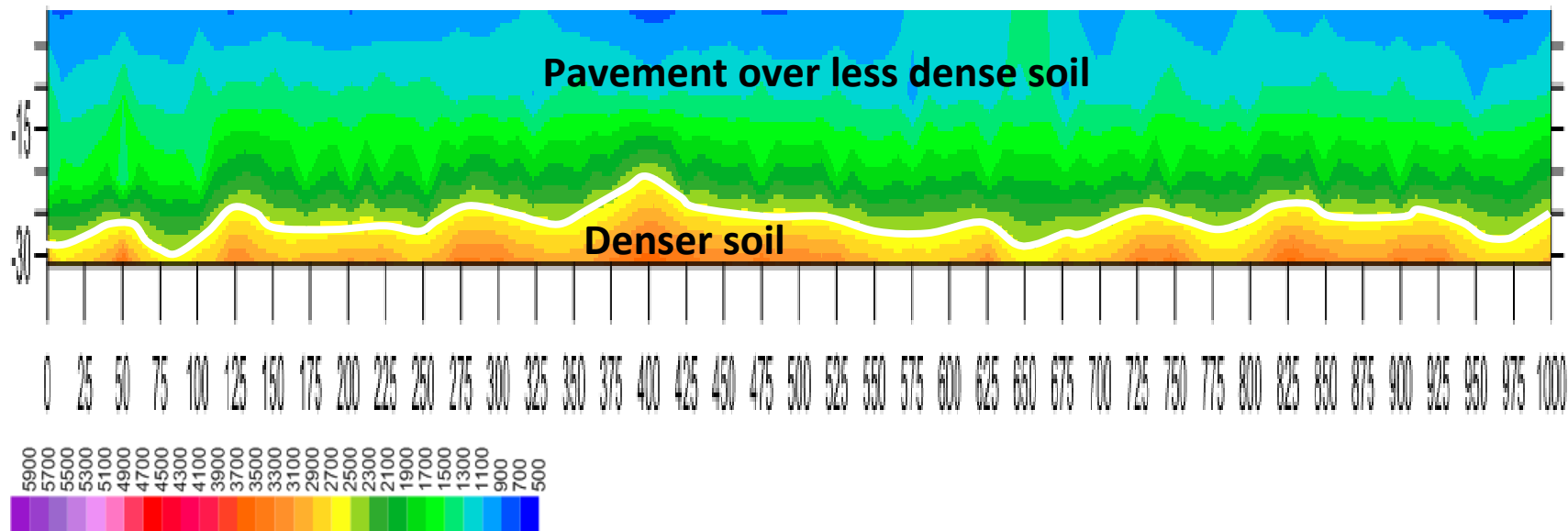


Fig. 6.22—Site 5: Example interpreted 2-D MASW shear-wave velocity profile with elevation control. Elevation control cannot be applied using the software provided by the MASW manufacturer (Kansas Geological Survey). The 0 ft mark on the 2-D MASW profile corresponds to the top of pavement (approx. 1-2 ft above ERT datum). The MASW data were acquired using a 1.5 ft geophone spacing. Distances and depths are in units of feet. Velocities are in units of ft/sec.

6.4.6 Project-Level Site 6 (I-55 Perry County)

6.4.6.1 Electrical Resistivity Tomography Data

An interpreted version of the 2-D ERT profile generated for Site 6 is shown in Fig. 6.23. At Site 6, intact/dry rock (as per interpretation) is characterized by resistivity values in excess of 1500 ohm-m and weathered rock by values between 50 and 1500 ohm-m. The soils at Site 6 are characterized by a broad range of resistivity values. Moist clayey soils are characterized by resistivity values less than about 10 ohm-m; dry fill, in places, is characterized by resistivity values in excess of 250 ohm-m. Indeed, where dry fill or dry soil overly rock, the contact between the two layers cannot be differentiated.

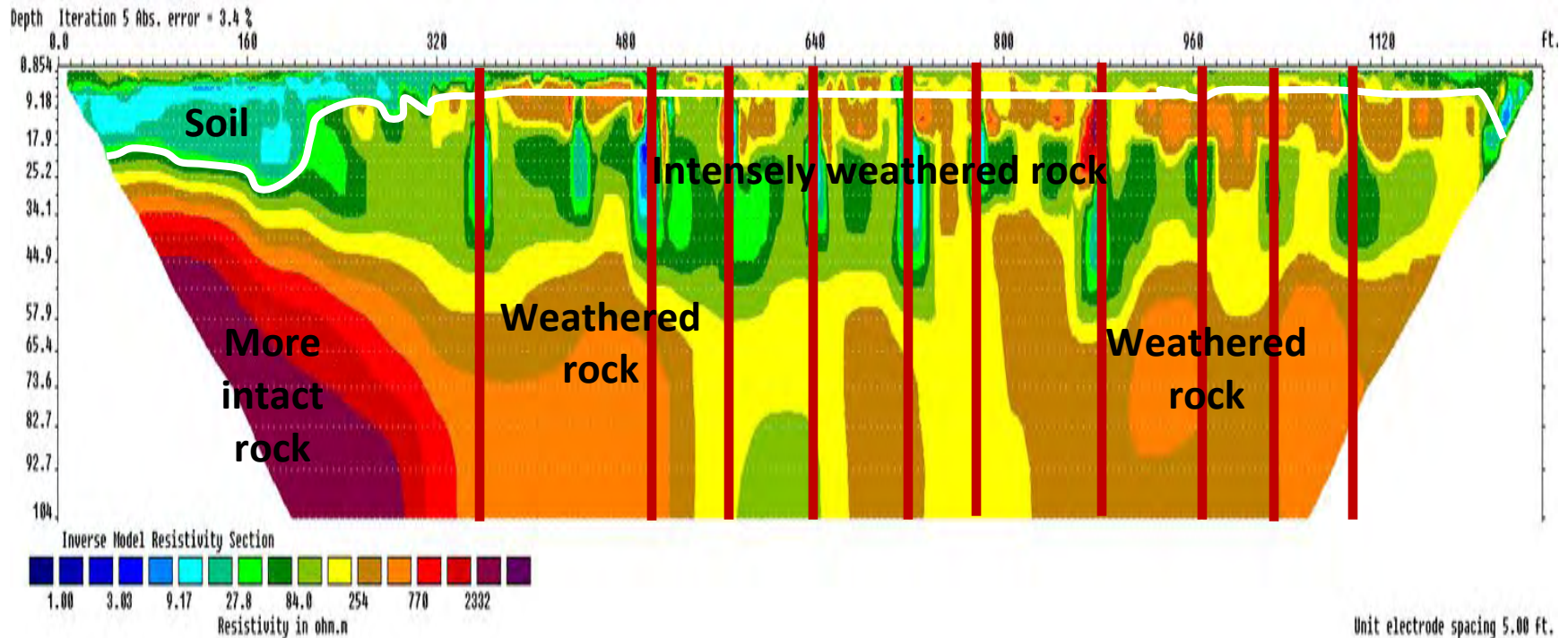


Fig. 6.23—Example interpreted Site 6 ERT profile without elevation control. Elevation control was not applied in order to facilitate comparison to the Site 6 MASW data (Figs. 6.24 and 6.25). The datum is the ground surface in the DOT ROW (approx. 1-2 ft below pavement surface). ERT data were acquired using a 5 ft electrode spacing. Distances and depths are in units of feet. Resistivity is in units of ohm-m. The locations of interpreted solution-widened joints are shown by thick vertical red lines.

6.4.6.2 Multi-Channel Surface Wave Analyses Data

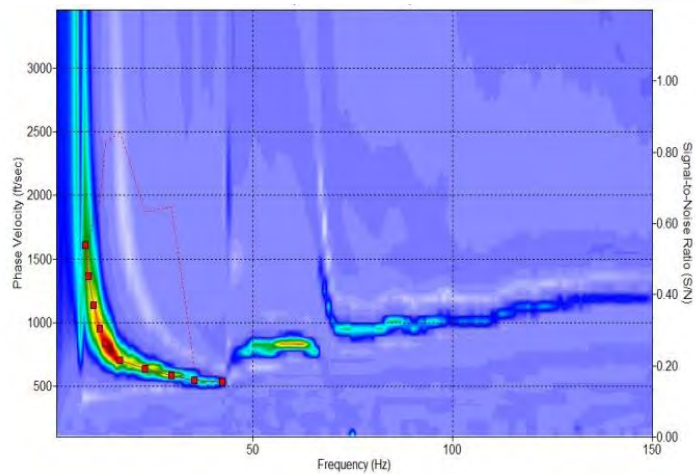
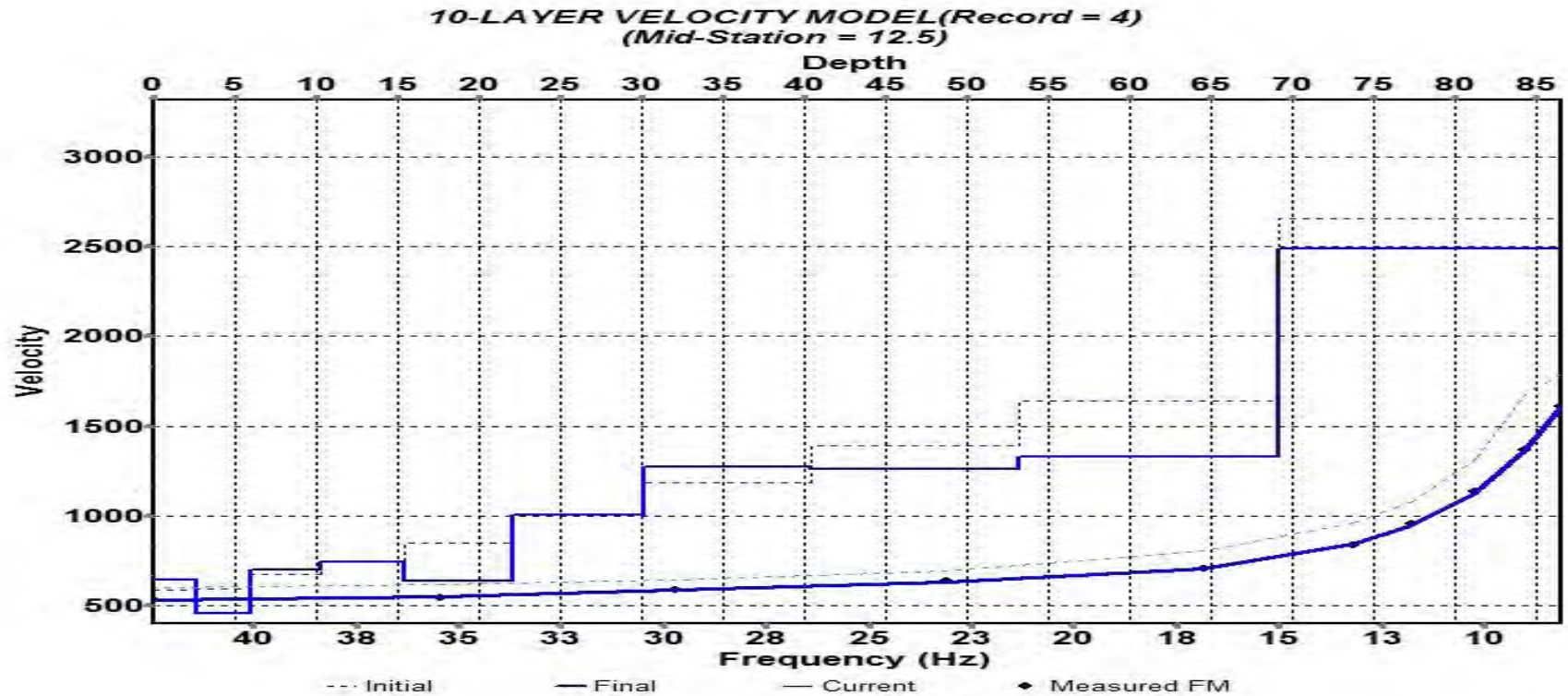


Fig. 6.24—Site 6 basic MASW data (station 75): dispersion curve and corresponding 1-D shear-wave velocity profile. Interpreted top of rock (1000 ft/s) is at a depth of approx. 22 ft. Data quality is excellent.

A representative 1-D shear-wave velocity profile from Site 6 is shown in Fig. 6.24. The interpreted top of rock (shear-wave velocity >1000 ft/sec) is at a depth of 22 ft. This depth estimate is consistent with the interpreted ERT profile (Fig. 6.23) where the depth to interpreted top of dense soil is about 20 ft.

An interpreted version of the 2-D MASW profile generated for Site 6 is shown in Fig. 6.25. Boring control was not available to constrain the geologic interpretations. At Site 6, the top of rock (as per interpretation) is characterized by velocities greater than 1000 ft/sec. Pavement and shallow soils are characterized by velocities less than 1000 ft/sec. A comparison of Fig. 6.23 and Fig. 6.25 indicate that the ERT and MASW data compare rather favorably. The ERT data are more definitive and almost certainly slightly more reliable.

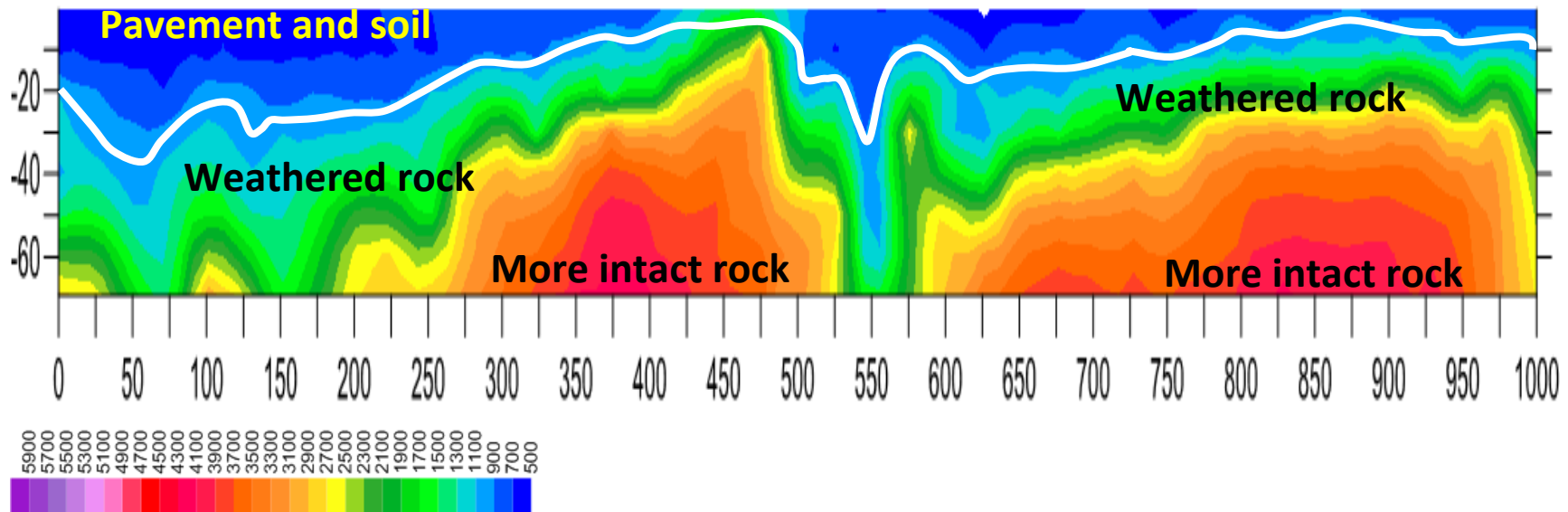


Fig. 6.25–Site 6: Example interpreted 2-D MASW shear-wave velocity profile with elevation control. Elevation control cannot be applied using the software provided by the MASW manufacturer (Kansas Geological Survey). The 0 ft mark on the 2-D MASW profile corresponds to the top of pavement (approx. 1-2 ft above ERT datum). The MASW data were acquired using a 1.5 ft geophone spacing. Distances and depths are in units of feet. Velocities are in units of ft/sec.

6.4.7 Project-Level Site 7 (HWY U)

6.4.7.1 Electrical Resistivity Tomography Data

An interpreted version of the 2-D ERT profile generated for Site 7 is shown in Fig. 6.26. At Site 7, intact/dry rock (as per interpretation) is characterized by resistivity values in excess of 1500 ohm-m and weathered rock by values between 50 and 1500 ohm-m. The soils at Site 7 are characterized by a broad range of resistivity values. Moist clayey soils are characterized by resistivity values less than about 10 ohm-m; dry fill and soil, in places, is characterized by resistivity values in excess of 250 ohm-m. Indeed, where dry fill or dry soil overly rock, the contact between the two layers cannot be differentiated.

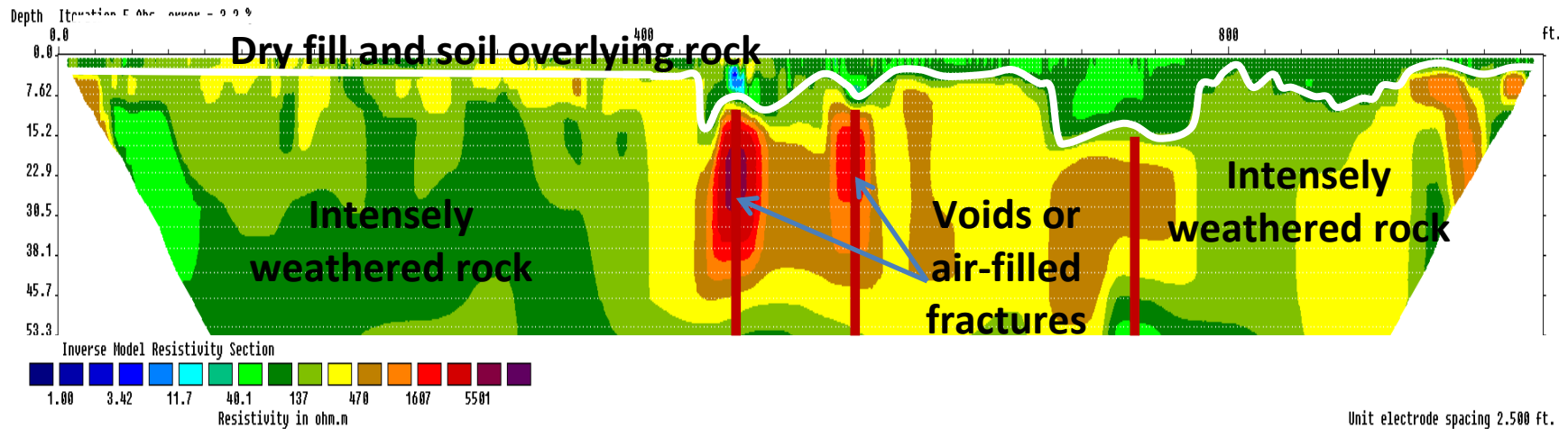


Fig. 6.26—Example interpreted Site 7 ERT profile without elevation control. Elevation control was not applied in order to facilitate comparison to the Site 7 MASW data (Figs. 6.27 and 6.28). The datum is to the ground surface in the DOT ROW (approx. 1-2 ft below pavement surface). ERT data were acquired using a 5 ft electrode spacing. Distances and depths are in units of feet. Resistivity is in units of ohm-m. The iteration error was 3.2%. This error value is typical of excellent quality ERT data acquired in karst terrain. The term “excellent quality,” in this sense, refers to the extent to which the acquired ERT field data and the output ERT profile correlate. The locations of interpreted solution-widened joints are shown by thick vertical red lines.

6.4.7.2 Multi-Channel Surface Wave Analyses Data

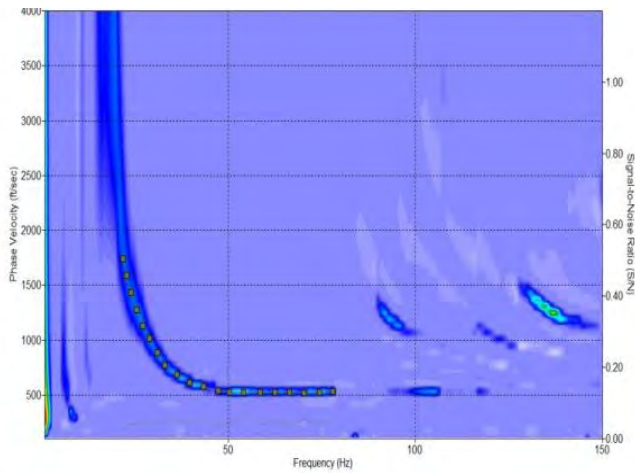
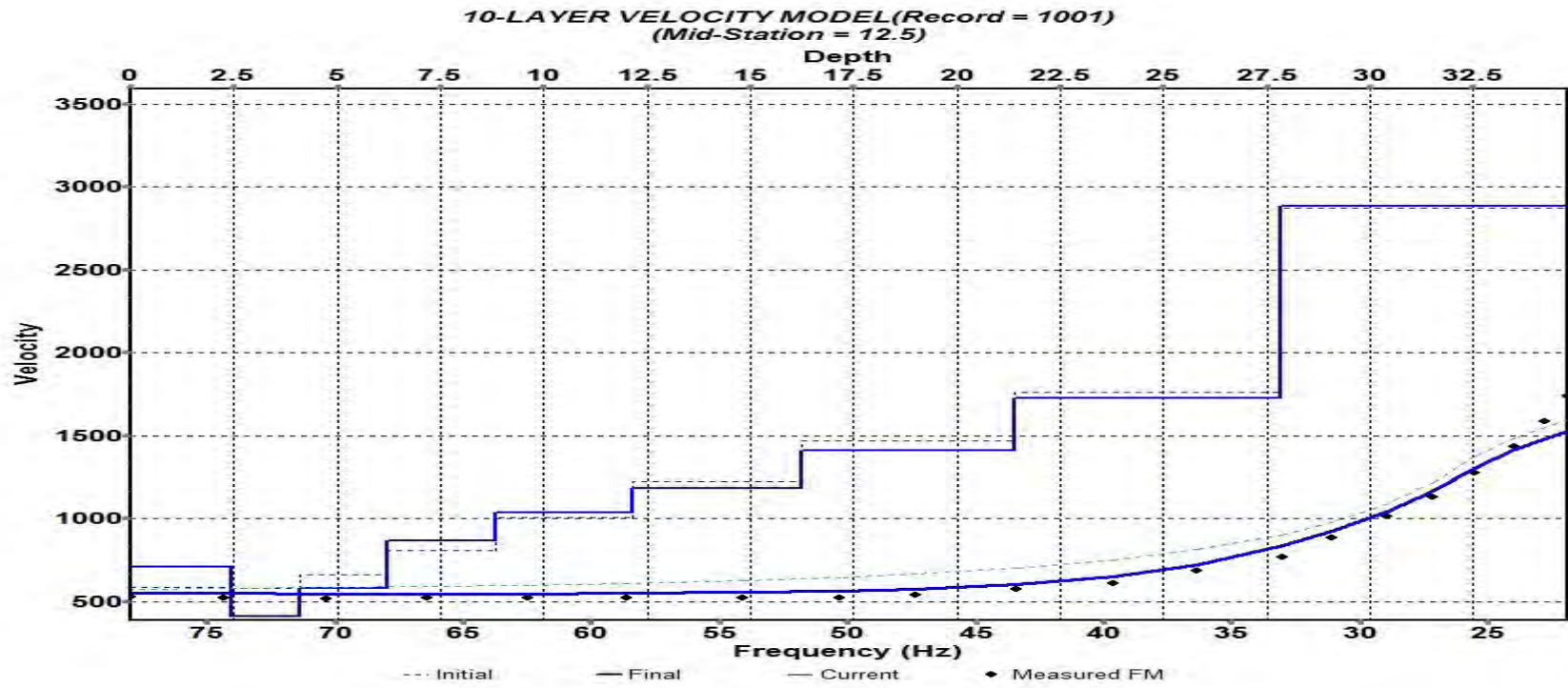


Fig. 6.27—Site 7 basic MASW data (station 675): raw record, corresponding dispersion curve and corresponding 1-D shear-wave velocity profile (inversion curve). Interpreted top of rock (1000 ft/sec) is at a depth of approx. 8.5 ft. Data quality is excellent.

A representative 1-D shear-wave velocity profile from Site 7 is shown in Fig. 6.27. The interpreted top of rock (shear-wave velocity >1000 ft/sec) is at a depth of 7.5 ft. This depth estimate is consistent with the interpreted ERT profile (Fig. 6.26) where the depth to interpreted top of dense soil is approximately 6 ft.

An interpreted version of the 2-D MASW profile generated for Site 7 is shown in Fig. 6.28. Boring control was not available to constrain the geologic interpretations. At Site 7, the top of rock (as per interpretation) is characterized by velocities greater than 1000 ft/sec. Pavement and shallow soils are characterized by velocities less than 1000 ft/sec. A comparison of Fig. 6.26 and Fig. 6.28 indicate that the ERT and MASW data compare rather favorably. The ERT data are more definitive and almost certainly slightly more reliable.

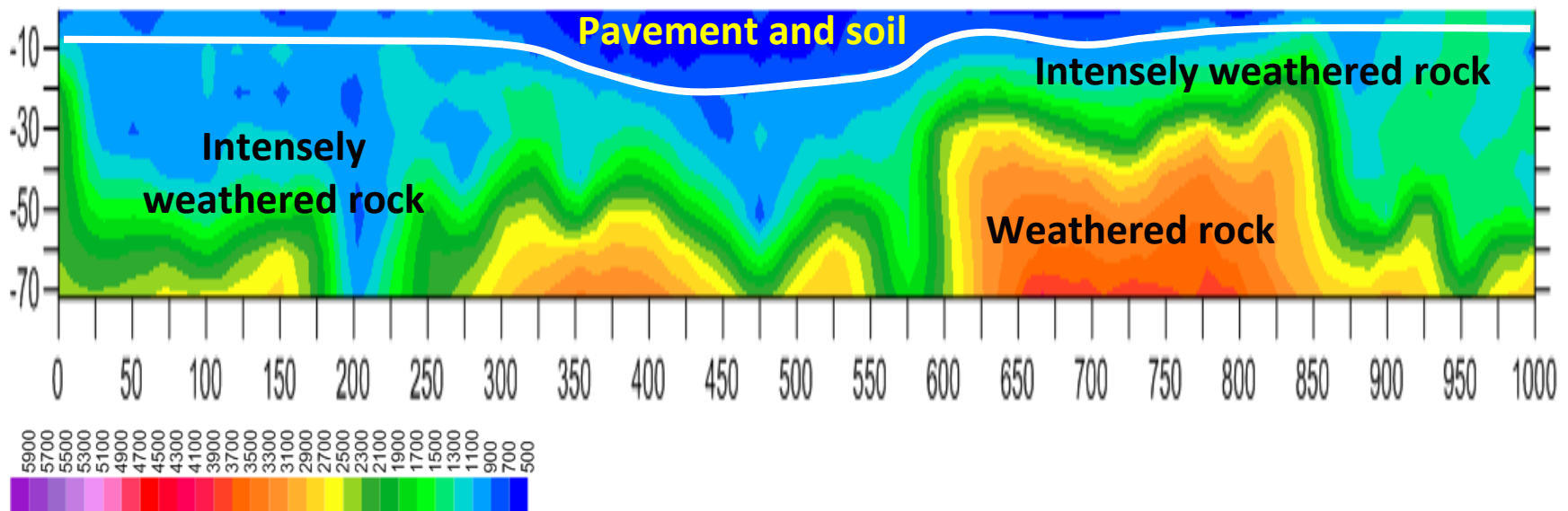


Fig. 6.28—Site 7: Example interpreted 2-D MASW shear-wave velocity profile with elevation control. Elevation control cannot be applied using the software provided by the MASW manufacturer (Kansas Geological Survey). The 0 ft mark on the 2-D MASW profile corresponds to the top of pavement (approx. 1-2 ft above ERT datum). The MASW data were acquired using a 1.5 ft geophone spacing. Distances and depths are in units of feet. Velocities are in units of ft/sec.

6.4.8 Project-Level Site 8 (I-35)

6.4.8.1 Electrical Resistivity Tomography Data

An interpreted version of the 2-D ERT profile generated for Site 8 is shown as Fig. 6.29. At Site 8, weathered rock (as per interpretation) is characterized by values between 20 and 1500 ohm-m. The soils at Site 8 are characterized by a broad range of resistivity values. Moist clayey soils are characterized by resistivity values less than about 10 ohm-m; dry fill, in places, is characterized by resistivity values in excess of 100 ohm-m.

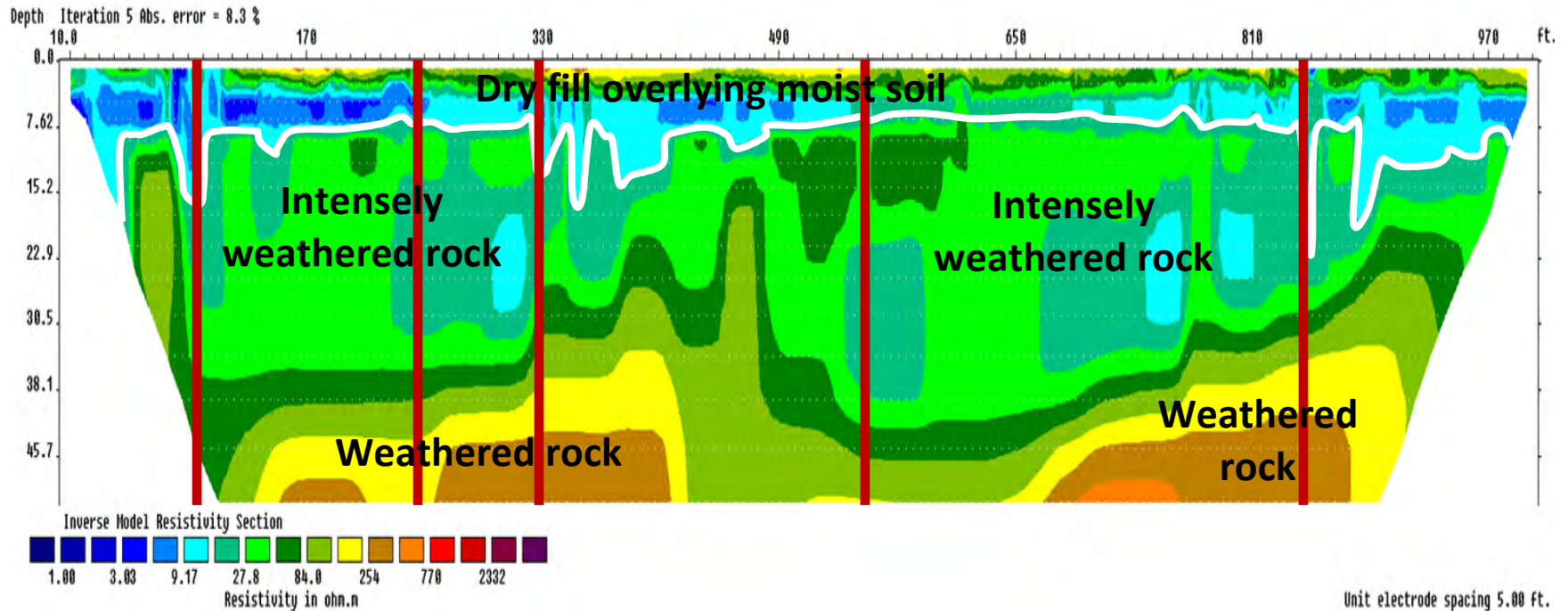


Fig. 6.29—Example interpreted Site 8 ERT profile without elevation control. Elevation control was not applied in order to facilitate comparison to the Site 8 MASW data (Figs. 6.30 and 6.31). The datum is the ground surface in the DOT ROW (approx. 1-2 ft below pavement surface). Distances and depths are in units of feet. Resistivity is in units of ohm-m. The iteration error was 8.3%. This error value is typical of good-excellent quality ERT data acquired in karst terrain. The term “good-excellent quality,” in this sense, refers to the extent to which the acquired ERT field data and the output ERT profile correlate. The locations of interpreted solution-widened joints are shown by thick vertical red lines.

6.4.8.2 Multi-Channel Surface Wave Analyses Data

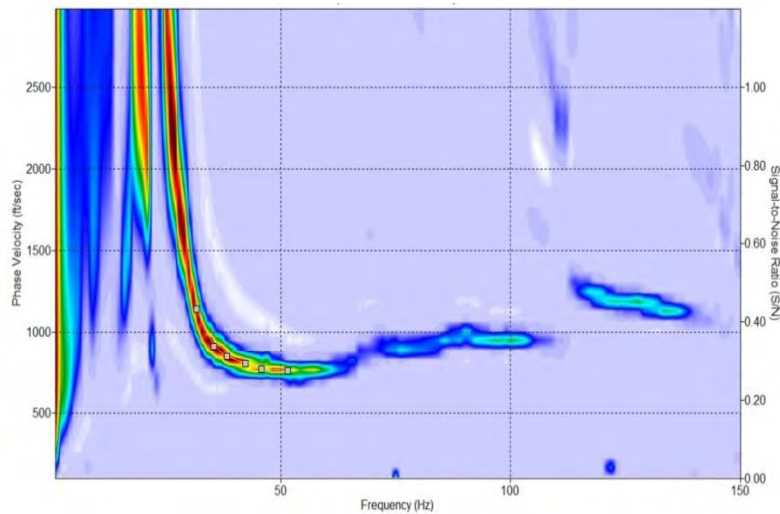
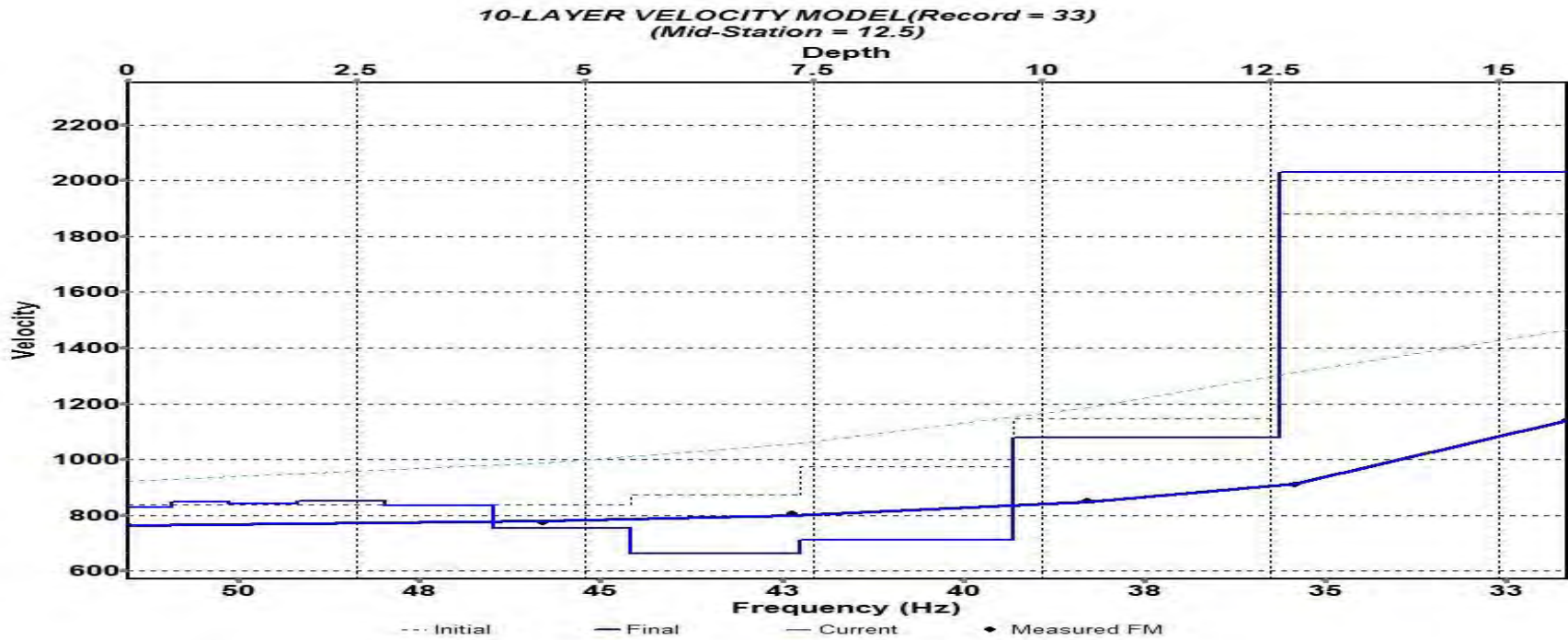


Fig. 6.30—Site 8 basic MASW data (station 675 ft): raw record, corresponding dispersion curve and corresponding 1-D shear-wave velocity profile (inversion curve). Interpreted top of rock (1000 ft/s) is at a depth of approx. 9 ft. MASW data quality is excellent.

A representative 1-D shear-wave velocity profile from Site 8 is shown in Fig. 6.30. The interpreted top of rock (shear-wave velocity >1000 ft/sec) is at a depth of 9 ft. This depth estimate is consistent with the interpreted ERT profile (Fig. 6.29) where the depth to interpreted top of dense soil is approximately 7 ft.

An interpreted version of the 2-D MASW profile generated for Site 8 is shown as Fig. 6.31. Boring control was not available to constrain the geologic interpretations. At Site 8, the top of weathered rock (as per interpretation) is characterized by velocities greater than 1000 ft/sec. Pavement and shallow soils are characterized by velocities less than 1000 ft/sec. A comparison of Fig. 6.29 and Fig. 6.31 indicates that the ERT and MASW data compare rather favorably. The ERT data are more definitive and almost certainly slightly more reliable.

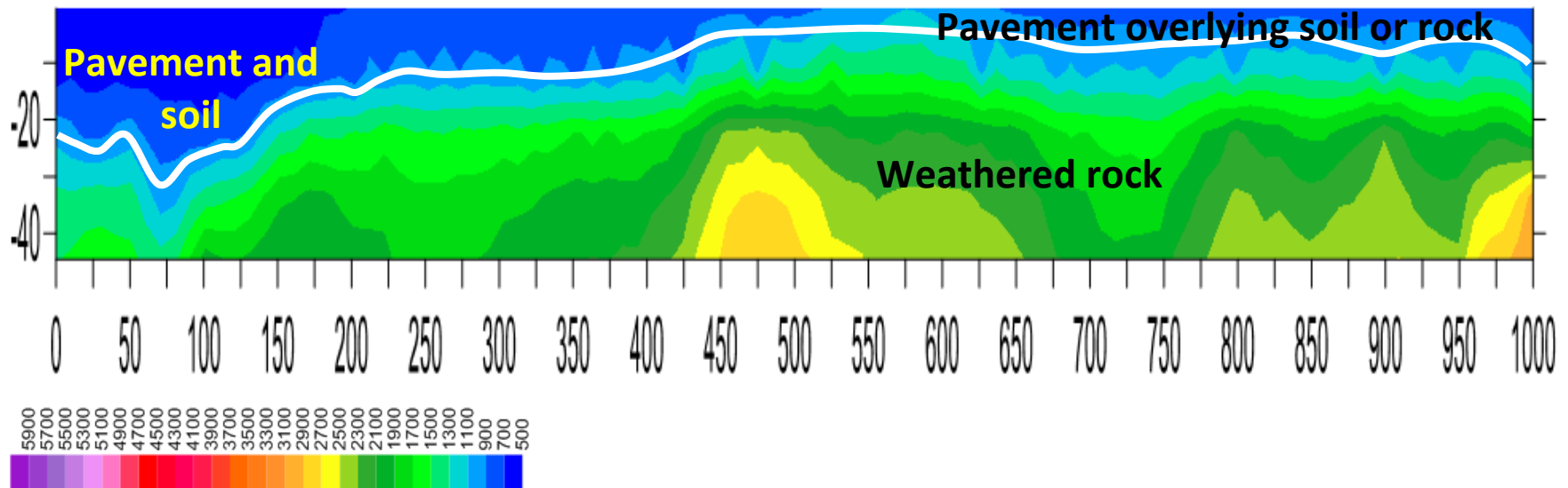


Fig. 6.31—Site 8: Example interpreted 2-D MASW shear-wave velocity profile with elevation control. Elevation control cannot be applied using the software provided by the MASW manufacturer (Kansas Geological Survey). The 0 ft mark on the 2-D MASW profile corresponds to the top of pavement (approx. 1-2 ft above ERT datum). The MASW data were acquired using a 1.5 ft geophone spacing. Distances and depths are in units of feet. Velocities are in units of ft/sec.

6.5 Concluding Remarks

Two-dimensional (2-D) electrical resistivity tomography (ERT) were generated for each project-level site with the objective of illustrating the utility of this subsurface imaging technology. As illustrated in Section 6.4 of this report, 2-D resistivity profiles can be transformed into 2-D geologic images (interpretations) of the subsurface. These geologic interpretations are based on the assumption that variations in the resistivity of the subsurface reflect correspond to changes in lithology (and moisture content). Generally, intact rock is characterized by high resistivity values; weathered rock is characterized by intermediate resistivity values; soil is characterized by low to intermediate resistivity values; and clays are characterized by very low resistivity values. Geologic interpretations are generally reliable, especially if ground truth is available to constrain and/or verify interpretations.

As illustrated by the ERT data acquired at project-level sites 1-8, interpreted 2-D ERT profiles can be of significant utility to those engaged in highway construction and/or maintenance. Interpretations of interest include, but are not limited to, the mapping/identification of the following:

- depth to top of rock
- variations in rock quality
- variations in rock lithology
- pattern, placement and density of solution-widened joints
- locations of air-filled voids
- locations of water- and clay-filled vugs in karst terrain
- distribution of dry soil
- distribution of moist soil
- distribution of sandy-silty soil
- distribution of clayey soil

Based on the assessment of the ERT data acquired at project-level sites 1-8, it was concluded that ERT can be useful to assess the condition of the base, sub-base, soil and rock beneath existing roadways, or prior to or during the construction of roadways, especially in karst terrain.

Active multi-channel analyses of surface wave (MASW) data were also acquired at each project-level site. The acquired MASW data were transformed into 2-D shear-wave velocity profiles that parallel the acquired 2-D ERT profiles (but were offset by 20 ft to 30 ft). As illustrated in Section 6.4 of this report, interpreted 2-D MASW profile can be of significant utility to those engaged in highway construction and/or maintenance. Interpretations of interest include, but are not limited to, the mapping/ identification of the following:

- depth to top of rock
- variations in soil and rock rigidity
- variations in soil and rock lithology

Based on the assessment of the MASW data, it was concluded that it would be useful to selectively acquire MASW data in regions where ERT data appear to be anomalous or where it is necessary to determine the engineering properties of the base material.

Borehole control was not available at each project-level site, so the interpretations of the 2-D ERT and 2-D MASW profiles could not be constrained by ground truth. Rather, the interpretation of each 2-D ERT profile was constrained by the corresponding 2-D MASW profile and vice-versa. The interpretations were also constrained by the field observations (outcropping rock, presence of thick fill, etc.), the author's familiarity with the geology of the various study areas, and geologic processes and principles.

7 ROLLING DYNAMIC DEFLECTOMETER (RDD) AND FALLING WEIGHT DEFLECTOMETER (FWD) INVESTIGATIONS

7.1 Introduction

Deflection-based non-destructive testing (NDT) measurements are commonly used to assess pavement quality, performance, and to determine pavement properties. Deflection-based measurements differ from the other NDT methods used in this study in that they measure the response of the pavement at load levels that are similar to those expected to be applied in service. In general, large pavement deflections under these loads indicate poor performance of the pavement structure. The large strains imposed on the pavement layers and subgrade may lead to premature failure of the pavement system under repeated cyclic loading. Therefore, tracking pavement deflections over time can be an effective pavement management tool to assess pavement performance and estimate remaining pavement life. In addition, deflection measurements can be used to quantitatively estimate the mechanistic properties, namely modulus, of the individual pavement layers using either empirical equations or back-calculation to match a measured deflection profile.



Fig. 7.1– Photograph of the Falling Weight Deflectometer (FWD) manufactured by Dynatest and operated by the Missouri Department of Transportation (MoDOT).

In current practice, deflection-based measurements are most commonly applied using the Falling Weight Deflectometer (FWD) device (Fig. 7.1). The FWD is a reliable and repeatable point-by-point deflection method that is employed to some degree by nearly all DOTs in assessing pavement properties and performance. The FWD applies an impact force to a loading plate on the pavement surface using a guided drop-weight. An array of geophones record the deflections of the pavement surface caused by the weight drop. Several different drop heights and/or impact weights can be used to measure the response under a wide range of applied pavement stresses. The FWD has been successfully used to evaluate individual components of the pavement system (e.g. Donovan and Tutumluer, 2009), characterize subgrade properties (e.g. Rahim et al., 2003), and support the decision making process for pavement management

and rehabilitation (e.g. Zaghoul and Elfino, 2000). However, one of the disadvantages of the FWD as a pavement management tool is that it is a point-by-point measurement with limited potential for complete and continuous coverage of pavement systems at the project or network level. The FWD is applied using a vehicle-towed device that must be completely stationary to take measurements. It is applied at discrete points along the pavement, with each measurement taking about 3 to 5 minutes to complete.

In recent years there has been progress in developing continuous deflection measurement devices to overcome some of the limitations of the FWD, namely the point-by-point implementation of the measurement. For this project the Rolling Dynamic Deflectometer (RDD) was studied as a tool for pavement assessment and management applications. The RDD was developed by the University of Texas and the Center for Transportation Research in Austin, Texas in the late 1990's as a proto-type device for measuring continuous profiles of pavement deflection (Bay, 1999). The RDD consists of a 50,000 lb (222.4 kN) Mertz Vibroseis truck (Fig. 7.2) which has been modified to allow for continuous dynamic loading and measurement of pavement deflections “on the fly”. The dynamic load is generated using a hydraulic loading system and is applied to the pavement through a pair of rolling wheels located under the truck (Fig. 7.3a). Ground motions are measured using several rolling geophones mounted to an aluminum frame that extends from the dynamically loaded roller underneath the truck (Fig. 7.3b).



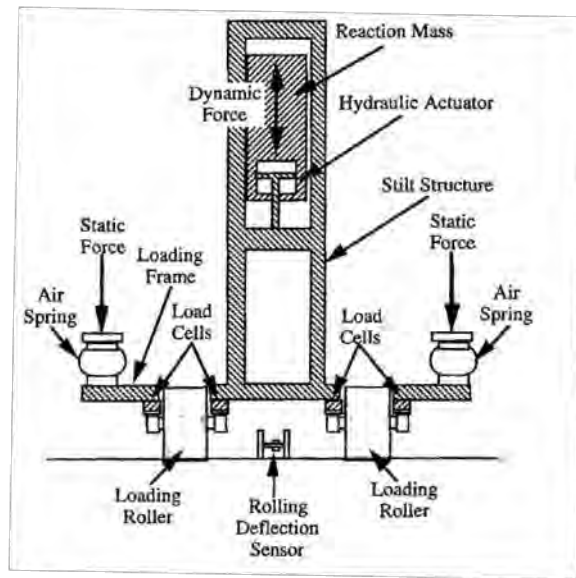
Fig. 7.2—Photograph of the first generation Rolling Dynamic Deflectometer (RDD) used in this project.

As the RDD profiles the surface at 1 to 2 mph (1.6 to 3.2 kph) the geophones record the deflection basin of the loaded pavement surface. The dynamic source typically tests pavement sections with a dynamic force of 10,000 lbs (44.5 kN) operating at a frequency of 30 Hz. One rolling geophone between the loading rollers aided by two or three additional rolling geophones attached to the aluminum frame capture the shape of the deflection basin in the

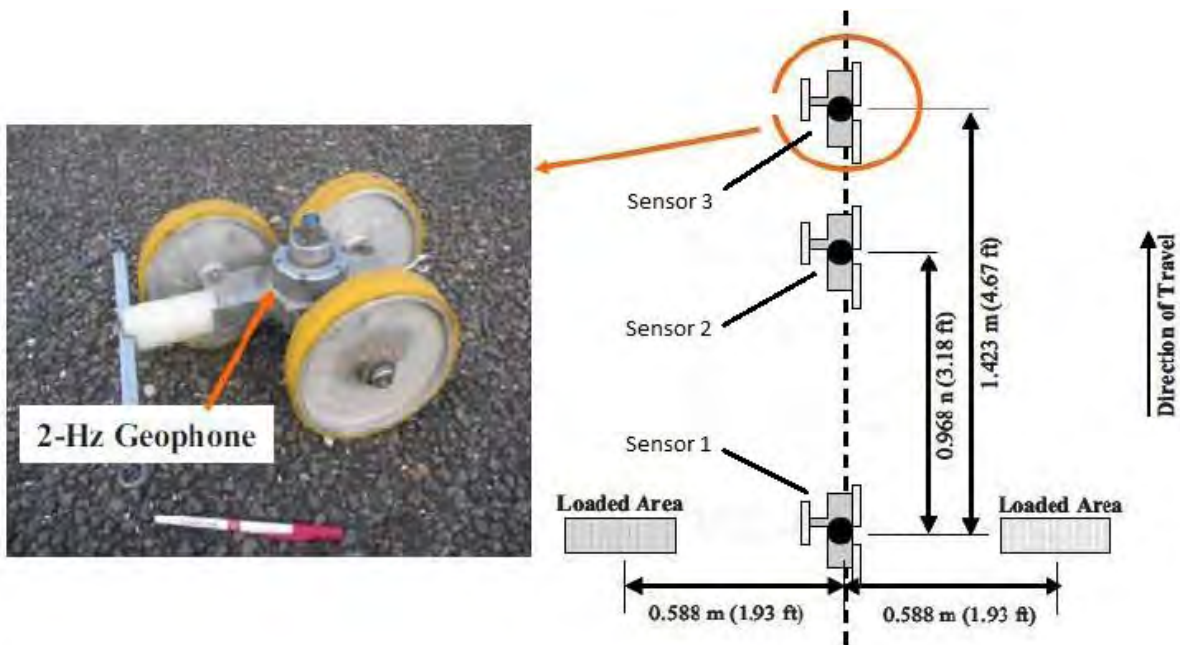
longitudinal travel direction. The rolling geophones have a natural frequency of 2 Hz with a peak-to-peak maximum motion of 0.25 in. (6.4 mm). The aluminum frame and sensors are isolated from the RDD system vibrations by steel cables. To ensure that the loading rollers keep contact with the ground surface during testing, a static hold down force is applied by hydraulic actuators reacting against the truck mass (Fig. 7.3a).

Over the past 15 years the RDD has been applied to many pavements, primarily in the state of Texas. The majority of studies have been focused on using the RDD to investigate the potential for reflective cracking in AC overlays of rigid pavements (Lee et al., 2004; Lee et al., 2005; Chen, 2007; Chen et al., 2008; Nam et al., 2010; Zhou et al., 2011; Chen et al., 2011). There have been only limited studies applying the RDD to flexible pavements (e.g. Bay et al., 1999).

In this study, the RDD was used at six pavement sites located around the state of Missouri to better understand the potential application of the RDD for pavement management in Missouri. Pavements tested in this study included: poor performing full-depth asphalt pavements, a recently overlaid jointed reinforced concrete pavement, poor performing unbonded concrete overlay pavements, unbonded concrete overlay that is performing well, and an unreinforced PCC pavement that is performing well. The objective of this portion of the research was to assess: (1) the type and quality of information that can be derived from the RDD for different pavement conditions and (2) evaluate the potential of the RDD to be used in MoDOT's pavement management program. Procedures used to acquire, analyze, and interpret the data are discussed below followed by results obtained from the test locations. Results from FWD measurements performed at these sites and three additional sites are also presented.



(a) RDD Load Application System (Bay & Stokoe, 1999)



(b) RDD Geophone Configuration (after Turner, 2003)

Fig. 7.3—Rolling Dynamic Deflectometer (RDD) loading and measurement configuration.

7.2 FWD Data Acquisition, Processing and Interpretation

7.2.1 FWD Data Acquisition

Falling Weight Deflectometer (FWD) data were collected on eight different Missouri roads in this study. Table 7.1 presents a summary of the dates of testing and weather conditions during the FWD measurements. Measurements were performed by MoDOT personnel at the request of the project investigators. The equipment used was a towed FWD device manufactured by Dynatest, as shown in Fig. 7.4. FWD data collection dates were scheduled to coincide with the NDT measurements performed by MS&T. However, a later review of the data indicated that the load plate geophone sensor was providing faulty readings at some of the sites. This problem was found to only affect measurements performed at sites tested in the summer of 2013 (Sites 5, 6, and 8). MoDOT fixed the problem on the FWD and performed another set of measurements at Sites 5 and 8 at a later date. Site 6 was not retested.

The FWD data collection was performed using nine receivers, as shown in Fig. 7.5. Load transfer measurements at joints were performed (at some sites) both entering the joint (Fig. 7.5) using receivers D1 and D3 and leaving the joint using receivers D1 and D8. In addition, at some sites, mid-slab deflection measurements were also performed. At flexible pavement sites, deflection measurements were performed at fixed intervals (typically 25 ft).

Table 7.1–Summary of RDD and FWD investigation dates and weather conditions of the pavement sites investigated.

Site No.	Pavement Site	Date of RDD Investigation	Weather Conditions	Date of FWD Investigation	Weather Conditions
1	US 63 North of Rolla (Site 1)	12/11/2013	28-35° F, sunny	10/30/12	33-46° F, no rain
2	US 54 Camden County (Site 2)	11/19/2013	50-56° F, sunny	11/14/12	37-42° F, no rain
3	MO 179 Jefferson City (Site 3)	12/10/2013	36-38° F, sunny	12/4/2012	26-29° F, cloudy, rain
4	HWY AT (Site 4)	N/A	N/A	08/05/2013	71-74° F, no rain
5	I-55 Pemiscot County (Site 5)	12/12/2013	28-35° F, sunny	4/30/14	49-53° F, no rain
6	I-55 Perry County (Site 6)	N/A	N/A	09/24/2013	51-71° F, no rain
7	HWY U (Site 7)	N/A	N/A	05/2/2013	57-65° F, no rain
8	I-35 (Site 8)	11/18/2013	38-45° F, sunny	5/28/2014	84-87° F, no rain
9	I-35 Daviess County (RDD Only)	11/18/2013	42-45° F, sunny	N/A	N/A



Fig. 7.4—Photo of falling weight deflectometer (FWD) equipment in operation at Site 1 (US 63).

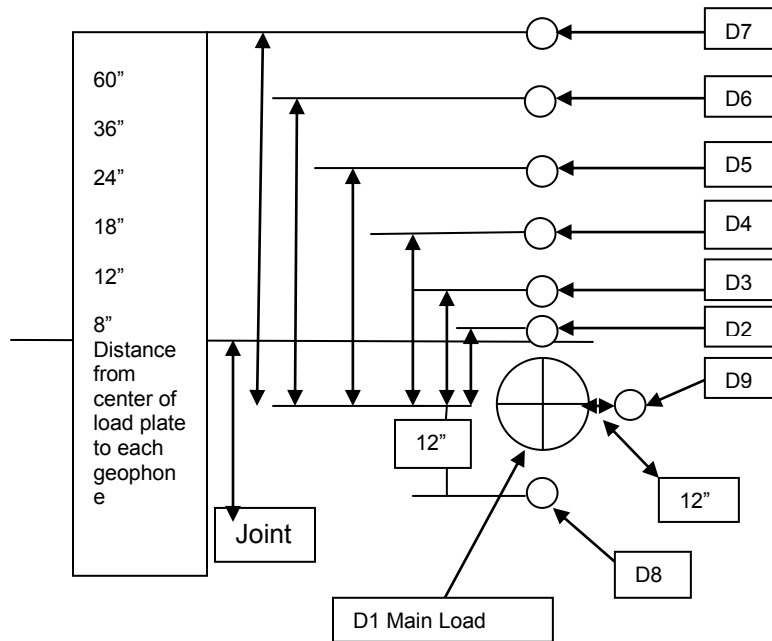


Fig. 7.5—FWD sensor arrangement and set-up for testing load transfer at a joint (entering slab).

7.2.2 FWD Data Processing and Interpretation

The output data files (F25 format) from the Dynatest system were supplied by MoDOT to the researchers after the completion of the measurements. The F25 files include information on location, loading parameters, temperature, measured loads and peak deflections at each receiver location. The FWD data collected in this study were used for two primary purposes.

First, at rigid pavement sites the FWD data were used to calculate load transfer efficiency (LTE_{FWD}) at joints in the pavement so that comparisons could be made with the results from the RDD and other NDT methods. The LTE_{FWD} was computed entering the slab as:

$$LTE_{FWD,E} = \frac{D3}{D1} * 100 \quad (1)$$

where, D3 and D1 are the deflections 12 inches from the load and at the load, respectively (Fig. 7.5). The LTE was also calculated leaving the slab with the load on the other side of the joint, as:

$$LTE_{FWD,L} = \frac{D8}{D1} * 100 \quad (2)$$

where, D8 and D1 are the deflections 12 inches from the load and at the load, respectively (Fig. 7.5). At, some sites only the leaving LTE measurements were made.

The FWD data were also used to develop profiles indicative of pavement parameters along the 1000-ft alignment tested by the RDD and NDT methods. For this purpose empirical forward calculation equations were used to develop estimates of subgrade modulus using the Hogg Model, as well as composite pavement modulus, and surface layer modulus using the AREA method. The procedures used in this study followed the methods described in Chapter 3 entitled “Forward Calculation Methodology” in the FHWA publication HRT-05-150 (Stubstal et al., 2006). Details of the methods used can be found in the appendix to this report. It should be noted that the modulus values from the forward calculations are only estimates, but serve the purpose of showing how properties changed along the pavement alignment. The more rigorous back-calculation procedure can provide better estimates of modulus values. However, due to the large number of measurements collected in this study (i.e. hundreds) and the time consuming nature of the back-calculation procedure it was not practical to use this approach for this study. In addition, since the RDD cannot be used to back-calculate modulus values and other methods used in this research (such as surface waves) determine the modulus at much smaller strain levels, no meaningful comparisons of modulus values would be possible. Instead the FWD data were used to provide qualitative information on changes in properties (i.e. lower surface stiffness, softer subgrade) that could be compared to the observations from other methods.

7.3 RDD Data Acquisition, Processing and Interpretation

7.3.1 RDD Data Acquisition

The RDD device was transported by truck from Texas to Missouri for field testing in November 2013. Due to scheduling conflicts with the RDD operator and cost considerations, it was not possible to bring the device to Missouri when the other NDT measurements were performed by Missouri S&T at each site. Measurements were first made on 11/18/2013 at the I-35 site in Daviess County followed by testing in the afternoon at a second site on I-35 near Bethany, MO (not tested with the other NDT methods). The HWY 54 site was tested on 11/19/2013. Due to

inclement weather (prolonged rainy conditions), it was not possible to perform the measurements at the remaining sites as planned. Therefore, the RDD was stored locally until the operators could return in December, 2013 to complete the testing at the remaining sites. Heavy snowfall at the I-55 site in Perry County (Site 5) prevented RDD measurements from being performed at this site during the second visit, and budget considerations precluded rescheduling measurements at this site.

The primary objective of the field testing program was to collect RDD data over the same 1000-ft test section where the other NDT methods performed by MS&T were applied. In addition, data were collected over one to two mile long sections at most sites. Table 7.2 presents a summary of the testing dates, pavement type, and length of RDD testing runs performed at each of the six sites tested.

Table 7.2–RDD testing summary

Site	Date	Pavement Type	Length of Run
US 63 NB: Phelps County	12/11/2013	AC overlay on PCC	1.5 miles
HWY 54 EB: Camdenton	11/19/2013	Full Depth AC	0.65 miles
HWY 179 SB: Jefferson City	12/10/2013	Full Depth AC	1000 ft
I-55 SB: Pemiscot County	12/12/2013	Unbonded PCC Overlay (good)	1.9 miles
I-35 NB: Daviess County	11/18/2013	Unbonded PCC Overlay (poor)	2.0 miles
I-35 SB: Bethany	11/18/2013	PCC	1.6 miles

The RDD data acquisition was performed by a two-man crew from the University of Texas. A M.S.-level graduate student, Dan Iffrig, from the University of Missouri-Columbia assisted with site access and recorded pavement distress observations as the RDD data were collected. At each site the RDD was driven to the site and positioned at the desired starting position. In all cases the loading was applied in the right lane. Lane drops were set up by MoDOT to allow for testing at most of the sites. In some cases, a moving lane closure (moving crash trucks behind the RDD) was used, which allowed traffic to pass around the RDD as the measurement was performed. Once positioned at the starting location, the aluminum frame was lowered to the ground and the three rolling sensors were positioned on the frame. The first sensor was positioned between the loading wheels, with the other sensors located 3.18 ft (sensor 2) and 4.67 ft (sensor 3) respectively from the first sensor. A static hold down force of nominally 10 kips was applied to the loading wheels and a dynamic force of ± 5 kips was applied to the wheels at a frequency of 30 Hz. The RDD was then moved along the pavement at about 1 to 2 mph. The distance travelled by the RDD was measured using an optical encoder wheel on the RDD, and landmarks along the test path (e.g. corehole locations, 100 ft intervals along

the 1000 ft test section) were noted to account for small cumulative measurement errors from the encoding wheel.

7.3.2 RDD Data Processing and Interpretation

The raw data collected by the geophones consists of the 30 Hz signal generated by the loading wheels along with any rolling noise from the sensors and road noise from passing vehicles. The 30 Hz signal is modulated by the deflection profile of the pavement created by the RDD. Processing of the data to reveal the deflection profile basically involves filtering to remove noise and demodulation to remove the 30 Hz signal and retain the deflection envelope. In addition, spatial averaging of the signal is applied to improve the reliability of the deflection values. For this study, the averaging procedure produced one deflection value for every two feet covered by the RDD. Therefore, over a typical 61.5 ft span of jointed reinforced PCC pavement, approximately 30 deflection values were measured in about 20 to 30 seconds. The dynamic force produced by the RDD is also measured and recorded using a load cell. The deflections are normalized to a 10 kip load and plotted in units of mils/10 kip. The processed output of the RDD consists of a plot of deflection vs. distance, as shown in Fig. 7.6. The red plot is the deflection measured between loading wheels, while the black and blue plots are the deflections from receiver 2 and receiver 3, respectively.

Interpretation of RDD data at this stage of development is largely qualitative. Currently, there is not a method available to back-calculate subgrade and pavement stiffness values from RDD deflections. The primary advantage of RDD measurements over conventional methods such as FWD is the dense spatial sampling of deflection values and the resulting high-resolution presentation of deflection data. Data can be presented over a long distance range, as shown in Fig. 7.6, to identify general regions of high or low deflections along the pavement, which can be identified for more detailed study using other methods. On rigid pavements, the RDD provides information on the quality of subgrade support and load transfer across joints and cracks. In Fig. 7.6 below, the sharp peaks in the deflection profile are locations of joints in the concrete pavement (in this case spaced at 61.5 ft). Fig. 7.7 presents the RDD deflection values over a much smaller distance range (about 100 ft). The quality of the joints can be evaluated by looking at the peaks in the Sensor 1 and Sensor 2 plots. As the loading wheel approaches a joint the deflections in Sensor 1 will increase resulting in a spike in the deflection profile. It is, therefore, easy to identify joint locations from the RDD profile even with the presence of an asphalt overlay (Fig. 7.6). Regions with poor support under the joint will result in larger spikes in the deflection profile. Additional information about the joints can be obtained by considering the motion of Sensor 2, which leads Sensor 1 by 3.18 ft, as illustrated in Fig. 7.8. As the rolling wheels approach the joint, Sensor 2 will move across the joint to the adjacent slab. If the motion of Sensor 2 mirrors the motion of Sensor 1 it indicates good load transfer across the joint. If, however, the response of Sensor 2 decreases abruptly as it crosses the joint, it indicates poor load transfer across the joint.

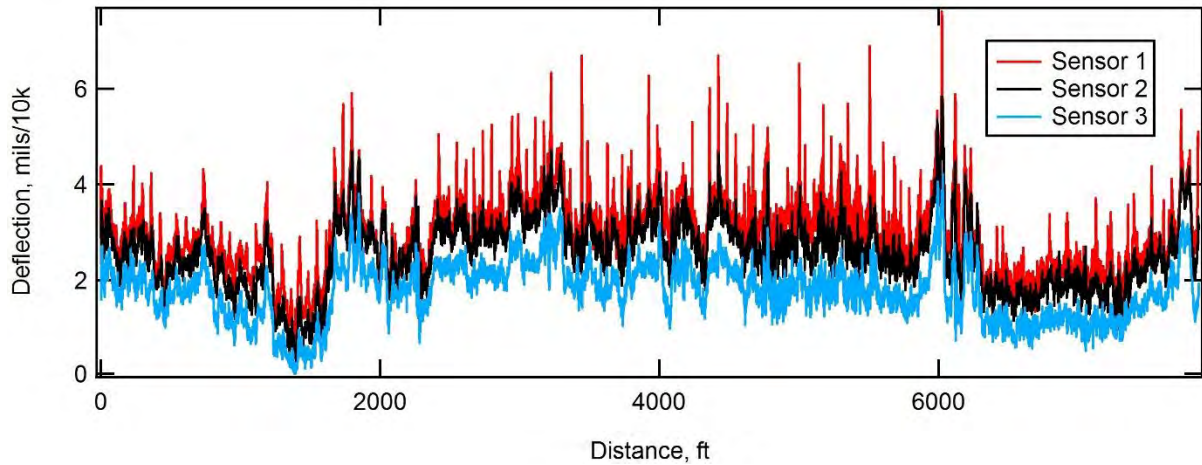


Fig. 7.6—Example of processed RDD data showing the deflection values from the three rolling sensors plotted vs. distance over a length of about 1.5 miles

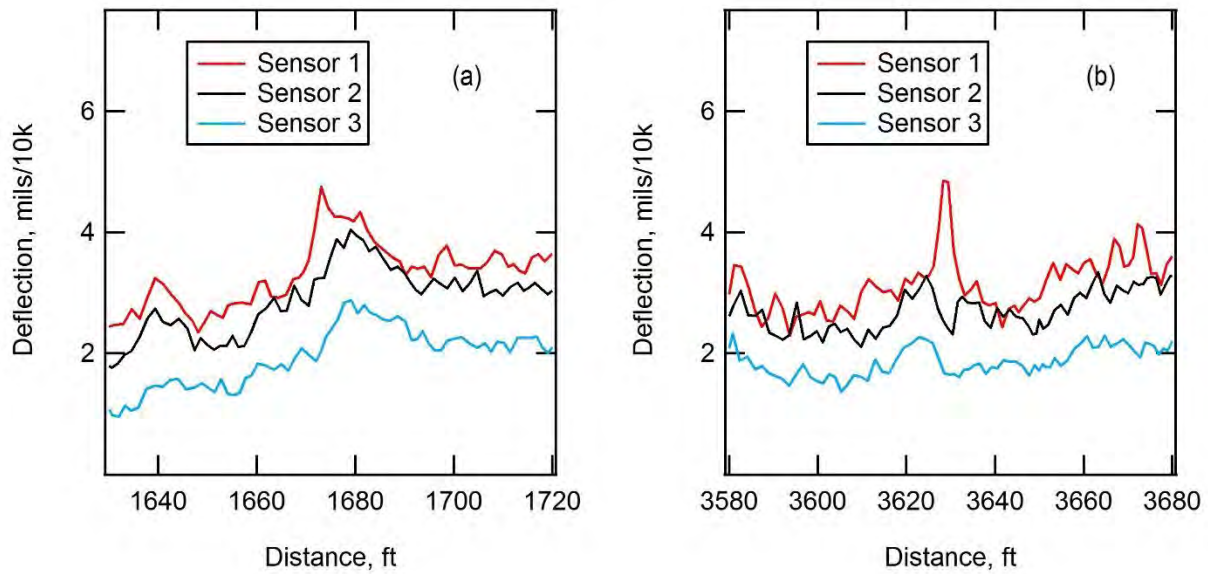


Fig. 7.7—Examples of load transfer evaluation using the RDD, showing (a) good load transfer and (b) poor load transfer at a joint.

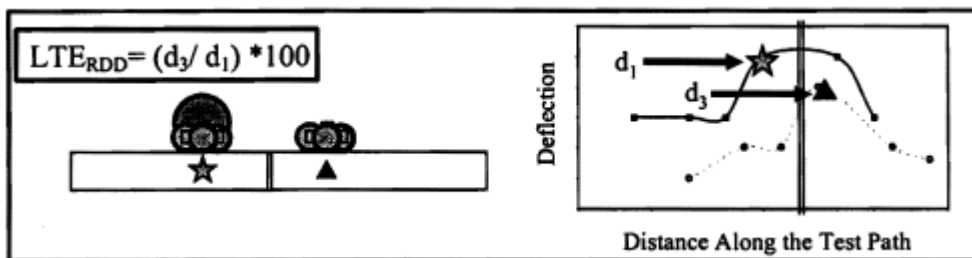


Fig. 7.8—Illustration of calculation of load transfer efficiency (LTE) from RDD data (from Lee et al., 2004).

The load transfer efficiency can also be calculated from the RDD (LTE_{RDD}) by:

$$LTE_{RDD} = \frac{W2}{W1} * 100 \quad (3)$$

where, W2 is the deflection from the Sensor 2 (located 3.18 ft from the loading wheel) after it passes the joint and W1 is the deflection from the Sensor 1 located between the loading wheel, as illustrated in Fig. 7.6. The receivers used in this calculation are spaced farther apart than those used in the FWD LTE calculation so the values may differ, but the trends should be the same.

Deflection profiles from the RDD can also provide information on support conditions under the concrete slabs. In rigid pavements, the deflection at the mid-point between joint locations is an indicator of slab support. As shown in Fig. 7.9, the midpoints between the joint locations (shown by the arrows) are largely unaffected by the presence of the joints, and therefore provides an indication of support conditions beneath the slab. The joints spaced at 61.5 ft intervals are clearly apparent, as is a crack in the mid-span of the slab at about 4650 ft. Much like the FWD, deflections from sensors far from the source (W3 in this case) are influenced primarily by the deeper structure and therefore provide qualitative information on the subsurface soil support conditions.

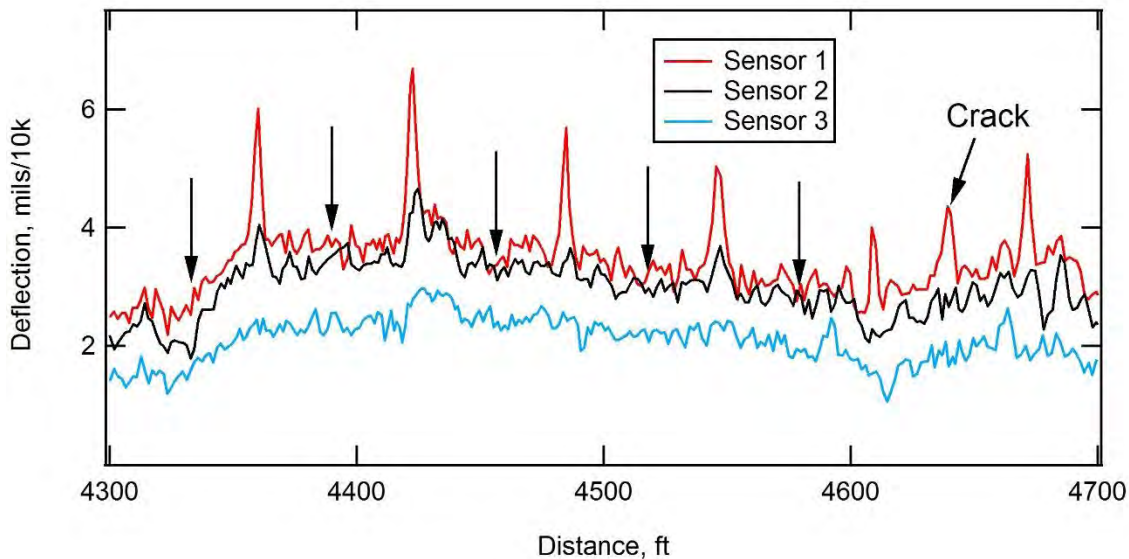


Fig. 7.9—Illustration of mid-slab support conditions evaluated from RDD data.

The data from the RDD can also be used to generate coarse representations of the deflection basin at a given location which may also provide qualitative information on support conditions under the pavements. An example of a deflection basin is shown in Fig. 7.10.

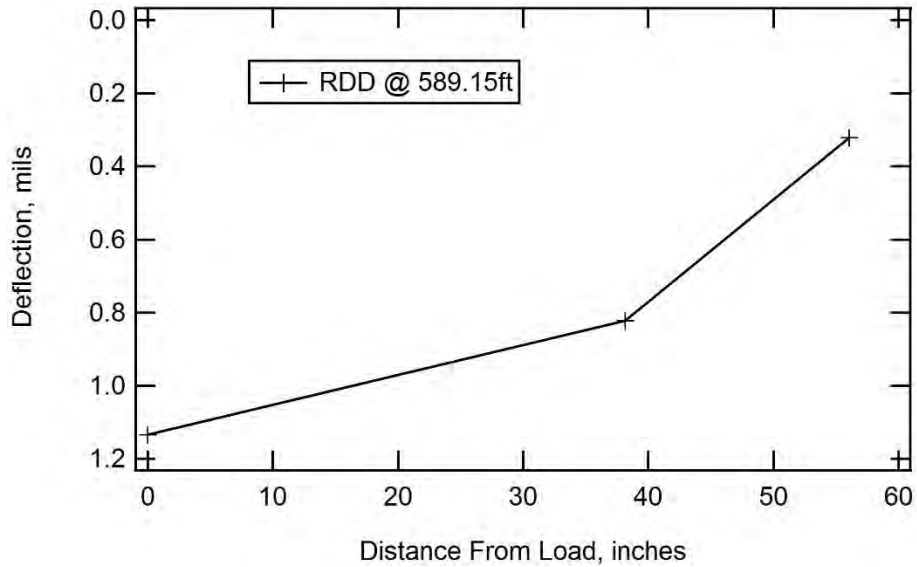


Fig. 7.10—Example deflection basin from RDD data.

7.4 RDD and FWD Results

7.4.1 Project Level Site 1 (US 63)

Project level Site 1 (US 63) is located near Rolla, Missouri. The pavement consists of two layers of bituminous mix (BM) over Portland cement concrete (PCC). Based on coring data collected at this site, the upper BM layer is about 1.5 in. thick, the lower BM layer is about 2 in. thick, and the lower PCC is 8.5 in.

RDD and FWD data were collected in the right lane in the northbound direction of US 63. Details of the data collection are described above and summarized in Table 7.1 and Table 7.2. At the time of the FWD measurements, the overlay was recently placed and no reflection cracks were apparent in the pavement. The joint locations were identified and marked for FWD testing using the GPR data collected at the site. The RDD data were collected about 14 months later and reflection cracks were apparent at nearly every joint location (e.g. see Fig. 7.11). Although the FWD and RDD data were collected at different times, no changes to the pavement profile (i.e. addition of asphalt) occurred during that time interval.

The RDD deflection profile collected over the full 1.5 mile span is shown in Fig. 7.12. The 1000-ft section of primary interest is indicated by the shaded region in Fig. 7.12. The 1000 ft test section is shown in expanded view in Fig. 7.13.



Fig. 7.11—Example of reflection crack observed at Site 1 (US 63) during RDD testing.

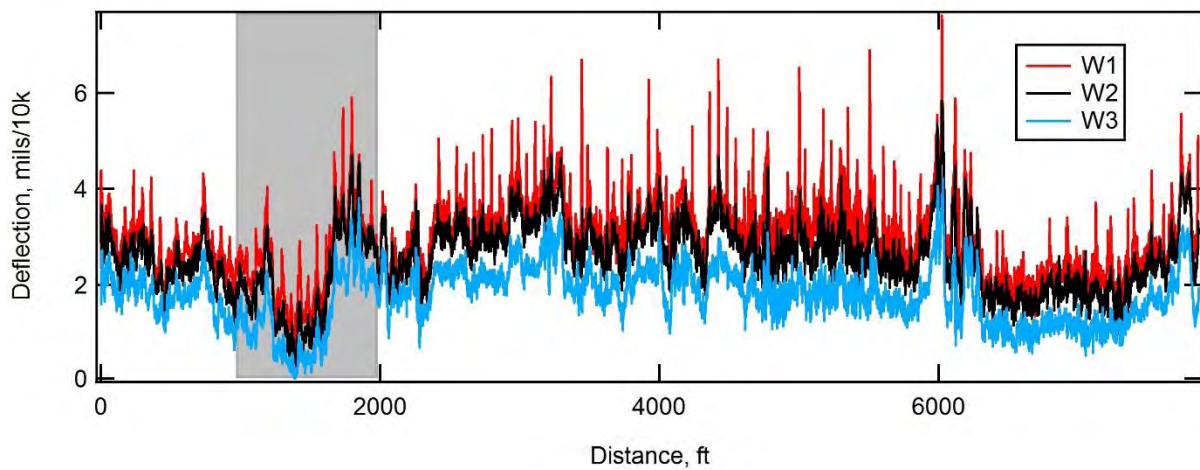


Fig. 7.12—RDD data over the full 1.5 mile extent on US 63 with the 1000 ft test section shaded.

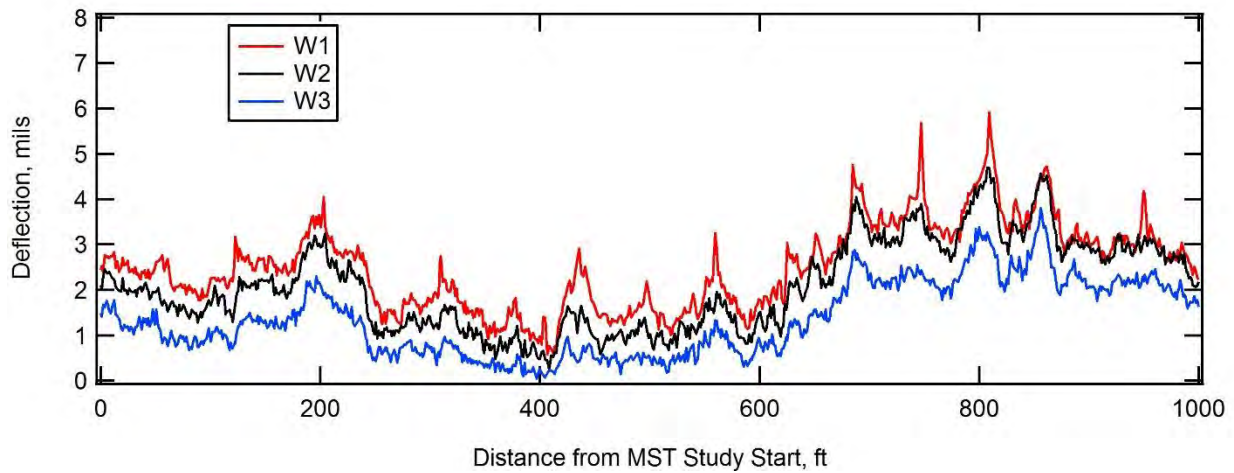


Fig. 7.13—RDD data over the 1000 ft test section on US 63.

Sensor 3 (W3 deflection profile) is located 4.18 ft from the point of loading, and therefore is primarily influenced by the subgrade support conditions. The W3 deflection profile presented in Fig. 7.12 shows significant variability in the support conditions along this 1.5 mile stretch of road. Likewise, the shorter 1000-ft section also shows significant variability in support conditions, as seen in Fig. 7.13. For example, between 250 ft and about 600 ft of the 1000 ft section the average deflection is 0.55 mils, while between 680 ft to 960 ft the average deflection was about 2.4 mils. The peak W3 deflection in the 1000 ft section was 3.8 mils while the minimum deflection was 0.04 mils. Histograms of the W3 deflections for the 1000-ft test section and the entire 1.5 mile section are presented in Figs. 7.13a and b, respectively. Table 3 summarizes statistical parameters from these sections.

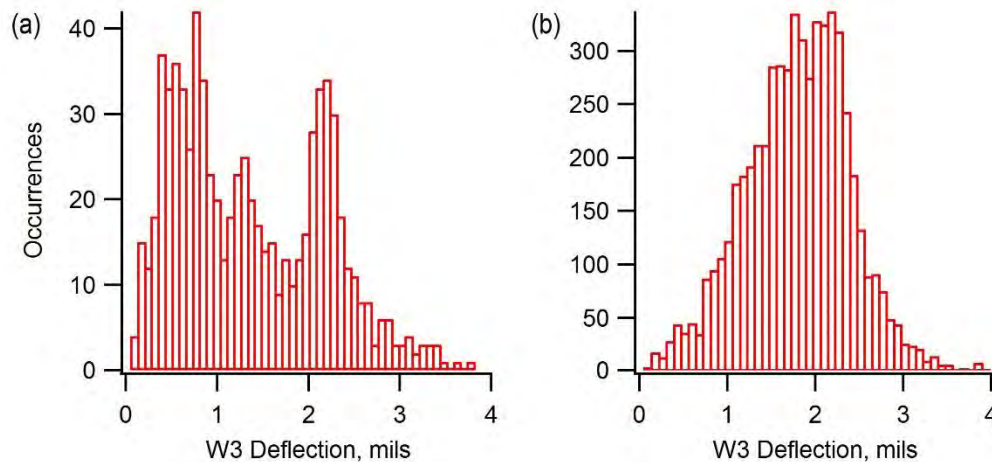


Fig. 7.14–Histogram of W3 displacement measured on the (a) 1000 ft section and the (b) 1.5 mile section.

Table 7.3–W3 deflection statistics for the 1.5 mile and 1000 ft section of US 63

Profile	Mean Deflection (mils)	Standard Deviation	Coefficient of Variation	Peak Deflection	Minimum Deflection
1000 ft	1.35	0.80	0.59	3.80	0.044
1.5 mile	1.78	0.59	0.33	4.21	0.044

Support conditions under the slab can also be inferred from the deflection measured by the W1 sensor (between the wheels) when passing over the midpoint of the slab, as illustrated in Fig. 7.9. Fig. 7.15 presents a comparison of the center slab deflections measured with the RDD and the FWD. In the regions where the RDD measured high deflections, the FWD values were consistent. However, between 200 and 600 ft the RDD showed much smaller deflections than were measured by the FWD.

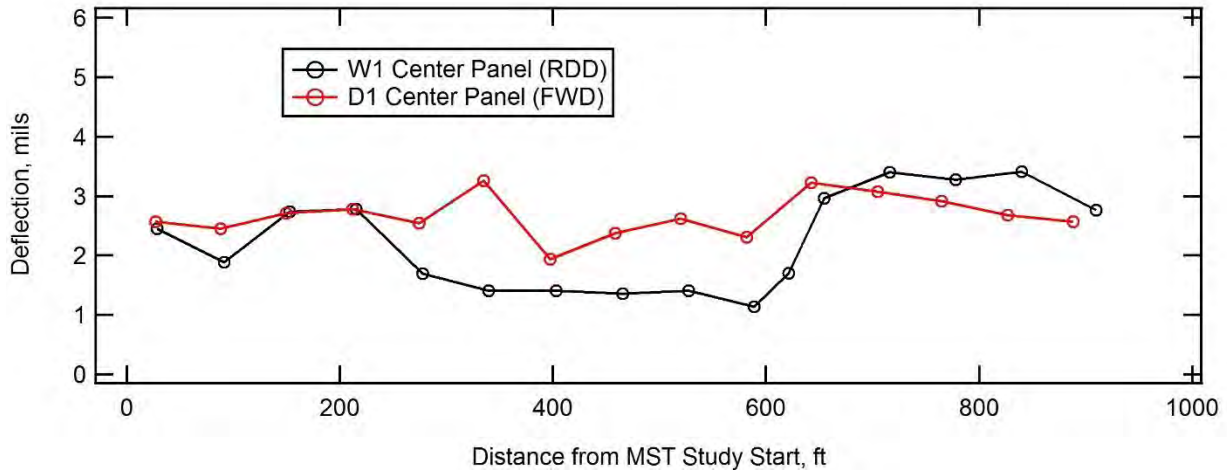


Fig. 7.15—Comparison of center slab deflections obtained from the RDD and the FWD at Site 1, US 63.

The locations of joints and cracks in the pavement are also apparent in the W1 profiles as spikes in the deflection plots, as shown in Fig. 7.12 and Fig. 7.13. The spikes in the profile indicate the increased deflection as the RDD approaches and passes over each joint and crack in the pavement. The magnitude of the joint deflections in the 1000-ft section recorded from the RDD and FWD are plotted and compared in Fig. 7.16. In this case the RDD showed lower joint deflections than the FWD over most of the profile, but slightly higher values for a few joints near the end of the section. Another way to isolate the performance of the joint using the RDD data is to subtract the W3 deflection from the W1 deflection (Chen, 2007), as shown in Fig. 7.17. Past studies by Chen, 2007 suggest threshold W1-W3 deflection value for reflection cracking of 4.4 mils. In this case, all of the W1-W3 values were less than 2 mils, although reflection cracking was apparent at nearly every joint location.

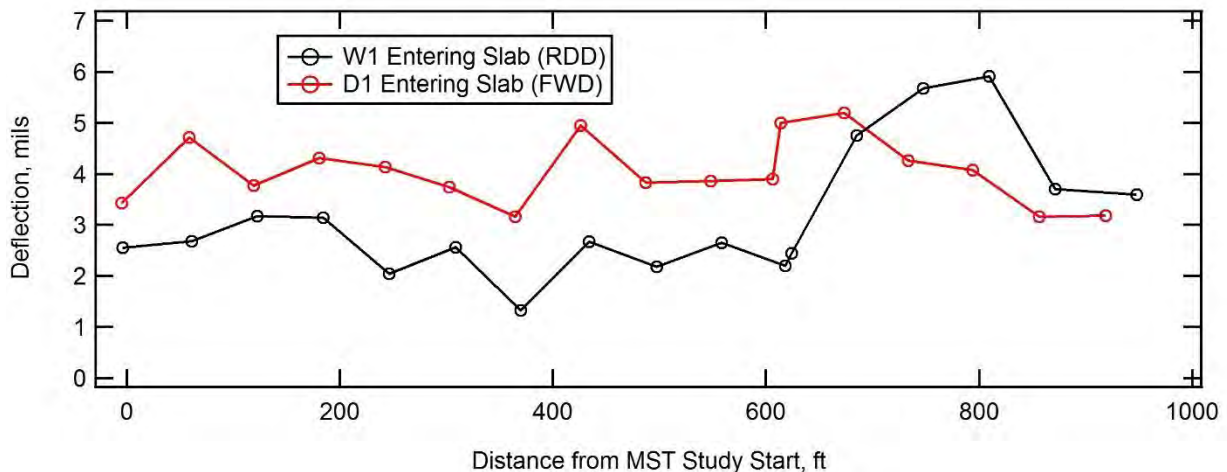


Fig. 7.16—Comparison of joint deflections obtained from the RDD and the FWD at Site 1, US 63.

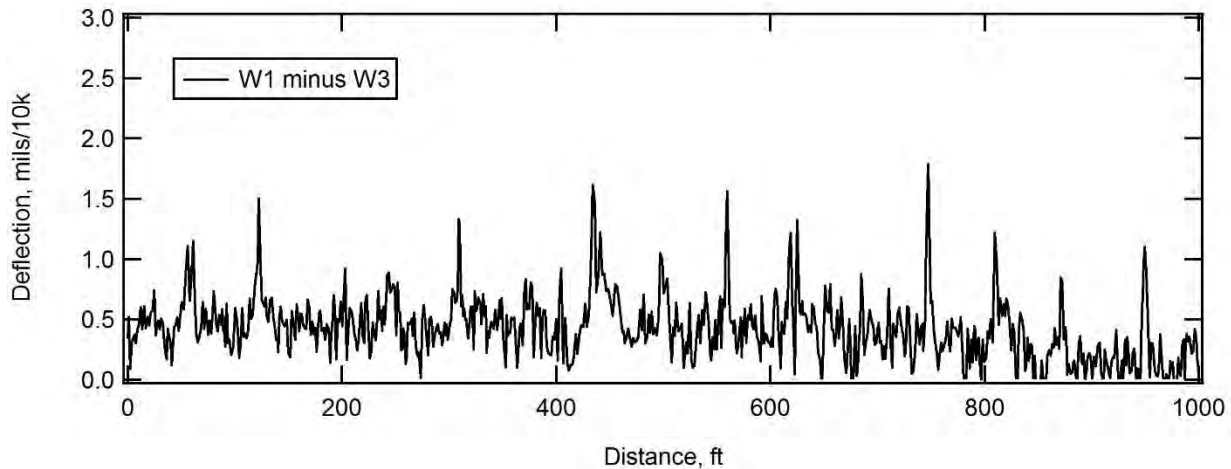


Fig. 7.17–Deflection difference ($W1-W3$) between Sensors 1 and 3 over 1000 ft test section at Site 1.

Load transfer efficiency was also calculated from the RDD and FWD data using equations (1) and (3). In this case there was a large difference in the LTE values obtained with the two methods, as shown in Fig. 7.18. The FWD showed very similar performance of the joints throughout the section (70 to 85%), while the RDD showed much lower values (40 to 60%) in the portion of the pavement where the deflections were low (200ft to 600 ft). The very low LTE values from the RDD may be partly due to the larger receiver spacing used in the RDD measurements (3 ft) as compared to the FWD measurements (1 ft). It should also be mentioned that the FWD measurements were performed shortly after the pavement was overlaid and no reflection cracking was evident, while the RDD was performed 14 months later when reflection cracking in the asphalt was evident at nearly all of the joint locations.

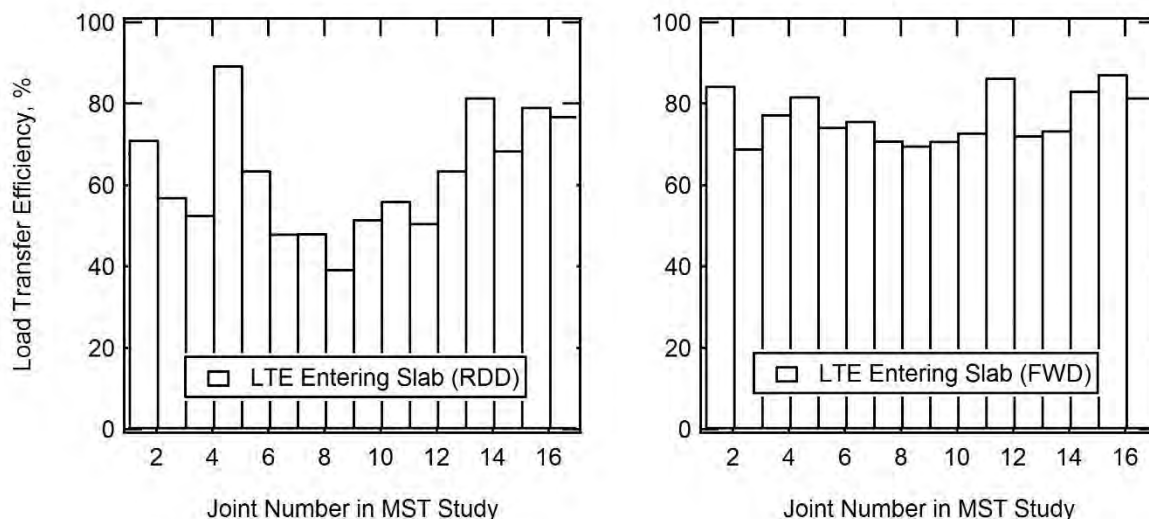


Fig. 7.18–Comparison of LTE at joints obtained from the RDD and the FWD at Site 1, US 63. Note: RDD measurements were performed approx. 14 months after the FWD measurements.

7.4.2 Project Level Site 2 (US 54)

Project level Site 2 is located on US 54 near Camden County, Missouri. The pavement profile when originally tested by the MS&T group (and MoDOT FWD) in November, 2013 consisted of approximately 11 in. of asphalt. At the time of the RDD testing there was no evidence of any surface distress or cracking in the newly overlaid section. Due to the different pavement conditions during the FWD and RDD testing it is difficult to make comparisons between the measurements. Fig. 7.19 shows a photograph of the RDD in operation at the newly overlaid US 54 site.

The RDD deflection profile collected over the full 0.65 mile span is shown in Fig. 7.20. The 1000-ft section of primary interest is indicated by the shaded region in Fig. 7.20. The 1000-ft test section is shown in expanded view in Fig. 7.21. Histograms of the deflection values from the W3 sensor are presented in Fig. 7.22, and values are shown in Table 7.4.



Fig. 7.19—Photograph of the RDD in operation at US 54.

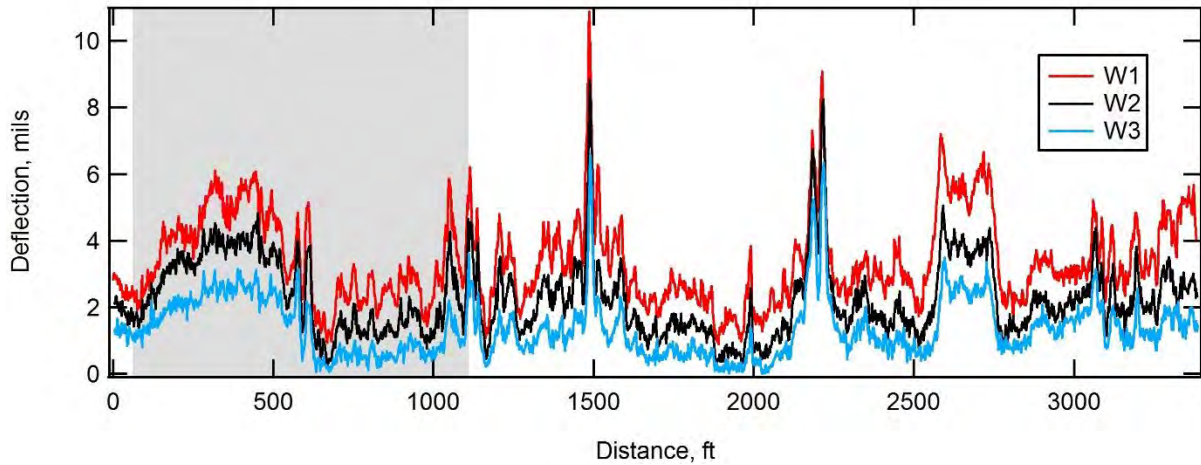


Fig. 7.20—RDD data over the full 0.65 mile extent on US 54 with the 1000 ft test section shaded.

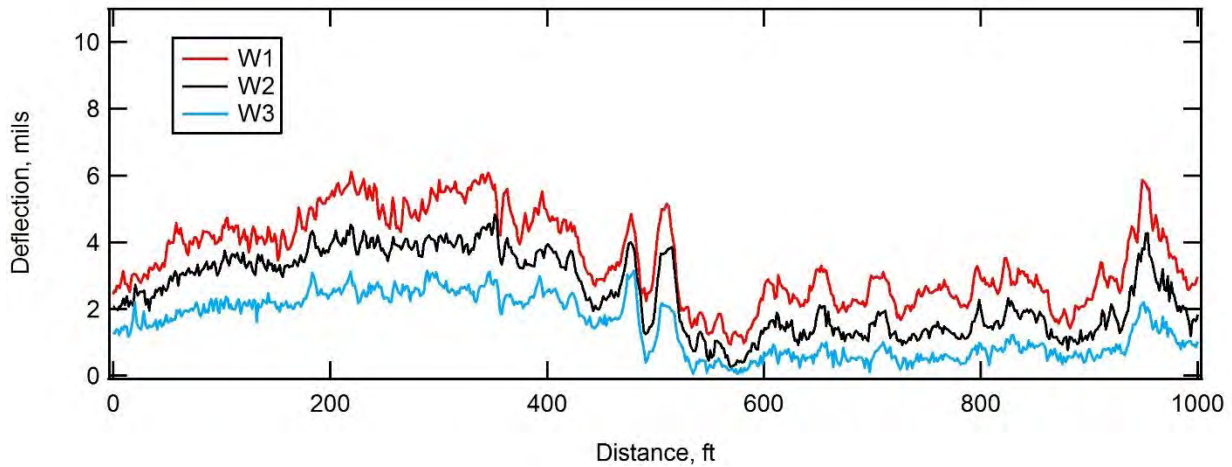


Fig. 7.21—RDD data over the 1000 ft test section on US 54.

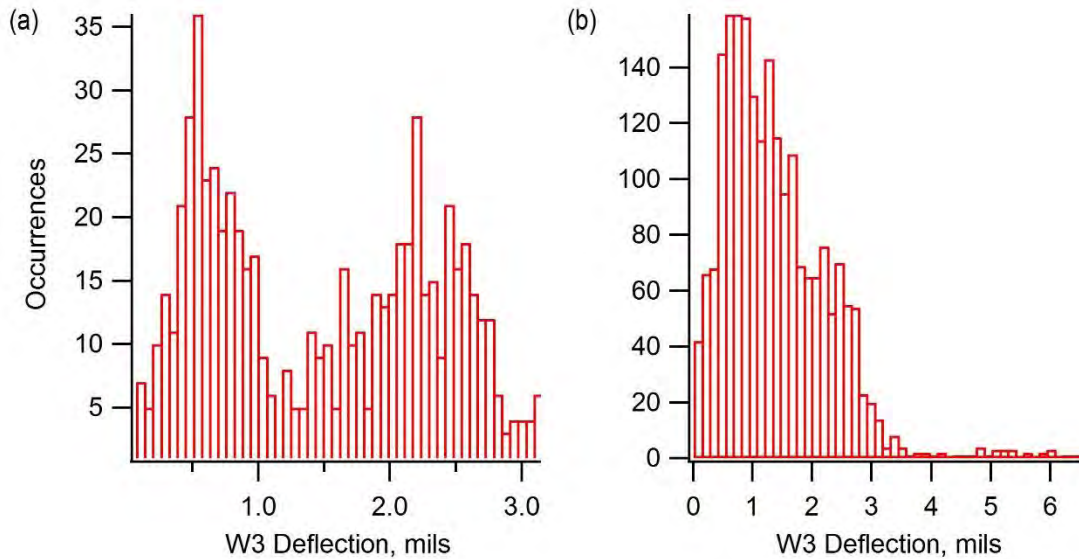


Fig. 7.22—Histogram of W3 displacement measured on the (a) 1000 ft section and the (b) 1.5 mile section.

Table 7.4–W3 deflection statistics for the 0.65 mile and 1000 ft section of US 54.

Profile	Mean Deflection (mils)	Standard Deviation	Coefficient of Variation	Maximum Deflection	Minimum Deflection
1000 ft	1.46	0.86	0.59	3.15	0.070
1.5 mile	1.37	0.89	0.65	6.59	0.014

A comparison of the deflection profiles measured using the first receiver of the RDD and FWD is presented in Fig. 7.23. As noted above, the pavement conditions were very different when these measurements were performed. Between the time of the FWD and RDD measurements a 2.75 in. asphalt overlay was placed at the site. The much higher deflections from the FWD as compared to the RDD are not surprising. A more meaningful comparison of the relative trends in deflection is presented in Fig. 7.24 where the deflection is normalized to the maximum value. The relative trend is nearly the same from the two measurements.

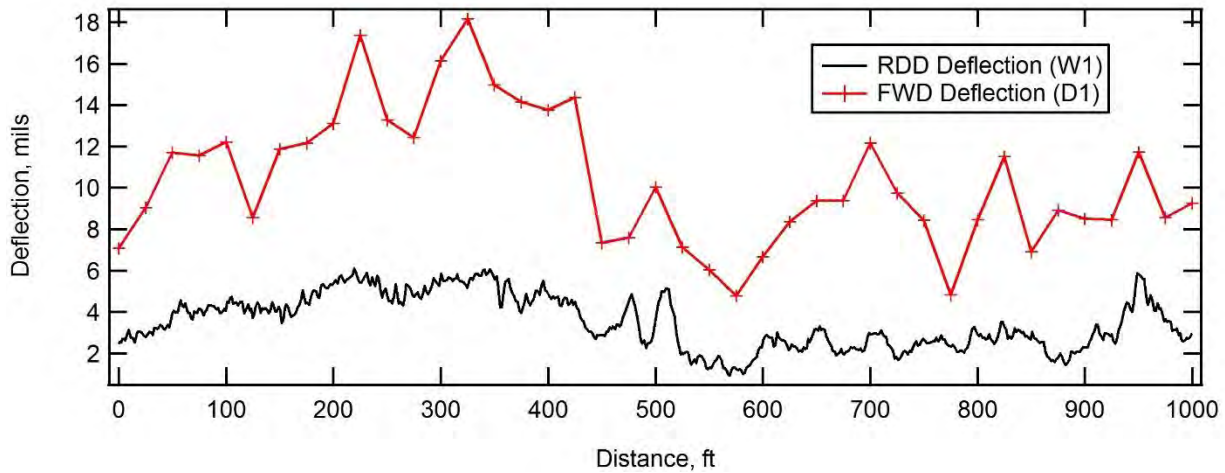


Fig. 7.23–Comparison of deflection profiles obtained from the first receiver of RDD and FWD measurements normalized to a load of 10 kips. Note RDD testing was performed after placement of a 2.75 in. asphalt overlay.

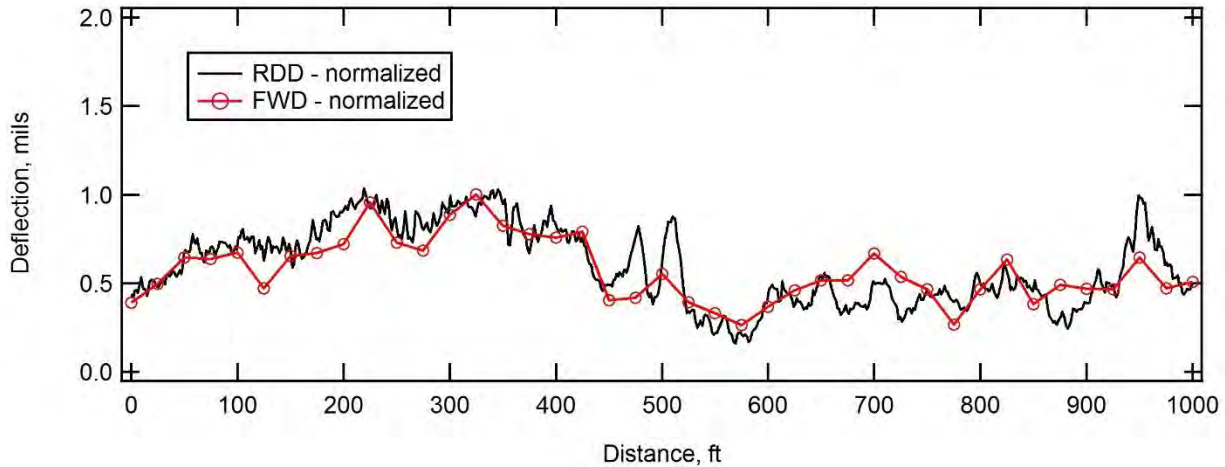


Fig. 7.24—Comparison of deflection profiles normalized by the maximum values obtained from the first receiver of RDD and FWD measurements showing the similarity in recorded trends over the 1000 ft section. Note RDD testing was performed after placement of a 2.75 in. asphalt overlay.

As discussed in Section 7.2.2, empirical forward calculation equations using FWD data can be used to develop estimates of subgrade modulus using the Hogg Model, as well as composite pavement modulus, and surface layer modulus using the AREA method. A plot of the subgrade modulus estimated using the Hogg method is shown in Fig. 7.25. The composite pavement modulus estimated from the AREA method is shown in Fig. 7.26. Estimates of the surface layer modulus from the AREA method (Fig. 7.27) are very sensitive to the thickness of the surface layer. Therefore, these values are only plotted at locations of cores and where FWD was applied nearby (typically within 5 to 10 ft). It should be noted that the estimates of surface stiffness assume a two-layer system consisting of continuous, elastic layers. Given the extensive cracking in the pavement at the time of the FWD testing, this assumption is likely not valid.

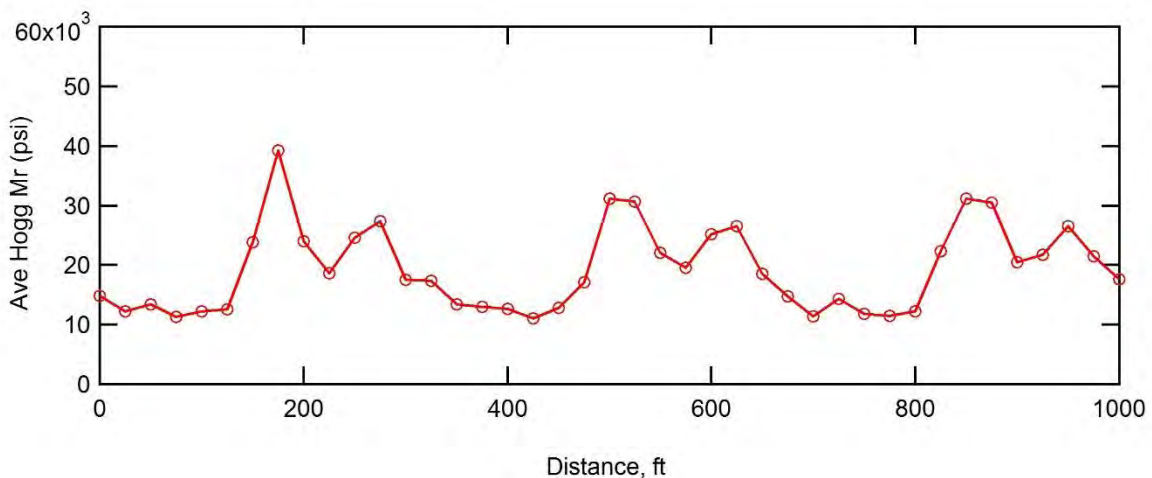


Fig. 7.25—Subgrade modulus estimated using the Hogg model from FWD data collected at Site 2 (US 54).

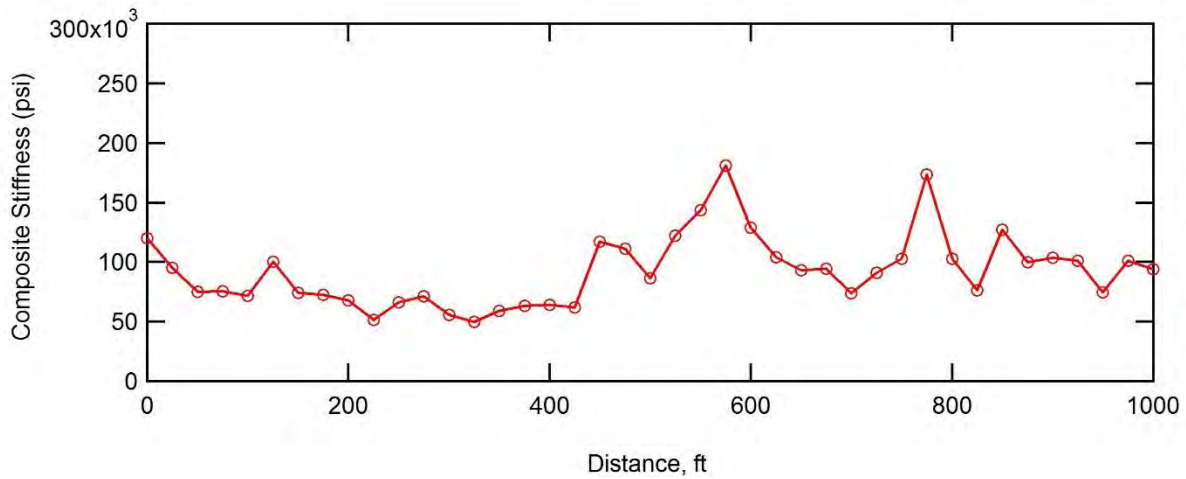


Fig. 7.26—Composite stiffness estimated using the AREA model from FWD data collected at Site 2 (US 54).

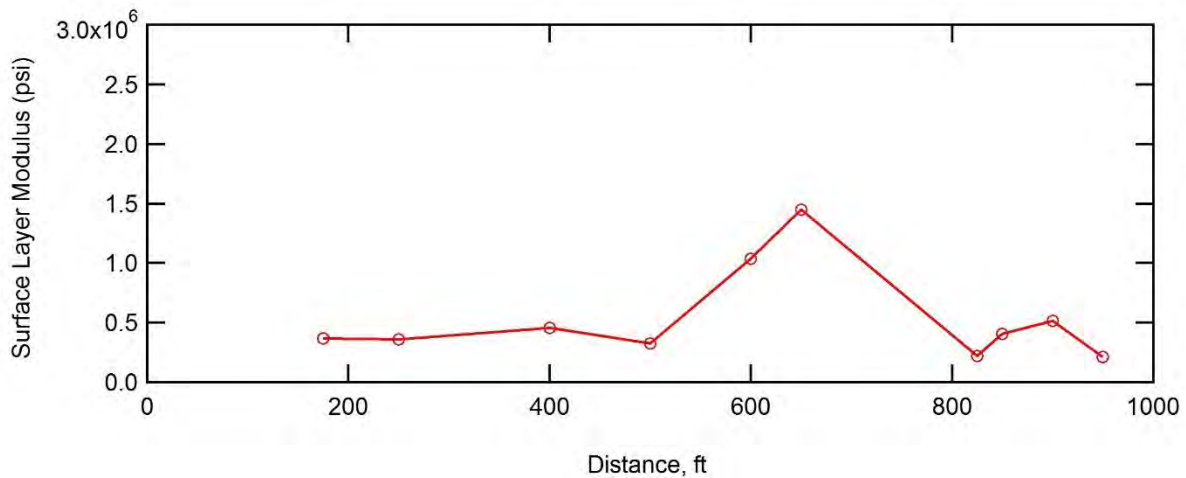


Fig. 7.27—Surface layer modulus estimated using the AREA model from FWD data collected at Site 2 (US 54). Note estimates were only made where nearby core control of surface layer thickness was available.

7.4.3 Project Level Site 3 (HWY 179)

Project level Site 3 is located on HWY 179 in Jefferson City, Missouri. The pavement surface layer consists of approximately 12 in. of asphalt. This site was originally tested by the MS&T group and MoDOT FWD in December, 2013. The RDD testing was performed one year later in December, 2014. The pavement profile was unchanged between the time of the original testing and the RDD measurements, and extensive transverse and longitudinal cracking was evident in the pavement at both times (Fig. 7.28).

A rolling road closure was used at this site and it was not possible to collect deflection data beyond the 1000 ft test section. Fig. 7.29 shows the deflection profile measured with the RDD at this site. A histogram of the deflections are presented in Fig. 7.30, and deflection values are shown in Table 5. A comparison of FWD center deflections to RDD W1 deflections are shown in Fig. 7.31. At this site, the magnitude of the deflections were similar, with FWD showing slightly higher values. However, unlike Site 2, the trends from the FWD and the RDD were different, with the FWD showing regions of high deflection that were not evident in the RDD profile.

The estimated subgrade modulus and composite modulus from the FWD deflections were relatively constant along the profile, as shown in Fig. 7.32 and Fig. 7.33. The estimated surface layer modulus was also relatively constant across the site, as shown in Fig. 7.34.



Fig. 7.28—Photograph of pavement surface at Site 3 during RDD testing showing extensive longitudinal and transverse cracking in the asphalt layer.

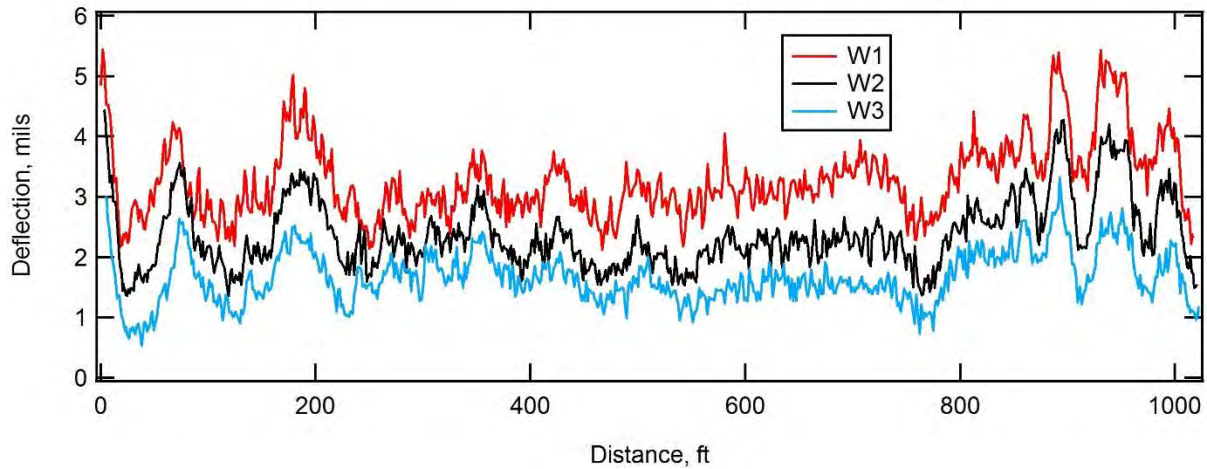


Fig. 7.29—RDD data over the 1000 ft test section on HWY 179.

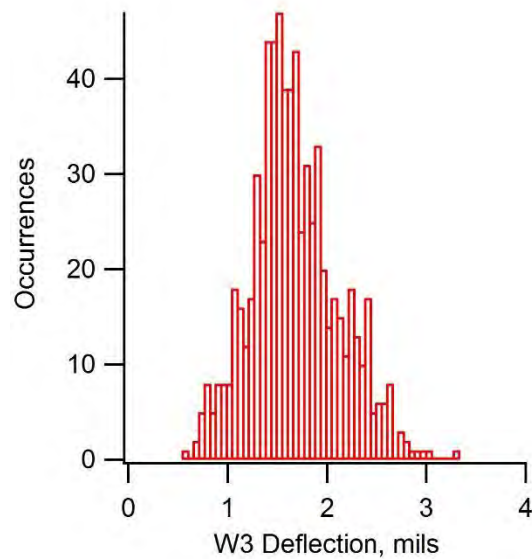


Fig. 7.30—Histogram of W3 displacement measured on the 1000 ft section at Site 3 (HWY 179).

Table 7.5—W3 deflection statistics for 1000 ft section of HWY 179

Profile	Mean Deflection (mils)	Standard Deviation	Coefficient of Variation	Peak Deflection	Minimum Deflection
1000 ft	1.66	0.44	0.27	3.32	0.53

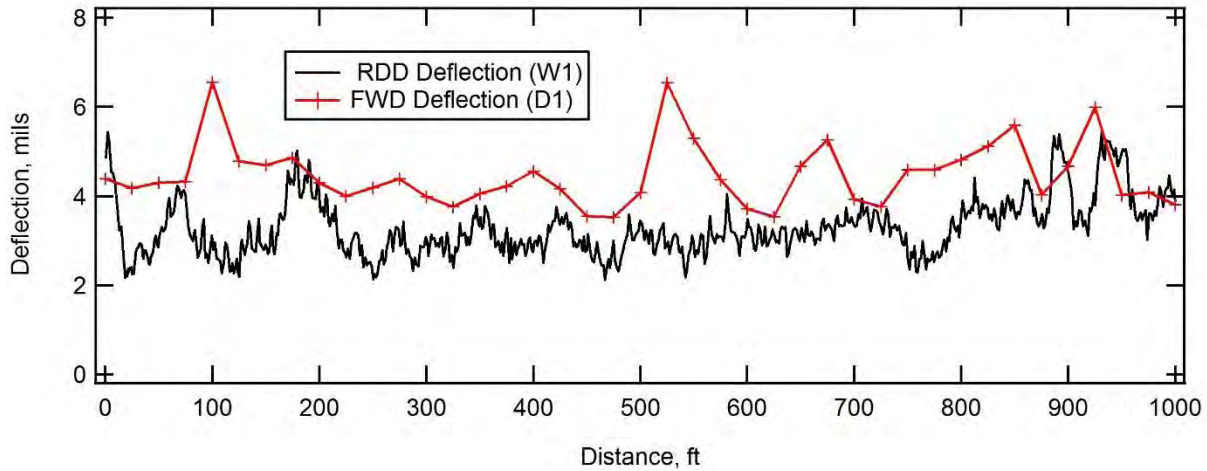


Fig. 7.31—Comparison of deflection profiles obtained from the first receiver of RDD and FWD measurements normalized to a load of 10 kips.

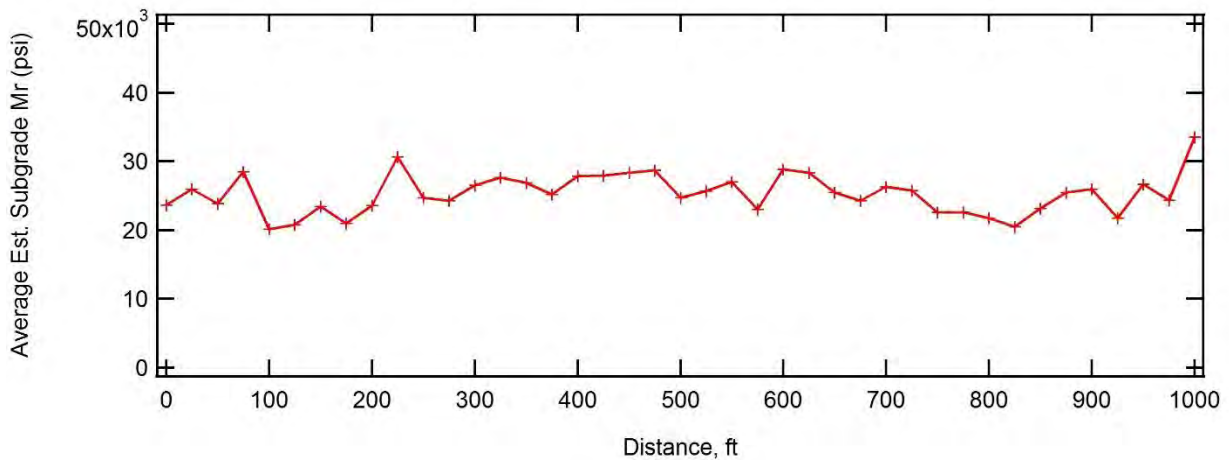


Fig. 7.32—Subgrade modulus estimated using the Hogg model from FWD data collected at Site 3 (HWY 179).

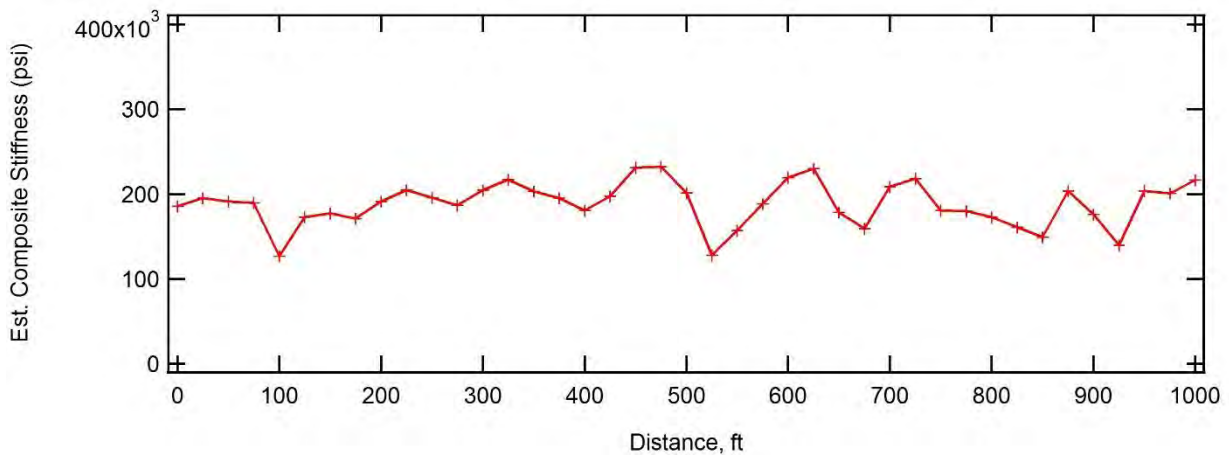


Fig. 7.33—Composite stiffness estimated using the AREA model from FWD data collected at Site 3 (HWY 179).

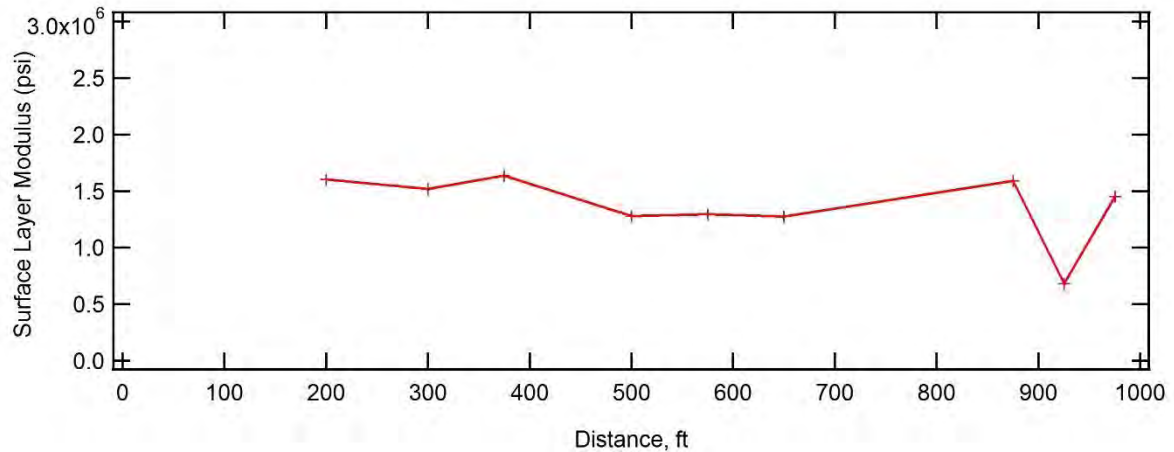


Fig. 7.34–Surface layer modulus estimated using the AREA model from FWD data collected at Site 3 (HWY 179). Estimates were only made where nearby core control of surface layer thickness was available.

7.4.4 Project Level Site 4 (HWY AT)

Project level Site 4 is located on HWY AT in Franklin County, Missouri. The pavement consists of a thin asphalt overlay over a 6 in. thick PCC layer. The thickness of the asphalt overlay and the total pavement thickness varied considerably across this site. Due to time and budget constraints, this site was not chosen for RDD testing. The FWD testing was performed in August, 2013 when the MS&T NDT measurements were performed. Fig. 7.35 shows the center deflections normalized to a 10 kip load as a function of distance. Fig. 7.36 shows the subgrade modulus estimated using the Hogg method, and Fig. 7.37 shows the estimated composite modulus from the AREA method.

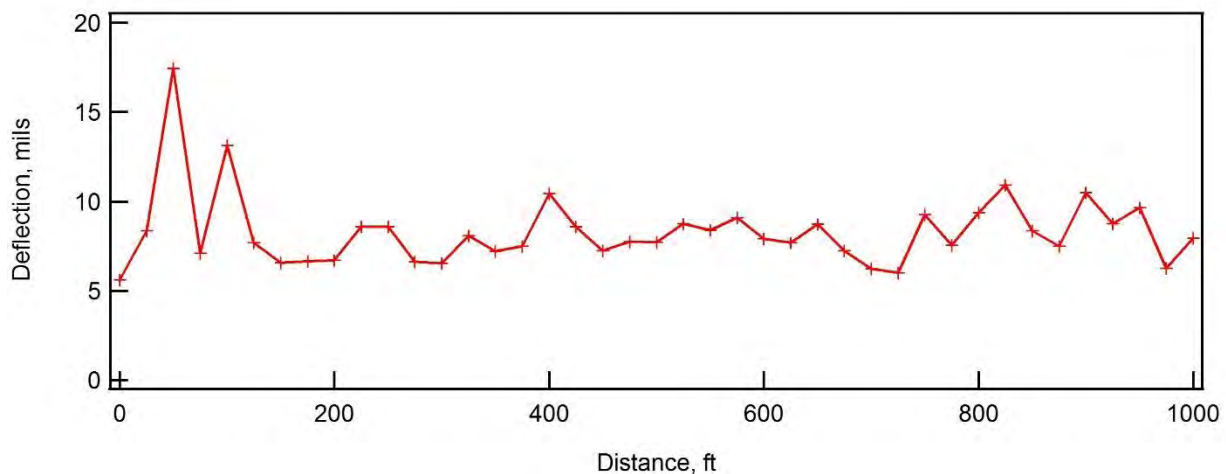


Fig. 7.35–Deflection profile obtained from the first receiver of FWD measurements normalized to a load of 10 kips.

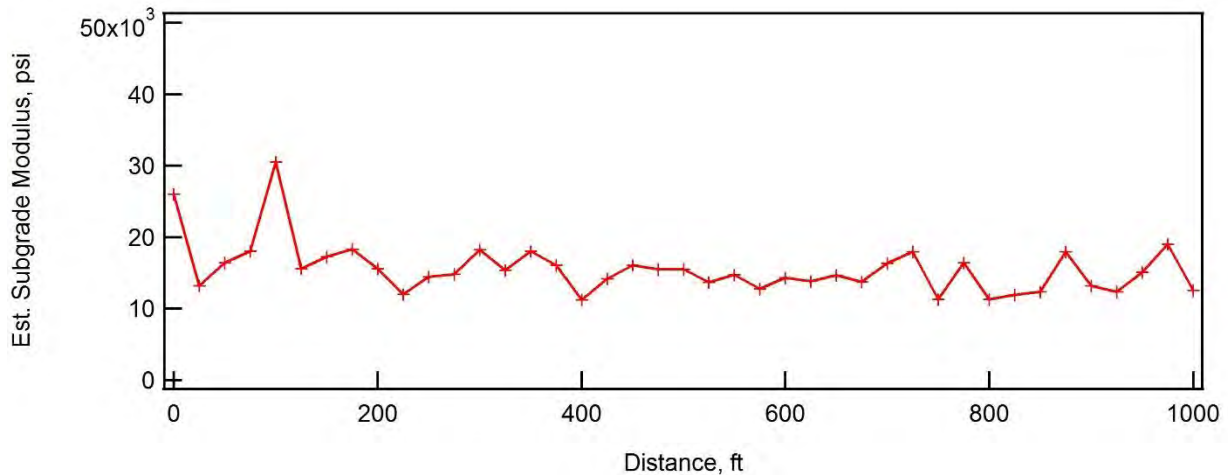


Fig. 7.36—Subgrade modulus estimated using the Hogg model from FWD data collected at Site 4 (HWY AT).

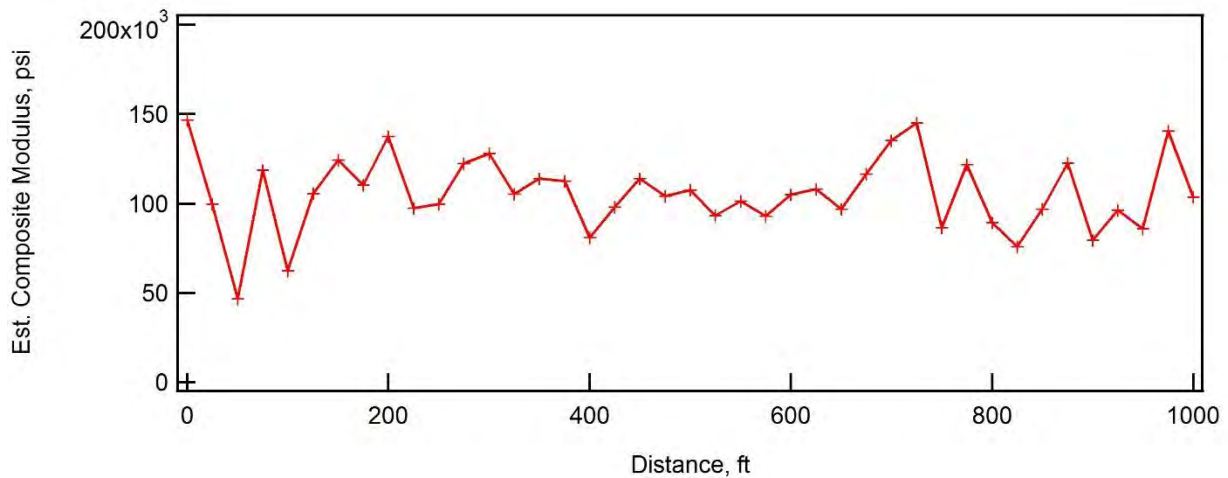


Fig. 7.37—Composite stiffness estimated using the AREA model from FWD data collected at Site 4 (HWY AT).

7.4.5 Project Level Site 5 (I-55, Pemiscot County)

Project level Site 5 is located in the southbound lane of Interstate 55 in Pemiscot County, Missouri. This pavement is an unbonded concrete overlay. The lowest layer of the pavement consists of the original PCC concrete pavement constructed in 1963 with 61.5 ft joint spacings. The PCC concrete pavement was overlaid with 1 to 3 in. of asphalt at a later date. In 2002, the asphalt was milled to about 1-in. thickness and a new 8 in. PCC surface layer was placed on the asphalt. The pavement has performed well with little evidence of surface distress (in contrast to the other unbonded overlay pavement tested at Site 8).

FWD measurements were performed in August, 2013 when the NDT testing by MS&T was performed. Later investigation of the FWD data showed a malfunctioning D1 receiver

which made most of the data useless for further interpretation. Therefore, MoDOT retested this site (only the joints) on April 30, 2014. The RDD testing at this site was performed on December 12, 2013.

The two-mile deflection section recorded with the RDD is shown in Fig. 7.38, with the 1000 ft test section shaded. An expanded view of the 1000 ft section is presented in Fig. 7.39. Histograms of the deflections from the 1000 ft and two mile sections are shown in Fig. 7.40. Tabular values are presented in Table 7.6.

As expected, the deflections are very small at this site due to the thick and stiff pavement. Deflections over the 1000 ft section are very small and fairly constant. Over the two-mile stretch, there are three regions – each about 800 ft in length- where the deflections are much higher. It is not clear what the cause of the higher deflections is in these regions.

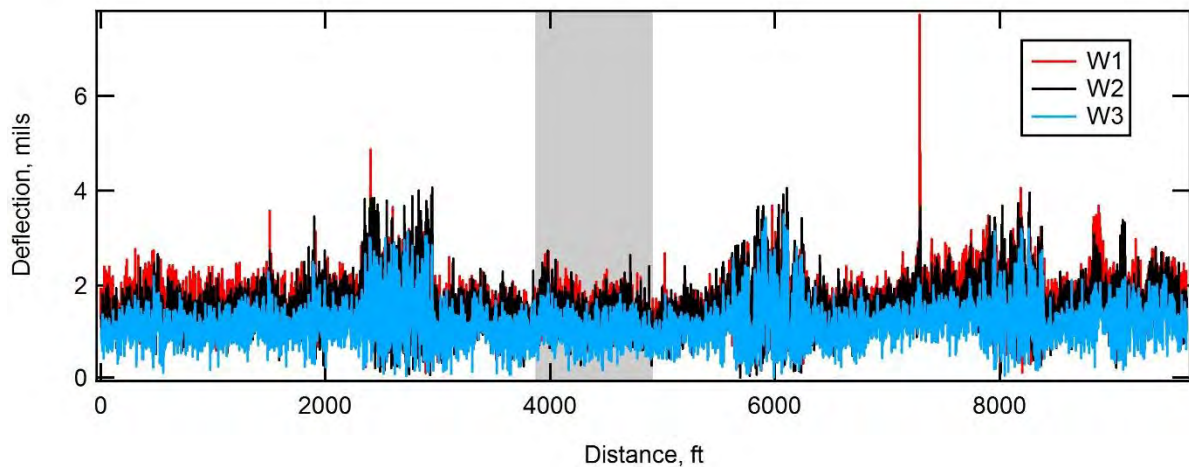


Fig. 7.38–RDD data over the full 2.0 mile extent on I-55 Pemiscot County with the 1000 ft test section shaded.

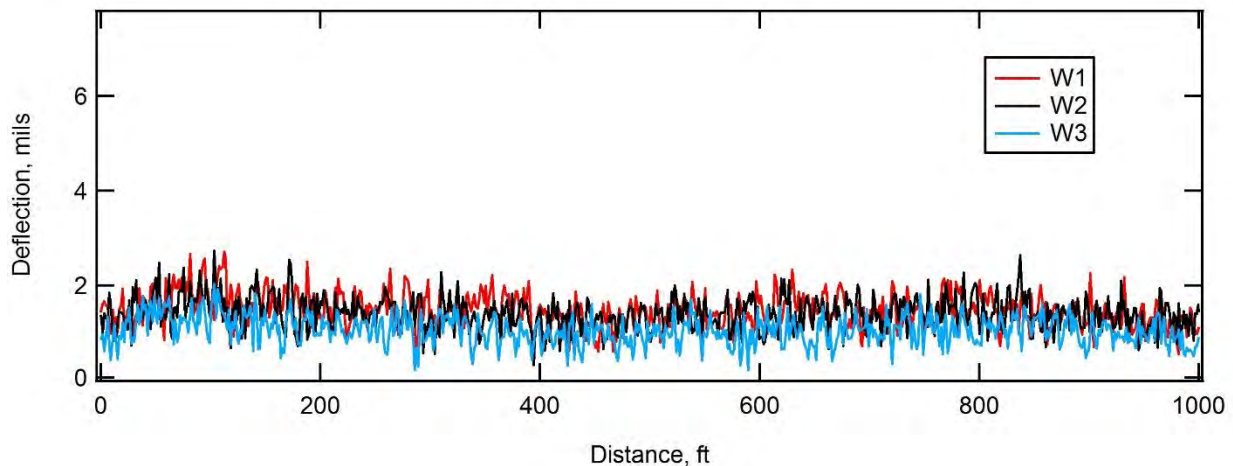


Fig. 7.39–RDD data over the 1000 ft test section on I-55 Pemiscot County.

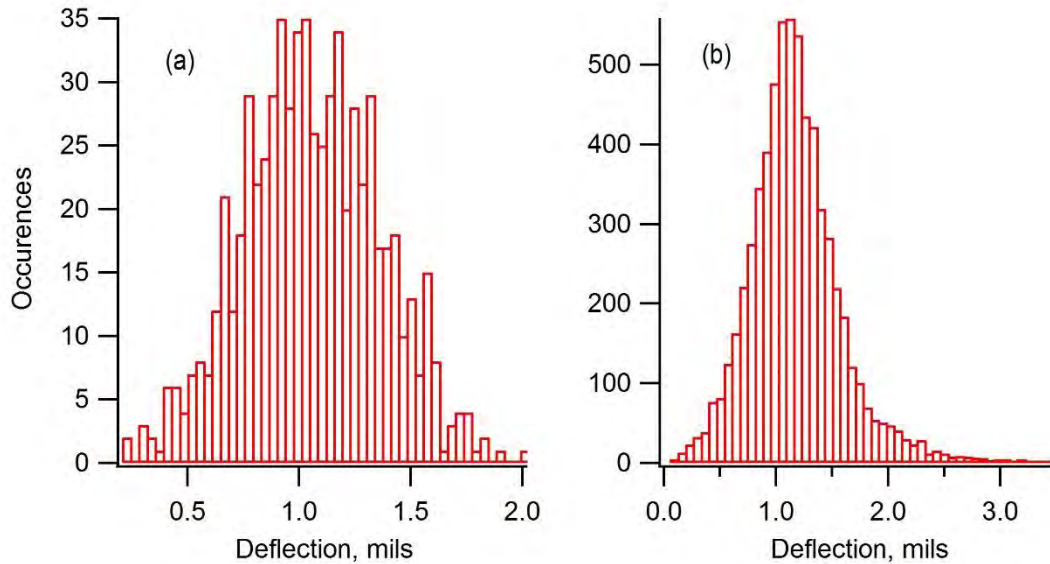


Fig. 7.40– Histogram of W3 displacement measured on the (a) 1000 ft section and the (b) 1.5 mile section.

Table 7.6–W3 deflection statistics for the 2.0 mile and 1000-ft section of I-55 in Pemiscot County

Profile	Mean Deflection (mils)	Standard Deviation	Coefficient of Variation	Peak Deflection	Minimum Deflection
1000 ft	1.66	0.44	0.27	3.32	0.53

The deflection characteristics changed greatly across this section also. Fig. 7.41 shows a typical 500 ft stretch where the location of the joints, spaced at 15 ft intervals, are clearly evident in the profile. This stretch of pavement is outside of the 1000 ft test section. In contrast, a 500 ft stretch of pavement within the 1000 ft section is shown in Fig. 7.42. In this case the locations of the individual joints are not apparent, as several peaks are evident. The surface of the pavement was similar in both cases, so the difference is likely due to some subsurface differences in the support conditions. Due to the inability to identify individual joints in the 1000 ft section, LTE was not calculated from the RDD data.

Another interesting aspect of the data in the 1000 ft section is that in some regions the deflection 3 ft away from the load (W2) was larger than the deflection under the load (W1), as shown with the arrows in Fig. 7.43. One possible explanation is that rocking of the slab is occurring.

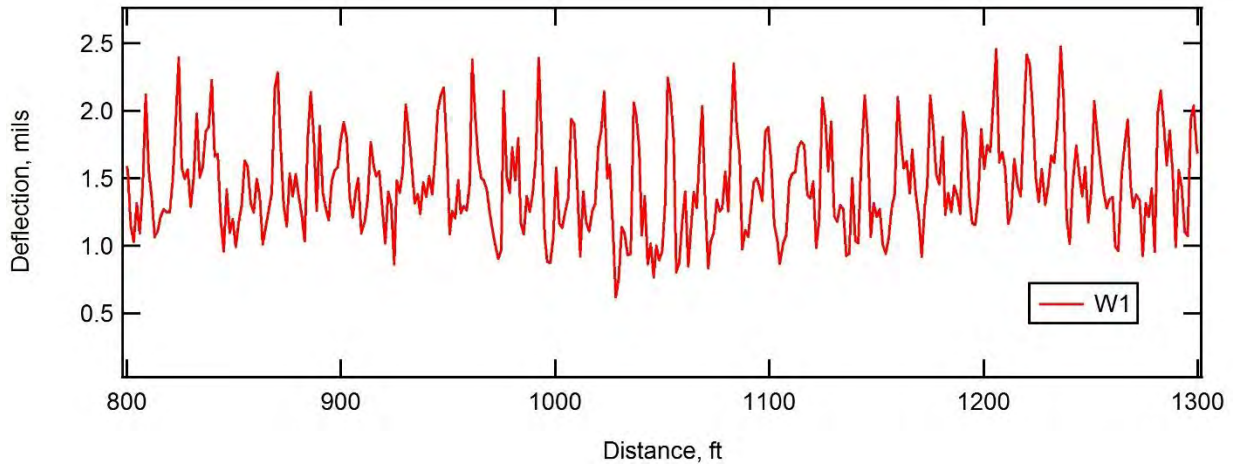


Fig. 7.41—RDD data over the 500 ft section where location of joints is clear.

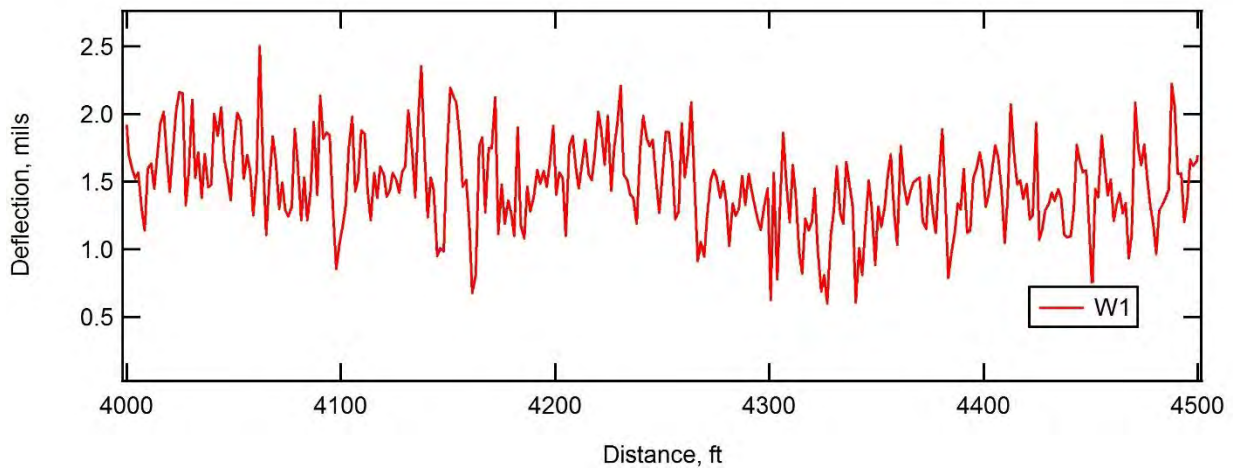


Fig. 7.42—RDD data over 500 ft length of 1000 ft test section showing difficulty identifying individual joints.

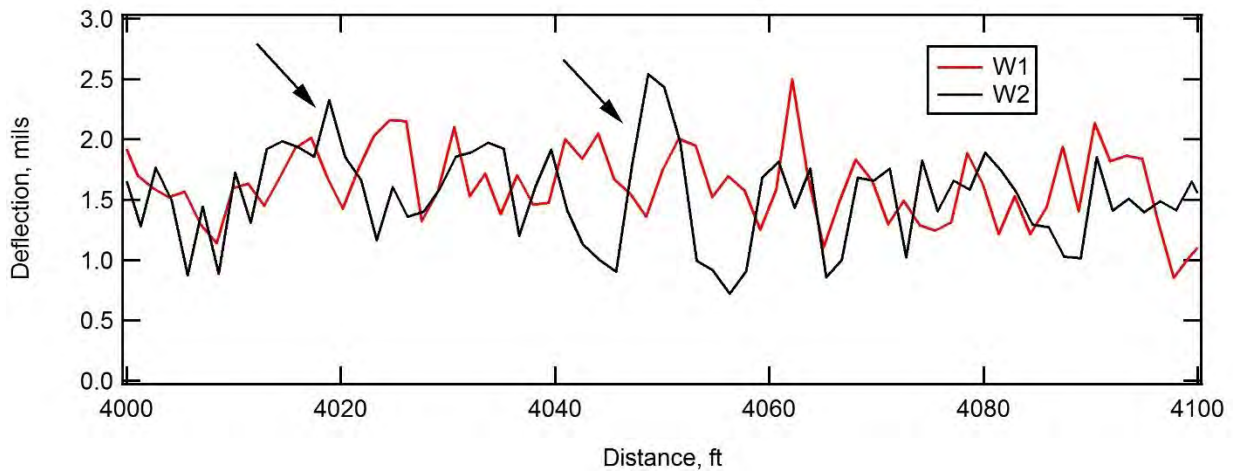


Fig. 7.43—RDD data over 500 ft length of 1000 ft test section showing difficulty locating joints.

Falling weight deflectometer data were collected at every third joint starting with the first joint in the 1000 ft profile. Load transfer efficiency values were calculated entering and leaving each joint for each from the three weight drops, as shown in Fig. 7.44. As expected, the LTE values were high (80 to 90%) and showed little change with the magnitude of the drop height (i.e. load).

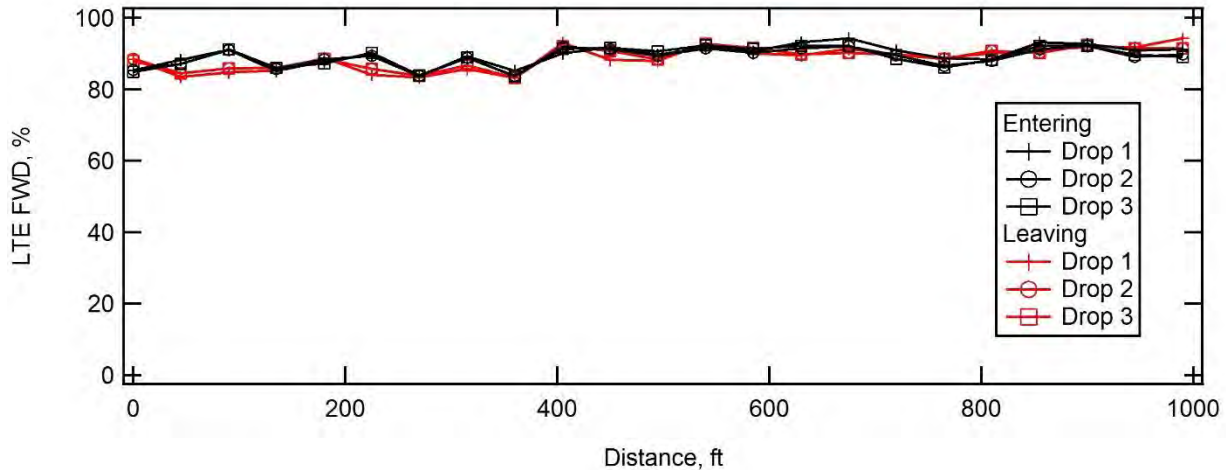


Fig. 7.44–Joint LTE measured using entering and leaving FWD deflections at every third joint.

7.4.6 Project Level Site 6 (I-55, Perry County)

Project level Site 6 is located in the southbound lane of Interstate 55 in Perry County, Missouri. This pavement is a 9 in. thick PCC pavement. Due to adverse weather conditions (rain and snow) when the RDD device was in Missouri it was not possible to perform RDD testing at this site. FWD testing was originally performed on September 24, 2014, however, as noted previously erroneous FWD data were collected on the D1 sensor due to a malfunction in the sensor. The D1 sensor is used for both entering and leaving LTE calculations so it was not possible to calculate LTE from this data. Retesting of this site was not performed.

7.4.7 Project Level Site 7 (HWY U)

Project level Site 7 is located on HWY U in Dent County, Missouri. The pavement section consists of a thin asphalt surface layer. Coring recovery ranged from 1 in. to 4 in. at this site. Surface cracking was evident through the test section. RDD testing was not performed at this site.

Fig. 7.45 shows the FWD center deflections normalized to 10 kip load as a function of distance. Fig. 7.46 shows the subgrade modulus estimated using the Hogg method, and Fig. 7.47 shows the estimated composite modulus from the AREA method. Due to the very thin asphalt pavement at this site the deflections were much higher and the composite stiffness was much lower than the other sites.

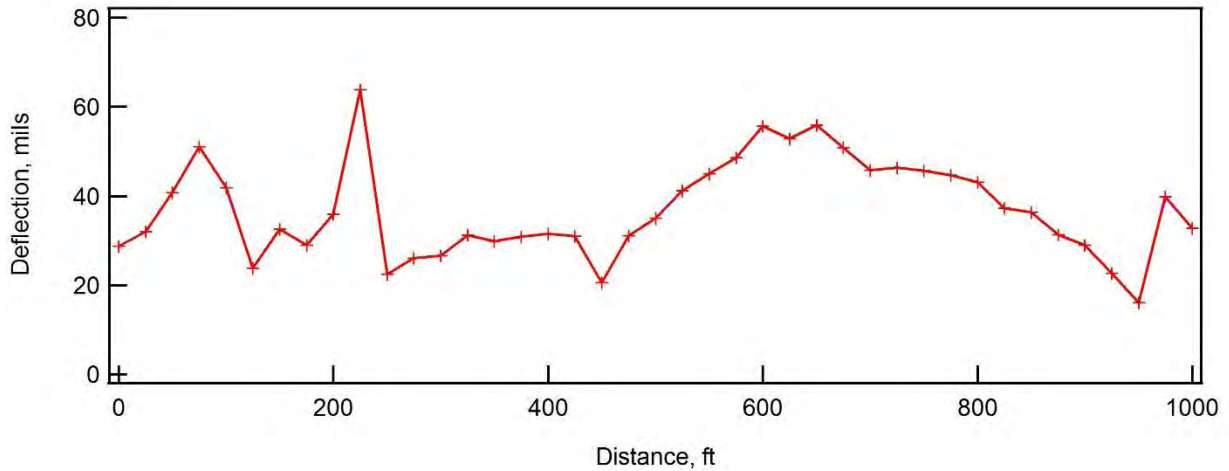


Fig. 7.45—Deflection profile obtained from the first receiver of FWD measurements normalized to a load of 10 kips.

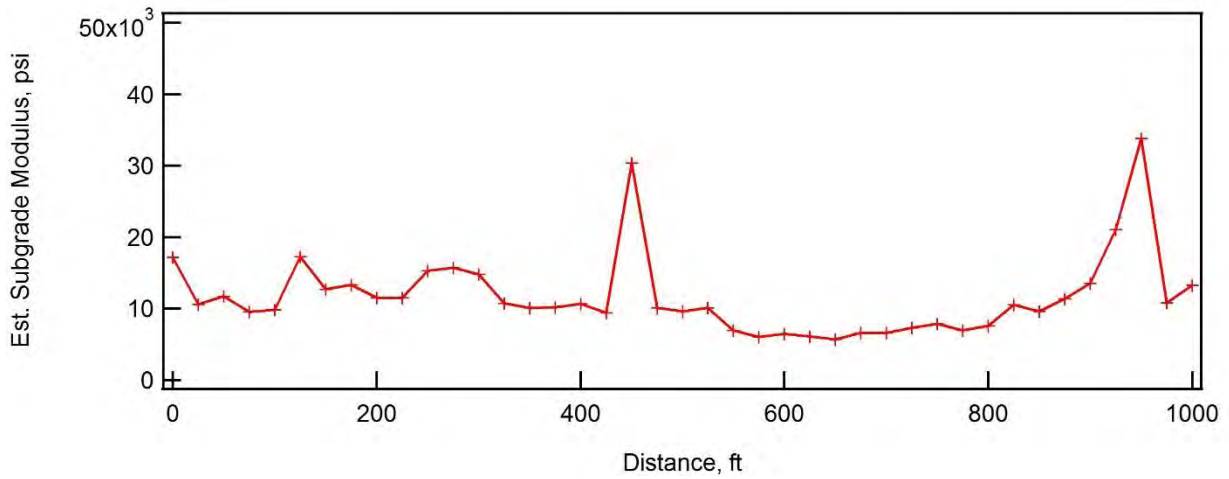


Fig. 7.46—Subgrade modulus estimated using the Hogg model from FWD data collected at Site 7 (HWY U).

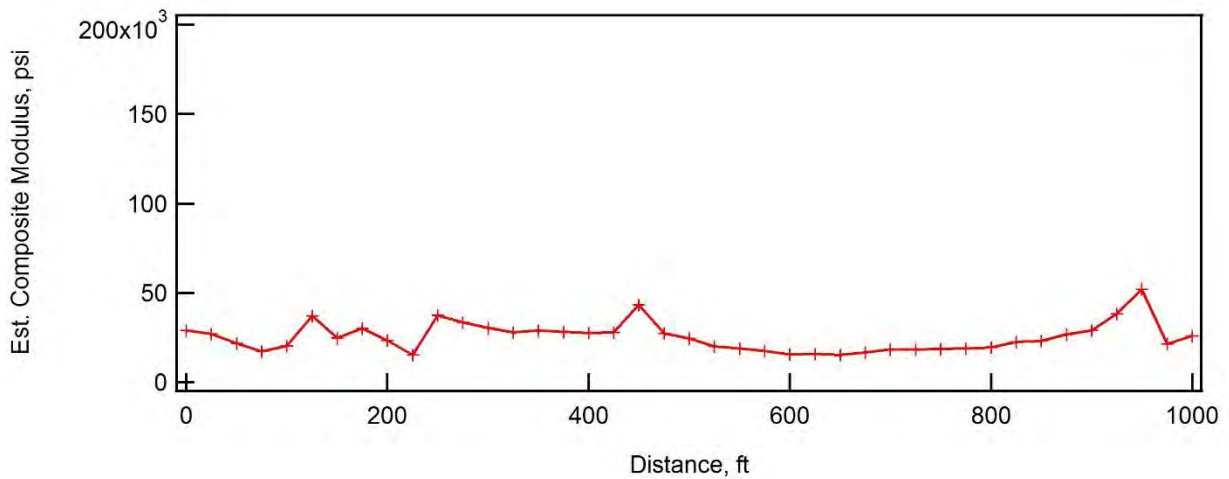


Fig. 7.47—Composite stiffness estimated using the AREA model from FWD data collected at Site 7 (HWY U).

7.4.8 Project Level Site 8 (I-35)

Project-level Site 8 is located on the north-bound lane of interstate I-35 near Daviess County, Missouri. The pavement at this site is a poorly performing unbonded concrete overlay. The original pavement at this site consisted of 9 in. thick PCC with 61.5 ft joint spacing. The pavement was overlaid with a 1.75 in. asphalt layer in 1994. The last rehabilitation in 2010 involved placement of a 7 in. PCC layer with 15 ft joint spacing on the asphalt layer. Since placement of the last concrete layer, this pavement has performed poorly with extensive cracking and slab shattering. The poor performance has been attributed to insufficient and inconsistent thickness of the concrete overlay when placed. The NDT measurements performed in August, 2013 by MS&T were performed prior to any rehabilitation at this site. FWD data were also collected in August 2013, but as noted earlier the data were erroneous due to a malfunctioning sensor. The RDD measurements were performed in November, 2013. Between the time of the NDT measurements and the RDD measurements rehabilitation measures were performed at this site. This included undersealing of shattered slabs (Fig. 7.48a) and full replacement of slabs (Fig. 7.48b). In addition, the concrete panels were saw-cut into quarters to minimize thermal deformations of the slab. Repeat FWD measurements (at the joints only) were performed by MoDOT in May, 2014. Due to the differences in pavement conditions at the time of the deflection measurements (FWD and RDD) and NDT testing, direct comparisons are difficult to make.

The RDD deflection profile recorded over the full two-mile section is shown in Fig. 7.49. The 1000 ft test section is shown as the shaded region in Fig. 7.49. An expanded view of the 1000 ft section is shown in Fig. 7.50. The 1000 ft section is in a region of high deflections relative to the other portions of the two-mile section. A comparison of W3 deflection histograms (Fig. 7.51) shows the much higher deflections measured in 1000 ft section. The W1 trace in Fig. 7.49 shows many spikes in the profile indicating the locations of joints at 15 ft intervals and the saw cuts used to quarter each slab.



Fig. 7.48—Photographs of 1000 ft test section on I-35NB showing (a) repair of cracked slabs (b) replacement of slabs.

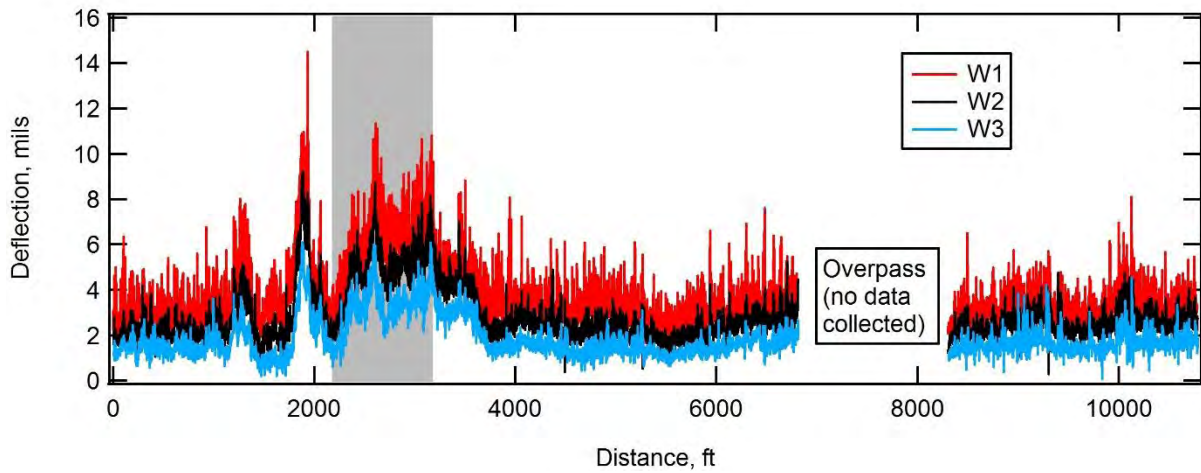


Fig. 7.49—RDD data over the full 2.0 mile extent on I-35 Northbound near Daviess County with the 1000 ft test section shaded.

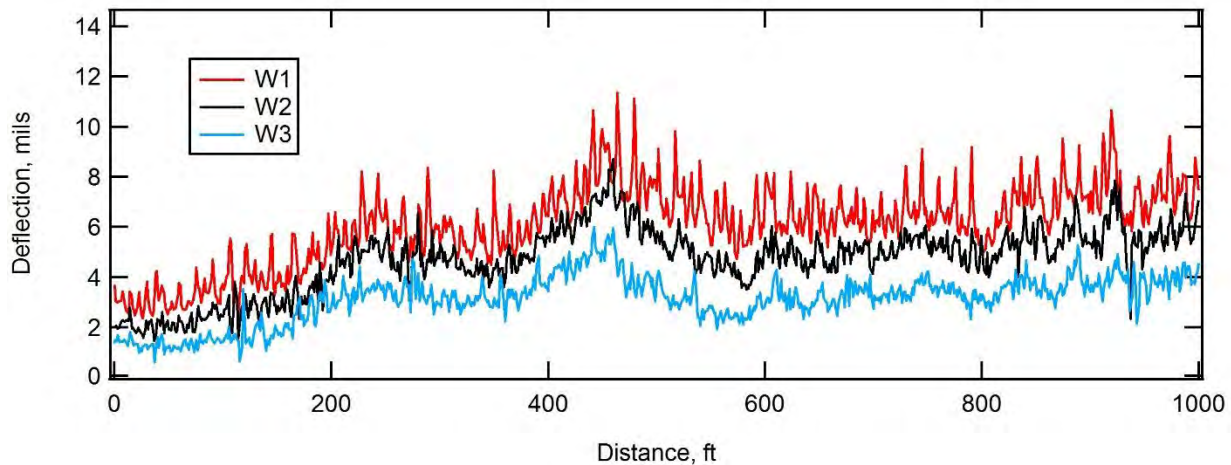


Fig. 7.50—RDD data over the 1000 ft test section on I-35 Northbound near Daviess County.

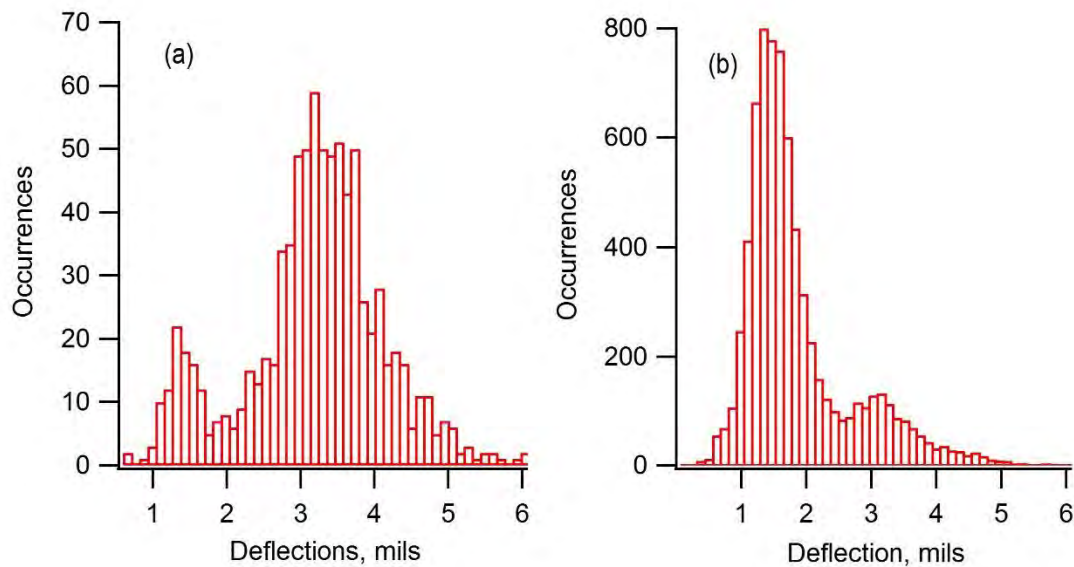


Fig. 7.51—Histogram of W3 displacement measured on the (a) 1000 ft section and the (b) 2.0 mile section of I-35 NB.

Table 7.7—W3 deflection statistics for the 2.0 mile and 1000 ft section of I-35 NB near Daviess County

Profile	Mean Deflection (mils)	Standard Deviation	Coefficient of Variation	Maximum Deflection	Minimum Deflection
1000 ft	3.16	0.94	0.30	6.08	0.592
2.0 mile	1.86	0.87	0.47	6.08	0.063

Deflections at joints were measured using the FWD in May, 2014 after problems with the malfunctioning D1 sensor were fixed. Measurements were performed at every third joint

using the D1 and D8 sensors (i.e. leaving the joint). Fig. 7.52 shows a comparison of deflection from the W1 and W2 sensors of the RDD with the D1 and D8 sensors of the FWD (all normalized to 10 kip load). From 200 to 1000 ft the magnitude of the deflections are similar between the FWD and RDD, but between 0 and 200 ft the joint deflections from the FWD are much higher. The LTE at the joints tested by the FWD were calculated and compared to LTE values measured at the same joints using the RDD. This comparison is shown in Fig. 7.53. The FWD showed very consistent and high LTE (50 to 70%) across the 1000 ft section. The RDD also showed fairly consistent LTE values but much lower efficiency (50 to 60%) as compared to the FWD results. These lower values are likely due to the much larger spacing between the sensors used for the RDD calculation (3.18 ft) as compared to the FWD calculation (1 ft).

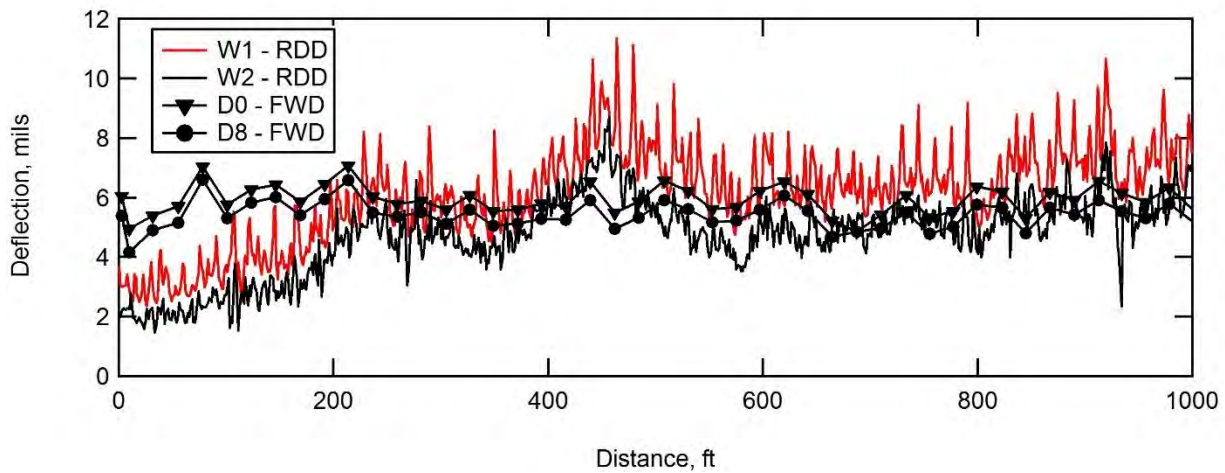


Fig. 7.52—Comparison of joint deflections from FWD testing with deflection profile from RDD measurements at Site 8.

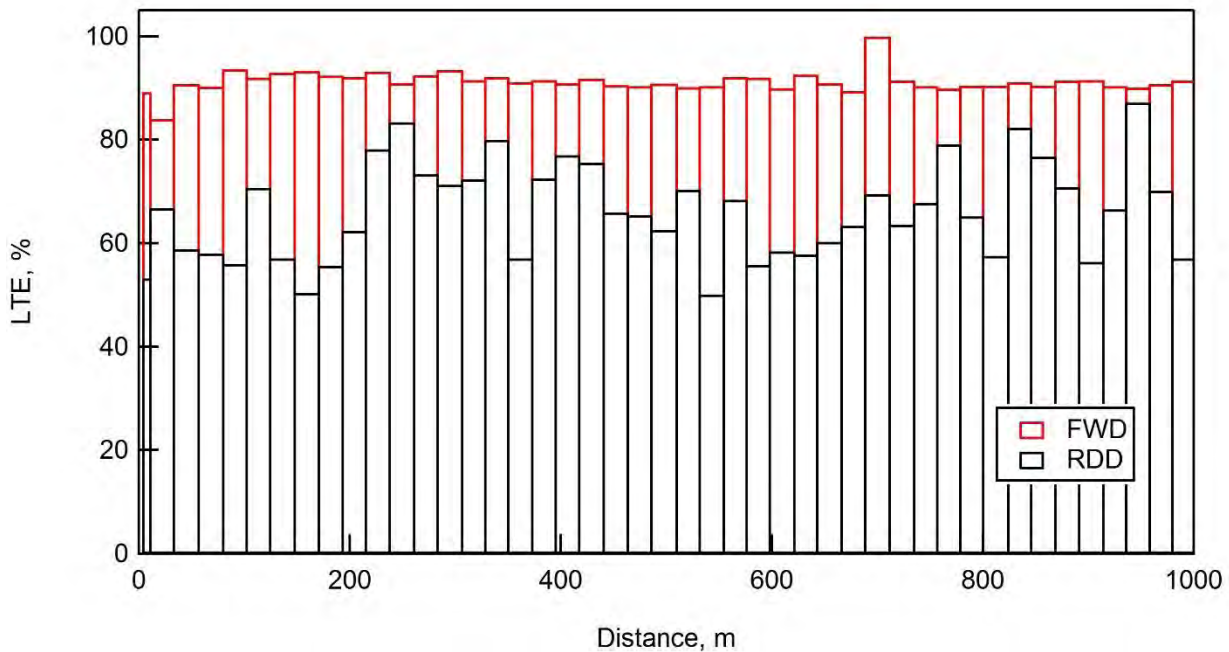


Fig. 7.53—Comparison of joint LTE measured with the FWD and the RDD at Site 8.

7.4.9 Additional Project-Level Site for RDD Testing (I-35 Southbound)

An extra site was tested on I-35 north of Site 8. This site was chosen because it is an example of a good-performing unreinforced PCC pavement. The pavement consists of a 14 in. thick PCC with 15 ft joint spacing. The pavement has been in service since 1996 and shows minimal surface distress. A photograph of the pavement is shown in Fig. 7.54.



Fig. 7.54—Photograph of section on I-35SB showing the good quality of pavement.

The RDD deflection profile recorded over the 1.6 mile section is shown in Fig. 7.55. A histogram of the W3 deflections is presented in Fig. 56 and a table of values is presented in Table 7.8. This profile differs from the others in a few ways. First, the deflections across this 1.6 mile section are remarkably consistent, as seen in the histogram of W3 deflections and the low coefficient of variation (COV) in Table 7.8. Also, the magnitude of the deflections on W3 are very low, with an average of 1.48 mils. In addition, the deflection profile has some unusual features. For example, the W3 profile shows downward spikes that are not as apparent in other profiles. Figure 7.57a shows an example of these downward spikes on W3 and W2. In other locations, the W2 deflection is greater than the W1 deflection at a joint, as shown in Figure 7.57b. Without other measurements at this site it is not possible to establish the cause of these unusual features in the RDD data. However, given the good performance of this pavement, these features do not appear to indicate problems with the pavement.

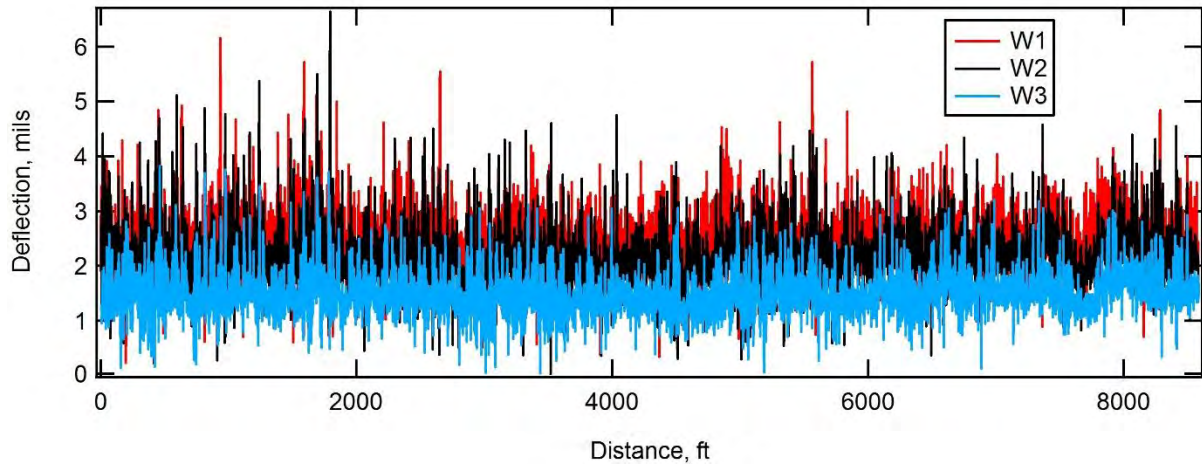


Fig. 7.55—RDD data over the full 1.6 mile extent on I-35 Southbound site.

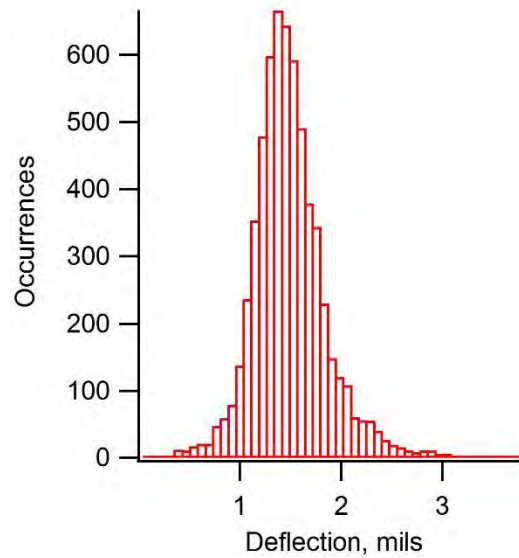


Fig. 7.56—Histogram of W3 displacement measured on the 1.6 mile section of I-35 SB.

Table 7.8—W3 deflection statistics for the 1.6-mile section of I-35 SB

Profile	Mean Deflection (mils)	Standard Deviation	Coefficient of Variation	Maximum Deflection	Minimum Deflection
1.6 mile	1.48	0.37	0.25	3.82	0.042

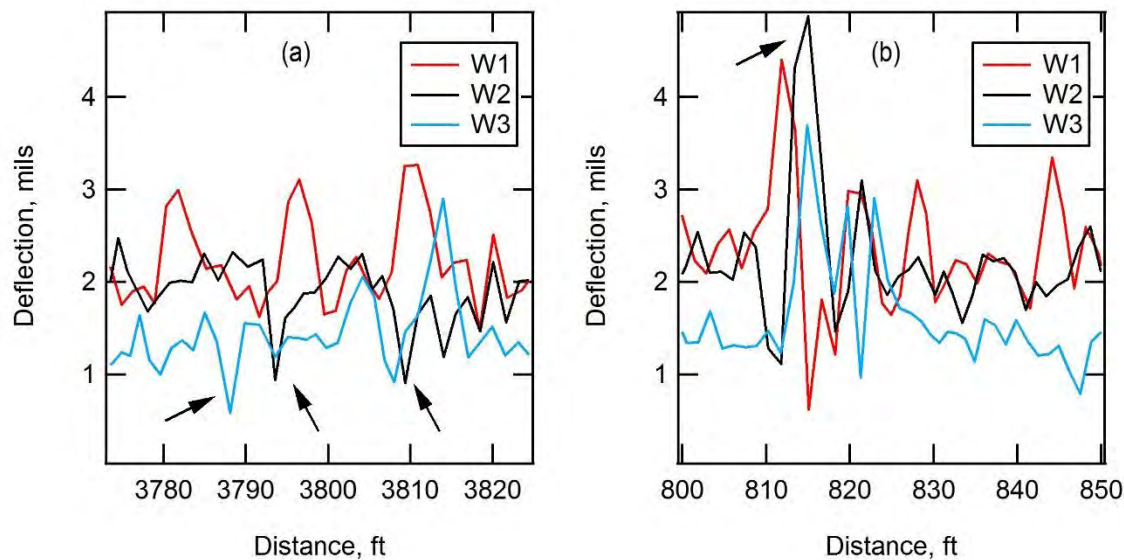


Fig. 7.57—Example deflection profiles at two locations showing unusual features in the profile, namely (a) downward spikes in the W3 profile, and (b) higher deflections on W2 than W1.

7.5 Concluding Remarks on Application of the RDD to Missouri Pavement Management

The objective of this portion of the study was to evaluate the potential application of a Rolling Dynamic Deflectometer (RDD) to Missouri’s pavement management program. Unlike the other technologies evaluated in Task 4 of this study, the RDD is not a commercial product that can be purchased off the shelf. There are only two in current existence; the first (used in this study) is the original prototype built from a modified Vibroseis truck, and the second is a custom-built buggy mounted device (termed the TPAD) that is operated by the Texas Department of Transportation (TxDOT). Implementing the RDD in Missouri’s pavement management program would require construction of a custom-built device.

In this study the RDD was applied to six pavement sites around Missouri representing different pavement types (PCC, full-depth asphalt, asphalt-overlaid PCC, and unbonded PCC pavements) and different levels of current performance. The RDD measurements at these sites were used to assess the quality of data that is obtained with the RDD and better understand the type of information that can be discerned about the pavement profile. The results from this study demonstrated that the RDD can effectively and quickly collect very high spatial-resolution (2 to 3 ft intervals) deflection data on a wide range of pavement systems. The unique view of the pavement deflection profile provided by the RDD is not practically obtainable with existing technologies. For example, the results from Site 2 (HWY 54) in Fig. 7.20 illustrate the great variability in pavement deflections that can be observed along this short 0.65 mile stretch of pavement using RDD data collected in about 30 minutes of testing time. To the extent that future pavement performance can be inferred from current deflections of the pavement system, the RDD provides valuable structural performance information that can supplement functional performance information in the pavement management program.

However, a significant limitation of the RDD is the current qualitative approach to data interpretation. At this stage of development, procedures have not been developed to back-calculate pavement parameters (such as thickness, stiffness, subgrade support) as can be done with FWD data. Therefore, the measured deflections provide a gross assessment of the pavement system (dominated primarily by the subgrade support, it appears). Detecting regions of stripping or debonding in surface asphalt layers, based on RDD deflection data alone, does not seem feasible at this stage. One of the quantitative assessments that can be performed with the RDD is load transfer efficiency (LTE) at joints in rigid pavements. The ability to rapidly and efficiently test every joint, even if covered by an asphalt overlay, is a great advantage of the RDD over the FWD.

As a pavement management tool, the RDD cannot be used at the network level to yearly evaluate structural performance information of all of Missouri's pavements, as the ARAN van does to collect functional performance information. However, the RDD could be used as a management tool to test pavements that are scheduled for rehabilitation in the near future. The ability to test at 1 to 2 mph will allow for extensive coverage of pavements in a relatively short amount of time. The structural information from the RDD could be used to identify regions in need of further study (due to anomalously high deflections) or to develop and apply more site-specific rehabilitation strategies based on structural performance. In addition, the RDD could be used as an effective quality control tool to evaluate newly constructed or rehabilitated pavements. For example, deflection criteria could be developed and the pavement assessed to detect poor performing joints, insufficient slab thickness or other construction defects.

8 NETWORK-LEVEL GROUND PENETRATING RADAR INVESTIGATIONS

8.1 Introduction

Network-level ground penetrating radar (GPR) data were acquired along two test sections of roadway: I-70 (network-level Site 9; Fig. 8.1) and MO 465 (network-level Site 10; Fig. 8.2). The test segment of I-70 extended from mile marker 84.2 to mile marker 20.8 and extended across three counties (Jackson, Saline and Lafayette); GPR data were acquired in the west-bound driving lane only. The test segment of MO 465 (Taney County only) extended from the intersection with HWY 76 to the intersection with US 65. GPR data were acquired in all four lanes (two southbound and two northbound). The objective of both network-level GPR surveys was to estimate pavement layer thicknesses.

8.2 Overview of Network-Level GPR Investigations

Network-level GPR data were acquired along two test sections of roadway: I-70 (network-level Site 9; Fig. 8.1) and MO 465 (network-level Site 10; Fig. 8.1).

Two higher-frequency 2.0 GHz horn antennae and one lower-frequency GSSI 400 MHz antenna were used to acquire example network-level GPR control. All three antennae were coupled to a vehicle (truck) with GPS capabilities. The 2.0 GHz horn antennae were mounted on the front of the truck; the 400 MHz antenna was mounted to the rear of the truck (Fig. 8.3). Acquisition parameters (4 scans/ft for 2.0 GHz antennae; 4 scans/ft for 400 MHz antenna; 325 scans/sec; 256 samples/scan for Site 9 and 6 scans/ft for 2.0 GHz antennae; 6 scans/ft for 400 MHz antenna; 325 scans/sec; 256 samples/scan for Site 10) were selected to enable quality GPR data collection at near-highway speeds (up to 50 miles per hour).



Fig. 8.1– Map showing network-level Site 9 (I-70). The test segment of I-70 extended from mile marker 84.2 to mile marker 20.8 and extended across three counties (Jackson, Saline and Lafayette). GPR data were acquired in the west-bound driving lane only.



Fig. 8.2– Map showing network-level Site 10 (MO 465). The test segment of MO 465 (Taney County only) extended from the intersection with HWY 76 to the intersection with US 65. GPR data were acquired in all four lanes (two north-bound; two south-bound).

8.3 Network-Level GPR Investigations

8.3.1 Network-Level Site 9 (I-70 WB)

The network-level Site 9 pavement consisted of approximately 10-12 in. of bituminous mix (BM) overlying 8-10 in. of portland cement concrete (PCC) with embedded wire mesh. The objective of the network-level Site 9 GPR investigation was two-fold: 1) to evaluate (at near-highway speeds) the condition of an extended segment (network-level) of pavement (BM overlying PCC); and 2) to estimate pavement layer thicknesses. The pavement surface along network-level Site 9 appeared (visually) to be in good condition. However, the network-level Site 9 bridge decks showed signs of cracks and patches. The objective of the network-level Site 9 GPR investigation was to estimate variations in estimated pavement layer thicknesses along an extended section (network-level) of pavement (BM over PCC).

GPR data were in the west-bound driving lane using a GSSI SIR-30 system equipped with two higher-frequency 2.0 GHz GSSI 42000S horn antennas (mounted on the front of the truck; Fig. 8.3) and one lower-frequency 400 MHz GSSI 5103 shielded antenna (mounted on the rear of the truck; Fig. 8.4). As depicted in Fig. 8.4 and Fig. 8.6, the two 2.0 GHz horn antennas were mounted with 4 ft center-to-center spacing. Antenna 1 (channel 1) was mounted on driver side; antenna 2 (channel 2) was mounted on the passenger side. The 400 MHz antenna was coupled to the trailer hitch of the truck and set up as channel 3. A mechanical distance measuring instrument (DMI) was mounted on the survey truck wheel to measure distances along the profile based on number of revolutions per unit of distance and to trigger the GPR

instruments (Fig. 8.5). For GPS coordinates control, a GPS antenna was mounted on the top of the survey truck as shown in Fig. 8.6.



Fig. 8.3– Two higher-frequency (2.0 GHz) GPR antennae were mounted to the front of the truck.



Fig. 8.4– The lower-frequency (400 MHz) GPR antenna was mounted to the back of the truck.



Fig. 8.5– Distance measuring instrument (DMI) mounted on the truck wheel.

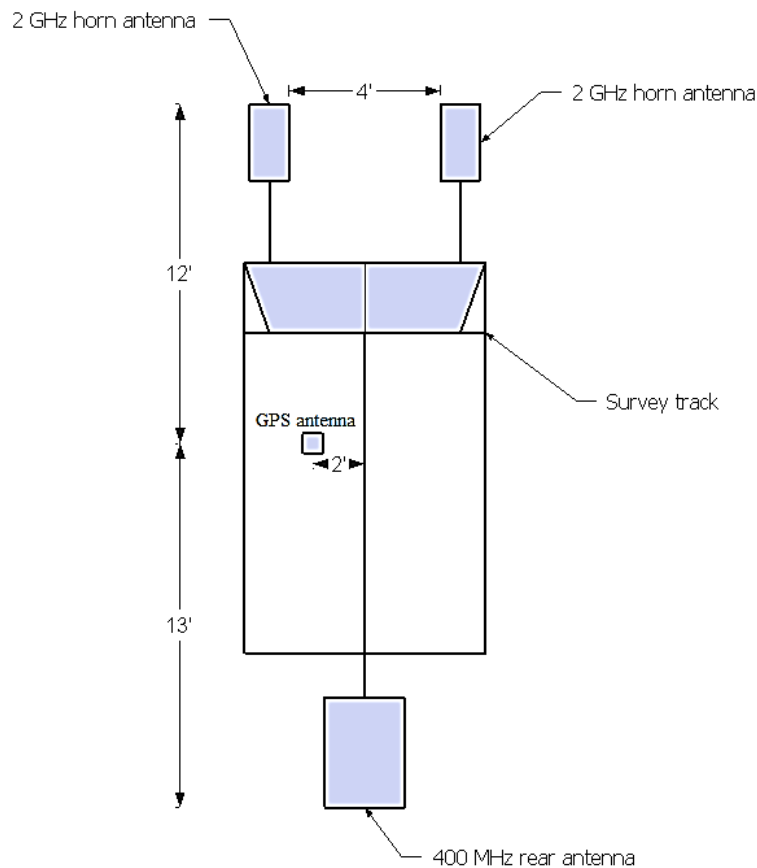


Fig. 8.6– Schematic drawing of survey system design (not to scale).

The GPR data were processed using GSSI RADAN 7 software. Initial processing steps included: time-zero correction, the application of basic filters for possible noise elimination and to enhance visual representation of data for interpretation purposes; and time-to-depth conversion. The reflection from the BM/PCC interface was identifiable on all acquired high-frequency and low-frequency GPR data. The reflection from the base of the PCC was confidently identified all low-frequency GPR data. However, the reflection from the base of the

PCC could not be confidently identified on all high-frequency GPR data, presumably because the pavement was more than 18 in. thick (the manufacturer indicates the effective investigative depth of the of the high-frequency GPR antennae is approximately 18 in.) and because of the presence of wire mesh (which masks the reflections from the underlying base PCC). Example segments of 2.0 GHz and 400 MHz GPR data are shown as Fig. 8.8 for comparison purposes.

Nine (9) core samples were acquired for correlation purposes. In-field descriptions of core properties included diameter, length, number of pieces, length of the specimen, quality of material, and signs of deterioration and/or defects. Example low- and high-frequency GPR data acquired in immediate proximity to core locations 01-09 are shown as Fig. 8.9 to Fig. 8.17, respectively.



Fig. 8.7– Schematic showing relative locations of the network-level Site 9 (segment of I-70) GPR traverses. Solid black lines represent the boundaries of west-bound driving lane. Mile marker 51 (MM 51) is shown for illustration purposes. The test segment of I-70 extended from mile marker 84.2 to mile marker 20.8 and extended across three counties (Jackson, Saline and Lafayette); GPR data were acquired in the west-bound driving lane only.

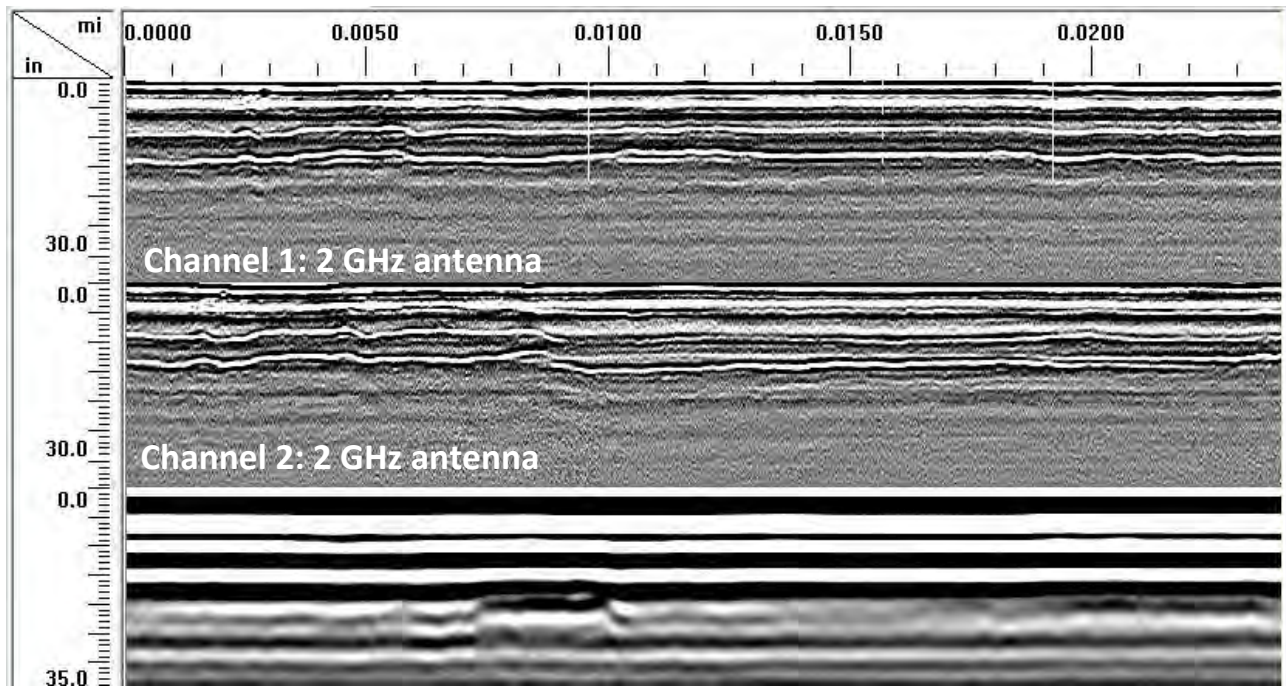


Fig. 8.8— Example of GPR data: Three parallel non-interpreted GPR profiles are presented. Two 2.0 GHz profiles and one 400 MHz GPR profile. A dielectric permittivity of 6.5 was used to convert reflection times to reflector depths. The horizontal axis is in units of feet; the vertical axis is in units of inches.

Table 8.1–Site 9 (I-70) core locations. The description is based on the visual assessment only, no lab testing was conducted.

Core	Mile mark	BM thickness and brief description	PCC thickness and brief description
01	74.3	BM layer has a total thickness of 12.0 in. Debonding/delamination is present at a depth of approximately 2 in.	PCC layer is intact and is approximately 7.5 in. thick
02	70.4	BM layer has a total thickness of 10.0 in. Debonding/delamination is present at a depth of approximately 2 in. and 7.5 in.	PCC layer is intact and is approximately 8.0 in. thick
03	67.5	BM layer has a total thickness of 10.25 in. Debonding/delamination is present at a depth of approximately 4 in.	PCC layer is intact and is approximately 8.0 in. thick
04	66.2	BM layer has a total thickness of 11.5 in. Debonding/delamination is present at a depth of approximately 7 in.	PCC layer is intact and is approximately 8.0 in. thick
05	62.2	BM layer has a total thickness of 9.5 in. The base of the BM layer appears to be deteriorated.	PCC layer is intact and is approximately 7.75 in. thick
06	52.3	BM layer has a total thickness of 8.5 in. with no visual evidence of deterioration	PCC layer is intact and is approximately 8.75 in. thick
07	44.0	BM layer has a total thickness of 8.5 in. Debonding/delamination is present at a depth of approximately 6.5 in. The base of the BM layer appears to be highly deteriorated.	PCC layer is approximately 8.5 in. thick. Delamination is present at a depth of approximately 12.5 in.
08	36.2	BM layer has a total thickness of 13.0 in. Debonding/delamination is present at a depth of approximately 3.5 in., 8.5 in., 10.5 in. and 12 in.	PCC layer is intact and is approximately 9.0 in. thick
09	30.2	BM layer has a total thickness of 13.0 in. Debonding/delamination is present at a depth of approximately 5.5 in. and 9.5 in.	PCC layer is approximately 9.0 in. thick. Delamination is present at a depth of approximately 13.5 in. and 20 in.

Core location 01: Two segments of Site 9 network GPR data acquired in proximity to core 01 are shown as Fig. 8.9. As noted, the reflection from the BM/PCC interface could be confidently identified on the high-frequency GPR data. The reflection from the base of the PCC could not be confidently identified on the high-frequency GPR profile, presumably because the pavement was more than 18 in. thick (the manufacturer indicates the effective investigative depth of the high-frequency GPR antenna is approximately 18 in.) and because of the presence of wire mesh (which masks the reflections from the underlying base PCC). Reflections from the BM/PCC interface, slab joints, the wire mesh, the base PCC and sub-PCC layers could be identified on the low-frequency GPR data.

Core location 02: Two segments of Site 9 network GPR data acquired in proximity to core 02 are shown as Fig. 8.10. As noted, the reflections from the BM/PCC interface and the wire mesh could be confidently identified on the high-frequency GPR data. The reflection from the base of the PCC could not be confidently identified on the high-frequency GPR profile, presumably because the pavement was more than 18 in. thick and because of the presence of wire mesh. Reflections from the BM/PCC interface, slab joints, the wire mesh, the base PCC and sub-PCC layers could be identified on the low-frequency GPR data.

Core location 03: Two segments of Site 9 network GPR data acquired in proximity to core 03 are shown as Fig. 8.11. As noted, the reflections from the BM/PCC interface and the wire mesh could be confidently identified on the high-frequency GPR data. The reflection from the base of the PCC could not be confidently identified on the high-frequency GPR profile, presumably because the pavement was more than 18 in. thick and because of the presence of wire mesh. Reflections from the BM/PCC interface, slab joints, the wire mesh, the base PCC and sub-PCC layers could be identified on the low-frequency GPR data.

Core location 04: Two segments of Site 9 network GPR data acquired in proximity to core 04 are shown as Fig. 8.12. As noted, the reflections from the BM/PCC interface and the wire mesh could be confidently identified on the high-frequency GPR data. The reflection from the base of the PCC could not be confidently identified on the high-frequency GPR profile, presumably because the pavement was more than 18 in. thick and because of the presence of wire mesh. Reflections from the BM/PCC interface, slab joints, the wire mesh, the base PCC and sub-PCC layers could be identified on the low-frequency GPR data.

Core location 05: Two segments of Site 9 network GPR data acquired in proximity to core 05 are shown as Fig. 8.13. As noted, the reflections from the BM/PCC interface and the wire mesh could be confidently identified on the high-frequency GPR data. The reflection from the base of the PCC could not be confidently identified on the high-frequency GPR profile, presumably because the pavement was more than 18 in. thick and because of the presence of wire mesh. Reflections from the BM/PCC interface, slab joints, the wire mesh, the base PCC and sub-PCC layers could be identified on the low-frequency GPR data.

Core location 06: Two segments of Site 9 network GPR data acquired in proximity to core 06 are shown as Fig. 8.14. As noted, the reflections from the BM/PCC interface and the wire mesh

could be confidently identified on the high-frequency GPR data. The reflection from the base of the PCC could not be confidently identified on the high-frequency GPR profile, presumably because the pavement was more than 18 in. thick and because of the presence of wire mesh. Reflections from the BM/PCC interface, slab joints, the wire mesh, the base PCC and sub-PCC layers could be identified on the low-frequency GPR data.

Core location 07: Two segments of Site 9 network GPR data acquired in proximity to core 07 are shown as Fig. 8.15. As noted, the reflections from the BM/PCC interface and the wire mesh could be confidently identified on the high-frequency GPR data. The reflection from the base of the PCC could not be confidently identified on the high-frequency GPR profile, presumably because the pavement was more than 18 in. thick and because of the presence of wire mesh. Reflections from the BM/PCC interface, slab joints, the wire mesh, the base PCC and sub-PCC layers could be identified on the low-frequency GPR data.

Core location 08: Two segments of Site 9 network GPR data acquired in proximity to core 08 are shown as Fig. 8.16. As noted, the reflections from the BM/PCC interface could be confidently identified on the high-frequency GPR data. The reflection from the base of the PCC could not be confidently identified on the high-frequency GPR profile, presumably because the pavement was more than 18 in. thick and because of the presence of wire mesh. Reflections from the BM/PCC interface, slab joints, the wire mesh, the base PCC and sub-PCC layers could be identified on the low-frequency GPR data.

Core location 09: Two segments of Site 9 network GPR data acquired in proximity to core 09 are shown as Fig. 8.17. As noted, the reflections from the BM/PCC interface could be confidently identified on the high-frequency GPR data. The reflection from the base of the PCC could not be confidently identified on the high-frequency GPR profile, presumably because the pavement was more than 18 in. thick and because of the presence of wire mesh. Reflections from the BM/PCC interface, slab joints, the wire mesh, the base PCC and sub-PCC layers could be identified on the low-frequency GPR data.

Based on the assessment of the GPR data acquired along network level Site 9 (I-70) it was concluded that the high-frequency GPR antenna was a useful tool for mapping layers within the pavement and variations in the thickness of the layers. The high-frequency GPR antenna was not capable of confidently imaging the reflection from the base of the PCC, presumably because the pavement was more than 18 in. thick (the manufacturer indicates the effective investigative depth of the high-frequency GPR antenna is approximately 18 in.) and because of the presence of wire mesh (which masks the reflections from the underlying base PCC).

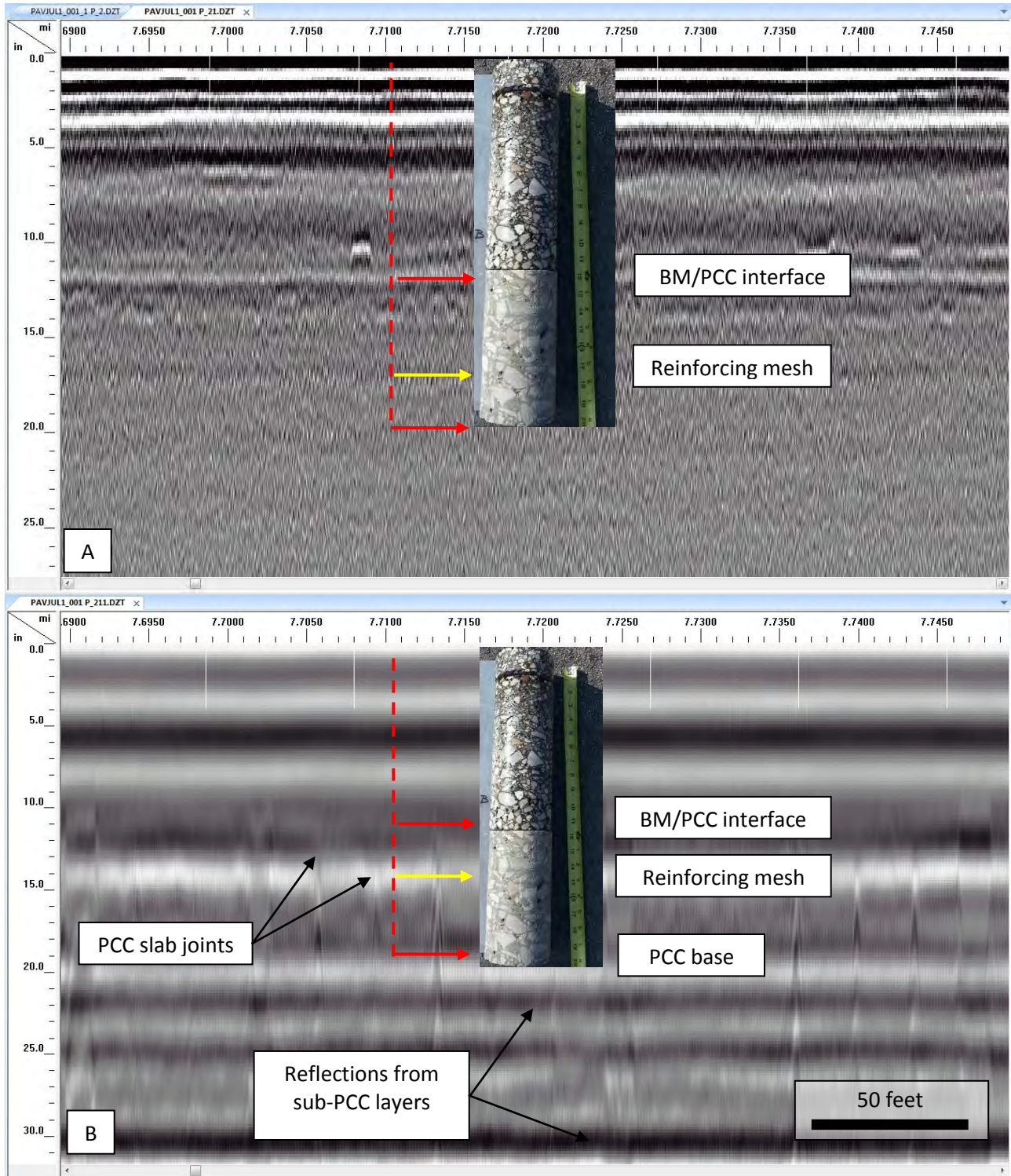


Fig. 8.9– Two segments of Site 9 network GPR data acquired in proximity to core 01: A) high-frequency GPR data acquired with 2.0 GHz air-launched antenna (one of two channels is shown); B) low-frequency GPR data acquired with 400 GHz antenna. Core 01 is superposed on the GPR data. A dielectric permittivity of 8.0 was used to convert reflection times to reflector depths. The horizontal axis is in units of feet; the vertical axis is in units of inches.

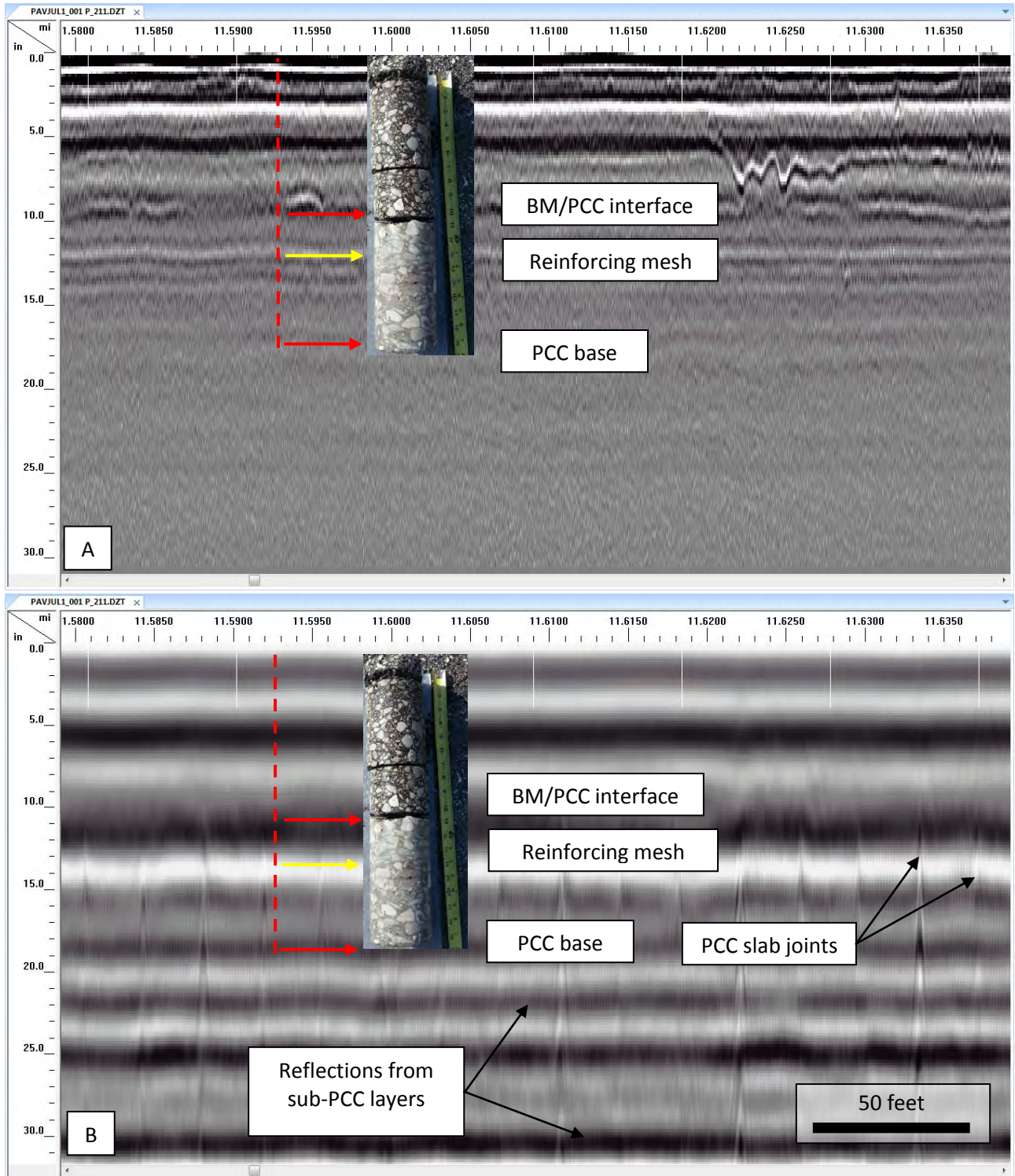


Fig. 8.10– Two segments of Site 9 network GPR data acquired in proximity to core O2: A) high-frequency GPR data acquired with 2.0 GHz air-launched antenna (one of two channels is shown); B) low-frequency GPR data acquired with 400 GHz antenna. Core O2 is superposed on the GPR data. A dielectric permittivity of 8.0 was used to convert reflection times to reflector depths. The horizontal axis is in units of feet; the vertical axis is in units of inches.

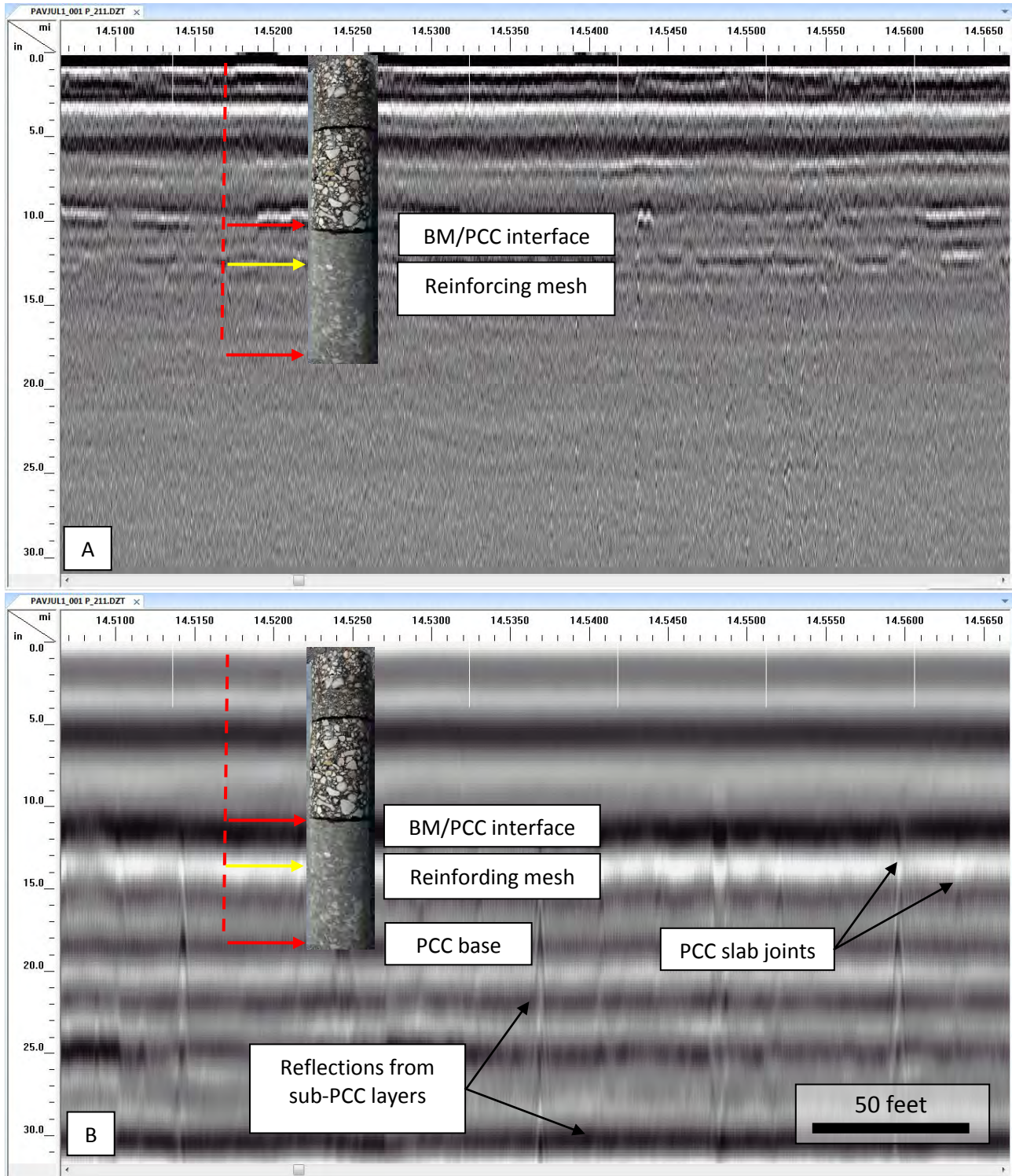


Fig. 8.11– Two segments of Site 9 network GPR data acquired in proximity to core O3: A) high-frequency GPR data acquired with 2.0 GHz air-launched antenna (one of two channels is shown); B) low-frequency GPR data acquired with 400 GHz antenna. Core O3 is superposed on the GPR data. A dielectric permittivity of 8.0 was used to convert reflection times to reflector depths. The horizontal axis is in units of feet; the vertical axis is in units of inches.

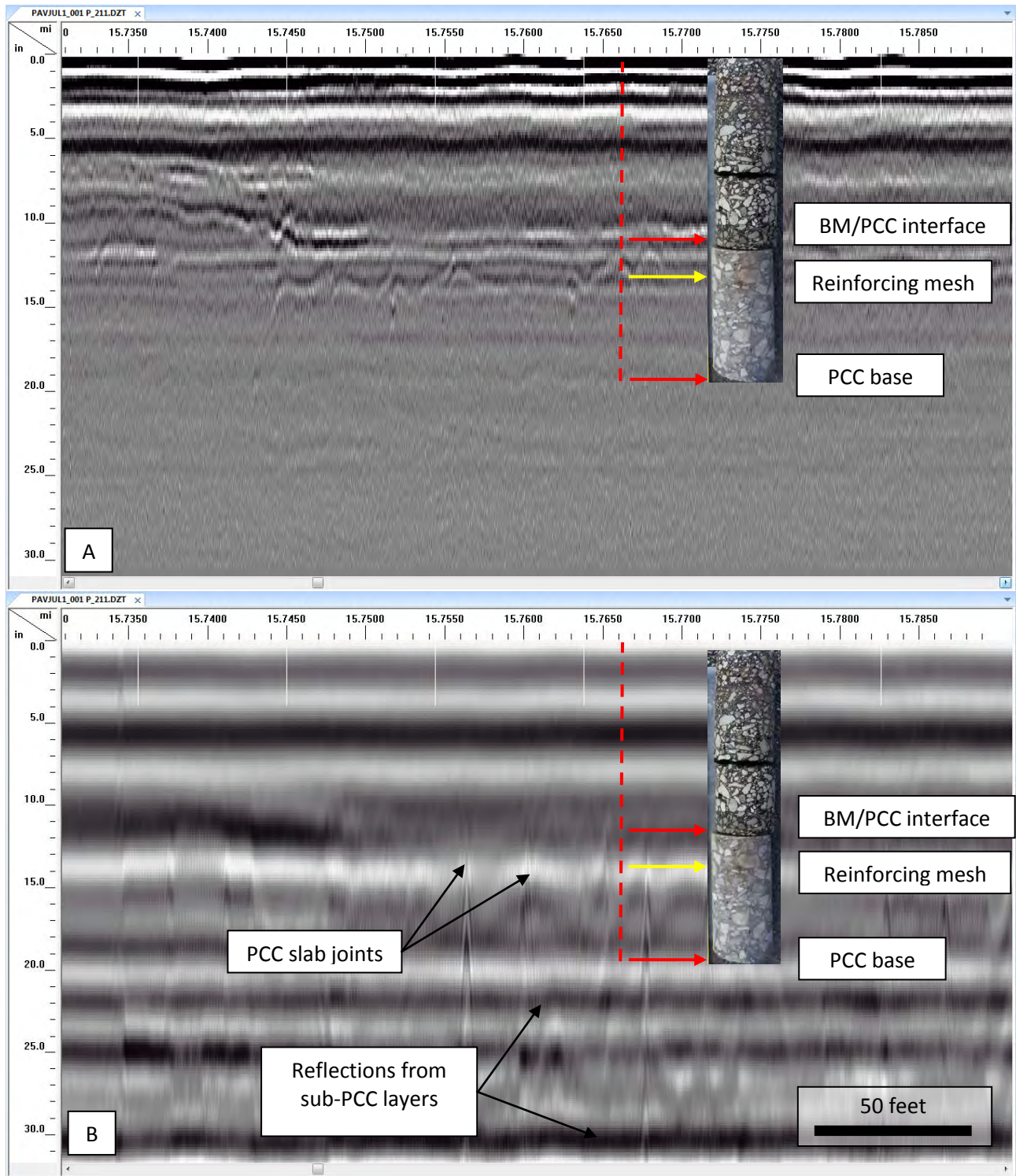


Fig. 8.12– Two segments of Site 9 network GPR data acquired in proximity to core 04: A) high-frequency GPR data acquired with 2.0 GHz air-launched antenna (one of two channels is shown); B) low-frequency GPR data acquired with 400 GHz antenna. Core 04 is superposed on the GPR data. A dielectric permittivity of 8.0 was used to convert reflection times to reflector depths. The horizontal axis is in units of feet; the vertical axis is in units of inches.

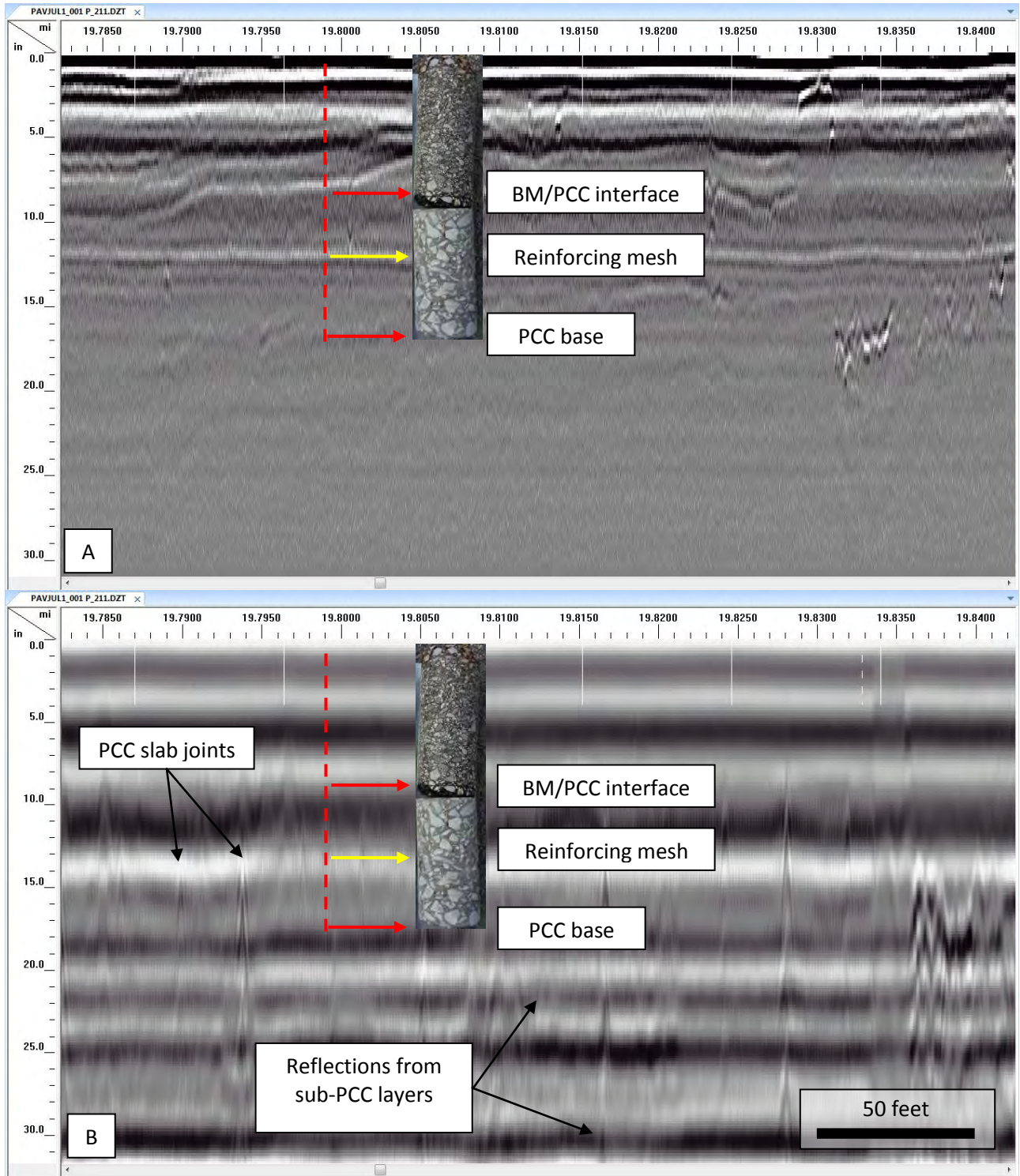


Fig. 8.13– Two segments of Site 9 network GPR data acquired in proximity to core 05: A) high-frequency GPR data acquired with 2.0 GHz air-launched antenna (one of two channels is shown); B) low-frequency GPR data acquired with 400 GHz antenna. Core 05 is superposed on the GPR data. A dielectric permittivity of 8.0 was used to convert reflection times to reflector depths. The horizontal axis is in units of feet; the vertical axis is in units of inches.

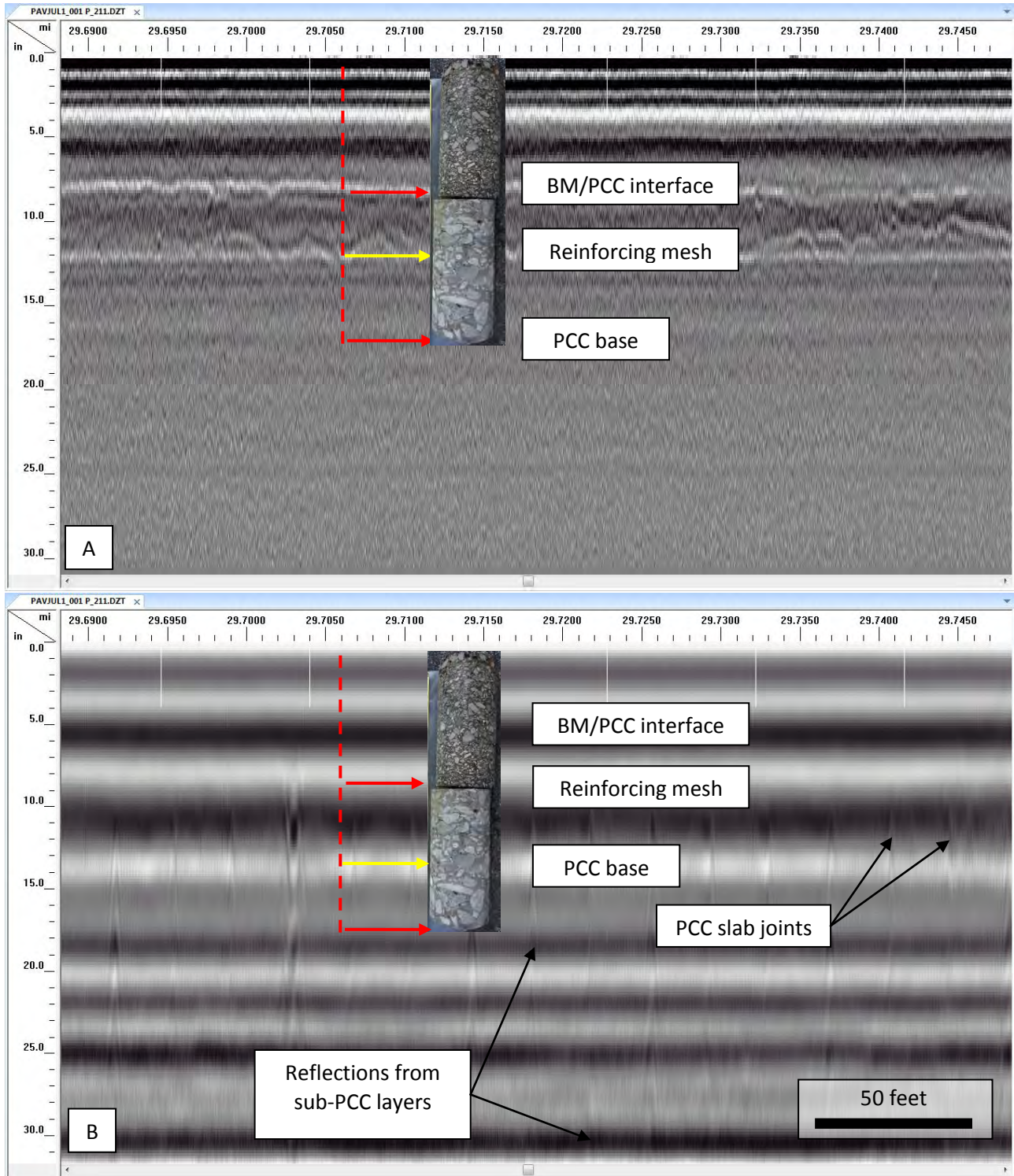


Fig. 8.14– Two segments of Site 9 network GPR data acquired in proximity to core 06: A) high-frequency GPR data acquired with 2.0 GHz air-launched antenna (one of two channels is shown); B) low-frequency GPR data acquired with 400 MHz antenna. Core 06 is superposed on the GPR data. A dielectric permittivity of 8.0 was used to convert reflection times to reflector depths. The horizontal axis is in units of feet; the vertical axis is in units of inches.

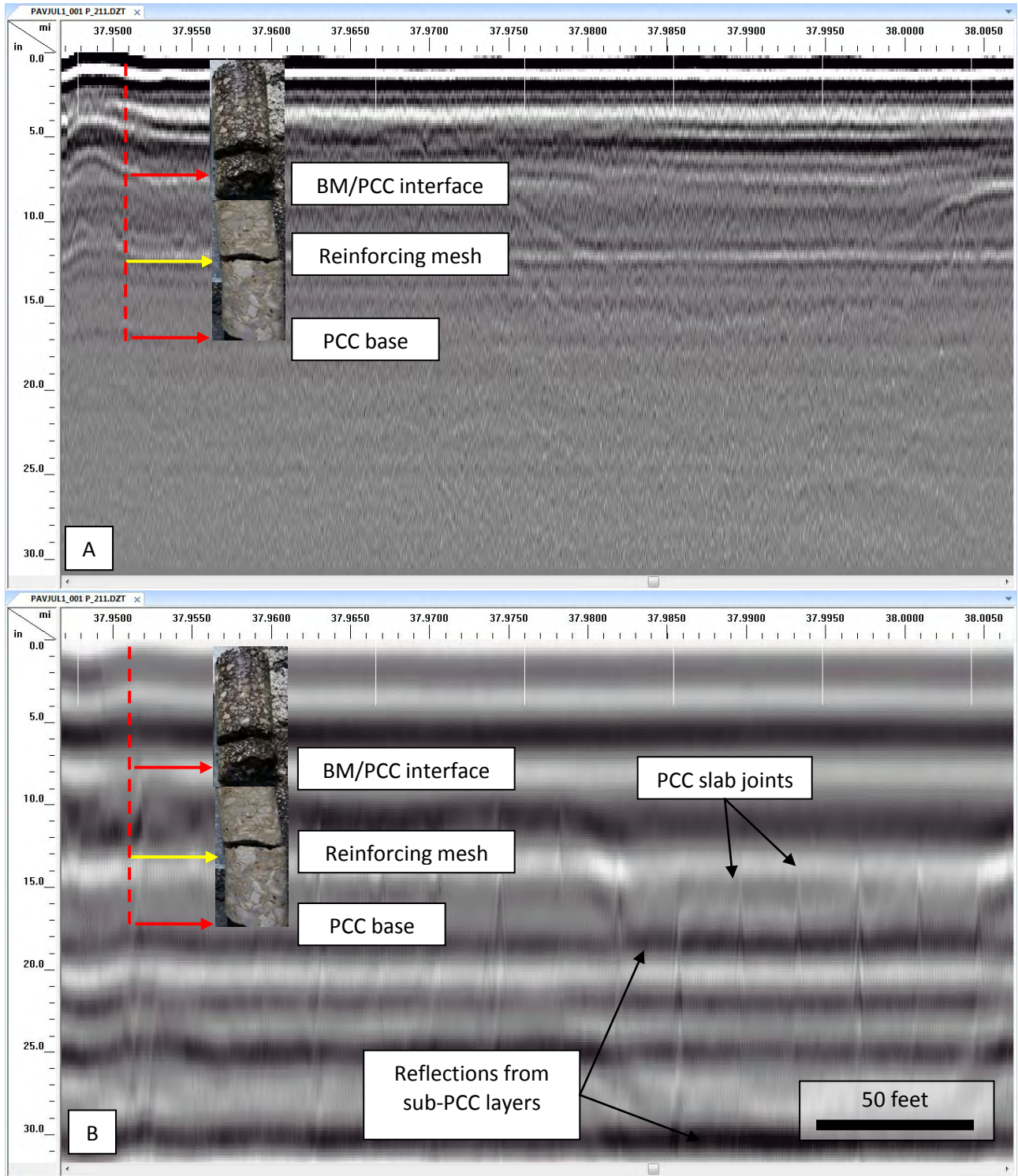


Fig. 8.15– Two segments of Site 9 network GPR data acquired in proximity to core 07: A) high-frequency GPR data acquired with 2.0 GHz air-launched antenna (one of two channels is shown); B) low-frequency GPR data acquired with 400 MHz antenna. Core 07 is superposed on the GPR data. A dielectric permittivity of 8.0 was used to convert reflection times to reflector depths. The horizontal axis is in units of feet; the vertical axis is in units of inches.

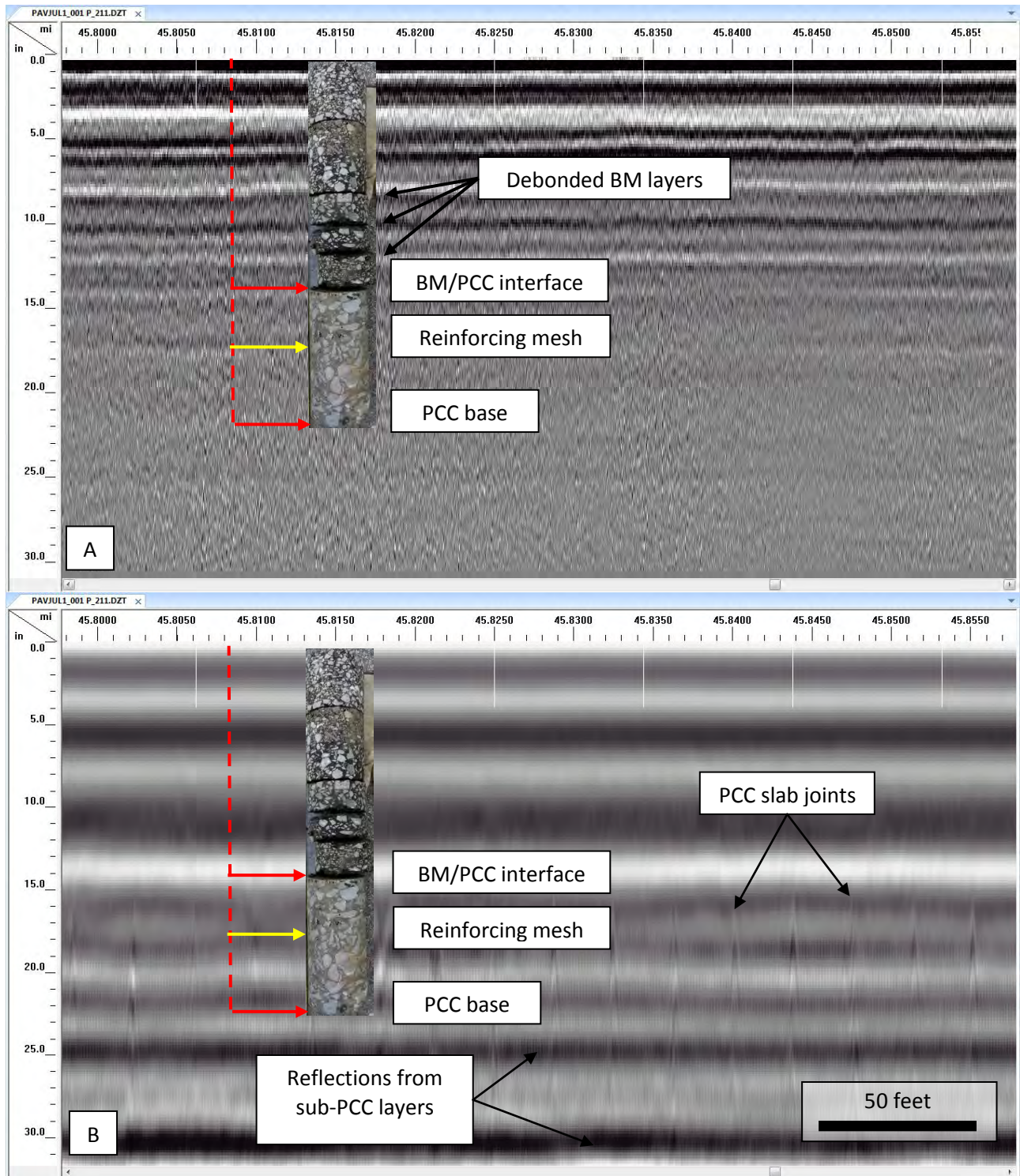


Fig. 8.16— Two segments of Site 9 network GPR data acquired in proximity to core 08: A) high-frequency GPR data acquired with 2.0 GHz air-launched antenna (one of two channels is shown); B) low-frequency GPR data acquired with 400 GHz antenna. Core 08 is superposed on the GPR data. A dielectric permittivity of 8.0 was used to convert reflection times to reflector depths. The horizontal axis is in units of feet; the vertical axis is in units of inches.

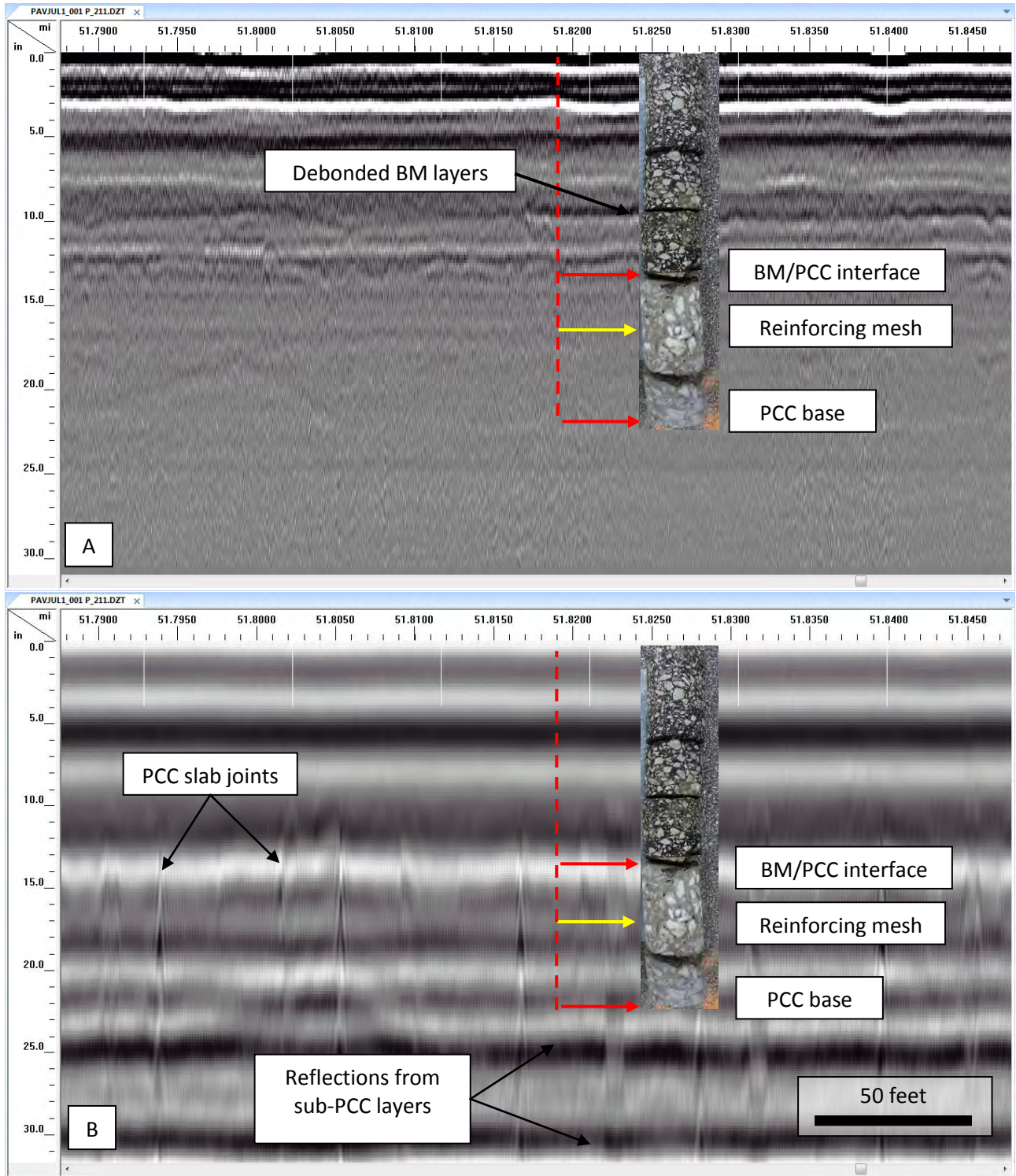


Fig. 8.17– Two segments of Site 9 network GPR data acquired in proximity to core 09: A) high-frequency GPR data acquired with 2.0 GHz air-launched antenna (one of two channels is shown); B) low-frequency GPR data acquired with 400 GHz antenna. Core 09 is superposed on the GPR data. A dielectric permittivity of 8.0 was used to convert reflection times to reflector depths. The horizontal axis is in units of feet; the vertical axis is in units of inches.

8.3.2 Network-Level Site 10 (MO 465)

The network-level Site 10 pavement is predominantly bituminous mix (BM) and appeared to be in good condition. The objective of the network-level Site 10 GPR investigation was two-fold: 1) to evaluate (at near-highway speeds) the condition of an extended segment (network-level) of pavement (mostly BM); and 2) to estimate pavement layer thicknesses.

GPR data were acquired in all four lanes (two northbound; two southbound; Fig. 8.18) using a GSSI SIR-30 system equipped with two higher-frequency 2.0 GHz GSSI 42000S horn antennas and one lower-frequency 400 MHz GSSI 5103 shielded antenna.

The GPR data were processed using GSSI RADAN 7 software. Initial processing steps included: time-zero correction, the application of basic filters for possible noise elimination and to enhance visual representation of data for interpretation purposes; and time-to-depth conversion. The reflection from the base of the BM was confidently identified all low-frequency GPR data.

Seven (7) core samples were acquired for correlation purposes (Table 8.2; Fig. 8.19). In-field descriptions of core properties included diameter, length, number of pieces, length of the specimen, quality of material, and signs of deterioration and/or defects. Example high-frequency GPR data acquired in immediate proximity to core locations 01-07 are shown as Figs. 8.20–8.26, respectively. As noted on Figs. 8.20-8.26, the reflections from the base of the BM pavement and from interfaces (BM/BM) within pavement can be confidently identified and mapped on all the high-frequency profiles.

Based on the assessment of the GPR data acquired along network level Site 10, it was concluded that the high-frequency GPR antenna was a useful tool for mapping layers within the BM and variations in the thickness of the BM layers.

MO 465 Network Level

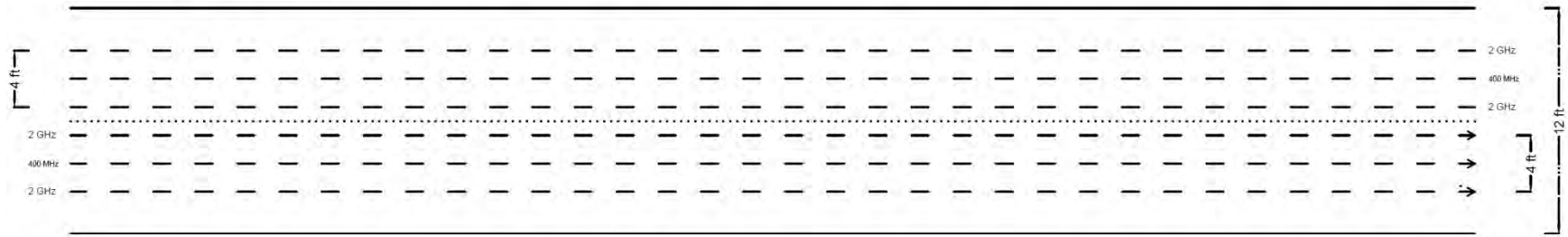


Fig. 8.18– Schematic showing locations of the GPR traverses along network-level Site 10 (MO 465). Solid black lines represent the boundaries of west -bound driving lane. Comparable GPR data were also acquired in east-bound lanes. Drawing is not to scale.

Table 8.2–Site 10 (MO 465) core locations. The description is based on the visual assessment only, no laboratory testing was conducted.

Core	Mile mark	BM thickness and brief description
1	1.04 (1.31 miles northeast of intersection MO 465 and MO 76); NB driving lane	BM layer has a total thickness of 12.5 in. and comprised of three layers (4.0 in., 4.5 in., and 4.0 in. from top to bottom accordingly). No visual evidence of deterioration is present.
2	2.96 (3.23 miles northeast of intersection MO 465 and MO 76); NB driving lane	BM layer has a total thickness of 12.0 in. and comprised of three layers (3.0 in., 4.5 in., and 4.5 in. from top to bottom accordingly). No visual evidence of deterioration is present.
3	4.84 (5.11 miles northeast of intersection MO 465 and MO 76); NB driving lane	BM layer has a total thickness of 12.5 in. and comprised of three layers (4.0 in., 4.5 in., and 4.0 in. from top to bottom accordingly). Debonding is present at a depth of 8.5 in.
4	5.78 (6.05 miles northeast of intersection MO 465 and MO 76); NB driving lane	BM layer has a total thickness of 11.5 in. and comprised of three layers (3.5 in., 4.0 in., and 4.0 in. from top to bottom accordingly). Debonding is present at a depth of 3.5 in. and 7.5 in.
5	0.03 (0.23 miles southwest of intersection MO 465 and US 65); SB driving lane	BM layer has a total thickness of 13.0 in. and comprised of four layers (1.5 in., 2.5 in., 4.5 in., and 4.5 in. from top to bottom accordingly). Debonding is present at a depth of 1.5 in. and 8.5 in.
6	1.00 (1.2 miles southwest of intersection MO 465 and US 65); SB driving lane	BM layer has a total thickness of 13.5 in. and comprised of four layers (1.5 in., 3.5 in., 5.0 in., and 3.5 in. from top to bottom accordingly). No visual evidence of deterioration is present.
7	3.03 (3.23 miles southwest of intersection MO 465 and US 65); SB driving lane	BM layer has a total thickness of 13.5 in. and comprised of four layers (2.0 in., 3.5 in., 4.5 in., and 4.5 in. from top to bottom accordingly). No visual evidence of deterioration is present.



Fig. 8.19—Network-level Site 10 core 07 (Table 8.2).

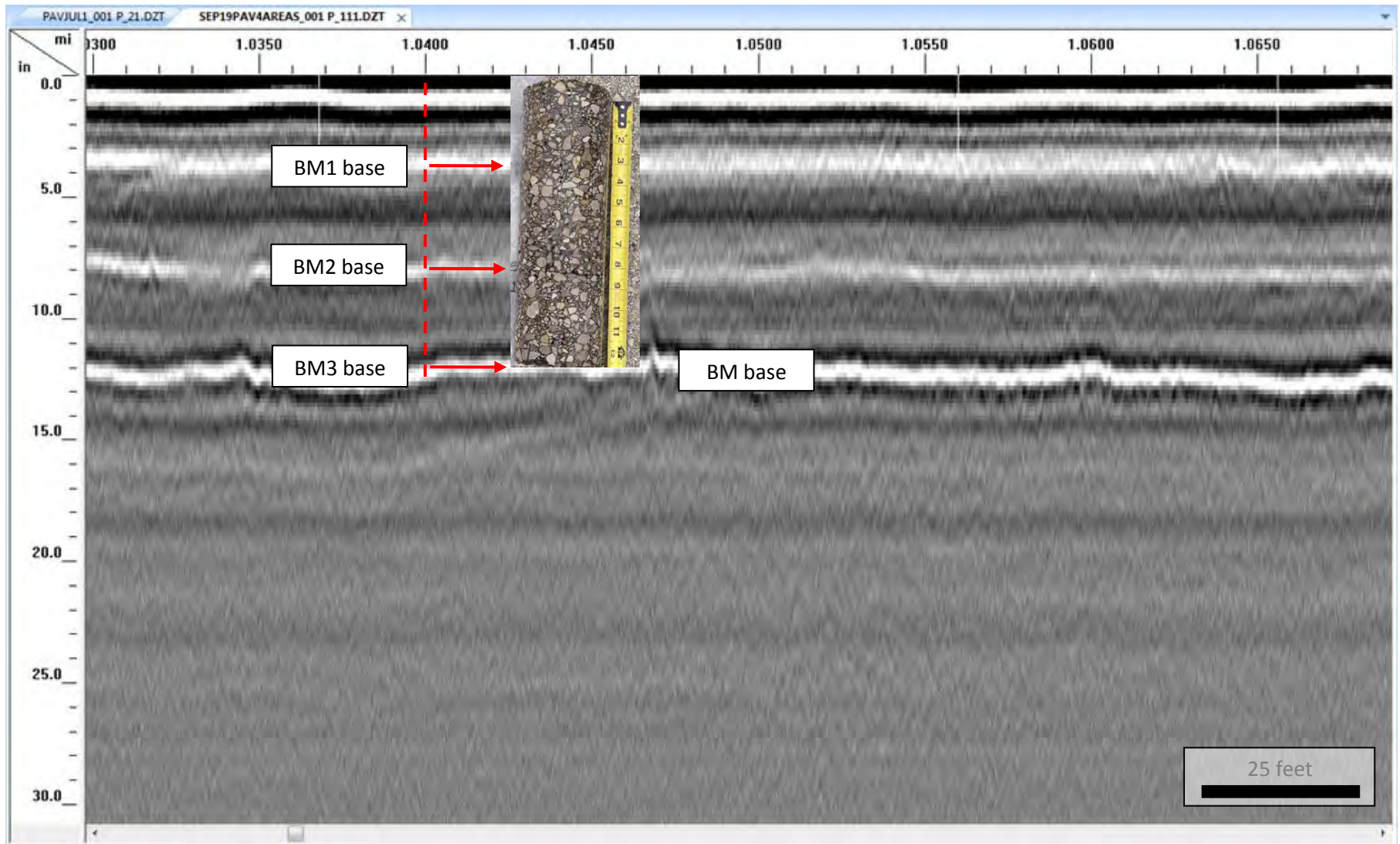


Fig. 8.20—Segment of network-level high-frequency GPR data (in proximity to network-level Site 10 Core 01; Core 01 is shown acquired using the high-frequency 2.0 GHz air-launched antenna (one of two channels is shown)). A dielectric permittivity of 6.5 was used to convert reflection times to reflector depths. The horizontal axis is in units of feet; the vertical axis is in units of inches.

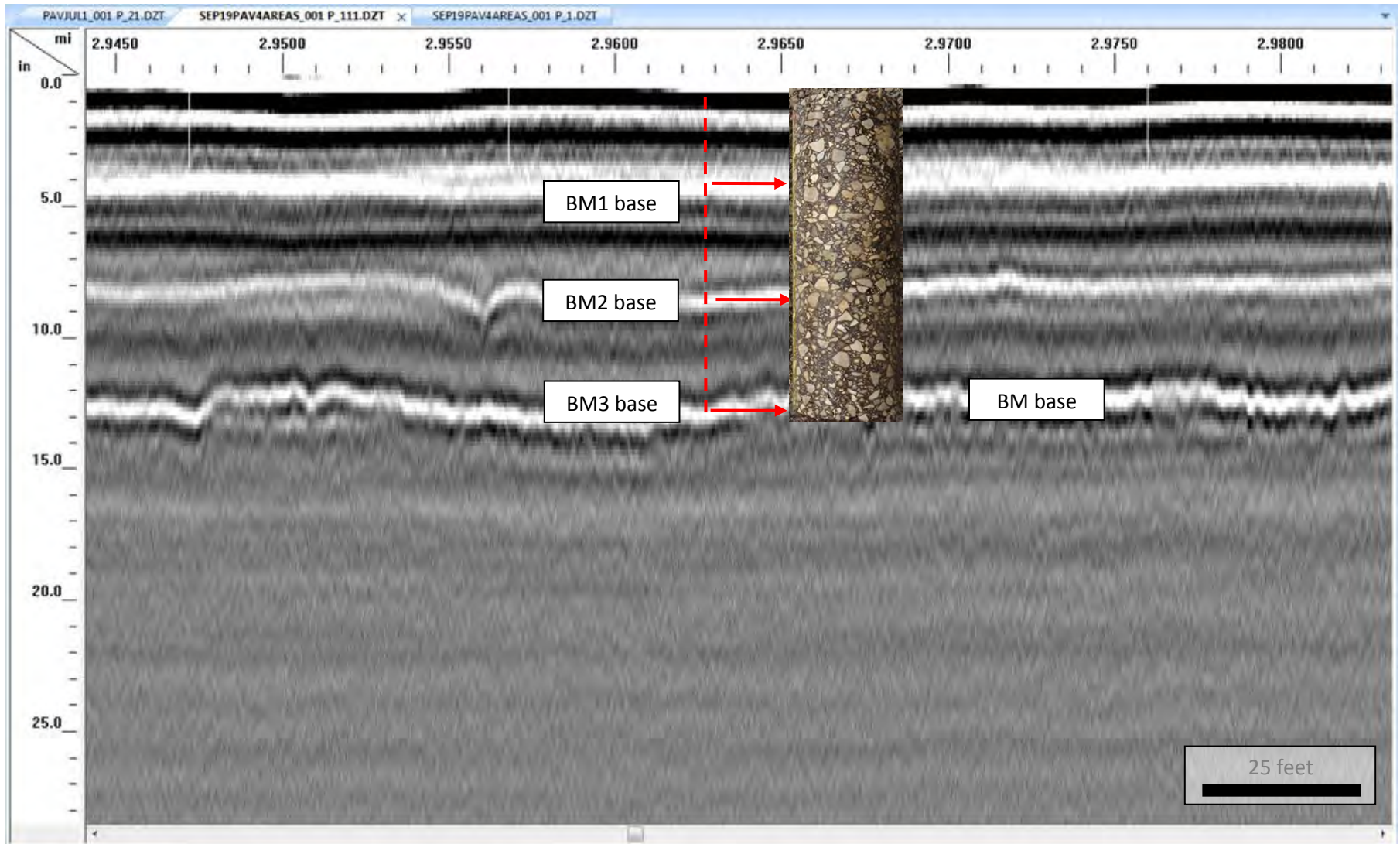


Fig. 8.21—Segment of network-level high-frequency GPR data (in proximity to network-level Site 10 Core 02; Core 02 is shown) acquired using the high-frequency 2.0 GHz air-launched antenna (one of two channels is shown). A dielectric permittivity of 6.5 was used to convert reflection times to reflector depths. The horizontal axis is in units of feet; the vertical axis is in units of inches.

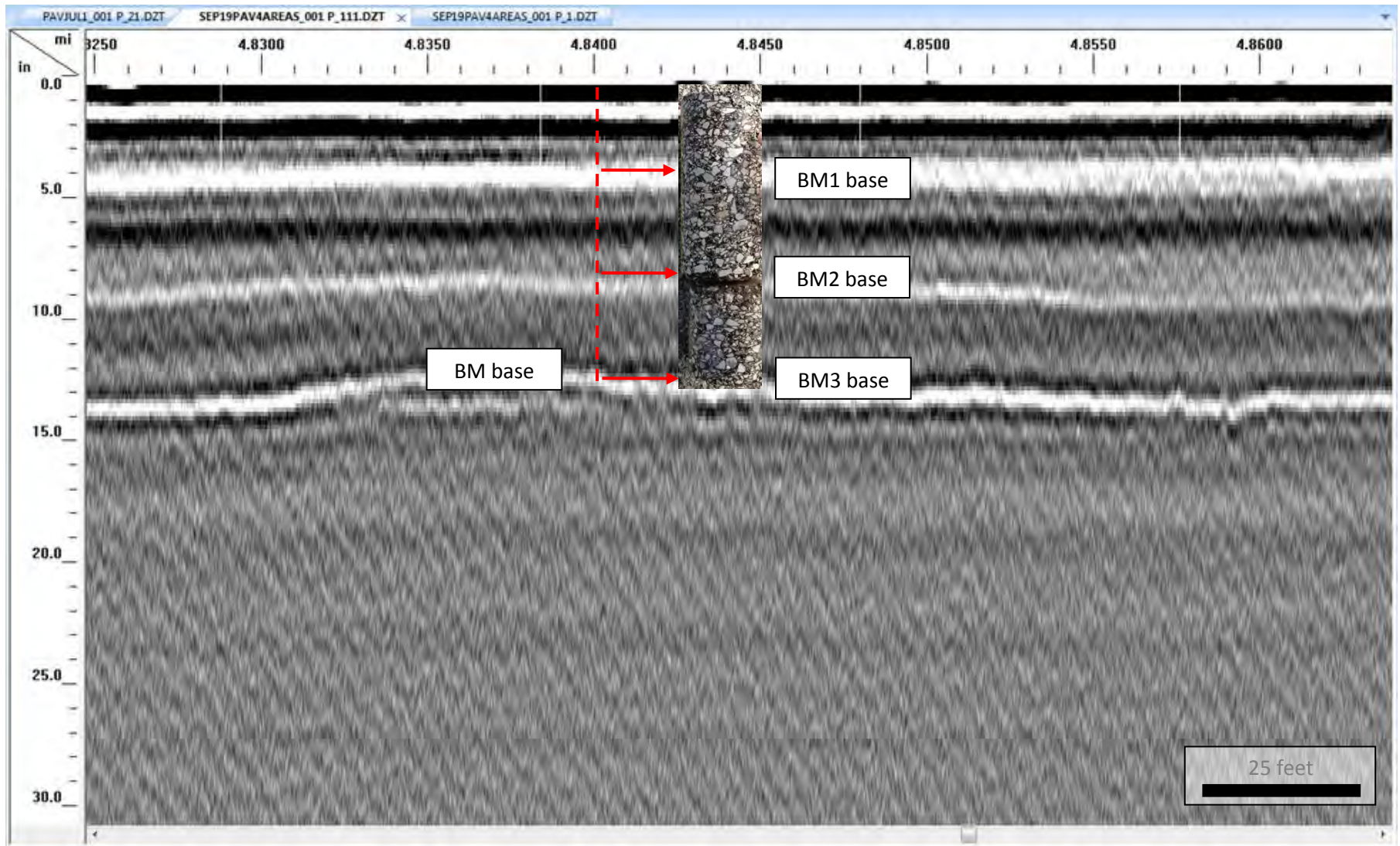


Fig. 8.22—Segment of network-level high-frequency GPR data (in proximity to network-level Site 10 Core 03; Core 03 is shown) acquired using the high-frequency 2.0 GHz air-launched antenna (one of two channels is shown) at Site 10. A dielectric permittivity of 6.5 was used to convert reflection times to reflector depths. The horizontal axis is in units of feet; the vertical axis is in units of inches.

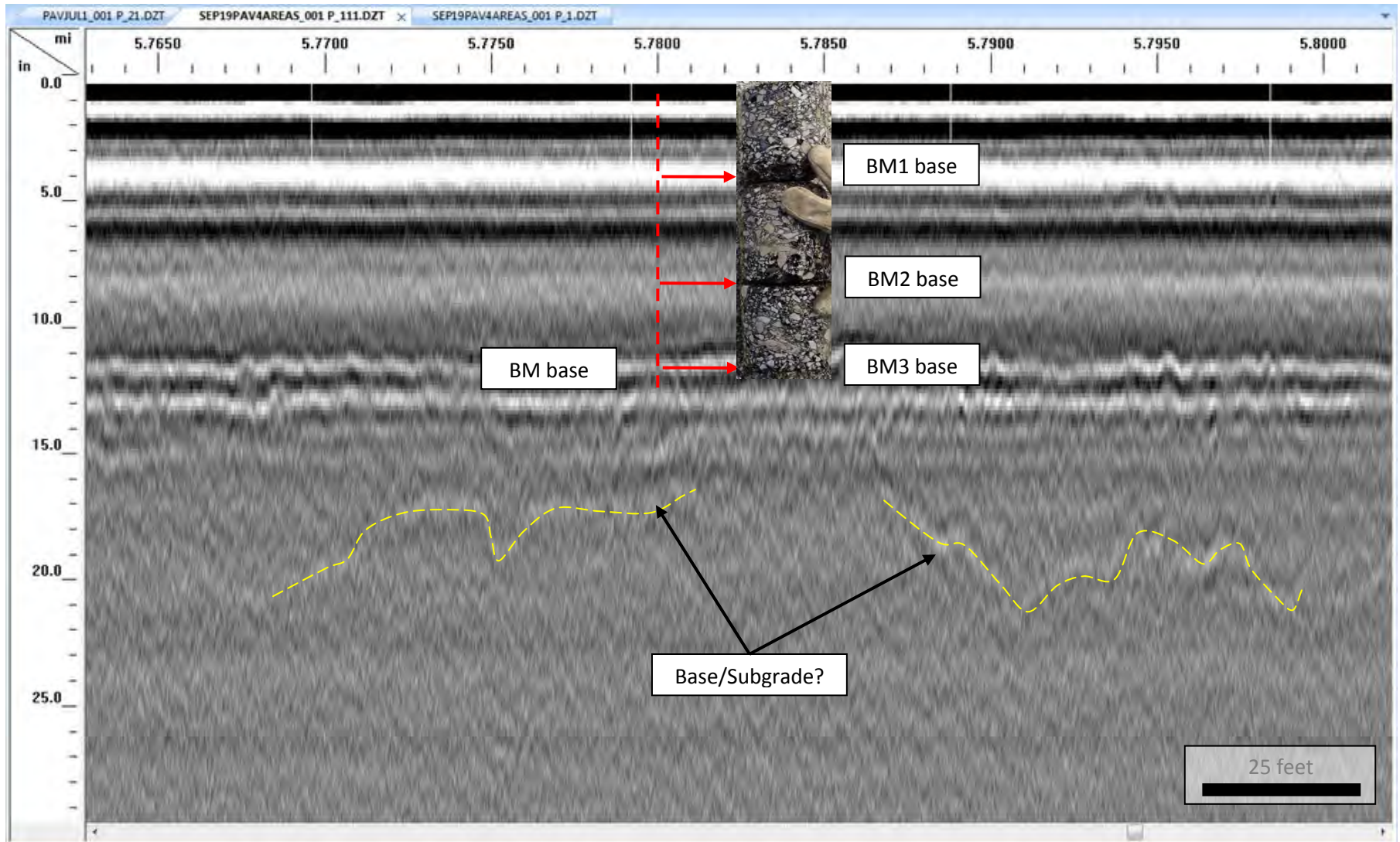


Fig. 8.23—Segment of network-level high-frequency GPR data (in proximity to network-level Site 10 Core 04; Core 04 is shown) acquired using the high-frequency 2.0 GHz air-launched antenna (one of two channels is shown) at Site 10. A dielectric permittivity of 6.5 was used to convert reflection times to reflector depths. The horizontal axis is in units of feet; the vertical axis is in units of inches.

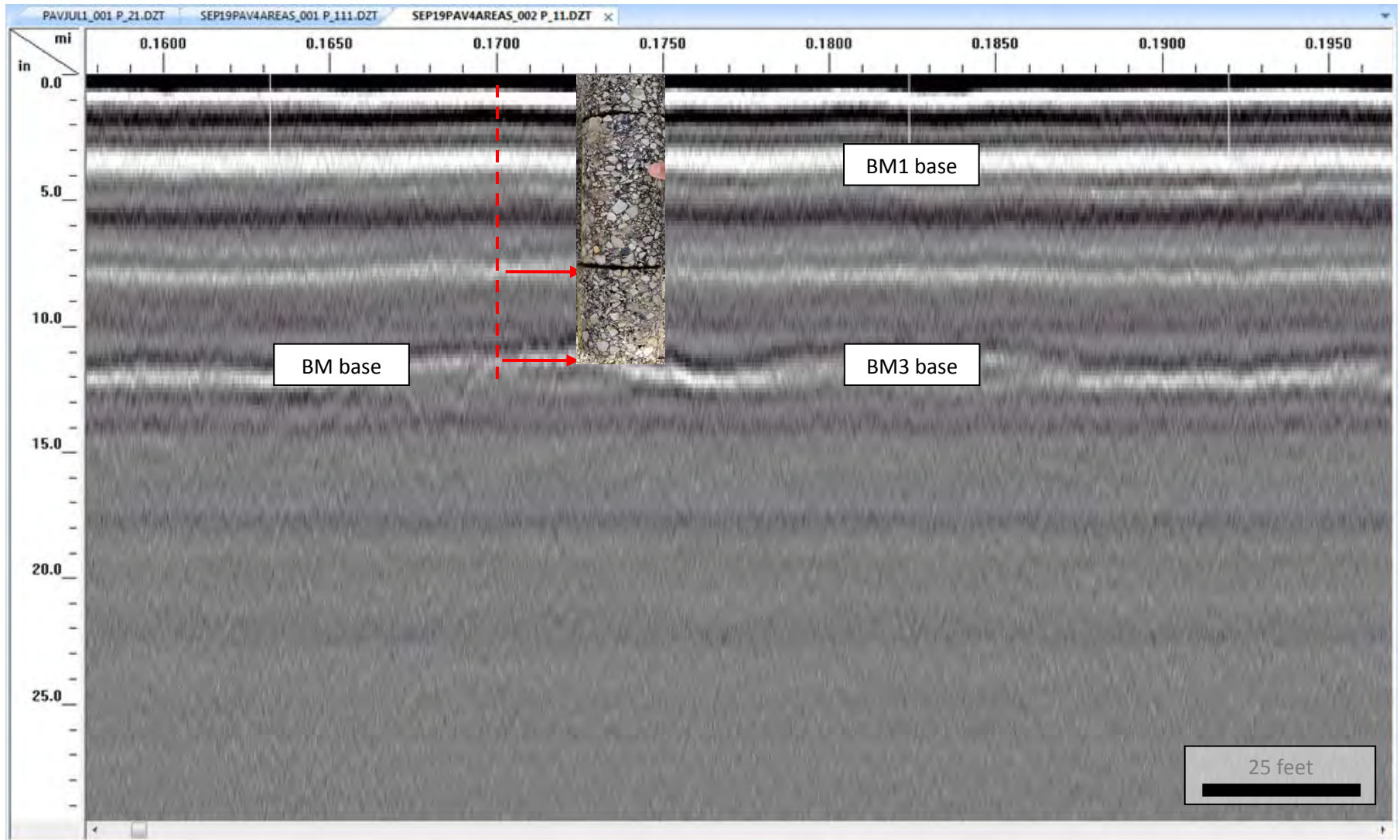


Fig. 8.24—Segment of network-level high-frequency GPR data (in proximity to network-level Site 10 Core 05; Core 05 is shown) acquired using the high-frequency 2.0 GHz air-launched antenna (one of two channels is shown) at Site 10. A dielectric permittivity of 6.5 was used to convert reflection times to reflector depths. The horizontal axis is in units of feet; the vertical axis is in units of inches.

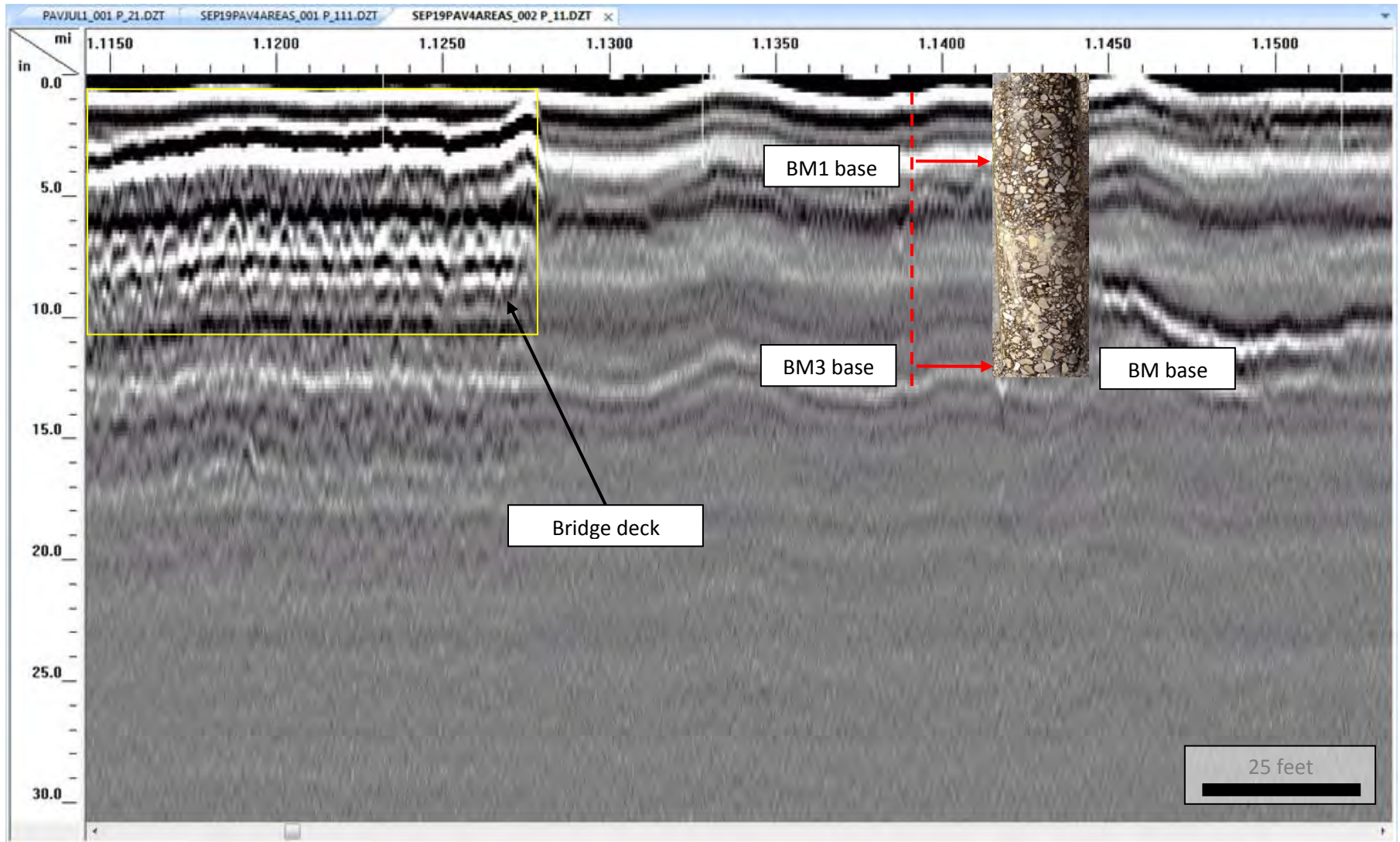


Fig. 8.25—Segment of network-level high-frequency GPR data (in proximity to network-level Site 10 Core 06; Core 06 is shown) acquired using the high-frequency 2.0 GHz air-launched antenna (one of two channels is shown) at Site 10. A dielectric permittivity of 6.5 was used to convert reflection times to reflector depths. The horizontal axis is in units of feet; the vertical axis is in units of inches.

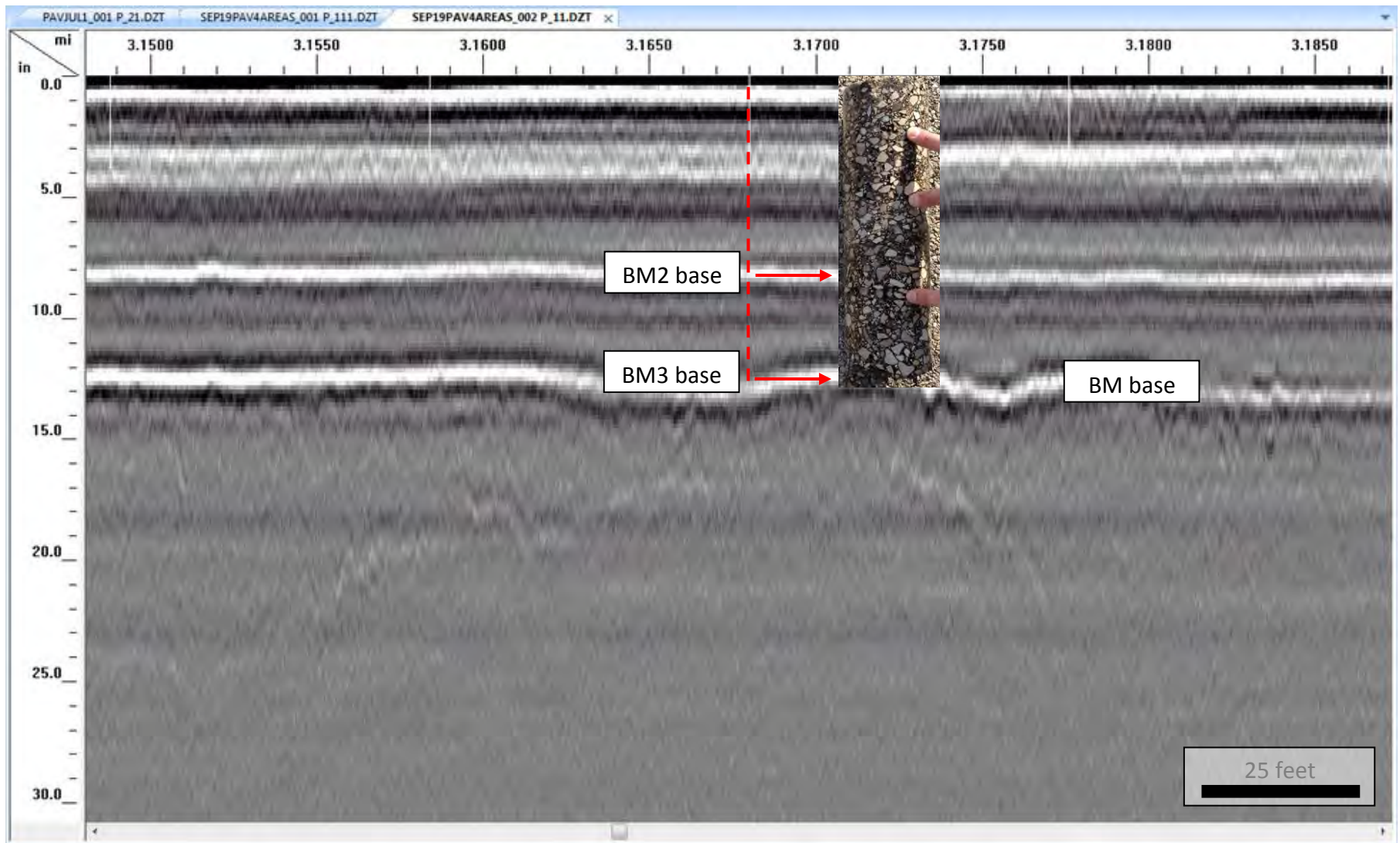


Fig. 8.26—Segment of network-level high-frequency GPR data (in proximity to network-level Site 10 Core 07; Core 07 is shown) acquired using the high-frequency 2.0 GHz air-launched antenna (one of two channels is shown) at Site 10. A dielectric permittivity of 6.5 was used to convert reflection times to reflector depths. The horizontal axis is in units of feet; the vertical axis is in units of inches.

8.4 Concluding Remarks

Low- and high-frequency network-level ground penetrating radar (GPR) data were acquired along two test sections of roadway: I-70 (network-level Site 9) and MO 465 (network-level Site 10). The test segment of I-70 extended from mile marker 84.2 to mile marker 20.8; GPR data were acquired in the west-bound driving lane only. The test segment of MO 465 extended from the intersection with HWY 76 to the intersection with US 65; GPR data were acquired all four lanes (two southbound and two northbound). The objective of both network-level GPR surveys was to estimate pavement layer thicknesses.

Based on the assessment of the GPR data acquired along network level Site 9 (I-70) it was concluded that the high-frequency GPR antenna was a useful tool for mapping layers within the BM and variations in the thickness of the BM layers. The high-frequency GPR antenna was not capable of confidently imaging the reflection from the base of the PCC, presumably because the pavement was more than 18 in. thick (the manufacturer indicates the effective investigative depth of the high-frequency GPR antenna is approximately 18 in.) and because of the presence of wire mesh (which masks the reflections from the underlying base PCC).

Based on the assessment of the GPR data acquired along network level Site 10, it was concluded that the high-frequency GPR antenna was a useful tool for mapping layers within the BM and variations in the thickness of the BM layers.

9 SUMMARY AND CONCLUSIONS

In Task 3, the following non-invasive technologies were identified as potentially most applicable to MoDOT roadways based on a review of published literature and the researchers' experience:

1. Ultrasonic Surface Waves (USW)
2. Impact Echo (IE)
3. Ground-coupled Ground Penetrating Radar (GPR) (400 MHz and 1500 MHz antennae)
4. Electrical Resistivity Tomography (ERT)
5. Multichannel Analyses of Surface Waves (MASW)
6. Falling Weight Deflectometer (FWD)
7. Rolling Dynamic Deflectometer (RDD)
8. Air-launched Ground Penetrating Radar (GPR)

To thoroughly assess the cost-effectiveness and utility of these technologies, corresponding field data were acquired across/along designated MoDOT roadways. Technologies 1-7 listed above were used to acquire non-invasive data along eight designated project-level roadways (Table 9.1); Technologies 3 (400 MHz only) and 8 listed above were used to acquire non-invasive data along two designated network-level roadways (Table 9.2).

In Table 9.1, the primary survey objectives (as defined by MoDOT) and related positive outcomes for each of the tested project-level roadway are presented. Positive outcomes were realized by six of the seven technologies (1-7) applied to the project-level roadways. The only technology that did not consistently generate positive outcomes was impact echo (IE; technology 2 above). The IE tool is designed to automatically output reliable estimates of the thicknesses of pavement layers and the depths to defects within the pavement layers. Unfortunately, the depth estimates automatically output by the IE tool at the test locations were not reliable. Hence, the outcomes of the IE tool were not deemed to be positive.

The ultrasonic surface wave (USW) technology, in contrast, proved to be very useful. The USW tool automatically outputs 1-D plots of the dynamic elastic modulus of the pavements to maximum depths of approximately 11 in. These elastic modulus plots are reliable (according to published literature) for uniform pavements and for the uppermost layer of non-uniform (e.g. PCC over BM) pavements. Pavement layers with contrasting elastic moduli (e.g. PCC over BM) could be identified on the 1-D elastic modulus plots, and **layer thicknesses could be estimated** (to a maximum depth of approximately 11 in.). **Zones of stripping in BM layers (where present) were characterized on the 1-D plots by anomalously low values of dynamic elastic modulus.** The only significant disadvantages to using this tool are that lane closures are required, and data acquisition is relatively slow.

The interpretations of the higher-frequency (1500 MHz) ground-coupled GPR antenna data were also useful. Different pavement layers (maximum depths of approximately 18 in.) and joints could be mapped with confidence at all project-level pavement sites. **The pattern, placement, and density of reinforcing steel could also be readily determined.** At some sites, there is a statistical correlation between debonded interfaces (confirmed by limited core

control) and corresponding GPR reflection amplitudes; at other sites it appears debonding could not be identified with confidence on the GPR profiles. However, core control was limited. In contrast, **zones of stripping in BM layers (where present) could be visually identified** on individual GPR profiles. **Voids beneath segments of one tested segment of roadway could be mapped** with apparent confidence (based on limited core and USW control). The only real significant disadvantage to using this tool is that lane closures are required. Data acquisition is relatively rapid.

The interpretations of the lower-frequency (400 MHz) ground-coupled GPR antenna data were somewhat less useful. This tool would be best used to image the base of thick (larger than 18 in.) pavements and base layers (to depths on the order of 4 ft.). The only real significant disadvantage to using this tool is that lane closures are required. Data acquisition is relatively rapid.

At each project-level roadway site, both 2-D MASW and 2-D ERT data were acquired. It should be noted that the interpretation of the ERT and MASW data (in the absence of constraining borehole control) provided potentially very useful information at each project-level site. More specifically:

1. Top of weathered rock (where present) could be mapped on each 2-D ERT profile.
2. Top of intact rock (where present) could be mapped on each 2-D ERT profile.
3. Solution-widened joints (where present) could be mapped on each 2-D ERT profile.
4. Dry soil and moist soil could be differentiated on each 2-D ERT profile.
5. Moist clayey soil could be differentiated on each 2-D ERT profile.
6. Top of weathered rock (where present) could be mapped on each 2-D MASW profile.
7. Top of intact rock (where present) could be mapped on each 2-D MASW profile.
8. Lateral and vertical variations in the shear-wave velocity of soil and rock (where present) could be mapped on each 2-D MASW profile.

The positive outcomes of the MASW and ERT surveys are listed above because they may be unrelated to the primary survey objectives (Table 9.1). The only significant disadvantages to using the MASW tool in the manner utilized for Task 4 investigations are that lane closures are required, and data acquisition is relatively slow. The only real significant disadvantage to using the ERT tool in the manner utilized for Task 4 investigations is that data acquisition is relatively slow.

The FWD is a well-established technique for pavement testing. The FWD provides useful information on the **structural performance of both rigid and flexible pavements** by measuring the deflection bowl produced from an impact load on the pavement surface. One of the advantages of the FWD is that it tests the pavements at strain levels that are similar to those experienced in service. The deflection measurements can be used in a variety of ways, including: to qualitatively assess of support conditions, to estimate stiffness parameters using empirical relationships, to calculate load transfer efficiency across joints, and to back-calculate stiffness parameters through inversion analyses. The primary disadvantages of the FWD for

pavement management applications are the point-by-point nature of the measurement, which limits its coverage for pavement management applications, and the time consuming analysis to back-calculate stiffness parameters.

The interpretations of the RDD data provided useful information about the pavement systems tested in this study. The unique high spatial-resolution (2 to 3 ft intervals) view of the pavement deflection profile provided by the RDD is not practically obtainable with existing technologies. The RDD appears to be most useful when applied to rigid pavements, particularly for assessing the quality of joints. Deflection measurements can be used to **determine load transfer efficiency across joints and cracks**, and due to the continuous nature of the RDD measurement it is possible to test every joint. At the current stage of development, the utility of the RDD for flexible pavements is largely as a means to qualitatively assess pavement support conditions. The deflection measurements from the RDD do not appear to be sufficiently sensitive to debonding and stripping within the surface materials. The ability to perform measurements at 1 to 2 mph allows for extensive coverage of pavements in a relatively short amount of time. The structural information from the RDD could be used to identify regions in need of further study (due to anomalously high deflections) or to develop and apply more site specific rehabilitation strategies based on structural performance. In addition, the RDD could be used as an effective quality control tool to evaluate newly constructed or rehabilitated pavements. The RDD requires lane closures, although it can be performed using moving lane closures in some cases.

To thoroughly assess the cost-effectiveness and utility of technologies 3 and 8, lower-frequency (400 MHz) and high-frequency (2000 MHz) air-launched GPR data were acquired along two designated MoDOT network-level roadways. In Table 9.2, the primary survey objectives (as defined by MoDOT) and related positive outcomes for each of the tested project-level roadway are presented.

The interpretations of the high-frequency (2000 MHz) air-launched GPR data were useful. **Pavement layers** (maximum depths of approximately 18 in.) **could be mapped** with confidence at both network-level pavement sites. The lower-frequency (400 MHz) antenna data could be used to image the pavement (and sub-pavement where applicable) to depths on the order of 4 feet. There are no significant disadvantages to acquiring network-level GPR data using truck mounted antennae.

As discussed in this report, pavement survey objectives can vary widely based on many factors (e.g., pavement type, base conditions, evaluation of existing vs. new construction, etc.), and there is not one technology that is best suited for all cases. Based on the findings summarized in this section, high-frequency air-launched GPR is recommended for primary consideration for network-level investigations of MoDOT pavements, and is recommended along all segments of pavement where ARAN data are collected. This data can be used to spot developing problems where further project-level investigations may be needed. USW, GPR, and FWD techniques are recommended for primary consideration for project-level investigations of MoDOT pavements, where in situ properties of the pavement are needed, or for quality

assurance purposes. At its current stage of development, RDD is recommended for secondary consideration for project-level investigations of MoDOT pavements. ERT is recommended for primary consideration of the base, and MASW is recommended for secondary consideration, or where engineering properties of the base material are desired.

Finally, a key deliverable from Task 4 is a guidance document focused on the utility and cost-effectiveness of project-applicable and network-applicable non-invasive imaging technologies. The guidance document is presented Appendix A.

Table 9.1–Positive outcomes from the eight project-level site investigations.

Project-level Roadway	Primary Survey Objective(s)	Positive Outcomes
US 63 Phelps County (Site 1)	Estimate pavement thickness and assess roadway condition	<ol style="list-style-type: none"> 1. USW tool could be used to estimate layer thicknesses (to a maximum depth of approx. 11 in.). 2. USW tool could be used to assess the actual (PCC) and/or relative (BM) condition of the pavement (to a maximum depth of approx. 11 in.). 3. Higher-frequency (1500 MHz) GPR tool could be used to estimate layer thicknesses (to base of lower PCC layer). 4. Higher-frequency (1500 MHz) GPR tool could be used to image wire mesh and joints. 5. Lower-frequency (400 MHz) GPR tool could be used to image joints and pavement to depths of approx. 4 ft. 6. RDD tool could be used to detect and test concrete joints and qualitatively assess pavement support conditions. High-deflection regions along the profile could be identified. 7. FWD tool could be used to test concrete joints, but the location had to be known a priori (due to the BM cover). FWD deflections could also used to qualitatively assess support conditions.
US 54 Camden County (Site 2)	Detect deep (>6 in.) stripping layer and assess roadway condition	<ol style="list-style-type: none"> 1. USW tool could be used to estimate layer thicknesses (to a maximum depth of approx. 11 in.). 2. USW tool could be used to assess the condition of the BM pavement (to a maximum depth of approx. 11 in.). Zones of stripping were identifiable. 3. Higher-frequency (1500 MHz) GPR tool could be used to estimate layer thicknesses (to base of BM). 4. Higher-frequency (1500 MHz) GPR tool could be used to image debonding/stripping. 5. Lower-frequency (400 MHz) GPR tool could be used to image pavement to depths of approx. 4 ft. 6. RDD tool could be used to qualitatively assess pavement support conditions (with high spatial resolution) and identify regions with anomalously high deflections. 7. FWD tool could be used to assess pavement deflections at discrete points along the profile. The deflections could be used to estimate pavement stiffness parameters using empirical relationships.
Rte 179 Cole County (Site 3)	Detect debonding and assess roadway condition	<ol style="list-style-type: none"> 1. USW tool could be used to estimate layer thicknesses (to a maximum depth of approx. 11 in.). 2. USW tool could be used to assess the condition of the BM pavement (to a maximum depth of approx. 11 in.). Zones of stripping and debonding were identifiable.

		<ol style="list-style-type: none"> 3. Higher-frequency (1500 MHz) GPR tool could be used to estimate layer thicknesses (to base of BM). 4. Higher-frequency (1500 MHz) GPR tool could be used to image debonding/stripping. 5. Lower-frequency (400 MHz) GPR tool could be used to image pavement to depths of approx. 4 ft. 6. RDD tool could be used to qualitatively assess pavement support conditions (with high spatial resolution) and identify regions with anomalously high deflections. 7. FWD tool could be used to assess pavement deflections at discrete points along the profile. The deflections could be used to estimate pavement stiffness parameters using empirical relationships.
HWY AT Franklin County (Site 4)	Detect shallow (<6 in.) stripping layer and assess roadway condition	<ol style="list-style-type: none"> 1. USW tool could be used to estimate layer thicknesses (to a maximum depth of approx. 11 in.). 2. USW tool could be used to assess the condition of the BM pavement (to a maximum depth of approx. 11 in.). Zones of stripping were identifiable. 3. Higher-frequency (1500 MHz) GPR tool could be used to estimate layer thicknesses (to base of BM). 4. Higher-frequency (1500 MHz) GPR tool could be used to image debonding/stripping. 5. Lower-frequency (400 MHz) GPR tool could be used to image pavement to depths of approx. 4 ft. 6. FWD tool could be used to assess pavement deflections at discrete points along the profile. The deflections could be used to estimate pavement stiffness parameters using empirical relationships.
I-55 Pemiscot County (Site 5)	Assess an unbonded concrete overlay (no flaws anticipated)	<ol style="list-style-type: none"> 1. USW tool could be used to estimate layer thicknesses (to a maximum depth of approx. 11 in.). 2. USW tool could be used to assess actual (PCC) and/or relative (BM) condition of pavement (to a maximum depth of approx. 11 in.). Zones of stripping were identifiable. 3. Higher-frequency (1500 MHz) GPR tool could be used to estimate layer thicknesses (to base of PCC). 4. Higher-frequency (1500 MHz) GPR tool could be used to image debonding/stripping in the BM layer. 5. Lower-frequency (400 MHz) GPR tool could be used to image pavement to depths of approx. 4 ft. 6. RDD tool could be used to qualitatively assess pavement support conditions (with high spatial resolution) and identify high-deflection regions. Detection of individual joints was not possible in the 1000-ft section. 7. FWD tool could be used to determine load transfer

		efficiency across concrete joints.
I-55 Perry County (Site 6)	Assess joint condition	<ol style="list-style-type: none"> 1. USW tool could be used to estimate layer thicknesses (to a maximum depth of approx. 11 in.). 2. USW tool could be used to assess the condition of the pavement (to a maximum depth of approx. 11 in.). 3. USW tool could be used to locate sub-PCC slab voids. 4. Higher-frequency (1500 MHz) GPR tool could be used to estimate layer thicknesses (to base of PCC). 5. Higher-frequency (1500 MHz) GPR tool could be used to locate sub-PCC slab voids. 6. Higher-frequency (1500 MHz) GPR tool could be used to image wire mesh and joints. 7. Lower-frequency (400 MHz) GPR tool could be used to image pavement to depths of approx. 4 ft.
HWY U Dent County (Site 7)	Assess a poor-condition asphalt roadway	<ol style="list-style-type: none"> 1. USW tool could be used to estimate layer thicknesses (to a maximum depth of approx. 11 in.). 2. USW tool could be used to assess the condition of the BM pavement (to a maximum depth of approx. 11 in.). Zones of stripping were identifiable. 3. Higher-frequency (1500 MHz) GPR tool could be used to estimate layer thicknesses (to base of BM). 4. Higher-frequency (1500 MHz) GPR tool could be used to image debonding/stripping. 5. Lower-frequency (400 MHz) GPR tool could be used to image pavement to depths of approx. 4 ft. 6. FWD tool could be used to assess pavement deflections at discrete points along the profile. The deflections could be used to estimate pavement stiffness parameters using empirical relationships.
I-35 Jackson County (Site 8)	Assess an unbonded concrete overlay (flaws are anticipated)	<ol style="list-style-type: none"> 1. USW tool could be used to estimate layer thicknesses (to a maximum depth of approx. 11 in.). 2. USW tool could be used to assess actual and/or relative condition pavement (to a maximum depth of approx. 11 in.). 3. Higher-frequency (1500 MHz) GPR tool could be used to estimate layer thicknesses (to base of lower PCC layer). 4. Higher-frequency (1500 MHz) GPR tool could be used to image wire mesh and joints. 5. Lower-frequency (400 MHz) GPR tool could be used to image joints and pavement to depths of approx. 4 ft. 6. RDD tool could be used test concrete joints and qualitatively assess support conditions. High-deflection regions along the profile were identified. 7. FWD tool could be used to determine load transfer across concrete joints and qualitatively assess support conditions.

Table 9.2–Positive outcomes from the two network-level site investigations.

Project Location	Survey Objective(s)	Positive Outcomes
I -70 (Site 9)	Estimate pavement layer thicknesses and assess roadway condition	<ol style="list-style-type: none"> 1. Air-launched antenna GPR tool could be used to estimate pavement layer thicknesses (to depths of approx. 18 in., but not to base of PCC layer). 2. Lower-frequency (400 MHz) GPR tool could be used to image pavement layers to depths of approx. 4 ft.
MO 465 (Site 10)	Estimate pavement layer thicknesses and assess roadway condition	<ol style="list-style-type: none"> 1. Air-launched antenna GPR tool could be used to estimate layer thicknesses (to base of BM). 2. Lower-frequency (400 MHz) GPR tool could be used to image pavement to depths of approx. 4 ft.

REFERENCES

- ASTM, C469/C469M-14 (2012). Standard Test Method for Static Modulus of Elasticity and Poisson's Ratio of Concrete in Compression. ASTM International, West Conshohocken, PA.
- Baker, M. R., K. Crain, and S. Nazarian (1995). "Determination of Pavement Thickness with a New Ultrasonic Device" *Research Report*, Center for Highway Materials Research, University of Texas, El Paso.
- Bay, J. A. (1997). *Development of a Rolling Dynamic Deflectometer for Continuous Deflection Testing of Pavements*. Ph.D. dissertation, University of Texas, Austin.
- Bay, J. A., K. H. Stokoe II, B. F. McCullough, and D. R. Alexander. (1999). Profiling Flexible Highway Pavement Continuously with Rolling Dynamic Deflectometer and at Discrete Points with Falling Weight Deflectometer. In *Transportation Research Record: Journal of the Transportation Research Board, No. 1655*, TRB, National Research Council, Washington, D.C., pp. 74–85.
- Carino, N.J., M. Sansalone, and N.N. Hsu (1986). "A Point Source - Point Receiver Technique for Flaw Detection in Concrete," *Journal of the American Concrete Institute*, Vol. 83, No. 2, April, pp. 199-208.
- Celaya, M. and S. Nazarian (2007). "Assessment of Debonding in Concrete Slabs Using Seismic Methods" *Transportation Research Record*, 2016, pp 65-75.
- Chen, D. (2007). "Using rolling dynamic deflectometer and overlay tester to determine the reflective cracking potential." *Journal of Testing and Evaluation*, 35(6), 644.
- Chen, D.-H., B.-H. Nam, and K.H. Stokoe (2008). "Application of Rolling Dynamic Deflectometer to Forensic Studies and Pavement Rehabilitation Projects." *Transportation Research Record: Journal of the Transportation Research Board* 2084(-1): 73-82.
- Donovan, P. and E. Tutumluer (2009). "Falling Weight Deflectometer Testing to Determine Relative Damage in Asphalt Pavement Unbound Aggregate Layers." *Transportation Research Record: Journal of the Transportation Research Board* 2104(-1): 12-23.
- Gucunski, N. and G. Slabaugh (2008). "Impact Echo Data from Bridge Deck Testing" *Transportation Research Record*, No. 2050, pp 111-121.
- Lee, J. L., D.-H. Chen , K. H. Stokoe, and T. Scullion (2004). "Evaluating Potential for Reflection Cracking with Rolling Dynamic Deflectometer." *Transportation Research Record: Journal of the Transportation Research Board*, 1869(-1), 16-24.

Lee, J., K.H. Stokoe, D.-H. Chen, M. Garrison, and B.-H. Nam (2005). "Part 1: Pavement Rehabilitation: Monitoring Pavement Changes in a Rehabilitation Project with Continuous Rolling Dynamic Deflectometer Profiles." *Transportation Research Record: Journal of the Transportation Research Board* 1905(-1): 2-16.

Nam, B-H, T. S., K. H. Stokoe II, J.-S. Lee (2010). "Rehabilitation Assessment of Jointed Concrete Pavement Using the Rolling Dynamic Deflectometer and Ground Penetrating Radar." *Journal of Testing and Evaluation* 39(3): 12.

Nazarian, S., M. Baker, and K. Crain (1997). "Assessing Quality of Concrete with Wave Propagation Techniques" *ACI Materials Journal*, Vol. 94, No. 4, pp. 296–306.

Rahim, A. and K. P. George (2003). "Falling Weight Deflectometer for Estimating Subgrade Elastic Moduli." *Journal of Transportation Engineering* 129(1): 100.

Stubstad, R. N., Y. J. Jiang, and E. O. Lukanen (2006). *Guidelines for Review and Evaluation of Backcalculation Results*. Report FHWA-HRT-05-152. FHWA., U.S. Department of Transportation, 2006

Turner, D., J. Lee, K.H. Stokoe, R. Boudreau, Q. Watkins, and G. Chang (2003). "Discrete and Continuous Deflection Testing of Runways at Hartsfield Atlanta International Airport, Georgia." *Transportation Research Record: Journal of the Transportation Research Board* 1860(-1): 76-89.

Zaghloul, S. and M. Elfino (2000). "Pavement Rehabilitation Selection Based on Mechanistic Analysis and Field Diagnosis of Falling Weight Deflectometer Data: Virginia Experience." *Transportation Research Record: Journal of the Transportation Research Board* 1730(-1): 177-186.

Zhou, F., S. Hu, D. Chen, and T. Scullion (2011). "RDD Data Interpretation and Its Application on Evaluating Concrete Pavements for Asphalt Overlays." *Journal of Performance of Constructed Facilities*, 26(5), 657-667.

APPENDIX A GUIDANCE DOCUMENT

The following eight non-invasive technologies were field tested in order to assess their applicability to MoDOT roadways:

1. Ultrasonic Surface Waves (USW)
2. Impact Echo (IE)
3. Ground-coupled Ground Penetrating Radar (GPR) (400 MHz and 1500 MHz antennae)
4. Electrical Resistivity Tomography (ERT)
5. Multichannel Analyses of Surface Waves (MASW)
6. Falling Weight Deflectometer (FWD)
7. Rolling Dynamic Deflectometer (RDD)
8. Air-launched Ground Penetrating Radar (GPR)

In Table A.1, the applicability of each of these technologies to the assessment of BM pavements is summarized. In Tables A.2, A.3 and A.4, the applicability of each of these technologies to the assessment of PCC pavements, the base and sub-base, and soil and rock, respectively, is summarized.

In Table A.5, a more detailed description of the USW technology is presented. Recommendations for the use of this technology are included. In Tables A.6-A.13, corresponding descriptions for the IE, 1500 MHz GPR, 400 MHz GPR, ERT, MASW, FWD, RDD, and GPR (2000 MHz air-launched), respectively, are presented.

In general, the use of the non-invasive technologies listed above is recommended in cases where more information is needed than that provided by traditional coring. While cores provide detailed information at discrete locations, it may not be appropriate in some cases to extrapolate the results based on limited data. Certain non-invasive imaging technologies (e.g. ground-coupled or air-launched GPR), have the benefit of providing continuity of data that cannot be achieved by coring at discrete locations. Additionally, cores are destructive, whereas non-invasive imaging technologies are nondestructive. Therefore, more data can be acquired with less damage and repair to the pavement. Examples of cases where non-invasive technologies would be useful to MoDOT include cases where:

- The condition of pavement appears to be highly variable
- The extent of voids at joints needs to be located
- Mesh position need to be located prior to grinding

It should be noted that the non-invasive technologies mentioned above are not intended to replace coring altogether, since core control is desirable or needed to constrain the interpretation of the results. However, the frequency (number) of cores may be reduced if non-invasive technologies are employed.

Table A.1–Applications to assessment of bituminous mix (BM) pavements (USW: ultrasonic surface wave; IE: impact echo; HF-GC-GPR: high-frequency ground-coupled ground penetrating radar; LF-GC-GPR: low-frequency ground-coupled ground penetrating radar; HF-AL-GPR: high-frequency air-launched ground penetrating radar; FWD: falling weight deflectometer; RRD: rolling wheel deflectometer; ERT: electrical resistivity tomography; MASW: multi-channel analyses of surface waves). D–Direct Measurement/Primary Application; d–Direct Measurement/Non-primary Application; I–Indirect Measurement/Primary Application; i–Indirect Measurement/Non-primary Application.

	BM layer thicknesses	BM layer condition	Debonding	Stripping	Cracking	Segregation	Rutting	Corrugation	Shoving	Depression	Overlay bumps	Patching	Raveling	Moisture below BM	Voids	Shallow utilities	Delaminations
USW	d	D	i	I		I							I		I		I
IE																	
HF-GC-GPR	D	I	D	I		I							I	I	D		I
LF-GR-GPR	d	i												i	d	D	
HF-AL-GPR	D	I	D	D		I								I	D		I
FWD																	
RDD																	
ERT																	
MASW																	

Table A.2–Applications to assessment of portland cement concrete (PCC) pavements (USW: ultrasonic surface wave; IE: impact echo; HF-GC-GPR: high-frequency ground-coupled ground penetrating radar; LF-GC-GPR: low-frequency ground-coupled ground penetrating radar; HF-AL-GPR: high-frequency air-launched ground penetrating radar; FWD: falling weight deflectometer; RRD: rolling wheel deflectometer; ERT: electrical resistivity tomography; MASW: multi-channel analyses of surface waves). D–Direct Measurement/Primary Application; d–Direct Measurement/Non-primary Application; I–Indirect Measurement/Primary Application; i–Indirect Measurement/Non-primary Application.

	PCC thickness	Spalling	PCC condition	Scaling	Cracking beneath BM	Segregation	Dowel bars	Wire mesh	Shallow utilities	Overlay thickness	Patching	Joint Load Transfer	Moisture below PCC	Joint Seal damage	Slab Cracking	Voids
USW	d		D		I	I				d	d				I	I
IE																
HF-GC-GPR	D		I		I	I	D	D	d	D	D		I	D	D	D
LF-GC-GPR	d		i		i	i	d	d	D	d	d		i	d		D
HF-AL-GPR	D		I		I	I	D	D	d	D	D		I	D	D	D
FWD												D				
RRD												D				
ERT																
MASW																

Table A.3–Applications to assessment of base and subbase (USW: ultrasonic surface wave; IE: impact echo; HF-GC-GPR: high-frequency ground-coupled ground penetrating radar; LF-GC-GPR: low-frequency ground-coupled ground penetrating radar; HF-AL-GPR: high-frequency air-launched ground penetrating radar; FWD: falling weight deflectometer; RRD: rolling wheel deflectometer; ERT: electrical resistivity tomography; MASW: multi-channel analyses of surface waves). D–Direct Measurement/Primary Application; d–Direct Measurement/Non-primary Application; I–Indirect Measurement/Primary Application; i–Indirect Measurement/Non-primary Application.

	Layer thicknesses	Moisture content	Layer rigidity	Voids	Locating utilities													
USW																		
IE																		
HF-GC-GPR	d	i		d	d													
LF-GC-GPR	D	I		D	D													
HF-AL-GPR	d	i		d	d													
FWD			I															
RRD			I															
ERT	D	D																
MASW	d		D															

Table A.4–Applications to assessment of soil and rock (USW: ultrasonic surface wave; IE: impact echo; HF-GC-GPR: high-frequency ground-coupled ground penetrating radar; LF-GC-GPR: low-frequency ground-coupled ground penetrating radar; HF-AL-GPR: high-frequency air-launched ground penetrating radar; FWD: falling weight deflectometer; RRD: rolling wheel deflectometer; ERT: electrical resistivity tomography; MASW: multi-channel analyses of surface waves). D – Direct Measurement/Primary Application; d – Direct Measurement/Non-primary application; I – Indirect Measurement/Primary Application; i – Indirect Measurement/Non-primary application.

	Soil thickness	Soil lithology	Soil moisture content	Soil clay content	Soil rigidity	Voids	Locating utilities	Depth to top of rock	Rock lithology	Rock rigidity	Solution-widened joints	Clay-filled vugs						
USW																		
IE																		
HF-GC-GPR																		
LF-GC-GPR																		
HF-AL-GPR																		
FWD					I	I				I								
RRD					I	I				I								
ERT	D	I	I	I		D	d	D	I	I	D	D						
MASW	D	I			D			D	I	D	d	d						

Table A.5–Ultrasonic surface wave (USW)

Recommendations	We recommend that the PSPA USW technique (or comparable tool) be used to assess the condition of BM and/or PCC pavement.
Capabilities	The USW tool can be used to estimate variations in the elastic modulus (Young’s modulus) of BM and/or PCC pavements. Secondary USW applications include estimating pavement layer thicknesses and identifying the locations and moduli of defective zones including those caused by stripping, raveling, delaminations and debonding.
Parameters measured	The USW tool generates surface wave energy at selected test locations and measures its phase velocities. The phase velocities are transformed into a 1-D plot of elastic modulus for that test location (depth ranges of either 2 in. to 7 in. or 3 in. to 11 in. for PSPA USW; other USW models may provide for different depths of investigation). An average elastic modulus for the pavement (over depth range analyzed) is also output.
How these parameters relate to condition of roadway	The elastic modulus of pavement is a direct function of the integrity of that pavement.
Optimum acquisition parameters	The operator need only follow the manufacturer’s instructions. The operator need only input pavement type, apparent pavement condition and temperature. Unfortunately, only one type of pavement can be input. If a pavement is multi-layered, the output modulus values will be reliable only for the upper layer.
Optimum weather conditions	PSPA USW data can be acquired under any weather conditions.
Crew size (vehicle-coupled, cart-mounted).	A single trained person can operate the PSPA USW tool.
Equipment costs (2015)	Approx. \$30,000 for PSPA system (including processing software and dedicated laptop).
Volume of data that can be acquired in 8 hour day	An experienced operator should be able to acquire PSPA USW data at more than 100 closely spaced locations in a single working day.
Potential acquisition problems	Traffic control is required. Output 1-D plots of elastic modulus extend over a limited depth range (2 in, to 7 in. or 3 in. to 11 in., only).
Optimum processing parameters	The user should simply follow the manufacturer’s instructions.
Software and hardware costs	Must be purchased as part of PSPA system.
Volume of data that can be processed in an 8-hour day	Data processing is automated. The user need only download the estimated thicknesses and/or depths. Average elastic modulus can be plotted on a base map to show variations in average quality of

	pavement. The 1-D elastic modulus profiles can be transformed into 2-D cross-sections.
Ease of processing	Processing is automated.
Potential processing problems	Processing is automated. The user need only have input the correct parameters (pavement type, temperatures, pavement condition).
Optimum interpretation parameters	The user need only understand the relationship between pavement condition and pavement elastic modulus (and the potential effect of ambient temperature). The user can interpret maps showing variations in the average elastic modulus of the pavement and/or interpret the output 2-D cross-sections (depicting vertical and lateral variations in elastic modulus).
Volume of data that can be interpreted in an 8-hour day	Data processing is automated. The user need only download the average modulus data and the 1-D modulus plots.
Deliverables	Maps showing variations in the average elastic modulus of the pavement and/or 1-D plots showing how the elastic modulus of pavement varies with depth at the test locations.
Ease and reliability of interpretations	The user need only understand the relationship between pavement condition and pavement elastic modulus (and the potential effect of ambient temperature).
Potential interpretation problems	The user need only understand the relationship between pavement condition and pavement elastic modulus (and the potential effect of ambient temperature).
Recommendations (including practices that could help MoDOT; cost-effectiveness)	USW technology should be the primary tool of choice for determining the in-situ dynamic elastic moduli of pavements to depths of approx. 11 in. depending on the specific USW tool employed. Ground truthing to constrain and verify interpretations will statistically improve the accuracy of the USW interpretations. The density of USW control should be a function of the user's need to know how the dynamic elastic modulus varies laterally and vertically within the tested segment of pavement.

Table A.6–Impact echo (IE)

Recommendations	Based on our experience with the portable seismic property analyzer (PSPA), we cannot recommend that the PSPA IE technique be used for BM and/or PCC pavement investigations. In our opinion, the layer thickness estimates generated by the PSPA IE tool are frequently unreliable. Other IE tools may be more reliable than the PSPA IE tool (for pavement investigations).
Capabilities	Ideally, the PSPA IE tool can be used to estimate the thickness of BM and/or PCC pavement and the depths to imperfections within the pavement. In our opinion, the layer thickness estimates and depth estimates generated by the PSPA IE tool are frequently unreliable.
Parameters measured	The PSPA IE tool estimates the recurrence frequency of reverberations (multiple reflections) from pavement layers and/or imperfections within the pavement. These frequencies are converted to depths based on PSPA estimated compressional wave velocities. In our opinion, the layer thickness estimates and depth estimates generated by the PSPA IE tool are frequently unreliable.
How these parameters relate to condition of roadway	Ideally, the PSPA IE tool can be used to estimate the thickness of BM and/or PCC pavement and the depths to imperfections within the pavement. In our opinion, the layer thickness estimates and depth estimates generated by the PSPA IE tool are frequently unreliable.
Optimum acquisition parameters	The operator need only follow the manufacturer’s instructions. The operator need only input pavement type, apparent pavement condition and temperature.
Optimum weather conditions	PSPA IE data can be acquired under any weather conditions.
Crew size (vehicle-coupled, cart-mounted).	A single trained person can operate the PSPA IE tool.
Equipment costs (2015)	Approx. \$30,000 for PSPA system (including processing software and dedicated laptop).
Volume of data that can be acquired in 8 hour day	An experienced operator should be able to acquire PSPA IE data at more than 100 closely spaced locations in a single working day.
Potential acquisition problems	Traffic control is required.
Optimum processing parameters	The user should simply follow the manufacturer’s instructions.
Software and hardware costs	Must be purchased as part of PSPA system.
Volume of data that	Data processing is automated. The user need only download the

can be processed in an 8-hour day	estimated thicknesses and/or depths.
Ease of processing	Processing is automated.
Potential processing problems	Processing is automated. However the output PSPA IE estimated depths/thicknesses are frequently unreliable.
Optimum interpretation parameters	The output PSPA IE estimated thicknesses/depths are frequently unreliable and cannot be interpreted.
Volume of data that can be interpreted in an 8-hour day	The output PSPA IE estimated thicknesses/ depths are frequently unreliable and cannot be interpreted.
Deliverables	Maps showing variations in estimated layer thicknesses or the depths to imperfections.
Ease and reliability of interpretations	The output PSPA IE estimated thicknesses/ depths are frequently unreliable and cannot be interpreted.
Potential interpretation problems	The output PSPA IE estimated thicknesses/ depths are frequently unreliable and cannot be interpreted.
Recommendations (including practices that could help MoDOT; cost-effectiveness)	The output PSPA IE estimated thicknesses/ depths are frequently unreliable and cannot be interpreted. We do not recommend use of the PSPA IE tool. Other IE tools may be more reliable than the PSPA IE tool (for pavement investigations).

Table A.7–High-frequency ground-coupled GPR

Recommendations	For a project-level site investigation where the intent is to image BM and/or PCC pavement a GPR system with a high-frequency ground-coupled antenna (1.5/1.6 GHz) is recommended.
Capabilities	<ol style="list-style-type: none"> 1. Tool can be used to measure thicknesses of existing pavement layers with an accuracy of $\pm 10\%$ if core control is available. 2. Tool can be used to estimate the thicknesses of new pavement layers with a higher degree of accuracy. 3. Tool can be used to accurately locate pattern, placement and density of reinforcing steel, wire mesh and dowel bars. 4. Tool can be used to locate joints. 5. Tool can be used to locate shallow utilities (embedded within pavement or immediately below pavement). 6. Tool can be used to identify areas of deteriorated bituminous mix pavement, especially if the BM pavement thickness is known or is uniform, or if stripping and/or delaminations are present. 7. Tool can be used to identify deteriorated Portland cement concrete pavement, especially if the pavement thickness is known or uniform. 8. Tool can be used to image shallow voids immediately beneath pavement. 9. Tool can be used to map (qualitatively) variations in the moisture content of soil immediately beneath uniform pavement. 10. Tool can be used for QA/QC of new pavement
Parameters measured and/or displayed	GPR systems are designed to generate visual displays depicting the arrival times and amplitudes of signal reflected from within the pavement. Reflectors include all pavement layers (top, base, PCC/BM, BM/PCC, BM/BM), delaminations, stripping, reinforcing steel, wire mesh, dowel bars, utilities and joints.
How these parameters relate to condition of roadway	<p>The amplitude of a reflection from a pavement layer is a function of the nature of the interface, the condition of the interface and the condition of the overlying pavement. Lateral variations in the condition of the interface and/or the condition of the overlying pavement cause corresponding changes in the amplitude of the reflection from that interface. Often, these amplitude variations can be measured, plotted and interpreted.</p> <p>The arrival time of a reflection from a pavement layer is a function of the nature of the interface, the condition of the interface and the condition of the overlying pavement. Lateral variations in the condition of the interface and/or the condition of the overlying pavement cause corresponding changes in the arrival time of the reflection from that interface. Often, these arrival time variations can be measured, plotted and interpreted.</p> <p>Reflection amplitudes and arrival times will also change if the depth to the interface changes (e.g. variations in pavement thickness). If</p>

	<p>pavement thicknesses are not uniform, it can be difficult to confidently identify the cause of plotted amplitude and/or travel time variations. Reflections can also be generated by stripping, delaminations, voids, utilities, reinforcing steel, dowel bars, wire mesh and utilities. These can often be confidently identified by an experienced interpreter.</p>
Optimum acquisition parameters	<p>Ground-coupled high-frequency GPR data can be acquired using a single antenna mounted on a push cart. The advantages to using a push cart are flexibility and cost, as data are readily acquired wherever the operator chooses to walk and single antenna systems are relatively inexpensive to operate.</p> <p>Ground-coupled high-frequency GPR data can also be acquired using multiple antennae coupled to the back of a slow moving vehicle. The advantages to using antennae coupled to the back of a vehicle are increased safety and decreased inconvenience to traffic as data can be acquired more rapidly.</p> <p>Acquisition parameters (including speed) depend on target size. If small targets (reinforcing steel) is to be imaged, denser sampling intervals (trace spacing) and slower antenna speeds are required.</p>
Optimum weather conditions	<p>Intact and deteriorated pavements are easiest to differentiate if moisture is present. GPR data acquired when the pavement is slightly moist are more interpretable and more definitive (re: pavement condition). Pavement layer thicknesses can be estimated during any weather condition (core control will result in more accurate estimates). Similarly, reinforcing steel, wire mesh, dowel bars, utilities, voids, stripping, can be mapped during all weather conditions.</p>
Crew size (vehicle-coupled, cart-mounted).	<p>A single trained person can operate a single antenna in a push cart. A driver and a trained operator can operate a multi-antennae system (coupled to slow moving vehicle).</p>
Equipment costs (2015)	<p>A ground-coupled GPR system with a 1.5GHz antenna and pushcart costs about \$25,000.</p>
Volume of data that can be acquired in 8 hour day	<p>10,000+ linear feet of GPR data can be acquired in a single day either a pushcart or vehicle-towed multi-antennae system.</p>
Potential acquisition problems	<p>Traffic control is required.</p>
Optimum processing parameters	<p>Generally, only basic processing is required. A trained processor is required.</p>
Software and hardware costs	<p>Commercial processing/interpretation software is about \$5000.</p>
Volume of data that can be processed in an 8-hour day	<p>Depends on the data quality and pavement condition. Frequently about 5,000+ lineal ft of GPR data can be processed in one day. The processing of GPR data acquired across multi-layered pavement or poor-quality</p>

	pavement requires is slower and requires greater expertise.
Ease of processing	An experienced processor is required. The processing of GPR data acquired across multi-layered pavement or poor-quality pavement requires greater expertise. Generally, the processor interprets the GPR data.
Potential processing problems	Poor quality data can be difficult to process. The conversion of reflection times to depths is very approximate unless ground truth (core control normally) is available.
Optimum interpretation parameters	Ideally, the processor should be able to plot (on a base map) the amplitudes and apparent depths of all reflectors of interest.
Volume of data that can be interpreted in an 8-hour day	Depends on the data quality and pavement condition. If ground truth is available, a skilled interpreter (normally the processor) can normally assess large volumes of mapped amplitude and apparent depth data in a few hours.
Deliverables	A suite of maps showing variations in the amplitudes and apparent depths of reflectors of interest with superposed interpretations highlighted features of interest.
Ease and reliability of interpretations	If ground truth is available, a skilled processor/interpreter will generate very reliable interpretations.
Potential interpretation problems	Interpretations are non-unique and can be somewhat ambiguous if additional data are not available (e.g. ground truth)
Recommendations (including practices that could help MoDOT; cost-effectiveness)	<p>The high-frequency ground-coupled cart-mounted GPR technology should be the primary tool of choice for the following project-level pavement condition assessment applications:</p> <ul style="list-style-type: none"> • Tool can be used to measure thicknesses of existing pavement layers with an accuracy of $\pm 10\%$ if core control is available. • Tool can be used to estimate the thicknesses of new pavement layers with a higher degree of accuracy. • Tool can be used to accurately locate pattern, placement and density of reinforcing steel, wire mesh and dowel bars. • Tool can be used to locate joints. • Tool can be used to locate shallow utilities (embedded within pavement or immediately below pavement). • Tool can be used to identify areas of deteriorated bituminous mix pavement, especially if the BM pavement thickness is known or is uniform, or if stripping and/or delaminations are present. • Tool can be used to identify deteriorated Portland cement concrete pavement, especially if the pavement thickness is known or is uniform. • Tool can be used to image shallow voids immediately beneath pavement.

	<ul style="list-style-type: none">• Tool can be used to map (qualitatively) variations in the moisture content of soil immediately beneath uniform pavement.• Tool can be used for QA/QC of new pavement <p>Ground truthing to constrain and verify interpretations will statistically improve the accuracy of the GPR interpretations.</p>
--	--

Table A.8–Low-frequency ground-coupled GPR

Recommendations	For a project-level or network-level site investigations where the objective is to map the base layers, sub-base layers and perhaps even the top of shallow rock. GPR system with a ground-coupled high-frequency antenna (200 MHz to 400 MHz) is recommended.
Capabilities	<ol style="list-style-type: none"> 1. Tool can be used to measure the thicknesses of base, sub-base and shallow soil layers with an accuracy of $\pm 10\%$ if core control is available. 2. Tool can be used to locate joints. 3. Tool can be used to locate shallow utilities and culverts. 4. Tool can be used to image shallow voids immediately beneath pavement. 5. Tool could be used to map top of shallow bedrock (to depths typically less than approx. 9 feet depending upon the frequency of GPR antenna employed).
Parameters measured	GPR systems are designed to generate visual displays depicting the arrival times and amplitudes of signal reflected from within the pavement. Reflectors include base, sub-base, and in some instances shallow bedrock.
How these parameters relate to condition of roadway	<p>The amplitude of a reflection from a layer (base, sub-base, top of soil, top of rock) layer is a function of the nature of the interface, the condition of the interface and the condition of the overlying pavement. Lateral variations in the condition of the interface and/or the condition of the overlying pavement cause corresponding changes in the amplitude of the reflection from that interface. Often, these amplitude variations can be measured, plotted and interpreted.</p> <p>The arrival time of a reflection from a layer is a function of the nature of the interface, the condition of the interface and the condition of the overlying pavement. Lateral variations in the condition of the interface and/or the condition of the overlying pavement layers cause corresponding changes in the arrival time of the reflection from that interface. Often, these arrival time variations can be measured, plotted and interpreted by an experienced interpreter.</p> <p>Reflection amplitudes and arrival times will also change if the depth to the interface changes (e.g. variations in pavement thickness). If pavement thicknesses are not uniform, it can be difficult to confidently identify the cause of plotted amplitude and/or travel time variations.</p>
Optimum acquisition parameters	Ground-coupled GPR data can be acquired using a single antenna mounted on a push cart or slow moving vehicle. Acquisition parameters (including speed) depend on target size. If smaller targets (joints) are to be imaged, denser sampling intervals (trace spacing) and slower vehicle speeds are required.
Optimum weather	Basal pavement layers can be mapped during almost any weather

conditions	condition (core control will result in more accurate interpretations).
Crew size (vehicle-coupled, cart-mounted).	A single trained person can operate a single antenna in a push cart. A driver and a trained operator can operate a system coupled to slow moving vehicle.
Equipment costs (2015)	Approx. \$20,000 for a ground-coupled GPR system with a 400 GHz antenna. Additional antenna's (200 MHz) cost about \$5000.
Volume of data that can be acquired in 8 hour day	A trained operator can easily acquire 10,000+ linear feet of low-frequency GPR data per day.
Potential acquisition problems	Traffic control is required. Low-frequency antennae may not be able to reliably image the subsurface beneath densely spaced reinforcing steel.
Optimum processing parameters	Generally, only basic processing is required. A trained processor is required.
Software and hardware costs	Commercial processing/interpretation software is about \$5000.
Volume of data that can be processed in an 8-hour day	Depends on the data quality and pavement condition. Frequently about 5,000+ lineal ft of GPR data can be processed in one day. The processing of poor quality data and/or GPR data acquired across multi-layered pavement or poor-quality pavement requires is slower and requires greater expertise.
Ease of processing	Poor quality data can be difficult to process. The conversion of reflection times to depths is very approximate unless ground truth (core control normally) is available.
Potential processing problems	Poor quality data can be difficult to process. The conversion of reflection times to depths is very approximate unless ground truth (core control normally) is available.
Optimum interpretation parameters	Ideally, the processor should be able to plot (on a base map) the amplitudes and apparent depths of all reflectors of interest.
Volume of data that can be interpreted in an 8-hour day	Depends on the data quality and pavement condition. If ground truth is available, a skilled interpreter (normally the processor) can normally assess large volumes of mapped amplitude and apparent depth data in a few hours.
Deliverables	A suite of maps showing variations in the amplitudes and apparent depths and thicknesses of layers of interest with superposed interpretations highlighted features of interest (culverts, utilities, etc.)..
Ease and reliability of interpretations	If ground truth is available, a skilled processor/interpreter will generate very reliable interpretations.
Potential interpretation problems	Interpretations are non-unique and can be somewhat ambiguous if additional data are not available (e.g. ground truth)
Recommendations (including practices	The low-frequency ground-coupled cart-mounted GPR technology should be the primary tool of choice for the following project-level

that could help MoDOT; cost-effectiveness)	<p>pavement condition assessment applications:</p> <ul style="list-style-type: none">• Tool can be used to measure the thicknesses of base, sub-base and shallow soil layers with an accuracy of $\pm 10\%$ if core control is available.• Tool can be used to locate shallow utilities and culverts.• Tool can be used to image shallow voids immediately beneath pavement. <p>Ground truthing to constrain and verify interpretations will statistically improve the accuracy of the GPR interpretations.</p>
--	--

Table A.9—Electrical resistivity tomography (ERT)

Recommendations	We recommend that the ERT technique be used to assess the condition of the base, sub-base, soil and rock beneath existing roadways or prior to or during the construction of roadways on an as needed basis.
Capabilities	The ERT tool can be used to map variations in the lithology of the subsurface and to estimate variations in the moisture content of the base, sub-base, soil and rock. The competency of rock can be estimated in a qualitative manner.
Parameters measured	The ERT tool is normally used to generate 2-D resistivity images of the subsurface. If a correlation between lithology and resistivity can be established, ERT profiles can be essentially transformed into geologic profiles. The resistivity of rock is often a function of its integrity.
How these parameters relate to condition of roadway	The ERT tool is normally used to generate 2-D resistivity images of the subsurface (to depths in excess of one hundred feet). If a correlation between lithology and resistivity can be established, ERT profiles can be essentially transformed into geologic profiles. The resistivity of rock is often a function of its integrity.
Optimum acquisition parameters	Acquisition parameters vary. Guidelines are available. Longer arrays are used to image the subsurface to greater depths. More closely spaced electrodes provide for higher spatial; resolution. There is a trade-off between higher resolution and acquisition costs.
Optimum weather conditions	ERT cannot be acquired while it is raining as moisture can damage the electrodes.
Crew size (vehicle-coupled, cart-mounted).	An ERT crew normally consists of four persons.
Equipment costs (2015)	Approx. \$80,000 for an ERT system equipped with 56 electrodes.
Volume of data that can be acquired in 8 hour day	Experienced operators should be able to acquire about 1000 lineal feet of ERT data in a single working day (56 electrodes; 5 ft electrode spacing).
Potential acquisition problems	If ERT data are acquired on paved roadway traffic control is required and holes must be drilled through the BM and or PCC to ensure electrodes are in contact with moist base or soil. ERT data are most commonly acquired in ROW.
Optimum processing parameters	Significant training and experience is required.
Software and hardware costs	Software is about \$5000. Dedicated computer is extra.
Volume of data that can be processed in an 8-hour day	An experienced operator can normally process 1000 lineal ft of ERT data in a single day. It normally takes more time to process poor quality field records.
Ease of processing	Training and experience is required. An experienced operator can

	normally process 1000 lineal ft of ERT data in a single day. It normally takes more time to process poor quality field records.
Potential processing problems	Training and experience is required. In certain instances, poor or suspect quality data must be removed from the data set prior to inversion. Processor must be able to recognize suspect data.
Optimum interpretation parameters	Training and experience is required. Ground truth is essential if resistivity profiles are going to be transformed into reliable 2-D geologic images.
Volume of data that can be interpreted in an 8-hour day	Training and experience is required. Ground truth will help the processor ensure that geologic interpretations are reasonable. Interpreter needs to understand the relationship between resistivity and lithology.
Deliverables	Normally, each ERT data set is transformed into a 2-D geologic image.
Ease and reliability of interpretations	Ground truth will help the processor ensure that geologic interpretations are reasonable. Interpreter needs to understand the relationship between resistivity and lithology.
Potential interpretation problems	Interpreter needs to understand the relationship between resistivity and lithology.
Recommendations (including practices that could help MoDOT; cost-effectiveness)	The ERT tool can be used to map lateral and vertical variations in the resistivity of the subsurface (normally soil and rock, unless electrodes are inserted into top of paved roadway). Output 2-D resistivity plots can be transformed into corresponding geologic models. Ground truthing to constrain and verify the ERT interpretations will increase the reliability of the output geologic models. The maximum depth of investigation is determined mostly by the size of the ERT array employed. A shorter electrode spacing will provide for higher vertical and lateral resolution.

Table A.10—Multi-channel analyses of surface waves (MASW)

Recommendations	We recommend that the MASW technique (or comparable tool: ReMi) be used to assess the condition of the base, the sub-base, soil and rock beneath existing roadways or prior to or during the construction of roadways on an as needed basis.
Capabilities	The MASW tool can be used to estimate variations in the rigidity of base, sub-base, soil and rock.
Parameters measured	The MASW tool generates surface wave energy at selected test locations and measures its phase velocities. The phase velocities are transformed into a 1-D plot of shear-wave velocity of the pavement and subsurface at that test location (to depths in excess of 100 ft).
How these parameters relate to condition of roadway	The shear wave velocity of pavement, soil and rock is a direct function of the rigidity (shear modulus) of that pavement. If ground truth is available, shear-wave velocities can often be correlated to lithology.
Optimum acquisition parameters	Acquisition parameters vary. Guidelines are available. Heavier sources and longer geophone arrays are generally used to image the subsurface to greater depths.
Optimum weather conditions	MASW data can be acquired under any weather conditions.
Crew size (vehicle-coupled, cart-mounted).	An MASW crew normally consists of three persons.
Equipment costs (2015)	Approx. \$30,000 for engineering seismograph, 24-channel cable and 24 low-frequency geophones.
Volume of data that can be acquired in 8 hour day	Experienced operators should be able to acquire MASW at 20 closely spaced locations in a single working day.
Potential acquisition problems	Traffic control is required is data are acquired on paved roadway. Data can also be acquired in ROW.
Optimum processing parameters	Training and experience is required. Processor input is necessary.
Software and hardware costs	Software is about \$2000. Dedicated computer is extra.
Volume of data that can be processed in an 8-hour day	An experienced operator can normally process 25 MASW records in a single day. It normally takes more time to process poor quality field records.
Ease of processing	Training and experience is required. Each MASW data set is transformed into a 1-D shear-wave velocity profile. If MASW data are acquired at multiple locations along a traverse, a 2-D shear-wave velocity profile can be constructed.
Potential processing problems	Training and experience is required. Ground truth will help the processor ensure that fundamental mode surface wave data are

	analyzed.
Optimum interpretation parameters	Training and experience is required. Ground truth will help the processor ensure that fundamental mode surface wave data are analyzed and that geologic interpretations (if any) are reasonable.
Volume of data that can be interpreted in an 8-hour day	Training and experience is required. Ground truth will help the processor ensure that geologic interpretations (if any) are reasonable. Interpreter needs to understand the relationship between shear-wave velocity and material integrity.
Deliverables	Each MASW data set is transformed into a 1-D shear-wave velocity profile. If MASW data are acquired at multiple locations along a traverse, a 2-D shear-wave velocity profile can be constructed.
Ease and reliability of interpretations	The user need only understand the relationship between shear modulus and the integrity of the tested material. Ground truth will be very useful if the interpreter intends to superpose geologic interpretations on the 1-D and 2-D shear-wave velocity profiles.
Potential interpretation problems	The user need only understand the relationship between shear modulus and the integrity of the tested material, and the relationship between shear modulus and lithology.
Recommendations (including practices that could help MoDOT; cost-effectiveness)	The MASW tool can be used to map lateral and vertical variations in the rigidity of base, sub-base, soil and rock. Output 1-D and/or 2-D shear-wave velocity plots can be transformed into corresponding geologic models. Ground truthing to constrain and verify the MASW interpretations will increase the reliability of the output geologic models. The maximum depth of investigation is determined mostly by the size of the acoustic source employed. If 2-D data are acquired, the spacing between adjacent 1-D traces should be a function of the anticipated complexity of the subsurface. For example, if the subsurface is essentially horizontally stratified, it can be effectively modelled using as few as one MASW field record. It is the opinion of the researchers that shorter geophone arrays should be employed if shallower depths of investigation are desired. The use of shorter arrays will minimize the potential for lateral smoothing. Interpretation of a narrower range of high-frequencies will provide for shallower depths of investigation but higher resolution over that depth range.

Table A.11–Falling weight deflectometer (FWD)

Recommendations	The FWD can be used for project level site investigations where information on joint quality or pavement stiffness is desired. The primary drawback is the point-by-point nature of the measurement and the resulting limited pavement coverage.
Capabilities	The FWD is a well-established technology and the capabilities of the FWD for various applications have been studied and documented extensively. The FWD can be used for a variety of applications including: evaluating joint conditions in rigid pavements, qualitative assessment of pavement condition based on deflection magnitudes, estimating pavement stiffness using empirical relationships, back-calculating pavement stiffness parameters, and detecting voids beneath the pavement.
Parameters measured	The FWD records the deflection profile created from an impact load designed to simulate traffic loading applied to the surface of the pavement. The peak deflections recorded at each receiver are the primary parameters measured by the FWD, along with the peak magnitude of the applied load.
How these parameters relate to condition of roadway	The pavement deflections measured by the FWD provides information on the pavement structural stiffness, as opposed to a functional performance indicator such as surface roughness. Pavements experiencing higher deflections will generally have a shorter life and require rehabilitation or reconstruction sooner than pavements with smaller deflections. Also, changes in the magnitude of deflections can indicate degradation of material performance in the pavement system. The deflections can be used in either empirical equations or back-calculations procedures to estimate pavement and subgrade stiffness parameters.
Optimum acquisition parameters	Data is typically acquired using multiple drop heights resulting in a range of applied loads to the pavement. The plate should be positioned on a clean surface free of rocks and debris. Acquisition parameters such as drop height, plate size, number of sensors and locations of sensors will vary depending on the type of pavement and purpose of the FWD measurement.
Optimum weather conditions	RDD operation is often subject to temperature restrictions to avoid frozen ground conditions and excessively high pavement temperatures. Criteria will vary from state to state. Testing may also be restricted under conditions of high winds, wet roads, icy or snowy road conditions, or limited visibility conditions.
Crew size (vehicle-coupled, cart-mounted).	An RDD crew normally consists of two people.

Equipment costs	Equipment is already owned by MoDOT so acquisition is not required
Volume of data that can be acquired in 8 hour day	FWD testing at a single locations can be completed in several minutes. Typically the FWD can cover 100 to 200 test locations in an 8-hr day.
Potential acquisition problems	Traffic control is required. Proper seating of the load plate is important. The plate should be placed on a clean surface free of rocks and debris. The equipment should be calibrated to ensure reliable readings.
Optimum processing parameters	Data processing parameters vary depending on the analysis being performed and the purpose of FWD measurement.
Software and hardware costs	Equipment is already owned by MoDOT so acquisition is not required
Volume of data that can be processed in an 8-hour day	Raw data collected by the load sensor and geophones are processed by the manufacturer software to produce output files of peak deflection and peak load for each weight drop performed. Time required for further processing of data depends on the analysis being performed and purpose of the FWD measurement.
Ease of processing	Processing of FWD data for calculating load transfer efficiency (LTE) of joints and empirical stiffness parameters can be performed easily from the FWD deflection data. Processing of the data using back-calculation procedures can be more time-consuming and requires experience and pavement input parameters.
Potential processing problems	Back-calculation of modulus values requires knowledge of layer thickness, Poisson's ratio, and an initial "seed" modulus value for each layer. The reliability of stiffness values obtained depends on the validity of these input parameters. Also, the back-calculation procedures typically assume static loadings and disregard dynamic effects, which can be important, particularly if a shallow stiff layer is present.
Optimum interpretation parameters	Processed FWD data produces numerical values of pavement parameters, such as stiffness, joint LTE, and peak deflection. The reliability of back-calculated and empirically derived values is dependent on the validity of the input parameters and analysis procedure or empirical equation.
Volume of data that can be interpreted in an 8-hour day	Processed FWD data produces numerical values of pavement parameters, such as stiffness, joint LTE, and peak deflection. The reliability of back-calculated and empirically derived values is dependent on the validity of the input parameters and analysis procedure or empirical equation.
Deliverables	Deliverables will depend on the application and purpose of the FWD measurement. They may include: back-calculated layer stiffness

	values, empirically estimated stiffness parameters, LTE of joints, or peak deflections.
Ease and reliability of interpretations	FWD measurements do not require subjective interpretation of the results as with some NDE methods. However, the reliability of the processed FWD data, particularly estimates of pavement stiffness parameters, depend on the validity of the assumptions used in the analysis procedure.
Potential interpretation problems	Stiffness estimates may be unreliable if the assumptions in the analysis procedure do not represent the actual conditions.
Recommendations (including practices that could help MoDOT; cost-effectiveness)	The FWD is already in use by MoDOT personnel and its utility and limitations for various pavement applications have been demonstrated by numerous studies. The FWD is a very effective tool for project-level studies of pavement and joint performance. Back-calculation procedures to estimate layer stiffness values can be time consuming and may not be easily implemented in a state-wide pavement management program due to the extensive amount of data that would be collected. Simpler parameters such as peak deflection or empirically-based estimates of stiffness may be better alternatives to track pavement performance for implementation into a pavement management program. The primary drawback of the FWD measurement is the point-by-point nature of the measurement which limits its coverage for network-level applications.

Table A.12—Rolling dynamic deflectometer (RDD)

Recommendations	For a project-level site investigation where there is a need for high-resolution structural information about the pavement or for rapid testing of load transfer across joints in rigid pavements
Capabilities	The RDD can be used to provide a continuous profile of pavement deflections for both rigid and flexible pavements. For flexible pavement the RDD provides a qualitative assessment of pavement support conditions. In rigid pavements the RDD can be used to measure the performance of joints and support conditions under joints. The RDD is not likely to be effective for detecting flaws or problems within the pavement surface layer.
Parameters measured	The RDD makes a direct and continuous measurement of the deflection (mils) of the pavement under a dynamic, sinusoidal load applied through a rolling wheel.
How these parameters relate to condition of roadway	The RDD provides an indicator of pavement structural performance by measuring pavement deflection (indicating pavement stiffness), as opposed to a functional performance indicator such as surface roughness. Pavements experiencing higher deflections will generally require rehabilitation or reconstruction sooner than pavements with smaller deflections. Also, changes in the magnitude of deflections can indicate degradation of material performance in the pavement system
Optimum acquisition parameters	Data is typically acquired using a nominal peak-to-peak sinusoidal force of 10 kips applied at a frequency of about 30 Hz. The force and frequency are adjustable and can be changed if needed. The pavement deflections are measured using rolling sensors (typically three) located between the loading wheels and 3.2 and 4.7 ft away from the loading wheels.
Optimum weather conditions	For safety, RDD testing is ideally performed under dry pavement conditions with good visibility.
Crew size (vehicle-coupled, cart-mounted).	An RDD crew normally consists of two people (one driver and one data recorder).
Equipment costs (2015)	Approx. \$300,000 for an RDD system (must be custom built)
Volume of data that can be acquired in 8 hour day	Four to eight miles of data can be acquired under ideal circumstances at one site
Potential acquisition problems	Should be no problems if equipment is operating properly and traffic control is in place. Very rough pavements (highly fractured, cracked sections) may cause problems with tracking of the rolling wheels.
Optimum processing parameters	Data processing is largely automated and produces a profile in near-real time.
Software and	Computer and data acquisition card are required. Software

hardware costs	development will be necessary to process the raw data. The software is not purchased off the shelf at this stage of development.
Volume of data that can be processed in an 8-hour day	Data processing as implemented by the University of Texas operators of the RDD is automated and produces a profile in near-real time.
Ease of processing	Data processing is largely automated and produces a profile in near-real time. Experiences is needed to assure high-quality data.
Potential processing problems	Averaging larger blocks of data will produce better signal to noise ratios at the expense of spatial resolution. Selection of the proper processing parameters requires experience.
Optimum interpretation parameters	Selection of processing parameters will depend on the quality of the data collected and may vary from site to site.
Volume of data that can be interpreted in an 8-hour day	The time required for data interpretation depends on the application and quality of the data.
Deliverables	Normally, a continuous profile of pavement deflection vs. distance at a minimum. Interpretations of load transfer efficiency at joints for rigid pavements
Ease and reliability of interpretations	Site dependent.
Potential interpretation problems	Identifying the proper points in the deflection plots around joints to calculate load transfer efficiency.
Recommendations (including practices that could help MoDOT; cost-effectiveness)	As a pavement management tool, the RDD could be used to test pavement systems that are scheduled for rehabilitation in the near future. The ability to test at 1 to 2 mph will allow for extensive coverage of pavements in a relatively short amount of time. The structural information from the RDD could be used to identify regions in need of further study (due to anomalously high deflections) or to develop and apply more site specific rehabilitation strategies based on structural performance. In addition, the RDD could be used as an effective quality control tool to evaluate newly constructed or rehabilitated pavements to verify, for example, the joint reconstructions have been performed properly.

Table A.13–High-frequency air-launched GPR

Recommendations	For a regional-level site investigation where the intent is to image BM and/or PCC a GPR system with a high-frequency air-launched antenna (2 GHz) is recommended.
Capabilities	<ol style="list-style-type: none"> 1. Tool can be used to measure thicknesses of existing pavement layer with an accuracy of $\pm 10\%$ if core control is available. 2. Tool can be used to estimate the thicknesses of new pavement layers with a higher degree of accuracy. 3. Tool can be used to accurately locate pattern, placement and density of reinforcing steel, wire mesh and dowel bars. 4. Tool can be used to locate joints. 5. Tool can be used to locate shallow utilities (embedded within pavement or immediately below pavement). 6. Tool can be used to identify areas of deteriorated bituminous mix pavement, especially if the BM pavement thickness is known or uniform, or if stripping and/or delaminations are present. 7. Tool can be used to identify deteriorated Portland cement concrete pavement, especially if the pavement thickness is known or uniform. 8. Tool can be used to image shallow voids immediately beneath pavement. 9. Tool can be used to map (qualitatively) variations in the moisture content of soil immediately beneath uniform pavement. 10. Tool can be used for QA/QC of new pavement.
Parameters measured and/or displayed	GPR systems are designed to generate visual displays depicting the arrival times and amplitudes of signal reflected from within the pavement. Reflectors include all pavement layers (top, base, PCC/BM, BM/PCC, BM/BM), delaminations, stripping, reinforcing steel, wire mesh, dowel bars, utilities and joints.
How these parameters relate to condition of roadway	<p>The amplitude of a reflection from a pavement layer is a function of the nature of the interface, the condition of the interface and the condition of the overlying pavement. Lateral variations in the condition of the interface and/or the condition of the overlying pavement cause corresponding changes in the amplitude of the reflection from that interface. Often, these amplitude variations can be measured, plotted and interpreted.</p> <p>The arrival time of a reflection from a pavement layer is a function of the nature of the interface, the condition of the interface and the condition of the overlying pavement. Lateral variations in the condition of the interface and/or the condition of the overlying pavement cause corresponding changes in the arrival time of the reflection from that interface. Often, these arrival time variations can be measured, plotted and interpreted.</p> <p>Reflection amplitudes and arrival times will also change if the depth to</p>

	the interface changes (e.g. variations in pavement thickness). If pavement thicknesses are not uniform, it can be difficult to confidently identify the cause of plotted amplitude and/or travel time variations. Reflections can also be generated by stripping, delaminations, voids, utilities, reinforcing steel, dowel bars, wire mesh and utilities. These can often be confidently identified by an experienced interpreter.
Optimum acquisition parameters	Air-launched high-frequency GPR data are normally acquired in a fast moving (highway speeds) vehicle. Acquisition parameters (including speed) depend on target size. If small targets (reinforcing steel) is to be imaged, denser sampling intervals (trace spacing) and slower vehicle speeds are required.
Optimum weather conditions	Intact and deteriorated pavements are easiest to differentiate if moisture is present. GPR data acquired when the pavement is slightly moist are more interpretable and more definitive (re: pavement condition). Pavement layer thicknesses can be estimated during any weather condition (core control will result in more accurate estimates). Similarly, reinforcing steel, wire mesh, dowel bars, utilities, voids, stripping, can be mapped during all weather conditions.
Crew size	Typically 2 persons; a driver and an operator.
Equipment costs (2015)	An air-launched GPR system with a twin 2-GHz antennae and all mounts costs about \$80,000.
Volume of data that can be acquired in 8 hour day	A 2-person field crew using a commercial vehicle can acquire air-launched GPR data at highway speeds.
Potential acquisition problems	The operator must be able to mount both the GPR and GPS systems on the vehicle and interface the data.
Optimum processing parameters	Generally, only basic processing is required. A trained processor is required.
Software and hardware costs (2015)	Commercial processing/interpretation software is about \$5000.
Volume of data that can be processed in an 8-hour day	Depends on the data quality and pavement condition. Frequently about 5,000+ lineal ft of GPR data can be processed in one day. The processing of GPR data acquired across multi-layered pavement or poor-quality pavement requires is slower and requires greater expertise.
Ease of processing	An experienced processor is required. The processing of GPR data acquired across multi-layered pavement or poor-quality pavement requires greater expertise. Generally, the processor interprets the GPR data.
Potential processing problems	Poor quality data can be difficult to process. The conversion of reflection times to depths is very approximate unless ground truth (core control normally) is available.
Optimum	Ideally, the processor should be able to plot (on a base map) the

interpretation parameters	amplitudes and apparent depths of all reflectors of interest.
Volume of data that can be interpreted in an 8-hour day	Depends on the data quality and pavement condition. If ground truth is available, a skilled interpreter (normally the processor) can normally assess large volumes of mapped amplitude and apparent depth data in a few hours.
Deliverables	A suite of maps showing variations in the amplitudes and apparent depths of reflectors of interest with superposed interpretations highlighted features of interest.
Ease and reliability of interpretations	If ground truth is available, a skilled processor/interpreter will generate very reliable interpretations.
Potential interpretation problems	Interpretations are non-unique and can be somewhat ambiguous if additional data are not available (e.g. ground truth)
Recommendations (including practices that could help MoDOT; cost-effectiveness)	<p>The high-frequency air-launched GPR technology should be the primary tool of choice for the following network-level pavement condition assessment applications:</p> <ul style="list-style-type: none"> • Tool can be used to measure thicknesses of existing pavement layers with an accuracy of $\pm 10\%$ if core control is available. • Tool can be used to estimate the thicknesses of new pavement layers with a higher degree of accuracy. • Tool can be used to accurately locate pattern, placement and density of reinforcing steel, wire mesh and dowel bars. • Tool can be used to locate joints. • Tool can be used to locate shallow utilities (embedded within pavement or immediately below pavement). • Tool can be used to identify areas of deteriorated bituminous mix pavement, especially if the BM pavement thickness is known or is uniform, or if stripping and/or delaminations are present. • Tool can be used to identify deteriorated Portland cement concrete pavement, especially if the pavement thickness is known or is uniform. • Tool can be used to image shallow voids immediately beneath pavement. • Tool can be used to map (qualitatively) variations in the moisture content of soil immediately beneath uniform pavement. • Tool can be used for QA/QC of new pavement <p>Ground truthing to constrain and verify interpretations will statistically improve the accuracy of the GPR interpretations. We recommend acquiring data using two air-launched GPR antennae.</p>

APPENDIX B PAVEMENT CORES AND AUGER SAMPLES